PEROXIDE BLEACH ACTIVATION: KINETICS AND MECHANISMS OF SOME ACYL TRANSFER REACTIONS

MICHAEL EDWARD DEARY

A thesis submitted in partial fulfilment of the
requirements of the Council for National Academic Awards
for the degree of Doctor of Philosophy

November 1990

Newcastle Upon Tyne Polytechnic in collaboration
with Warwick International Ltd.

CONTENTS

This thesis is dedicated, with much love, to my wife Katherine and my baby daughter Hannah.

ABSTRACT

This research has been concerned with a kinetic and mechanistic study of peroxide bleach activation, which is an important process with regard to detergent formulations. Bleach activation occurs *in situ* in the laundry liquor and utilises the reaction of alkaline hydrogen peroxide with a peroxyacid precursor (the bleach activator), such as tetraacetylethylene-diamine (TAED) or pentaacetylglucose (PAG), to yield an organic peroxyacid - usually peracetic acid. Peroxyacids are more efficient than the traditionally used hydrogen peroxide at stain removal in today's preferred low temperature washes. The studies contained herein will have hopefully contributed to a greater understanding of the process of bleach activation, facilitating developments in this area. Our approach to this study was to initially work on a bleach activator, p-nitrophenylacetate (PNPA) for which the activation reaction scheme was relatively easy to elucidate. An important feature to arise from the PNPA study was that, in addition to the reaction of hydrogen peroxide with PNPA to yield peracetic acid, peracetic acid itself reacts with PNPA, yielding diacetyl peroxide, which subsequently undergoes hydrolysis and perhydrolysis. It was essential during this study to be able to measure peracetic acid in the presence of excess hydrogen peroxide. This was made possible by the development, by us, of an iodimetric spectrophotometric technique capable of rapidly and accurately measuring peracetic acid concentrations as low as 1×10^{-5} M in the presence of up to 1000 - fold excess of hydrogen peroxide.

The methods and approach developed in the study of PNPA were successfully applied to the study of two commercially used bleach activators, TAED and PAG. Our studies of the reactivity of various nucleophiles towards TAED revealed enhanced reactivity for the hydrogen peroxide anion compared to other peroxide species. A cyclic intermediate mechanism is proposed by us to explain this observation; the hydrogen peroxide anion acts as both nucleophile and general acid catalyst in it's reaction with TAED. From work done on PAG we have shown that, despite the often quoted yield of 2.5 moles of peracetic acid per mole of PAG, all 5 acetyl groups are available for transfer to nucleophiles. Also suggested from the PAG studies is the possibility that rate limiting acetyl migration may be important for these reactions.

CHAPTER 1 MECHANISMS OF ACYL TRANSFER REACTIONS OF AMIDES AND ESTERS

1.1 General Introduction

The research described within this thesis is concerned with the process of bleach activation.

Up to the early 1970's, the boil wash formed the basis for washing practice in the UK and Western Europe; however, since then, major changes have taken place due to increased use of coloured cottons[1], increased use of synthetics and synthetic blends[1], and a drastic rise in electricity prices.[2] Consequently, low-temperature washes, typically 60°C or less, are now preferred. Hydrogen peroxide, the traditional bleach used in European detergent formulations (in the form of sodium perborate), is inefficient at stain removal below temperatures of 60°C and, therefore, an alternative bleaching moiety is required in order to obtain effective bleaching at low temperatures. The removal of oxidisable stains from fabrics by means of peroxygen bleaches at temperatures less than 60°C customarily involves the use of organic peroxides[3,4,5] (peracids). The most commonly-used peracid is peracetic acid, normally generated *in situ* in the laundry liquor by the reaction of alkaline hydrogen peroxide with a peracid precursor (the bleach activator). The process of *in situ* peracid generation is known as bleach activation, so called because we are essentially activating the poor low-temperature bleaching performance of hydrogen peroxide. In addition to this reaction, the bleach activator also undergoes hydrolysis; this is wasteful from the point of view of bleach activation since a bleaching moiety is not generated.

The first patent for a bleach activator, tetraacetylethylenediamine (TAED), appeared in 1959[6] and, whilst numerous other bleach activators

have been patented, TAED remains by far the most commonly-used bleach activator in European detergent formulations, having over 90% of the market share (1986/7 figures).[7] The two other main bleach activators used in European formulations are isononanoyloxibenzenesulphonate (ISONOBS) and penta-o-acetylglucose (PAG), with 1.5% and 5% of the activator market share, respectively.[7] The commercially-used alternative to bleach activation is to add peracids to the wash preformed, such as H48[3,4] (active ingredient, magnesium monoperoxyphthalate hexahydrate). The advantages and disadvantages of *in situ* generation and preformed addition of peracids have been discussed in the literature.[3,4]

Scheme 1.1 shows the general form of the reaction of hydrogen peroxide with bleach activators; in TAED and PAG R = CH_3, whilst for ISONOBS R = $(CH_2)_7CH_3$.

Scheme 1.1

These reactions are acyl (or aroyl where R = Ar) transfer reactions, general reviews of which can be found in the literature (see for example Jencks[8,9,10]; Williams and Douglas[11]; Bender[12]). In this chapter we have reviewed the more limited field of acyl and aroyl transfer reactions of esters and amides, since the bleach activators that we have studied (p-nitrophenylacetate, TAED and PAG) belong to these groups. Experimentally, because of the stability conferred upon amides by resonance of the nitrogen lone pair electrons with the carbonyl function, the study of the reaction of a range of nucleophiles with all but the most highly activated amides, such as imides[13,14], acetylimidazole[15,16] and N - acylated pyridiniums[17], is difficult. Consequently,

reflecting the much larger body of literature on the reaction of esters with nucleophiles, there is necessarily a bias towards these reactions in this review.

1.2 Structural Considerations

This section is a brief review of the effects on reactivity of various structural features of amides and esters. Table 1.1 contains a list of 74 structurally different esters and amides and compares their reactivities, based on the rate of reaction with the hydroxide ion. The rate constant k_{OH} was used as the basis of the comparison of reactivities because it is the most commonly available rate constant in the literature. A glance through Table 1.1 will reveal the wide range of reactivities exhibited by amides and esters. For the limited number of amides listed in Table 1.1, the k_{OH} values span the range $1.9 \times 10^{-6} M^{-1}s^{-1}$ (paramethoxyacetanilide [7][18]) to $1.6 \times 10^{6} M^{-1}s^{-1}$ (N-Acetyl-4-methylpyridinium [12][17]). Similarly, for the esters illustrated in Table 1.1, the range is $8.4 \times 10^{-5} M^{-1}s^{-1}$ (ethyl-p-aminobenzoate [55][19,20]) to $2.83 \times 10^{4} M^{-1}s^{-1}$ [51][21]. The structural features of amides and esters, which appear to be primarily accountable for the extremely wide range of reactivities at the carbonyl carbon, are discussed below.

1.2.1 Resonance Stabilisation

Compared to the corresponding esters, most amides generally exhibit a lower reactivity towards OH^- [22,23], as is evidenced by the respective k_{OH} values for diacetylamine [15][24] (0.88 $M^{-1}s^{-1}$) and acetic anhydride [74][25] (966.7 $M^{-1}s^{-1}$); similarly, metanitroacetanilide [6][18] ($1.1 \times 10^{-5} M^{-1}s^{-1}$) and m-nitrophenylacetate [37] (6.867 $M^{-1}s^{-1}$)[25]. The mechanism of reaction of an amide or an ester with OH^-, in alkaline conditions, is generally considered to be of the form shown below.

Table 1.1 Comparison of rate constants for the alkaline hydrolysis of amides and esters in water at 25°C.

Name of compound	Structure		$k_{OH}/M^{-1}s^{-1}$	Reference
Formamide	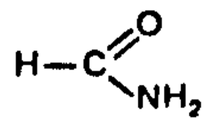	[1]	0.211 (80°C)	23
Trimethylacetamide	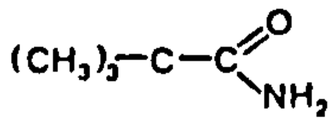	[2]	2.50×10^{-5} (50°C)	33
Benzamide	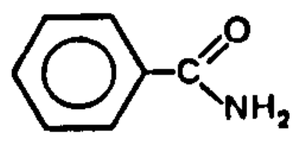	[3]	4.00×10^{-5} (40.3°C) 2.70×10^{-4} (70°C)	34 33
N-Methylformanilide	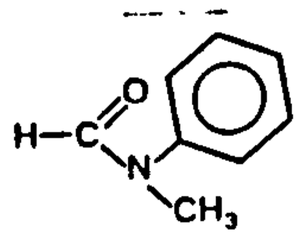	[4]	2.33×10^{-4}	30
N-Methyl-2,2,2-trifluoroacetanilide	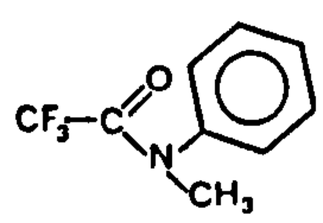	[5]	2.45	30
m-Nitroacetanilide	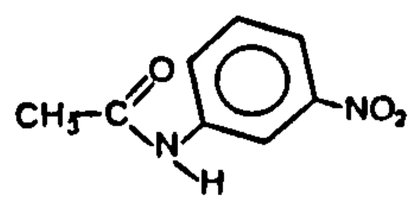	[6]	1.10×10^{-5}	18
p-methoxyacetanilide	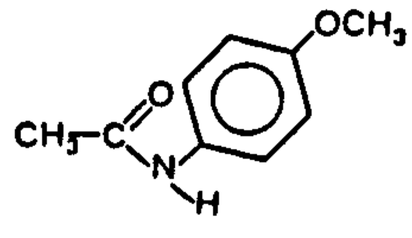	[7]	1.90×10^{-6}	18
3-Formyl-2-nitromethylene-tetrahydro-2H-1,3-thiazine	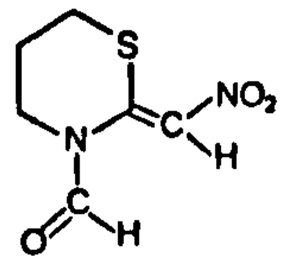	[8]	140	26
Acetylimidazole	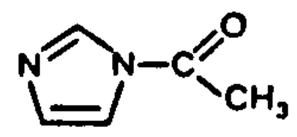	[9]	266	15

Table 1.1 continued.

Name of compound	Structure		$k_{OH}/M^{-1}s^{-1}$	Reference
Acetylimidazolium	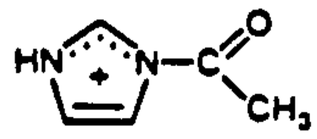	[10]	1.17×10^6	15
N-Acetyl-3,4-lutidinium	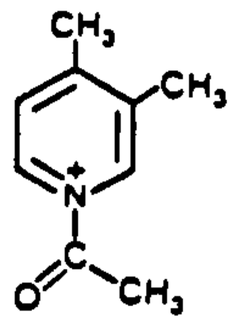	[11]	1.48×10^6	17
N-Acetyl-4-methylpyridinium	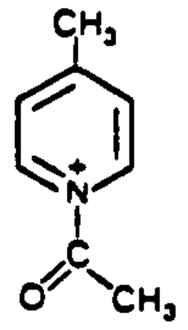	[12]	1.60×10^6	17
N-methyldiacetamide	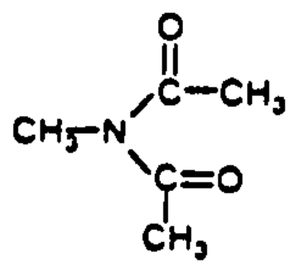	[13]	1.91	35
			1.54	37
N-Methylsuccinimide	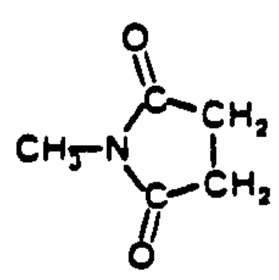	[14]	0.51	37
Diacetylamine	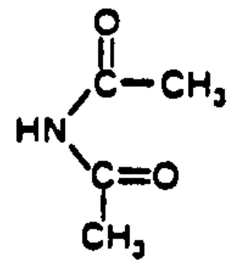	[15]	0.88	24
Succinimide	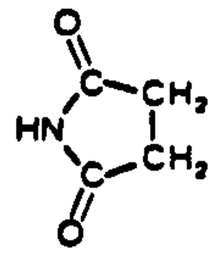	[16]	3.16	24
Substituted maleimides	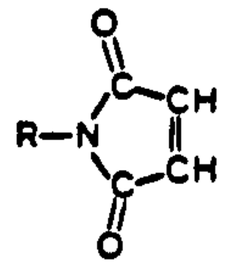			
Maleimide	R = H	[17]	95.7	37
N-Methylmaleimide	R = CH_3	[18]	58.9	37
N-Ethylmaleimide	R = CH_3CH_2	[19]	46.8	37
N-Hydroxymethylmaleimide	R = CH_3O	[20]	110	37

Table 1.1 continued.

Name of compound	Structure		$k_{OH}/M^{-1}s^{-1}$	Reference
Substituted phthalimides	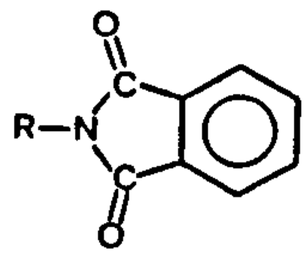			
N-Carboxymethyl-phthalimide	R = $CH_2C(O)O^-$	[21]	12.13 28.8	38 39
N-Carboxyethyl-phthalimide	R = $CH_2CH_2C(O)O^-$	[22]	15.31	38
N-(3-bromopropyl)-phthalimide	R = $CH_2CH_2CH_2Br$	[23]	33.50	38
N-(2-bromoethyl)-phthalimide	R = CH_2CH_2Br	[24]	31.30	38
N-(hydroxymethyl)-phthalimide	R = CH_2OH	[25]	32.70	38
N-(hydroxymethyl)-phthalimide (ionised)	R = CH_2O^-	[26]	3.44×10^{-3}	38
N-Carbethoxy-phthalimide	R = $C(O)CH_2CH_3$	[27]	2196	38
Alkylacetates	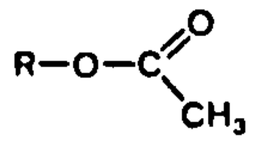			
Ethylacetate	R = CH_2CH_3	[28]	0.075	40
Methoxyethylacetate	R = $CH_2CH_2OCH_3$	[29]	0.113	25
2-Chloroethylacetate	R = CH_2CH_2Cl	[30]	0.283	40
Propargylacetate	R = CH_2CCH	[31]	0.467	40
Trifluoroethylacetate	R = CH_2CF_3	[32]	1.70	40
Methylformate	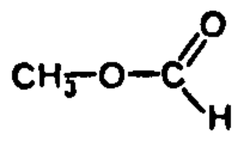	[33]	33.30	40

Table 1.1 continued.

Name of compound	Structure		$k_{OH}/M^{-1}s^{-1}$	Reference
Substituted phenylacetates	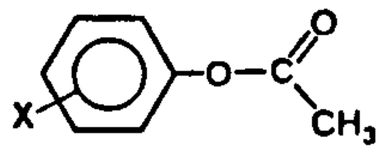			
p-Methylphenylacetate	X = p-CH_3	[34]	0.98	25
Phenylacetate		[35]	1.27	25
p-Chlorophenylacetate	X = p-Cl	[36]	2.20	25
m-Nitrophenylacetate	X = m-NO_3	[37]	6.87	25
p-Nitrophenylacetate	X = p-NO_3	[38]	9.50	25
2,4-Dinitrophenylacetate	X = 2,4-NO_3	[39]	53.67	25
1-Acetoxy-4-methoxy-pyridinium perchlorate	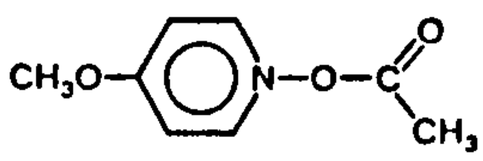	[40]	9500	41
Substituted phenylacetates (all at 30°C)	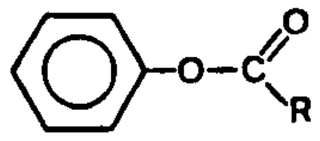			
	R = CH_3	[41]	3.71	21
	R = CH_2CH_3	[42]	2.51	21
	R = CH_2OCH_3	[43]	82.50	21
	R = CH_2Cl	[44]	990	21
	R = $CHCl_2$	[45]	28333	21
	R = CH_2Br	[46]	1583	21
	R = $CH_2SCH_2CH_3$	[47]	27.5	21
	R = CH_2CN	[48]	1167	21
	R = $CH_2OC_6H_5$	[49]	875	21
	R = CH_2CH_2Br	[50]	5.67	21
	R = $CH_2CH_2NO_3$	[51]	283	21
p-Nitrophenylformate	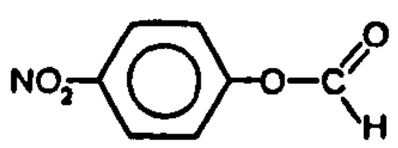	[52]	119	42

Table 1.1 continued.

Name of compound	Structure		$k_{OH}/M^{-1}s^{-1}$	Reference
p-Nitrophenylpivolate	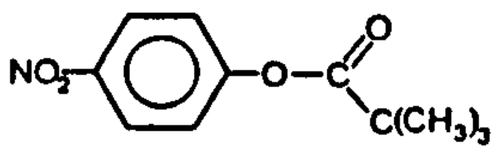	[53]	2.75	43
Phenylsalicylate (ionised)	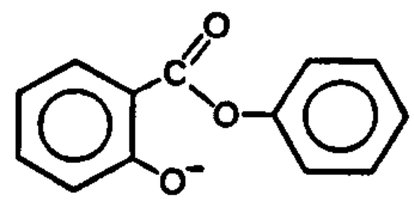	[54]	$12.4x10^{-4}$(30°C)	44
Ethyl-p-aminobenzoate	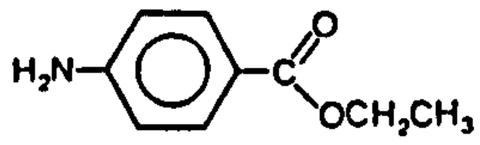	[55]	$8.40x10^{-5}$*	19,20
Ethyl-m-aminobenzoate	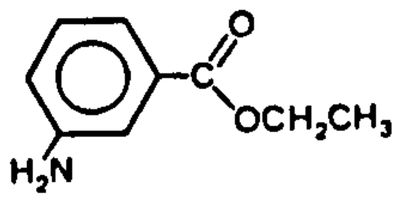	[56]	$164.7x10^{-5}$*	19,20
Substituted alkylacetates**	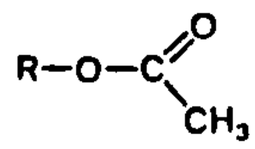			
Methylacetate	R = CH_3	[57]	$108x10^{-3}$	31
Ethylacetate	R = CH_2CH_3	[58]	$46.6x10^{-3}$	31
n-Propylacetate	R = $CH_2CH_2CH_3$	[59]	$27.0x10^{-3}$	31
i-Propylacetate	R = $CH(CH_3)_2$	[60]	$7.06x10^{-3}$	31
n-Butylacetate	R = $CH_2CH_2CH_2CH_3$	[61]	$23.0x10^{-3}$	31
i-Butylacetate	R = $CH_2CH(CH_3)_2$	[62]	$18.2x10^{-3}$	31
s-Butylacetate	R = $CH(CH_3)CH_2CH_3$	[63]	$3.27x10^{-3}$	31
t-Butylacetate	R = $C(CH_3)_3$	[64]	$0.27x10^{-3}$	31

*56 wt% acetone-water

**70 vol% acetone-water

Table 1.1 continued.

Name of compound	Structure	$k_{OH}/M^{-1}s^{-1}$	Reference
ω-Lactones* (all at 0°C)	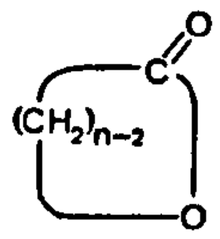		
n = 5	[65]	$1480x10^{-4}$	32
n = 6	[66]	$55000x10^{-4}$	32
n = 7	[67]	$2550x10^{-4}$	32
n = 8	[68]	$3530x10^{-4}$	32
n = 9	[69]	$116x10^{-4}$	32
n = 10	[70]	$0.22x10^{-4}$	32
n = 11	[71]	$0.55x10^{-4}$	32
n = 12	[72]	$3.30x10^{-4}$	32
n =13	[73]	$6.50x10^{-4}$	32
Acetic anhydride	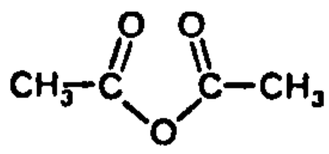	[74] 966.7	25

*60 vol% dioxane-water

Scheme 1.2

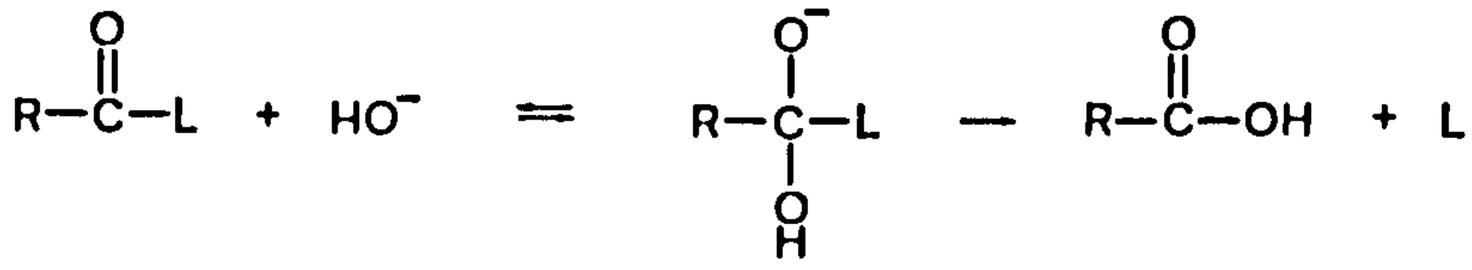

The structural features which appear to have the most significant effects are those which affect the electron density at the carbonyl carbon, that is, its electrophilicity.[26] With simple amides such as [1] to [7], the lone pair of the nitrogen atom is involved in resonance with the carbonyl carbon, thus giving a higher electron density at the carbonyl carbon, compared to the corresponding ester:

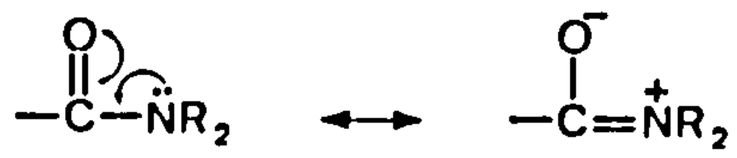

There are several structural features which can modify the extent of the resonance stabilisation of amides and, therefore, alter the reactivity. A good example is:

3-formyl-2-nitromethylenetetrahydro-2,4-1,3-thiazine [8], in which the delocalisation of the nitrogen lone pair electrons into the carbonyl function is considerably reduced by the presence of a nitroenamine system[26]; as well as delocalisation of the lone pair electrons into the carbonyl function, interaction with the nitroenamine system is also possible:

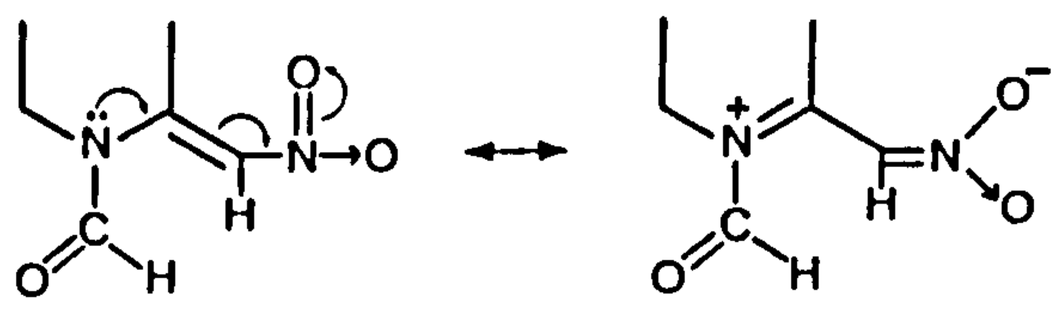

Further evidence for the reduced resonance stabilisation of [8] comes from crystalographic studies[26], which give bond lengths of C=O, 1.211 Å, and C-N, 1.364 Å, for the amide function. The C-N bond length is longer than that expected for a cyclic tertiary amide (1.336 Å[26]), and this indicates that the delocalisation is operating less effectively. The enhanced reactivity of [8] over the amides [1] to [7] is likely to be largely due to the effect of reduced resonance stabilisation. The high reactivity of acetylimidazole [9] is also explained[15] by reduced resonance stabilisation; the nitrogen lone pair electrons are involved in resonance with the aromatic ring, rather than the carbonyl function.

Some of the most reactive amides are the pyridiniums[17], [11] and [12], where clearly there is no possibility of resonance stabilisation. The imide function is another example where there is a reduction in the extent of resonance stabilisation, and enhanced reactivity over 'ordinary' amides. In the case of imides ([13] to 27]) the delocalisation of the nitrogen lone pair electrons occurs over both carbonyl functions:

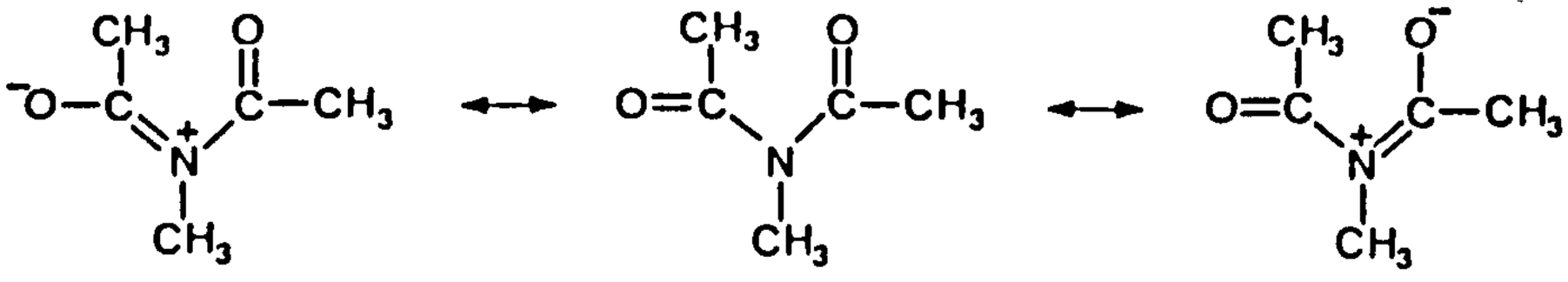

As might be expected, the bond length for the C-N bond in imides (1.40 Å for succinimide[27]) lies between the standard values[28] given for an amine (1.471 Å) and an ordinary amide bond (1.30 Å). Of course, some contribution to the enhanced reactivity of imides arises from the presence of an additional electron withdrawing carbonyl function.

Although resonance stabilisation is not a significant factor in determining the reactivity of esters, there are some cases where structural

features do result in reduced reactivity due to this effect. Ethyl-p-aminobenzoate [55], for example, reacts 20 times slower than the meta isomer[19] [56]. The p-amino group, unlike the m-amino group, can be involved in resonance stabilisation of the carbonyl function:

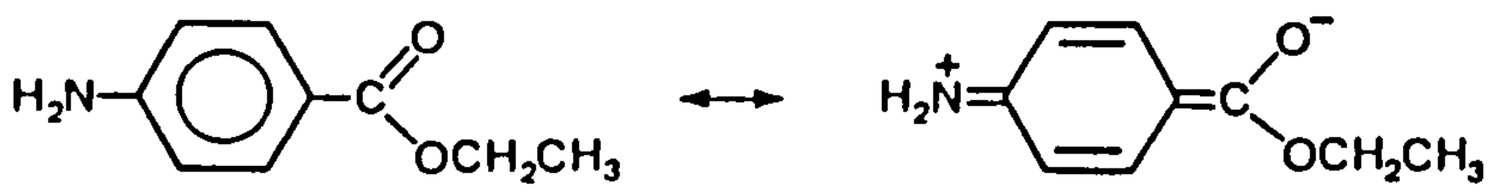

Additional evidence for this resonance effect was provided by Westheimer and Metcalf, in 1941[29], when they showed that ethyl-3,5-dimethyl-1,4-dimethylaminobenzoate, in which the two o-methyl groups prevent the dimethylamino group from lying in the same plane as the benzene ring, thus inhibiting resonance, hydrolyses some 24 times faster than the unhindered ester.

1.2.2 Polar Substituent Effects

Another factor affecting the electron density at the carbonyl carbon, and thus the reactivity, is the presence of electron donating or electron withdrawing substituents in the acyl or aroyl position. Thus, the presence of the highly electron withdrawing trifluoromethane group in N-methyl-2,2,2-trifluoroacetanilide [5] leads to an approximately 10,000-fold rate enhancement[30] over N-methylformanilide [4]. Other examples are the series of substituted phenyl acetates [41] to [51], where k_{OH} values range from 2.51 $M^{-1}s^{-1}$ for the electron donating group CH_3CH_2, to 28,333 $M^{-1}s^{-1}$ for the highly electron withdrawing group Cl_2CH.

1.2.3 The Nature of the Leaving Group

The nature of the leaving group is discussed more fully in Section 1.4, however, it is interesting at this point to compare the effect of leav-

ing group structure on the reactivities of some esters and amides. A good demonstration of leaving group effects on amides is given by acetylimidazole [9] and acetylimidazolium [10]. Acetylamidizole has a poor leaving group (pKa = 14.2[15]), however, protonation to form acetylimidazolium gives a good leaving group (pKa = 7.0[15]) and results in a 4,400-fold enhancement for k_{OH}[15]. For esters, the series of substituted phenyl acetates ([34] to [39]) demonstrates the dependence of k_{OH} on leaving group pKa. The values of k_{OH} range from 0.983 $M^{-1}s^{-1}$ for p-methylphenylacetate[25] (pKa of p-methylphenol ion = 10.185[25]) to 53.67 $M^{-1}s^{-1}$ for 2,4-dinitrophenylacetate[25] (pKa of 2,4-dinitrophenol ion = 4.02[25]).

1.2.4 Steric Considerations

Listed in Table 1.1 are a series of substituted alkyl actetates ([57] to [64]); the rate retarding effect in increasingly branched aliphatic groups is clearly demonstrated.

1.2.5 Configuration and Conformation

The temperature independence of dipole moments (1.7 - 1.9D) for esters has been explained in terms of inhibition of the free rotation of the alkoxyl group; the molecule being orientated in the trans conformation[12]:

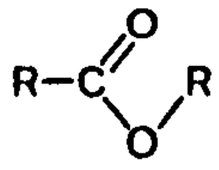

With 5 to 9 membered ring ω-lactones, however, ([65] to [69])[32] the conformation is enforced cis and it is proposed[20] that this results in a situation where the free energy of the ground state is higher than

the prevailing trans formation in open chain esters, and in ω-lactones with 10 or more atoms in the ring ([70] to [73]). This results in a higher rate of reaction for ω-lactones containing up to 9 atoms in the ring.

1.3 The Nature of the Intermediate for Acyl Transfer Reactions

Scheme 1.3 shows the general form of the reaction that we are concerned with.

Scheme 1.3

The nucleophile, such as OH^-, as in the discussion in the previous section, interacts with the carbonyl carbon, utilizing the orbital which was originally used to form the π bond of the double bond C = O; the leaving group is expelled.[8] However, questions arise as to the nature of the transition state(s) for these reactions, and also as to the timing of the formation of the carbonyl carbon bond to the nucleophile and the breaking of the bond to the leaving group.

There are three[9,10] extremes of timing of bond formation and fission for nucleophilic acyl substitution reactions, as shown in Schemes 1.4 to 1.6. Schemes 1.4 and 1.5 represent stepwise mechanisms, whereas Scheme 1.6 is a concerted mechanism.

Scheme 1.4

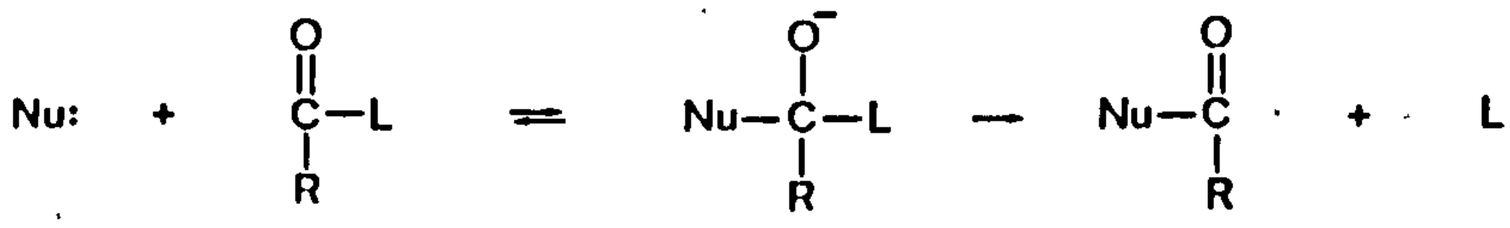

Scheme 1.5

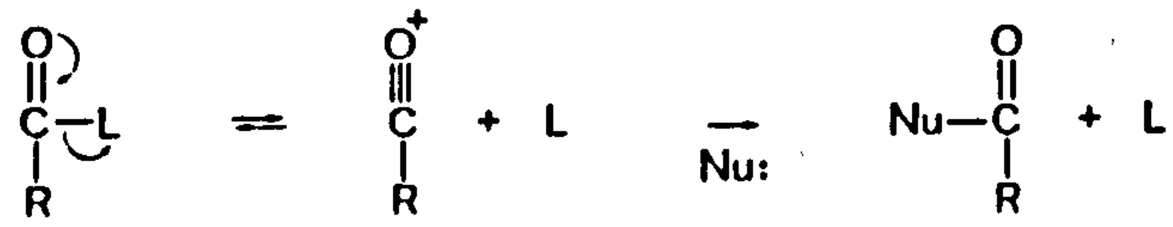

Scheme 1.6

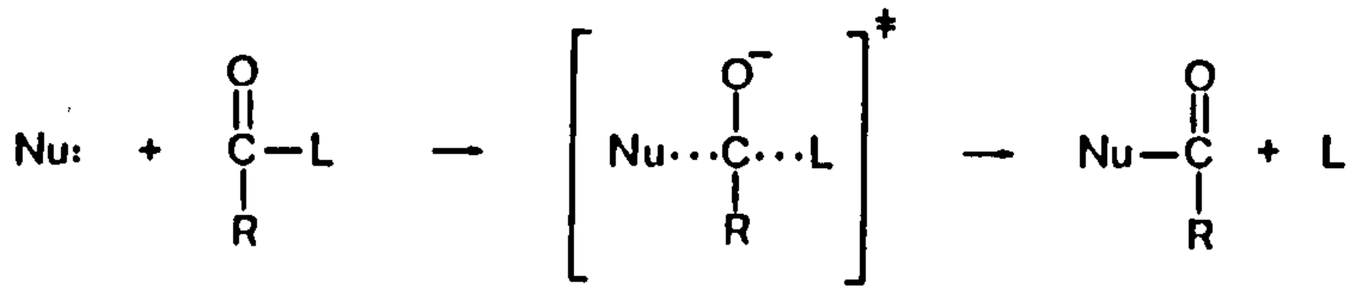

An intermediate can be said to exist if its lifetime is greater than one molecular vibration, which is about 10^{-13}s at 25°C[9,10]. With the tetrahedral intermediate (Scheme 1.4) the nucleophile bond to the carbonyl carbon, and the consequent loss of negative charge at the nucleophilic centre, is formed before the fission of the carbonyl carbon from leaving group. The reverse process operates in the acylium ion intermediate mechanism (Scheme 1.5) where the leaving group departs, forming the acylium ion before nucleophilic attack at the carbonyl carbon.[11] The final mechanism (Scheme 1.6) involves no stable intermediate struc-

ture, rather, there is coupling between the bond formation and fission processes. This is known as a concerted acyl transfer reaction.[45,46]

From a review of the literature, it is clear that, in addition to the well-established tetrahedral[47] and acylium ion[11] intermediate mechanisms, there has recently been good evidence obtained to support the existence of the concerted and transfer mechanisms.[45,46]

1.3.1 Tetrahedral Intermediates

Bender[47] was first to demonstrate a nucleophilic acyl substitution reaction proceeding via a tetrahedral intermediate, when he showed, using O^{18}, that carbonyl oxygen exchange accompanies the hydrolysis of carboxylic acid derivatives (Scheme 1.6).

Scheme 1.6

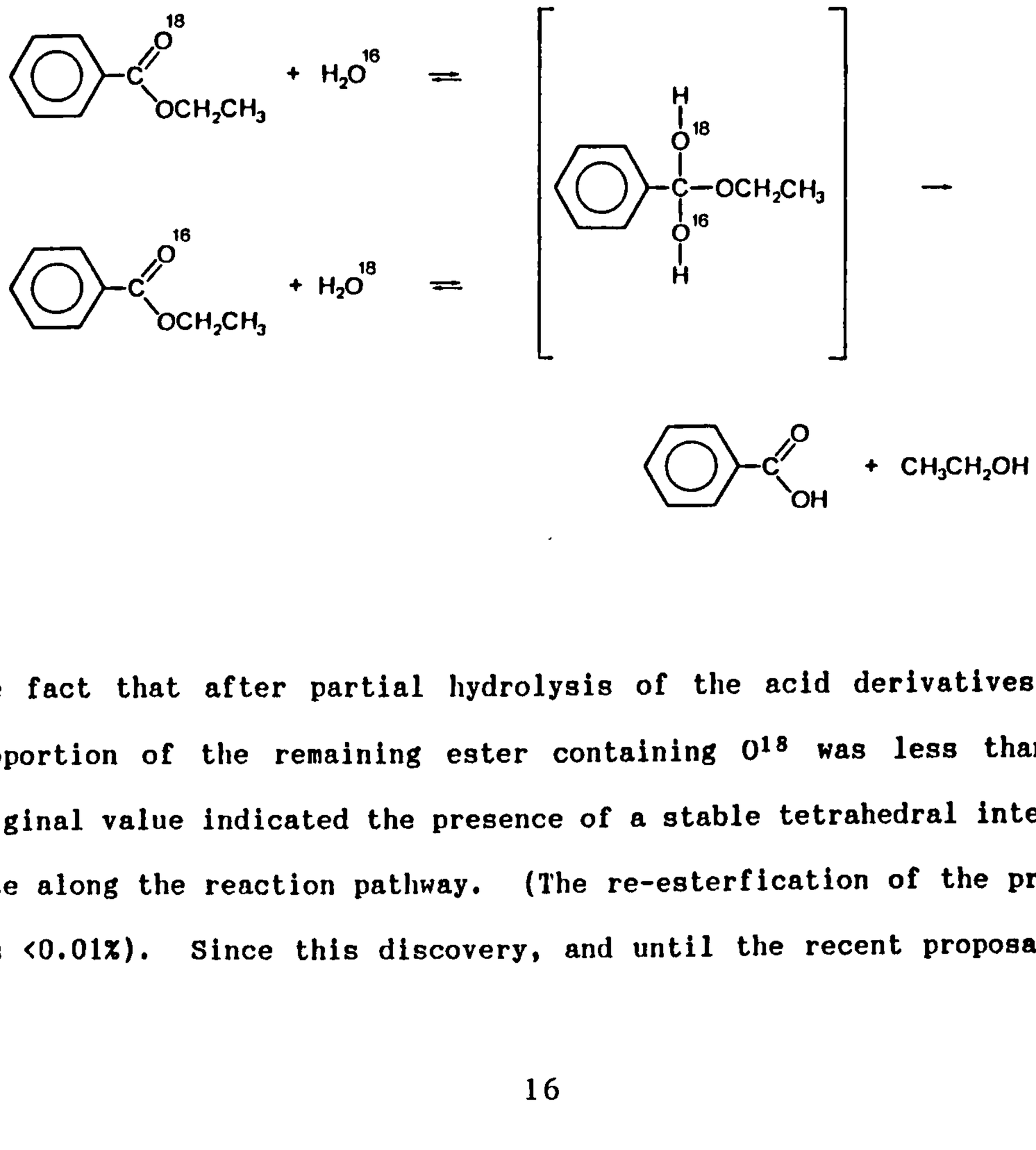

The fact that after partial hydrolysis of the acid derivatives, the proportion of the remaining ester containing O^{18} was less than the original value indicated the presence of a stable tetrahedral intermediate along the reaction pathway. (The re-esterfication of the product was <0.01%). Since this discovery, and until the recent proposals of

concerted mechanisms, most of the literature, other than for cases where there is an obvious acylium ion intermediate, was discussed in terms of tetrahedral intermediates.

Apart from the isotope evidence and breaks in Brønsted-type plots of log k against pKa, which will be discussed in Section 1.4, there is other excellent, and direct evidence for the presence of stable tetrahedral intermediates.

Recently, two groups of researchers have found ways of directly observing hemiorthoester intermediates of O,O-acetyl transfer using UV[48] and NMR techniques.[49] Indeed, Mclelland and Santry[48], using UV measurements, have been able to make accurate kinetic determinations of the breakdown of these intermediates. The basic principle of these studies is summarised in Scheme 1.7.

Scheme 1.7

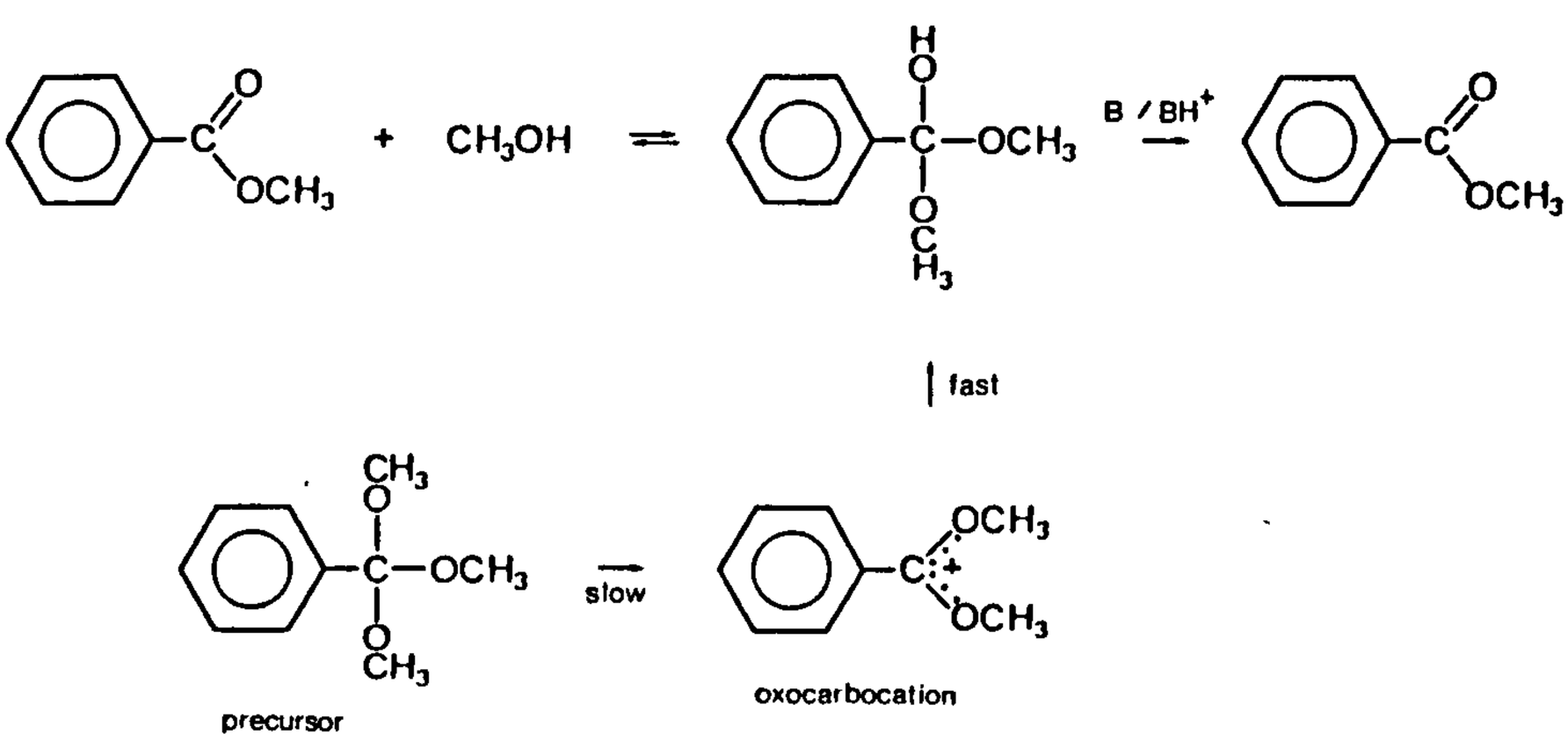

If the hemiorthoester tetrahedral intermediates are generated from highly energetic precursors via an oxocarbocation, then they have a sufficient lifetime to be observed in an aqueous solution. For exam-

ple, around pH 4, which corresponds to the maximum lifetime of the hemiorthoesters, the half-life is of the order of magnitude of 1 second[48]; acid and base catalysis results in much reduced lifetimes, above and below pH 4.0.

1.3.2 Acylium Ion Intermediates

Evidence for acyl transfer reactions which proceed via an acylium ion intermediate (SN1) has been reviewed by Williams and Douglas.[11] Such a reaction mechanism occurs for acyl groups which possess good leaving functions, most likely with pKa's below 2.[46] The acylium ion intermediate may be stabilised by charge neutralisation.

Cryoscopic measurements[50] of methyl mesitoate hydrolysis (Scheme 1.8) in 100% sulphuric acid have suggested acylium ion formation:

Scheme 1.8

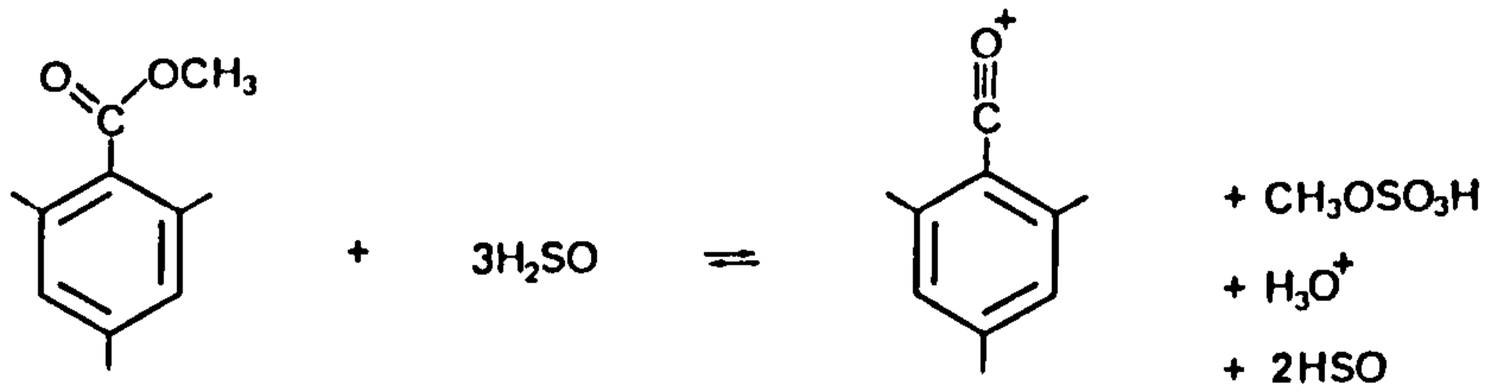

Positive entropies of activation close to zero, and the lack of carbonyl oxygen exchange during hydrolysis has also been taken to indicate SN1 mechanisms. During the diazotization of benzamide[51], for example, there is no exchange of the carbonyl carbon, which is consistent with Scheme 1.9.

Scheme 1.9

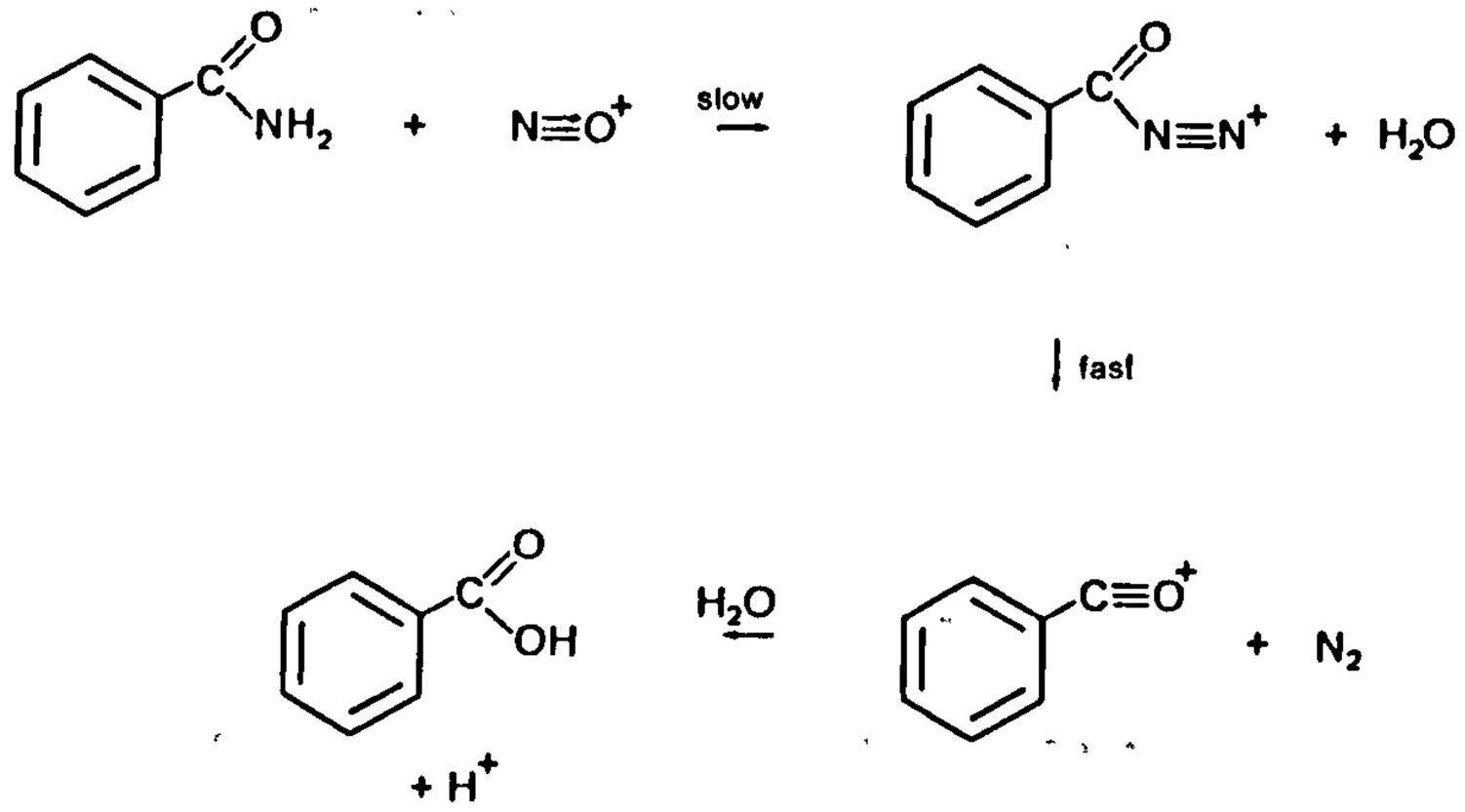

The hydrolysis of benzoyl chlorides has been shown to proceed via the formation of a tetrahedral intermediate in solvents containing a low proportion of water, whereas, at higher water concentrations, the mechanism becomes SN1. More direct evidence has come from infra-red and NMR techniques, which have been employed to demonstrate the presence of acylium ions such as the free oxocarbonium ion ($CH_3-C{\equiv}O^+$)[52].

1.3.3 Concerted Acyl Transfer Mechanisms

The most convincing evidence for the existence of acyl transfer reaction mechanisms whereby the bond breaking and bond fission processes are coupled, is provided by linear free energy studies[45,46], and these are reviewed in Section 1.4. The work, which was conducted on the reaction of phenyl esters with phenolate anions, has revealed a wide spectrum of concerted mechanisms existing between the boundaries defined by acyl transfer reactions which proceed via acylium ion and tetrahedral intermediates.

1.4 Linear (and non-Linear) Free Energy Relationships: Evidence of Concerted and Stepwise Mechanisms

1.4.1 General

Linear free energy relationships (LFER's) are a powerful tool for probing the nature of the transition state for a particular reaction. The free energy ΔG of equilibria and rate processes are proportional to the logarithm of the equilibrium (Eqn 1.1) or rate constants (Eqn 1.2).

$$\Delta G^{\circ} = -2.3\ RT\ \log K \qquad \text{Eqn 1.1}$$

$$\Delta G^{\ddagger} = -2.3\ RT\ \log K = -2.3\ RT \log k \frac{h}{kT} \qquad \text{Eqn 1.2}$$

Equation 1.2 is defined by transition state theory, where K is the pseudo equilibrium constant for the formation of the transition state, k is the observed rate constant, and h and k are Planck's and Boltzman's constants, respectively. In a LFER study, the free energy required to form the transition state from a series of different nucleophiles and substrates is correlated with the free energy change of other rate or equilibria processes (Equation 1.3).

$$\delta\Delta G_x = \alpha\delta\Delta G_y \qquad \text{Eqn 1.3}$$

If α is 1.0, for example, then it might be inferred that the same factors are contributing to both processes. One should, however, be aware that in correlations between rate and equilibrium processes there are factors which may contribute to the transition state which may be absent in the ground state, or vice versa. Strict interpretation of the degree of correlation may, therefore, be difficult in these cases.

1.4.2 Brønsted-type Plots - General

One of the most widely-used LFER's is the correlation between nucleophilicity and basicity (Equation 1.4).

$$\log k = \beta\ pK + C \qquad \text{Eqn 1.4}$$

where β is the Brønsted coefficient, and C a constant. Brønsted coefficients have been traditionally used as a measure of the amount of

bond formation and charge development/loss in the transition state.[8] In an acyl transfer reaction there is donation of an electron pair from the nucleophile to the substrate, with partial formation of a bond and the loss of formal negative charge on the nucleophile. Similarly, in either a concerted or consecutive process, there is partial fission of the bond between the carbonyl carbon and the leaving group, with the development of formal negative charge on the leaving group. In the Brønsted correlation, processes are compared with protonation and deprotonation, respectively (Equations 1.5 and 1.6).

$$Nu: + H^{+} \overset{K}{\rightleftharpoons} NuH \qquad \text{Eqn 1.5}$$

$$LH \overset{K}{\rightleftharpoons} L^{-} + H^{+} \qquad \text{Eqn 1.6}$$

Consider, for example, the protonation of a nucleophile (Equation 1.5). If an electron donating substituent R is added to Nu: then this increases the nucleophilic basicity, favouring NuH, thus increasing K and, consequently reducing the standard free energy of reaction (ΔG°). Now, for the attack of this same compound, Nu: at a carbonyl carbon: if the higher energy transition state resembles a structure where there is complete loss of the formal negative charge on Nu, then one might expect that the addition of the electron donating substituent R would result in a similar free energy charge ($\Delta G^{\ddagger}$) to that produced in ΔG°, thus:

$$\frac{\Delta G}{\Delta G^{\circ}} = \alpha \sim 1 \qquad \text{Eqn 1.7}$$

A Brønsted-type plot of log k against pKa should give a ß value of about 1.0. If, however,the highest energy transition state resembled a structure where only a third of the charge on Nu: had been lost, then one would expect the addition of substituent R to have only an intermediate effect on $\Delta G^{\ddagger}$, compared to ΔG° (i.e. ~ a third of the effect), and a Brønsted-type plot might yield a value of 0.3. (These arguments

apply equally to the leaving group substituent effects.) Thus, in its simplest interpretation, assuming that polar substituent effects work in one direction only, and that they apply equally to transition and ground state, then ß may be taken as a measure of the transition state structure. In particular, ß is numerically equal to the fractional extent of proton transfer at the transition state of the reaction being correlated.[8]

1.4.3 Brønsted-type Plots: Evidence for a Stepwise Nucleophilic Acyl Transfer Mechanism

Consider Scheme 1.10, where a nucleophile RX^- adds to the carbonyl carbon to form a tetrahedral intermediate, followed by expulsion of the leaving group YR^1-

Scheme 1.10

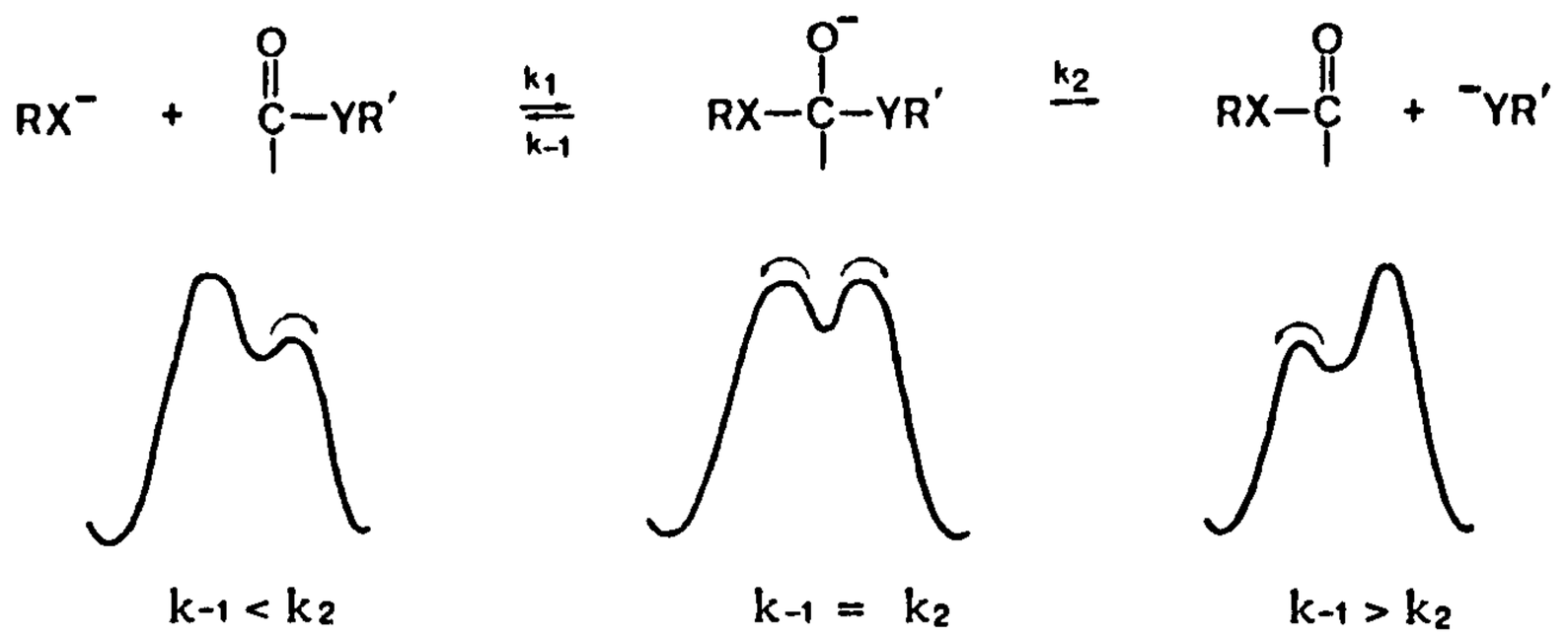

For a completely symmetrical reaction, where RX = R^1Y, then, clearly, the tetrahedral intermediate will break down equally into products and reactants, since $k_{-1} = k_2$. If, however, we have the case where RX^- is a stronger nucleophile and, therefore, a poorer leaving group than R^1Y, then upon attack of RX^- the tetrahedral intermediate will prefer-

entially break down to products ($k_{-1} < k_2$) and the attack of the nucleophile will be rate determining. For the converse case, where R^1Y^- is a better nucleophile than RX^- and, therefore, a poorer leaving group ($k_{-1} > k_2$), the tetrahedral intermediate will preferentially break down into reactants and, thus, the breakdown of the tetrahedral intermediate is the rate determining step.

Now, in the case where, RX^- is a poorer nucleophile than R^1Y^- ($k_{-1} > k_2$) and tetrahedral intermediate breakdown is the rate determining step, then, clearly, at the rate determining step the reaction has passed through the tetrahedral intermediate, and the transition state resembles a structure where there is a high degree of bond formation between nucleophile and substrate, and a loss of almost all of the formal negative charge on the nucleophile. Similarly, there is only a small amount of bond formation between R^1Y and the carbonyl carbon, with the development of almost 1 unit of formal negative charge on the leaving group. Therefore, from a Brønsted-type plot of log k against the pKa of the nucleophile or leaving group, a high value for βnuc and βlg might be expected (β^- 0.7 to 1.0) (Figure 1.1).

For the case where RX is a better nucleophile than R^1Y, and where the rate determining step is attack of the nucleophile, then the transition state at the rate determining step occurs before the formation of a tetrahedral intermediate; at this transition state there will only be partial bond formation between substrate and nucleophile, and only part of the formal negative charge on the nucleophile will be lost. The leaving group will have quite a large degree of bond formation to the carbonyl carbon and will only have gained a proportion of formal negative charge. Polar substituent effects will, therefore, have a smaller effect and, consequently, low values of βnuc and βlg should be expected ($\sim$ 0.2 - 0.3) (Figure 1.1).

Figure 1.1

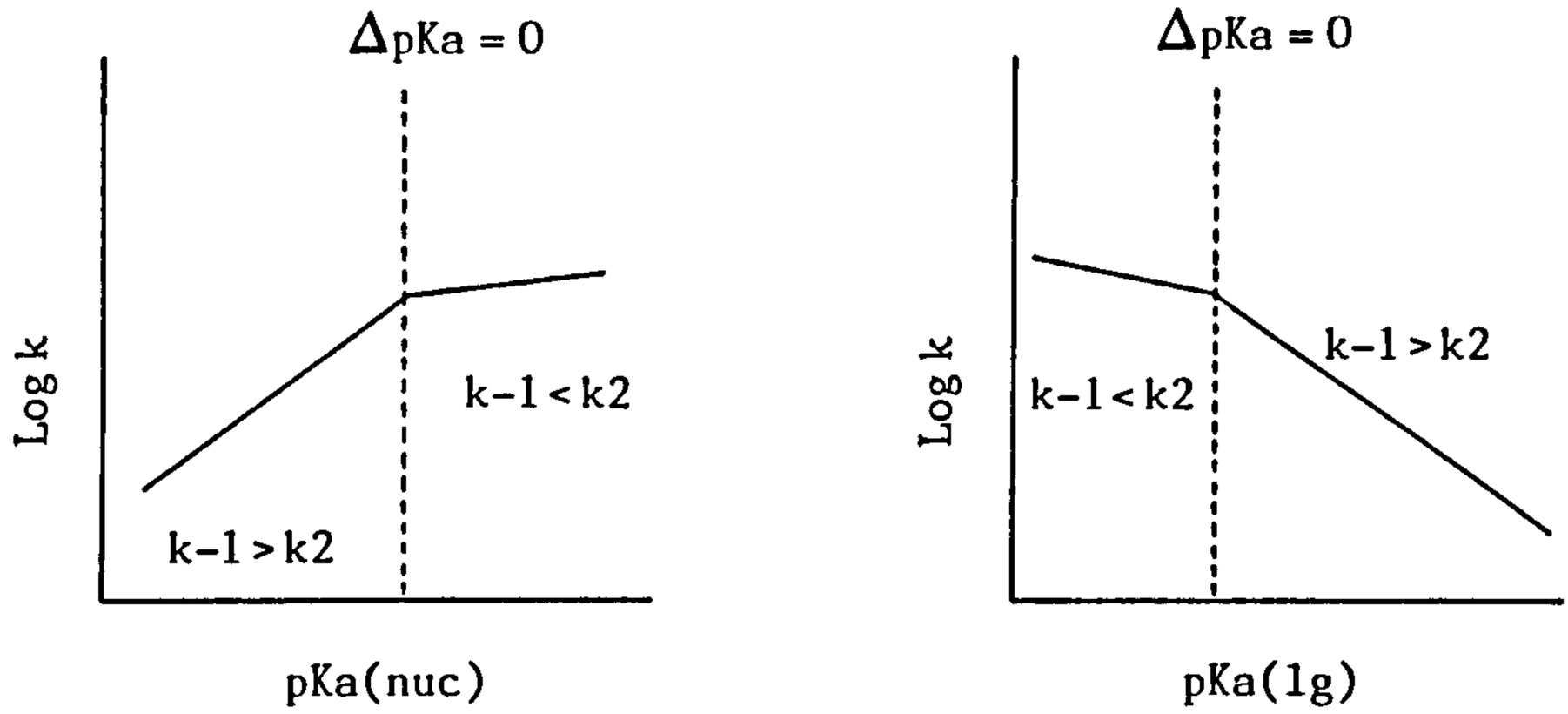

Thus, if an acyl transfer reaction accurs via the formation of a stable tetrahedral intermediate, then a break in a Brønsted-type plot would be good evidence of this. For reactions between structurally similar nucleophiles and substrates, then the break in the Brønsted-type plot might be expected to occur where $\Delta pKa = 0$ for the nucleophile and leaving group of the substrate. This may not be necessarily so for structurally dissimilar nucleophiles and substrates[45]; different leaving atoms have different bond strengths to carbon, and there are also electronic and steric effects.[54,55]

The most convincing evidence for an unambiguous break in a Brønsted-type plot, indicating a change in rate determining step and the presence along the reaction coordinate of a stable tetrahedral intermediate, has been obtained for acyl transfer reactions between esters[53] (and thioesters[42]) and thiol anions. Figure 1.2 shows a Brønsted-type plot for the reaction of a series of thiol anions with various substituted

Figure 1.2 The dependence on basicity of the rate constants for the reactions of a series of thiol anions with $AMPP^+$, DNPA, PNPA, and PA. The points represent aryl thiols (O) and alkyl thiols (Δ). The solid lines have slopes of $\beta_1 = 0.27$ and $\beta_2 = 0.84$. (From reference 53).

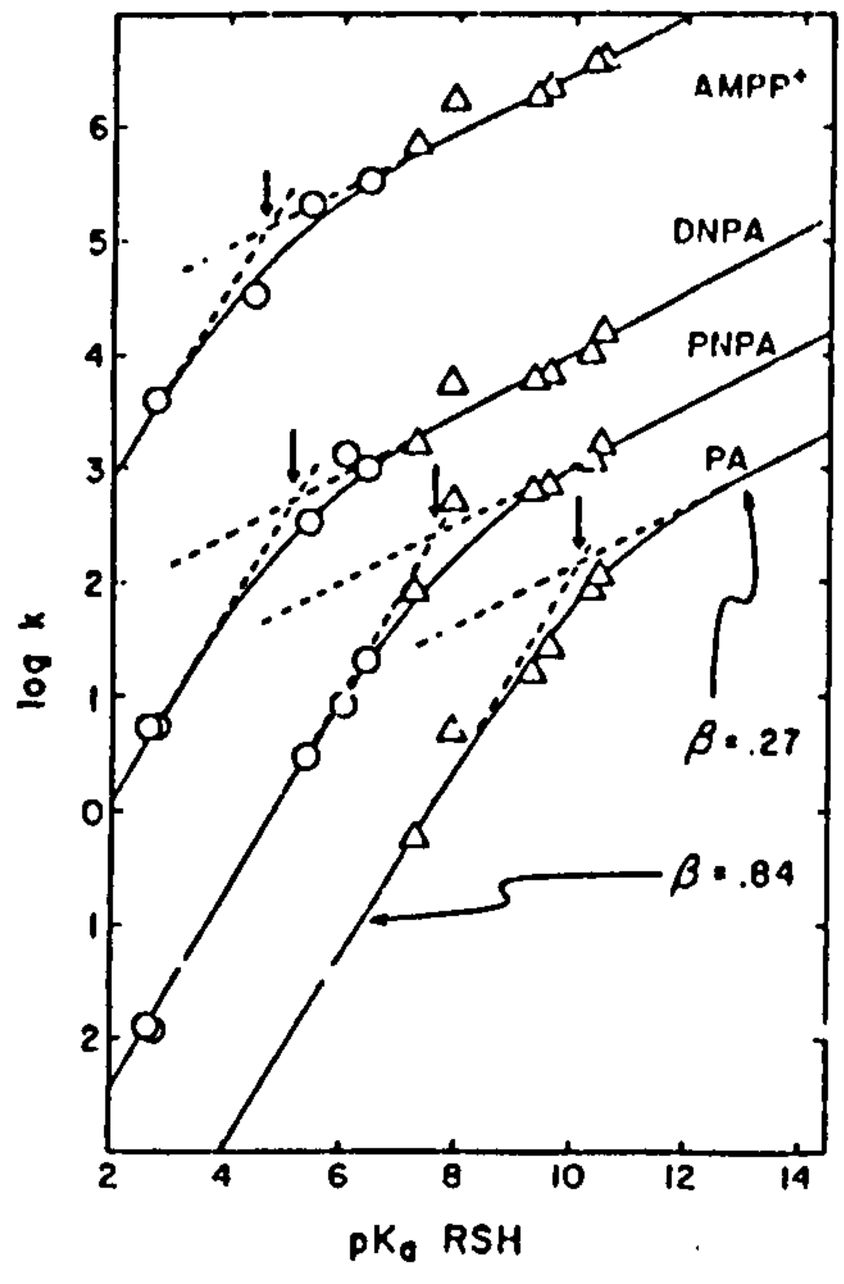

Figure 1.3 The dependence on basicity of the leaving group of the rate constants for the reactions of RS^- with substituted phenyl esters. The lines drawn through the points have a slope of $\beta = -0.33$ and $\beta' = 0.87$. (From reference 53).

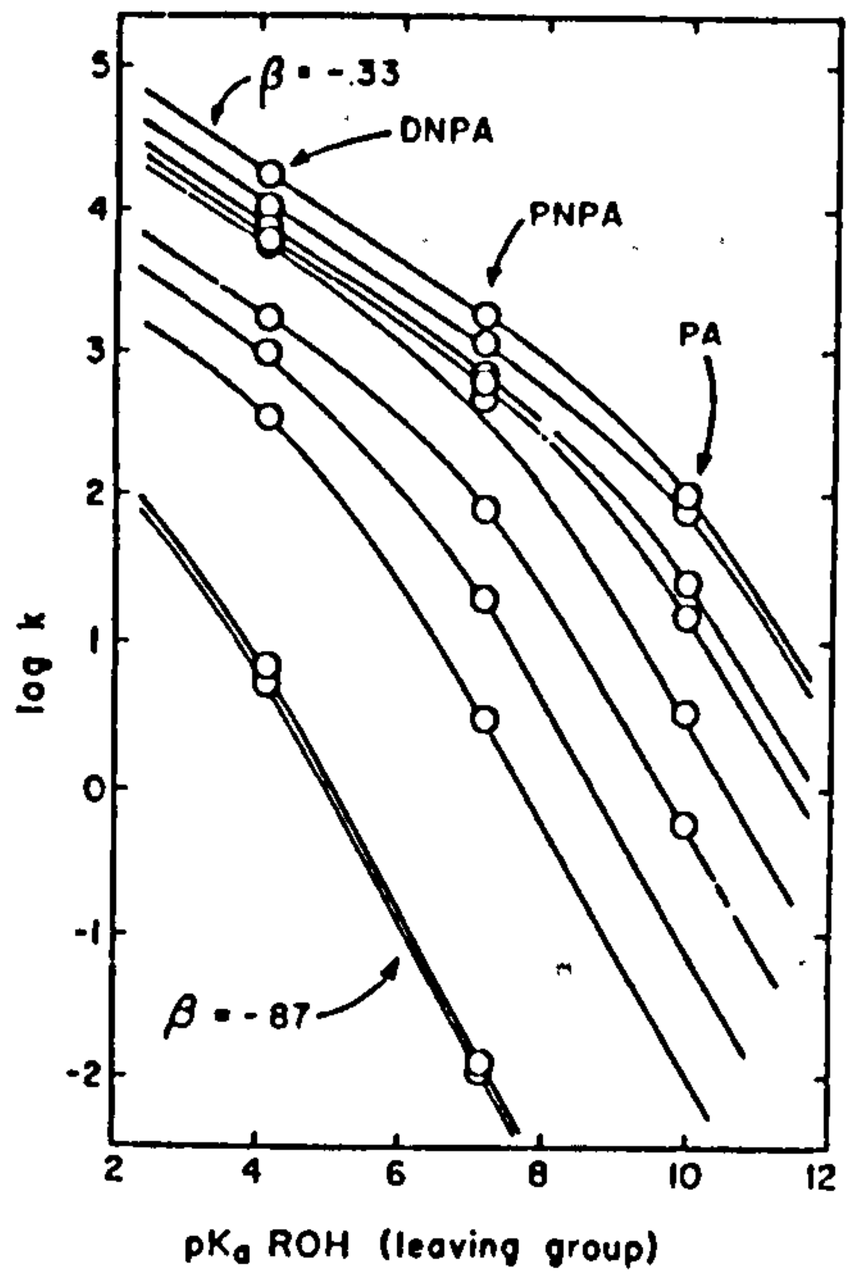

phenyl esters.[53] The breaks in the plots are well defined and correspond roughly to the point where ΔpKa = 0. For each of the substituted phenyl esters, βnuc is observed to change from ~ 0.8 before the break to ~ 0.3 after the break. A break in a Brønsted-type plot is also observed for a plot of log k against leaving group basicity for the reaction of thiol ions with substituted phenyl esters[53] (Figure 1.3), as might be expected. The βlg values obtained, -0.87 and -0.33, are consistent with the βnuc values in Figure 1.2 for the plot of log k against nucleophile basicity; again, this is to be expected on the basis of the previous results.

Work on ester aminolysis has suggested that these reactions also proceed via the formation of a stable tetrahedral intermediate along the reaction coordinate.[41,54] Unlike the reactions of thiols with esters[53] and thioesters[42], however, the break in the Brønsted plot of log k against the pKa of the nucleophile occurs some 4 to 5 pKa units[41,54,56] above the point where ΔpKa = 0; this is shown in Figure 1.4 for the reaction of a series of primary, secondary, and tertiary amines with substituted phenyl acetates[41] (leaving group range of 4 to 10). The breaks in the Brønsted-type plots are not as clear as those observed for the reaction of esters with thioesters[53] (Figure 1.5). For the substituted phenyl esters with lower leaving group basicities (phenyl acetate and paranitrophenylacetate) there is no observable break at all. Where breaks in the Brønsted-type plot are observed, the βnuc value changes from 0.9 before the break to approximately 0.2 afterwards. It might, however, be argued that the curvature observed in the plots in Figure 1.4 are simply a manifestation of solvation effects of highly basic nitrogen nucleophiles; similar curvature observed in Brønsted-type plots for the reaction of esters with oxygen anions, which was originally thought to correspond to a change in r.d.s. for these

Figure 1.4 Logarithmic plot of the rate constants for reactions of phenylacetate, p-nitrophenylacetate, 2,4-dinitrophenylacetate, and 1-acetoxy-4-methoxypyridinium cation with structurally similar primary, secondary, and tertiary amines as a function of amine basicity at 25°C. (From reference 41).

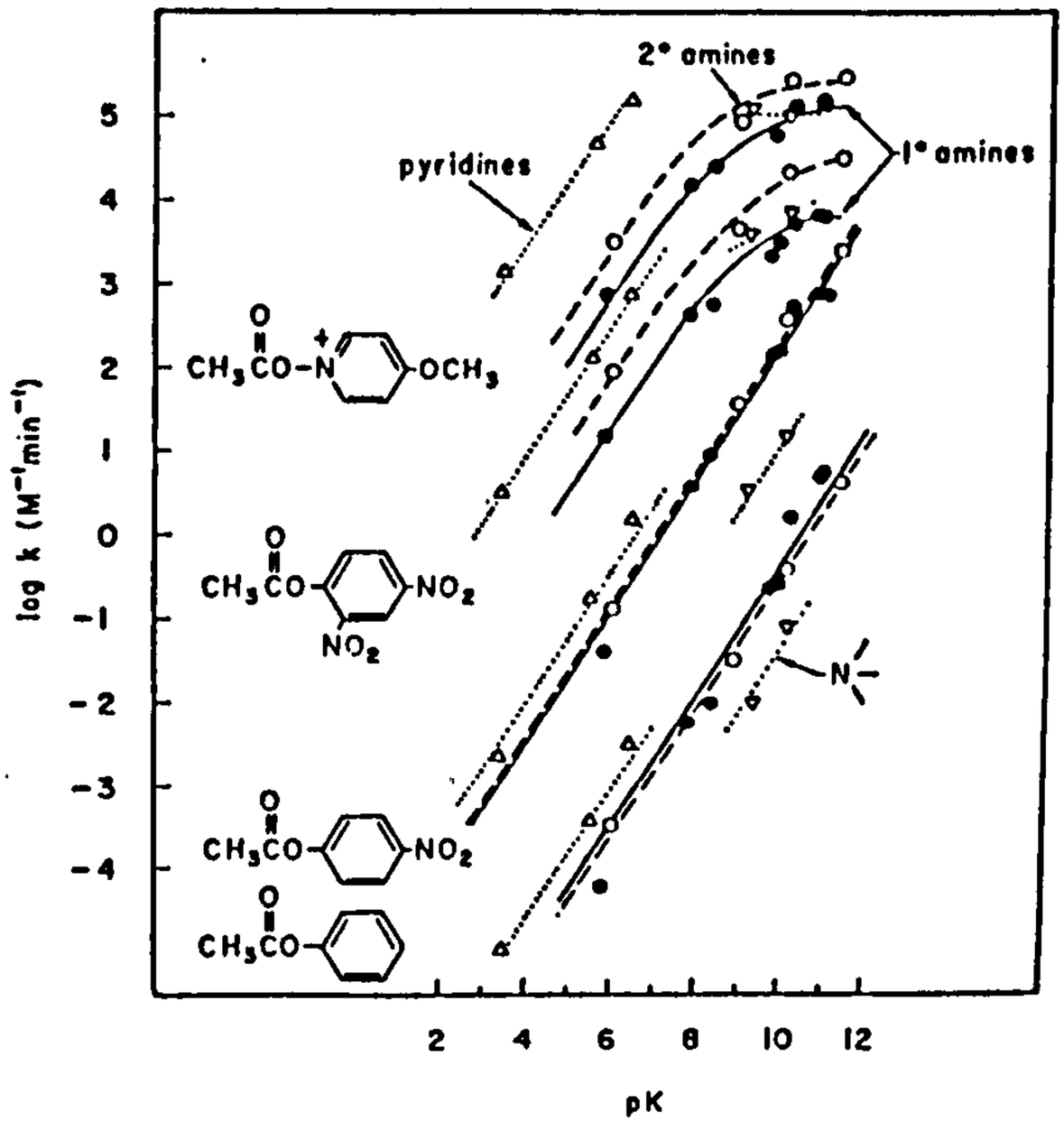

Figure 1.5 A Bronsted-type plot for the reaction of thiol anions with the thioesters p-nitrothiophenylformate, p-nitrothiophenylacetate, and p-nitrothiophenylpivalate, in order of decreasing rate. The solid lines represent the least-squares slopes for those points above pK = 4.5, which represent rate-determining attack. These have values of 0.29 (0.96), 0.29 (0.96), and 0.41 (0.95) in order of decreasing rate. (From reference 42).

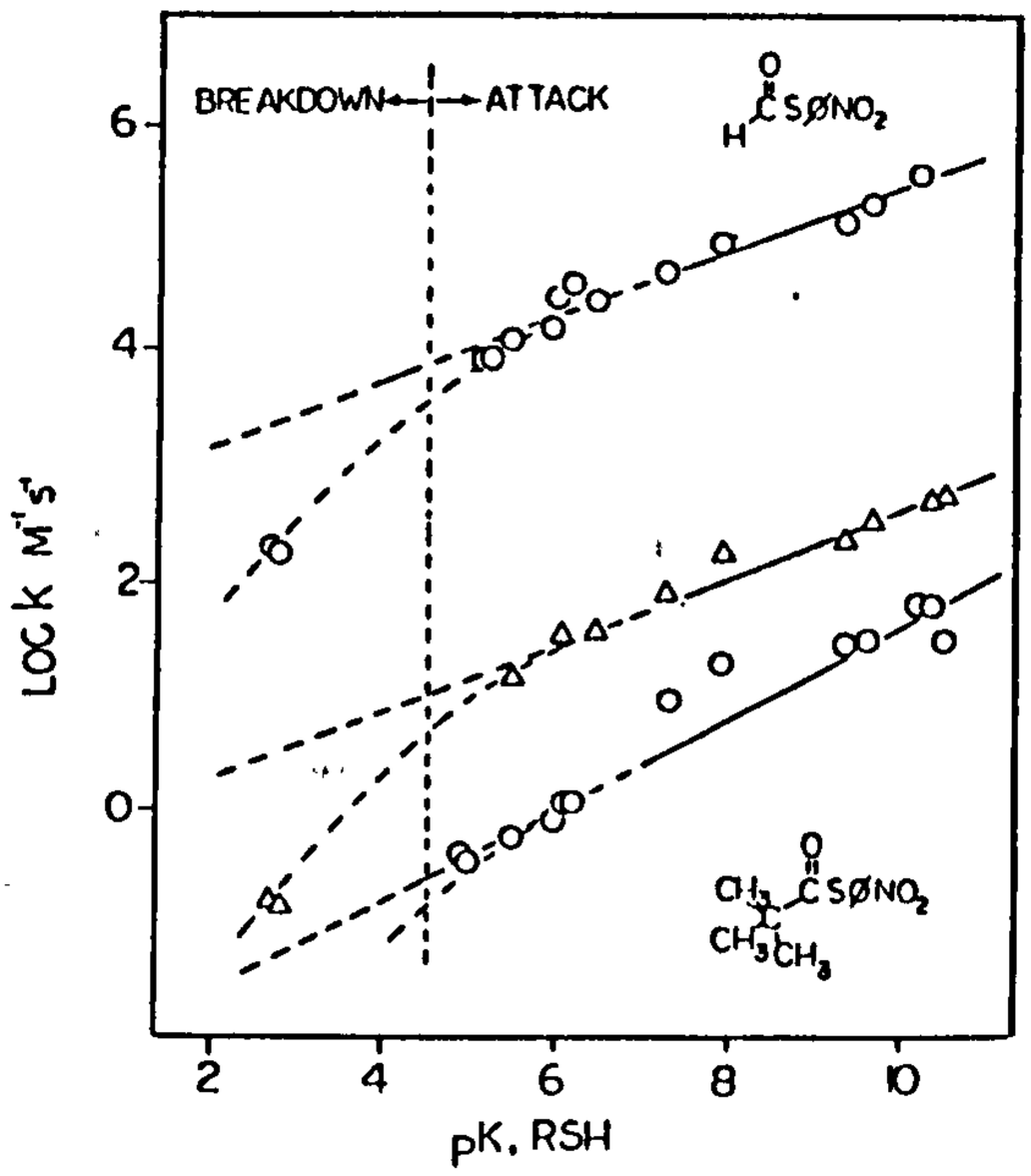

reactions[43], is now thought to be due to desolvation effects of highly-basic oxygen anions.[45,46] Despite these latter observations, Gresser and Jencks[54] appear to have confirmed that the curvature observed in Brønsted-type plots for ester aminolysis reactions is due to a change in r.d.s. rather than solvation effects. Figure 1.6 shows Brønsted-type plots for the reactions of substituted diphenyl carbonates [75] with a series of substituted quinuclidines [76].

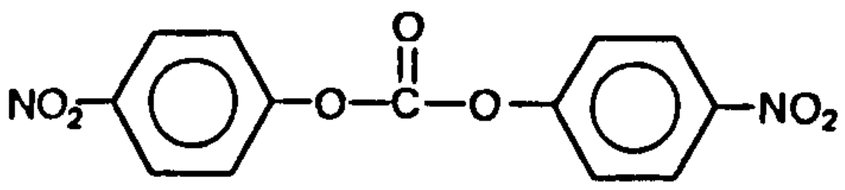

[75]

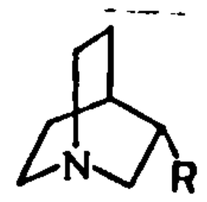

[76]

Significant curvature is obvious in the plots for 3,4 and 2,4 substituted diphenyl carbonates. The general trend observed in these plots is that the value of ΔpKa at which the break in r.d.s. occurs increases with increasing basicity of the substituted diphenyl carbonate leaving group. It appears that in the reaction of amines with esters, the partitioning of the tetrahedral intermediate reflects factors other than the relative basicities; there is obviously a greater stability for the ester than the cationic amide. Castro[56] in 1985 observed similar results for the reaction of a series of substituted pyridines with 2,4-dinitrophenylbenzoate (in aqueous ethanol), obtaining a value of ΔpKa ~ 5 (Figure 1.8).

For the reactions of activated amides with oxygen nucleophiles[15] and amines[15,14,13], the existence of a tetrahedral intermediate along the reaction coordinate has also been suggested, although for the reaction of a series of amines with the activated amide acetylimidazole[16], a concerted mechanism has been postulated. This will be discussed in the next section.

Figure 1.6 Logarithmic plot of the rate constants for reactions of m-nitrophenylphenylcarbonate,▽; p-nitrophenylphenylcarbonate,○; 3,4-dinitrophenylphenylcarbonate,△; and 2,4-dinitrophenylphenylcarbonate, □, with substituted quinuclidines as a function of amine basicity at 25°C and ionic strength 1.0M (tetramethylammonium chloride). (From reference 54).

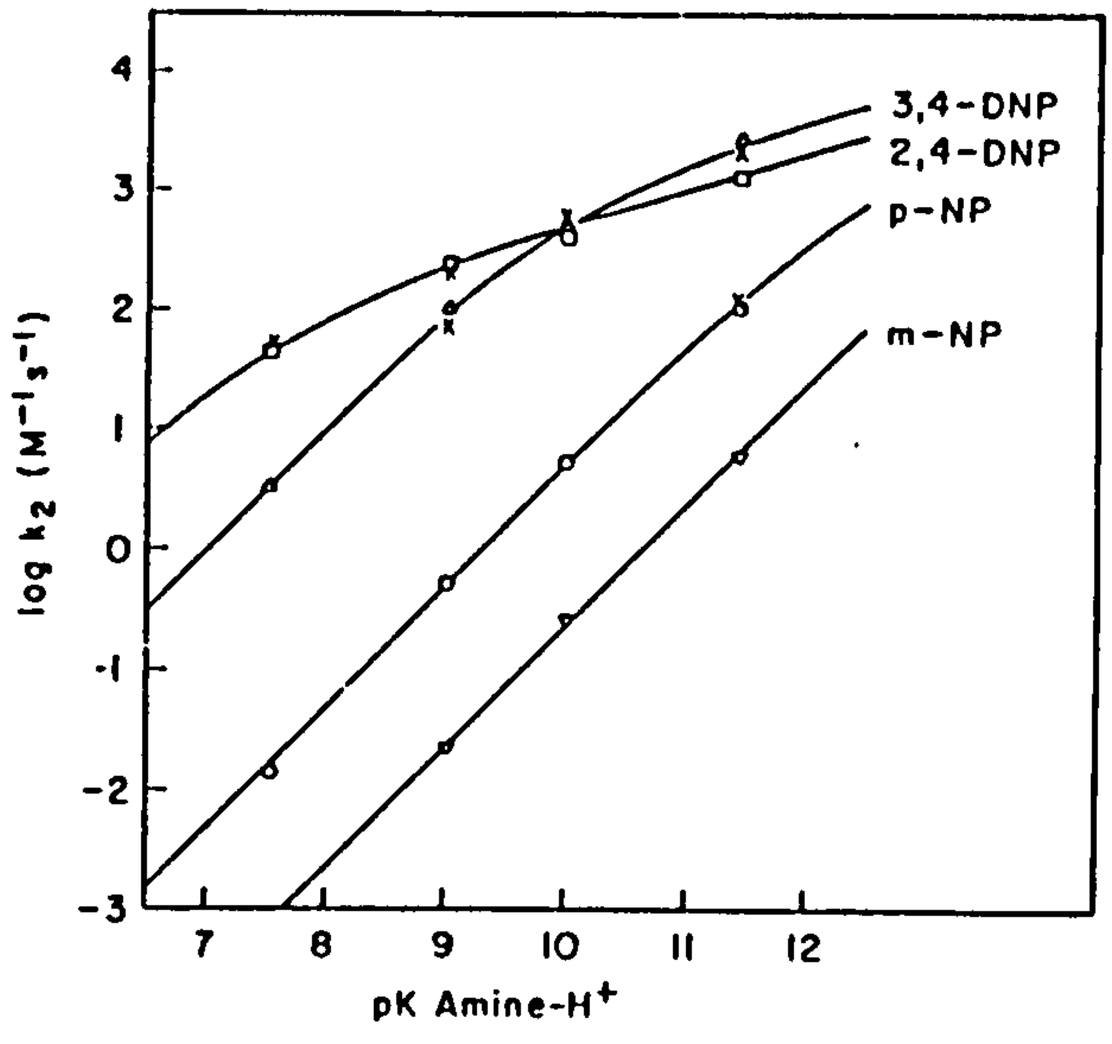

Figure 1.7 Effect of basicity on the rate constants for reactions of oxyanions with acetylimidazolium ion at 25°C. (From reference 15).

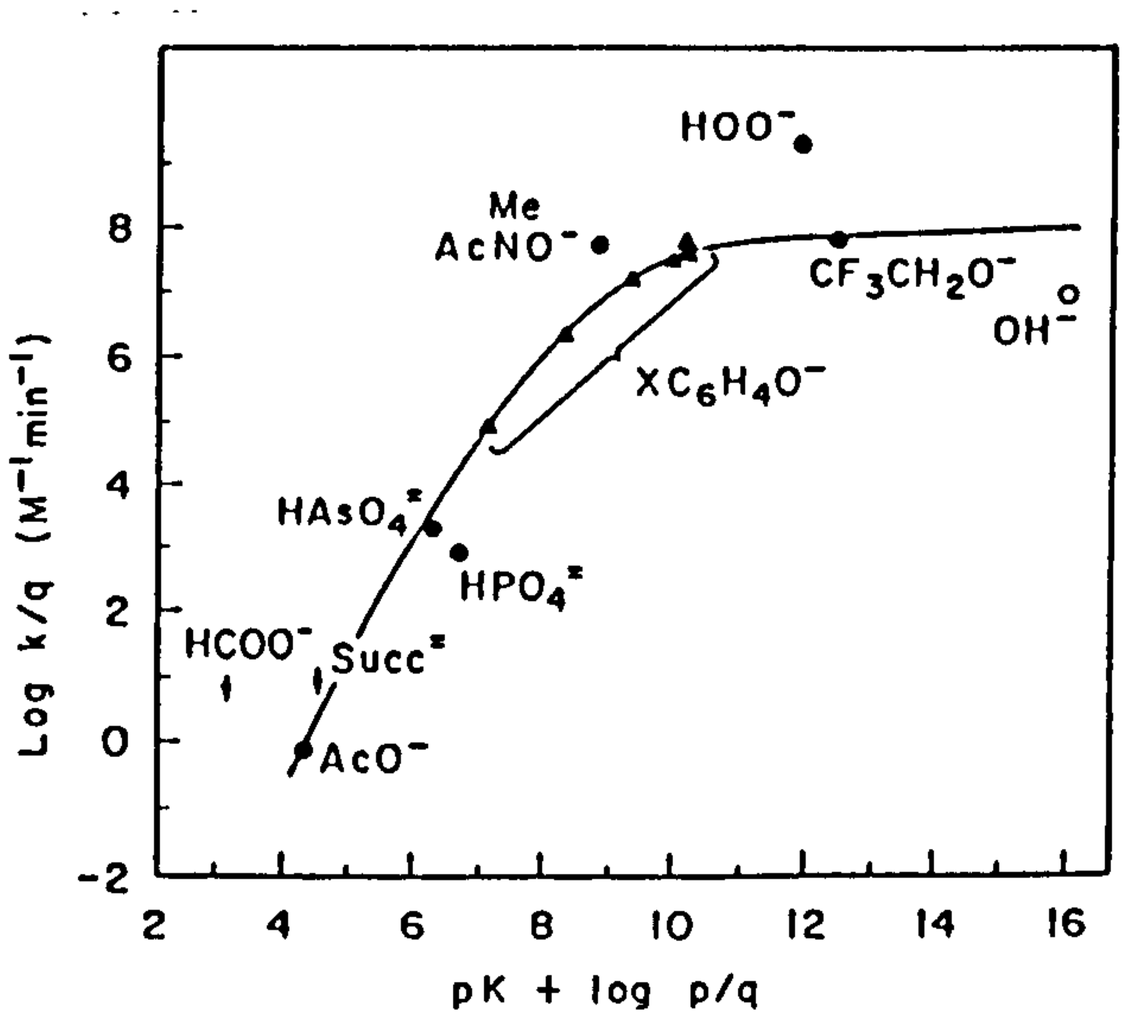

Figure 1.8 Bronsted-type plot for the pyridinolysis of 2,4-dinitrophenylbenzoate in 44 wt% aqueous ethanol at 25°C, ionic strength 0.2M (KCl).

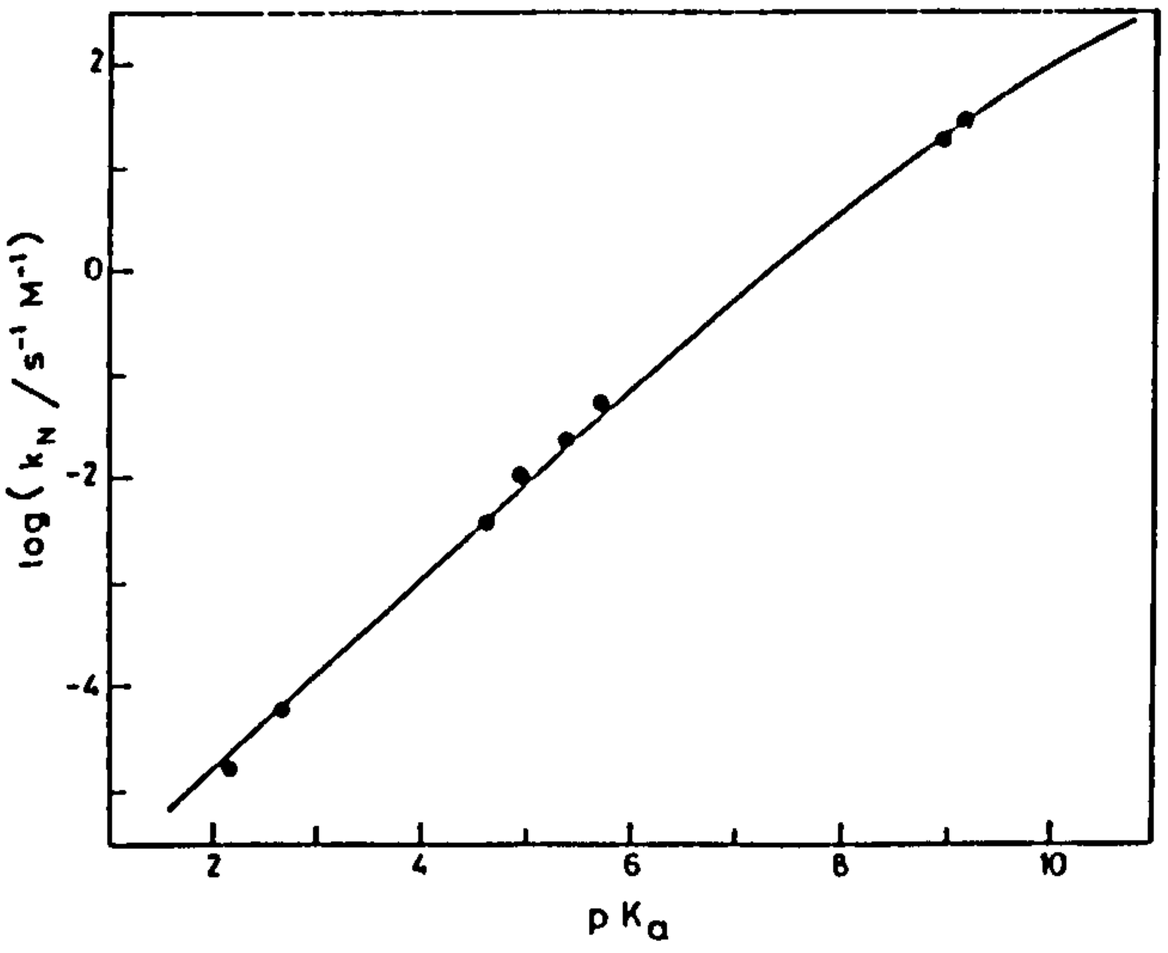

1.4.4 Brønsted-type Plots: Evidence for a Concerted Mechanism of Acyl Transfer

From the previous discussion of stepwise acyl transfer mechanisms it is clear that a change in r.d.s. corresponds to a change in the kinetically significant transition state and, thus, a change to either an earlier or later reaction coordinate. Since the reaction coordinate is a measure of bond order and charge development, then one would expect that at two different reaction coordinates, the degree of bond order and charge development, as measured by ßnuc abd ßlg, would be different. In a concerted mechanism, however (Scheme 1.11), there is only one kinetically significant transition state and, therefore, there can be no change in r.d.s. as one varies the nucleophile or leaving group pKa's.

Scheme 1.11

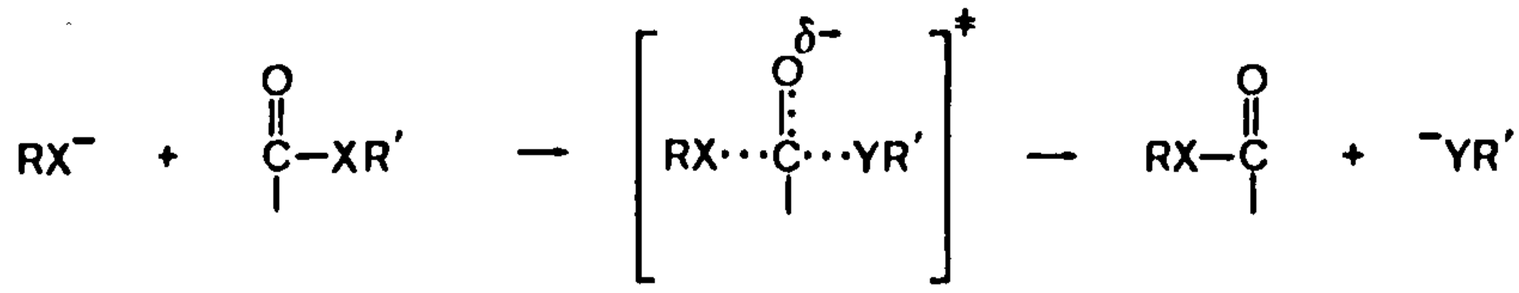

Oakenfull and Jencks[16] and Ba-Saif et al.[45,46] have recognised that, for a reaction series in which the nucleophiles and leaving groups are structurally similar, the observation of a Brønsted-type plot which is linear for a significant nucleophile pKa range either side of the leaving group pKa (or vice versa), is good evidence of a concerted acyl transfer mechanism. The alternative explanation for such a plot is that the reaction proceeds via a stepwise mechanism in which the electronic structures for the transition states corresponding to tetrahedral intermediate breakdown and nucleophilic attack (representing two different reaction coordinates) are similar; polar substituent effects

on nucleophiles and substrates would, therefore, be responsible for similar free energy changes.[45]

The reaction of substituted phenyl acetates with oxygen anions of a considerable range of pKa's has been investigated[41,57,42] and it is clear that whilst for nucleophiles of low pKa's the Brønsted-type plot is linear, at much higher pKa's, typically about 12, there was curvature. This was also the case for p-nitrophenylformate and pinitrophenylpivalate.[42] As mentioned earlier, it is now thought that such curvature does not reflect a change in r.d.s. rather, it is a consequence of the desolvation requirements of nucleophiles[57]; a nucleophile may need to become partially or wholly desolvated in order to reach a transition state during nucleophilic attack.[57,58] It has been proposed that the process is more difficult for the most basic oxygen anions.[57] Solvation effects will be discussed in Section 1.5.

Ba-Saif et al. in 1987[45], obtained a value of ßnuc = 0.75 for aryl oxygen anions and could detect no break in the plot, either above or below the pKa of the p-nitrophenol leaving group (pKa = 7.14). They calculated that the single transition state resembled a structure in which the loss of formal negative charge on the attacking group (0.75 units) was virtually balanced by the formation of a formal negative charge on the leaving group (0.95), with virtually no change in charge on the carbonyl group. These results are not conclusive proof of concertedness for reasons described above, however, Ba-Saif et al. have conducted further experiments[46] which appear to confirm the coupling of the bond formation and bond breaking processes. They have determined ßnuc values at several different leaving group pKa's and, similarly, ßlg at several different nucleophile pKa's for the reaction of oxygen nucleophile with esters. Linear Brønsted-type plots were obtained in all cases (Figures 1.9 and 1.10), however, ßnuc and ßlg were found to

Figure 1.9 Dependence of β_{nuc} on pK_{lg} for attack of phenolate ions of varying structure on phenyl esters.

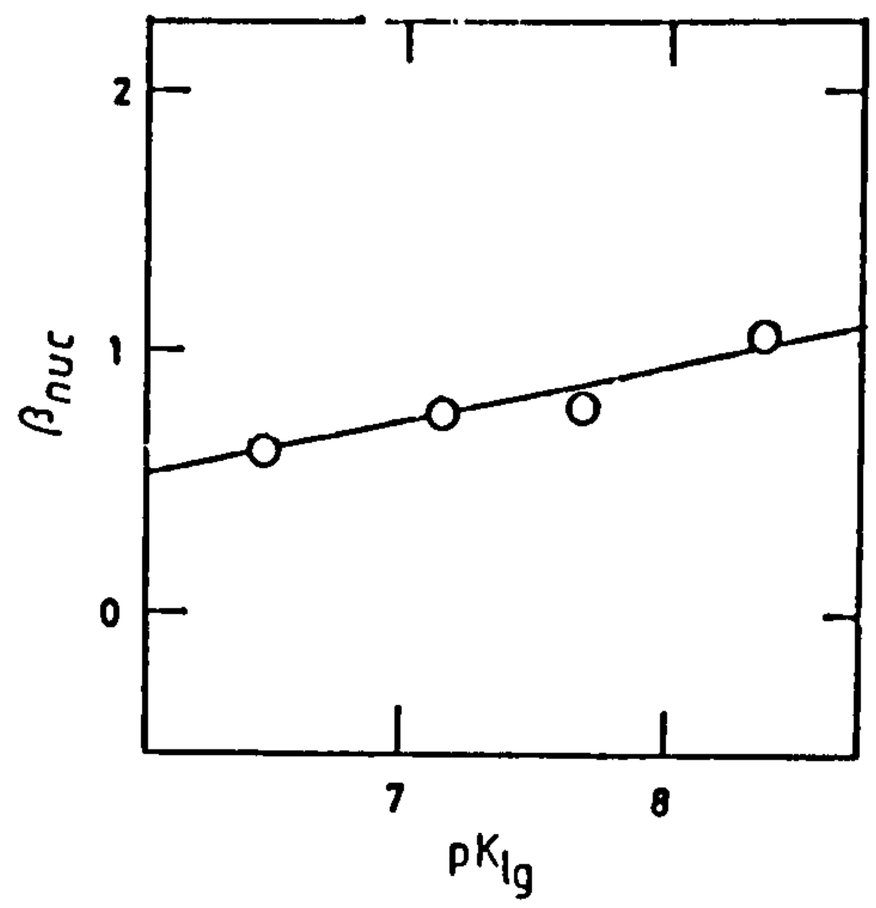

Figure 1.10 Dependence on pK_{nuc} of β_{lg} for attack of phenolate ions on aryl esters with leaving groups of varying structure.

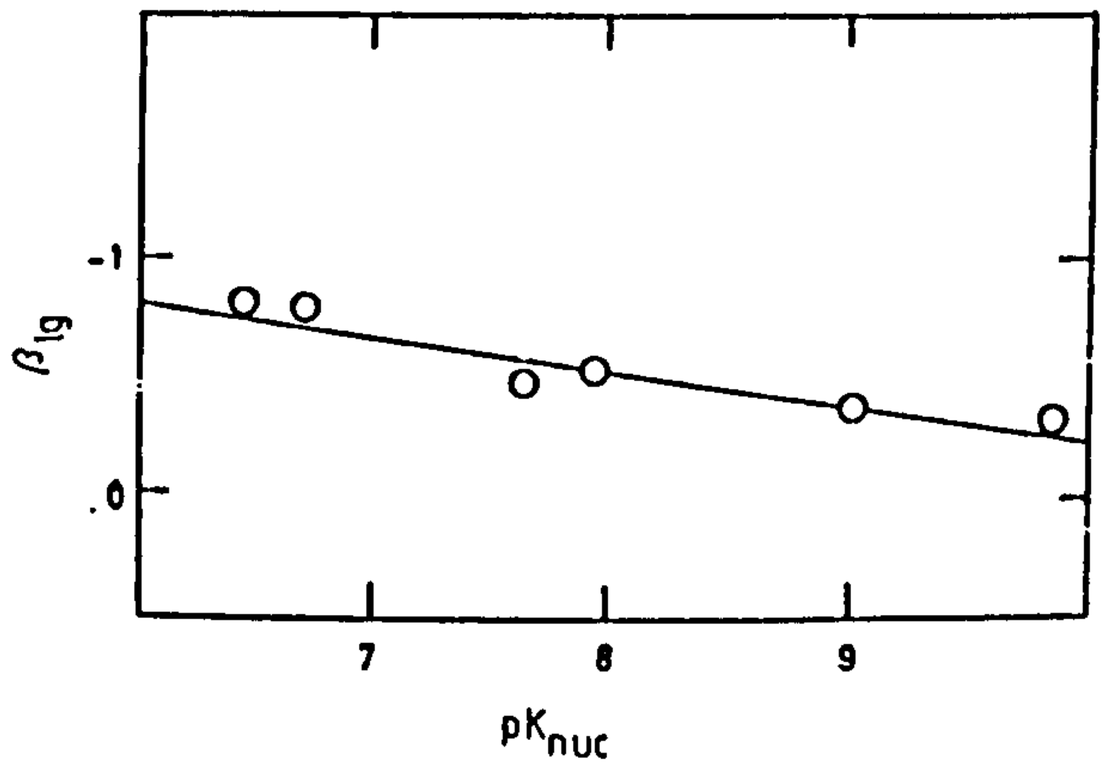

vary linearly with pka_{lg} and pKa_{nuc}, respectively; this indicates a change in transition state structure, that is, the position of the transition state on the reaction coordinate has shifted. Moreover, there is cross-correlation between the variation of ßnuc and ßlg with pka, indicating a coupling between the bond breaking and bond formation processes. For those reactions which are known to proceed via a stepwise mechanism, such as the reaction of thiols with phenylesters (Figure 1.2) and amines with phenylesters (Figure 1.4). It will be noted that the slope of the plots (ßnuc), in the region where there is rate determining breakdown of the tetrahedral intermediate, does not vary as the pKa of the leaving group is altered; a change in pKa of the leaving group does, of course, have the general effect of making the carbonyl carbon less electrophilic, thus altering the constant, C, of the Brønsted plot (Equation 1.4).

As can be seen from Figures 1.9 and 1.10, for the results of Ba-Saif et al[46], when pKa_{lg} was increased from 6.46 to 8.35, the ßnuc value increased from 0.64 to 1.04, indicating an increase in bond formation and charge development in the transition state. For the ßlg values, an increase in pKa_{nuc}, from 6.72 to 9.86, results in a change in ßlg, from -0.79 to -0.33. For the range of phenolate ions and esters studied, the degree of change in ßnuc with pKa_{lg}, and in ßlg with pKa_{nuc}, correlates (the slopes are 0.20 $\pm$ 0.04 and 0.15 $\pm$ 0.03, respectively). Ba-Saif et al. speculate on the basis of these data that, for hypothetical substituted phenyl acetates with leaving group pKa's of above 11.7 and below 2.0, the reactions will proceed via stable tetrahedral intermediates and acylium ion intermediates, respectively. It is interpolated from the data that effective charge development and loss on leaving and attacking oxyanions is fully balanced in the transition state when entering and leaving nucleophiles have a pKa of 7.1. In terms of

potential energy surface diagrams (Figure 1.11a and 1.11b) they perceive the concerted mechanisms occupying the area bounded by the stepwise mechanisms. Increasing the pKa of the leaving group causes the reaction to take a path which is nearer to the tetrahedral intermediate mechanism (Figure 1.11b). Ba-Saif et al. propose[45] that there is a smooth transition between concerted and stepwise mechanisms.

Finally, Oakenfull and Jencks[15] have also discussed the possibility of concerted acyl transfer reactions, on the basis of results obtained for the reaction of acetyimidazolium (pKa_{lg} = 7.2) with various nitrogen nucleophiles; a Brønsted-type plot yielded a linear relationship (Bnuc = 1.0) over a pKa_{nuc} range of 6 to 12.

1.5 Solvation, Polarisability and the 'α Effect'

1.5.1 General

The acyl transfer reactions which have been discussed in the previous sections are Lewis acid-base reactions. Ritchie[58] states that, from attempts to understand the rates and equilibria of Lewis acid-base reactions, it appears that the important factors are Brønsted basicity, which was discussed extensively in the previous sections, polarisability and solvation. Edwards and Pearson[59], in discussing the factors determining the reactivity of nucleophile reagents, also consider basicity and polarisability important, however, additionally, they list as important the presence on the nucleophile of unshared pairs of electrons on the atom adjacent (α) to the nucleophilic atom; this is termed the α effect.

Figure 1.12 shows data for the reactions of a range of different nucleophile types with p-nitrophenylacetate (PNPA), compiled from some[41,45,53,60,61,62,63,64,65] of the many literature studies of nucleophilic reactions with substituted phenyl acetates. This demonstrates

Figure 1.11 Contour diagram of the potential energy surface for the transfer of the acetyl group between phenolate ion nucleophiles.

(a)

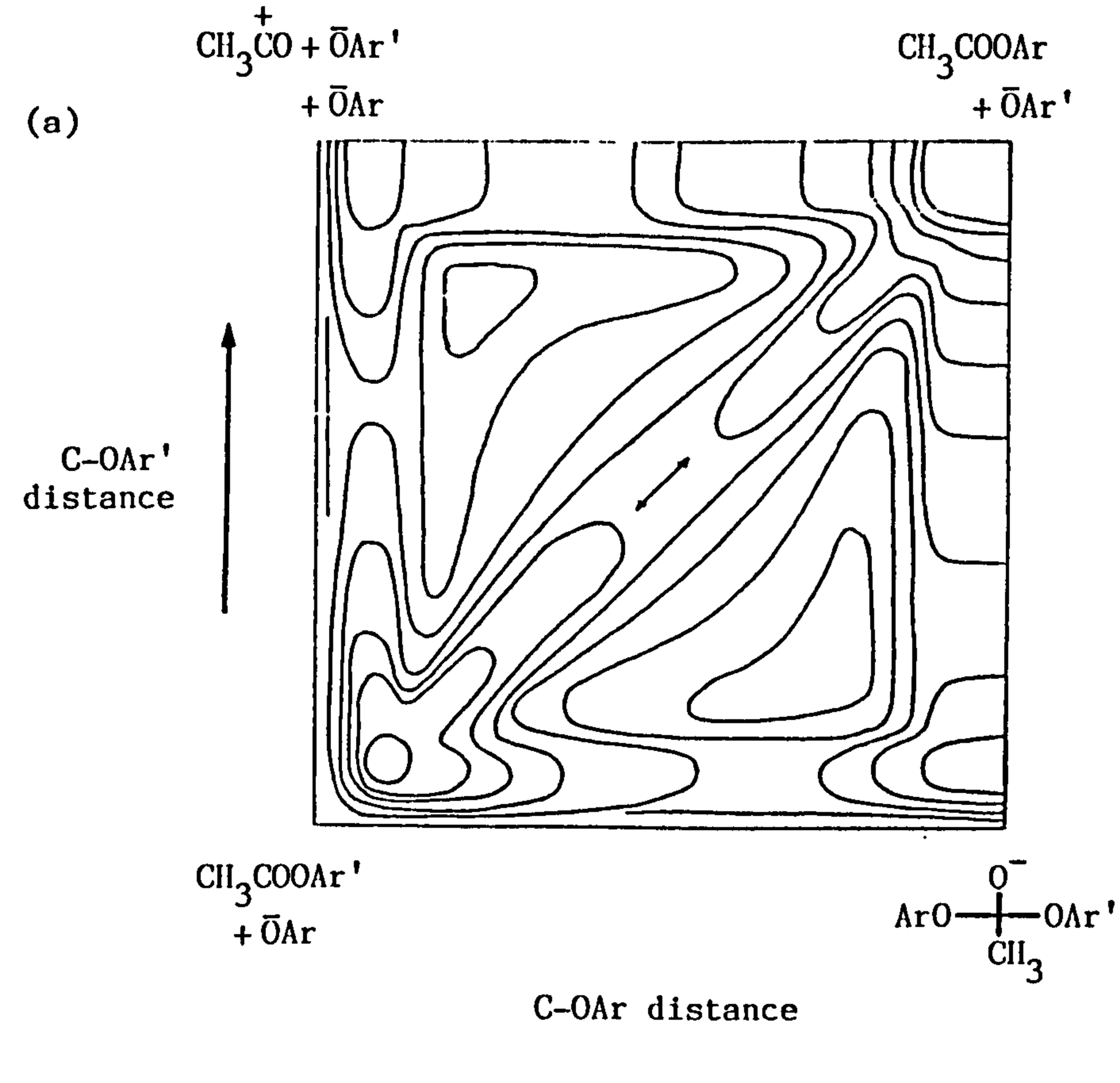

(b)

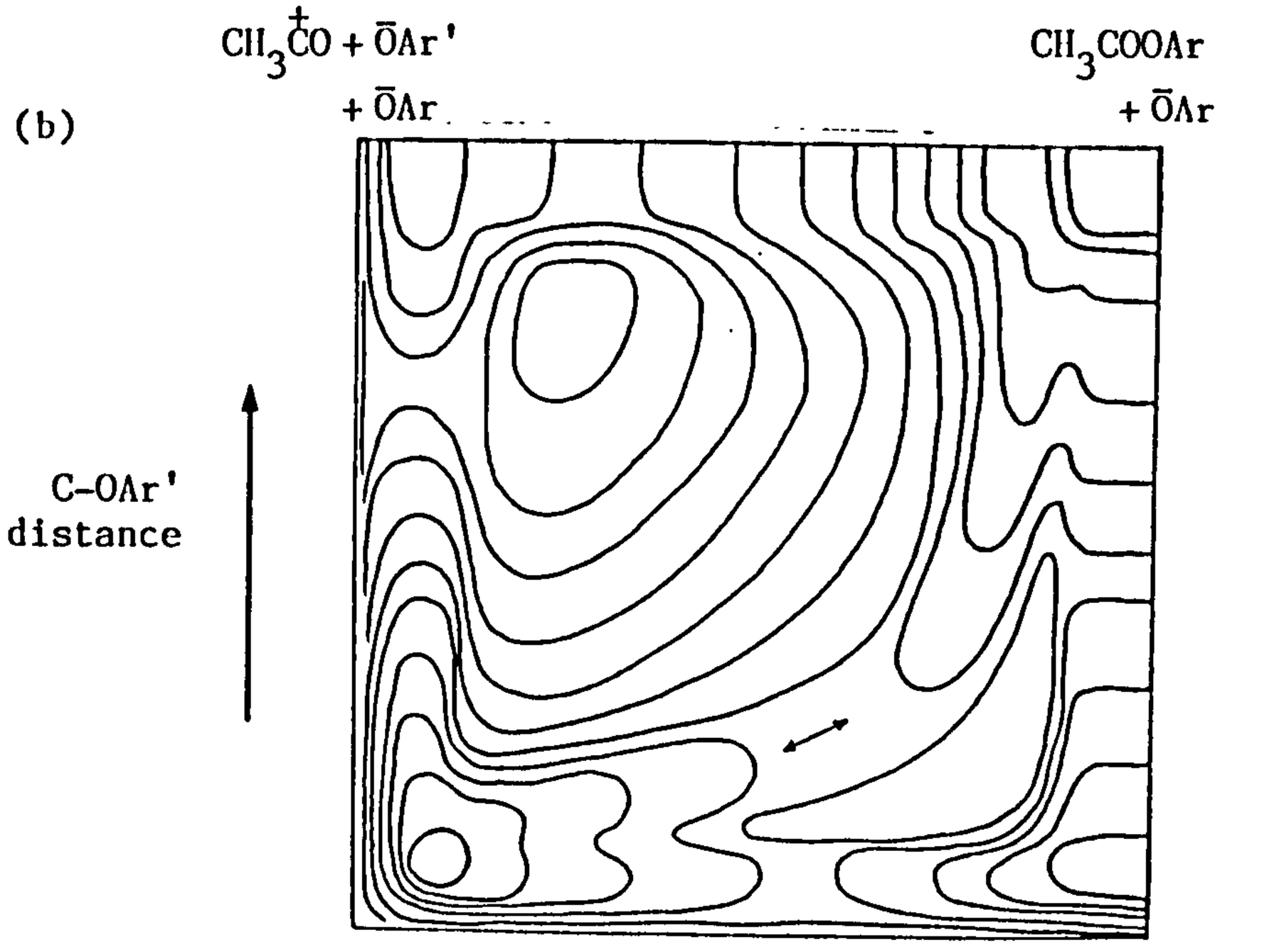

Figure 1.12 Bronsted-type plot for the reaction of a range of nucleophiles with p-nitrophenylacetate in aqueous solution at 25°C. The points represent hydro peroxides,▲; peroxyacids,Δ; thiols,□; primary amines,∇; secondary amines,▼; tertiary amines,◈; phenolate ions,O; alcoholate ions,●; the hydroxide ion,✱; other oxygen ions,■. (see Appendix 1 for rate constants)

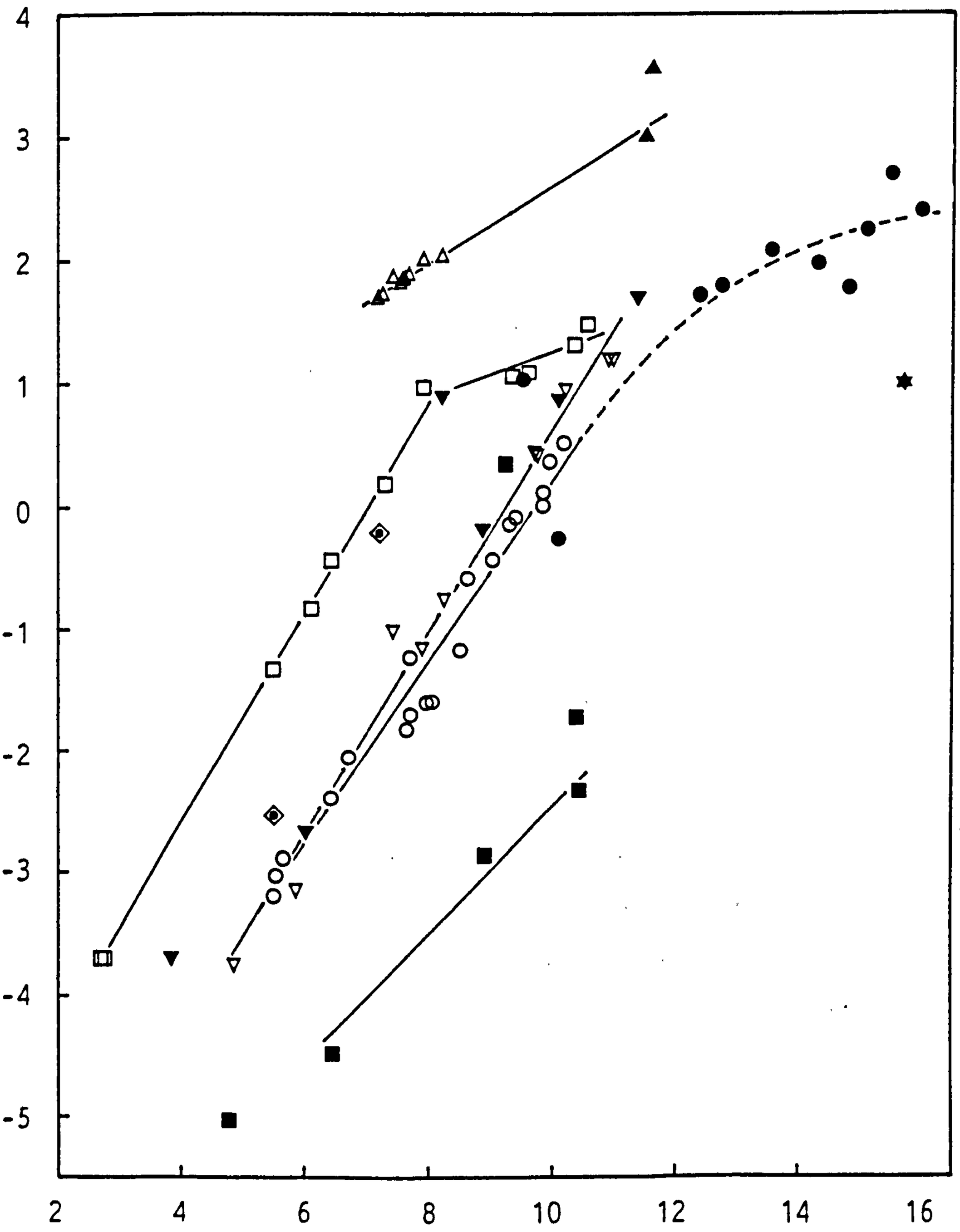

the wide spectrum of nucleophilic reactivities over and above the reactivity series that structurally similar nucleophiles form.

This section discusses factors other than Brønsted basicity which may contribute to nucleophilicity in acyl and aroyl transfer reactions.

1.5.2 Solvation

It is often forgotten when dealing with mechanisms of reactions in aqueous solution that, as well as the changes occurring in bonds between reactant molecules, there will also be a change in the interactions between the reactants and the surrounding solvent molecules. Thus, in the previous discussion on the nature of transition states when talking about bond formation and bond breaking, it is more strictly true to talk about the total bond order[46], which encompasses both the bonding process and solvation effects.

Ritchie[58] has demonstrated the importance, indeed, the dependence, of some reactions of cations with anions on solvation effects. In a range of studies on the reaction of cations (triaryl-methyl cations, aryldiazonium ions, and tropylium ions) with anionic nucleophiles, in water and methanol, a reactivity series of N_3^- > CH_3O^- > CN^- was found in all cases. Thus, the reactivity of the nucleophiles was related to some property of the nucleophile other than basicity or polarisability, since cyanide is more basic and more polarisable than the azide anion. The reaction series was experimentally shown to be qualitatively related to the solvation energy, with the better nucleophiles, such as CN^-, being those with the lower solvation energies. The cation-anion reaction is thought to occur as shown in Scheme 1.12

Scheme 1.12

$$R^+ + X^- \rightleftharpoons [R^+][X^-] \rightleftharpoons [R^+X^-] \rightleftharpoons RX$$

solvent separated ion pair — intimate ion pair — product

The transition state for this reaction is believed to be a one-solvent molecule separated ion pair, in which it is the anion which becomes desolvated; the cationic solvation shell remaining little perturbed from the ground state. Thus, the lower the solvation energy of the anion, the easier it is to form the transition state, and the greater the reactivity.

Jencks et al.[57] have also addressed the question of solvation, with respect to the curvature observed for the reaction of the more basic oxygen ions with substituted phenyl acetates. However, they advise caution, because: "they [solvation effects] can be used to 'explain' almost anything". Jencks et al.[57] suggest that it is likely that at least one of the three hydrogen bonded solvating water molecules around the basic oxygen anion is likely to be removed in the early phase of the reaction, and that this removal, given the high solvation energies, would be likely to contribute to the free energy changes in forming the transition state. The desolvation requirements are, necessarily, non-linear, for the most strongly basic oxygen anions, otherwise, the Brønsted plot would be linear, although altered in slope. For the less basic oxygen nucleophile, the Gibbs free energy required for the removal of a water molecule decreases and, eventually, becomes negligible.

1.5.3 Polarisability

It has been stated[8] that on examination of a wider series of reactions than those of $B_{Ac}2$ type, the correlation of rates of reaction with basicity is more the exception than the rule; many nucleophilic displacements at saturated centres, for example, show no detectable dependence on basicity of the nucleophile. Clearly, other factors, of which polarisability is considered an important one, must come into play in determining the reactivity in these cases. Polarisabilty, or 'softness', is a measure of the mobility of the electrons of a nucleophile, and has been used as a parameter in the second Edwards[66] equation, relating properties of the nucleophile with rates of reaction:

$$\log \frac{k}{k_o} = P + \beta H \qquad \text{Eqn 1.8}$$

Here, (k/k_o) is the rate relative to the 'water' reaction; P is the polarisability, which can be determined from the molar refractivity (R_N/RH_2O) in uncomplicated cases[8]; (it is related to the oxidation potential of the nucleophile), H is a measure of basity. Polarisability is much less important for reactions at the carbonyl carbon than at the sp^3 hybridised carbon[8]; however, it is still a factor which must be examined.

In a nucleophilic substitution reaction at a carbonyl carbon, the orbital which was originally used to form the π bond of the double bond is available for the interaction with the attacking nucleophile, allowing bond formation at close range.[8] This is obviously analogous to basicity which involves bond formation at short distance with a proton. Now, consider the case of a nucleophilic displacement reaction at a sp^3 hybridised carbon centre. It is believed[8] that bond formation between the nucleophile and the carbon atom must take place at a distance in this transition state owing to the unavailability of unoccupied orbit-

als for bond formation, and the increased steric demands of the pentavalent transition state.[8] It follows, that any feature of the nucleophile (or substrate) which promotes full or partial bond formation in the transition state between nucleophile and substrate at a considerable distance will increase the rate of reaction. If, therefore, a nucleophile possesses a high degree of polarisability, and the polarisation of the bonding electrons takes place in the direction from the nucleophile towards the substrate, then this permits good electrostatic interaction without necessitating bringing the nucleophile close to the substrate.[59] Obviously, then, when discussing polarisability, such factors as the size of the nucleophilic atom are important[8], since outer electrons of the large atoms are held more loosely than in smaller atoms. Thus, sulphur nucleophiles might be expected to be more reactive than oxygen nucleophiles.

Obviously, polarisability will not be as important for reactions at the carbonyl carbon, however, looking again at Figure 1.12, it can be seen that although in many cases, nucleophile series show a clear dependence of nucleophilicity on basicity, as might be expected for these types of reaction, different groups of structurally similar nucleophiles form different reactivity series.[8] Some of these differences may be ascribed to the intrinsic polarisability, or lack of polarisability, of some groups of structurally similar nucleophiles. In Figure 1.12, the sulphur nucleophiles (thiols) are indeed more reactive than the phenoxide oxygen nucleophiles. However, another characteristic of many polarisable or 'soft' nucleophiles, such as thiols, is the availability of unoccupied d or π orbitals with which an electron pair of a substrate can interact by back-bonding.[8] For example, the insensitivity of the reaction of thiol anions with aldehydes may be due to back-bonding, in

which the electron density of the carbonyl oxygen is transferred to a d orbital on the attacking sulphur atom in the transition state[53]:

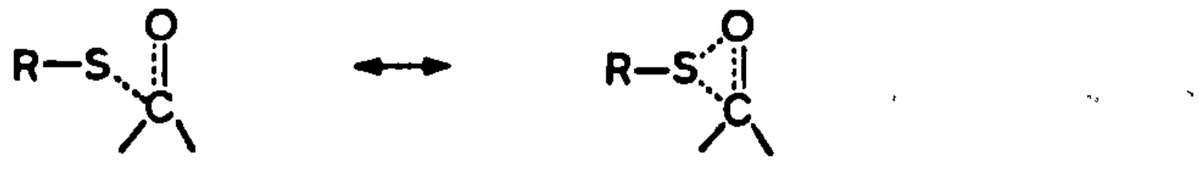

This may also be possible with other carbonyl containing compounds.

Where nucleophiles exhibit enhanced reactivity which cannot be accounted for by polarisability and basicity, then this is known as the 'α effect'[59], and is discussed in the next section. Peroxides, for example, which are not observed to have any extraordinary polarisability[62], are often cited examples of this α effect. (See Figure 1.12.)

1.5.4 The 'α Effect'

The term ' α effect' was applied by Edwards and Pearson in 1962[59] to describe nucleophiles whose reactivity exceeded that which might have been expected from their basicity and polarisability. Nucleophiles demonstrating this α effect, as indicated by positive deviations from Brønsted-type plots of log k against pKa, are structurally characterised by an unshared pair of electrons on the atom adjacent, or α, to the nucleophilic atom. Anionic nucleophiles, such as peroxy anions[62] and ClO^-, as well as neutral nucleophiles, such as hydroxylamine[67] and hydrazine[68,69] have been shown to demonstrate the α effect, although the type of substrate does influence the extent of this effect[62]; the α effect is most significant for reactions at unsaturated carbons[70] such as the carbonyl carbon of amides and esters.

Recent studies[70,71] have provided good evidence to suggest that the enhanced reactivity shown by some α nucleophiles is a manifestation,

either wholly or partly, of solvation effects. DePuy et al. in 1983[70], demonstrated that, in the gas phase, HOO^-, compared to HO^-, showed no enhanced reactivity towards the carbonyl carbon. This is contrary to the data presented in Figure 1.12, which clearly show that, for the reaction with PNPA, in aqueous solution, HO^- is much less reactive than HOO^-, whilst having a larger pKa. It is argued[70], that if the α effect is an intrinsic property of the anion, then it should manifest itself in the gas phase, as well as in the aqueuos phase. Additionally, Buncel and Um[71] have shown that, for the reaction of PNPA with the nucleophile, butane-2,3-dionemonoximate anion and the 'normal' nucleophile, p-chlorophenoxide ion, the degree and rate enhancement (α effect) shown by the αnucleophile is dependent on the nature of the solvent; the α effect was markedly increased by increasing the composition of the dimethylsulphoxide (DMSO) - water mixture to 50 mole % DMSO.

Of the arguments advanced to explain the α effect, which are not based on solvation effects, two of the more recent ascribe the effect to either ground state destabilisation of anionic nucleophiles[72,73,74,75] or transition state stabilisation.[75,76] Some of the earlier explanations for the α effect have been based on intramolecular general base catalysis[67,72,73,74] and stabilisation of the transition state by hydrogen bonding to the carbonyl carbon by a hydrogen on the α atom.[67,77,78]

1.6 Catalysis Mechanisms of Acyl Transfer Reactions

This section examines the mechanisms of catalysis of acyl transfer reactions, and considers the conditions under which such mechanisms are expected to occur. The main types of catalysis examined are specific and general acid-base catalysis (Section 1.6.1), and nucleophilic cata-

lysis (Section 1.6.3). In addition, bifunctional general acid-base reactions are discussed (Section 1.6.2).

1.6.1 General and Specific Acid-Base Catalysis

The main routes through which general and specific acid-base catalysis can operate in acyl transfer reactions of esters and amides are detailed in Scheme 1.13.

Scheme 1.13

(i) General acid catalysis: protonation of the anionic carbonyl oxygen in the tetrahedral intermediate.[40]

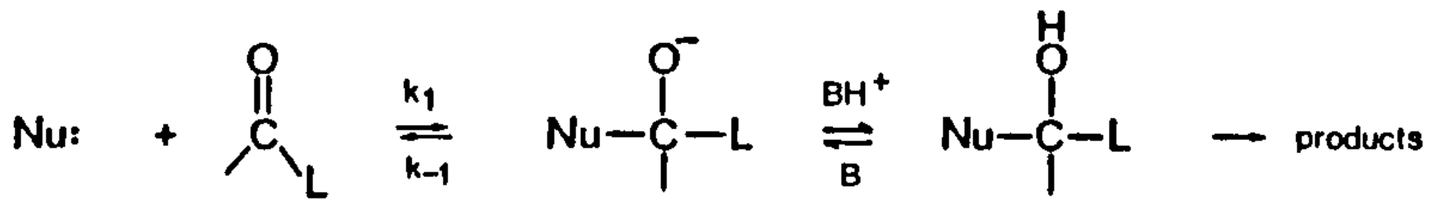

(ii) General acid catalysis: protonation of the leaving group.[35,16]

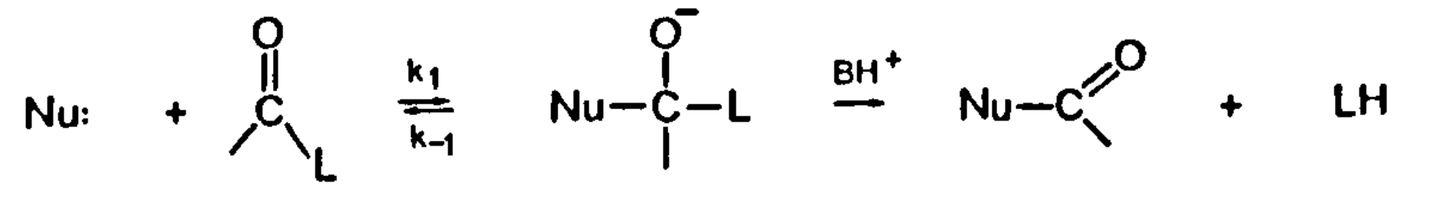

(iii) General base catalysis: proton abstraction from nucleophile in the tetrahedral intermediate.[14,15,40,79]

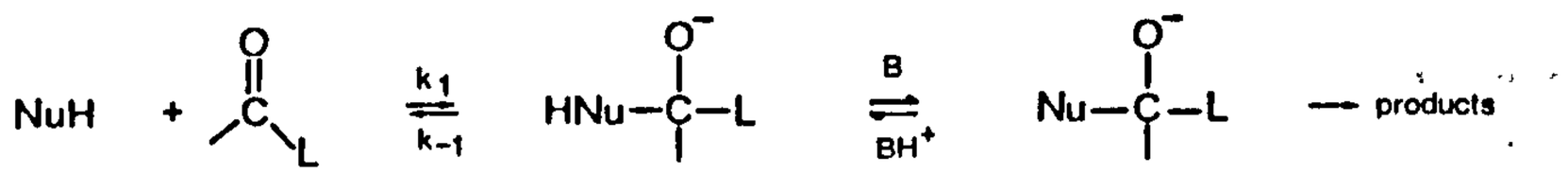

(iv) Specific base catalysis: proton abstraction from nucleophile in a rapid pre-equilibrium step before the nucleophile attacks.[80,81,82]

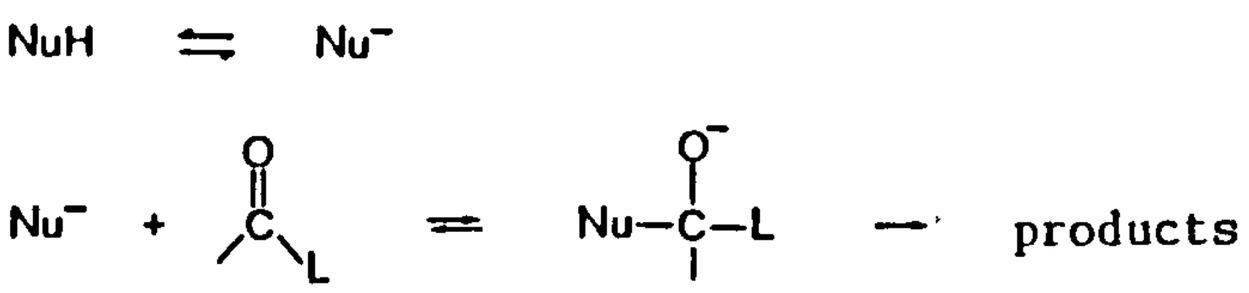

(v) Specific acid catalysis: protonation of the substrate in a rapid pre-equilibrium step.[35]

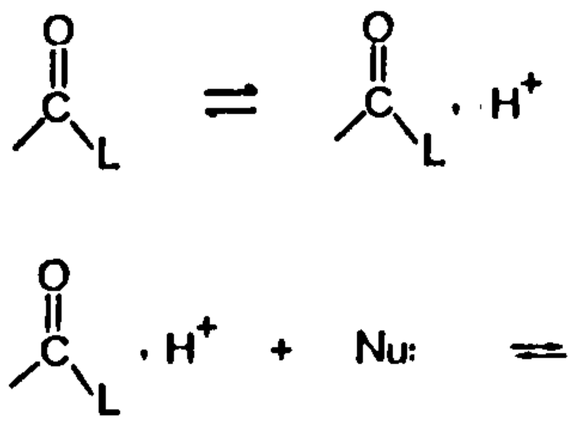

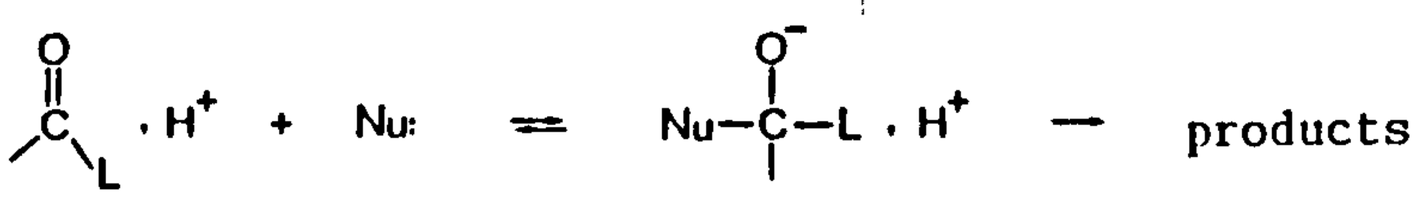

In the catalysis mechanisms detailed in the above scheme, catalysis can be effected by making the nucleophile more reactive (iv), making the substrate more reactive (v), or by stabilising the tehrahedral interme-diate with respect to the k_{-1} back-reaction to reactants (i, ii and iii). Note, that in Scheme 1.13, the catalysis mechanisms have been detailed for reactions which proceed via the formation of a tetrahedral intermediate; general acid and general base catalysis of reactions which proceed via a concerted mechanism, in which there is no stable

tetrahedral intermediate formed, is a special case and will be discussed later in this section.

Having defined the types of catalysis expected, it is important now to examine the circumstances under which catalysis will and will not occur. The three main factors which appear to determine this are: the position on the reaction coordinate of the kinetically significant transition state with respect to the proton transfer step; the pKa changes which occur on the bonding of heavy atoms; and the lifetime of the tetrahedral intermediate. These are discussed below.

As we have discussed ealier in this chapter, in reactions which proceed via a stepwise mechanism, the kinetically significant transition state can either occur before or after the stable tetrahedral intermediate on the reaction coordinate; this is termed rate determining formation and rate determining breakdown of the tetrahedral intermediate, respectively. In cases where rate determining formation of the tetrahedral intermediate is the kinetically significant transition state then, clearly, any catalytic mechanism which occurs via stabilisation of the tehrahedral intermediate (i, ii, and iii) is not likely to have any effect on the rate of reaction, since the proton transfer step occurs after the kinetically significant transfer state.[83] Of course, specific acid-base catalysis may be observed in cases of rate determining formation, since these mechanisms occur via a rapid pre-equilibrium proton transfer step. For specific acid-base catalysis, the rate of reaction will be directly proportional to either $[H_3O^+]$ or $[OH^-]$.[83] In cases where breakdown of the tetrahedral intermediate is rate determing, then all of the catalysis mechanisms listed in Scheme 1.13 could apply.

Another factor to be considered in determining whether catalysis is expected to occur is the pKa changes which occur on the bonding of

heaving atoms. Jencks[10,84] has proposed that the driving force behind general acid-base catalysis is the large and sudden changes in pKa which occur on the binding of heaving atoms (Scheme 1.14). Such large changes in pKa give rise to unstable transition states and intermediates (where intermediates exist) and the catalysts act to stabilise these intermediates and transition states, forming a lower energy pathway for the reaction.

Scheme 1.14 Changes in pKa on the bonding of heavy atoms.[10]

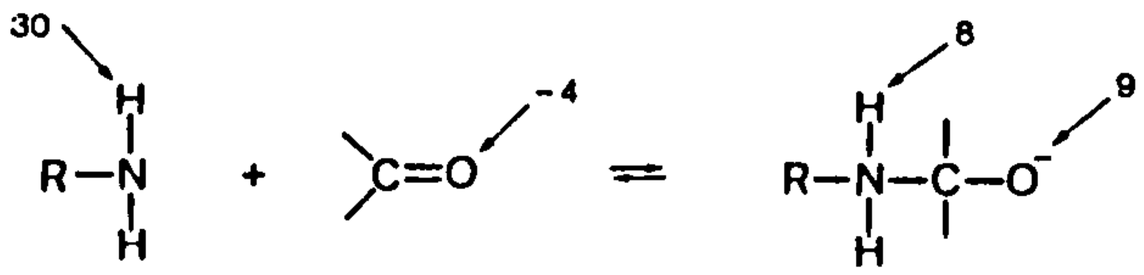

The final factor to be considered, in determining whether acid-base catalysis is to be expected, is the lifetime of the tetrahedral intermediate. Jencks[9,10] has suggested that the lifetime of the intermediate formed during an addition reaction is of critical importance in determining whether catalysis will or will not occur. As we have seen in Section 1.3, there is a whole gamut of lifetimes of tetrahedral intermediates, ranging from those which are stable as molecules in their own right, to those with lifetimes with the order of one molecular vibration (~10^{-13}s). In the latter case, the intermediate can be said not to exist, and the reaction proceeds via a concerted mechanism. The reason for this range of lifetimes is the presence of stabilising or destabilising structural features in the tetrahedral intermediate.[49] Depending on the lifetime of the tetrahedral intermediate, the catalysis mechanisms detailed in Scheme 1.13 can occur via (a) interaction with the solvent alone, (b) interaction with an external general acid or general base (enforced catalysis) and (c) interaction with an exter-

nal general acid or base which is present in a preassociation complex with the nucleophile and substrate prior to the addition reaction (enforced preassociation mechanism).[9,10] Reactions which proceed via a concerted mechanism, without the formation of a tetrahedral intermediate, are a special case of the enforced preassociation mechanism.[9,10] These points are eloborated upon below.

Solvent mediated proton transfer. Where the lifetime of an intermediate is sufficiently long, the proton transfer steps detailed in Scheme 1.13 may occur by interaction with the solvent alone, in which case no discernable catalytic effect would be observed with added general acid or general base. Consider Scheme 1.15, where a nucleophile adds to a carbonyl centre to form a tetrahedral intermediate.

Scheme 1.15

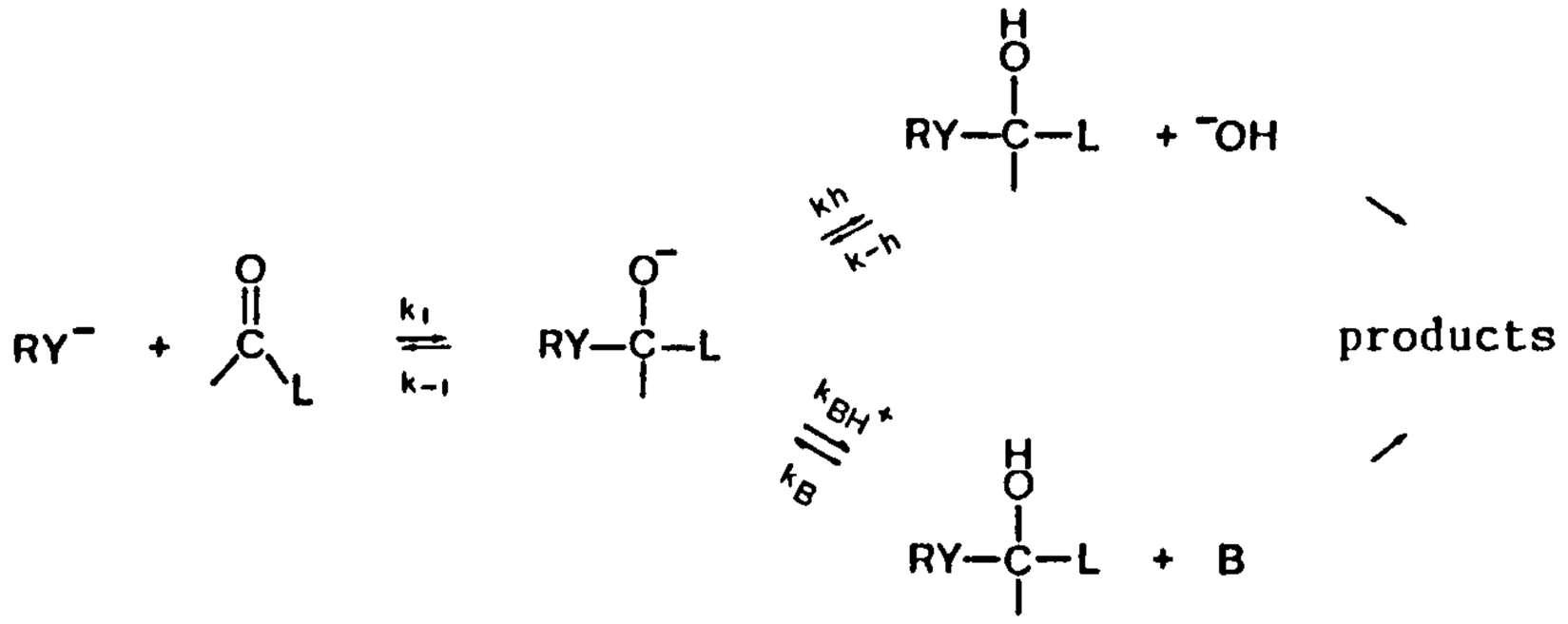

k_h is the rate of proton abstraction from the solvent which, in the case of water, is given by Equation 1.9.

$$k_h = k_{-h}\ Kw/Ka \qquad \text{Eqn 1.9}$$

Where Ka is the acid dissociation constant of the tetrahedral intermediate, and k_{-h} is diffusion controlled abstraction of a proton by hydroxide (10^{10} m^{-1} s^{-1}).[10] (Thus, the higher the basicity of the anionic carbonyl carbon of the tetrahedral intermediate, the greater the value of k_h.) If in Scheme 1.15, $k_h > k_{-1}$ then the intermediate can diffuse throught the solvent, and abstract a proton from it, faster than the nucleophile is expelled. In this case, every intermediate that is formed is 'trapped' by a solvent proton and there is, therefore, no requirement for general acid catalysis. This is true of the reaction of EtS^- with acetaldehyde[10], where $k_{-1} = 6x10^6$ s^{-1} and $kh = 8x10^8$ s^{-1} and no catalysis is observed. Where the attacking nucleophile contains a proton which becomes acidic when the addition compound is formed, such as in aminolysis reactions, a solvent mediated 'proton switch' mechanism has been proposed[10], as shown is Scheme 1.16.

Scheme 1.16

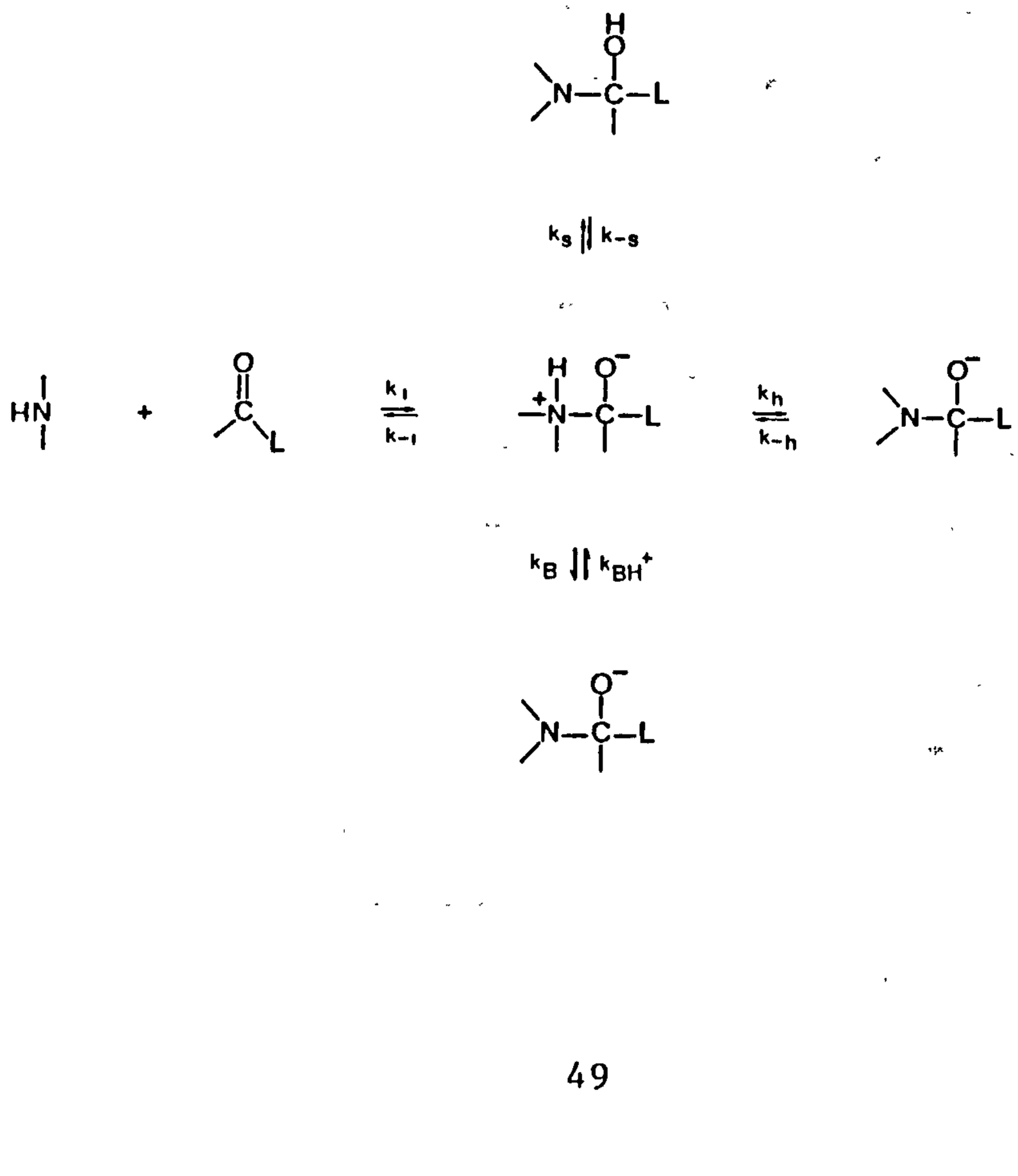

Here, the acidic proton is transferred, probably through two solvent molecules to the anionic carbonyl oxygen with a rate constant k_s of approximately 10^6 - 10^8 s^{-1}. If k_s or k_h > k_{-1} then no catalysis will be observed.

Enforced catalysis. General acid-base catalysis *will* be observed in the above examples when k_{-1} becomes larger than either k_h or k_s (where appropriate). In this case, not every molecule of the addition intermediate that is formed is 'trapped' by the solvent before the molecule is expelled and, therefore, there is a role for catalysis to play in increasing the number of the more stable 'trapped' intermediates. Such catalysis is described by the Brønsted equations[8] 1.10 and 1.11, for which the same factors discussed in Section 1.4 apply. If bond formation

$$\text{Log } k_B = C + \beta \text{ pKa} \qquad \text{Eqn 1.10}$$

$$\log k_{HA} = C - \alpha \text{ pKa} \qquad \text{Eqn 1.11}$$

between B and the acidic proton of an addition intermediate is complete in the kinetically significant transfer state, then $\beta \sim 1.0$. If an intermediate value between zero and unity is obtained for β, then this implies that there is only partial bond formation. It is generally found with the general acid and general base catalysis discussed above, that for weaker acids and bases, the Brønsted slopes, α and β, are close to unity[85], since the proton transfer step is thermodynamically unfavourable, and the observed rate is proportional to the strength of the acid or base. For strong acids and bases, the activation energy for the proton transfer is so small that the observed rate is dependent on the rate of diffusion together of the reactants.[85] The value of the diffusion controlled limit, k_d, is $\sim 10^8 - 10^{10} m^{-1}s^{-1}$ in water, and differs little for various compounds.[86] In this region, the values of α and β are close to zero. If a plot of log k against the pKa of the

catalyst is made for a particular reaction, such as the general acid catalysis of intermolecular S-acetymercaptoethylamine aminolysis (Scheme 1.17), as shown in Figure 1.13, then α changes from -1.0 to zero as the catalysis becomes diffusion controlled. This type of plot is known as an 'Eigen curve' and is indicative of this type of general acid-base catalysis. The break point in the curve, between the region of dependence on acid strength, and the diffusion controlled process, generally, occurs when the pKa of the catalyst approaches the pKa of the protonated intermediate.

Scheme 1.17

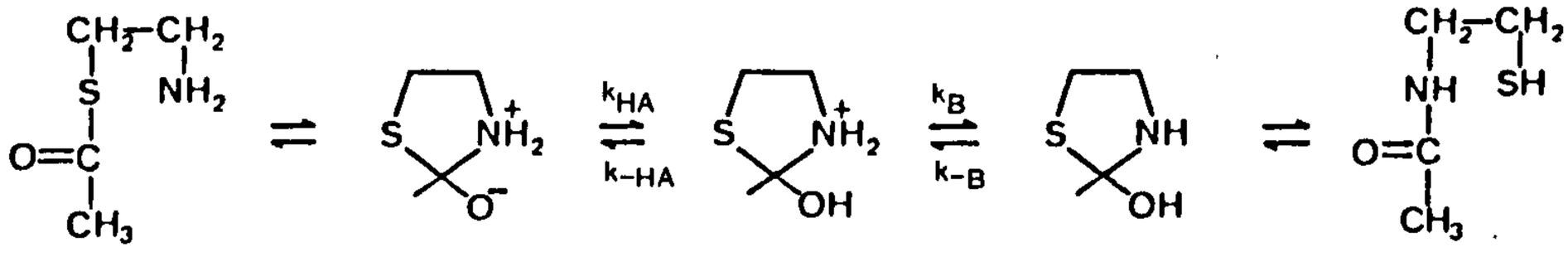

In Scheme 1.17, there is both general acid and general base catalysis, and it is interesting to note, from Figure 1.13, that the observed rate for the bifunctional catalyst bircarbonate shows a large positive deviation from the Brønsted plot, almost approaching the diffusion controlled limit. This is most likely due to[85] the bicarbonate acting as both general acid and general base in a concerted* cyclic proton transfer mechanism (Scheme 1.18). Catalytic species which can act in this manner are termed bifunctional catalysts.

---

* In this case, the term 'concerted' simply describes the proton transfer and is not a reference to the nature of the acyl transfer reaction as a whole.

Scheme 1.18

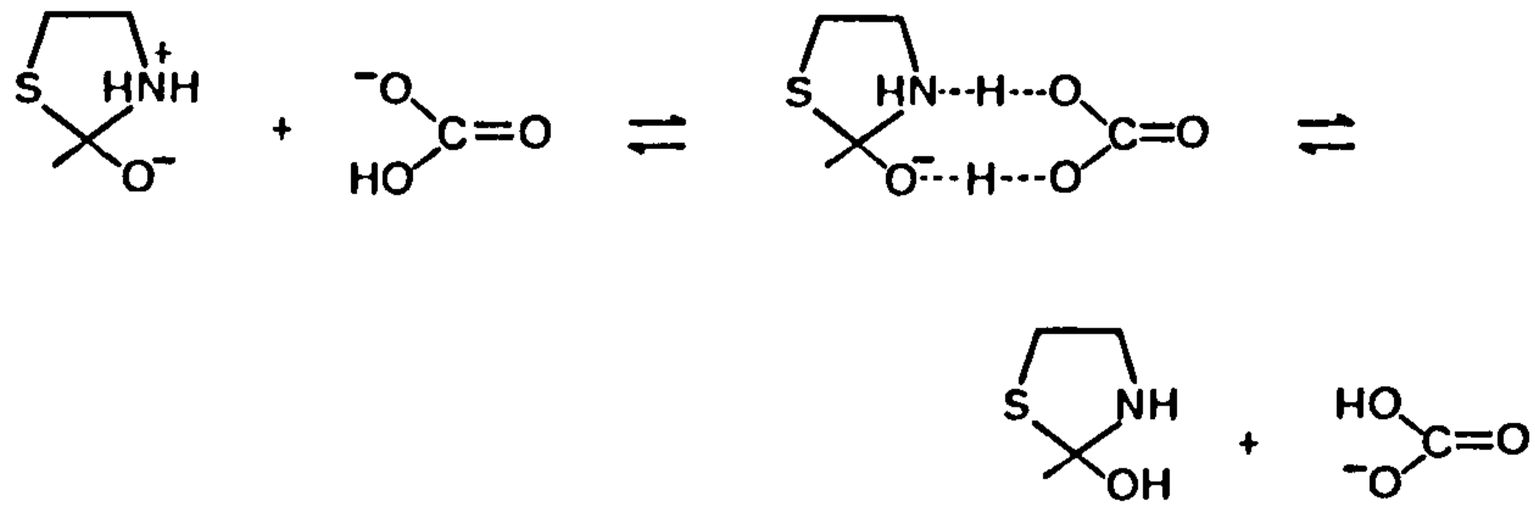

In Figure 1.13, the phosphate monoanion and the carboxylic acids could also act as bifunctional catalysts. However, these catalysts already lie in the diffusion controlled region and cannot, therefore, increase the rate of reaction further. The hydroxonium, H_3O^+, has a value which is 20 times higher than expected for the diffusion controlled process, and it is speculated that this is because the proton transfer can occur rapidly through adjacent water molecules in a 'proton jump mechanism'.[85] The topic of bifunctional catalysts is discussed further in Section 1.6.2.

Another experimental manifestation of enforced catalysis is that the observed rate constant, k_{obs}, levels off with increasing buffer concentration. Such a relationship was found by Khan[14] for general base catalysed hydroxylaminolysis of the activated amide, N-ethoxycarbonylphthalimide (ECPH) in acetate buffer (Scheme 1.19).

Scheme 1.19

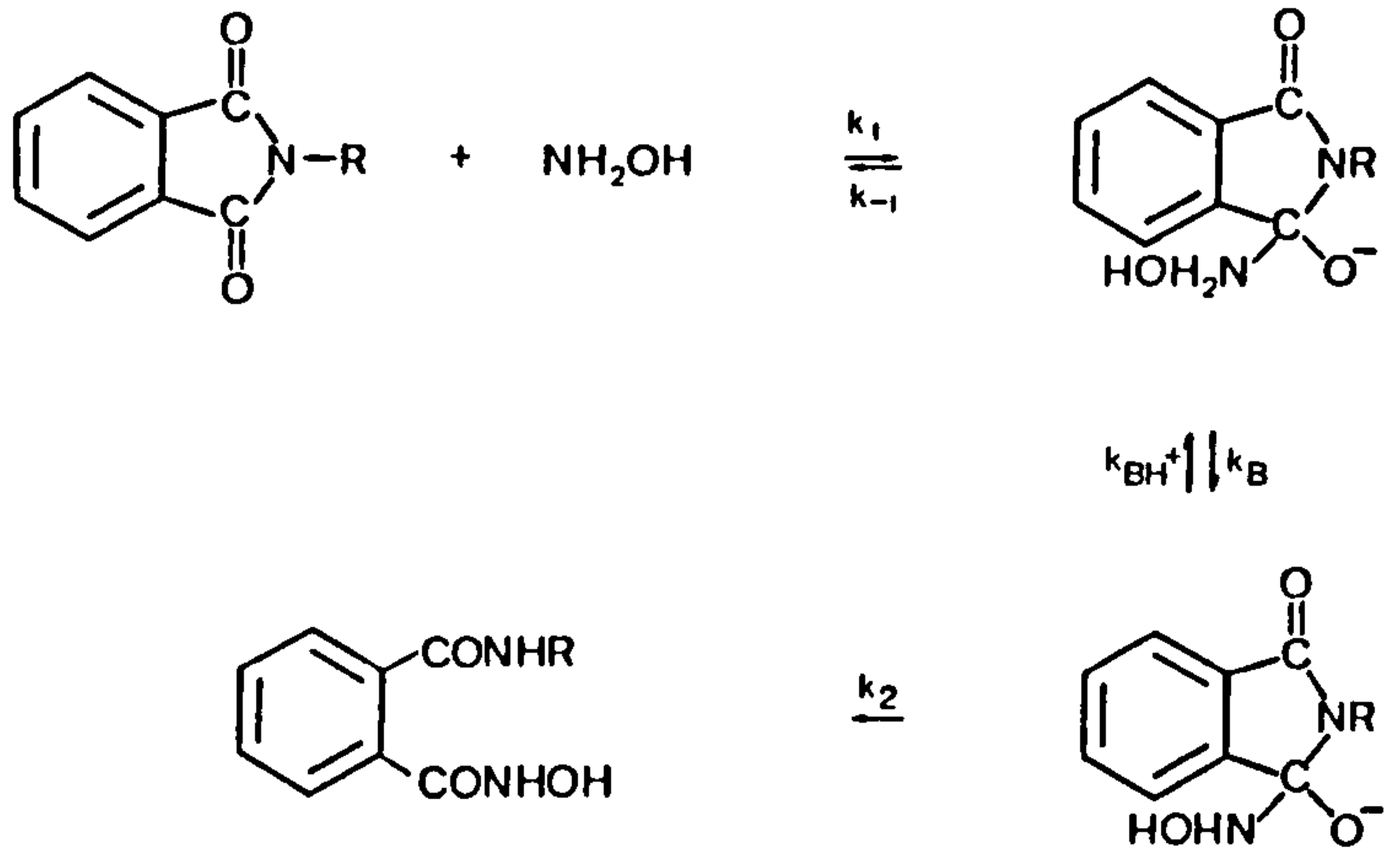

As the buffer concentration is increased, then all of the initially formed tetrahedral intermediate is trapped by the general base, acetate; k_2, the breakdown of the intermediate, becomes rate determining. This is also excellent evidence of a tetrahedral intermediate on the reaction pathway, provided that the curvature in the plot can be shown not to be due to other factors, such as changing pH with increasing buffer concentrations.

This discussion of enforced catalysis has, so far, centred on the catalysis mechanisms detailed in Scheme 1.13 (i) and 1.13 (iii). For reactions involving carbonyl compounds where the leaving ability of the leaving group is poor, then there is a requirement for the leaving group to be protonated, making it a much better leaving group. The reactions of amides, for example, are generally dominated by the requirement for protonation of the leaving group in order to avoid the unstable RN^- anion.[16] Drake et al.[86] have found, in studies of the hydrolysis of amides, that simple proton transfer to the leaving group of the tetrahedral intermediate is the rate determining step for poor

leaving groups (pKa > 9), and is followed by rapid cleavage of the C-N bonds; good leaving groups have a rate determining step of C-N cleavage, which is followed by rapid protonation of the leaving group. The protonation of the carbonyl oxygen in such reactions is not likely to be a significant route for catalysis, because of the importance of protonation of the leaving group.

Oakenfull et al.[16] have conducted a series of experiments on catalysis of the aminolysis of acetylimidazole, which has a leaving group pKa of 14.2. Imidazole (the imidazolium ion) was found to act as a general acid catalyst for the reaction of ammonia and ethylamine with acetylimidazole. For the reasons discussed above, imidazole must act to protonate the leaving group:

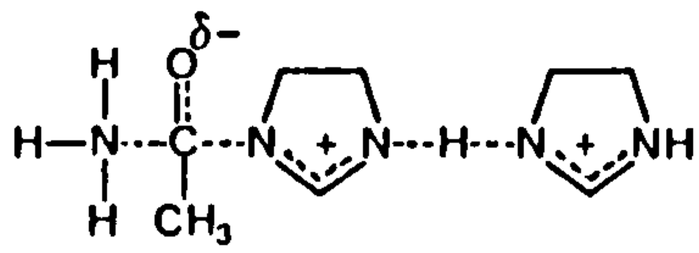

Additionally, a general base catalysed term was detected, and this was assigned to free imidazole acting to abstract an acidic proton from the attacking amine:

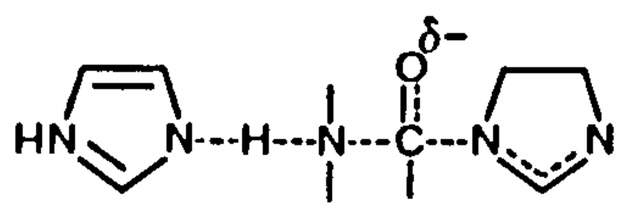

Removal of the proton in accordance with the above mechanism prevents expulsion of the attacking reagent to regenerate starting materials, and provides sufficient electron density at the reaction centre to expel the imidazole anion, which is now the best leaving group. It is,

of course, well-established that in nucleophilic reactions of amines, the catalysis is effected by a second molecule of amine acting as a general base, giving on overall pseudo first order rate constant, k_{obs}, defined by Equation 1.12

$$k_{obs} = k_1[RNH_2] + k_2[RNH_2]^2 \qquad \text{Eqn 1.12}$$

Enforced preassociation mechanism.[9,10] This is a form of enforced catalysis, as discussed above, since the lifetime of the intermediate is insufficient for solvent alone to be involved in the protonation/-deprotonation steps. The essential difference between this mechanism and the 'normal' cases of enforced catalysis is that the lifetime is so small that there is a requirement for a termolecular preassociation of nucleophile, substrate and catalyst before the formation of the tetrahedral intermediate. This is illustrated in Figure 1.14, for an acid catalysed addition reaction.

Figure 1.14

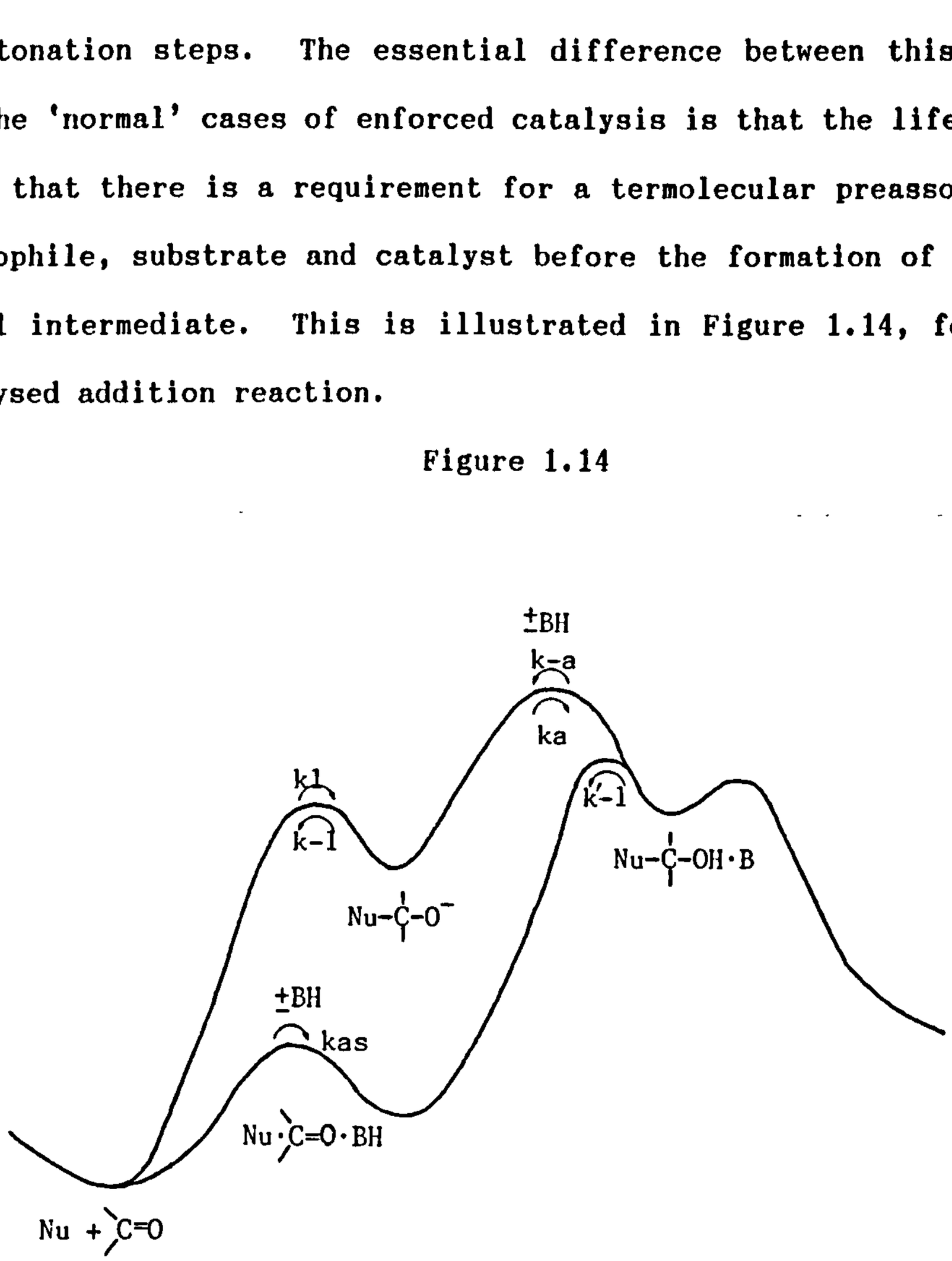

When the lifetime of a tetrahedral intermediate is very small (~ 10^{-8} to 10^{-10}s) then the intermediate-catalyst complex is so unstable that it reverts to reactants (k'_{-1}) faster than the catalyst can diffuse away from it (k_{-a}). Since this is the lowest energy pathway for the *breakdown* of the tetrahedral intermediate to reactants, then by the principle of microscopic reversibility, the termolecular preassociation complex must be the lowest energy pathway for the *formation* of the tetrahedral intermediate. Such a mechanism is likely to occur for the addition of pentafluorothiophenolate to acetaldehyde[9], as shown in Scheme 1.20:

Scheme 1.20

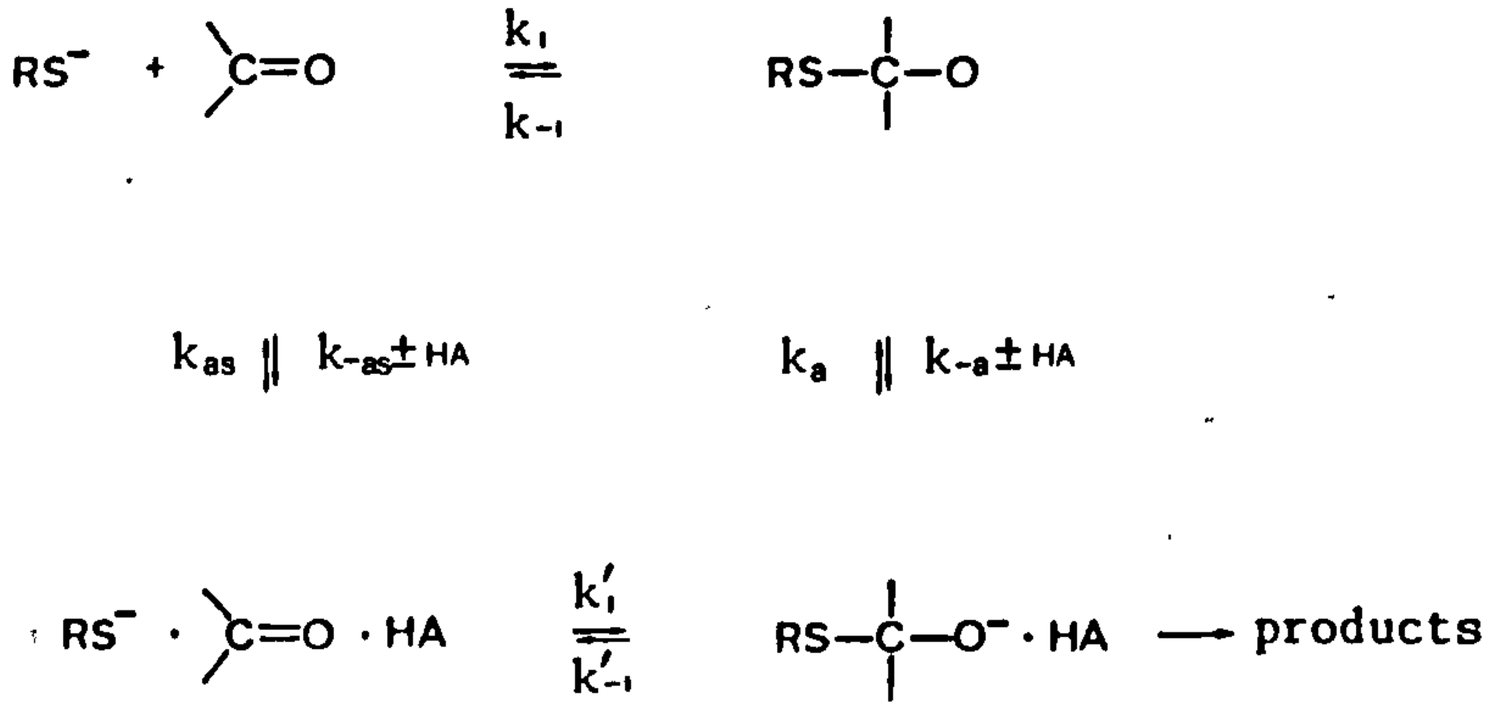

The route where RS^- adds to acetaldehyde, followed by a 'trapping' encounter with the general acid, HA, is the highest energy pathway. There is also good evidence to suggest that the general acid-base catalysis of the methoxyaminolysis of phenylacetate occurs via a preassociation mechanism.[87] This is discussed in Section 1.6.2, which deals with bifunctional catalysis.

Jencks[9,10] has also defined a further case of the preassociation mechanism where, for example, for the general acid catalysis of a nucleophilic substitution reaction, the general acid catalyst is actually hydrogen bonded to the carbonyl oxygen in the preassociation complex. The carbonyl carbon is thus protonated immediately that the intermediate is formed.

It is clear that, for reactions which occur via a concerted reaction mechanism, there must be a preassociation of nucleophile, substrate and catalyst. All of the catalysis mechanisms listed in Scheme 1.13 could equally well apply to a concerted process provided that the catalyst was present in a preassociation complex.

Finally, it should be noted that in a discussion of conditions under which catalysis should and should not be expected to occur, structural factors should also be considered. Khan[14] found general acid and general base catalysis for maleimide aminolysis by secondary amines and general acid catalysis by tertiary amines, yet no catalysis was observed with primary amines. The proposed explanation involved an internally hydrogen bonded structure which discouraged the probable occurrence of intermolecular general acid - general base catalysis:

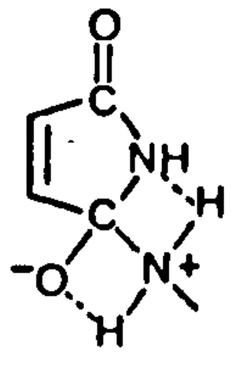

1.6.2 Bifunctional General Acid and General Base Catalysis

In reactions, such as the aminolysis of esters, which are susceptible to both general acid and general base catalysis, some catalysts, such as phosphate and bicarbonate are theoretically capable of acting as

fully concerted bifunctional catalysts. This is because they contain both acidic and basic groups. By concerted bifunctional catalysts it is meant[87] that one molecule performs both the general acid and general base catalysis (bifunctional) and that the two processes occur with no intermediate step (concerted).*

It has already been mentioned in Section 1.6 that bircarbonate may act as a bifunctional catalyst in the intramolecular aminolysis of S-acetyl-mercaptoethylamine[85] (Figure 1.13); compared to monofunctional catalysts of similar basicities, bicarbonate accelerates the rate to a value approaching the diffusion controlled limit. Nevertheless, it has been argued[84] that concerted bifunctional catalysis should be rare or non-existant, because of the low probability of meeting all of the requirements of the two simultaneous proton transfers in a single low-energy transition state, that is, whilst a molecule may, for example, be an effective general base catalyst, it is unlikely that the conditions will exist, simultaneously, under which it is also an effective general acid catalyst.

Cox and Jencks[87] however, in a study of general acid and general base catalysis of the methoxyaminolysis of phenylacetate, have produced excellent evidence for the existence of concerted bifunctional catalysis. General acid and general base catalysis of the methoxyaminolysis of phenylacetate is likely to proceed via an enforced preassociation mechanism.[87] This is demonstrated[87] by the good fit of Brønsted plot data for the general acid and general base catalysis of this reaction, to a theoretical curve defined by the enforced preassociation mechan-

---

* Note, that whilst the proton transfer step may be concerted, the reaction as a whole can still be stepwise.

Figure 1.13 Bronsted plot for general acid catalysis of the acetyl transfer reaction of S-acetylmercaptoethylamine at 50°C and ionic strength 1.0 M, based on a value of $k_{H_3O^+} = 6.5 \times 10^{10}\ M^{-1}\ sec^{-1}$. (From reference 85).

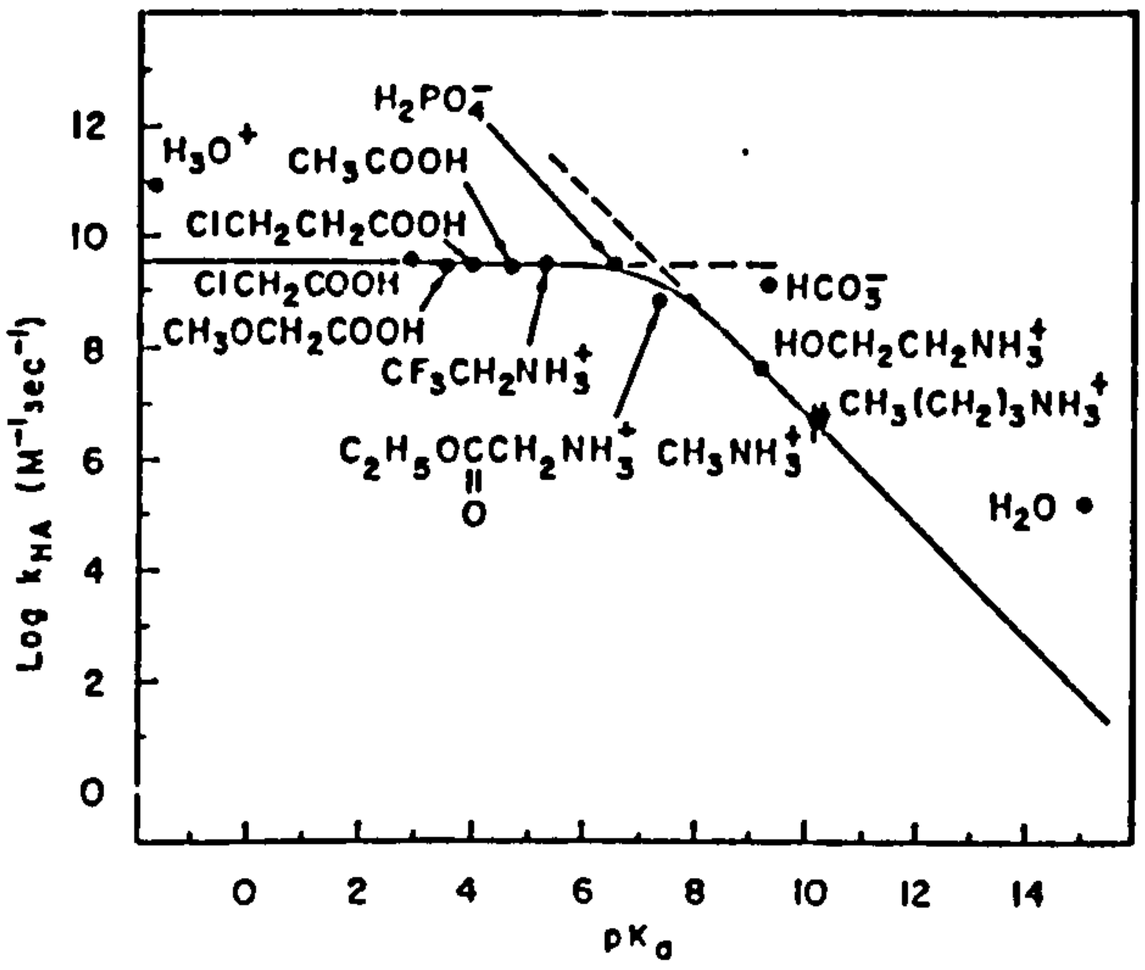

ism, as opposed to that for the Eigen mechanism. Figure 1.15a shows a Brønsted plot for the general acid-base catalysis of this reaction. For catalysts with pKa values < 4, there is a slope of $\alpha = -0.16$, after which the plot for catalysis by monofunctional acids of pk = 4-7 curves downwards to a limiting slope of $\alpha = -1.0$. Rate constants for catalysts containing both acidic and basic functions, however, (cacodylic acid, and the monoanions of phosphate, methylarsenate, bicarbonate and a series of substituted phosphates) fall on an extension of the Brønsted slope of $\alpha = -0.16$. In the enforced preassociation mechanism, as we have seen in Section 1.6.1, the reaction proceeds via an initial termolecular association of substrate, nucleophile, and catalyst according to Scheme 1.21

Scheme 1.21

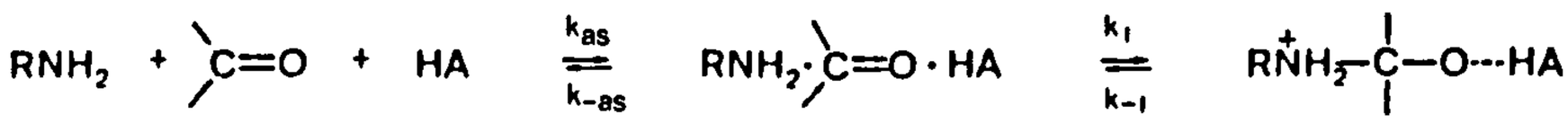

For strong acid catalysis (pKa < 4 in this case), the rate limiting step is assumed to be attack of the methoxyamine at the carbonyl carbon, with the carbonyl oxygen hydrogen bonded to the acid catalyst (k_1). The subsequent proton transfer step is rapid. For weaker monofunctional acids (pKa > 4), the proton transfer step itself is rate limiting, since it is no longer strongly thermodynamically favourable. In this region the rate of catalysis is dependent on the strength of the acid, as in the case of the Eigen function obtained for the diffusion controlled 'trapping' mechanism. (See Section 1.6.1.) The fact that those catalysts capable of acting via a bifunctional mechanism fall on the extension of the Brønsted slope of $\alpha = -0.16$ defined by the

Figure 1.15 (A) Bronsted plot for catalysis of the methoxyaminolysis of phenylacetate by bifunctional acids (open symbols) and monofunctional acids (closed symbols): carboxylic acids,□; cacodylic acid, phosphate, substituted phosphonate, methylarsonate and bicarbonate monoanions,O; protonated amines,●; upper limits for catalysis by fluoroacetone hydrates, hexafluoro-2-propanol and 2-chloroethylammonium ion,|. (B) Solvent deuterium isotopes effects for catalysis by monofunctional (●) and bifunctional (O) acids. (From reference 87).

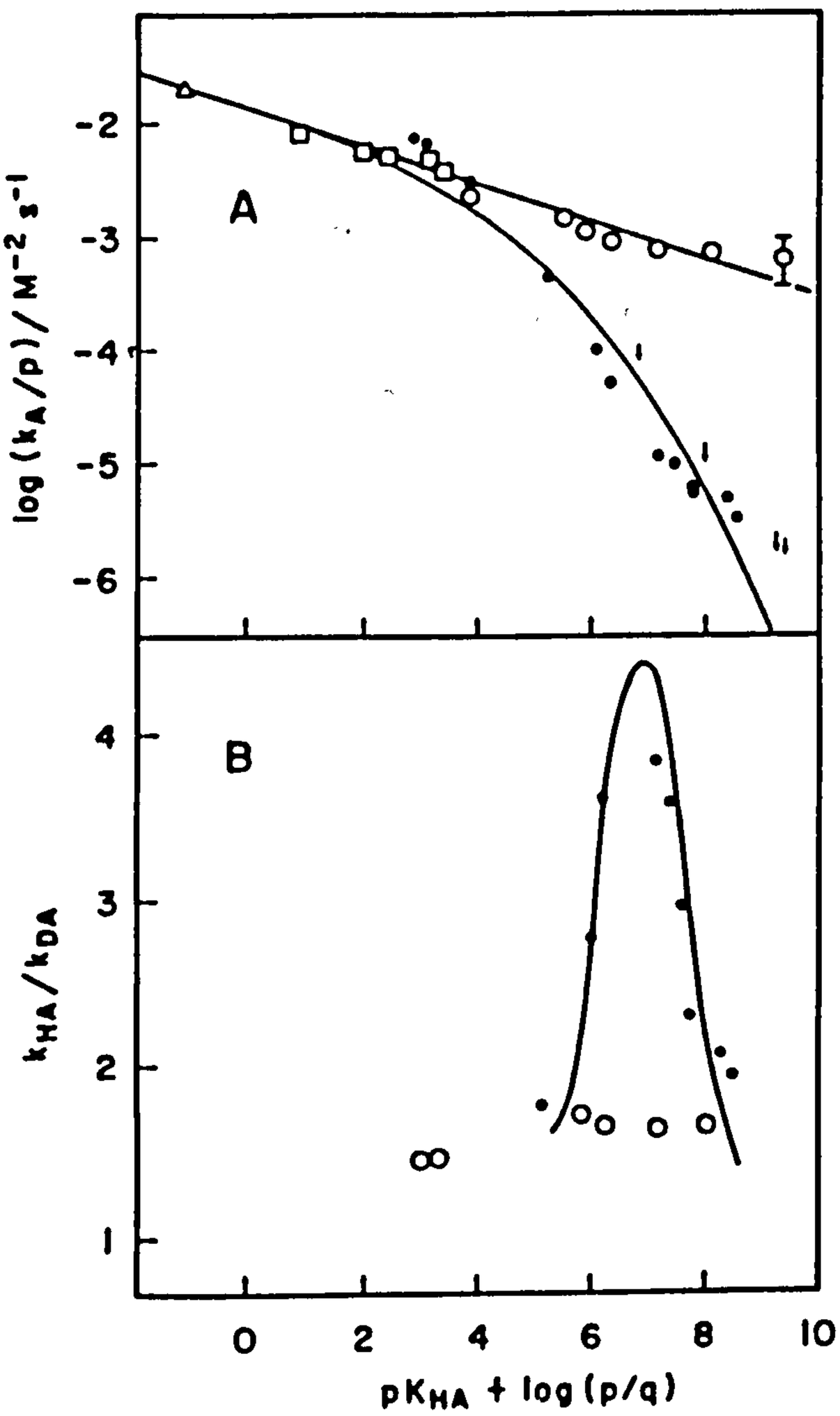

rate limiting step of k_1 (Scheme 1.21) indicates that the thermodynamically unfavourable proton transfer steps have been circumvented. Further evidence to support this is provided by the solvent deuterium isotope effect[87] (Figure 1.15b). There is a sharp peak for k_{HA}/k_{DA} at pKa = 6.8 for monofunctional catalysts, indicating a kinetically significant proton transfer step, whilst for bifunctional catalysts there is no such peak, indicating that the rate limiting proton transfer steps have been circumvented. The data for general base catalysis of this reaction by monofunctional and bifunctional catalysts follows exactly the same patterns for general acid catalysis.

An attractive explanation[87] for the effectiveness of concerted bifunctional catalysis is shown diagrammatically in Scheme 1.22 for the catalysis, by the phosphate monoanion, of phenylacetate methoxyaminolysis.

Scheme 1.22

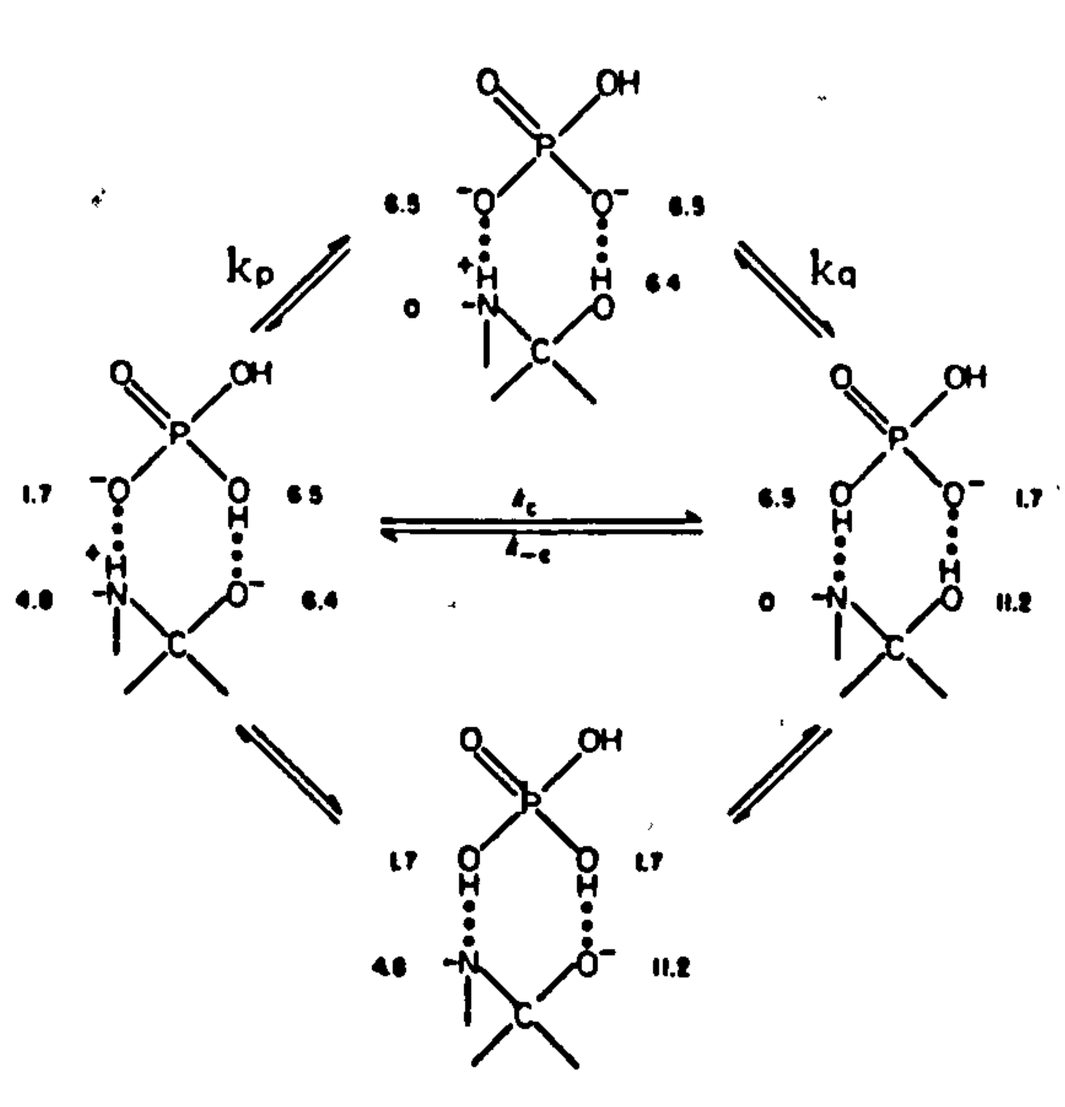

The effectiveness of concerted bifunctional catalysis lies in the changes in pKa which occur upon transfer of a proton in a cyclic system. In Scheme 1.22, initially, proton transfer from the amine to the basic site of the phosphate monoanion is thermodynamically unfavourable, whilst the transfer of a proton from the acidic site of the phosphate to the carbonyl oxygen is thermoneutral. Now, consider the case where the catalyst acts via a *stepwise* one-encounter bifunctional mechanism (k_p then k_q) in which there is an intial proton transfer from the catalyst to the carbonyl oxygen (k_p). The subsequent proton transfer from the amine to the catalyst is now strongly thermodynamically favourable and proceeds with little or no barrier (k_q). We can see from an examination of the initial and final pKa values that the *overall* proton transfer process (k_c) is strongly favourable thermodynamically. Thus, the primary reason for the effectiveness of *concerted* bifunctional catalysis arises from the rapid simultaneous proton transfers made possible by the concerted mechanism. This allows the reaction to proceed via the low-energy k_c pathway.

1.6.3 Nucleophilic Catalysis

The imidazole catalysed hydrolysis of activated acyl compounds, and the catalysis of other acyl transfer reactions of these compounds, is probably the best-known example of nucleophilic catalysis.[8] This is shown in Scheme 1.23, for the hydrolysis of PNPA.

Scheme 1.23

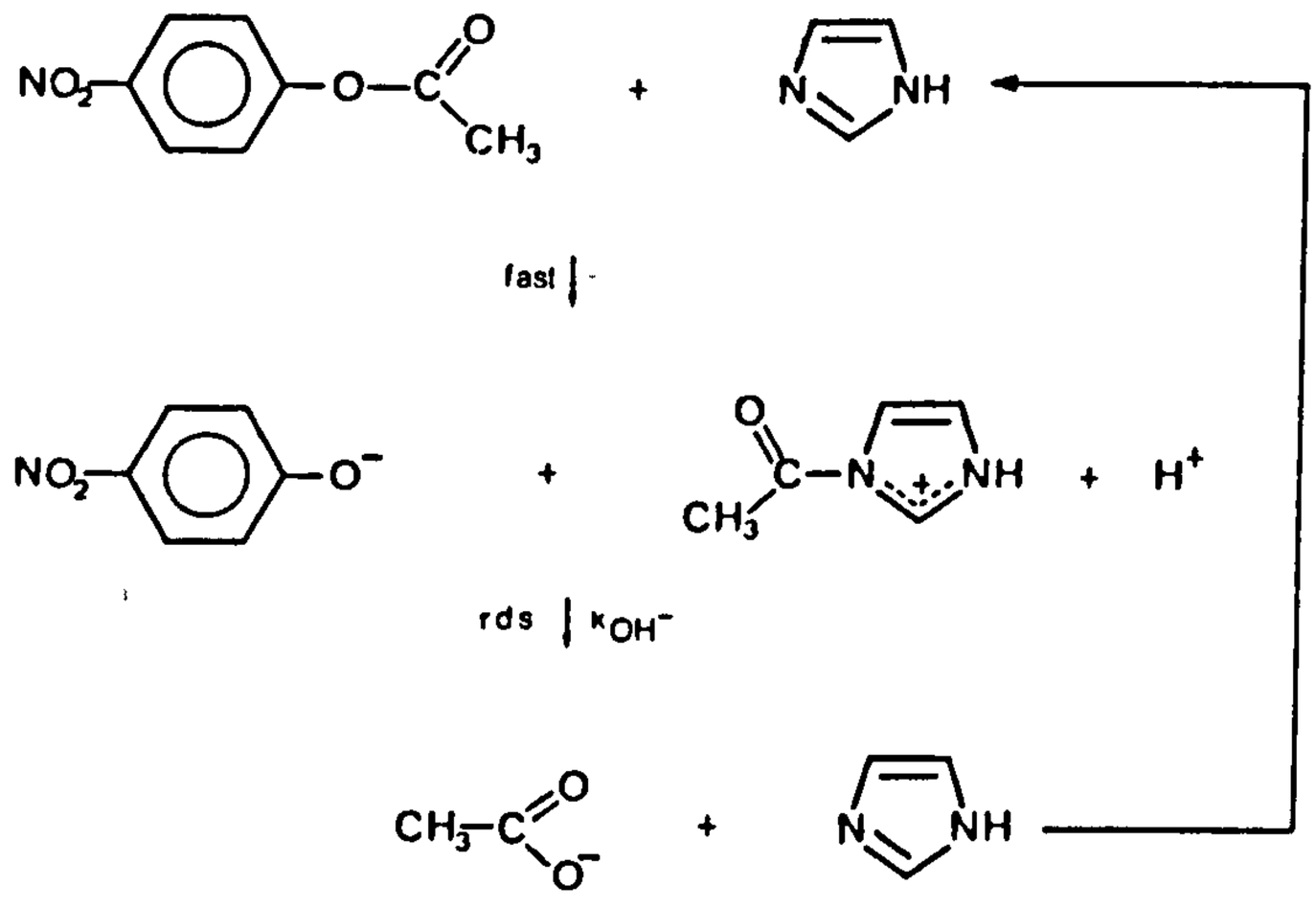

The acetylimidazolium ion intermediate which is formed is hydrolysed ca. 10^5 times faster than PNPA (k_{OH^-} values of $1.17 \times 10^6 M^{-1}s^{-1}$ and $9.5 M^{-1}s^{-1}$, respectively). When present, other nucleophiles, such as amines and thiols, will also react with the Acetylimidazolium intermediate, giving an accelerated rate of reaction for these acyl transfer reactions. Jencks[8] has defined three essential requirements for effective nucleophilic catalysis:

(1) The catalysts must have a higher nucleophilic reactivity than the final acyl group acceptor.

(2) The intermediate which is formed by reaction of the substrate with the catalyst must be more reactive than the substrate.

(3) The intermediate must be thermodynamically less stable than the product, so that it does not accumulate instead of the final product.

It has been demonstrated[54] that the reaction of tertiary amines, such as substituted quinuclidines, with substituted diphenylcarbonates, proceed via a nucleophilic catalysis mechanism. Tertiary amines can, of course, catalyse a reaction by either a nucleophilic (Scheme 1.24) or a general base catalysis mechanism (Scheme 1.25).

Scheme 1.24

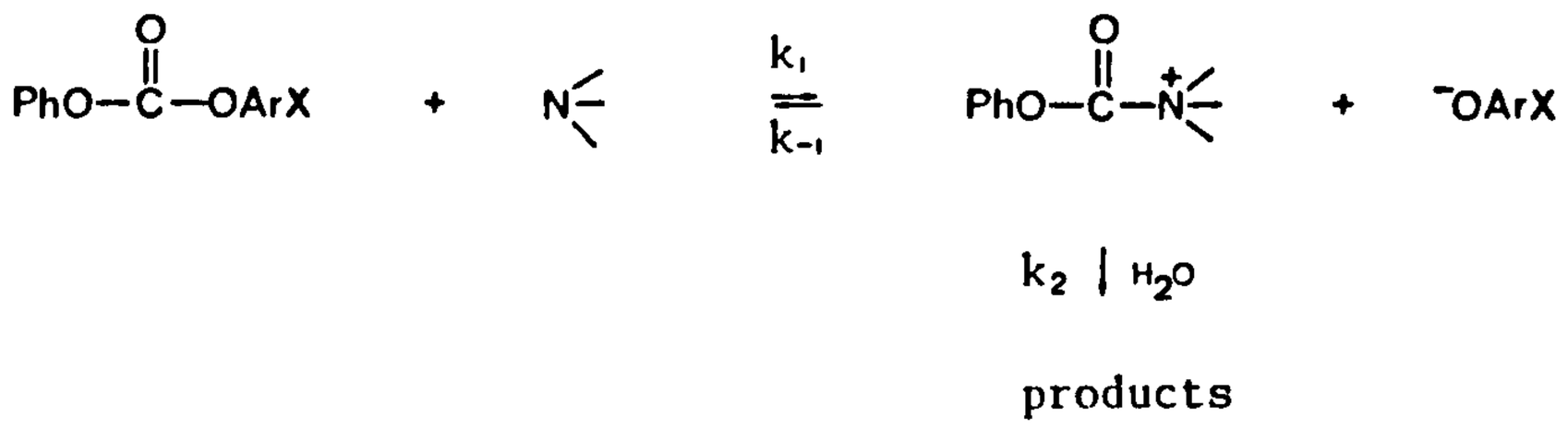

Scheme 1.25

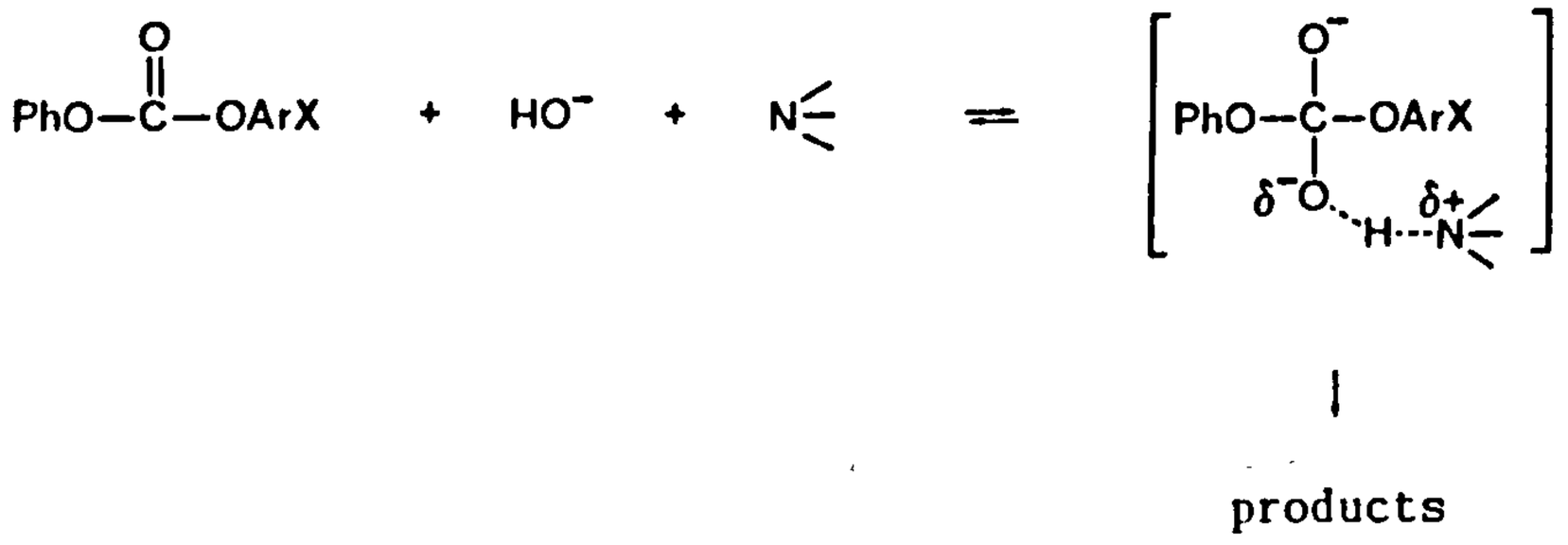

In this case, the demonstration of significant inhibition of the catalysis reaction by added $^{-}$OArX is evidence that the reaction proceeds via the nucleophilic catalysis mechanism. Low concentrations of added $^{-}$OArX should not have any effect on the rate of general base catalysed hydrolysis.

Acetate has also been shown to act as a nucleophilic catalyst of the hydrolysis of several aryl acetates[88], and the methanolysis of PNPA.[89] Gold et al.[88] have demonstrated that for substituted phenylacetates

with good leaving functions (pKa < 8.0), a significant proportion of the acetate catalysed hydrolysis reactions (70% to 80%) proceeds via nucleophilic catalysis (Scheme 1.26), with the remainder being general base catalysis.

Scheme 1.26

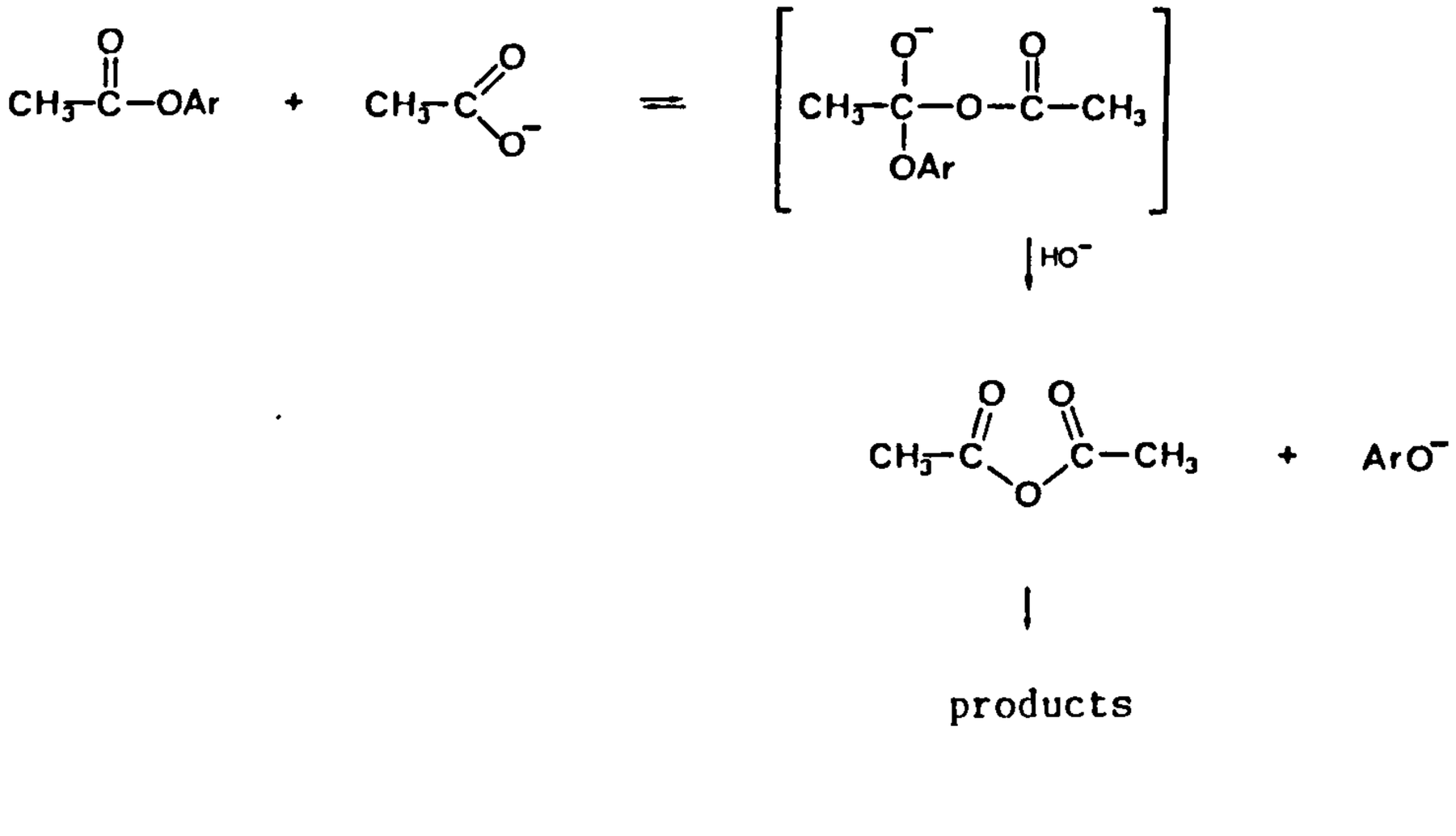

Nucleophilic catalysis by acetate converts the substrate into the more reactive substance, acetic anhydride, which is then rapidly hydrolysed to regenerate the catalyst. Gold et al.[88] measured the nucleophilic catalysis, by trapping the acetic anhydride intermediate with aniline or m-toluidine. For substituted phenylacetates with leaving group pKa's > 8.0, the acetate catalysed reaction was found to proceed almost exclusively via general base catalysis. This is also true of the acetate catalysed hydrolysis N-acetylbenzotriazole[90] (leaving group pKa of 8.32). However, Showen and Behn[89] have shown, using tritium labeled acetate ions, that the methanolysis of PNPA (in absolute methanol) proceeds exclusively by the nucleophilic catalysis mechanism.

1.7 Intramolecular Interactions

Whilst the rate enhancing effects of intramolecular reactions and intramolecular catalysis, compared to the corresponding intermolecular interactions, are well established[8]; there have been, very recently, a number of papers[44,91,92,93,94] published on this subject. The interest in intramolecular interactions arises because of their relevance to the processes which occur within the active sites of enzymes.

1.7.1 Intramolecular Acyl Transfer Reactions

The presence, on one molecule, of neighbouring groups which are capable of acting as nucleophile and substrate, greatly enhances their reaction compared to the case where the nucleophilic and substrate groups are on separate molecules. The rate enhancement is due, in part, to the close proximity of the neighbouring groups, resulting in an increase in 'effective concentration' of reactants.[8] This cannot account for all the rate increase, however, since a comparison of rate constants for the inter- and intramolecular aminolysis and phenylacetate[8], for example, implies an effective concentration in the case of the intermolecular reaction of 1250 M; this is obviously unobtainable. The rapid rate of the intramolecular reaction, in this case, was ascribed to the difference in entropies and activation of the two reactions. Nevertheless, intramolecular reactions are still often quoted in terms of 'effective concentrations'.

A recent example of a study of intramolecular acyl transfer reactions has been provided by Briffett and Hibbert, in 1989[94], for the hydroxide ion-promoted reaction between ester and amide groups in 1-Acyloxy-8-acylaminonapthalene-3-6-disulphonates (Scheme 1.27).

Scheme 1.27

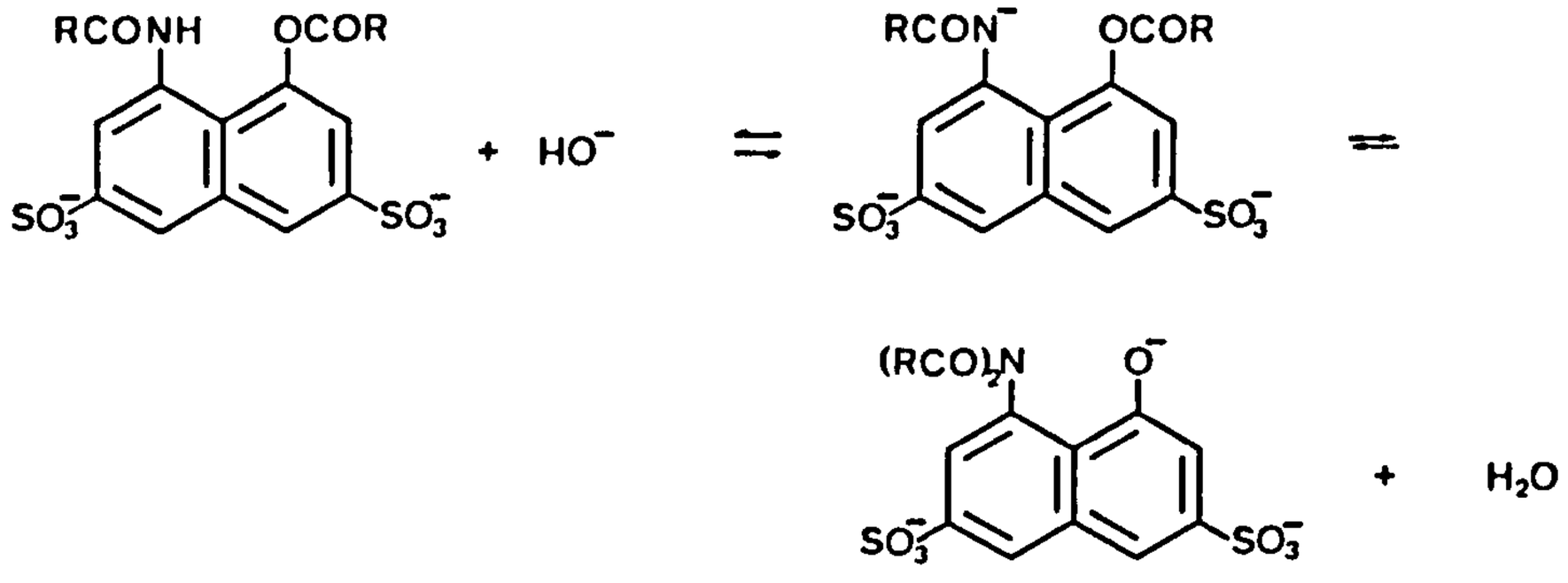

It is proposed that the hydroxide ion acts to ionise the amide by proton abstraction in a rapid pre-equilibrium step. In a comparison with data for related intermolecular reactions an effective molarity for the intramolecular acyl transfer of ~ 10^5 M is obtained.

1.7.2 Intramolecular General Acid-base Catalysis

The other main form of intramolecular interaction is that of catalysis. Some molecules which undergo a reaction with an external nucleophilic species at the carbonyl carbon may also contain a group which is capable of acting as an intramolecular general acid, general base or nucleophilic catalyst. Such intramolecular catalysis can produce large rate enhancements. Intramolecular general base catalysis of the hydrolysis of salicylate esters[44], for example, has been shown to produce a rate enhancement of ~ 10^6. Evidence[44] has also been obtained for the intramolecular general base catalysis of the aminolysis of ionised phenyl salicylates (PS) (Scheme 1.28a). It is suggested that general base catalysis is effected via a mechanism involving proton abstraction from the attacking primary or secondary amine by the anionic oxygen. The absence of enhanced nucleophilicity of tertiary amines towards PS, whilst primary and secondary amines demonstrated enhanced reactivity, indicates that the theoretically possible intramolecular or general acid catalysis mechanism (Scheme 1.28b) is not observed in this case.

Scheme 1.28

(a)

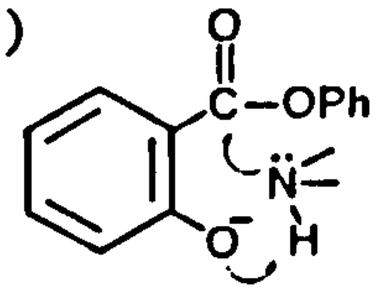

(b)

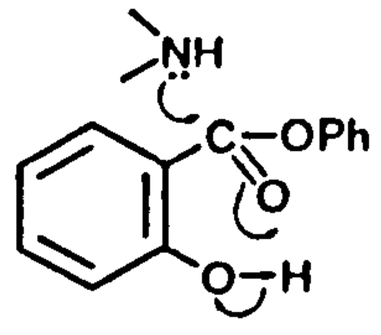

1.7.3 Intramolecular Nucleophilic Catalysis

An example of intramolecular nucleophilic catalysis is demonstrated by the carboxy-group in the hydrolysis of substituted maleamic acids.[95] The proposed mechanism for the reaction, which is also subject to external general acid catalysis (protonation of the leaving amine), is shown in Scheme 1.29. Catalysis is effected by one of the carboxy-group oxygens reacting with the carbonyl carbon to form a more reactive cyclic anhydride structure in a manner analagous to the external nucleophilic catalysis mechanism already discussed for the acetate anion (Section 1.6.3). After departure of the amine leaving group the cyclic anhydride structure undergoes hydrolysis by H_3O^+, regenerating the carboxy group.

Scheme 1.29

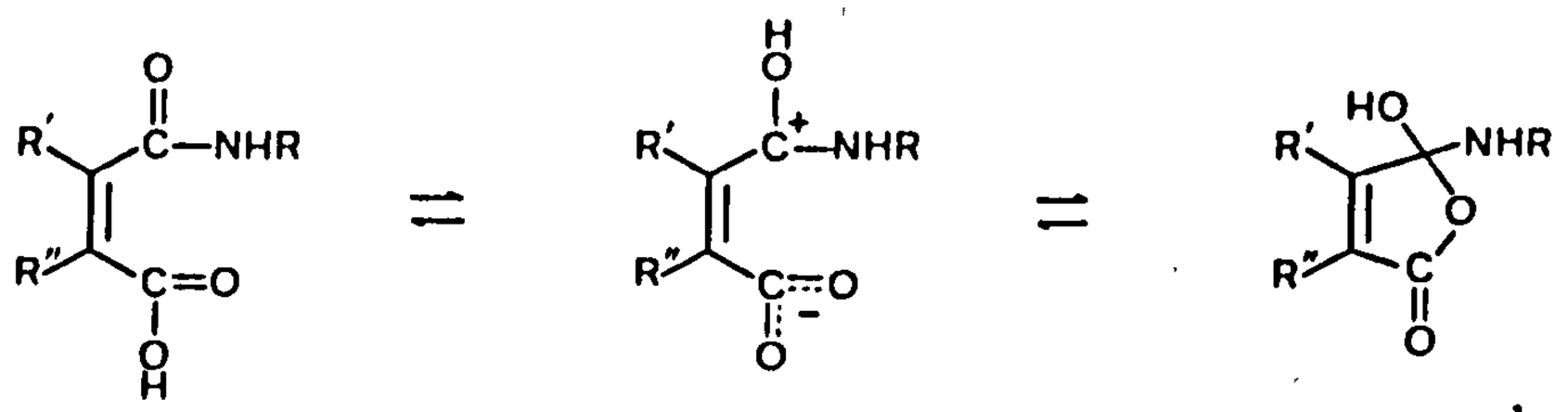

For N N-dimethylmaleamic acid, intramolecular catalysis by the carboxy group produces a rate enhancement of 44 compared to the hydrolysis of the corresponding secondary amide.[95]

1.8 Summary

A wide range of acyl transfer reactions of esters and amides has been reviewed and the major factors affecting them have been considered. A summary of these factors is given below.

1. The main structural features which affect the reactivity of amides and esters towards nucleophiles appear to be resonance stabilisation with the carbonyl function and polar substituents in the acyl position altering the electrophilicity of the carbonyl carbon; the nature of the leaving group; the presence of substituents such as branched aliphatic groups which cause steric hindrance of the reaction at the carbonyl carbon; ring structures which enforce a more energetic ground state configuration compared to the preferred orientation in open chain structures. Resonance stabilisation is particularly important in ami-

des since the lone pair electrons of the amide nitrogen are delocalised into the carbonyl function, this generally results in lower reactivities for amides with nucleophiles compared to the corresponding esters.

2. For the actual reaction mechanism of nucleophiles with amides and esters, there exist three possible extremes of bond formation and bond fission at the carbonyl carbon: reactions may proceed via the formation of a stable tetrahedral intermediate in which the nucleophile adds to the carbonyl carbon before the leaving group is expelled; alternatively, an acylium ion intermediate may be formed where the leaving group is expelled before the nucleophile adds to the carbonyl carbon; the third possibility is a concerted mechanism where bond formation between nucleophile and carbonyl carbon occurs simultaneously with bond fission between the leaving group and the carbonyl carbon. There is literature evidence for all three possibilities, although that for the existence of stable tetrahedral intermediates and acylium ion intermediates is most conclusive. Stable tetrahedral intermediate mechanisms are likely for the reactions of thiols with phenylesters. Acylium ion mechanisms are likely to apply to acyl groups which possess good leaving functions (pKa's below 2). Reactions where evidence that concerted mechanism exists are those for phenolate anions with phenylesters, and amines with amides, that is, those cases where the nucleophile and leaving group are structurally similar.

3. The main factors which have been shown to affect nucleophilicity of a nucleophile (as measured by log k_2) are basicity, solvation, polarisability, and the α effect. Polarisability and the α effect are important in determining the relative reactivities of different series of structurally similar nucleophiles (e.g. thiols, phenoxides, alkoxides, amines, and peroxides) towards a particular amide or ester, whilst within the group of structurally similar nucleophiles basicity is the

most important factor. Effects due to solvation such as desolvation requirements of a nucleophile in the transition state appear to be important for the most basic oxygen nucleophiles. In addition, recent evidence has suggested that the α effect is, perhaps, a manifestation of solvation requirements of so-called α nucleophiles.

4. The three main types of catalysis of acyl transfer reactions considered important in this review were specific and general acid-base catalysis, and nucleophilic catalysis. For general acid-base catalysis the three determinant factors of whether catalysis will be observed are: the position on the reaction coordinate of the kinetically significant transition state (catalysis will not be observed if a proton transfer occurs after the kinetically significant transfer state); the large changes in pKa which occur upon the bonding of heavy atoms; the lifetime of the tetrahedral intermediate. The lifetime of the intermediate is important since this determines whether 'trapping' of the tetrahedral intermediate with respect to the back-reaction to reactants occurs by interaction with the solvent alone (no catalysis), by interaction with a general acid or general base catalyst (enforced catalysis); or by interaction with a general catalyst in which the catalyst substrate and nucleophile form a termolecular preassociation complex prior to the reaction (enforced preassociation mechanism).

5. Where reactions are susceptible to both general acid and general base catalysis, it has been demonstrated that for some catalysts such as phosphate, which possesses both acidic and basic groups, two rapid, simultaneous (concerted) proton transfers can occur, leading to enhanced catalytic activity of these bifunctional catalysts over the monofunctional catalysts of comparable pKa.

6. The presence on one molecule of neighbouring groups which are capable of acting as nucleophile and substrate greatly enhances their reactivity compared to the case where nucleophile and carbonyl carbon are on separate molecules. In addition, some molecules which undergo reactions with external nucleophilic species at the carbonyl carbon may also contain a group which is capable of acting as an intramolecular general acid, general base or nucleophilic catalyst. Intramolecular catalysis can result in large rate enhancements.

CHAPTER 2 PEROXIDE MEASUREMENT TECHNIQUES

This chapter describes the method of peroxide measurement employed throughout the course of this research into bleach activation. Most important to the study has been the development of a rapid and convenient spectrophotometric method for the determination of peroxyacids (peracids) in the presence of a large excess of hydrogen peroxide. This method is described in Section 2.2.

The relevant literature concerning peroxide measurement techniques, and in particular those techniques which enable quantitative determination of peroxides in the presence of other peroxides, is surveyed in Section 2.1.

2.1 Selective Peroxide Determination Techniques

We were particularly interested in determining peracid concentrations in the presence of excess hydrogen peroxide in order to follow peracid release during the bleach activation reaction. Hydrogen peroxide and peracid are both highly reactive oxidising agents and tend to have similar reactivities with many reagents used in peroxide determination, making resolution of a mixture of these peroxides difficult. For example, Frew et al. in 1983[96], have studied spectrophotometric methods for hydrogen peroxide determination based on phenolphthalein oxidation, iodide oxidation (with added molybdate catalyst) catalytic dye bleaching, coupled oxidation of NADPH, and horseradish peroxidase-coupled oxidation. Of the four assays in which the reactions with hydrogen peroxide and peracids were compared (not catalytic dye bleaching), three showed no selectivity for hydrogen peroxide at all, whilst for the coupled oxidation of NADPH assay significant colour development was found when using metachloroperbenzoic acid (MCPBA).

Nevertheless, there are a number of assay reagents which are selective for hydrogen peroxide and will not react with peroxyacids (although it is more difficult to find assay reagents with the converse properties). Eisenberg, in 1943[97], described a colourimetric method specific for hydrogen peroxide determination, which utilizes the yellow coloured complex formed between the titanium (IV) ion and hydrogen peroxide according to Scheme 2.1.[97]

Scheme 2.1

$$Ti^{4+} + H_2O_2 + 2H_2O \longrightarrow H_2TiO_4 + 4H^+$$

The complex is often written as TiO_2^{2+}.[98] Titanium (IV) sulphate is mixed with the peroxide in acidic conditions and the (instantly developed) colour measured at 410 nm with a molar absorptivity, ε = 720 l mol^{-1} cm^{-1} [96]. Eisenberg[97] determined hydrogen peroxide concentrations as low as 5.29 x 10^{-5} M using this method (4 cm path length). Sellers , in 1980[98], refined this method by using titanium (IV) oxalate, which gave an improved molar absorptivity of ε = 935 l mol^{-1} cm^{-1}. Although this titanium (IV) complex method is selective for hydrogen peroxide at room temperature, at high temperatures the colour development is proportional to the total peroxide concentration in a solution.[99] Ogleby and Williams[99] utilized this property to measure both peracetic acid and hydrogen peroxide concentrations in a mixed solution (approximately 15% peracetic acid, 14% hydrogen peroxide). A sample is divided into two aliquots, one of which is heated at 90-95°C, whilst the other remains at room temperature. The titanium (IV) oxide assay reagent is added simultaneously and the colour development in the two aliquots compared, allowing the calculation of the respective percentages of the two peroxides. In practice, in a fully automated system, sodium molybdate, which reacts with peroxides in a similar way, replaced the titanium (IV) oxalate which is unstable, especially at high temperatures.

The titrimetric ceric sulphate assay is also specific for hydrogen peroxide. Ceric sulphate has been found to satisfy the requirements of a stoichiometrical reaction with hydrogen peroxide in the presence of peracid, and non-reactivity with the peracid.[100] This reaction, which is conducted under acidic conditions, is the standard method for hydrogen peroxide determination.[101] Greenspan and Mackellar[100] have utilized this method to determine peracetic acid in the presence of hydrogen peroxide by first titrating the hydrogen peroxide with cerium (IV) sulphate and then determining the residual peracetic acid iodimetrically. The titrations must be carried out rapidly and at a fairly low temperature (below 10°C) in order to avoid significant equilibration of the peroxides in the acidic conditions.[102] This method is widely used to resolve solutions containing hydrogen peroxide and paracetic acid.

An alternative to this method is the iodimetric assay developed by Sully and Williams in 1962.[102] This assay does not employ a totally selective reagent as in the previous methods, rather, it utilizes the much greater reactivity of iodide (no molybdate catalyst added) with peracid than with hydrogen peroxide. The liberated iodine is titrated with thiosulphate over a period of several minutes and a linear graph of titre versus time is extrapolated back to zero time to give a value, corrected for the slow reaction of hydrogen peroxide, which corresponds to the peracid. The hydrogen peroxide concentration is calculated from the total titre. A comparison of the method with the ceric sulphate method of Greenspan and Mackellar[100] yielded roughly similar results. The reliability of the assays is very good when the two peroxide species are present in comparable amounts. However, they will be subject to inaccuracies when one of the species is present in a large excess over the other; Di Furia et al.[103] found that the ceric sulphate method

fails to give accurate results when small amounts of peracetic acid are determined in a large excess of hydrogen peroxide.

Di Furia et al.[103] have described a gas-liquid chromatographic assay which has been used determine accurately $2x10^{-2}$ M peracid concentrations (MCPBA) in the presence of up to one hundred-fold excess of hydrogen peroxide. The procedure is based on the fact that under the appropriate experimental conditions, the oxidation of organic sulphides to the corresponding sulphoxide is rapid with peracids and very slow with hydrogen peroxide. Upon addition of a known excess of methyl-p-tolylsulphide to the peroxide mixture the peracid reacts within seconds whereas the hydrogen peroxide is not consumed. After 5-10 minutes the reaction is quenched and the concentrations of remaining sulphide and the formed sulphoxide are measured simultaneously by G.L.C. from which the peracid concentration can be calculated.

The spectrophotometric determination of I_3^- at 352 nm greatly enhances the sensitivity of iodide-reduction methods used for peroxide determination[96,104,105,106] because of the high molar absorptivity, $\varepsilon \sim 25000$ mol^{-1} cm^{-1} [104]. Frew et al.[96] have determined μM concentrations of peroxides using the spectrophotometric assay of Allen et al.[104]

By following I_3^- formation, a technique known as kinetic spectrophotometry has been used to resolve mixtures of peroxides obtained from atmospheric samples.[105,106,107] The method is standardised by calculating the rate constants for formation of the triiodide complex in a single component peroxide system. Binary and ternary mixtures of peroxides can then be resolved by following I_3^- release until completion and then employing a graphical analysis method to identify, and estimate, the concentrations of the peroxide compounds, making use of their rate constants for I_3^- formation. Peracetic acid and hydrogen peroxide con-

centrations can be easily resolved using this method since their respective half-lives (under the conditions used) are 0 and 14 minutes.[107]

None of the methods above reviewed was found to be applicable to this study of bleach activation for various reasons. In particular, we wish to measure very low concentrations of peracetic acid, yet the method which does give acceptable sensitivity, kinetic spectrophotometry, is too time consuming and would allow very few measurements to be made during the course of a reaction. A suitable spectrophotometric method was, therefore, developed and is described in Section 2.2.3.

2.2 Determination of Peracids in the Presence of Excess Hydrogen Peroxide

This section describes an assay for peracid determination in the presence of excess hydrogen peroxide; preliminary work on molar absorptivities (2.3.1.) and UV interference is also reported. A Hewlett Packard HP 8451 diode array spectrophotometer, fitted with thermostatted cell holder was used for all spectrophotometric determinations.

2.2.1 Apparent Molar Absorptivities (ε) for Iodimetric Spectrophotometric Methods of Peroxide Determination

The main method of peroxide measurement employed throughout the course of this research has been based on the spectrophotometric determination of iodine, in the form of I_3^-, liberated from the oxidation of iodide by the peroxide under acidic condition. This reaction is rapid for peracids and also for hydrogen peroxide when the ammonium heptamolybdate catalyst is present.[107]

Literature values for $\varepsilon_{I}{}^{3-}$ at λmax (usually reported as 352 nm), determined under various conditions show poor agreement[96,104,105], possibly due to interference by iodine reducing substances in assay solutions. Consequently, the value of the apparent $\varepsilon_{I}{}^{3-}$ was determined for both hydrogen peroxide and peracids under the assay condition used

in this research. This was done by measuring I_3^- liberation spectrophotometrically[96,104] (at 352 nm), using the potassium iodide/potassium hydrogen phthalate reagent of Allen et al.[104], for solutions of hydrogen peroxide and metachloroperbenzoic acid (MCPBA) standardised by the standard cerimetric[101] and iodimetric titrations[108], respectively.

Table 2.1 shows a comparison of literature values of apparent ε_{I3^-} with those that we have determined. In addition, Figure 2.1 shows a plot of MCPBA concentration (in the cuvette) against A_{352}; Clearly for I_3^- the Beer-Lambert law is obeyed for absorbances up to at least 1.65. The slope of this plot gave an apparent ε_{352} for I_3^- of 26097 $\pm$ 254* $M^{-1}cm^{-1}$ and the error of the intercept (4.648 $\pm$ 94.72)*x10^{-4}, included the origin.

In agreement with literature work[106], we have found from this study that the value of ε_{I3^-} for the liberated iodine shows a dependence on the concentration of iodide in the assay solution; the results are consistent with the reported[109] equilibrium constant for the formation of I_3^- from I_2 and I^-. We also found that slightly higher values of ε_{I3^-} were obtained when the potassium iodide reagents contained the heptamolybdate catalyst; similar effects have previously been observed.

2.2.2 Effect of UV Light on Triiodide Formation

The HP 8451 diode array spectrophotometer provides radiation throughout the range 190 to 820 nm; this was found to cause problems during iodimetric spectrophotometric determinations. Radiation in the UV region was found to interact with iodide, promoting triiodide formation, most probably via a photooxidation reaction, which is shown in Scheme 2.2.

Note * 90% Confidence Limits

Table 2.1 Apparent molar absorbtivities (ϵ).

	ϵ^{*}/l mol^{-1} cm^{-1}			
	MCPBA		H_2O_2	
KI**/gl^{-1}	Uncatalysed	Catalysed	Catalysed	Reference
3.1	24100	24400	23700	This work
10[c]	26200	28800	27000	Reference 105
13	-	-	25000	Reference 104
13	-	-	23000	Reference 96
31	26100	26500	25800	This work

* Determined in potassium hydrogen phthalate buffer unless otherwise stated.

** Concentrations are those in cuvette.

[c] Potassium dihydrogen phosphate - disodium hydrogen phosphate buffer.

Figure 2.1 Plot demonstrating the relationship between m-chloroperbenzoic acid (MCPBA) concentration and absorbance at 352nm due to the formation of triiodide in a potassium hydrogen phthalate buffer containing 31 gl^{-1} potassium iodide at 25°C. Concentrations refer to those in the cuvette

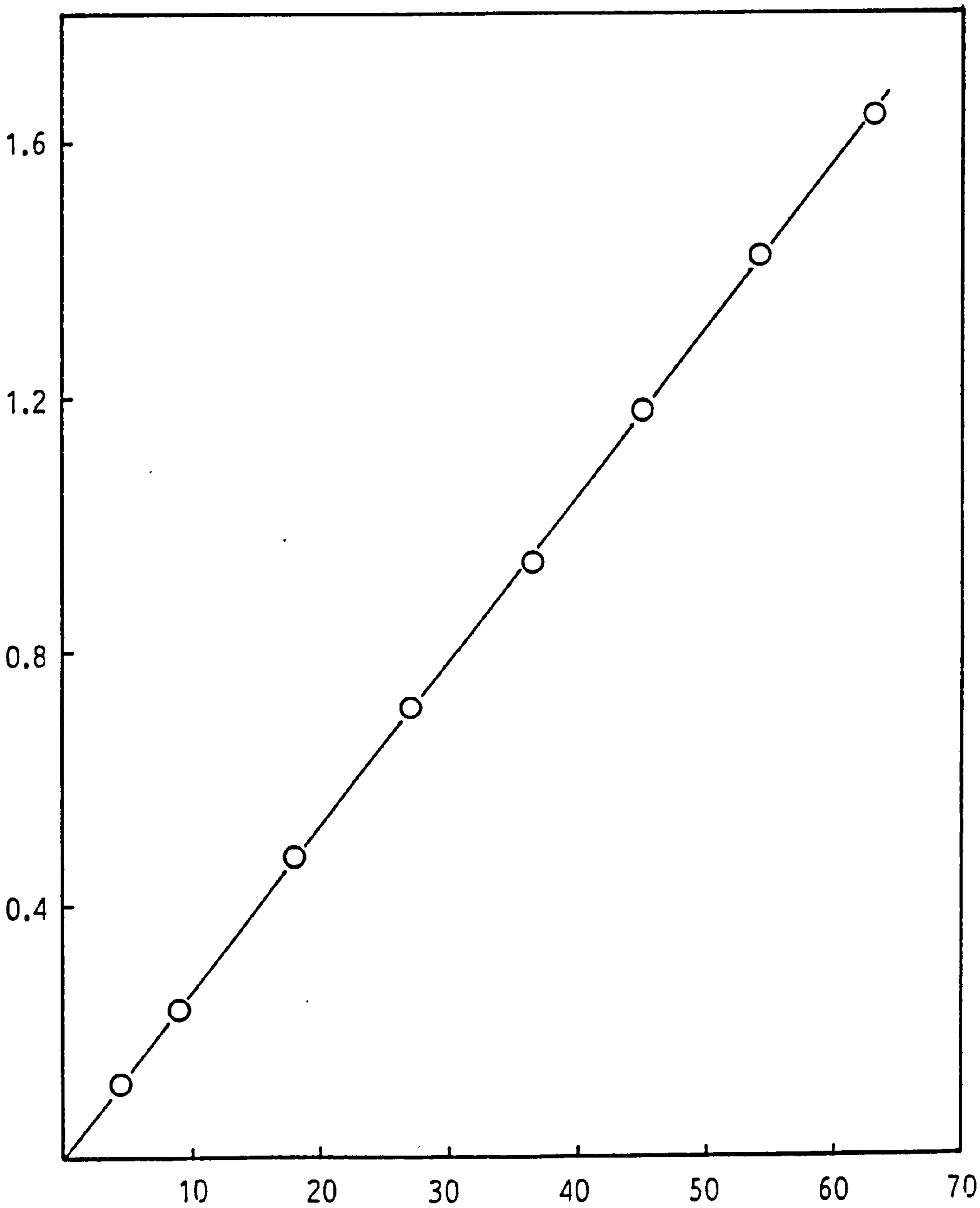

Scheme 2.2

$$\text{(i)}\quad I^- + I^- \xrightarrow{h\nu} I_2 + 2e^-$$

$$\text{(ii)}\quad 2e^- + \tfrac{1}{2}O_2 + 2H^+ \longrightarrow H_2O$$

$$\text{(iii)}\quad I_2 + I^- \rightleftharpoons I_3^-$$

The problem was alleviated by modification of the incident radiation on the sample cell, using a 295 nm UV cut-off filter (the filter has the characteristics shown in Figure 2.2). Figure 2.3 details the time-course of absorbance increase at 352 nm upon exposure of a potassium iodide/phthalate buffer solution to unmodified radiation, and also shows the fall in absorbance at 352 nm subsequent to the modification of the incident radiation using the 295 nm UV cut-off filter. Figure 2.4 shows absorbance spectra of the iodide phthalate buffer solution, both before (a) and after (b) exposure to unmodified radiation; the peak at 352 nm in (b) corresponds to I_3^-. The levelling off of the absorbance increase in Figure 2.3 is due to the fact that only part of the sample cell is irradiated by the spectrophotometer beam; the plateau region corresponds to the situation where diffusion of triiodide away from the irradiated region equals the rate of triiodide formation. The fall in absorbance after modification of the incident radiation is due to the process of diffusion alone.

2.2.3 Assay for the Determination of Peracids in the Presence of a Large Excess of Hydrogen Peroxide

In the study of bleach activation it is essential that we are able to measure the release of the peracetic acid. If we attempt to measure peracetic acid in the presence of excess hydrogen peroxide, using the uncatalysed KI/phthalate reagent of Allen et al.[104], then although the peracetic acid will react rapidly to form I_3^- (Scheme 2.3), there is

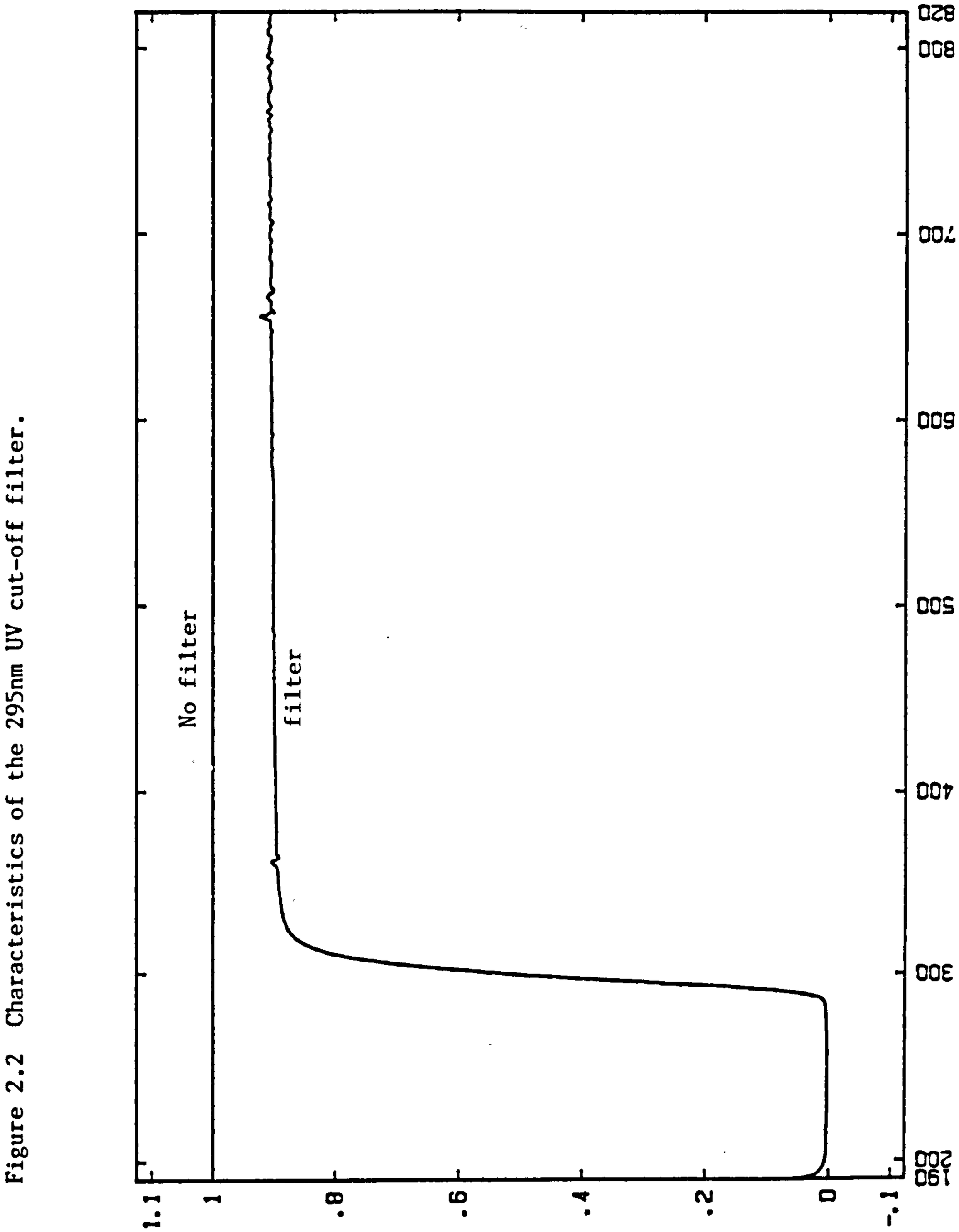

Figure 2.2 Characteristics of the 295nm UV cut-off filter.

Figure 2.3 Effect of irradiation on absorbance at 352nm due to triiodide formation in a sample containing potassium iodide reagent in a potassium hydrogen phthalate buffer at25°C.

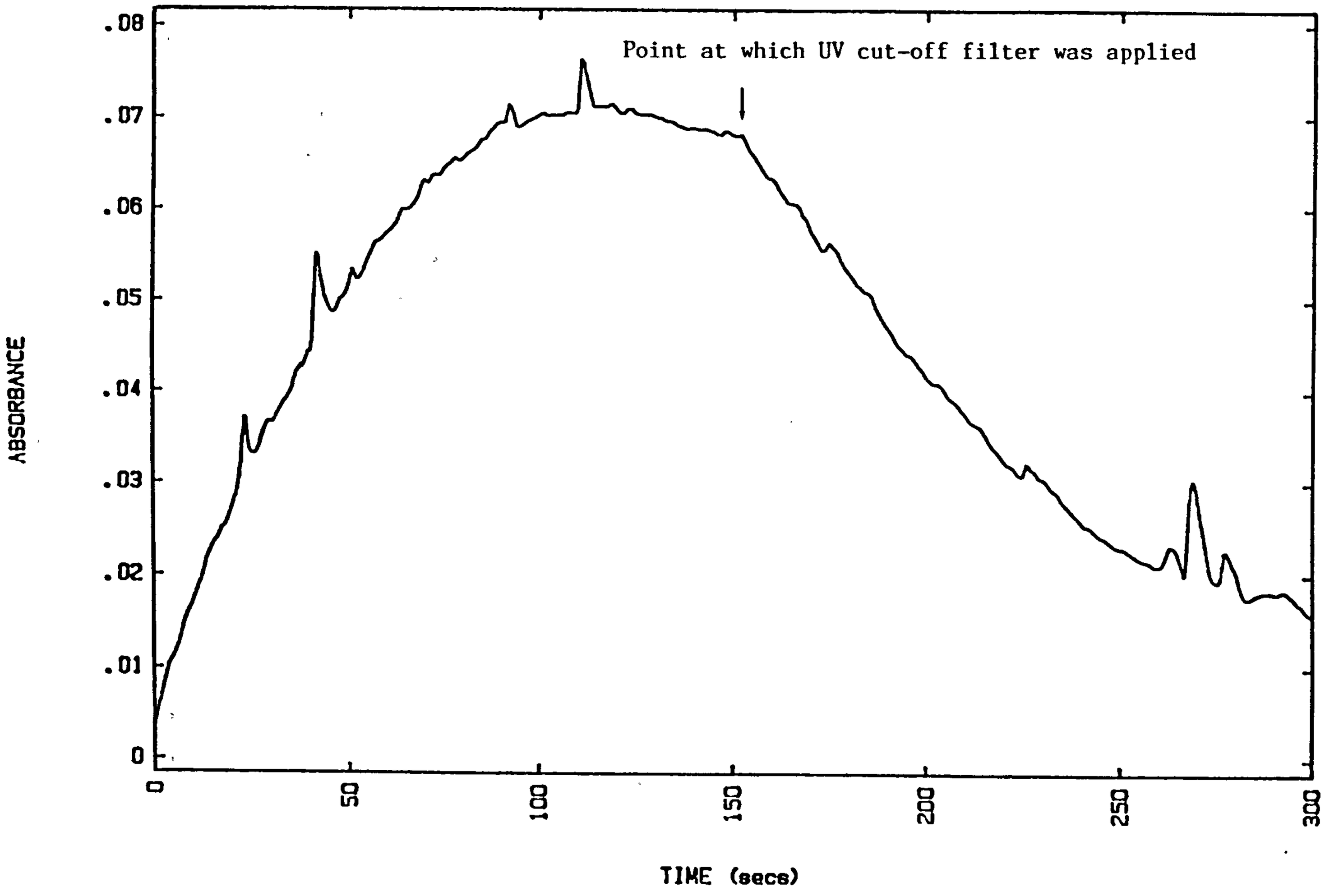

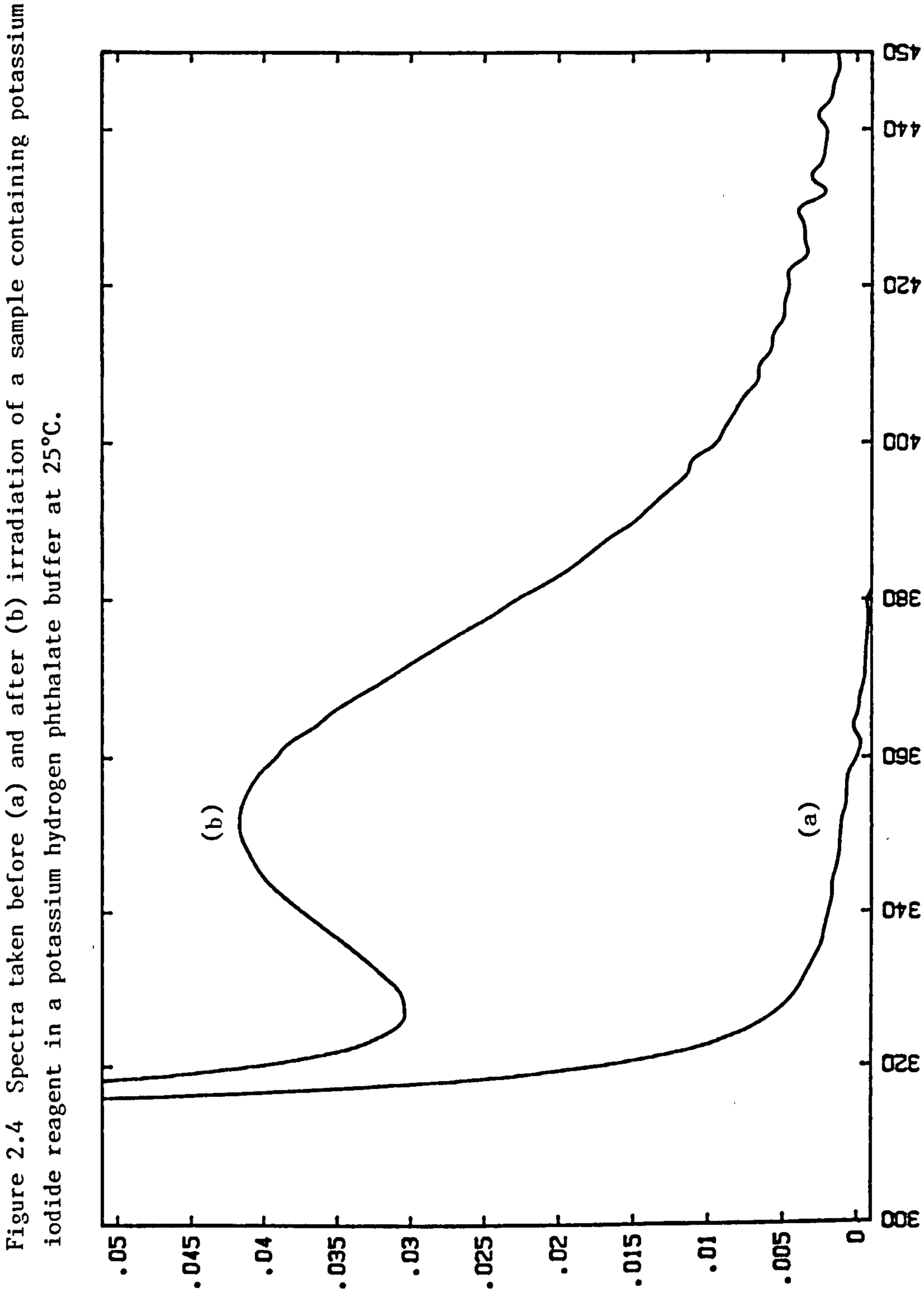

Figure 2.4 Spectra taken before (a) and after (b) irradiation of a sample containing potassium iodide reagent in a potassium hydrogen phthalate buffer at 25°C.

also the interfering slow reaction of hydrogen peroxide with iodide (Scheme 2.3).

Scheme 2.3

$$H_2O_2 + 2I^- \xrightarrow{\text{Slow}} I_2$$

$$CH_3C(O)OOH + 2I^- \xrightarrow{\text{Fast}} I_2$$

$$I_2 + I^- \rightleftharpoons I_3^-$$

A single spectrophotometric measurement would not, therefore, correspond to the peracetic acid concentration. It is, however, possible to make use of this interfering slow reaction of H_2O_2 with iodide since it was observed that the increase in absorbance at 352 nm is linear for up to 1 minute after adding a sample to the assay mix.

The assay theory is a simple one:

As shown diagrammatically in Figure 2.5, we inject a mixture of peracid in excess hydrogen peroxide into the iodide assay mix in a cuvette. There is an initial rapid increase in absorbance, due to oxidation of iodide by peracid, followed by a slow linear increase in absorbance due to the reaction H_2O_2 (the initial rate). At a known time after adding the sample to the assay mix, the absorbance increase is followed for a short period of time. Knowing the interval between addition of the sample (A) and taking the first absorbance measurement (B), then the linear increase in absorbance followed between times B and C can be extrapolated back to zero time, corresponding to the absorbance due to the rapid reaction of peracid alone with iodide to form I_3^-. The concentration of the peracid is then simply calculated from the absorbance using the appropriate apparent molar absorptivity, as detailed in Table 2.1.

Figure 2.5

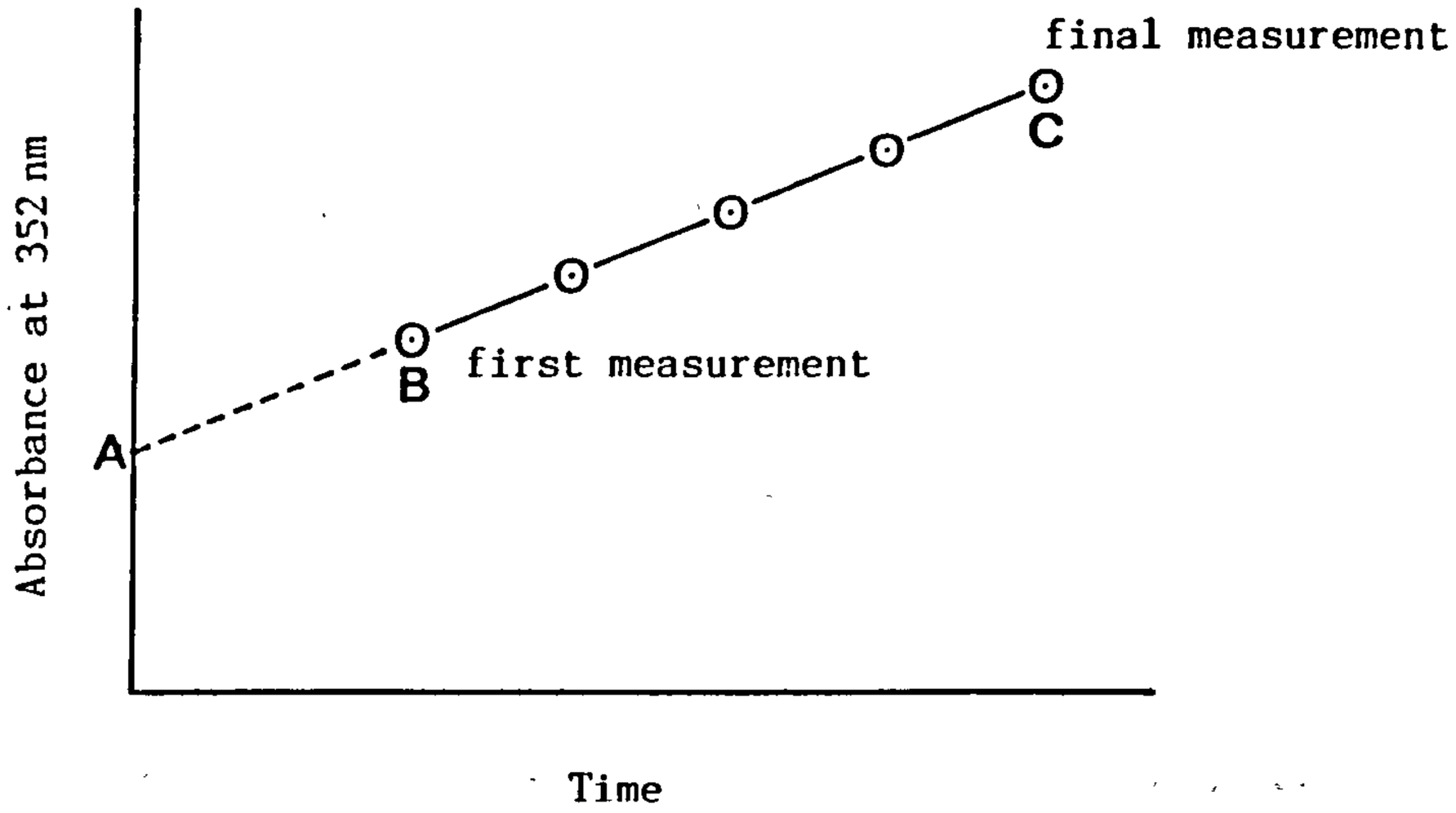

Throughout the course of this research there have been several improvements to the basic method regarding precision and the level of excess hydrogen peroxide in which it is possible to accurately determine the peracid. The final format of the assay is described below.

Experimental

Absorbance measurements were made at 25°C using a Hewlett Packard HP 8451A diode array spectrophotometer fitted with a 290 nm UV cut-off filter and thermostatted cell holder.

Reagents

Analytical grade reagents were used wherever possible. The assay solutions were as follows:

Solution A containing potassium iodide (Analar, BDH, recrystalised from distilled water), 6.6 gl^{-1}; sodium hydroxide, 2 gl^{-1}

Solution B containing potassium hydrogen phthalate, 20 gl^{-1}

Metachloroperbenzoic acid and hydrogen peroxide mixtures were prepared by diluting standardised stock solutions with distilled water contain-

ing $1x10^{-5}$ M ethylenediaminetetramethylenephosphonic acid (EDTMP).

Assay

A 0.1 ml aliquot of the sample solution is added to a 1 cm cuvette containing 1 ml of solution A and 1 ml of solution B and the timer on the spectrophotometer is started simultaneously. The cuvette is quickly stoppered and shaken and the liberated iodine is measured at λ_{max} = 352 nm for 0.1 s every 1.0 s for a total of 5 s. The absorbance at zero time is calculated by regression analysis, assuming a linear relationship between absorbance and time. The concentration of peracid is calculated from the absorbance at zero time using an apparent molar absorptivity of 24100 l mol^{-1} cm^{-1}.

Results and discussion

The interval between starting the timer and taking the first absorbance reading is about 12 seconds. Figure 2.6 shows a plot of absorbance versus time for a $1x10^{-5}$M solution of peracetic acid in the presence of a range of hydrogen peroxide concentrations. For peracid samples containing no hydrogen peroxide, the slope of the graph is zero. This shows that the reaction between peracid acid and iodide is complete before the first absorbance measurements is made.

Table 2.2 shows the linear response of the method. The presence of reducing impurities in the iodide, however, causes a fixed negative bias (results not shown). And it was, therefore, necessary to recrystalise the potassium iodide.

Table 2.3 shows that the assay is accurate within experimental error, for ratios of hydrogen peroxide to peracid of up to 1000. The precision of the method is less at the higher ratios of hydrogen peroxide to peracid. The random error involved in starting the timer causes an

Figure 2.6 Plot showing the effect of hydrogen peroxide concentration on the rate of absorbance increase at 352nm due to triiodide formation in an assay reagent containing potassium hydrogen phthalate buffer and 3.1 gl^{-1} KI.

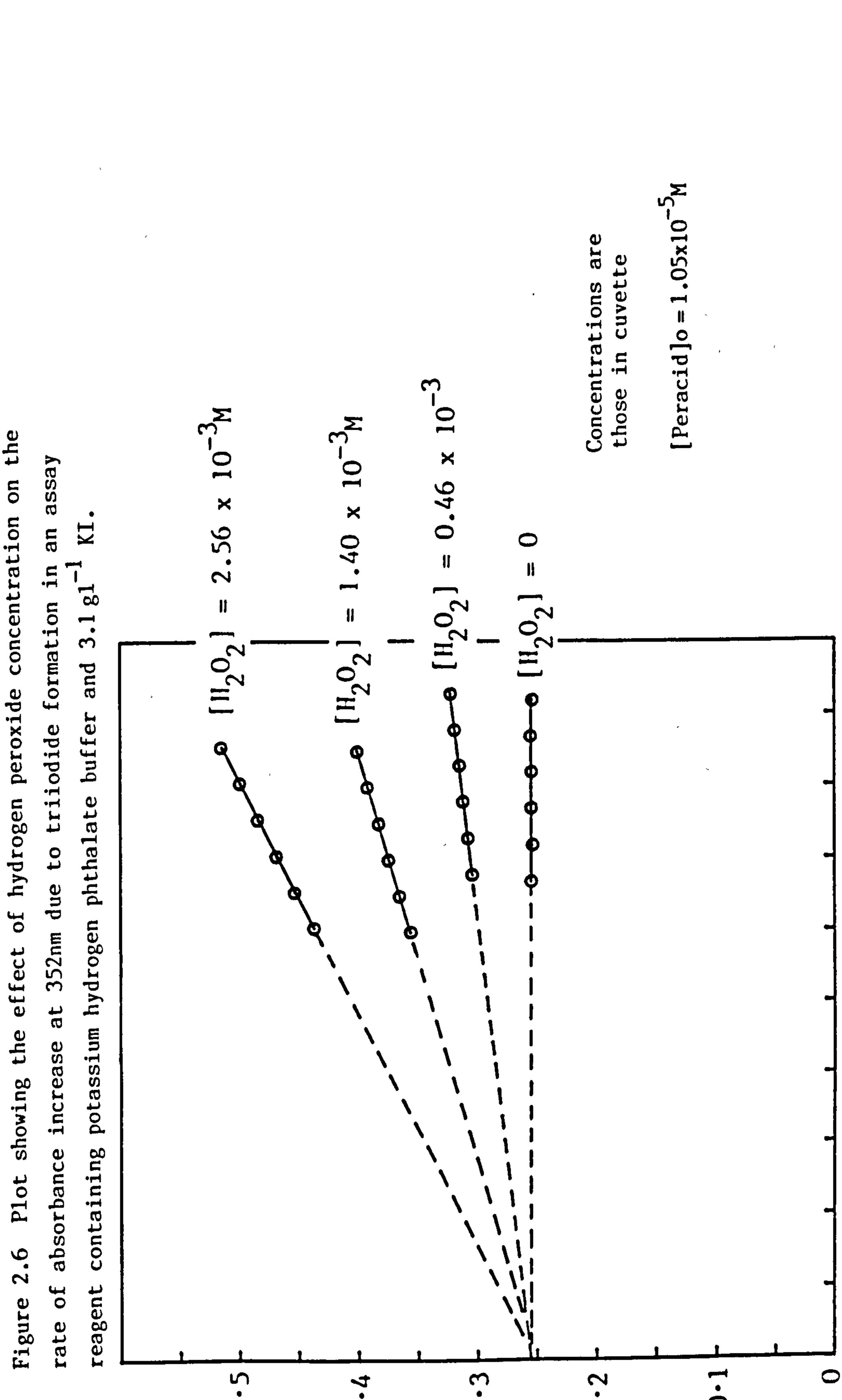

Table 2.2 Determination of m-chloroperbenzoic acid (MCPBA) in the presence of hydrogen peroxide; response of the assay. Concentrations in the cuvette: H_2O_2, 2.51 mM; KI, 3.1 gl^{-1}

10^5[MCPBA]*/M**	98% Confidence limits¢ of 10^5[MCPBA]/M
0.49	0.49 ± 0.01
0.98	0.97 ± 0.01
1.96	1.94 ± 0.01
2.83	2.96 ± 0.02
3.93	3.89 ± 0.04
4.92	4.89 ± 0.05
5.90	5.89 ± 0.07
6.88	6.83 ± 0.12

* Concentrations are those in the cuvette.

** Prepared by mixing known volumes of titrated solutions of MCPBA and H_2O_2.

¢ n = 5.

Table 2.3 Determination of MCPBA in the presence of hydrogen peroxide: effect of hydrogen peroxide concentration and amount of potassium iodide used.

Ratio of $[H_2O_2]$ to [MCPBA]	10^5[MCPBA]/M	98% Confidence limits of 10^5[MCPBA]/M	
		Assay 3.1 gl^{-1} of KI	Alternative 31 gl^{-1} of KI
0	1.05	1.05 ± 0.01	1.06 ± 0.01
4.0	1.05	1.06 ± 0.01	1.08 ± 0.01
10.5	1.05	1.06 ± 0.01	1.10 ± 0.02
21.4	1.05	1.07 ± 0.01	1.14 ± 0.02
54	1.05	1.06 ± 0.02	1.17 ± 0.06
99	1.04	1.04 ± 0.05	1.23 ± 0.06
217	1.03	1.07 ± 0.05	-
530	1.03	1.12 ± 0.03	-
1050	1.03	1.06 ± 0.05	-

error in the calculated absorbance at zero time; this error is larger at the higher hydrogen peroxide concentrations at which the change of absorbance with time is also larger.

If the time interval between starting the timer and taking the first absorbance reading is appreciably greater than about 12s or if absorbance readings are taken for much longer than 5 s, then at high ratios of hydrogen peroxide to peracid a positive systematic error in the measured peracid concentration occurs (data not shown). This is because the measured absorbance change no longer represents adequately the initial rate of the reaction of hydrogen peroxide with iodide. Ensuring that the concentration of iodide in the cuvette is always 3.1 gl^{-1} the method is easily modified to allow the use of larger samples of more dilute peracid solutions.

A set of results from an assay procedure in which solution A was replaced by an alternative solution containing ten times as much iodide is shown in Table 2.3. A positive systematic error occurs at the higher hydrogen peroxide to peracid ratios. This is because at the higher iodide concentration the time course of the reaction of hydrogen peroxide is faster and the initial rate phase of the reaction is complete before the first absorbance measurement has been made. During this research into bleach activation assay solutions containing both iodide concentrations have been used as reagents to determine peroxides. The higher KI concentration was used as a reagent for the bulk of the work described in Chapter 3; despite the systematic errors shown in Table 2.3, for the typical concentrations of hydrogen peroxide used, the assay was perfectly adequate. Also, in this earlier version of the assay, absorbance readings were taken for 10 seconds.

The improved method described above was used for the bulk of the work in Chapters 5 and 7.

CHAPTER 3 STUDIES ON A MODEL BLEACH ACTIVATOR: p-NITROPHENYL-ACETATE (PNPA)

The approach employed in this study of bleach activation has been initially to work on a bleach activator, PNPA, for which the activation reaction scheme was relatively easy to elucidate; the methods and approach used in the study of this 'model' bleach activator were then applied successfully to the study of the commercially-used bleach activators, tetraacetylethylenediamine (Chapters 4 to 7) and penta-o-acetylglucose (Chapter 8).

PNPA is a bleach activator in the sense that peracetic acid is liberated as one of the products of activation, however, it cannot be used commercially, for the good reason that the anionic form of the other product, paranitrophenol (PNP) is bright yellow in colour. Scheme 3 shows the perhydrolysis and hydrolysis reactions of PNPA; from the point of view of bleach activations the hydrolysis reaction is wasteful since peracetic acid is not produced.

Scheme 3.1

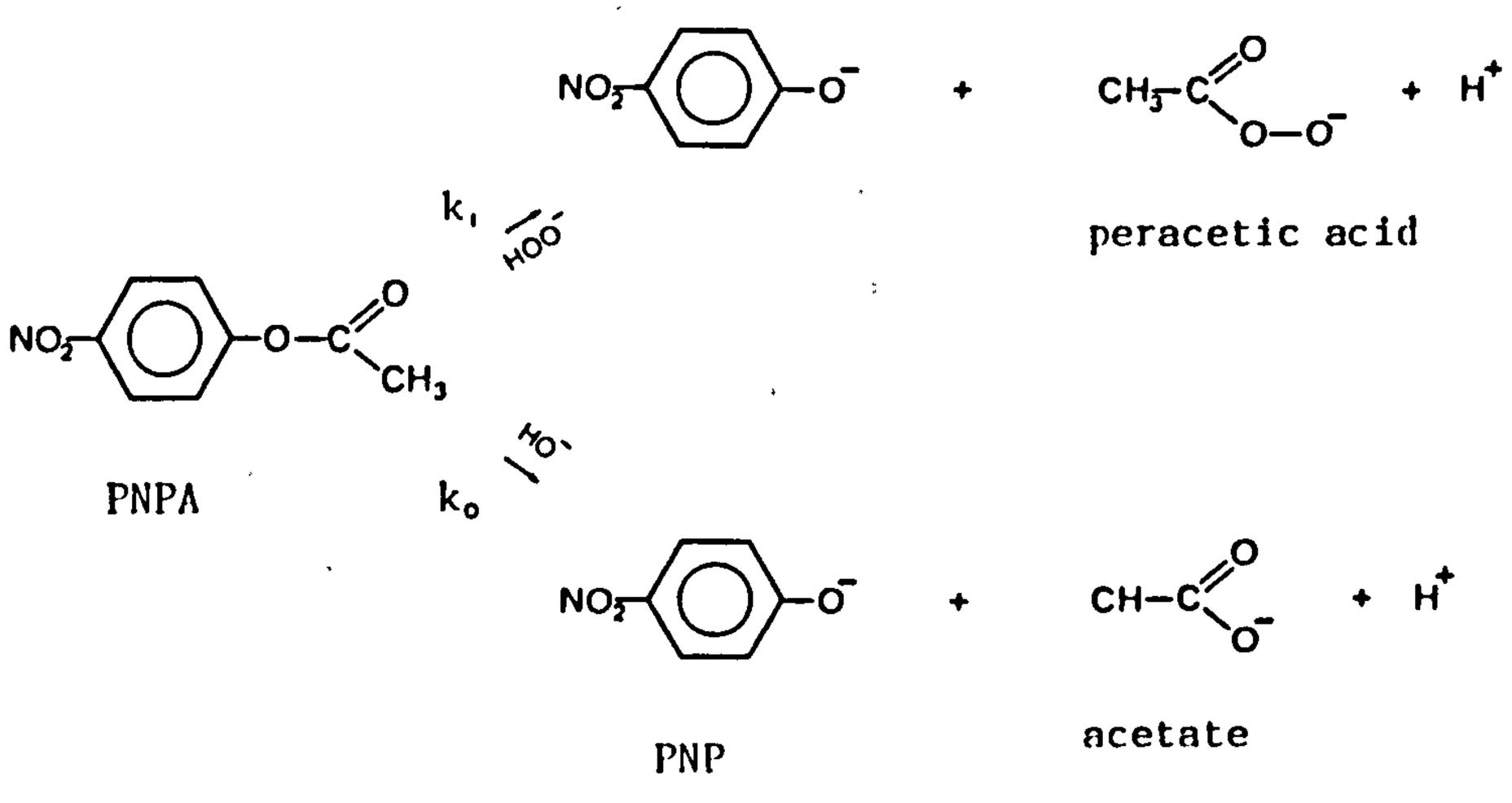

The formation of PNP can be followed easily spectrophotometrically since the anion has a maximum absorptivity at 400 nm, well away from the absorbances of other species involved in the reaction, such as peracetic acid, hydrogen peroxide and buffer components, which all absorb in the UV region of the spectrum. For this reason, and the fact that the strongly electron withdrawing nature of the nitro group makes oxidation of PNP unlikely, PNPA is the ideal bleach activator on which to begin studies. Additionally, there is a substantial body of literature on the reaction of PNPA with nucleophiles, as is evidenced by Figure 1.12 in Chapter 1.

All spectrophotometric measurements were conducted at 25.0 $\pm$ 0.1°C using a Hewlett Packard diode array spectrophotometer fitted with thermostatted cell holder.

3.1 Timecourse of Bleach Activation using PNPA as a Model Activator

During the course of the reaction of hydrogen peroxide with PNPA (k_1 in Scheme 3.1), the concentrations of the products, PNP and peracetic can both be followed; peracetic acid can be determined in the presence of hydrogen peroxide using the assay described in Section 2.2.3, and PNP can be determined spectrophotometrically by measuring the absorbance at 400 nm. In addition, the total iodide reactable peroxide concentration, that is, the sum of the hydrogen peroxide and peracetic acid, can also be followed using the catalysed potassium iodide assay mix (solution A in Section 2.2.3, containing 0.2 g $^{-1}$ ammonium heptamolybdate). This section describes the study of the timecourse of the reaction of PNPA with hydrogen peroxide.

Experimental

Materials

Analytical grade materials were used wherever possible. Hydrogen peroxide solutions were standardised cerimetrically.[101]

An approximately $2x10^{-3}$ M solution of PNPA was prepared by stirring 0.36 g PNPA in 1000 ml distilled water for about 4 hours. Undissolved PNPA was removed by filtering the solution through a No. 4 scinter under vacuum. The PNPA solution was standardised as follows: 0.05 ml PNPA solution was dispensed by micropipette into an optical cell containing 2 ml of an approximately 0.1 M hydrogen peroxide solution in pH 10.0 carbonate buffer. Under these conditions the PNPA rapidly hydrolyses and perhydrolyses, liberating PNP. The absorbance of 400 nm was followed until A_∞ was reached (almost instantaneous) and the concentration of PNP liberated was calculated using the molar absorptivity of 18300 M^{-1} cm^{-1} for the PNP anion. The concentration of PNP is related to the initial concentration of PNPA according to Equation 3.1

$$[PNP] = [PNPA]_o + [PNP]_o \qquad \text{Eqn 3.1}$$

Where $[PNP]_o$ is the initial concentration of PNP in the PNPA solution (due to the slow hydrolysis of PNPA during preparation of the solution and during storage). $[PNP]_o$ was determined by adding 0.1 ml PNPA solution to 2 ml of pH 6.8 phosphate buffer (I = 0.1) in an optical cell, and measuring the absorbance at 400 nm. The concentration was calculated using a molar absorptivity of 7344 M^{-1} cm^{-1} for the PNP anion at pH 6.8. $[PNPA]_o$ was then simply calculated from Equation 3.1. All solutions contained $1x10^{-5}$ M EDTA, which was added at least 2 hours before the comencement of the reaction.

Procedure

The reaction was started by mixing equal volumes of hydrogen peroxide/-phosphate buffer solution and PNPA solution. Initial conditions upon

mixing the solution were: $[H_2O_2]_o$, 2.018×10^{-3} M; $[PNPA]_o$, 9.103×10^{-4} M; $[PNP]_o$, 4.486×10^{-5} M; pH 6.8 phosphate buffer (I = 0.1); $[EDTA]_o = 1 \times 10^{-5}$ M.

The concentrations of PNP, peracetic acid and total iodide reactable peroxide were monitored during the course of the reaction (about 18000 seconds duration). PNP concentration was determined as follows: 0.1 ml reaction mix was added to 2 ml pH 6.8 phosphate buffer (I = 0.1 M) and a spectrum was taken over the range 200 to 500 nm. [PNP] was calculated using a molar absorptivity of 7344 M^{-1} cm^{-1} at 400 nm for PNP at pH 6.8. The peracetic acid and total iodide reactable peroxide concentrates were measured using the assays described in Chapter 2 (KI = 66 gl^{-1}). However, these assays rely upon measuring the absorbance of triiodide at 352 nm yet PNP also absorbs at this wavelength. This background absorbance is corrected for by measuring the absorbance due to PNP in the reaction mixture at 352 nm in a potassium hydrogen phthalate/sodium hydroxide buffer (i.e. the conditions used for the peroxide assays.)

A BASIC computer program was written for the HP 8451 to prompt each measurement, record the time, and store the absorbance values and spectra on disc.

Results and Discussion

Figure 3.1 shows plots for the concentrations of PNP, peracetic acid and total iodide reactable peroxide over the duration of the reaction; the concentration of hydrogen peroxide was simply calculated by subtracting the peracetic acid concentration from the total iodide reactable peroxide concentration. Figure 3.2 shows sequential spectra taken of the reaction mixture over a period of 2000 to 7000 seconds; the main

Figure 3.1 Change in the concentrations of: peracetic acid plus H_2O_2, ▽; peracetic acid, ○; H_2O_2 calculated from the previous concentrations, □; and p-nitrophenol, △. Conditions were: pH 6.8 phosphate buffer (I = 0.1 M); $[H_2O_2]_o = 2.02 \times 10^{-3}$ M; $[PNPA]_o = 9.10 \times 10^{-4}$ M; [EDTA] = 1×10^{-5} M; 25°C.

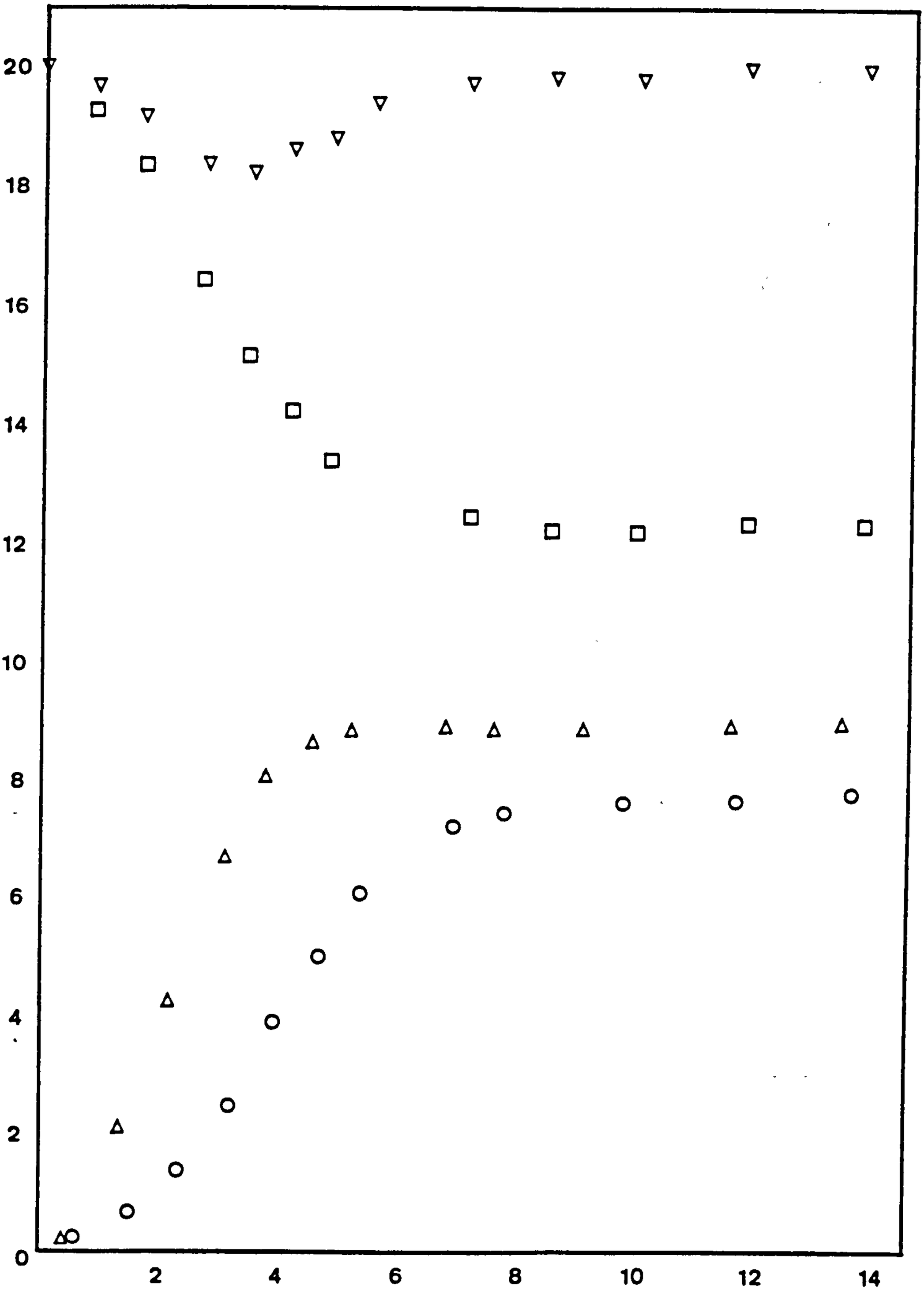

Figure 3.2 Sequential spectra taken subsequent to mixing solutions of p-nitrophenylacetate (PNPA) and hydrogen peroxide: pH 6.80 phosphate buffer (I = 0.02M); $[H_2O_2] = 1.956 \times 10^{-3}$M; $[PNPA]_o = 0.903 \times 10^{-3}$M; [EDTA] = 1×10^{-5}M; 25°C.

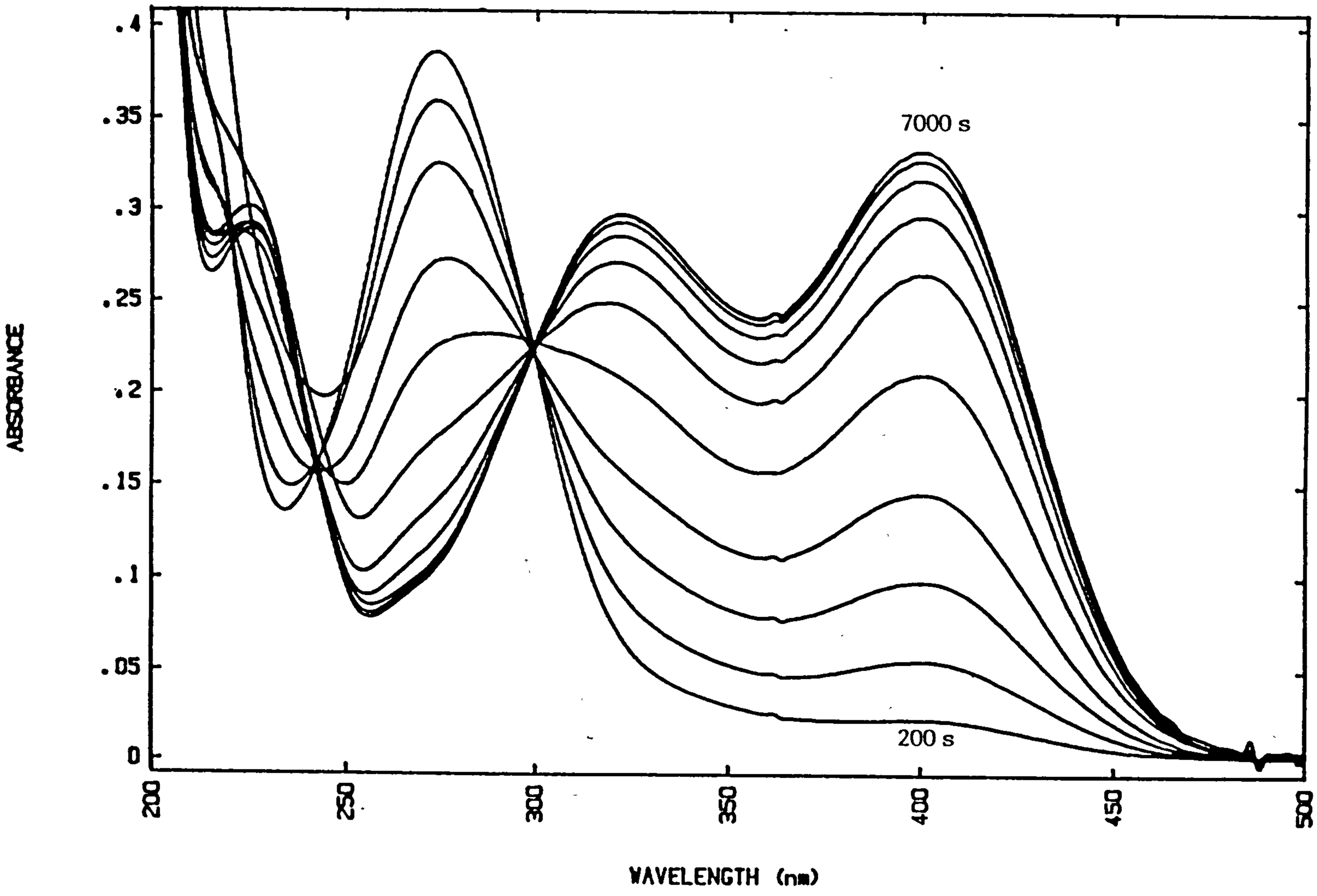

peaks represent PNPA (274 nm), protonated PNP (322 nm) and the anionic form of PNP (400 nm). There is an isobestic point at 300 nm.

If the reaction of PNPA with hydrogen peroxide was as simple as suggested in Scheme 3.1, that is, perhydrolysis and the competing hydrolysis reaction to form PNP and peracetic acid or acetic acid, then the results plotted in Figure 3.1 would be unexpected. The concentration of total iodide reactable peroxide during the course of the reaction would be expected to remain constant since according to Scheme 3.1 the only peroxide species present in the reaction solution are peracetic acid and hydrogen peroxide.

However, a trough in total iodide reactable peroxide concentration is observed, eventually returning to the original level. Other points to note which are not consistent with Scheme 3.1 are that the concentrations of peracetic acid lagged well behind that of PNP and continued to increase after the point when all of the PNPA had reacted to form PNP (as indicated by an infinity concentration of PNP). Also, the hydrogen peroxide concentration continues to decrease after all the PNA has reacted. Clearly, then, after all the PNPA has reacted, hydrogen peroxide is still reacting and peracetic acid is still being formed.

The proposed explanation is summarised in Scheme 3.2 and is consistent with suggestions that in addition to the reactions in Scheme 3.1, peracetic acid also reacts with PNPA, to form PNP and diacetyl peroxide.

Scheme 3.2

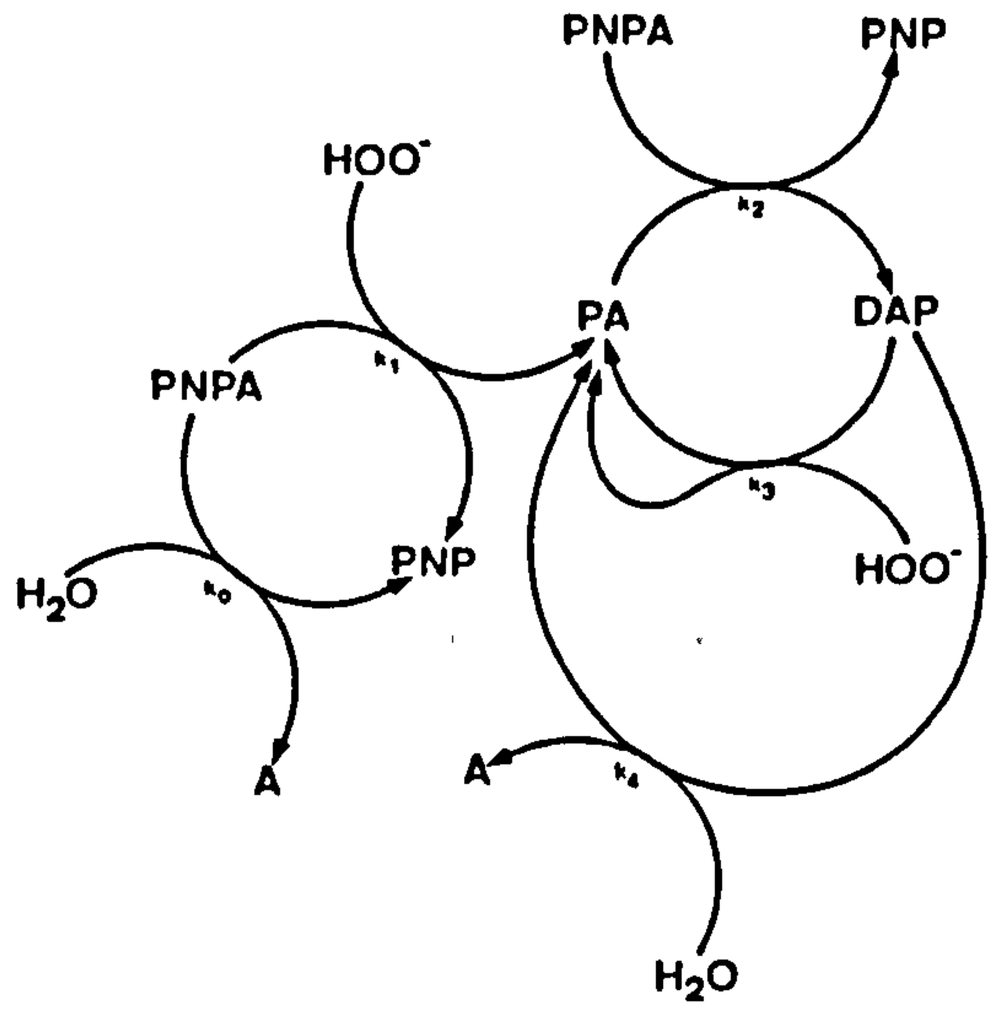

PNP = p-Nitrophenol; PA = Peracetate; A = Acetate
DAP = Diacetyl peroxide

Diacetyl peroxide reacts very slowly with iodide, even in the presence of the ammonium molybdate[107] catalyst. Thus, its build-up is characterised by a trough in total iodide reactable peroxide. Peracetic acid is regenerated from diacetyl peroxide by either hydrolysis to yield peracetic acid and acetic acid, or by perhydrolysis to yield two molecules of peracetic acid. The reason for the lag in peracetic acid concentration in Figure 3.1, is that as soon as it is formed from the activation reaction it is 'tied up' in the form of the diacetyl peroxide. A similar scheme has been suggested on the basis of complex kinetics observed for the reaction of a surfactant paranitrophenol ester and H_2O_2 in borate buffer.[110]

The next stage of this research was to independently determine the rate constants for all of the reactions shown in Scheme 3.2, with the ultimate aim being to simulate the reaction on mixing PNPA with hydrogen peroxide. This is described in the following section. Decomposition reactions of diacetyl peroxide and the other peroxide components are

assumed to be negligible under these reaction conditions since the total iodide reactable peroxide concentration is regenerated completely.

3.2 Determination of Rate Constants for the Reactions Occurring upon Mixing PNPA and Hydrogen Peroxide

This section describes the determination of the individual rate constants listed in Scheme 3.2; the experimental conditions employed were identical to those used in the previous sections, that is, pH 6.80 phosphate buffer (sodium salts), I = 0.1, 25°C. All solutions contained 1×10^{-5} M EDTA.

Experimental

Materials

PNPA solutions were prepared and standardised as described in Section 3.1. Hydrogen peroxide solutions were standardised by cerate titrimetry.[101] Peracetic acid solutions were prepared from Proxitane 4200 (Interox Ltd). Proxitane 4200 contains a significant proportion of hydrogen peroxide and this must obviously be removed before conducting kinetic measurements. The reaction of peracetic acid and hydrogen peroxide, which at high pH is catalysed by minute trace quantities of metal ions[111] was utilized to remove the hydrogen peroxide as follows: 10 ml of Proxitane was added to about 70 ml water and the pH raised to 10.5 using 2 M NaOH. After 5 minutes the pH was lowered to that of the buffer solution (pH 6.80) using 2 M H_2SO_4. One ml of this solution was added to 50 ml of phosphate buffer to give a solution approximately 4×10^{-3} M in peroxyacetic acid. Diacetyl peroxide was generated *in situ* by mixing, in equal proportions, solutions of 0.49 mM PNPA and 0.92 mM peracetic acid (in a pH 6.80 phosphate buffer, I = 0.1); this yielded an approximately 0.5 mM solution of diacetyl peroxide.

Procedure

The rate constants corresponding to k_o to k_5 in Scheme 3.2 were determined as follows:

(a) PNPA hydrolysis (k_o): This was followed by measuring the release of PNP at 400 nm in a solution containing PNPA (2.04×10^{-4} M) in buffer alone. PNP release was followed over 23000 seconds and the first order rate constant, k_o, was obtained from linear regression of $\ln(A_\infty - A)$ against time. A_∞(1.579) was calculated using a molar absorptivity of 7344 M^{-1} cm^{-1} for the PNP anions at 400 nm.

(b) Reaction of PNPA with H_2O_2 (k_1): Under pseudo first order conditions, the rate of release of PNP at 400 nm was followed for solutions of PNPA (1.094×10^{-4} M) in the presence of excess hydrogen peroxide (ranging from 1.68×10^{-2} M to 9.58×10^{-2} M). Pseudo first order rate constants were obtained from non-linear regression using Equation 3.2.

$$A = A_\infty + (A_o - A_\infty)e^{-k_{obs}\, t} \qquad \text{Eqn 3.2}$$

where A_o, A_∞ and kobs are the initial absorbance, the infinity absorbance and the pseudo first order rate constant, respectively. PNP formation was followed for at least 4 half-lives, when Equation 3.2 was used; in every case in which the reaction was followed to virtual completion the calculated A_∞ value was in good agreement with the measured value.

(c) Reaction of PNPA with Peracetic Acid (k_2): The procedure outlined in (b) was repeated, using peracetic acid instead of hydrogen peroxide ($[PNPA]_o = 0.901 \times 10^{-4}$ M; peracetic acid range from 1.362×10^{-3} M to 3.746×10^{-3} M). Pseudo first order rate constants were again obtained by non-linear regression using Equation 3.2.

(d) Hydrolysis of Diacetyl Peroxide (k_4): Following *in situ* generation of diacetyl peroxide (see materials) the subsequent generation of pera-

cetic acid in buffer alone was followed; the first order rate constant for the reaction was obtained from non-linear regression using Equation 3.3.

$$[PA] = [PA]_\infty + ([PA]_o - [PA]_\infty)e^{-k_{obs}\, t} \qquad \text{Eqn 3.3}$$

(e) Reactions of Diacetyl Peroxide with Hydrogen Peroxide (k_5): Under pseudo first order conditions, the formation of peracetic acid was measured for solutions of diacetyl peroxide (ranging from 0.567×10^{-4} to 2.246×10^{-4} M) in the presence of excess hydrogen peroxide (ranging from 2.402×10^{-3} M to 10.425×10^{-3} M).

Results

Figure 3.3 shows a plot of $\ln(A_\infty - A)$ against time for PNPA hydrolysis from which the first order rate constant is obtained. Figures 3.4 and 3.5 show absorbance data from first order kinetic runs for the reaction of PNPA with hydrogen peroxide and peracetic acid, respectively. The data have been plotted in the form $(A - A_o)/(A_\infty - A_o)$ against time; the curves are defined by Equation 3.2, from which the pseudo first order rate constants listed in Tables 3.1 and 3.2 have been obtained. Plots of pseudo first order rate constants against nucleophile concentration, for hydrogen peroxide and peracetic acid, which are linear, are shown in Figures 3.6 and 3.7. The observed second order rate constants, kobs, were obtained from linear regression of the pseudo first order rate constants; the 90% confidence limits of the intercept included the independently determined value for PNPA hydrolysis. No literature values for the reactivities of peroxyacetic acid towards PNPA have previously been reported. Figure 3.8 shows the change in concentration of peroxyacetic acid during and after the reaction with PNPA. The curve is defined by Equation 3.2, from which the first order rate constant is obtained for the hydrolysis of diacetyl peroxide. Figure 3.9 shows a typical plot of peracetic acid formation on reacting diacetyl

peroxide with hydrogen peroxide; the concentration of peracetic acid eventually reached a value, corresponding to Equation 3.4, greater than its original concentration.

$$[Peracid]_\infty = [Peracid]_o + 2([peracid]_{orig} - [Peracid]_o) \quad \text{Eqn 3.4}$$

The subscripts ∞, o, and orig indicate the final concentration, the concentration at any time after addition of hydrogen peroxide, and the original concentration, respectively; these data are contained in Table 3.4 The curve in Figure 3.9 is defined by Equation 3.3 from which the pseudo first order rate constants listed in Table 3.3 were obtained. Figure 3.10 shows a plot of pseudo first order rate constants against hydrogen peroxide concentration; the mean observed second order rate constant was obtained by dividing the first order rate constant by the nucleophile concentration (the pseudo first order rate constants were corrected for diacetyl peroxide hydrolysis).

This study was also conducted in pH 6.8 phosphate buffer at a lower ionic strength (I = 0.02); first, pseudo first, and second order plots pertaining to this study are contained in Figures 3.11 to 3.19 and the resulting rate constants are contained in Tables 3.5 to 3.8. The values for all rate constants measured in the studies described in this section are contained in Table 3.11. Equation 3.5 was used to estimate the rate constant for the reaction of PNPA and diacetyl peroxide with hydrogen peroxide and peracetic acid anions, using pKa values[113] of 11.6 and 8.2, respectively.

$$k = kobs(K_a + [H^+])/K_a \quad \text{Eqn 3.5}$$

3.3 General Discussion

3.3.1 Reaction Scheme

It has been shown that during the reaction of PNPA with peracetic acid, a species is formed which reacts with water to yield one mole of peracetic acid, and with hydrogen peroxide to give two moles of peracetic

Table 3.11 A summary of rate data for the reaction of various nucleophiles with acyl species. k_o values are first order rate constants and k_{obs} values are observed second order rate constants.

Acyl Species	Nucleophile	Buffer	pH	Ionic Strength / M	k_o / s^{-1}	k_{obs} / $M^{-1}s^{-1}$ *	k / $M^{-1}s^{-1}$
PNPA	Buffer	Phosphate	6.8	0.02	5.55×10^{-6}	-	-
PNPA	Buffer	Phosphate	6.8	0.10	7.32×10^{-6}	-	-
PNPA	HOO^-	Phosphate	6.8	0.02	-	$(4.753\pm0.351)\times10^{-2}$	3002
PNPA	HOO^-	Phosphate	6.8	0.10	-	$(5.565\pm0.181)\times10^{-2}$	3511
PNPA	HOO^-	Borate	9.25	0.10	-	3.84 ± 0.26	862
PNPA	HOO^-	Carbonate	10.0	0.10	-	92.80 ± 5.37	3789
PNPA	$CH_3CO_3^-$	Phosphate	6.8	0.02	-	3.98 ± 0.17	104
PNPA	$CH_3CO_3^-$	Phosphate	6.8	0.10	-	3.88 ± 0.06	101
$(CH_3CO_2)_2$	Buffer	Phosphate	6.8	0.02	9.69×10^{-5}	-	-
$(CH_3CO_2)_2$	Buffer	Phosphate	6.8	0.10	16.50×10^{-5}	-	-
$(CH_3CO)_2$	HOO^-	Phosphate	6.8	0.02	-	0.352 ± 0.047	22221
$(CH_3CO_2)_2$	HOO^-	Phosphate	6.8	0.10	-	0.544 ± 0.060	34300

* 90% Confidence Limits.

acid; the results are consistent with Scheme 3.2 in which this species is diacetyl peroxide. The occurrence of diacetyl peroxide has not been confirmed by independent analysis, however, the results obtained in Section 3.2 are considered satisfactory evidence of its identity. Ogata and Sawaki[112] have reported good yields of peroxybenzoic acid during the perhydrolysis of benzoyl peroxide (in alkaline aqueous organic solvents) which is analagous to the perhydrolosis of diacetyl peroxide.

Figure 3.19 shows the concentration changes which occur upon mixing PNPA and hydrogen peroxide in a 2:1 mole ratio, obtained from the experimental described in Section 3.1. The curves were computer generated by numerical solution to the differential equations corresponding to Scheme 3.2, and using the rate constants contained in Table 3.11 (program contained in Appendix 2). There is excellent agreement between the calculated and observed concentrations indicating that the reaction Scheme 3.2 completely describes the system. Good agreement was also obtained for the similar course of studies conducted at the lower ionic strength buffer (I = 0.02 M) (Figure 3.20) for which the rate constants contained in Table 3.11 apply.

3.3.2 The Importance of Adding EDTA to Reaction Solutions

The importance of adding EDTA to the PNPA and peroxide/buffer solutions two hours prior to the reactions is demonstrated by three studies conducted at pH 6.80 at the lower ionic strength (I = 0.02 M) (Figures 3.21 to 3.23); the concentration changes were followed upon mixing hydrogen peroxide and PNPA in a 2:1 mole ratio; EDTA was added only to the hydrogen peroxide/buffer solution. The total iodide reactable peroxide concentration does not return to the original concentration, indicating peroxide decomposition during the course of the reaction. It is interesting to note from the comparison of the experimentally-

Figure 3.19 Change in the concentrations of: peracetic acid plus H_2O_2, ∇; peracetic acid, O; H_2O_2 calculated from the previous concentrations, □; p-nitrophenol, ∇. The curves represent the numerical solution of differential rate equations corresponding to Scheme 3.2. Conditions were: pH 6.8 phosphate buffer (I = 0.1M); $[H_2O_2]_o = 2.02 \times 10^{-3}$M; $[PNPA]_o = 9.10 \times 10^{-4}$M; $[EDTA] = 1 \times 10^{-5}$M.

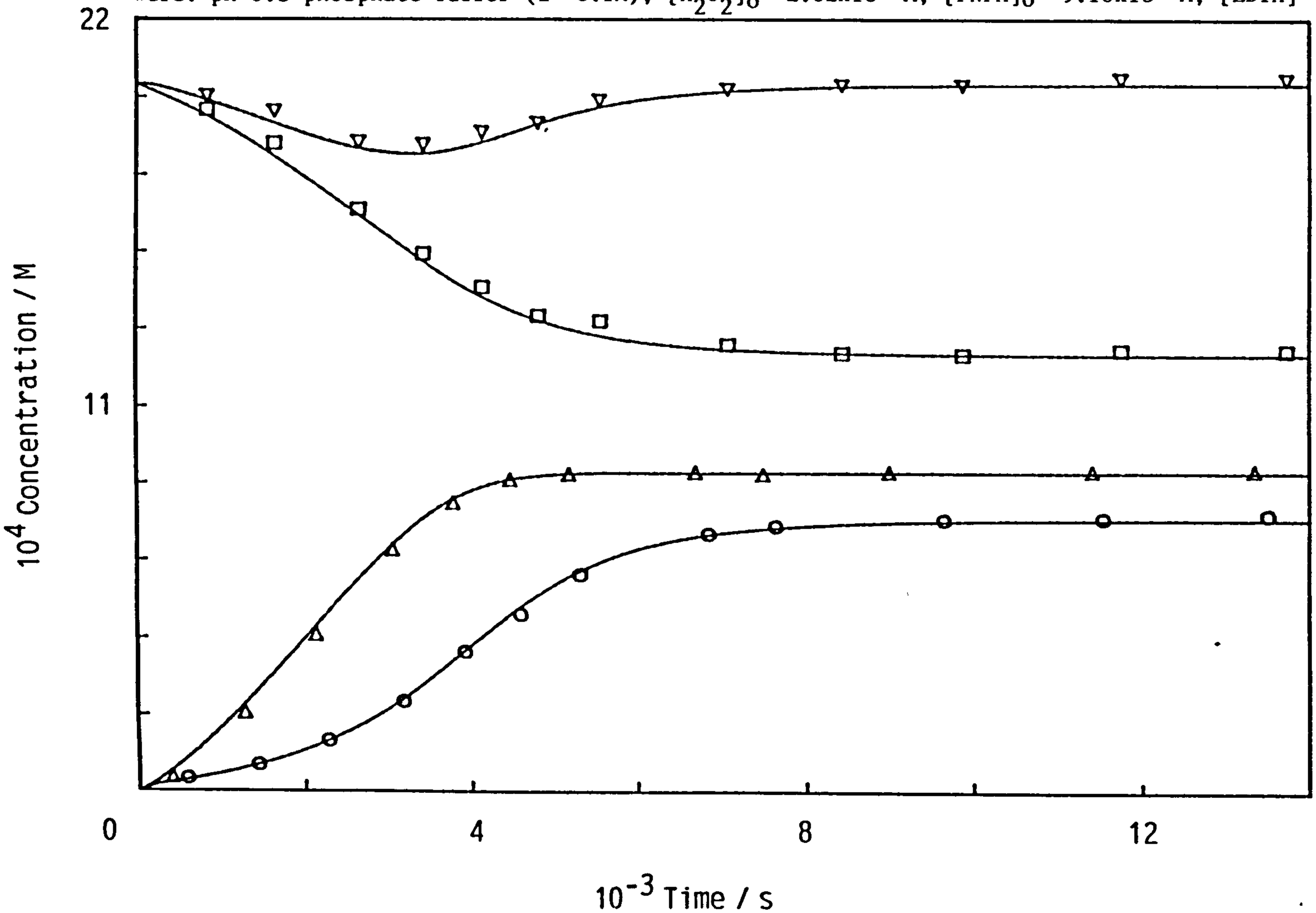

Figure 3.20 Change in the concentrations of: peracetic acid plus H_2O_2, ∇; peracetic acid, O; H_2O_2 calculated from the previous concentrations, □; p-nitrophenol, Δ. The curves represent the numerical solution of differential equations corresponding to Scheme 3.2. Conditions were: pH 6.8 phosphate buffer (I = 0.02M); $[H_2O_2]_o = 1.961 \times 10^{-3}$M; $[PNPA]_o = 0.766 \times 10^{-3}$M; $[EDTA] = 1 \times 10^{-5}$M.

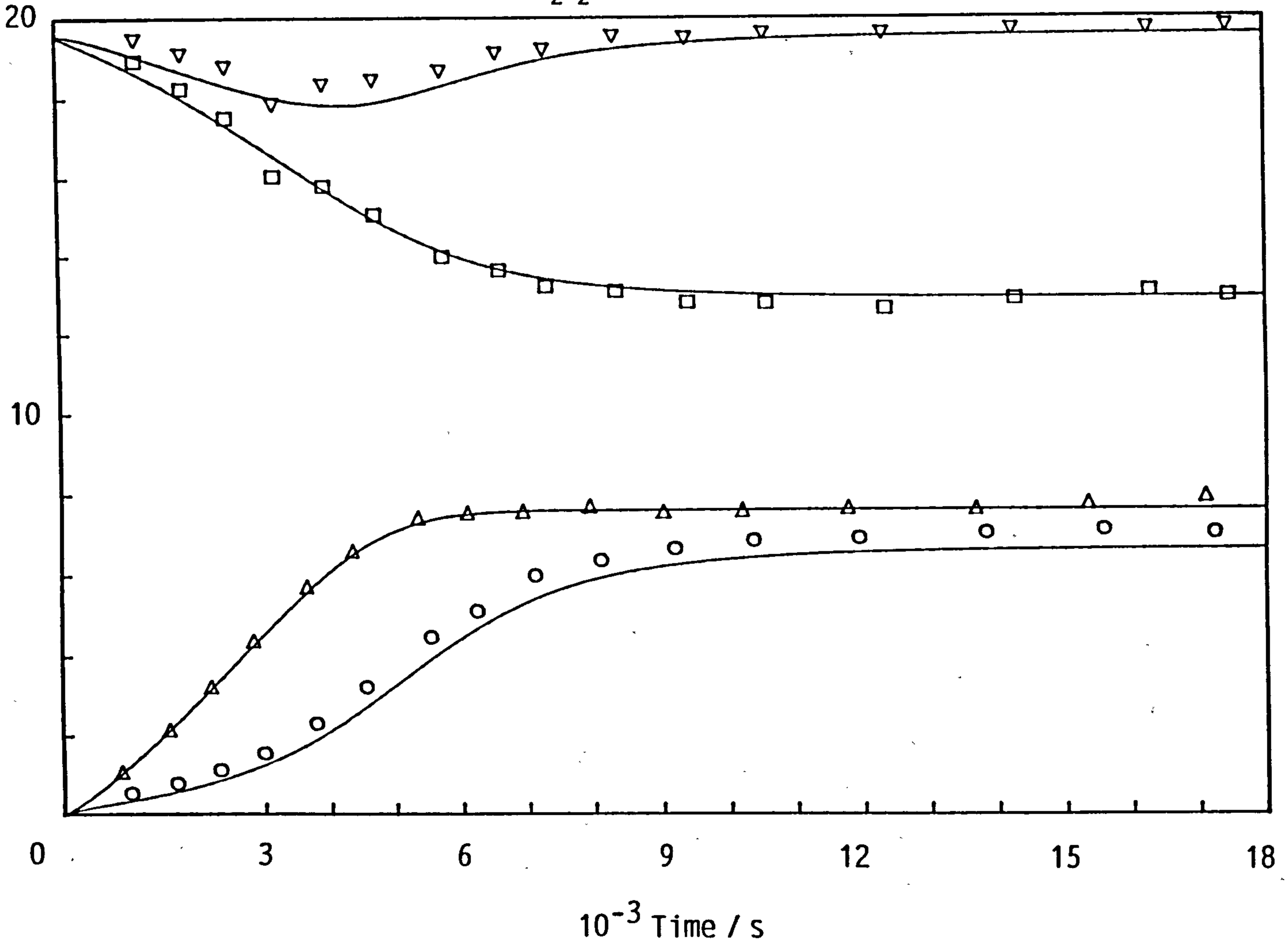

determined and the computer-generated concentration data in Figures 3.21 to 3.23 (based on rate constants contained in Table 3.11) that the peroxide loss appears to be mainly due to hydrogen peroxide since, in most cases, the peracetic acid concentration data are described perfectly by the computer generated data.

3.3.3 General Discussion of Rate Constants Corresponding to Scheme 3.2

The rate constants have been determined at pH 6.8 at two ionic strengths (I = 0.1 and I = 0.02). In addition, rate constants for the reaction of PNPA with hydrogen peroxide (k_1) were determined in a pH 9.25 sodium hydroxide/sodium borate buffer (I = 0.1) and a pH 10.00 carbonate buffer (I = 0.1), at 25°C. Pseudo first order rate constants were obtained from linear regression of $\ln(A_\infty - A)$ and Figures 3.24 and 3.25 show the first order plots for borate and carbonate buffers, respectively. The observed second order rate constants were obtained from linear regresssion of the pseudo first order rate constants and these plots are shown in Figures 3.26 and 3.27 for borate and carbonate buffers, respectively. The data for these plots are contained in Table 3.10

3.3.4 Ionic Strength/Phosphate Buffer Effects

The rate constants listed in Table 3.11 corresponding to Scheme 3.2, were determined at two phosphate buffer concentrations, also corresponding to two different ionic strengths (no salt added). Except for the reaction of peracetic acid with PNPA, all the reactions showed a rate acceleration at the higher phosphate buffer concentration. It has been shown[25,114] that for alkaline hydrolysis of esters the kinetic salt effects are negative and usually small[114], although the latter is not always the case since trifluoroethyl acetate[25] exhibits an unusually large negative salt effect for esters (40% smaller rate constant in 1M KCl than at an ionic strength close to zero). Similar negative salt

Figure 3.21 Change in the concentrations of: peracetic acid plus H_2O_2, ∇; peracetic acid, O; H_2O_2 calculated from the previous concentrations, □; p-nitrophenol, Δ. The curves represent the numerical solution of differential rate equations corresponding to Scheme 3.2. Conditions were: pH 6.8 phosphate buffer (I = 0.02M); $[H_2O_2]_o = 2.26\times10^{-3}$M; $[PNPA]_o = 1.06\times10^{-3}$M; $[EDTA] = 1\times10^{-5}$M.

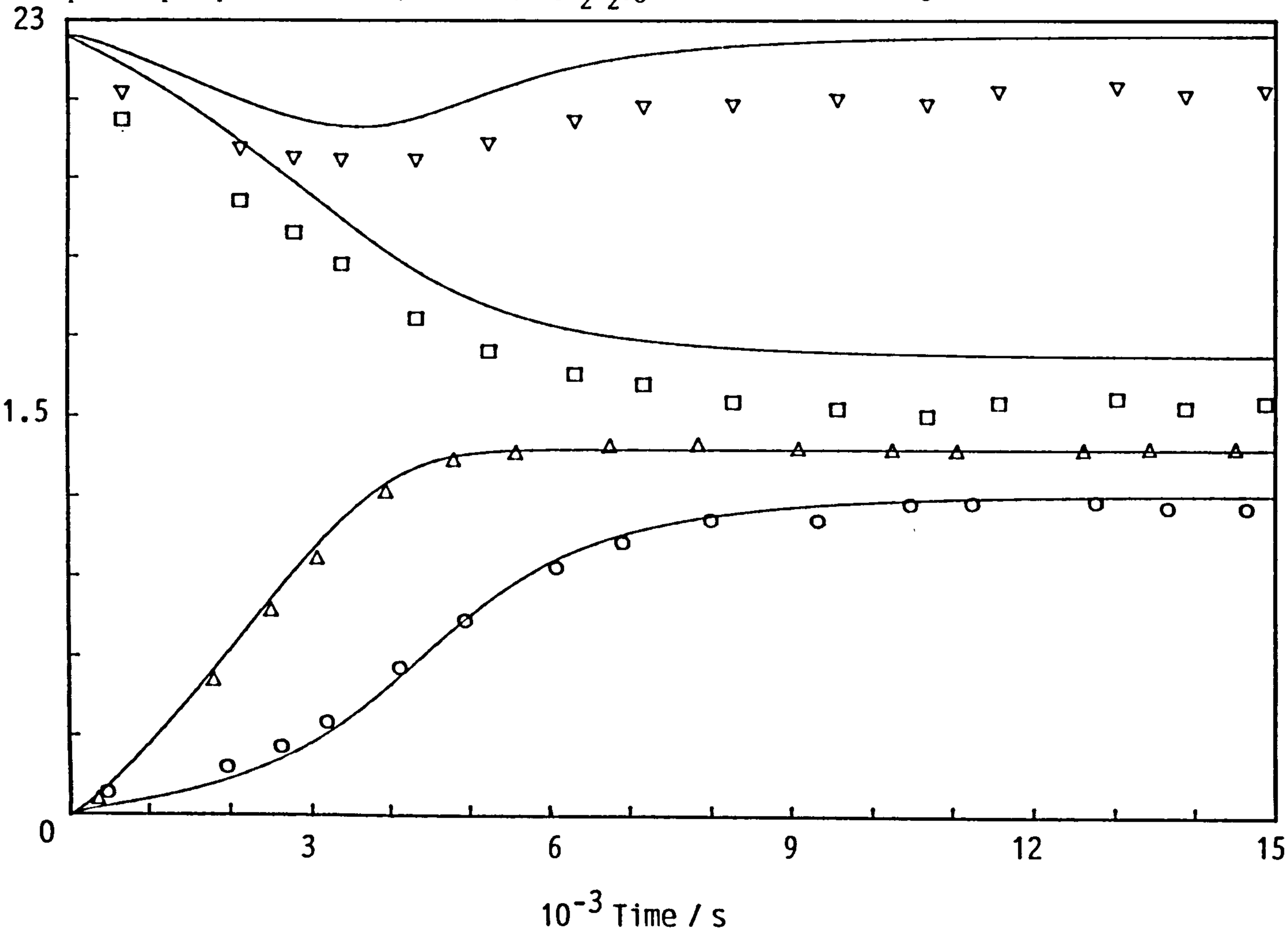

Figure 3.22 Change in the concentrations of: peracetic acid plus H_2O_2, ▽; peracetic acid, ○; H_2O_2 calculated from the previous concentrations, □; p-nitrophenol, Δ. The curves represent the numerical solution of differential equations corresponding to Scheme 3.2. Conditions were: pH 6.8 phosphate buffer (I = 0.02M); $[H_2O_2]_o = 2.34 \times 10^{-3}$M; $[PNPA]_o = 0.85 \times 10^{-3}$M; no EDTA present; 25°C.

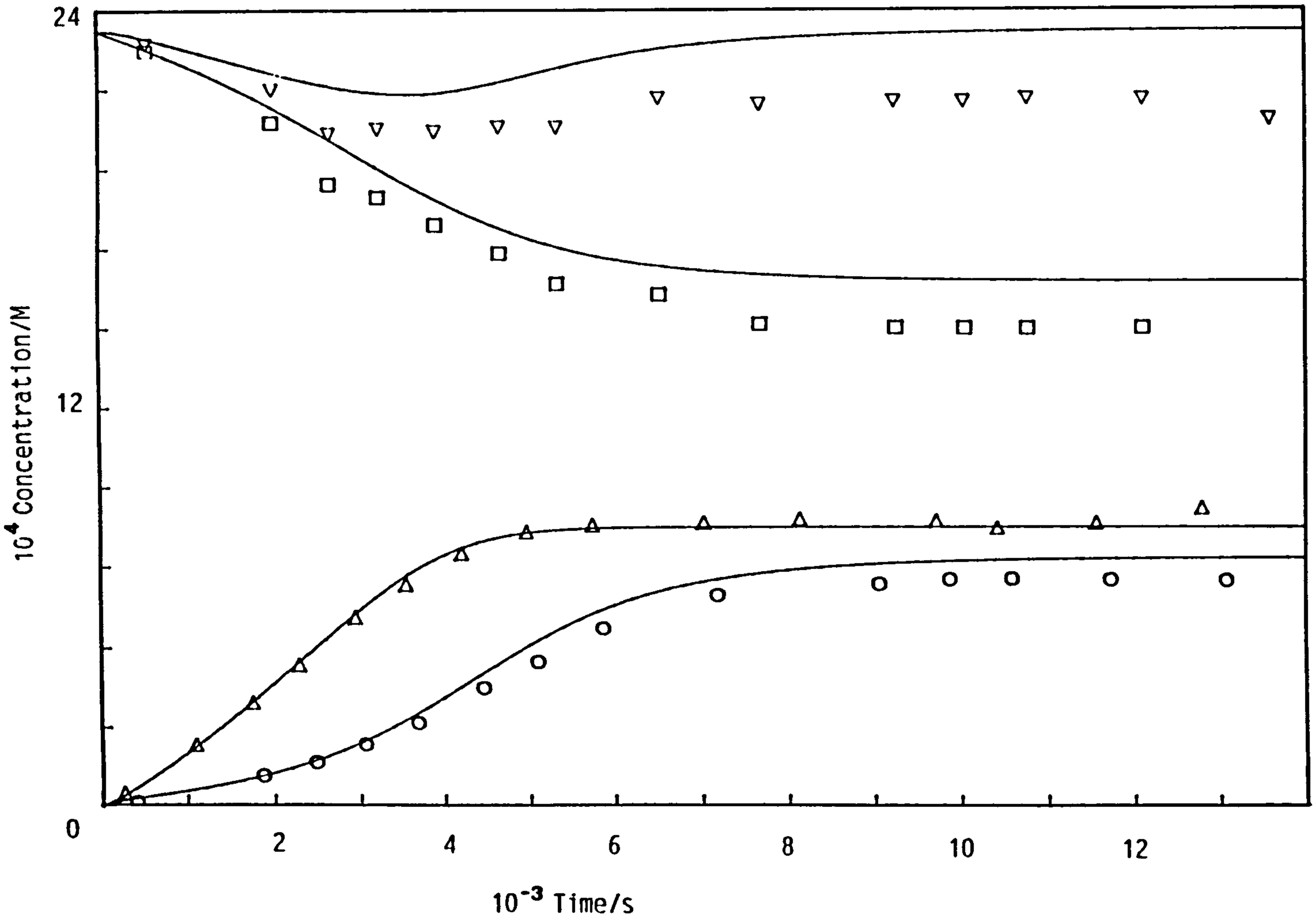

Figure 3.23 Change in the concentrations of: peracetic acid plus H_2O_2, ▽; peracetic acid, O; H_2O_2 calculated from the previous concentrations, □; p-nitrophenol, Δ. The curves represent the numerical solution of differential equations corresponding to Scheme 3.2. Conditions were: pH 6.8 phosphate buffer (I = 0.02M); $[H_2O_2]_o = 1.956 \times 10^{-3}$M; $[PNPA]_o = 0.903 \times 10^{-3}$M; [EDTA] = 1×10^{-5}M; 25°C.

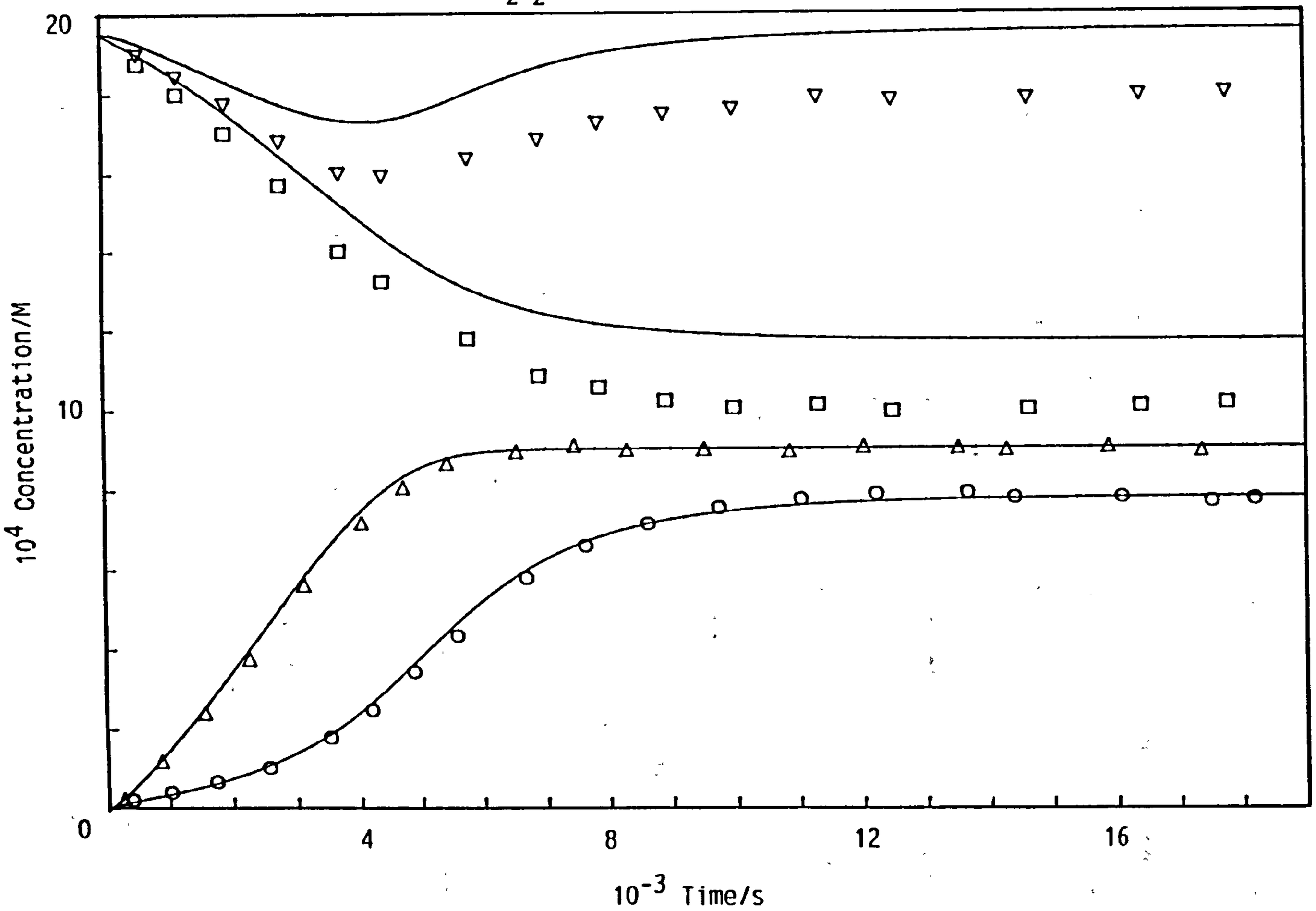

effects should be expected for other nucleophile substitution reactions with esters, and so the observed rate acceleration at higher ionic strength in this study cannot be due to salt effects. General acid base mechanisms must therefore be involved.

No general acid-base catalysis is observed for the reaction of peracetic acid with PNPA and, according to the review and discussion of acid-base catalysis in Chapter 1, there are likely to be two main reasons for this. Firstly, for reactions which exhibit general acid-base catalysis and proceed via a stable tetrahedral intermediate (as is likely to be the case with the reaction of peroxides with PNPA, since they are good nucleophiles) then a change in rate determining step and consequent levelling off of general acid-base catalysis is observed with increasing buffer concentration.[14,10] It is possible, though unlikely, that the phosphate buffer concentrations used in this study lie above the change in r.d.s. More likely is, that this reaction belongs to the class where the lifetime of the intermediate is sufficient to diffuse through solution and abstract a proton to the carbonyl oxygen. In this case, or a borderline case, general acid-base catalysis would be absent or insignificant. If this applies to peracetic acid then it will also apply to the better nucleophile, hydrogen peroxide, and so this leaves only the possibility of general base catalysis for the reaction of hydrogen peroxide with PNPA. The general base catalyst must interact in some way with the hydrogen atom of the hydroperoxide anion to stabilise the transition state. The hydrolysis of PNPA in phosphate buffer alone shows a 36% rate acceleration at the higher buffer concentration. This is probably due to both general acid and general base catalysis and the observed first order rate constants are likely to include the terms in Equation 3.6.

$$k_o = k_{H2O}\,[H_2O]^n + k_{OH^-}\,[OH^-] + k_H\,[H^+] + k_{BH^+}\,[BH^+] + k_B\,[B]$$

Eqn 3.6

The hydrolysis and perhydrolysis reactions of dicetyl peroxide show the largest buffer effects (70% and 55% increases at the higher buffer concentrations, respectively). The hydrolysis of the analagous acetic anhydride shows a similarly large dependence on phosphate buffer concentration.[25]

3.3.5 Comparison of Rate Constants with Literature Values

To our knowledge there have been no previous reports of the reactivity of peracetic acid towards PNPA. However, it is evident from Figure 3.28 that the estimated rate constant for peracetic acid fits on a Brønsted-type plot for reactions of PNPA with para and meta substituted peroxybenzoate anions.[64]

The estimated values of k (3002 and 3511 $M^{-1}\ s^{-1}$) for the reaction of the hydroperoxy anion with PNPA in phosphate buffer compare well to those estimated by Jencks and Gilchrist[41] (3667 $M^{-1}\ s^{-1}$, with pKa = 11.6, I = 1M). McIsaac et al.[62] (1972) have quoted a value of 2267 $M^{-1}\ s^{-1}$ for the same reaction in phosphate buffer using the lower pKa of 11.37 (I = 1.0M) Re-calculating using a pKa of 11.6 gives a value of 3850 $M^{-1}\ s^{-1}$. The estimated value, k, obtained in carbonate buffer (3789 $M^{-1}\ s^{-1}$) is similar to our value and the literature values in phosphate buffer. All the estimated values for k quoted above show a positive deviation from the Brønsted-type plot in Figure 3.28. It has been suggested that this higher-than-expected reactivity is due to (i) the presence of two potentially reactive oxygens in the unsubstituted hydrogen peroxide molecule,[41] (ii) stabilisation of the transition state by a hydrogen bonding interaction,[77,78] (iii) the αeffect. Point (ii) will be considered in more detail in Chapter 10.

Figure 3.28 Bronsted type plot for the reaction of a range of substituted peroxybenzoic acids and peracetic acid with p-nitrophenylacetate in aqueous solution at 25°C. The points represent p-NO_2-PBA,▽, m-NO_2-PBA,●, m-Cl-PBA,□, p-SO_3-PBA,▼, p-Cl-PBA,○, PBA,■, p-MeO-PBA,△, and peracetic acid,▲. The line represents the best fit using the linear least squares method.

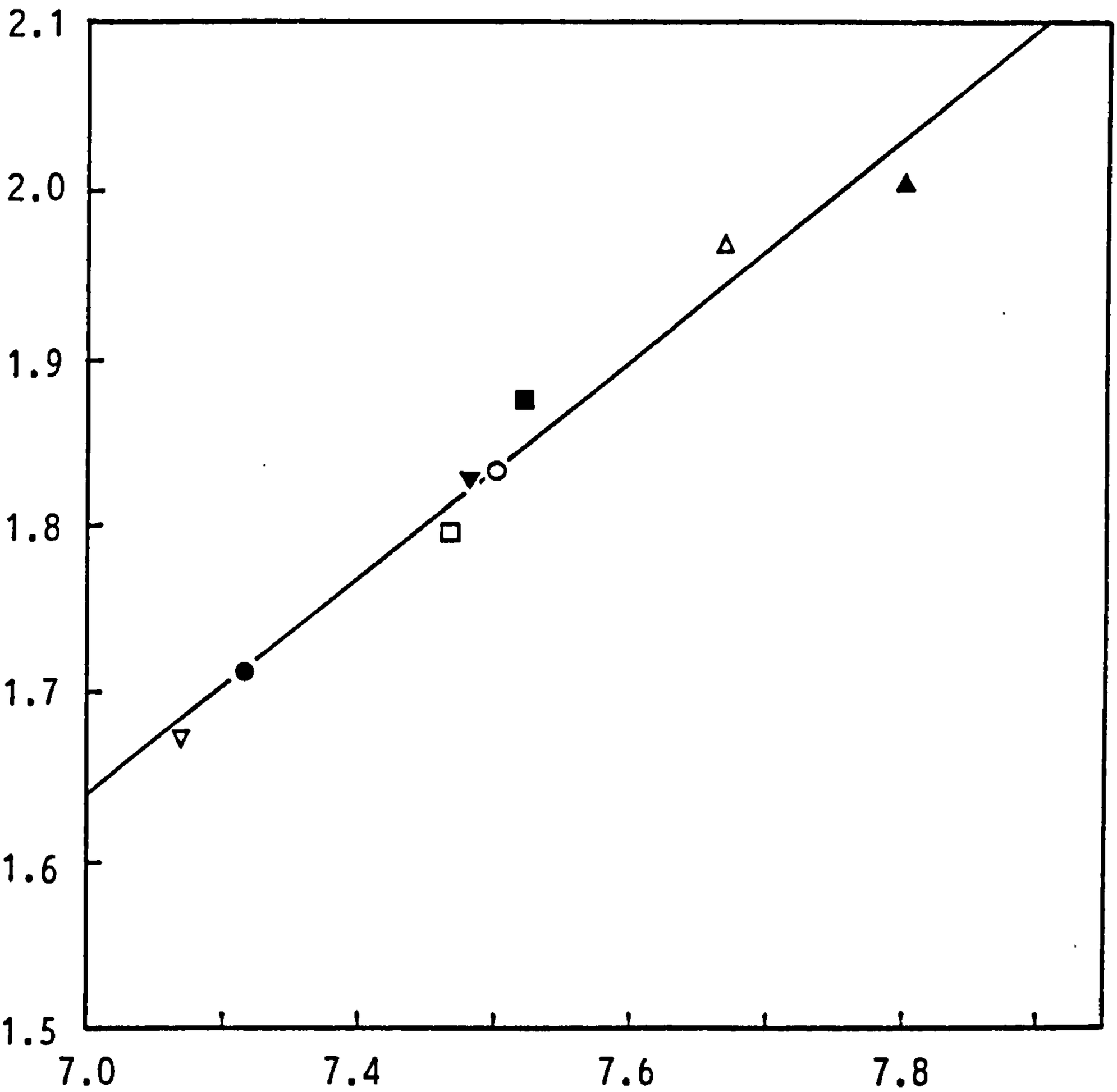

3.3.6 Borate Buffer Effects

The estimated values of k for the reactivities of HOO^- towards PNPA in borate buffer are about four times lower than those obtained in phosphate and carbonate buffers. It is well-known that hydrogen peroxide interacts with borate buffers; indeed, in detergent formulations, hydrogen peroxide is supplied to the wash liquor in the form of sodium perborate. It has recently been shown[115] that around pH 9.0 at low hydrogen peroxide concentration the predominant equilibrium is:

$$B(OH)_3 + H_2O_2 \overset{K}{\rightleftharpoons} (HO)_3BOOH^- + H^+ \qquad \text{Eqn 3.7}$$

Since the hydrogen peroxide concentrations used in the present study are much less than the concentration of boric acid (0.1M) in the buffer $[B(OH)_3]$ can be equated to $[B(OH)_3]_T$ without significant error, and Equation 3.8 can be used to estimate the second order rate constant k, provided it is assumed that $(HO)_3BOOH^-$ does not react with PNPA.

$$k = k_{obs}\,(K_a + [H^+] + K\,[B(OH)_3]_T)/K_a \qquad \text{Eqn 3.8}$$

Using the value of K reported (2.0×10^{-8})[115] a value of $k = 3920\ M^{-1}\ s^{-1}$ is obtained, which is similar to those in phosphate and carbonate buffers and supports the assumption that $(HO)_3BOOH^-$ is a poor nucleophile compared with HOO^-. The plots of $\ln(A_\infty - A)$ against time for the reaction of PNPA and hydrogen peroxide in borate buffer (Figure 3.25) showed negative deviations from linearity after one or two half-lives. Similar results are reported[110] for the reaction of a surfactant paranitrophenyl ester in borate buffer. These results indicate that under these particular conditions the PNPA reacts with the released peroxyacid faster than it does with hydrogen peroxide. These observations of an approximately 75% lower rate of reaction in borate buffer than phosphate or carbonate buffers has important implications for detergent formulations where the hydrogen peroxide is delivered in the form of sodium perborate, and the buffering capacity of the wash

liquor is maintained by borate buffer. Clearly, in such systems, the formation of $(HO)_3BOOH^-$ will serve as a slow release mechanism for peroxide. This could mean that the competing hydrolysis reaction in bleach activation could be more significant than in cases where the hydrogen peroxide is delivered by other means such as in sodium percarbonate.

Finally, the hydrolysis reaction and the reaction of HOO^- with diacetyl peroxide are roughly an order of magnitude higher than the the corresponding reactions with PNPA. However, this should not be entirely unexpected since acid anhydrides are more reactive than the corresponding esters[25] and the rates of substitution on the carbonyl carbon of diacetyl peroxides should parallel those for the analagous anhydrides. The rate of alkaline hydrolysis, k_{OH} (corrected to [B] = 0) and acetic anhydride, for example, is approximately 100 times larger than for PNPA.[25] The only reported value for the reaction of diacetyl peroxide with hydrogen peroxide (85000 M^{-1} s^{-1}) that we are aware of[110] was obtained indirectly from the analysis of the complex kinetics of PNP formation for the reaction of a surfactant paranitrophenol ester in 0.05 M borate buffer.

Table 3.1 Observed first order rate constants (kobs) for the reaction between p-nitrophenylacetate and hydrogen peroxide. Conditions were: pH 6.80 sodium hydrogen phosphate - disodium hydrogen phosphate buffer (I = 0.1); [PNPA] = 1.094×10^{-4}M; [EDTA] = 1×10^{-5}M; 25°C.

$10^2[H_2O_2]/M$	$10^3 kobs/s^{-1}$
0	7.323×10^{-3}
1.680	1.229
3.825	2.517
5.769	3.534
7.690	4.649
9.580	5.632

Table 3.2 Observed first order rate constants (kobs) for the reaction between p-nitrophenylacetate and peracetic acid. Conditions were: pH 6.80 sodium dihydrogen phosphate - disodium hydrogen phosphate buffer (I = 0.1); [PNPA] = 0.901×10^{-4}M; [EDTA] = 1×10^{-5}M; 25°C.

10^3[Peracetic acid]/M	$10^3 kobs/s^{-1}$
0	7.323×10^{-3}
1.362	5.454
1.882	7.420
2.367	9.275
2.824	11.080
3.299	13.023
3.746	14.610

Table 3.3 Observed first order rate constants (kobs) for the reaction between diacetyl peroxide and hydrogen peroxide. Conditions were: pH 6.80 sodium dihydrogen phosphate - disodium hydrogen phosphate buffer (I = 0.1); [diacetyl peroxide] ranging from 0.58×10^{-4} to 2.25×10^{-4}M; [EDTA] = 1×10^{-5}; 25°C.

$10^3[H_2O_2]$/M	10^3kobs/s^{-1}
0.000	0.1584
2.402	1.056
4.800	2.739
5.064	2.494
6.505	3.361
8.624	4.385
10.425	5.584

Table 3.4 Initial (o) and infinity (∞) concentrations of peracetic acid for the reaction between diacetyl peroxide and hydrogen peroxide. Conditions were those listed in table 3.3.

$10^3[H_2O_2]$/M	$10^4[PA]_o$/M	$10^4[PA]_\infty$/M	$10^4(([PA]_\infty-[PA]_o)/2 + [PA]_o)$/M
2.402	4.626	8.246	6.436
4.800	4.126	8.619	6.372
4.871	5.625	7.359	6.492
5.064	4.421	6.770	5.595
8.624	5.208	7.429	6.318
10.425	4.759	7.949	6.354

Table 3.5 Observed first order rate constants (kobs) for the reaction between p-nitrophenylacetate and hydrogen peroxide. Conditions were: pH 6.80 sodium dihydrogen phosphate - disodium hydrogen phosphate buffer (I = 0.02); [PNPA] = 0.833×10^{-4}; 25°C; no EDTA was present.

$10^2[H_2O_2]/M$	$10^3 kobs/s^{-1}$
0.000	5.554×10^{-3}
3.560	1.793
7.120	3.566
10.680	5.407
14.240	7.122
17.800	8.476

Table 3.6 Observed first order rate constants (kobs) for the reaction between p-nitrophenylacetate and peracetic acid. Conditions were: pH 6.80 sodium dihydrogen phosphate - disodium hydrogen phosphate buffer (I = 0.02); [PNPA] = 0.833×10^{-4}; 25°C; no EDTA was present.

10^3[Peracetic acid]/M	$10^3 kobs/s^{-1}$
0.000	5.554×10^{-3}
0.794	3.163
1.144	4.699
1.245	5.197
1.474	5.541
1.532	5.980

Table 3.7 Observed first order rate constants (kobs) for the reaction between diacetyl peroxide and hydrogen peroxide. Conditions were: pH 6.80 sodium dihydrogen phosphate - disodium hydrogen phosphate buffer (I = 0.02M); [diacetyl peroxide] ranging from 1.93×10^{-4} to 3.88×10^{-4}M; 25°C; no EDTA was present.

$10^3[H_2O_2]$/M	10^3kobs/s^{-1}
0.000	9.695×10^{-2}
4.465	1.787
6.282	2.238
8.077	3.157
9.872	3.605
11.667	4.272

Table 3.8 Initial (o) and infinity (∞) concentrations of peracetic acid (PA) for the reaction between diacetyl peroxide and hydrogen peroxide. Conditions were those listed in table 3.7.

$10^3[H_2O_2]$/M	$10^3[PA]_o$/M	$10^3[PA]_\infty$/M	$10^3(([PA]_\infty - [PA]_o)/2 + [PA]_o)$/M
4.465	0.924	1.699	1.311
6.282	1.017	1.655	1.336
8.077	1.068	1.594	1.331
9.872	1.098	1.561	1.329
11.667	1.123	1.509	1.316

Table 3.9 Observed first order rate constants (kobs) for the reaction between p-nitrophenylacetate and hydrogen peroxide. Conditions were: pH 10.00 sodium carbonate - sodium hydrogen carbonate buffer (I = 0.1M); [PNPA] = 1.0×10^{-5}M; [EDTA] = 1×10^{-4}M; 25°C.

$10^4[H_2O_2]$/M	10^2kobs/s^{-1}
1.320	1.492
2.660	2.700
4.407	4.210
6.170	5.730
7.930	7.831
9.690	9.129

Table 3.10 Observed first order rate constants (kobs) for the reaction between p-nitrophenylacetate and hydrogen peroxide. Conditions were: pH 9.24 sodium hydroxide - sodium borate buffer (I = 0.1M); [PNPA] = 4×10^{-5}M; [EDTA] = 1×10^{-4}M; 25°C.

$10^3[H_2O_2]$/M	10^2kobs/s^{-1}
4.98	2.225
9.96	4.349
14.94	6.328
19.92	7.817
24.90	10.310
29.88	11.720

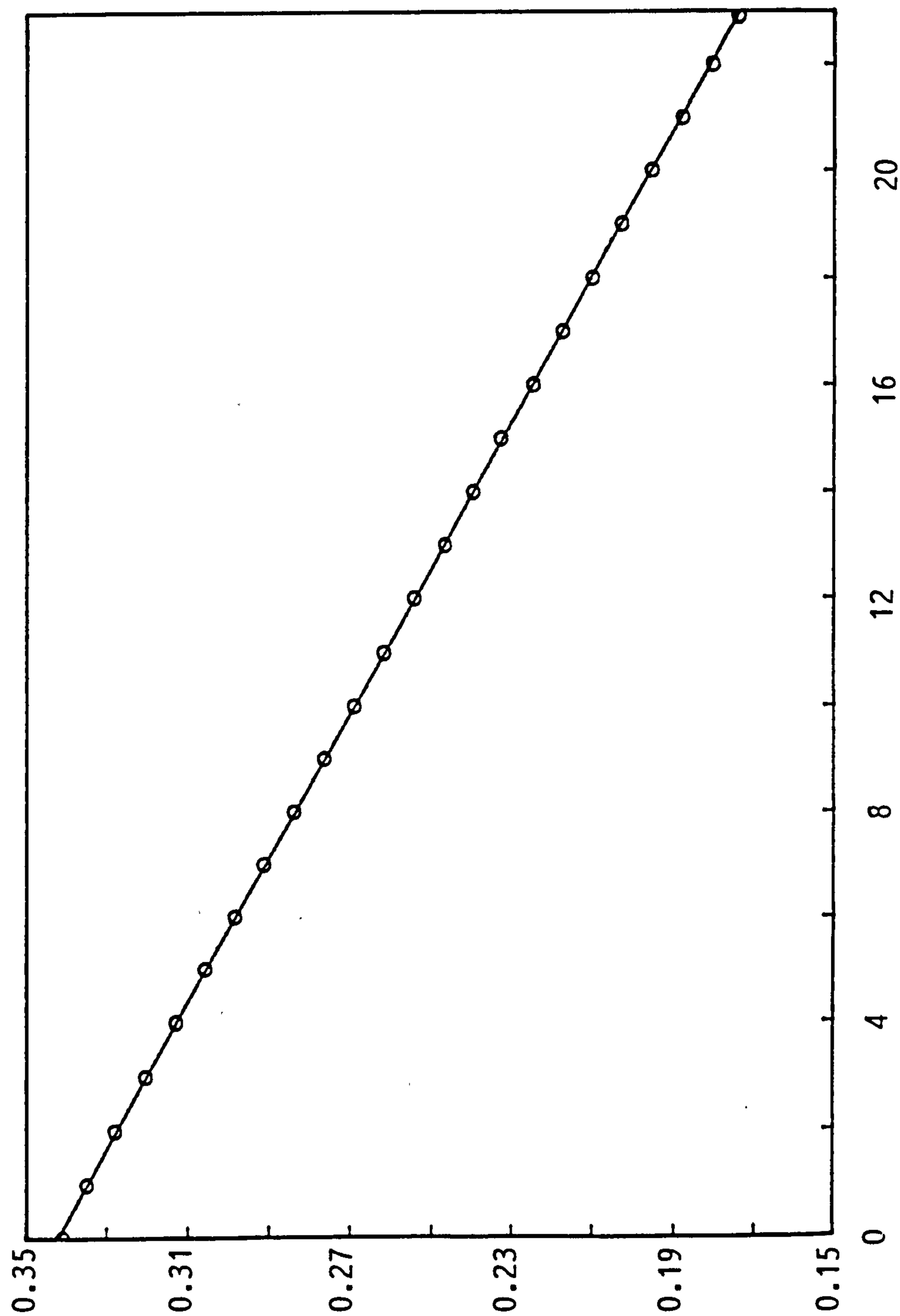

Figure 3.3 First order plot for the hydrolysis of p-nitrophenylacetate in a pH 6.80 sodium dihydrogen phosphate - disodium hydrogen phosphate buffer (I = 0.1M) at 25°C. [EDTA] = $1x10^{-5}$M. The line represents the best fit using the linear least squares method.

Figure 3.4 Plot showing the increase in absorbance at 400nm due to p-nitrophenol formation during the reaction between p-nitrophenylacetate and hydrogen peroxide: pH 6.80 phosphate buffer (I = 0.1M); $[PNPA]_o = 1.094 \times 10^{-4}$M; $[H_2O_2]$ as indicated on graph; 25°C; $[EDTA] = 1 \times 10^{-5}$M. The curves represent the best fits to Equation 3.2.

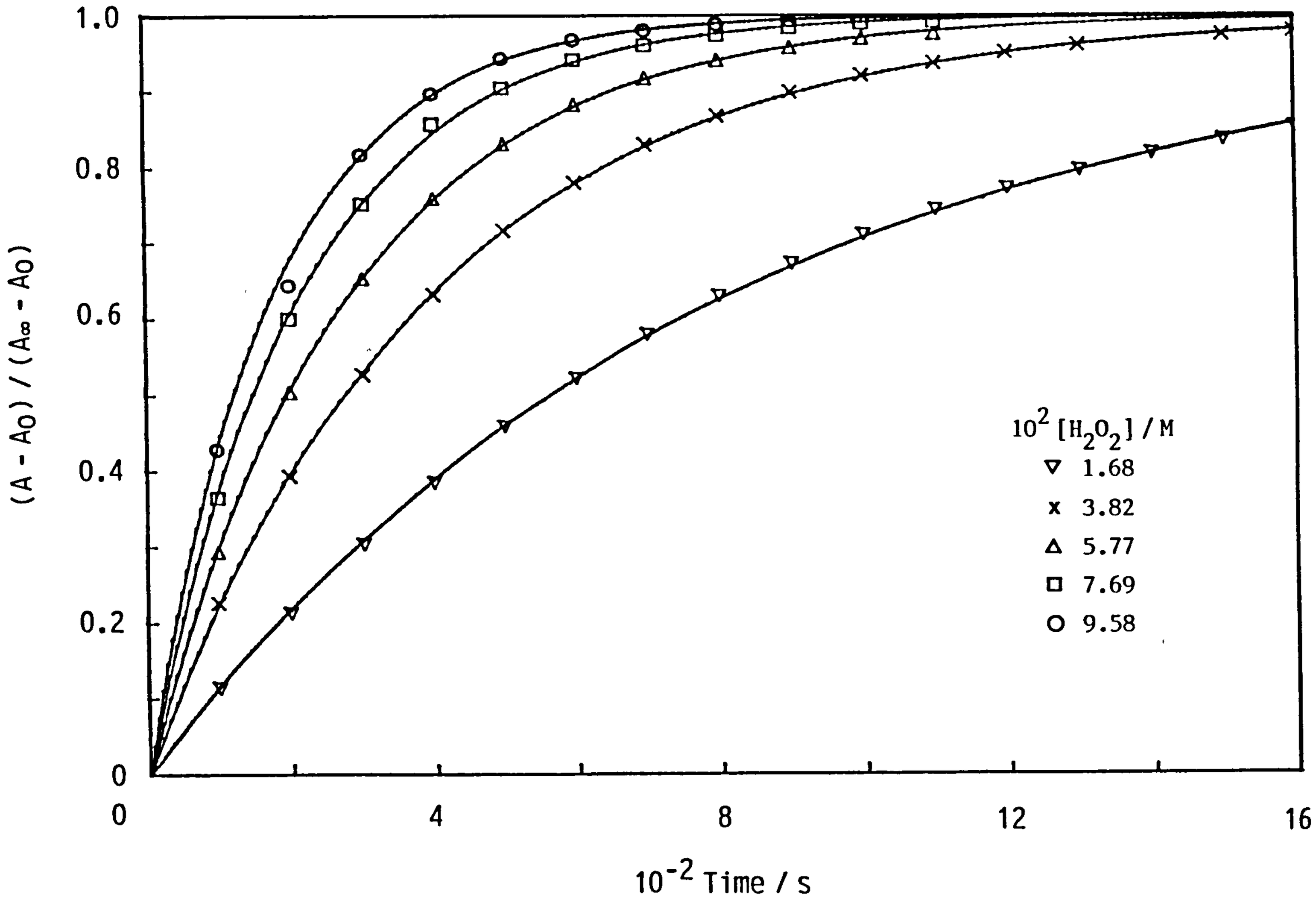

Figure 3.5 Plot showing the increase in absorbance at 400nm due to p-nitrophenol formation during the reaction between p-nitrophenylacetate and peracetic acid: pH 6.80 phosphate buffer (I = 0.1M); $[PNPA]_o = 0.901 \times 10^{-4}$M; [Peracetic acid] as indicated on graph; 25°C; $[EDTA] = 1 \times 10^{-5}$M. The curves represent the best fits to Equation 3.2.

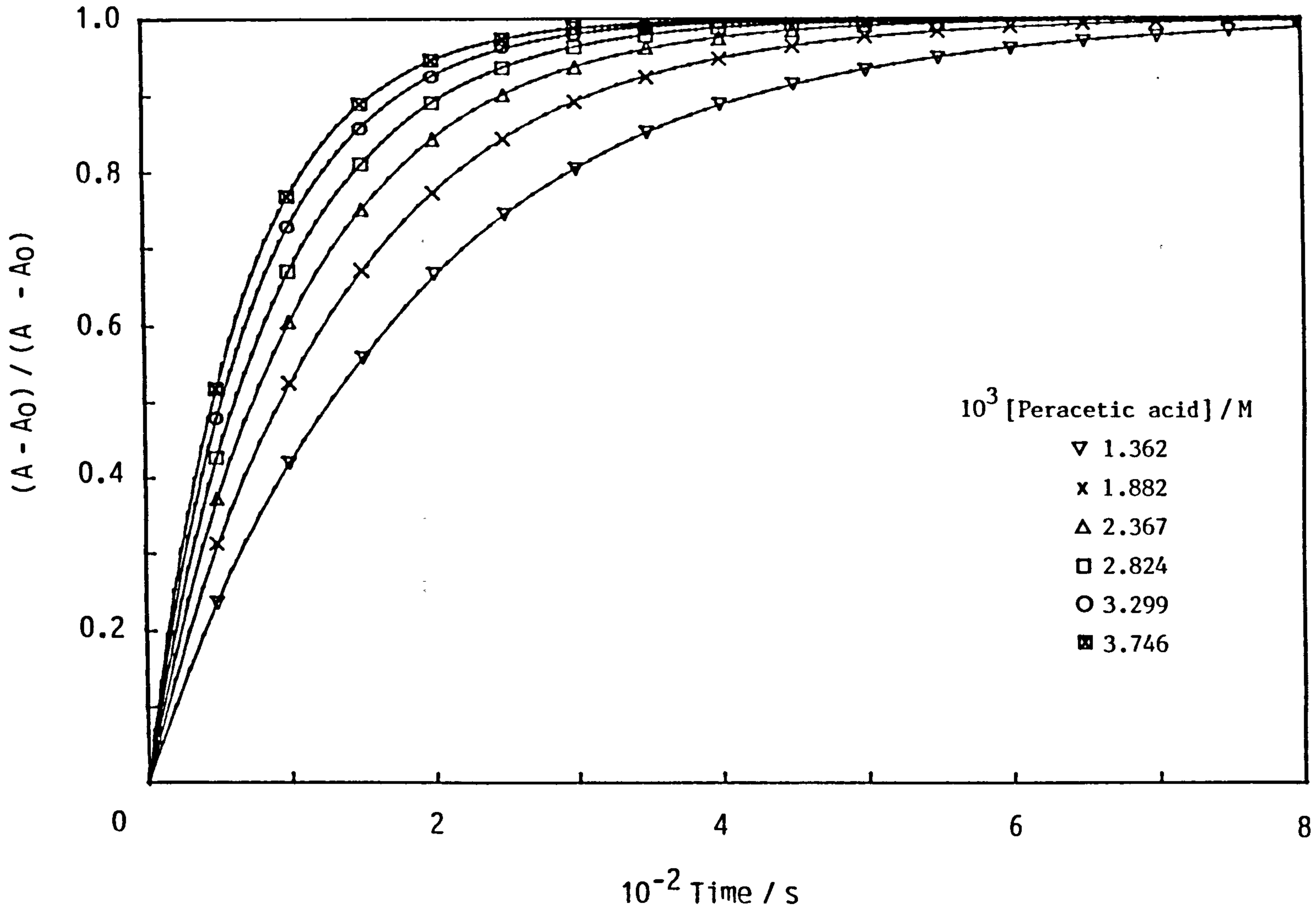

Figure 3.6 Plot of pseudo first order rate constant (kobs) against nucleophile concentration for the reaction between hydrogen peroxide and p-nitrophenylacetate. Conditions were: pH 6.80 sodium hydrogen phosphate - disodium hydrogen phosphate buffer (I = 0.1M) containing $1x10^{-5}$M EDTA; $[PNPA]_o = 1.094x10^{-4}$M; 25°C. The line represents the best fit using the linear least squares method.

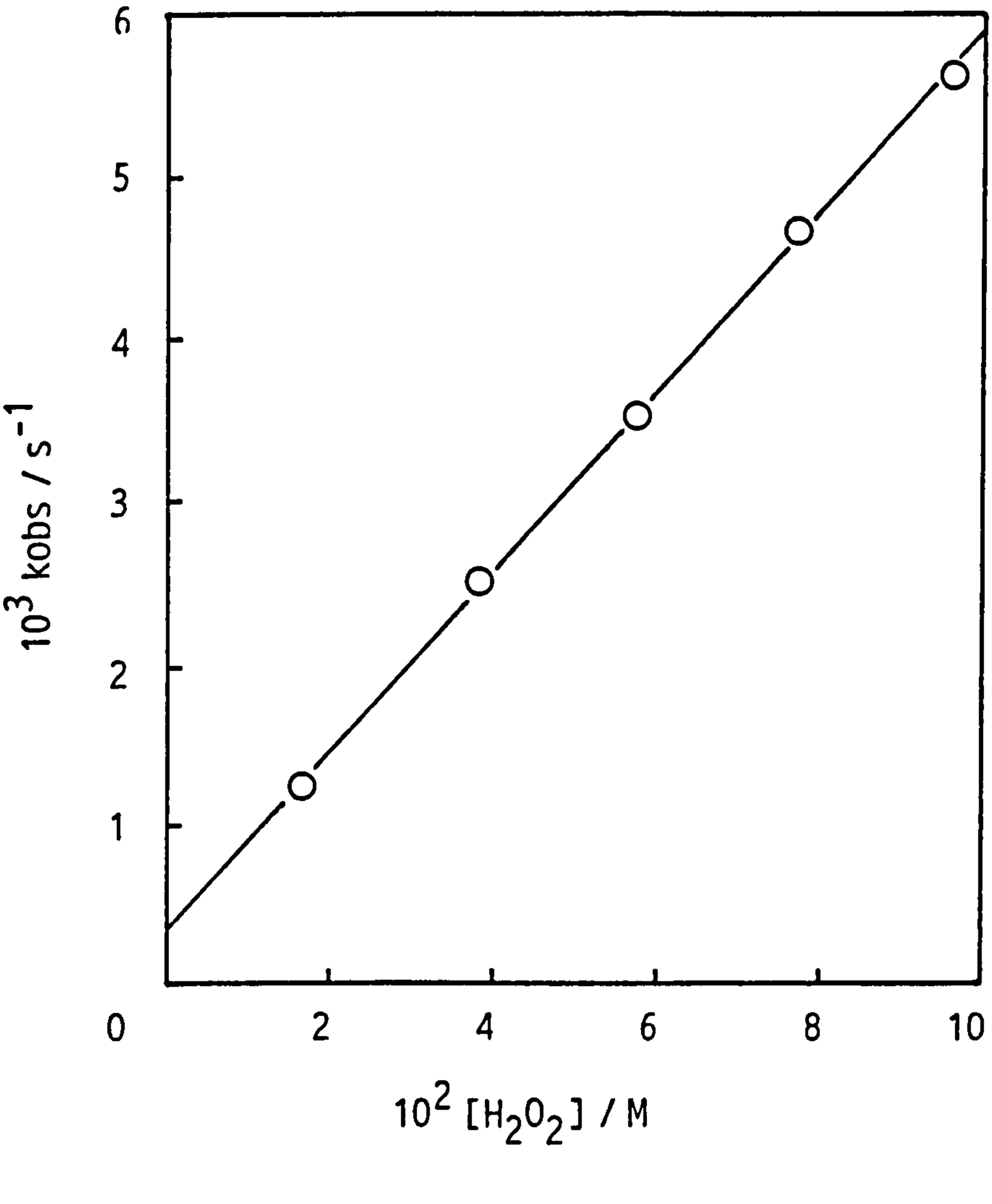

Figure 3.7 Second order plot of pseudo first order rate constant (kobs) against nucleophile concentration for the reaction between peracetic acid and p-nitrophenylacetate. Conditions were: pH 6.80 sodium dihydrogen phosphate - disodium hydrogen phosphate buffer (I = 0.1M) containing $1x10^{-5}$M EDTA; $[PNPA]_o = 0.901x10^{-4}$M; 25°C. The line represents the best fit using the linear least squares method.

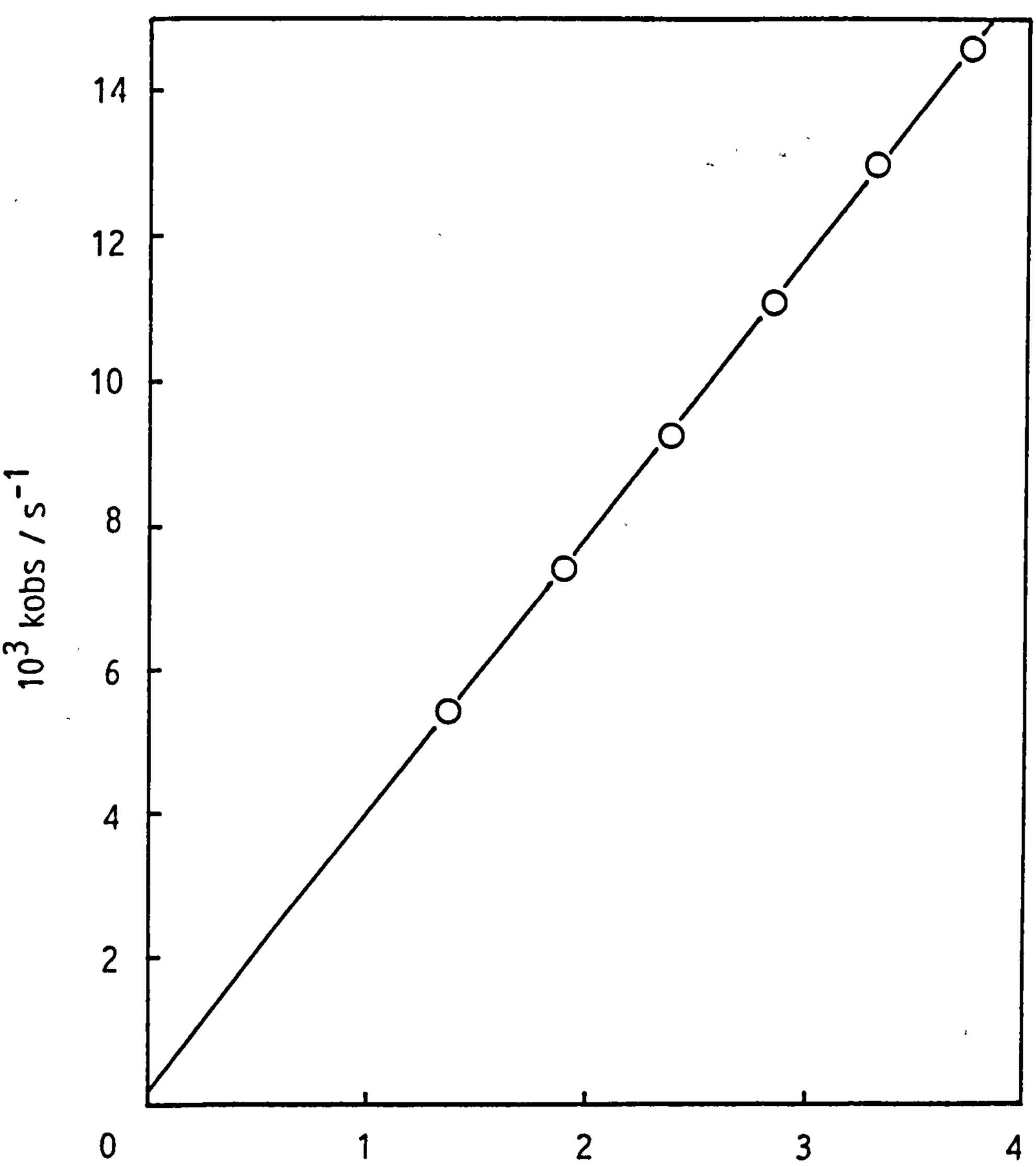

Figure 3.8 Change in the concentrations of peracetic acid, O, and p-nitrophenol, Δ, during and after the reaction between peracetic acid and p-nitrophenylacetate. Conditions were: pH 6.80 sodium dihydrogen phosphate - disodium hydrogen phosphate buffer (I = 0.1M) containing $1x10^{-5}$M EDTA; $[PNPA]_o = 4.9x10^{-4}$M; $[peracetic\ acid]_o = 9.2x10^{-4}$M; 25°C. The curve represents the best fit to equation 3.3.

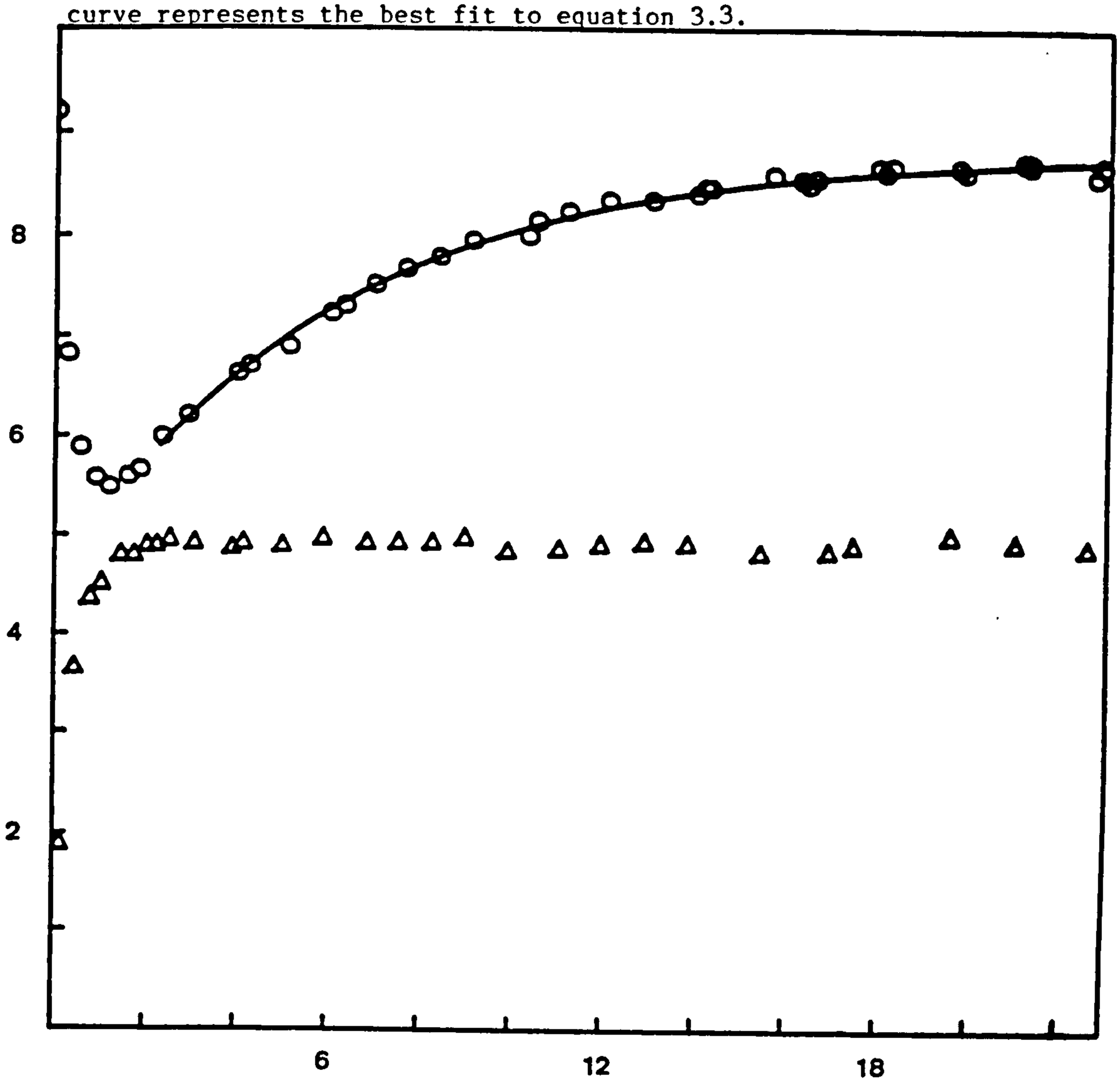

Figure 3.9 Increase in the concentration of peracetic acid after addition of excess hydrogen peroxide to diacetyl peroxide. Conditions were: pH 6.80 sodium dihydrogen phosphate - disodium hydrogen phosphate buffer (I = 0.1M); $[H_2O_2] = 5.06 \times 10^{-3}$M; [EDTA] = 1×10^{-5}M. The curve represents the best fit to equation 3.3 with [peracetic acid] = 6.77×10^{-4}M and kobs = 2.49×10^{-3} s^{-1}.

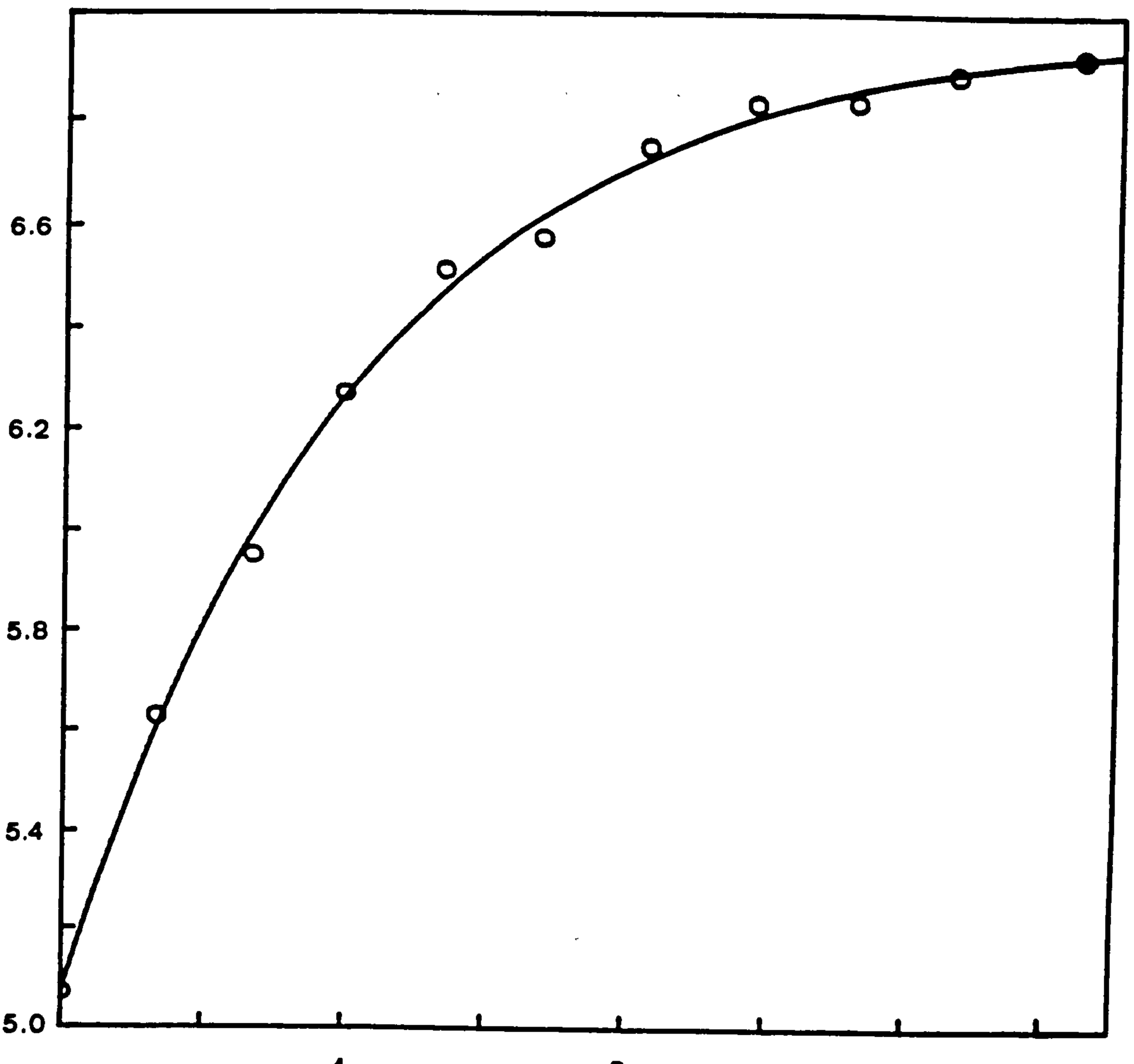

Figure 3.10 Plot of pseudo first order rate constant (kobs) against nucleophile concentration for the reaction between hydrogen peroxide and diacetyl peroxide. Conditions were: pH 6.80 sodium dihydrogen phosphate - disodium hydrogen phosphate buffer (I = 0.1M) containing $1x10^{-5}$M EDTA; $[diacetyl\ peroxide]_o$ ranging from $0.58x10^{-4}$ to $2.25x10^{-4}$M; 25°C. The line represents the best fit using the linear least squares method.

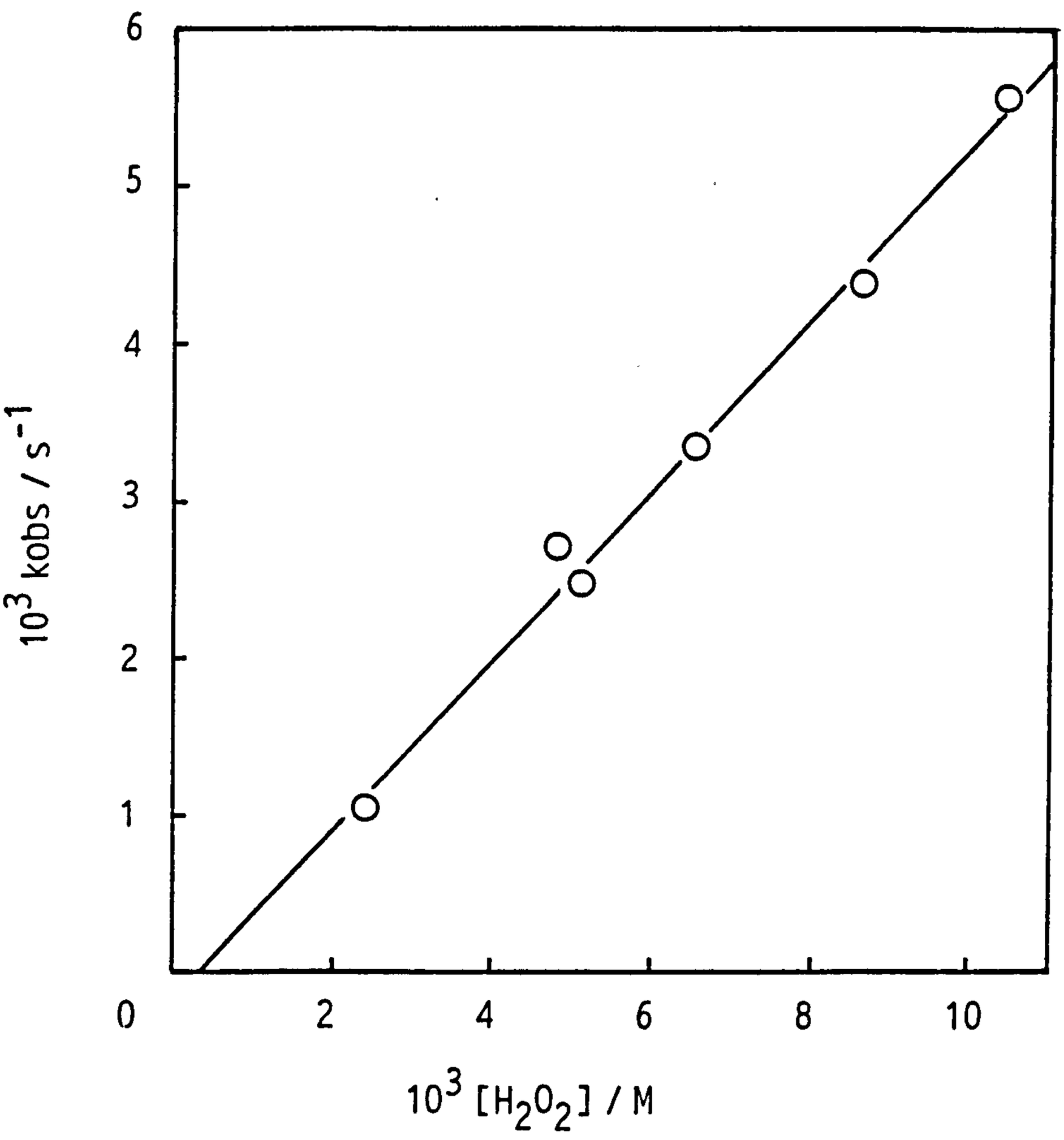

Figure 3.11 First order plot for the hydrolysis of p-nitrophenylacetate in a pH 6.80 sodium dihydrogen phosphate - disodium hydrogen phosphate buffer (I = 0.02M) at 25°C. No EDTA was present. The line represents the best fit using the linear least squares method.

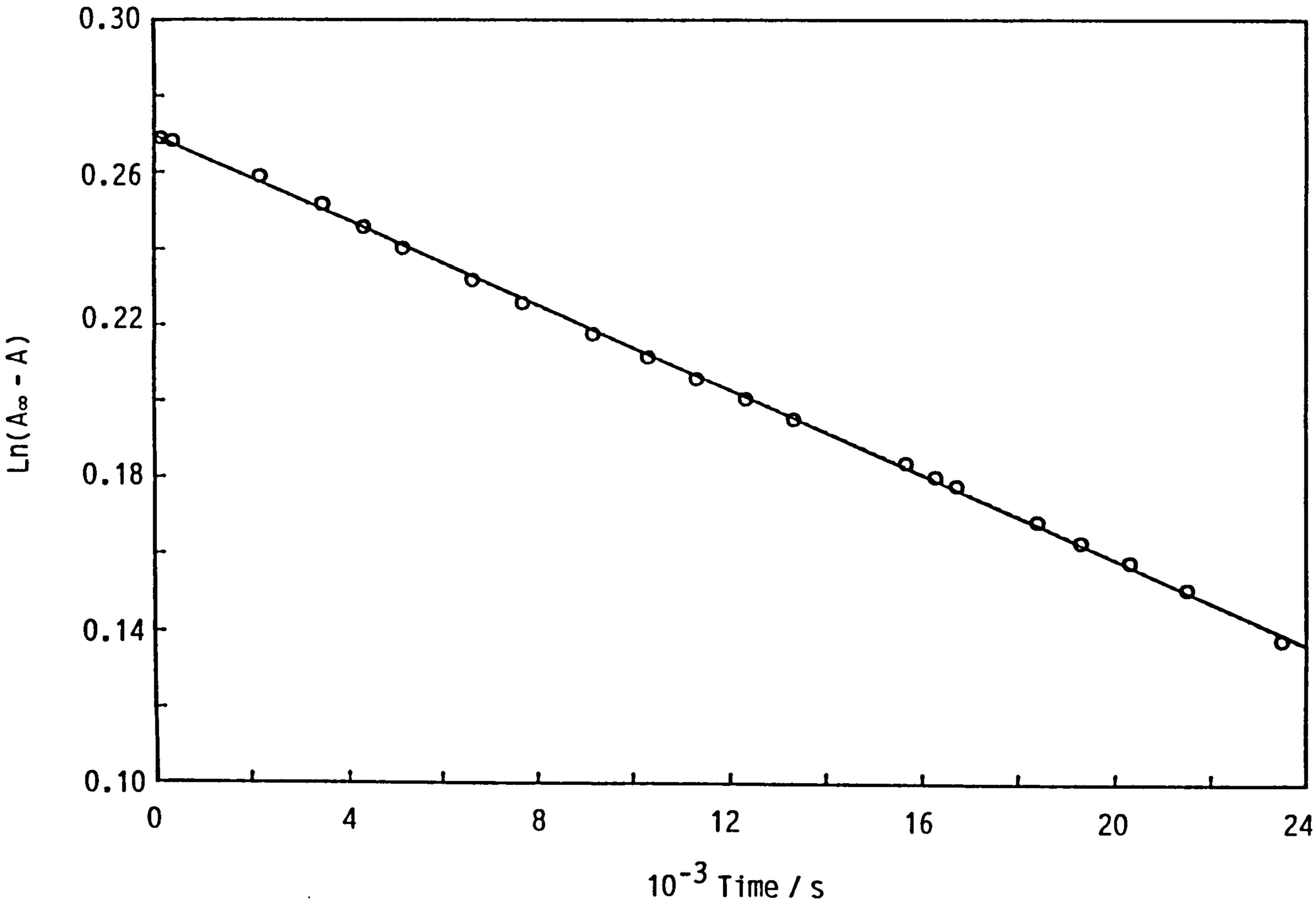

Figure 3.12 Plot showing the increase in absorbance at 400nm due to p-nitrophenol formation during the reaction between p-nitrophenylacetate and excess hydrogen peroxide. Conditions were: pH 6.80 sodium dihydrogen phosphate - disodium hydrogen phosphate buffer (0.02M); $[PNPA]_o = 0.833 \times 10^{-4}$M; [hydrogen peroxide] as indicated on graph; 25°C; No EDTA.

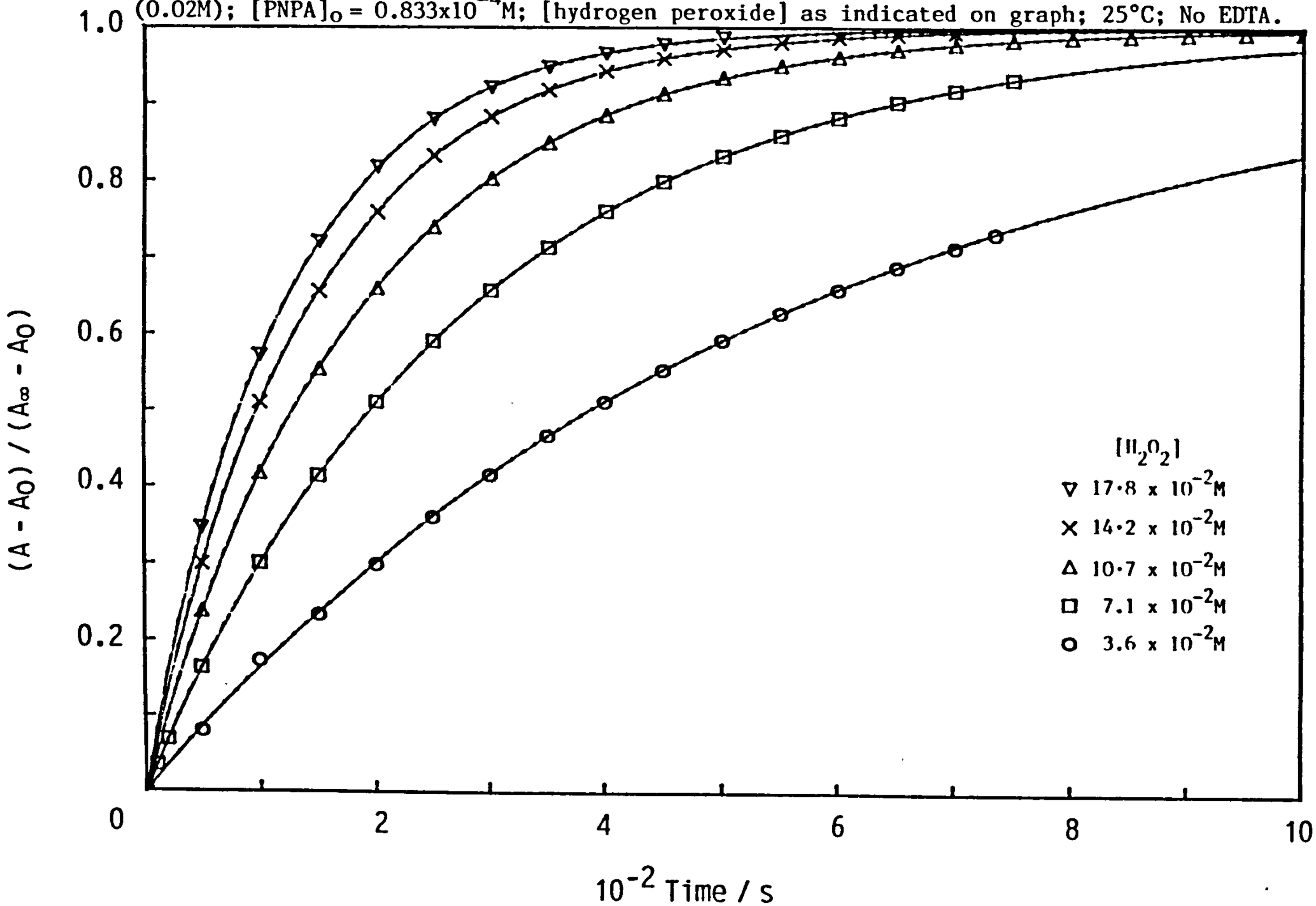

Figure 3.13 Plot showing the increase in absorbance at 400nm due to p-nitrophenol formation during the reaction between p-nitrophenylacetate and excess peracetic acid. Conditions were: pH 6.80 sodium dihydrogen phosphate - disodium hydrogen phosphate buffer ($I = 0.02M$); $[PNPA]_o = 0.833 \times 10^{-4}M$; [peracetic acid] as indicated on graph; 25°C. No EDTA.

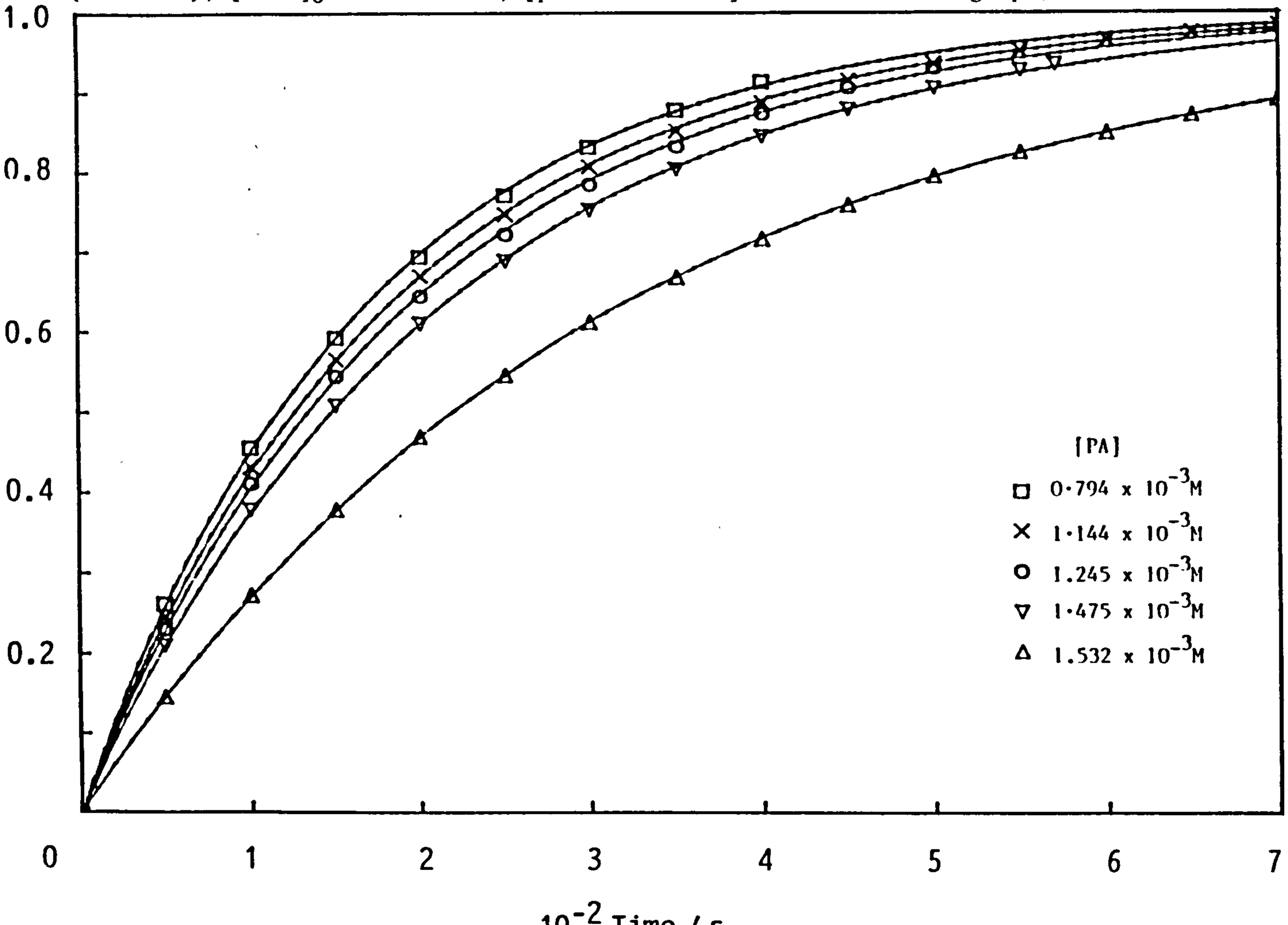

Figure 3.14 Plot of pseudo first order rate constant (kobs) against nucleophile concentration for the reaction between hydrogen peroxide and p-nitrophenylacetate. Conditions were: pH 6.80 sodium dihydrogen phosphate - disodium hydrogen phosphate buffer (I = 0.02M); $[PNPA]_o = 0.833 \times 10^{-4}$M; 25°C; no EDTA was present. The line represents the best fit using the linear least squares method.

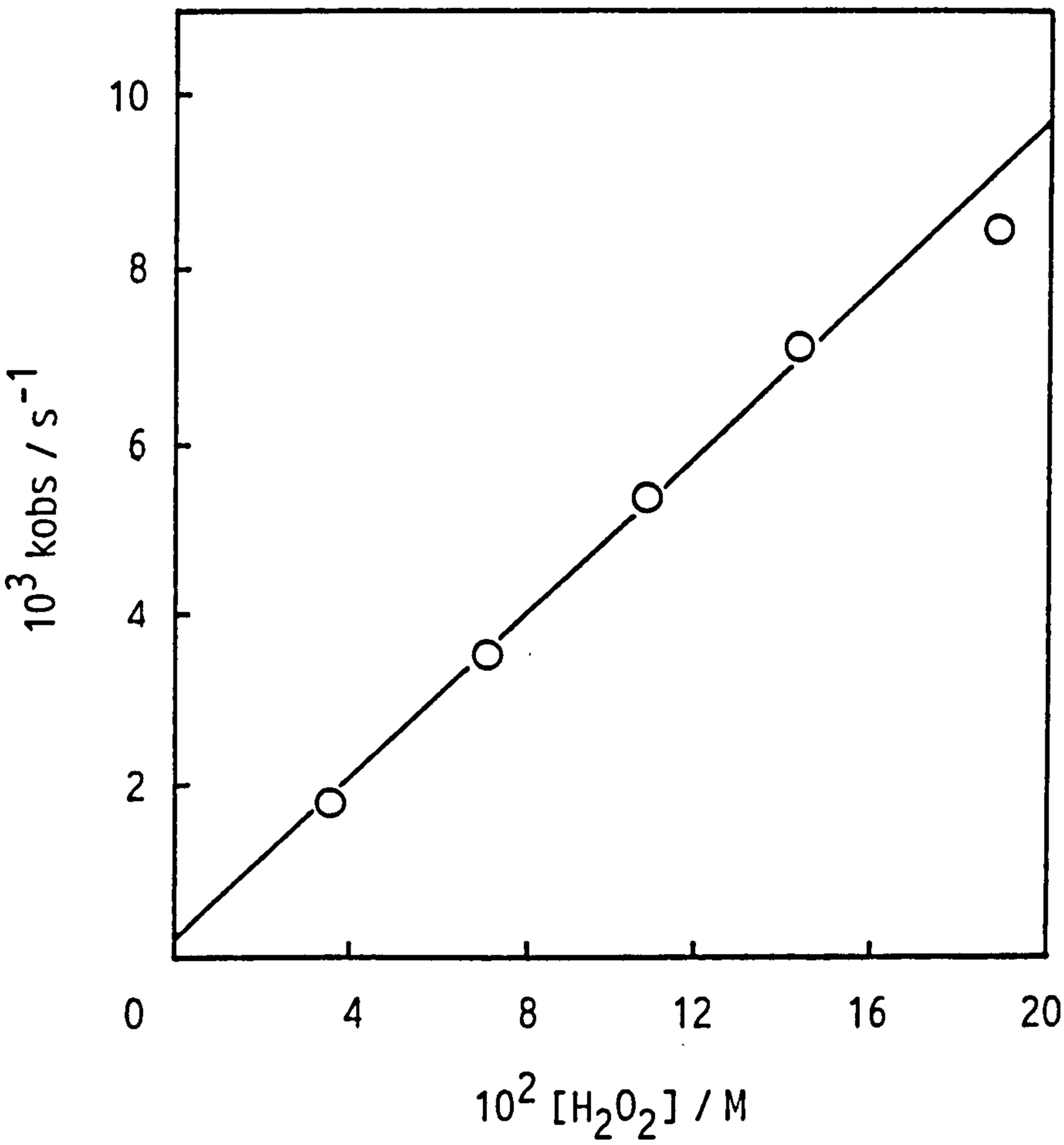

Figure 3.15 Plot of pseudo first order rate constant (kobs) against nucleophile concentration for the reaction between peracetic acid and p-nitrophenylacetate. Conditions were: pH 6.80 sodium dihydrogen phosphate - disodium hydrogen phosphate buffer (I = 0.02M); $[PNPA]_o = 0.833 \times 10^{-4}$M; 25°C; no EDTA was present. The line corresponds to the mean value of kobs (corrected for hydrolysis) devided by the nucleophile concentration.

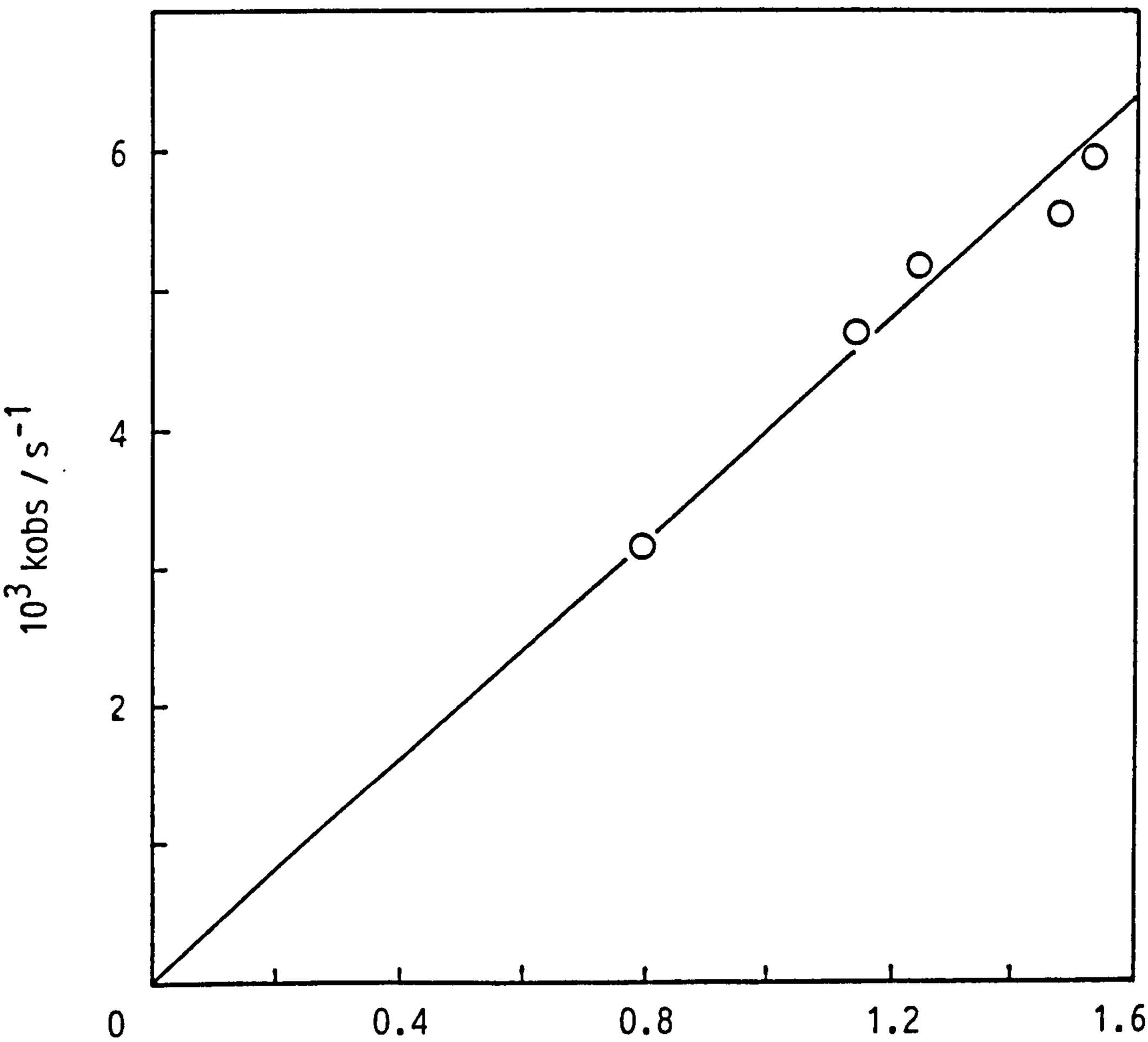

Figure 3.16 Change in the concentrations of peracetic acid, O, and p-nitrophenol, □, during and after the reaction between peracetic acid and p-nitrophenylacetate. Conditions were: pH 6.80 sodium dihydrogen phosphate - disodium hydrogen phosphate buffer (I = 0.02M); $[PNPA]_o = 0.9C3 \times 10^{-4}$M; [peracetic acid]$_o = 1.832 \times 10^{-3}$M; 25°C. No EDTA was present.

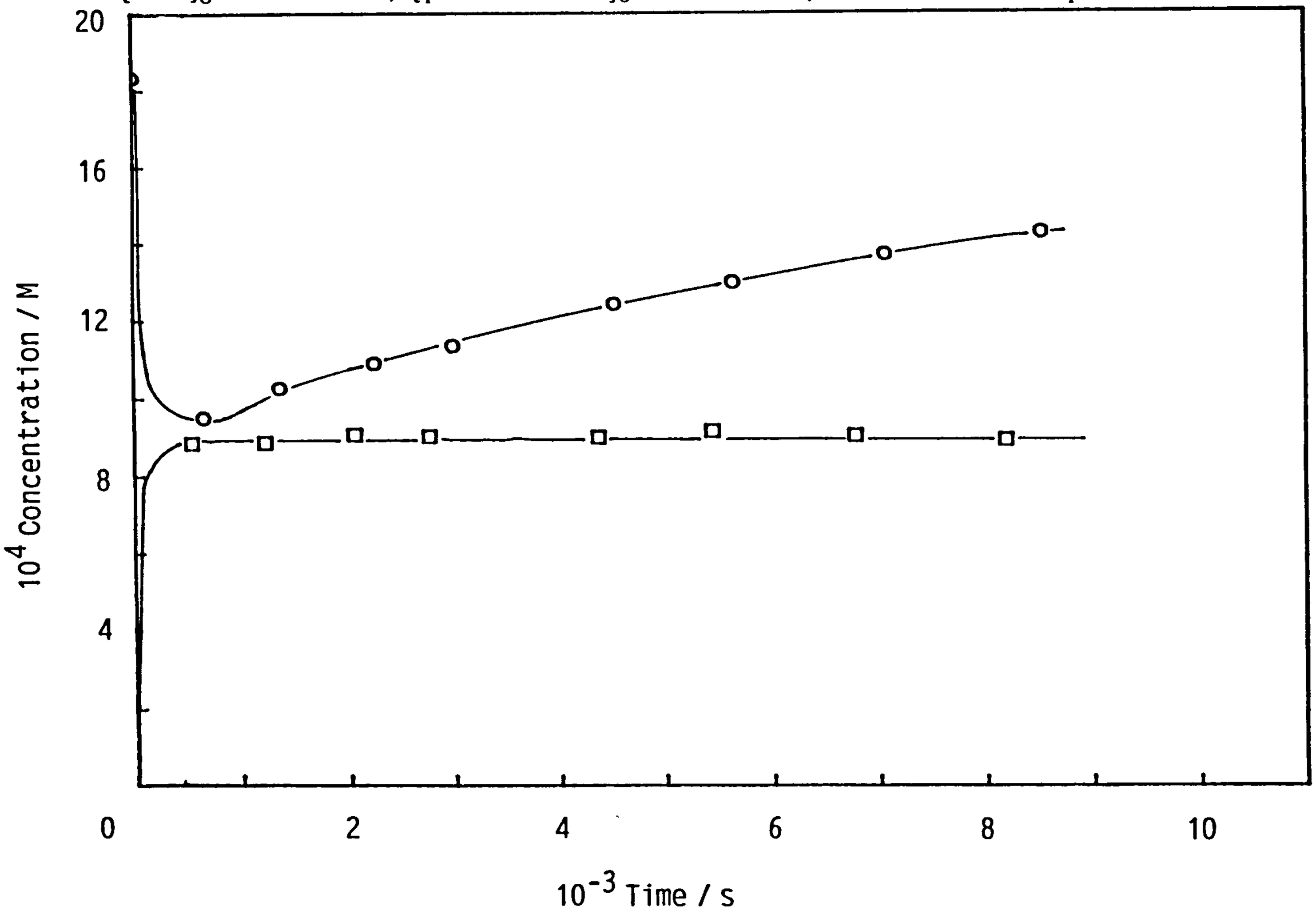

Figure 3.17 Increase in the concentration of peracetic acid after the addition of excess hydrogen peroxide to diacetyl peroxide.Conditions were: pH 6.80 sodium dihydrogen phosphate – disodium hydrogen phosphate buffer (I = 0.02M); $[H_2O_2] = 4.465 \times 10^{-3}$M; 25°C. No EDTA was present. The curve respresents the best fit to Eqn 3.3.

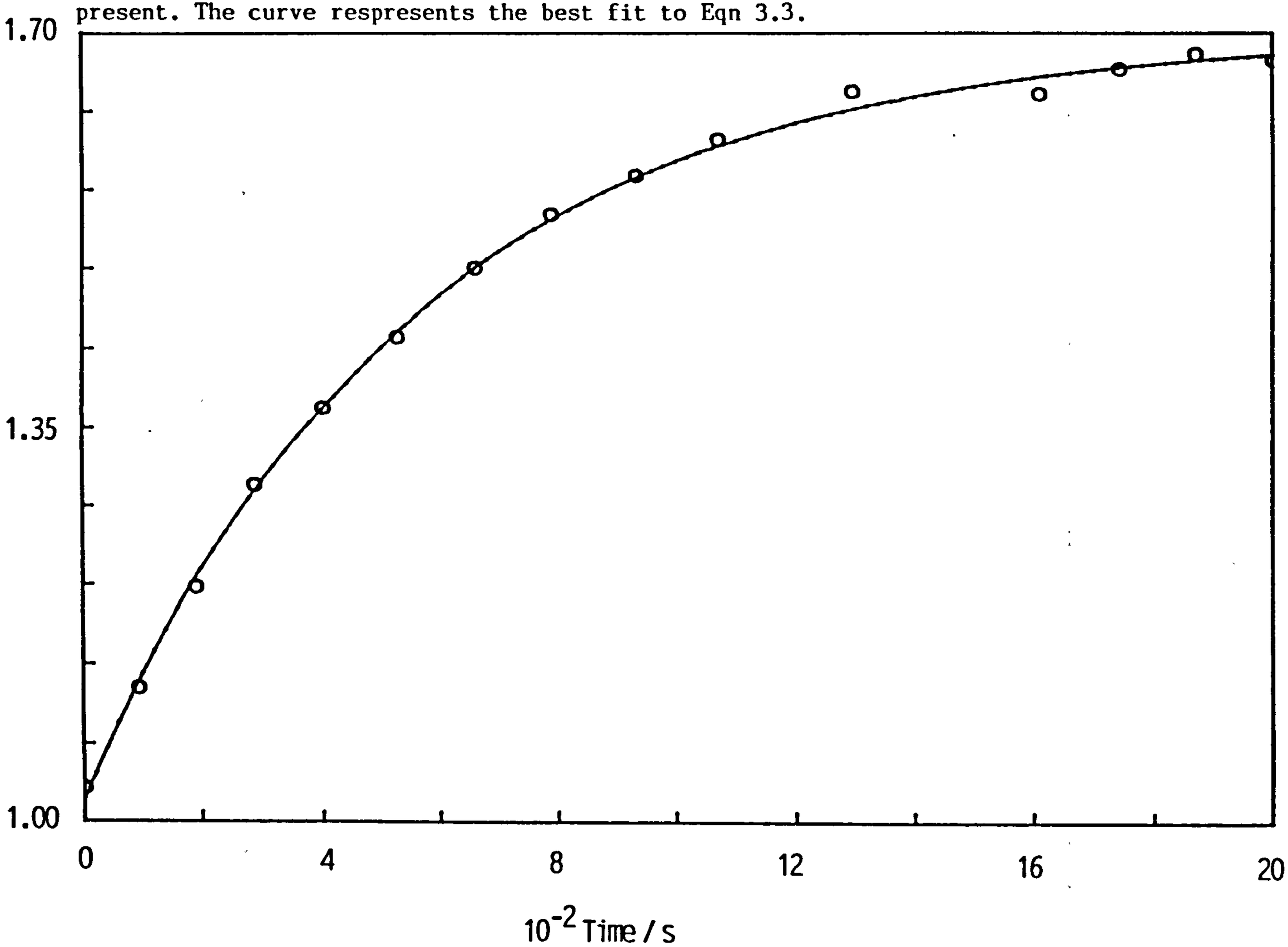

Figure 3.18 Plot of pseudo first order rate constant (kobs) against nucleophile concentration for the reaction between hydrogen peroxide and diacetyl peroxide. Conditions were: pH 6.80 sodium dihydrogen phosphate - disodium hydrogen phosphate buffer (I = 0.02M); [diacetyl peroxide]$_o$ ranging from 1.93×10^{-4} to 3.88×10^{-4}M; 25°C; no EDTA was present. The line represents the best fit using the linear least squares method.

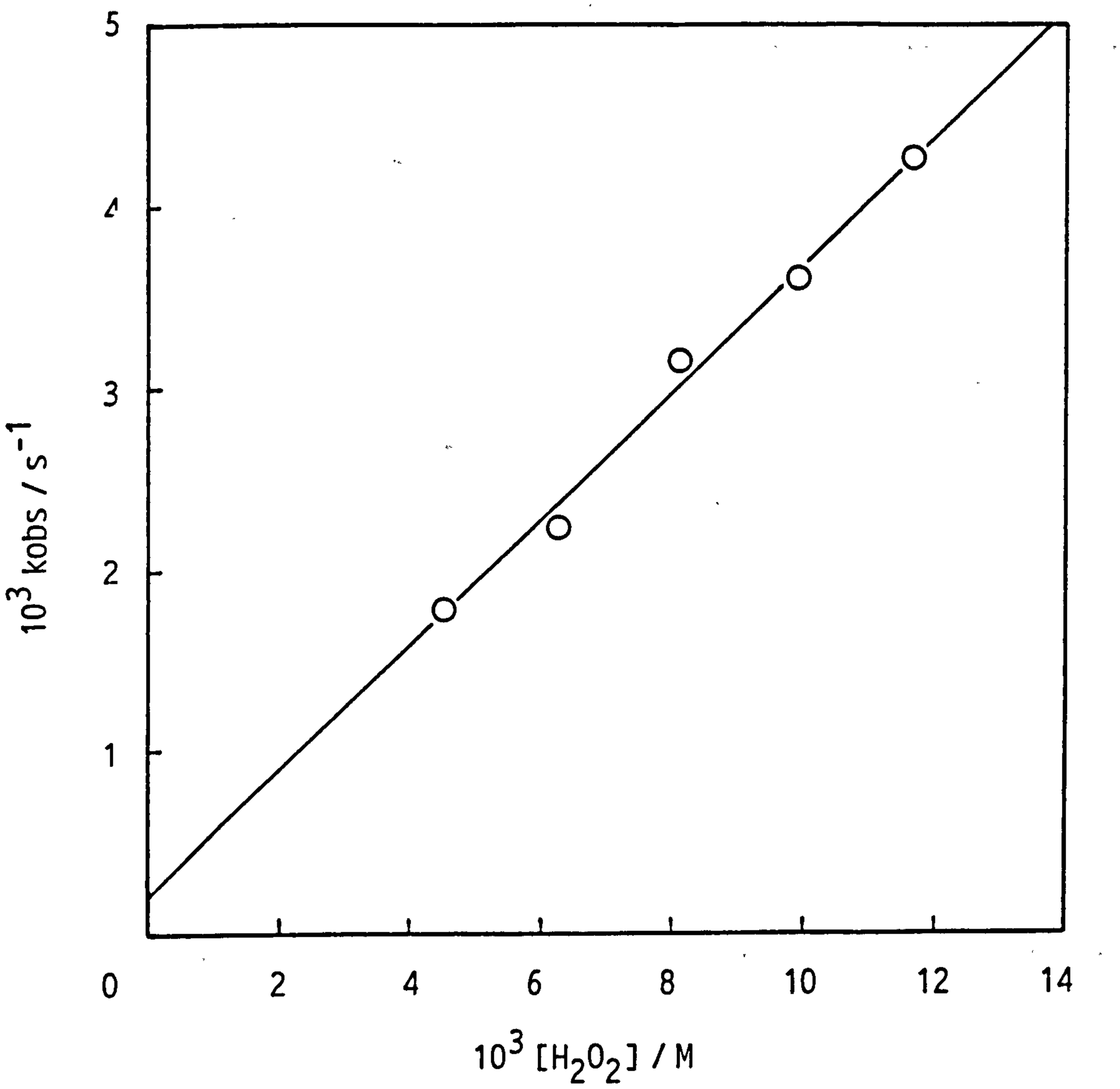

Figure 3.24 Pseudo first order plots for the reaction between p-nitrophenylacetate and hydrogen peroxide. Conditions were: pH 10.00 sodium carbonate - sodium hydrogen carbonate buffer (I = 0.1M) containing $1x10^{-4}$M EDTA; $[PNPA]_o = 1x10^{-5}$M; [hydrogen peroxide] ranging from $1.32x10^{-4}$M to $9.69x10^{-4}$M; 25°C. The lines represent the best fit using the linear least squares method*.

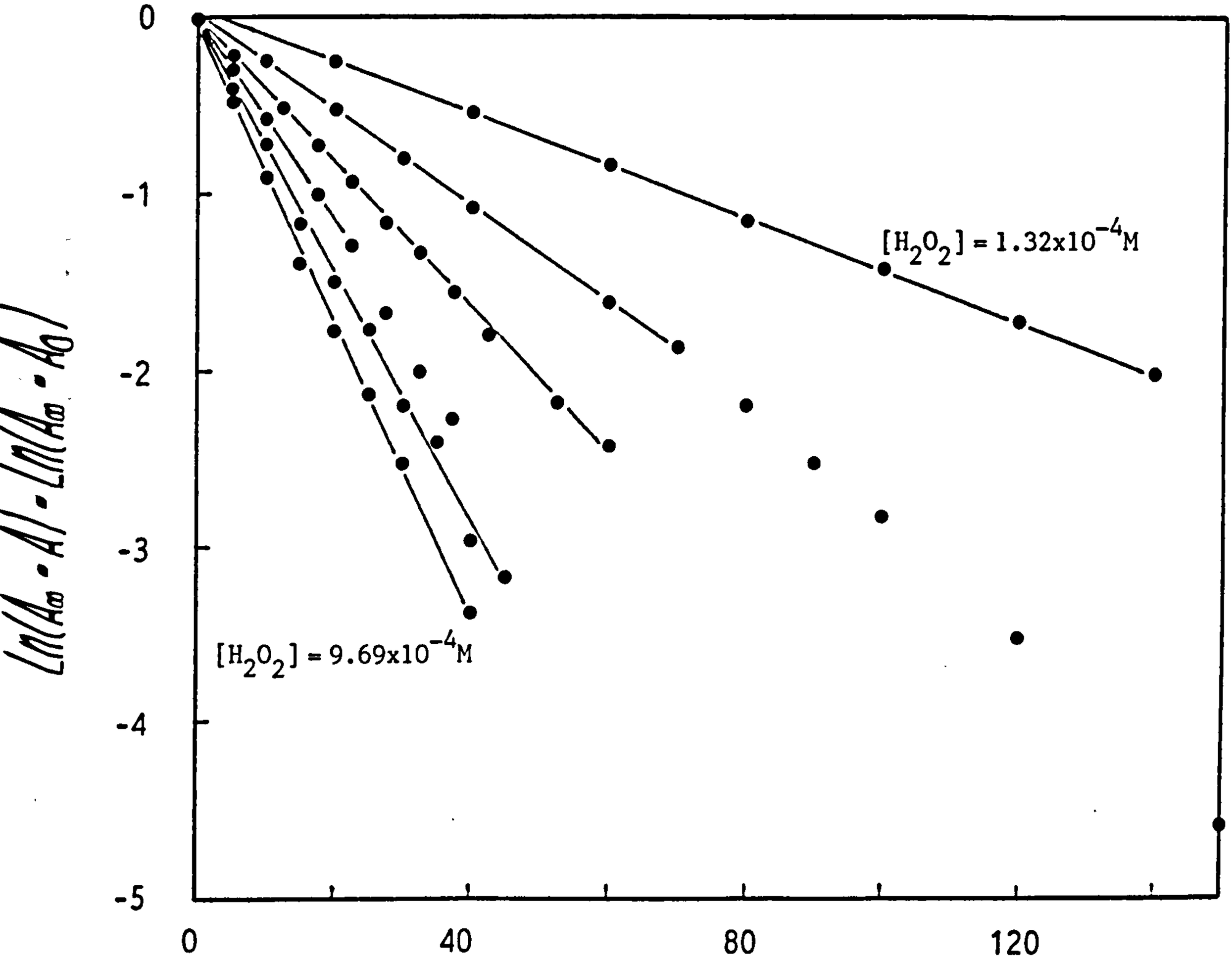

*Only data in the initial linear region of the plots was used.

Figure 3.25 Pseudo first order plots for the reaction between p-nitrophenylacetate and hydrogen peroxide. Conditions were: pH 9.24 sodium hydroxide - sodium borate buffer (I = 0.1M) containing $1x10^{-4}$M EDTA; $[PNPA]_o = 4x10^{-5}$M; [hydrogen peroxide] ranging from $4.98x10^{-3}$M to $29.88x10^{-3}$M; 25°C. The lines represent the best fit using the linear least squares method for data in the initial linear region of the plot.

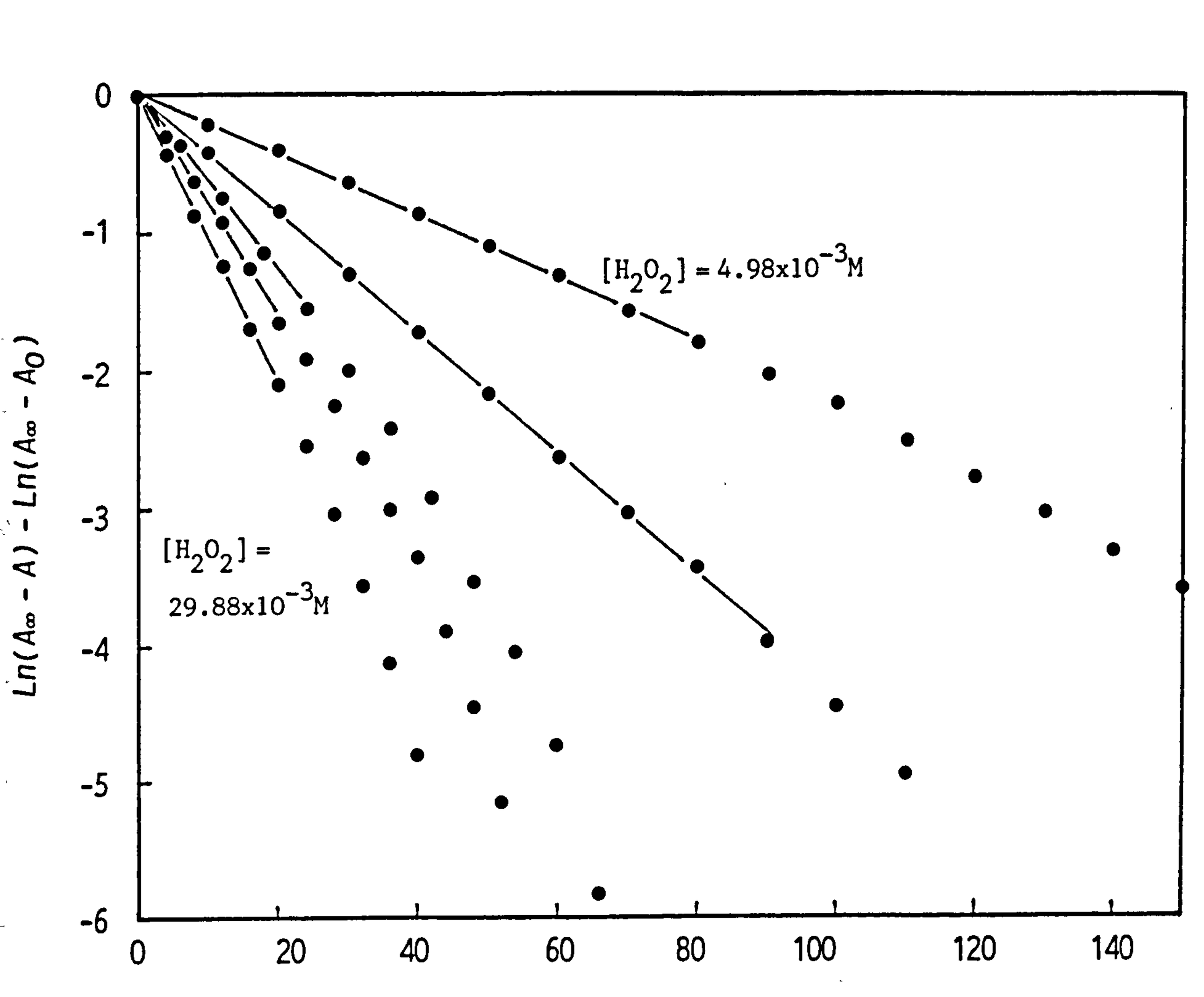

Figure 3.26 Second order plot of pseudo first order rate constant (kobs) against nucleophile concentration for the reaction between hydrogen peroxide and p-nitrophenylacetate. Conditions were: pH 9.24 sodium hydroxide - sodium borate buffer (I = 0.1M); $[PNPA]_o = 4x10^{-5}M$; $[EDTA] = 1x10^{-4}M$; 25°C. The line represents the best fit using the linear least squares method.

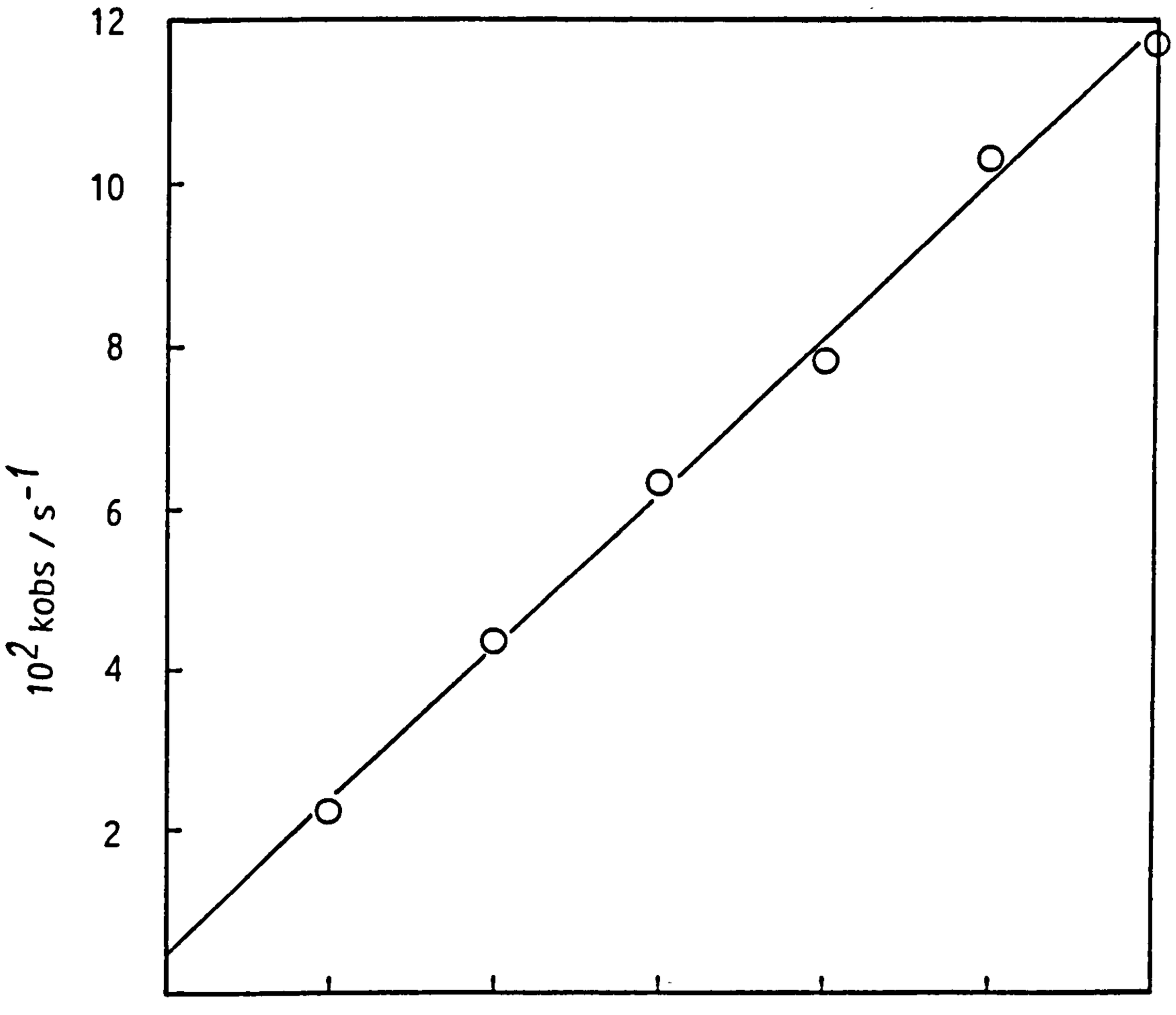

Figure 3.27 Second order plot for the reaction between p-nitrophenyl acetate and hydrogen peroxide. Conditions were: pH 10.00 sodium carbonate - sodium hydrogen carbonate buffer (I = 0.1M); $[PNPA]_o$ = $1x10^{-5}$M; [EDTA] = $1x10^{-4}$M; 25°C. The line represents the best fit using the linear least squares method.

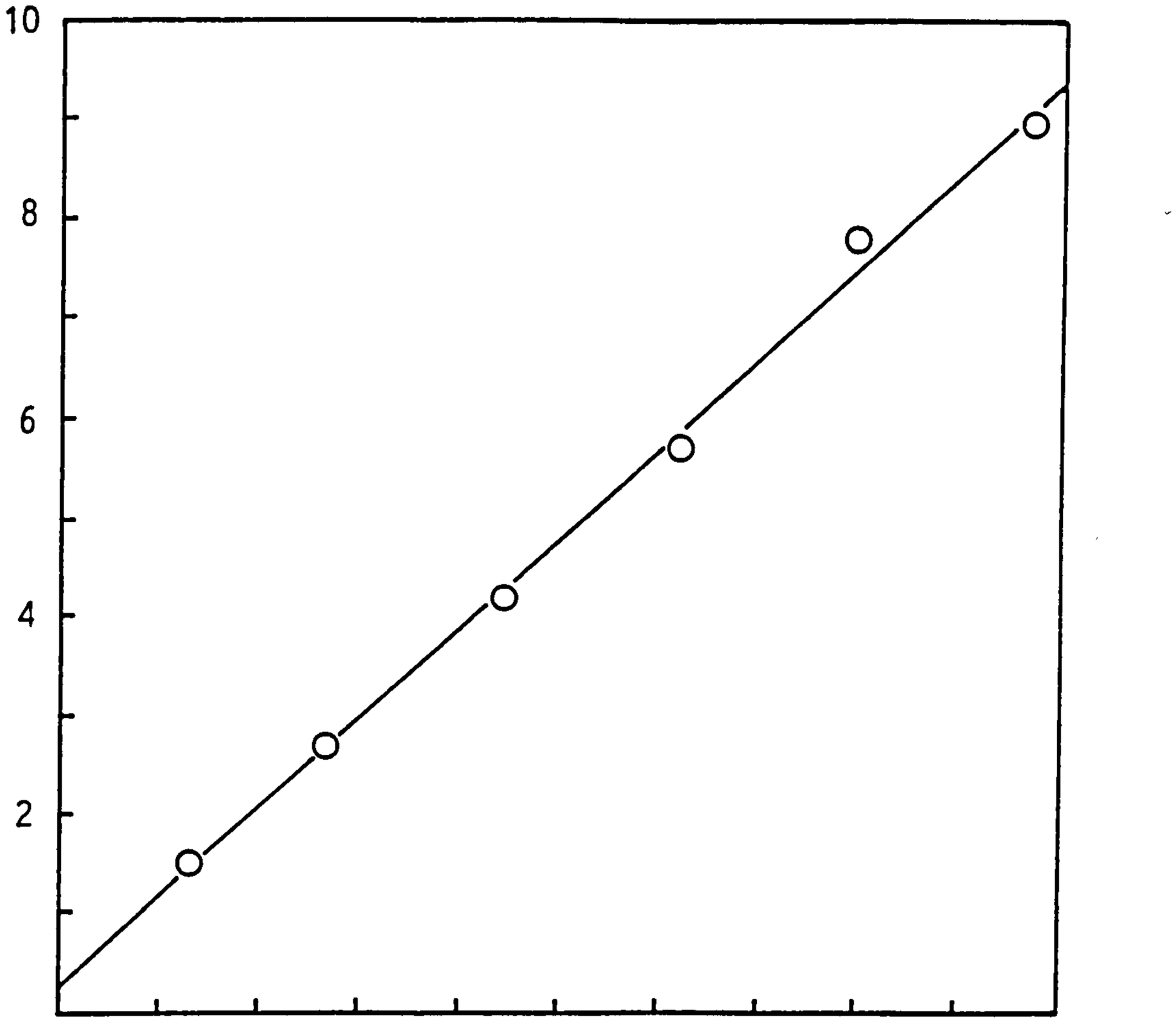

CHAPTER 4 A STUDY OF TETRAACETYL-ETHYLENEDIAMINE HYDROLYSIS

Having successfully elucidated the scheme for the reaction between hydrogen peroxide and PNPA, the methods and approach used in that study were applied to the study of the bleach activator tetraacetylethylenediamine (TAED). This chapter describes a study conducted into TAED hydrolysis: a particularly important reaction from a commercial point of view since it competes with the perhydrolysis reaction, thus reducing the yield of the desired product of bleach activation, peracetic acid. Structural aspects of TAED, obtained from crystalographic studies, are discussed in Section 4.1, and comparisons are made with other amides. Section 4.2 contains details of an initial spectrophotometric study which was conducted in order to determine rate constants for TAED hydrolysis; TAED undergoes hydrolysis to triacetylethylenediamine (TriAED), which, in turn, undergoes hydrolysis to the final product, diacetylethylenediamine (DAED). Section 4.3 describes a pH dependence study of TAED and TriAED hydrolysis. Two such studies were conducted, one at an ionic strength of 0.1 M, using sodium salts, and the second at an ionic strength of 1.0 M, using potassium salts. The latter study used isolated TriAED which was supplied by Warwick Chemicals Ltd. The hydrolysis data for this latter study was collected from the aminolysis, alcoholysis, and perhydrolysis experiments detailed in Chapters 6 and 7. Section 4.4 describes a study of the effect of carbonate buffer concentration on TriAED hydrolysis and, also, the effect of the cation used in the buffer solutions. Finally, Section 4.5 is a general discussion of TAED and TriAED hydrolysis.

In the experimental procedures described in this chapter, all absorbance measurements were made using the HP 8451 diode array spectrophotome-

ter, fitted with thermostatted cell holder. All absorbance measurements were within the region where the Beer-Lambert law was obeyed.

4.1 Crystalographic Studies of TAED

Crystalographic data for TAED were obtained from Warwick International Ltd. Molecular graphics used in this section were plotted using the CHEMOD computer facility of Warwick International Ltd.

Figure 4.1 shows the structure of TAED in crystaline form together with the bond angles and distances obtained from crystalographic analysis. Figure 4.2 (a-c) shows the crystal structure from three different perspectives, and Figure 4.2 (d) shows the charge distribution on the molecule (calculated using the Del Re program). The molecule consists of two approximately planar imide groups in the E,Z configuration separated by an ethylene group. The E,Z configuration is consistent with the studies of Lee and Kumler[166] who predicted this configuration for N-methyldiacetamide on the basis of the observed dipole moment (3.2D). They concluded that the presence of the bulky methyl groups does not allow the compound to assume the otherwise more favoured E,E conformation (predicted dipole moment of 2.6-2.9 D in dioxane). The presence of an approximately planar imide group in TAED is expected since, as discussed in Chapter 1, there is strong mesmerism involving the C = O) and C - N bond electrons which holds the group essentially flat, as with succinimide[27] (Scheme 4.1).

Figure 4.1

(a) Crystal structure for TAED

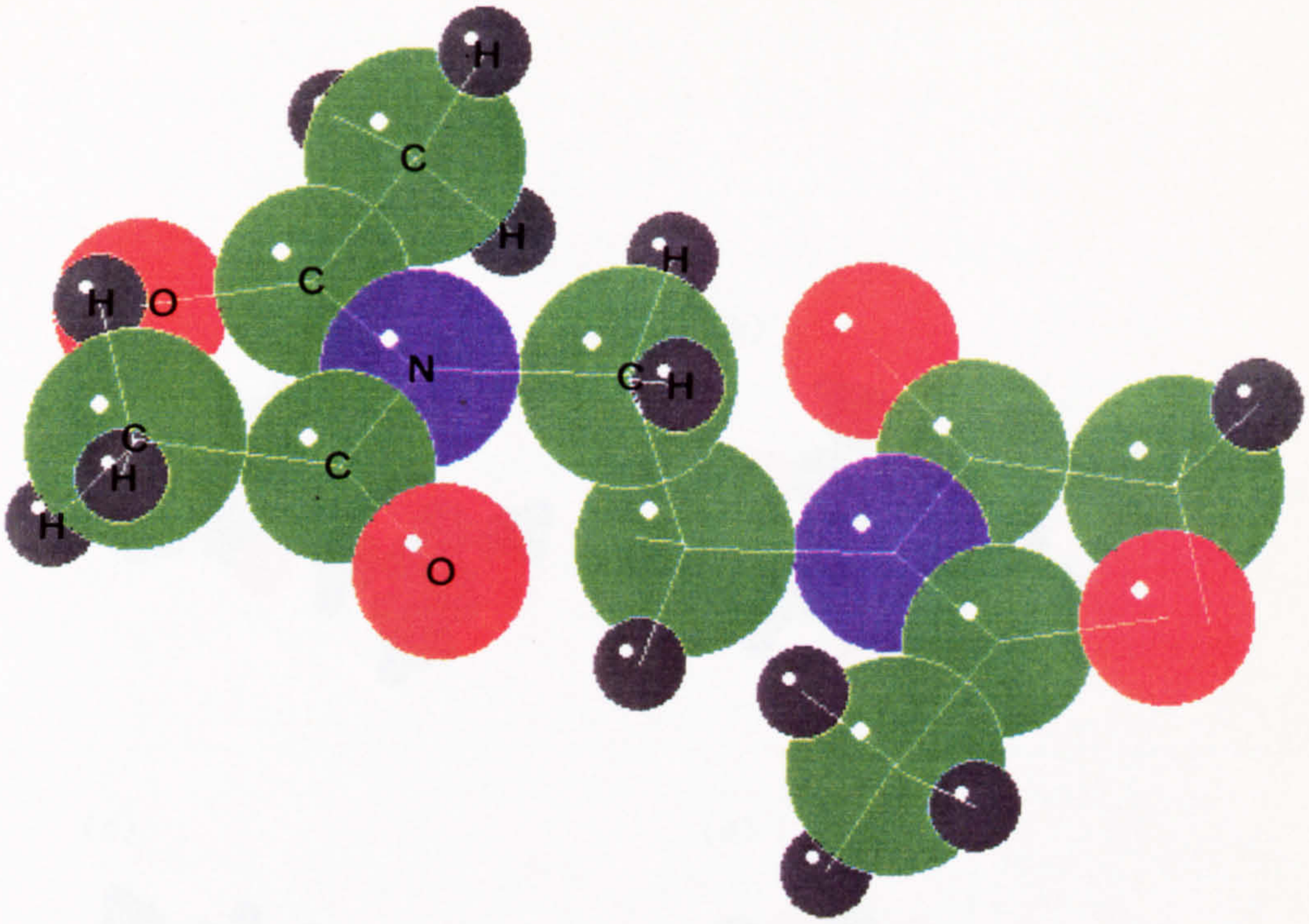

(b) Principal bond lengths and angles obtained from crystalographic analysis.

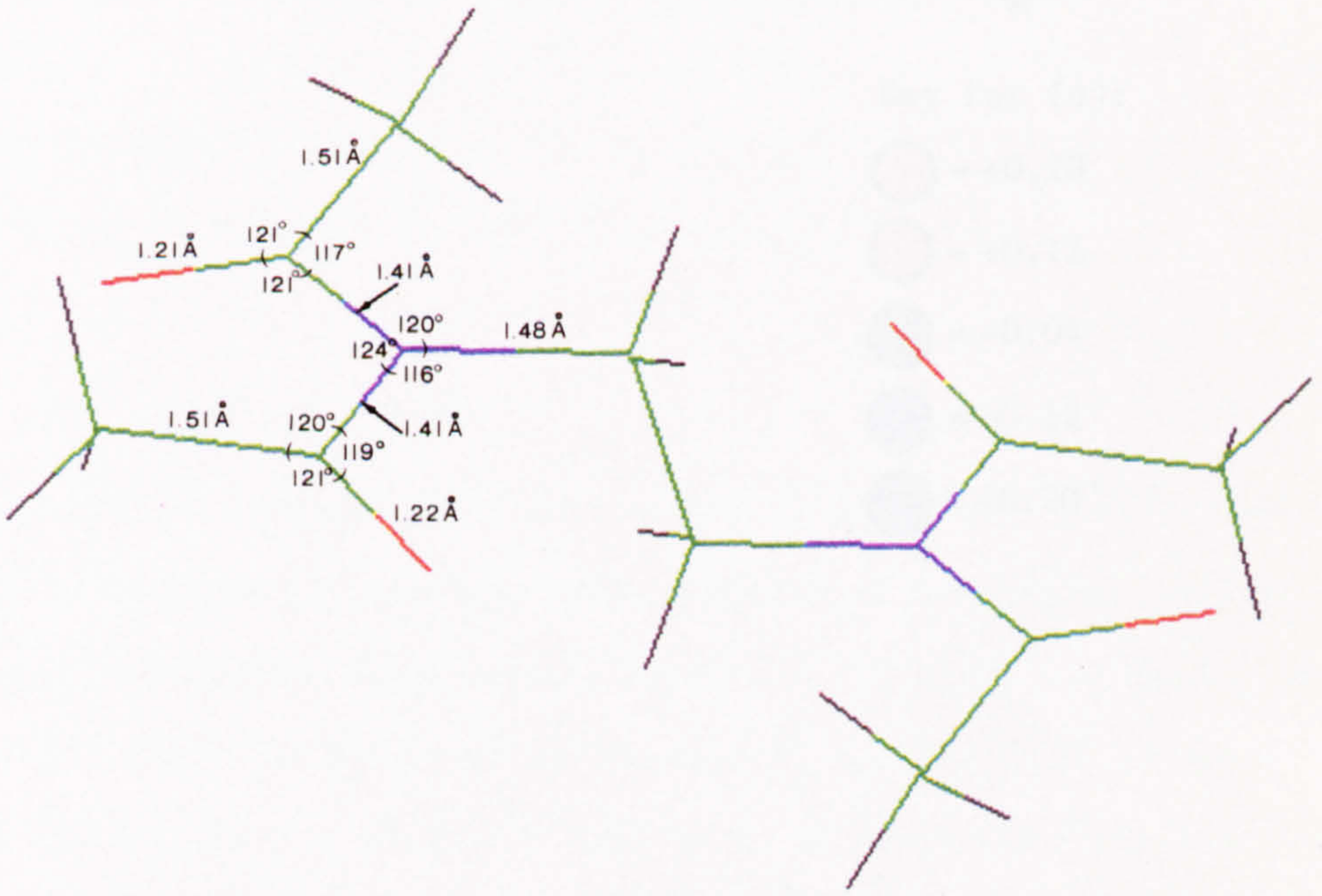

Figure 4.2 Crystal structure for TAED from three different perspectives (a - c) and charge distribution on the molecule calculated using the Del Re program (d).

(a)

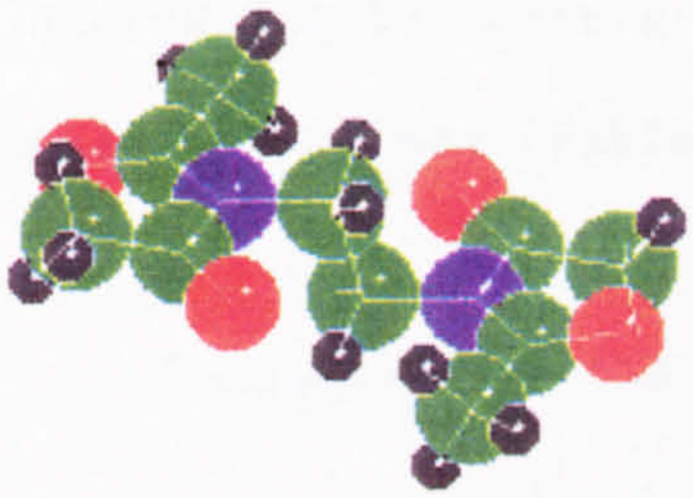

(b)

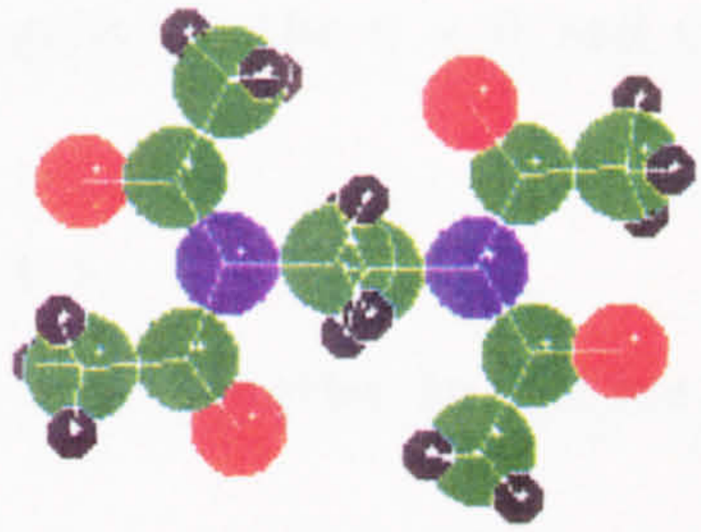

(c)

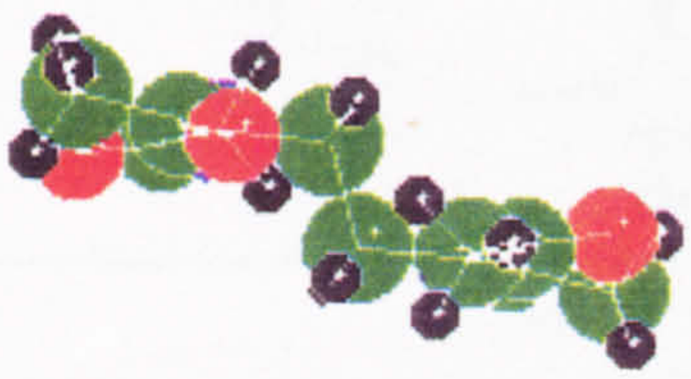

(d)

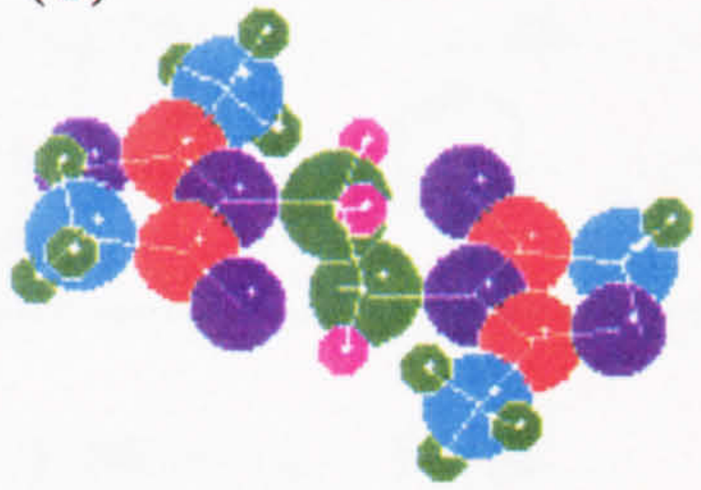

Key for (d):

= +0.20

= +0.12

= -0.04

= -0.12

= -0.20

Scheme 4.1

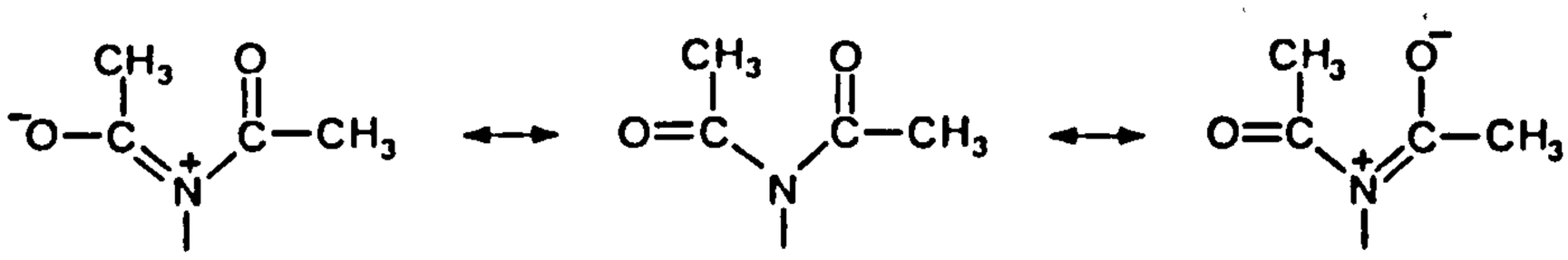

It is interesting to compare bond lengths of the C - O and C - N groups for a series of amides (Table 4.1).

Table 4.1

Comparison of C-N and C-O bond lengths in amides.

	Bondlength/nm				
Bond	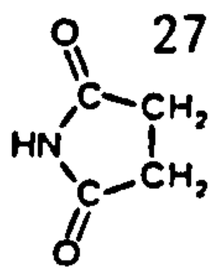 27	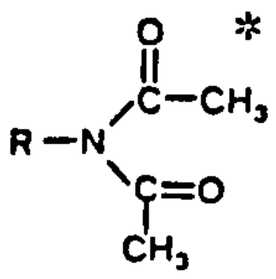 *	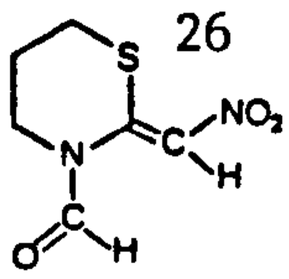 26	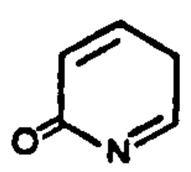 26	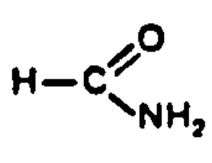 117
C-N	1.40	1.41	1.36	1.336	1.30
C-O	1.21	1.22	1.21	1.23	1.26

*TAED, this work, $R = CH_2CH_2N(COCH_3)_2$

Compared to Formamide and cyclic tertiary amides, succinimide, TAED, and 3-formyl-2-nitromethylenetetrahydro-2H-1,3-thiazine (FNMTHT) have longer and shorter bond lengths for the C - N and C - O bonds, respectively. This, as discussed in Chapter 1, implies that in these amides the delocalisation of the N lone pair of electrons into the carbonyl function is operating less effectively than in 'ordinary' amides. In

the case of FNMTHT, this is due to resonance of the nitrogen lone pair electrons with the nitroenamine system, whilst, with the amides, the lone pair electrons are delocalised over two carbonyl functions. This reduced resonance with the carbonyl function is also responsible for the increased reactivity of imides and compounds like FNMTHT compared to 'ordinary' amides. The similarity of bond lengths for succinimide and TAED, together with their planar configuration suggest that succinimide is a reasonable model for TAED, at least regarding the extent of nitrogen lone pair electron delocalisation over the carbonyl functions. The main difference, of course, is the ring structure in succinimide which reduces the CNC angle (112.6°) compared to TAED (124°) and which also enforces the Z,Z configuration. It was noted, however, in Chapter 1 that the reactivity of N-methyldiacetamide and succinimide towards the hydroxide ion is very similar (1.908[35] and 3.16[24] M^{-1} s^{-1}, respectively) and TAED also should be expected to show a similar reactivity.

4.2 Spectrophotometric study of TAED Hydrolysis

Figure 4.3 shows spectra of equimolar concentrations (2.6 x 10^{-5} M) of DAED and TAED, in distilled water; DAED was obtained from Warwick Chemicals Ltd. TAED has a maximum absorbance of 216 nm for which the molar absorptivity is 17240 M^{-1} cm^{-1}. DAED has a maximum absorbance at the lower limit of the wavelength range available on the HP 8451 spectrophotometer. There appears to be a maximum absorbance at 192 nm although it is quite likely that this is due to stray light effects. The molar absorptivity of DAED at 196 nm is 13334 M^{-1} cm^{-1}. Clearly, the λ_{max} values of DAED and TAED are sufficiently separated for the two spectra to be easily resolved and, therefore, the transition of TAED to DAED (via triacetylethylenediamine (TriAED)) due to hydrolysis and perhydrolysis can be followed spectrophotometrically. The hydroly-

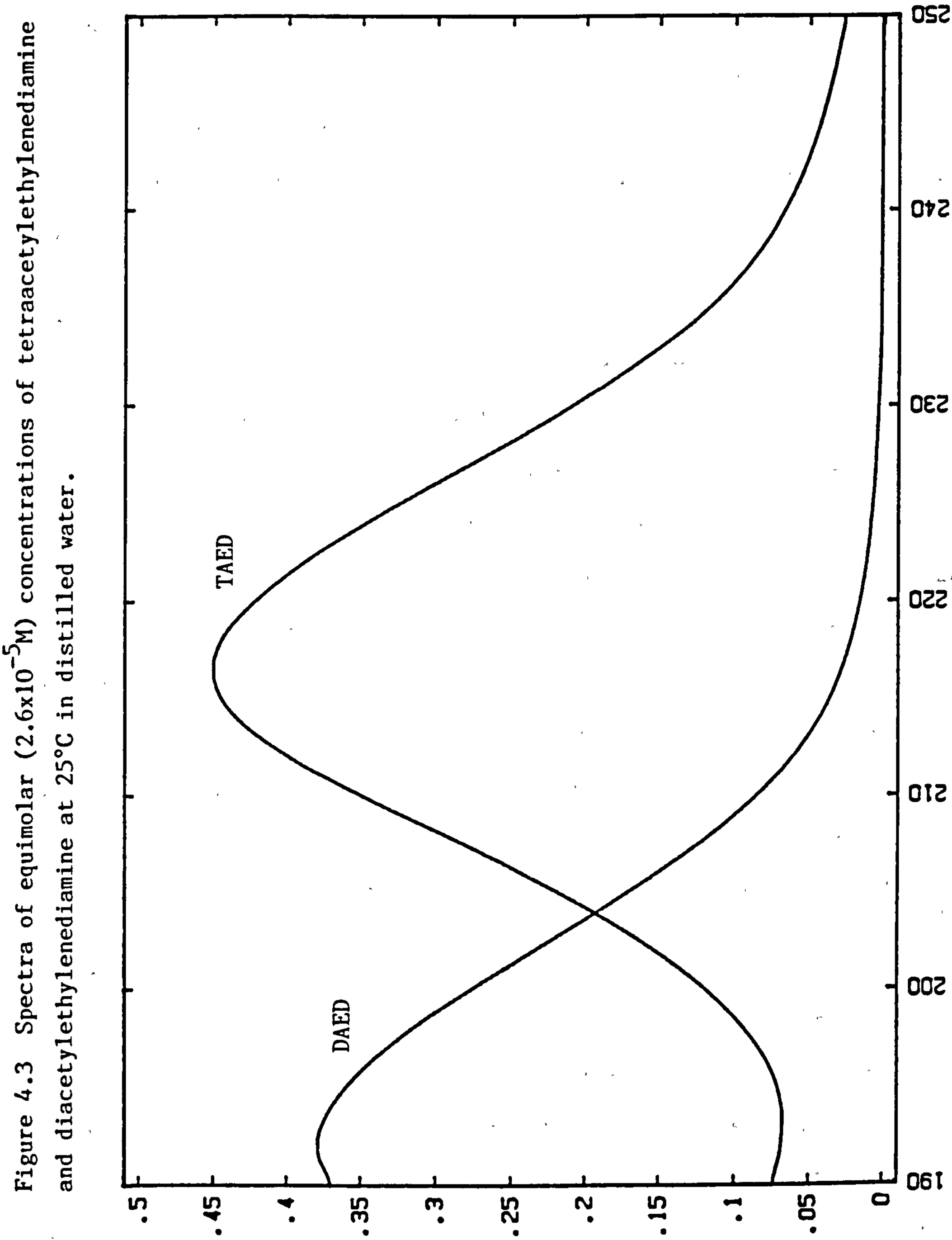

Figure 4.3 Spectra of equimolar ($2.6x10^{-5}$M) concentrations of tetraacetylethylenediamine and diacetylethylenediamine at 25°C in distilled water.

sis of N-methyldiacetamide, an analagous compound to TAED, has been followed spectrophotometrically (at 216 nm) in literature studies.[35]

Experimental

The hydrolysis of TAED was followed by measuring absorbance changes over the wavelength range 190 to 250 nm; the Beer-Lambert law was found to be obeyed up to absorbances of at least 1.0 in this wavelength range.

Materials

Analytical grade reagents were used wherever possible. A 2×10^{-3} M TAED solution was prepared by adding TAED (Warwick Chemicals Ltd. 99% purity by GLC) to a beaker containing 800 ml distilled water which is being quite vigorously stirred using a magnetic stirrer. After one hour the TAED solution is decanted into a 1000 ml volumetric flask and made up to the mark with distilled water. Carbonate buffer solutions were prepared using sodium carbonate (decahydrate) and sodium hydrogen carbonate. All solutions contained 1×10^{-5} M ethylenediaminetetramethylenephosphonic acid hexasodium salt (EDTMP) (Warwick Chemicals Ltd. 96% purity by GLC) which is metal ion chelater; EDTMP was used in place of EDTA which was used for the same purpose in the previous chapter.

Procedure

Upon mixing the TAED and buffer solutions in equal proportions the TAED hydrolysis reaction was followed spectrophotometrically, as detailed below. Successive spectra of the reaction solution were taken by adding 0.1 ml samples to 2 ml distilled water in a cuvette. It was necessary to dilute the sample in distilled water because the carbonate buffer absorbs strongly in the UV region, with the consequence that direct measurement of the reaction solution would give absorbances exceeding the range where the Beer-Lambert law is obeyed. The reaction

was followed for about 20000 seconds (about 4 half-lives), with additional measurements taken after 24 and 48 hours, in order to obtain an infinity absorbance. Initial conditions upon mixing the solutions were: $[TAED]_o$, 1 x 10^{-3} M; carbonate buffer, pH 9.6, I = 0.1 M; EDTMP, 1 x 10^{-5} M.

Results

Figure 4.4 shows the sequential spectra for the TAED hydrolysis reaction. Clearly, there is a reduction in absorbance due to TAED, and a corresponding rise in absorbance in the wavelength range attributable to DAED. There is a good isosbestic point for DAED and TAED at 203.5 nm. If a plot of ln $(A - A_\infty)$ against time is made for λ = 216 nm (Figure 4.5), then two distinct linear phases are apparently indicating, as might be expected, that there are two rates involved in TAED hydrolysis corresponding to the hydrolysis of TAED and TriAED.

$$\text{TAED} + H_2O \xrightarrow{k_1} \text{TriAED} + \text{acetate} \qquad \text{Eqn 4.1}$$

$$\text{TriAED} + H_2O \xrightarrow{k_2} \text{DAED} + \text{acetate} \qquad \text{Eqn 4.2}$$

Looking at the structures of TAED [77] and TriAED [78]:

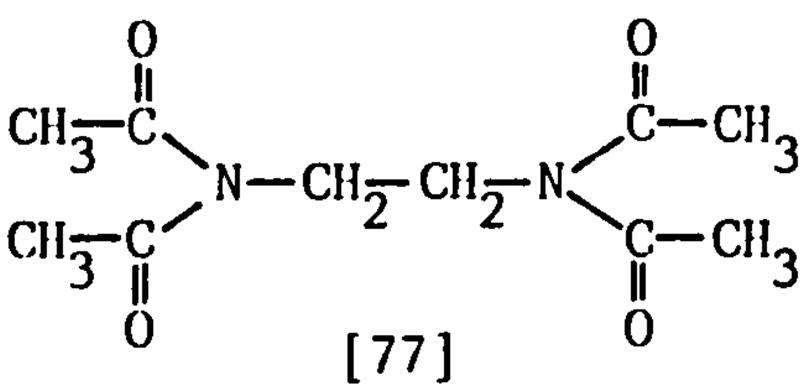

[77]

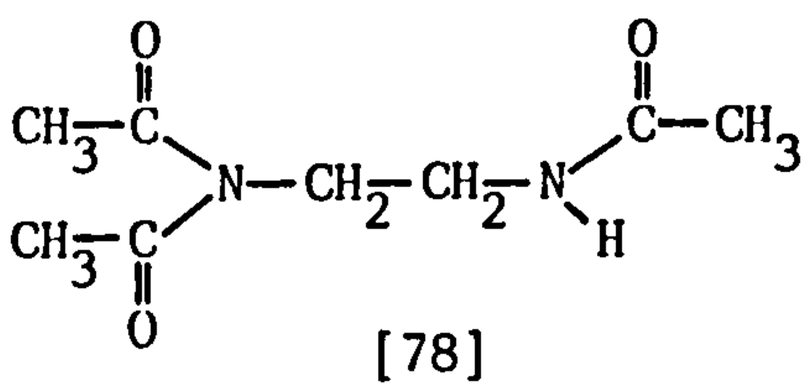

[78]

on statistical grounds it would be expected that the hydrolysis reactions of TAED will be two times faster than those for TriAED, since only the imide groups are reactive to nucleophilic attack.

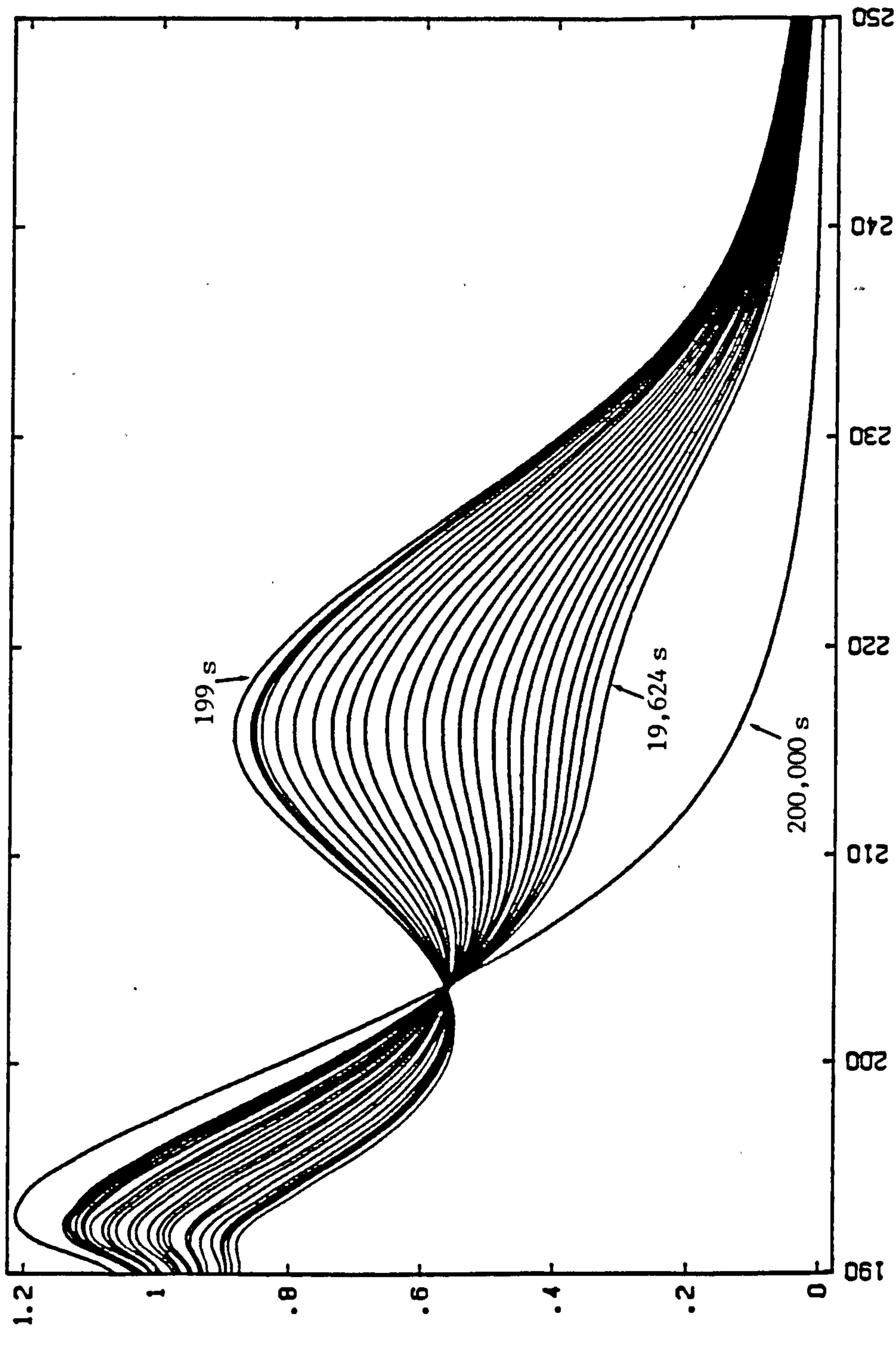

Figure 4.4 Sequential spectra taken during the hydrolysis of tetraacetylethylenediamine (TAED) in a pH 9.60 sodium carbonate - sodium hydrogen carbonate buffer (I = 0.1M) at 25°C.

Figure 4.5 First order plot for the hydrolysis of tetraacetyl-ethylenediamine at 25°C in a pH 9.60 sodium carbonate - sodium hydrogen carbonate buffer (I = 0.1M): [TAED] = $1x10^{-3}$M; [EDTMP] = $1x10^{-5}$M. The lines represent the best fit to data in the two phases of the plot using the linear least squares method. Absorbance measurements were made at 218 nm.

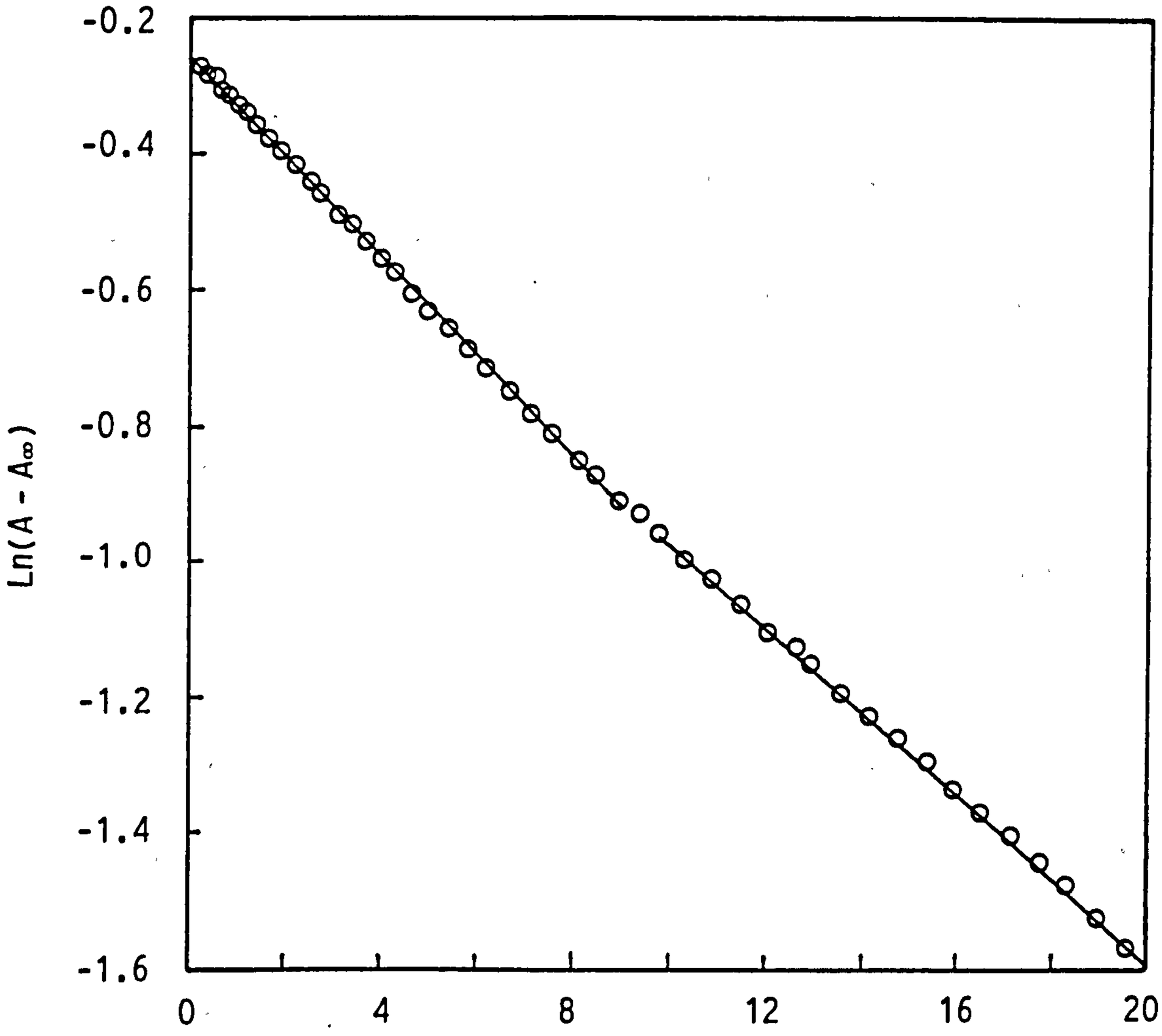

Rate Constants

Using the ELORMA computer program, the first order rate constants k_1 and k_2 were obtained from non-linear regression, according to Equation 4.3.

$$A = A_\infty + A_1 e^{-k1t} + A_2 e^{-k2t} + A_B \qquad \text{Eqn 4.3}$$

Where A_B is the background absorbance and A_1 and A_2 are constants. Absorbance data from 194 to 230 nm, at 4 nm intervals were used in the calculation. k_1 and k_2 were calculated as 1.399×10^{-4} s^{-1} and 0.499×10^{-4} s^{-1}, respectively. The ratio, $k_1:k_2$ is approximately 2.8 and, so, there is another factor involved in the reaction in addition to the statistical effect mentioned above, which would predict a ratio of 2. This effect is discussed in Section 4.5. Figure 4.6 shows the absorbance data for TAED hydrolysis drawn with a curve defined by Equation 4.3.

TriAED spectrum

The spectrum for TriAED cannot be determined directly during the hydrolysis reaction since it is masked by those of TAED and DAED. It is possible, however, using the obtained absorbance data, to *calculate* a spectrum for TriAED. The theory for this calculation, which is based on the work of Alcock et al.[118] is described below.

The hydrolysis reaction of TAED, in which account must also be taken of the acetate formed, can be expressed as follows:

$$\begin{array}{ccccc} & \xrightarrow{k_1} & & \xrightarrow{k_2} & \\ X & & Y & & Z \\ & & + & & + \\ & & Ac & & Ac \end{array} \qquad \text{Eqn 4.4}$$

The respective concentrations of X, Y, and Z are defined by Equations 4.5, 4.6, and 4.7.

$$[X] = [X]_o e^{-k1t} \qquad \text{Eqn 4.5}$$

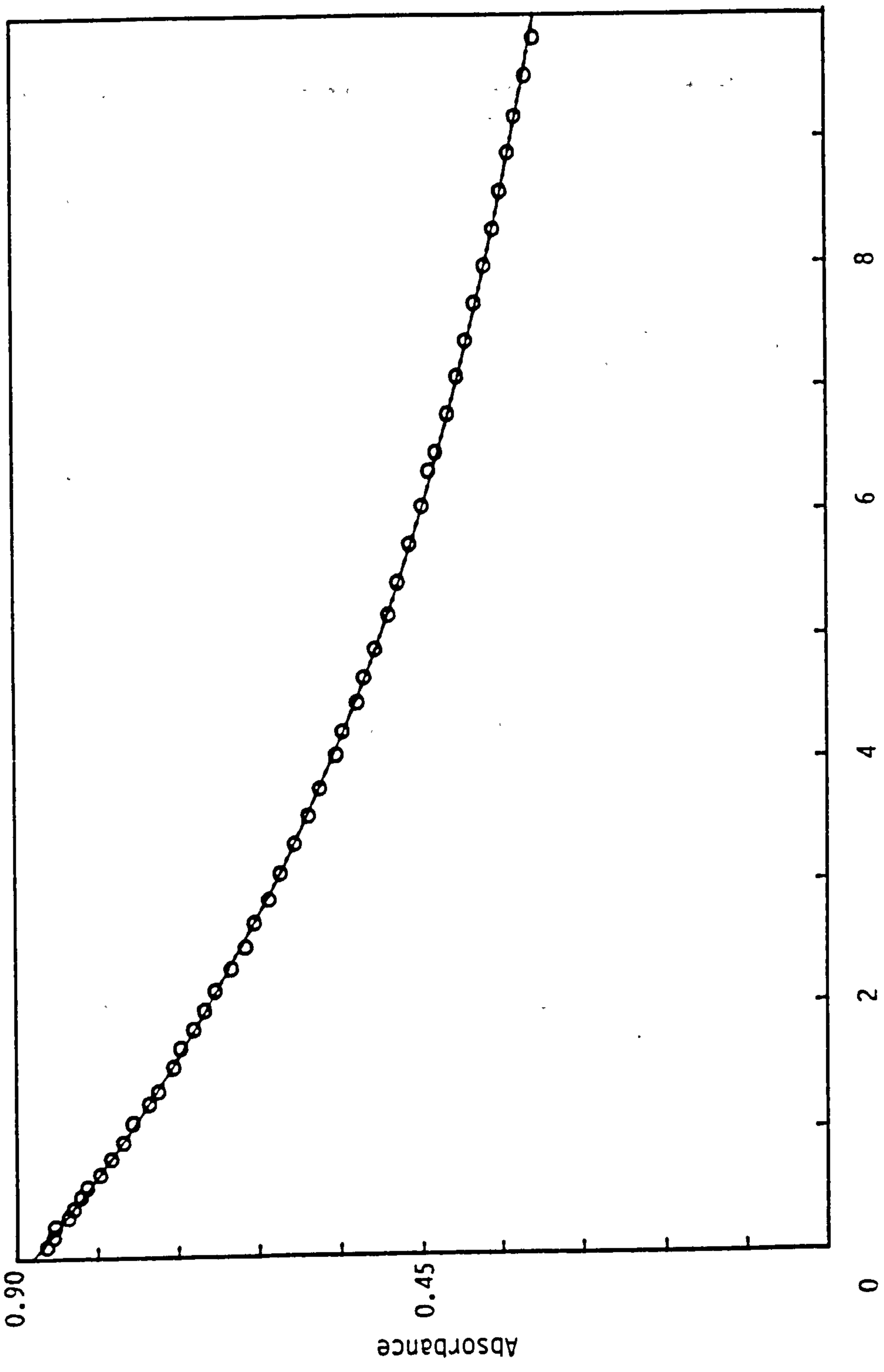

Figure 4.6 Plot of absorbance decrease at 218nm during the hydrolysis of tetraacetylethylene-diamine (TAED) at 25°C in pH 9.60 sodium carbonate - sodium hydrogen carbonate buffer (I = 0.1M). The curve represents the best fit to Equation 4.3.

$$[Y] = [X]_o \frac{k_1}{k_1 - k_2} (e^{-k2t} - e^{-k1t}) \qquad \text{Eqn } 4.6$$

$$[Z] = [X]_o + [X]_o \left(\frac{k_2\, e^{-k1t} - k_1\, e^{-k2t}}{k_1 - k_2}\right) \qquad \text{Eqn } 4.7$$

For $[A_c]$, the amount formed equals the amount of X lost plus the amount of Z formed:

$$[A_c] = ([X_o] - [X]) + [Z] \qquad \text{Eqn } 4.8$$

Substituting from Equation 4.7:

$$[A_c] = [X]_o - [X]_o\, e^{-k1t} + [X]_o + \frac{[X]_o\, k_2\, e^{-k1t} - k_1\, e^{-k2t}}{k_1 - k_2} \qquad \text{Eqn } 4.9$$

$$\therefore [A_c] = [X]_o \left\{ 2 - e^{-k1t} + \left(\frac{k_2\, e^{-k1t} - k_1\, e^{-k2t}}{k_1 - k_2} \right) \right\} \qquad \text{Eqn } 4.10$$

The absorbance is thus given by:

$$A = \varepsilon_X [X] + \varepsilon_Y [Y] + \varepsilon_Z [Z] + \varepsilon_{Ac} [A_c] + A_B \qquad \text{Eqn } 4.11$$

Substituting Equations 4.5, 4.6, 4.7, and 4.10 into 4.11:

$$A = \varepsilon_X [X]_o\, e^{-k1t} + \varepsilon_Y [X]_o \frac{k_1}{k_1 - k_2} (e^{-k2t} - e^{-k1t}) \qquad \text{Eqn } 4.12$$

$$+ \varepsilon_Z [X]_o + [X]_o \left(\frac{k_2\, e^{-k1t} - k_1\, e^{-k2t}}{k_1 - k_2}\right)$$

$$+ \varepsilon_{Ac} [X]_o \left\{ 2 - e^{-k1t} + \left(\frac{k_2\, e^{-k1t} - k_1\, e^{-k2t}}{k_1 - k_2} \right) \right\} + A_B$$

Dividing by $[X]_o$ and rearranging:

$$\frac{A}{[X]_o} = \frac{A_B}{[X]_o} + \varepsilon_Z + 2\,\varepsilon_{Ac} \left(\varepsilon_X - \varepsilon_Y \frac{k_1}{k_1 - k_2} + \varepsilon_Z \frac{k_2}{k_1 - k_2} + \varepsilon_{Ac} \frac{k_2}{k_1 - k_2} - \varepsilon_{Ac} \right) e^{-k1t}$$

$$+ \left(\varepsilon_Y \frac{k_1}{k_1 - k_2} - \varepsilon_Z \frac{k_1}{k_1 - k_2} - \varepsilon_{Ac} \frac{k_1}{k_1 - k_2} \right) e^{-k2t} \qquad \text{Eqn } 4.13$$

which gives

$$A = A_B + \varepsilon_Z [X]_o + 2\varepsilon_{Ac} [X]_o + \left(\varepsilon_X - \varepsilon_Y \frac{k_1}{k_1 - k_2} + \varepsilon_Z \frac{k_2}{k_1 - k_2} + \frac{\varepsilon_{Ac} k_2}{k_1 - k_2} - \varepsilon_{Ac} \right) [X]_o e^{-k_1 t} + \left(\varepsilon_Y \frac{k_1}{k_1 - k_2} - \varepsilon_Z \frac{k_1}{k_1 - k_2} - \varepsilon_{Ac} \frac{k_1}{k_1 - k_2} \right) [X]_o e^{-k_2 t}$$ Eqn 4.14

This compares with

$$A = A_B + A_\infty + A_1 e^{-k_1 t} + A_2 e^{-k_2 t}$$ Eqn 4.15

Therefore,

$$A_\infty \equiv \varepsilon_Z [X]_o + 2 \varepsilon_{Ac} [X]_o$$ Eqn 4.16

and because the measured absorbance at infinity time, A_∞', incorporates A_B then

$$A_\infty' - A_B = \varepsilon_Z [X]_o + 2 \varepsilon_{Ac} [X]_o$$ Eqn 4.17

$$A_1 \equiv \left(\varepsilon_X - \varepsilon_Y \frac{k_1}{k_1 - k_2} + \varepsilon_Z \frac{k_2}{k_1 - k_2} + \varepsilon_{Ac} \frac{k_2}{k_1 - k_2} - \varepsilon_{Ac} \right) [X]_o$$ Eqn 4.18

$$A_2 \equiv \left((\varepsilon_Y - \varepsilon_Z - \varepsilon_{Ac}) \frac{k_1}{k_1 - k_2} \right) [X]_o$$ Eqn 4.19

From Equations 4.17 and 4.19

$$A_2 = \left(\varepsilon_Y - \frac{A_\infty' - A_B}{[X]_o} + \varepsilon_{Ac} \right) \frac{k_1}{k_1 - k_2} [X]_o$$ Eqn 4.20

$$\Rightarrow \varepsilon_Y [X]_o = A_\infty' - A_B - \varepsilon_{Ac} [X]_o + \frac{k_1 - k_2}{k_1} A_2$$ Eqn 4.21

Values for A_1 and A_2 at each wavelength, obtained from linear regression using Equation 4.15 are contained in Table 4.2. Values for A_B due to the carbonate buffer were measured independently. ε_{Ac} values at each wavelength were obtained using a solution of sodium acetate. Using Equation 4.21, $\varepsilon_Y[X]_o$ values were calculated and are also contained in Table 4.2.

From Equation 4.17 we get

$$\varepsilon_Z [X]_o = A_\infty' - A_B - 2 \varepsilon_{Ac} [X]_o = [DAED]$$ Eqn 4.22

Table 4.2 Linear constants, and values of $\varepsilon_X[X]_o$, $\varepsilon_Y[X]_o$ and $\varepsilon_Z[X]_o$, obtained from absorbance data for the hydrolysis of tetraacetylethylenediamine in pH 9.60 sodium carbonate - sodium hydrogen carbonate buffer ($I = 0.1M$). $[x]_o = 4.76 \times 10^{-5}M$ in the cuvette.

λ / nm	A_B	$A_\infty' - A_B$	$A_c[X]_o$	A_1	A_2	$\varepsilon_X[X]_o$	$\varepsilon_Y[X]_o$	$\varepsilon_Z[X]_o$
194	0.6442	0.5453	0.0228	-0.2343	-0.1817	0.1293	0.4057	0.4997
198	0.4211	0.5398	0.0129	-0.1608	-0.2032	0.1758	0.3962	0.5140
202	0.2601	0.4103	0.0074	-0.0391	-0.0852	0.2860	0.3481	0.3955
206	0.1696	0.2657	0.0045	0.0965	0.0843	0.4465	0.3154	0.2567
210	0.1195	0.1465	0.0027	0.2203	0.2743	0.6411	0.3202	0.1411
214	0.0885	0.0720	0.0016	0.2736	0.4510	0.7966	0.3605	0.0688
218	0.0630	0.0339	0.0009	0.2183	0.5668	0.8190	0.3976	0.0321
222	0.0415	0.0165	0.0005	0.1176	0.5830	0.7171	0.3910	0.0155
226	0.0257	0.0085	0.0003	0.0396	0.5091	0.5572	0.3357	0.0079
230	0.0154	0.0045	0.0002	-0.0013	0.3841	0.3873	0.2513	0.0041

and it can also be shown that

$$[TAED] = \varepsilon x\ [X]_o = A_\infty' - A_B + A_1 + A_2 \qquad \text{Eqn 4.23}$$

Figure 4.7 shows plots of $\varepsilon_X[X]_o$, $\varepsilon_Y[X]_o$ and $\varepsilon_Z[X]_o$ at each wavelength which correspond to spectra of equimolar concentrations of TAED, Tri-AED, and DAED, respectively.

The UV spectrum of TriAED might be expected to show characteristics of both TAED and DAED, which it does to a large extent. The main difference is that the peak corresponding to the $\pi \dashrightarrow \pi^*$ transition of the imide group[27] (220 nm) occurs at a longer wavelength than it does in TAED. The reasons for the bathochromic shift, and its consequences are discussed in the general discussion (Section 4.5).

Finally, after this study had been completed, isolated TriAED was obtained from Warwick Chemicals Ltd. and the spectrum of this compound in distilled water is shown in Figure 4.8. Clearly, the calculated spectrum resembles the actual spectrum very closely, including the confirmation of the of a peak at 220 nm for the $\pi \dashrightarrow \pi^*$ transitions of the imide group.

4.3 pH Dependence of TAED and TriAED Hydrolysis

A pH dependence study of the TAED and TriAED hydrolysis reactions was necessary in order to ascertain whether there is a simple first order dependence on hydroxide ion cencentration, and to possibly determine the extent of the reaction with H_2O. In addition, information on general acid-general base catalysis by buffer components may be obtained.

The pH dependence studies were conducted in carbonate buffers at ionic strengths of 0.1 M (using sodium salts) and of 1.0 M (using potassium salts). For the study at I = 1.0 M, isolated TriAED was used and the data for this study were collected from the aminolysis, alcoholysis, and perhydrolysis experiments detailed in Chapters 6 and 7.

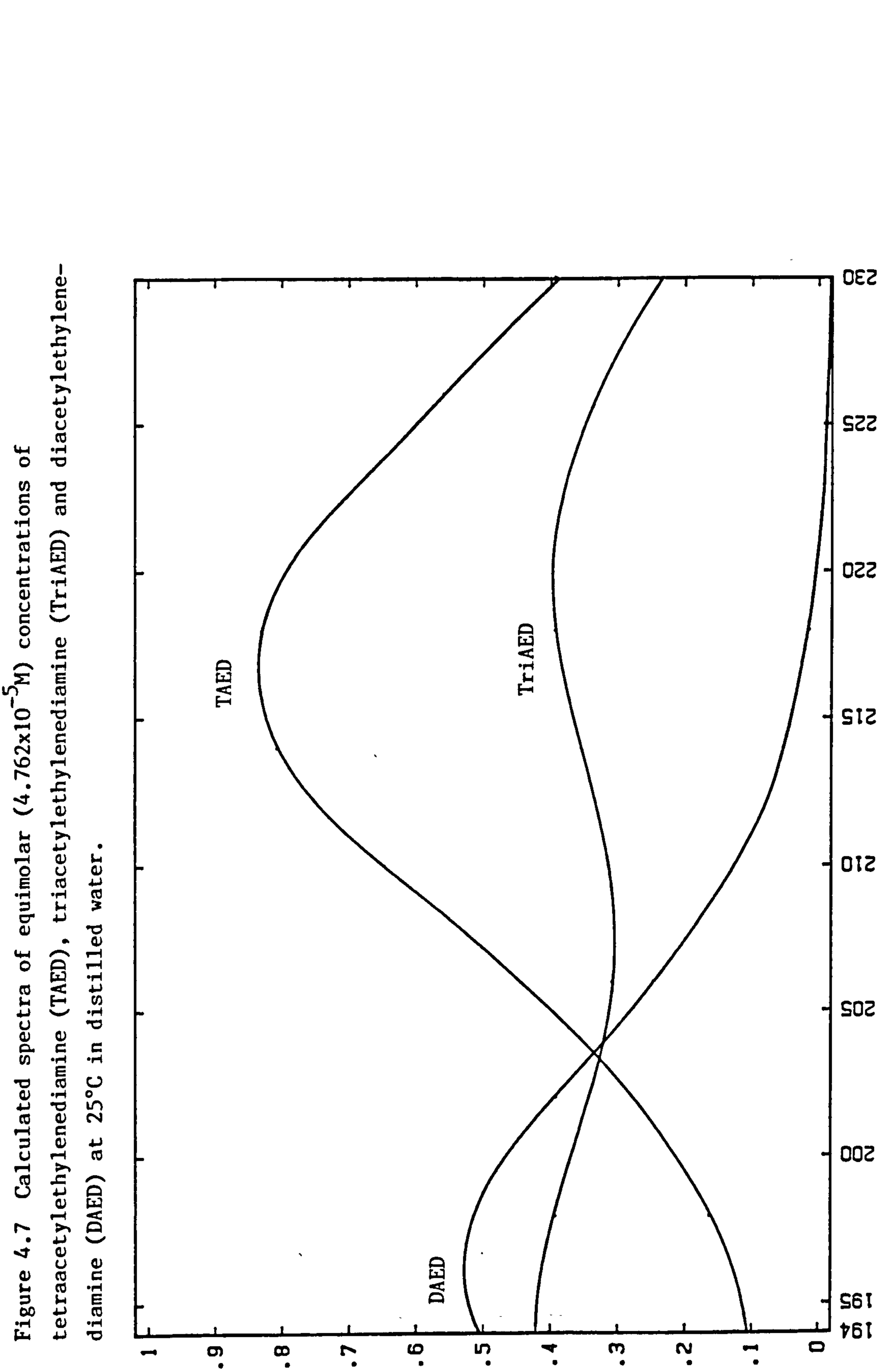

Figure 4.7 Calculated spectra of equimolar (4.762×10^{-5}M) concentrations of tetraacetylethylenediamine (TAED), triacetylethylenediamine (TriAED) and diacetylethylenediamine (DAED) at 25°C in distilled water.

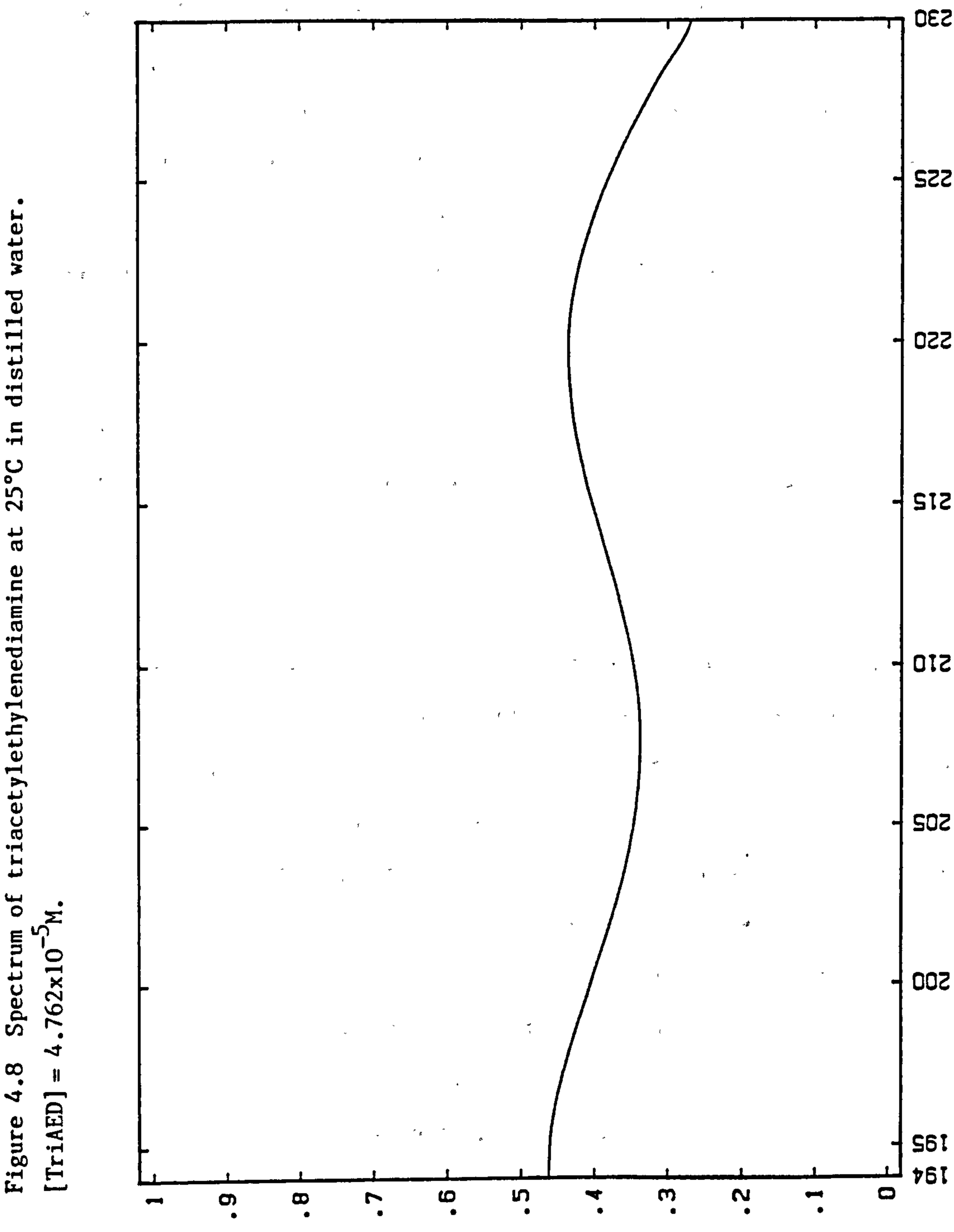

Figure 4.8 Spectrum of triacetylethylenediamine at 25°C in distilled water. [TriAED] = 4.762×10^{-5}M.

Experimental

For the study at I = 0.1 M rate constants for TAED and TriAED hydrolysis at pH 10.47 were obtained using the same procedure outlined in Section 4.2. Additionally, a value for hydrolysis at pH 9.99 was obtained; solutions for this run were made up as described in Section 4.2, however, the reaction was followed directly, by measuring the absorbances changes at 232 nm in the reaction solution. For the pH dependence study at I = 1.0 M, the hydrolysis of TriAED was followed in 0.05 M potassium carbonate buffers, with the ionic strength being made up to 1.0 using added KCl. These runs were conducted as part of a study of the reaction of various nucleophiles with TriAED. Chapters 6 and 7 should be consulted for the experimental details and data treatment.

Results

I = 0.1 M (sodium salts used)

Kinetic runs were conducted at pH's 9.6 (see Section 4.2), 9.99, and 10.47. For hydrolysis at pH 10.47, the data treatment described in Section 4.2 was employed and rate constants for both TAED and TriAED hydrolysis were obtained. Figure 4.9 shows a plot at ln $(A - A_\infty)$ against time for the run at pH 10.47, clearly, demonstrating the biphasic nature of the overall reaction. Figure 4.10 shows absorbance data at 216 nm for the run, plotted with a curve described by Equation 4.15. k_{TAED} and k_{TriAED} values of 7.093×10^{-4} s^{-1} and 2.568×10^{-5} s^{-1} were obtained from non-linear regression analysis using Equation 4.15. Absorbance data from 196 to 232 nm, at 4 nm intervals, were used in the calculation. Table 4.3 contains the values for the constants from Equation 4.15, and $\varepsilon y[X_o]$ values (molar absorptivity of TriAED) at each wavelength. The ratio of the rate constants k_{TAED} and k_{TriAED} at pH 10.47 is 2.76: similar to the value of 2.80 obtained at pH 9.6, indicating that the ratio is independent of pH.

Figure 4.9 First order plot for the hydrolysis of tetraacetylethylene-diamine at 25°C in a pH 10.47 sodium carbonate - sodium hydrogen carbonate buffer (I = 0.1M): $[TAED]_o = 1x10^{-3}M$; $[EDTPM] = 1x10^{-5}M$. The lines represent the best fit to data in the two phases of the plot using the linear least squares method. Absorbance measurements were made at 216 nm.

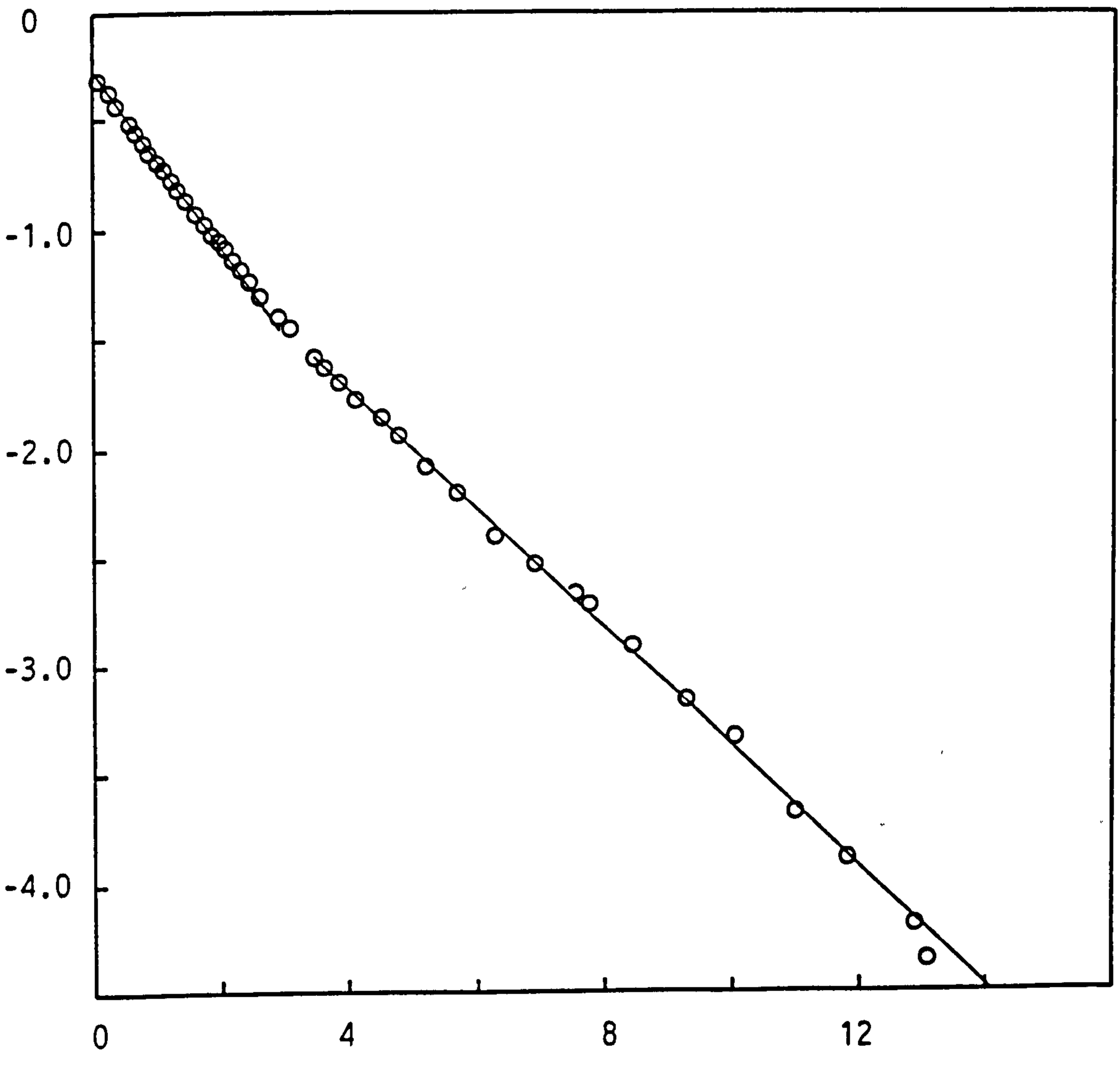

Figure 4.10 Plot of absorbance decrease at 216 nm during the hydrolysis reaction of tetraacetylethylenediamine at 25°C in pH 10.47 sodium carbonate - sodium hydrogen carbonate buffer (I = 0.1M). The curve represents the best fit to Equation 4.3. $[TAED]_o = 1x10^{-3}M$; [EDTMP] = $1x10^{-5}M$.

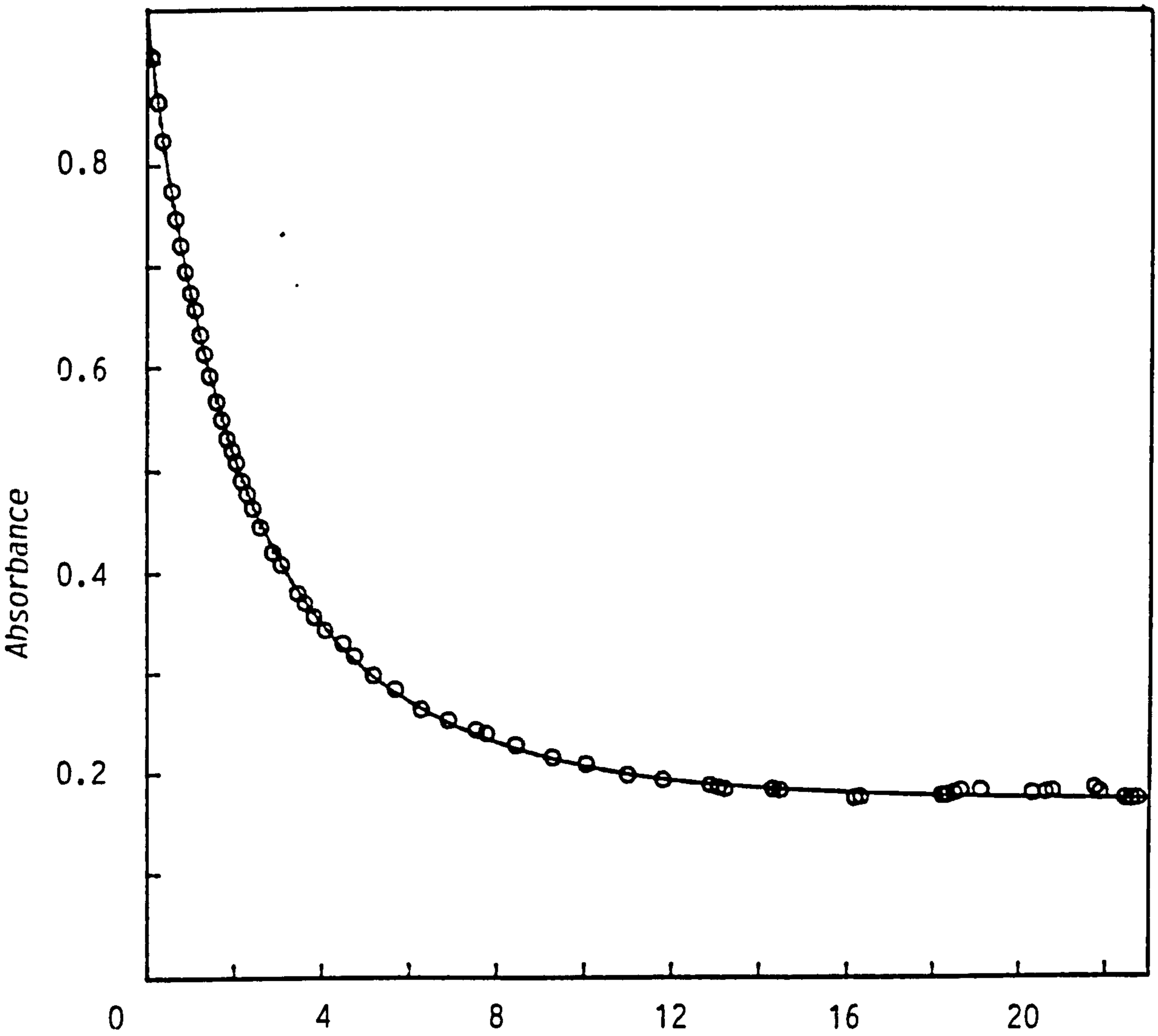

Table 4.3 Linear constants, and values of $\varepsilon_X[X]_o$, $\varepsilon_Y[X]_o$ and $\varepsilon_Z[X]_o$, obtained from absorbance data for the hydrolysis of tetraacetylethylenediamine in pH 10.47 sodium carbonate - sodium hydrogen carbonate buffer (I = 0.1M). $[X]_o = 4.76 \times 10^{-5}$M in the cuvette.

λ / nm	A_B	$A_\infty' - A_B$	$A_C[X]_o$	A_1	A_2	$\varepsilon_X[X]_o$	$\varepsilon_Y[X]_o$	$\varepsilon_Z[X]_o$
196	0.8446	0.4080	0.0172	-0.1991	-0.0863	0.1226	0.3357	0.3736
200	0.6052	0.4005	0.0097	-0.1218	-0.0881	0.1906	0.3345	0.3811
204	0.4120	0.2827	0.0057	-0.0320	0.0103	0.2610	0.2836	0.2713
208	0.2837	0.1633	0.0035	0.1922	0.1499	0.5054	0.2554	0.1563
212	0.2002	0.0777	0.0021	0.3140	0.3032	0.6949	0.2690	0.0735
216	0.1423	0.0307	0.0012	0.3261	0.4374	0.7942	0.3086	0.0283
220	0.0968	0.0088	0.0007	0.2425	0.5053	0.7566	0.3305	0.0074
224	0.0629	-0.0012	0.0004	0.1418	0.4852	0.6258	0.3080	-0.0020
228	0.0405	-0.0051	0.0002	0.0688	0.3964	0.4601	0.2476	-0.0055
232	0.0255	-0.0054	0.0001	0.0271	0.2806	0.3023	0.1735	-0.0056

For the run at pH 9.99, absorbance data were obtained for the latter part of the reaction only. Consequently, only the rate constant for TriAED hydrolysis, k_{TriAED} could be calculated. This was done by linear regression of ln $(A - A_\infty)$ against time for the region corresponding to $A = A_2\ e^{-k2t} + A_B$.

Rate constants for TAED and TriAED hydrolysis at pH 9.6, 9.99, and 10.47 are contained in Table 4.4, and a plot of log k_{TAED} and log k_{TriAED} against pH is shown in Figure 4.11. The slope for TriAED hydrolysis is 0.819 $\pm$ 0.136* and the slope for TAED hydrolysis, where only two values were obtained, is 0.810. These values compare with the expected value of 1.0 for a first order dependence on hydroxide ion concentration. The two most likely explanations for a value lower than 1.0 being obtained are (a) general acid catalysis by HCO_3^- and (b) a large contribution to the hydrolysis reaction from the nucleophile H_2O. This will be discussed in Section 4.5.

I = 1.0 M (potassium salts used)

Isolated Triaed was used in these runs. First order rate constants, k_{TriAED}, were obtained from linear regression of ln $(A - A_\infty)$ against time and are contained in Table 4.4. Figure 4.12 shows a plot of log k_{TriAED} against pH for TriAED. The data fit to a slope of 0.932 $\pm$ 0.090*; this value is higher than that obtained at I = 0.1 M (sodium salts used).

---

* 90% confidence limits

Table 4.4 pH dependence of the hydrolysis of tetraacetylethylenediamine (TAED) and triacetylethylenediamine (TriAED) at 25°C in a sodium carnonate - sodium hydrogen carbonate buffer. [EDTMP] = 1×10^{-5}M.

Ionic strength/M	pH	$10^4 k_{TAED}/s^{-1}$	$10^4 k_{TriAED}/s^{-1}$	Number of determinations
0.1*	9.60	1.400	0.4995	1
	9.99	-	1.0023	1
	10.47	7.093	2.568	1
1.0**	9.80	-	0.815	1
	10.00	-	1.140	2
	10.03	-	1.084	3
	10.16	-	1.790	2
	10.39	-	2.302	1
	10.42	-	2.488	1
	10.62	-	4.757	3
	11.04	-	11.200	1

*Using TAED. Buffer components were sodium salts.

**Using isolated TriAED. The ionic strength was made up to 1.0M with KCl. Buffer components were potassium salts.

Figure 4.11 Plot showing the pH dependence of the hydrolysis (ko) of tetraacetylethylenediamine, Δ, and triacetylethylenediamine, O, at 25°C. The reactions were carried out in sodium carbonate - sodium hydrogen carbonate buffers (I = 0.1M). The line for the TriAED data represents the best fit using the linear least squares method.

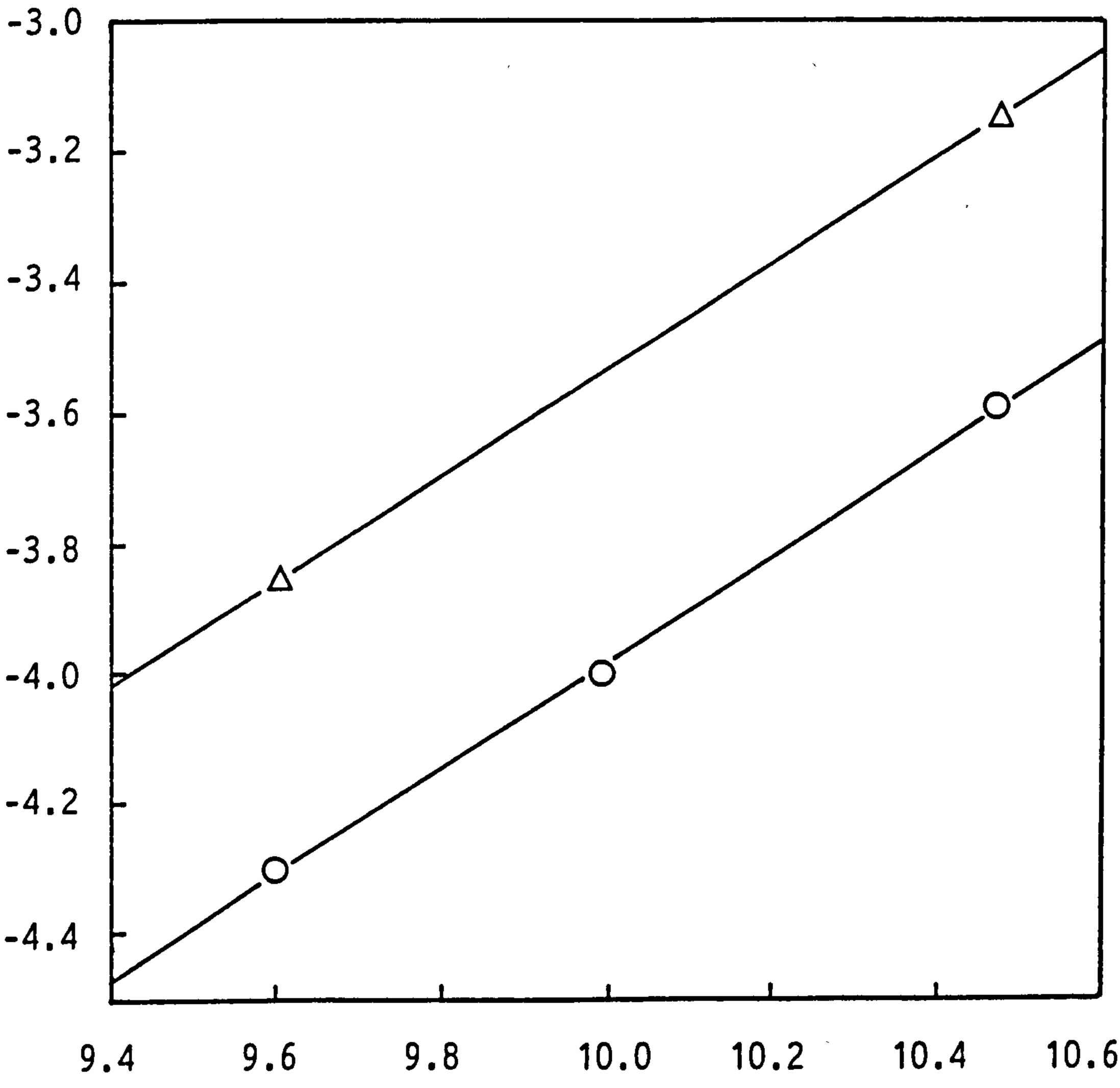

Figure 4.12 Plot showing the pH dependence of the hydrolysis (ko) of triacetylethylenediamine (TriAED) at 25°C. The reactions were carried out in potassium carbonate - potassium hydrogen carbonate buffers (I = 1.0M with KCl). The line represents the best fit using the linear least squares method.

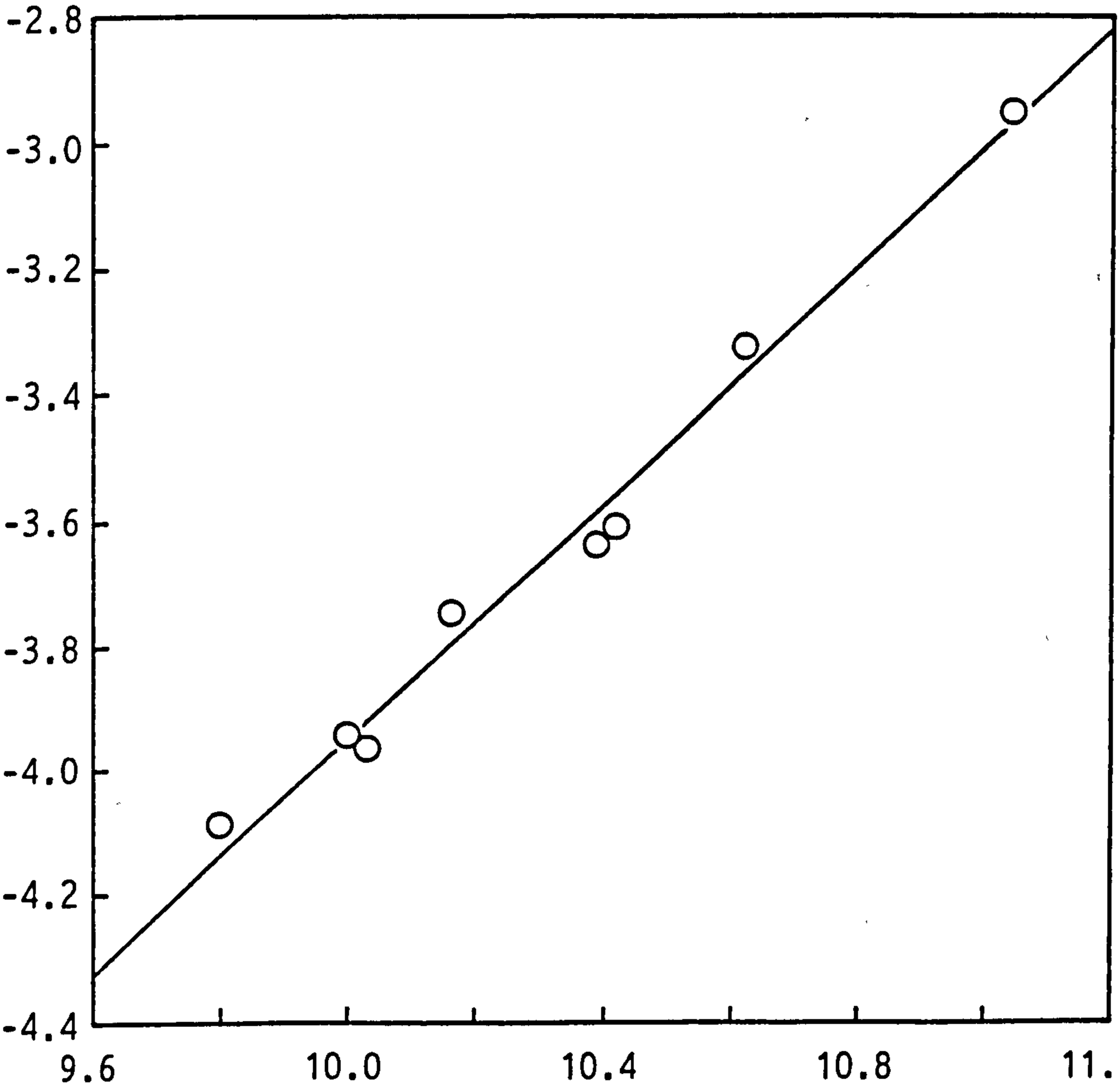

4.4 Effect of Buffer Components on TriAED Hydrolysis

A limited study was conducted in order to assess the effect of carbonate buffer concentration on the rate of TriAED hydrolysis. The two buffer components present are HCO_3^- and CO_3^{2-}. Whilst both are capable of acting as general base catalysts of the hydrolysis reaction, HCO_3^- can also act as a general acid catalyst. First order rate constants for TriAED hydrolysis were obtained at five carbonate buffer concentrations, whilst maintaining the ionic strength constant (I = 1.0 M). Potassium salts were used in this study. An additional value was also obtained for one buffer concentration using sodium salts.

Experimental

The CO_2-free experimental described in Section 6.1 was used during this study.

Reagents

TriAED, 2 x 10^{-3} M solution in distilled water (I = 1.0 M) with added KCl); carbonate buffer solution, pH 9.80, prepared by mixing 0.05 M potassium hydrogen carbonate (I = 1.0 M with KCl) and 0.05 M potassium carbonate (I = 1.0 M with KCl); KCl solution, 1.0 M.

Procedure

A range of carbonate buffer concentrations (0.01 to 0.05 M) was prepared from the stock buffer solution by diluting with KCl solution. Slight differences in pH resulting from the dilution of the stock buffer were corrected with KOH. TriAED hydrolysis was followed by adding 0.12 ml TriAED solution to 2.0 ml buffer solution in a cuvette and measuring the absorbance change at 230 nm. The hydrolysis reactions were carried out in parallel as described in Section 4.2. Additionally, a rate constant for TriAED hydrolysis was obtained at a buffer concentration of 0.05 M at pH 9.8 using sodium salts instead of potassium.

Results

First order rate constants for TriAED hydrolysis were obtained from linear regression of ln ($A - A_\infty$) against time and are contained in Table 4.5. Figure 4.13 shows a plot of K_{obs} against buffer concentration. These results suggest that there is buffer catalysis of the hydrolysis reaction and that the general acid or general base catalysis is levelling off at the higher buffer concentration. Such a levelling off with increasing buffer concentration is indicative of a change in rate determining step, as has been observed by Khan[14] and Laurent and Pellisier.[35] A change in rate determining step suggests that the reaction is stepwise as opposed to concerted. This will be discussed in Section 4.5

When the hydrolysis reaction is conducted using sodium salts instead of potassium salts then, for the same buffer concentration (0.05 M), there is a 43% increase in the rate of hydrolysis. Such cation effects are known to occur[66] and will be discussed in Section 4.5.

4.5 Discussion of the TAED and TriAED Hydrolysis Reaction

The hydrolysis reaction of TAED was initially followed spectrophotometrically over a wavelength range of 190 to 250 nm. Sequential spectra taken during the course of the reaction (Figure 4.4) showed a reduction in absorbance at the peak of 216 nm (corresponding to $\pi \rightarrow \pi^*$ transition for the C = O bond in conjunction with the non-bonded valence electron pair of the nitrogen[27]), and a corresponding increase in absorbance in the wavelength range attributable to DAED. There was quite a good isobestic point at 203.5 nm. On plotting ln ($A - A_\infty$) against time (Figure 4.5), it became evident that the hydrolysis reaction was biphasic, corresponding to the hydrolysis of TAED and TriAED. On statistical grounds it would be expected that the hydrolysis of TAED would be twice as fast as that for TriAED since TAED has twice the number of

Table 4.5 Effect of buffer concentration on the rate of hydrolysis of triacetylethylenediamine (TriAED). Conditions were: pH 9.80 potassium carbonate - potassium hydrogen carbonate buffer (I = 1.0M)*; 25°C.

[Buffer]/M	10^5kobs/s^{-1}
0.01	6.577
0.02	6.853
0.03	7.059
0.04	7.003
0.05	7.080
0.05**	10.136

*Ionic strength was made up to 1.0M using KCl.

**Using sodium salts as an alternative to potassium salts.

Figure 4.13 Effect of buffer concentration on the rate of hydrolysis (ko) of triacetylethylenediamine. The reactions were carried out in pH 9.80 potassium carbonate - potassium hydrogen carbonate buffer. The ionic strength was maintained at 1.0 M using KCl.

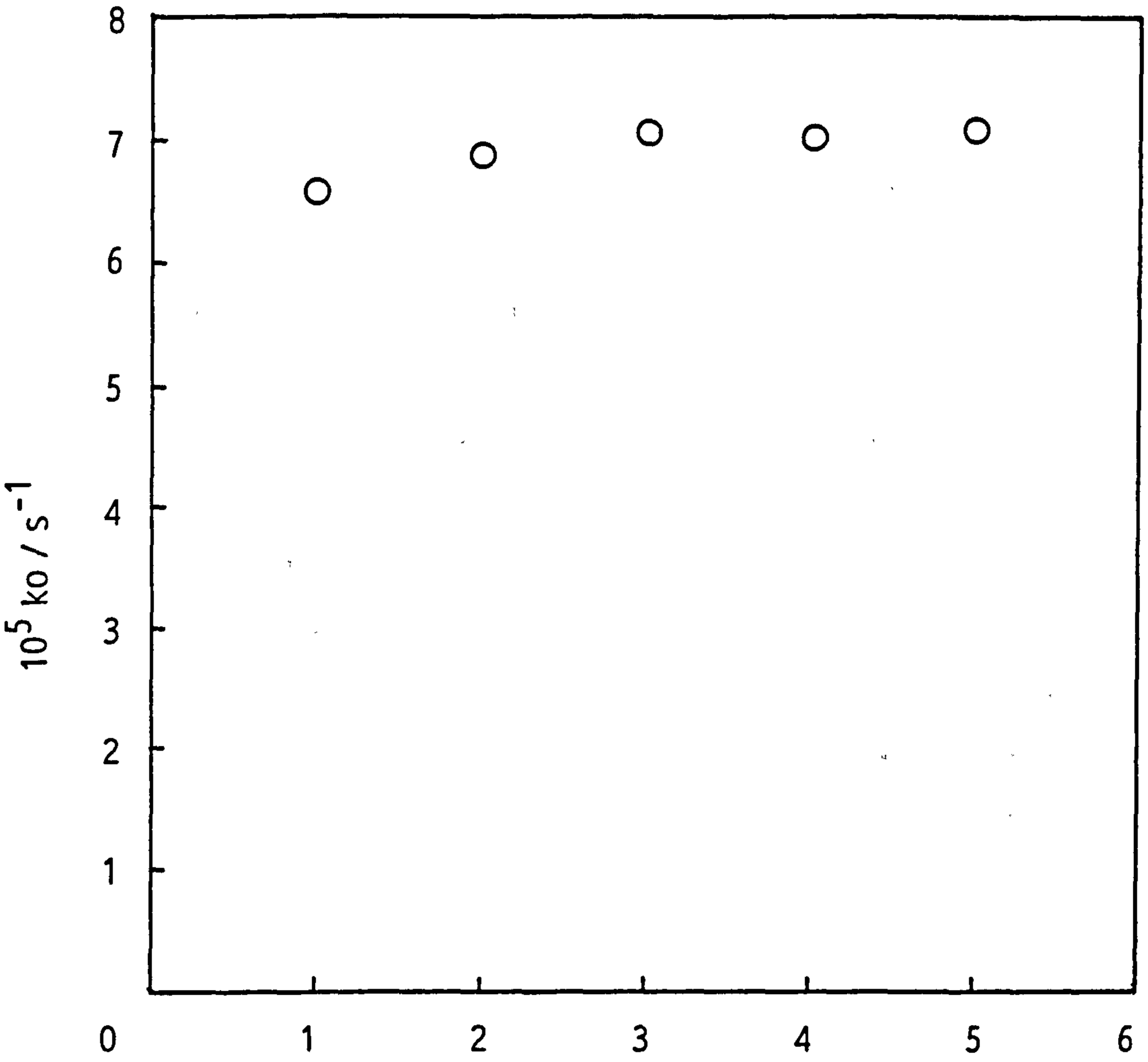

reactable acetyl groups. However, rate constants obtained from the ELORMA program gave a higher-than-expected ratio of 2.8. The explanation for this is attributed to the electron withdrawing nature of acetyl groups: in TAED, there are two opposite pairs of electron withdrawing acetyl groups, however, in TriAED, one acetyl group has reacted and has been replaced by a proton. The removal of the electron withdrawing acetyl group has the consequence, in TriAED, that the carbonyl carbons in the remaining imide group are slightly less electrophilic than in TAED and, therefore, less reactive.

Using data obtained from the ELORMA program at several different wavelengths, it was possible to calculate a spectrum for TriAED. The calculated spectrum compared well with the actual spectrum for isolated TriAED. The spectrum for TriAED generally shows the characteristics of both DAED and TAED, however, the peak corresponding to $\pi \rightarrow \pi^*$ transition in the imide group (220 nm) occurs at a longer wavelength than it does in TAED (216 nm). The explanation for the bathochromic shift is, again, due to the electron withdrawing nature of the acetyl groups: compared to TAED, the removal of an acetyl group in TriAED effectively means that there has been an addition of charge to the $\pi \rightarrow \pi^*$ transition in the remaining imide group, resulting in a bathochromic shift.[119]

From the results of the pH dependence study we can say, firstly, that the ratio of rate constants for TAED hydrolysis and TriAED hydrolysis (~ 2.8) is independent of pH over the pH range investigated (9.8 to 10.47). For the study conducted at I = 0.1 M (sodium salts), a slope of 0.819 was obtained from a plot of log k_{TriAED} against pH (Figure 4.1) for TriAED hydrolysis. The reason for the slope being less than the expected value of 1.0 for a simple first order dependence on hydro-

xide ion concentration, is likely to be due to general acid and general base catalysis by buffer components and/or a significant rate of reaction by the H_2O nucleophile. As the hydrolysis rate constants have not been extrapolated to zero buffer concentration for each pH, it is not possible to state which of the explanations is most valid. However, our limited study of buffer effects (Section 4.3) has indicated that there is catalysis of the hydrolysis reaction of TriAED. Laurent and Pellisier[35], working on the hydrolysis of the structurally similar N-methyldiacetamide [13], have shown that in the carbonate and phosphate buffers the reaction is likely to be catalysed only by the acid components of the buffer, that is, HCO_3^- and $H_2PO_4^-$. A similar situation should be expected for TAED and TriAED hydrolysis. Additionally, Laurent and Pellisier[35] proposed that the acid buffer components act as bifunctional catalysts, as is shown in Scheme 4.2.

Scheme 4.2

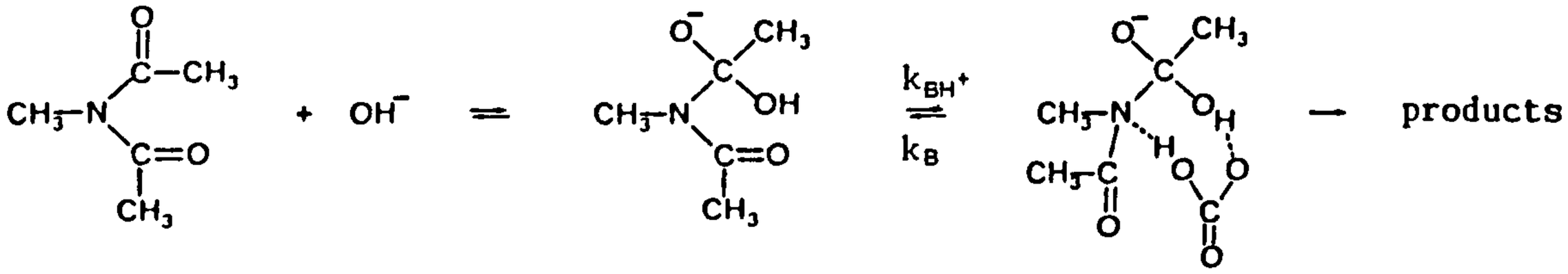

Although no evidence was produced for this particular mechanism, there is good evidence[85,87,120,121] for the existence of bifunctional catalysis, and its associated rate enhancement in comparison to monofunctional general acid and general base catalysts. (See Section 1.6.2 for a review of bifunctional catalysis.)

The existence of general acid catalysis for TAED and TriAED hydrolysis, with HCO_3^- acting as either a monofunctional or bifunctional catalyst, would explain the observed slope of 0.819 for the pH dependence study.

Laurent and Pellisier[35], in the absence of buffer, obtained a slope of 1.0 for a pH dependence study on the hydrolysis of N-methyldiacetamide.

There is also, of course, the contribution to the overall hydrolysis rate from the reaction of TAED and TriAED with H_2O to consider. Although no estimations of the extent of this reaction can be made from our data, Laurent and Pellisier[35] found that between pH 4.1 and 6.5 this reaction was the most significant, that is, the rate of hydrolysis was independent of pH in this region. (Below pH 4.1, the rate of hydrolysis showed a first order dependence on $[H^+]$.)

For our more extensive pH dependence study, conducted at I = 1.0 M (potassium salts), a slope of 0.938 was obtained. The same arguments used above to explain the slope being less than 1.0 apply. The fact that the slope for I = 1.0 M is higher than that for I = 0.1 M may be attributable to ionic strength effects and/or cation effects, and it is not possible, without further work on these effects, to say which is most valid.

Buffer Catalysis and Cation Effects. Section 4.4 described the limited study conducted into the effect of buffer concentration on the rate of TriAED hydrolysis. The results (Figure 4.13) show that there is catalysis by the buffer components, and these interactions have been discussed above. However, the observation that the rate increase levels off with increasing buffer concentrations is an interesting one. Laurent and Pellisier[35] have also observed such a levelling off, although they found this at higher buffer concentrations (0.1 M at pH 9.7) than our results suggest (0.03 M). They also found that, at pH 8.4, the limiting value for the rate constant was independent of the nature of the buffer, that is, phosphate or carbonate. The observed levelling off at higher buffer concentrations indicates a change in

rate determining step which, in turn, implies the formation of an intermediate along the reaction coordinate.[14] Khan, in 1988[14], observed such an effect for the general base catalysed hydroxylaminolysis of N-ethoxycarbonylphthalimide (ECPH) (Scheme 1.19 in Section 1.6.1). Of course, one must be sure when arriving at such conclusions that the levelling off, or non-linear dependence of the rate on buffer concentrations, is not due to other factors such as a changing pH with increasing buffer concentration. We observed that the pH of the buffer did change when diluted, however, this was corrected with added KOH. In a tentative conclusion from this limited study, and the work of Laurent and Pellisier on N-methyldiacetamide, we can suggest the following stepwise mechanism for TAED or TriAED hydrolysis.

Scheme 4.3

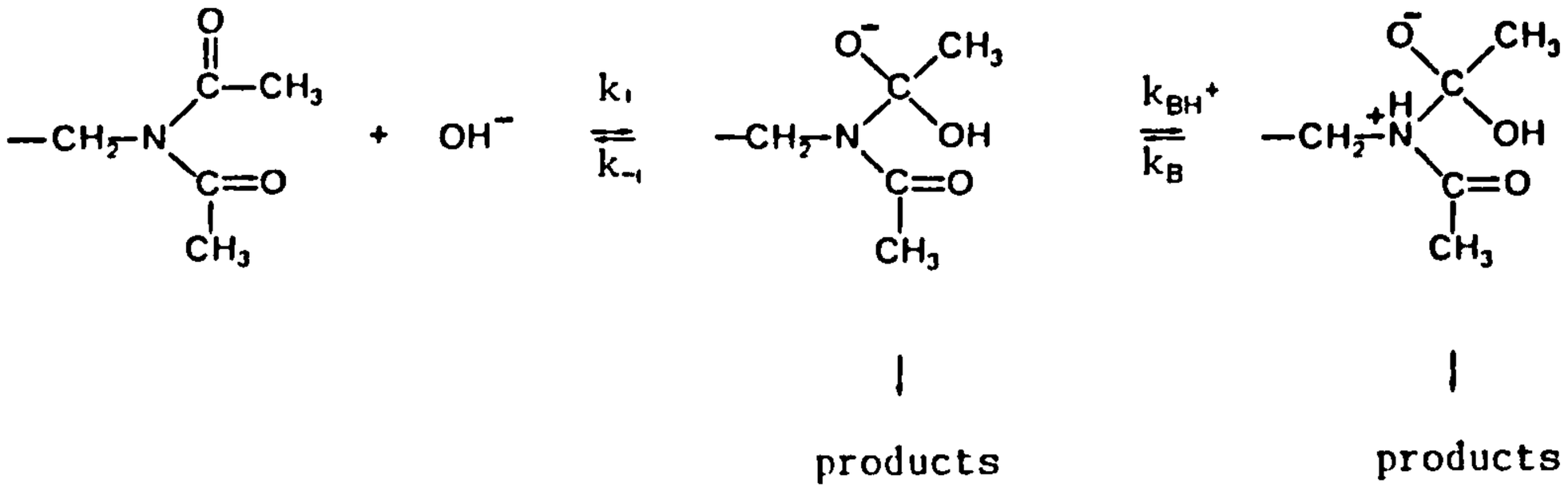

At higher buffer concentrations, k_1, the attack of the hydroxide ion becomes rate determining. It is likely, considering the discussion of catalysis in Section 1.6, that general acid catalysis is effected by protonation of the imide nitrogen rather than stabilization at the transition state by protonation of the carbonyl oxygen; protonation of the nitrogen allows the amide group to leave without the formation of the unstable RN^- anion.[16] The question of whether this catalysis

occurs by a monofunctional or bifunctional mechanism remains unanswered, although the bifunctional mechanism is appealing.

Finally, it was found that the cation used in the buffer components, and to maintain the ionic strength, had an effect on the rate of hydrolysis. In reactions carried out at 0.05 M carbonate buffer (I = 1.0 with KCl or NaCl) the rate of TriAED hydrolysis in the presence of sodium salts was 43% higher than in the presence of potassium salts. Bruice et al. in 1967[68], observed similar effects with the hydrolysis of phenylacetates. The ratio of values for hydroxide ion catalysed hydrolysis of phenylacetate in 1M salt solution was $(n\text{-}C_3H_7)_4NCl$: $(CH_3)_4NCl$: KCl : LiCl $\cong$ 0.63 : 1 : 2.4 : 2.9. Bruice et al.[68] suggested that this rate enhancement for potassium and, particularly, for lithium, was due to an interaction of the hydrated metal ion with the transition state of the ester, as shown in Scheme 4.4.

Scheme 4.4

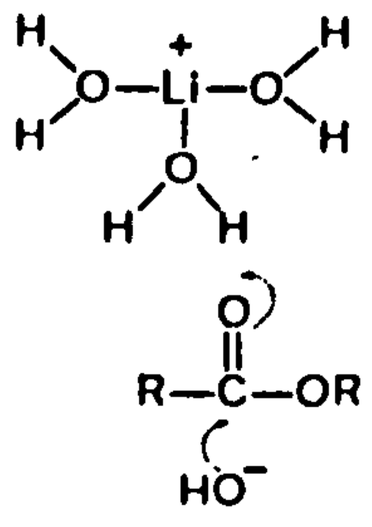

Here, the hydrated lithium ion, acts as a general acid catalyst. Thus, the rate enhancement shown by Na^+ ions and K^+ ions, for our results might be explained by such a catalytic mechanism in which hydrated Na^+ ions, like Hydrated Li^+ ions, were more effective than hydrated K^+ ions in protonating the transition state. This explanation would not, however, be consistent with the proposed Scheme 4.3 in which, at higher buffer concentration, the rate determining step became attack at the

hydroxide ion; these reactions were conducted at [Buffer] = 0.05 M, well above the point at which we observe attack of the hydroxide ion to become rate limiting and, therefore, catalysis by hydrated metal ions should have no effect. An alternative explanation is that the observed rate enhancements are due to the influence of the metal ion on the structure of water. The effect of an ion on water depends on its size and charge.[122] Small ions such as lithium (ionic radius 0.6 Å) increase the structure of water, whereas, the larger ions of potassium (1.33 Å), rubidium and caesium, disrupt the water structure.[122] The sodium ion, therefore (0.95 Å) is likely to have an intermediate effect between Li^+ and K^+.

CHAPTER 5 KINETIC STUDY OF THE TAED BLEACH ACTIVATION REACTION SCHEME

In Chapter 3, the studies of a model bleach activator, paranitrophenylacetate (PNPA) were described. Rate constants for the hydrolysis and perhydrolysis reaction were determined, and a computer program was used to simulate the overall activation reaction. This chapter describes how the same methods and approach were applied to the study of tetraacetylethylenediamine (TAED).

Using as a basis the model study on PNPA, and taking the results of the TAED hydrolysis investigation into account (Chapter 4), it was initially thought that Equations 5.1 to 5.8 would adequately describe the TAED bleach activation system.

$$TAED + H_2O \longrightarrow TriAED + Acetate \qquad \text{Eqn } 5.1$$

$$TriAED + H_2O \longrightarrow DAED + Acetate \qquad \text{Eqn } 5.2$$

$$TAED + H_2O_2 \longrightarrow TriAED + Peracetic\ acid \qquad \text{Eqn } 5.3$$

$$TriAED + H_2O_2 \longrightarrow DAED + Peracetic\ acid \qquad \text{Eqn } 5.4$$

$$TAED + Peracetic\ acid \longrightarrow TriAED + Diacetyl\ peroxide \qquad \text{Eqn } 5.5$$

$$TriAED + Peracetic\ acid \longrightarrow DAED + Diacetyl\ peroxide \qquad \text{Eqn } 5.6$$

$$Diacetyl\ peroxide + H_2O \longrightarrow Peracetic\ acid + Acetate \qquad \text{Eqn } 5.7$$

$$Diacetyl\ peroxide + H_2O_2 \longrightarrow 2\ Peracetic\ acid \qquad \text{Eqn } 5.8$$

The rate constants for TAED and TriAED hydrolysis (Equations 5.1 and 5.2) have been determined in the previous chapter; this chapter describes the elucidation of the remaining rate constants (Equations 5.3 to 5.8). The kinetic studies were carried out in carbonate buffer (sodium salts) at pH 9.60 (I = 0.1 M) and 25°C.

5.1 Timecourse of Bleach Activation for TAED

From the results of preliminary experiments (results not shown), it was

decided to follow the timecourse of bleach activation at pH 9.60. Additionally, owing to problems encountered with peroxide decomposition in these preliminary experiments, EDTA was replaced with ethylenediaminetetramethylenephosphonic acid hexasodium salt (EDTMP), as in the previous chapter.

Experimental

Materials

Analytical grade reagents were used wherever possible. TAED and carbonate buffer solutions (sodium salts) were prepared as described in Section 4.2. Hydrogen peroxide was standardized cerimetrically.[101] All solutions contained 1 x 10^{-5} M EDTMP.

Procedure

The reaction was started by mixing equal volumes of hydrogen peroxide/-carbonate buffer solution and TAED solution. Initial conditions upon mixing the solutions were: $[H_2O_2]_o$, 1.015 x 10^{-3} M; $[TAED]_o$, 0.5 x 10^{-3} M; sodium carbonate (decahydrate)/sodium hydrogen carbonate buffer, pH 9.60 (I = 0.1 M); $[EDTMP]_o$, 1 x 10^{-5} M. The peracetic acid and total iodide reactable peroxide concentrations were monitored during the course of the reaction (9000 seconds), as for the similar study of paranitrophenylacetate (PNPA) described in Chapter 3.

Results and Discussion

Figure 5.1 shows plots for the concentrations of peracetic acid, total iodide reactable peroxide, and hydrogen peroxide over the duration of the reaction; the concentration of hydrogen peroxide was calculated simply by subtracting the peracetic acid concentration from the total iodide reactable peroxide concentration. No detectable peroxide decomposition was observed during the course of the reaction. The concentration of total iodide reactable peroxide remained relatively constant

Figure 5.1 Change in the concentrations of: peracetic acid plus H_2O_2, ∇; peracetic acid, Δ; H_2O_2 calculated from the previous concentrations, □. Conditions were: pH 9.60 sodium carbonate - sodium hydrogen carbonate buffer (I = 0.1M) containing $1x10^{-5}$M EDTMP $[H_2O_2]_o = 1.015x10^{-3}$M; $[TAED]_o = 0.5x10^{-3}$M; 25°C.

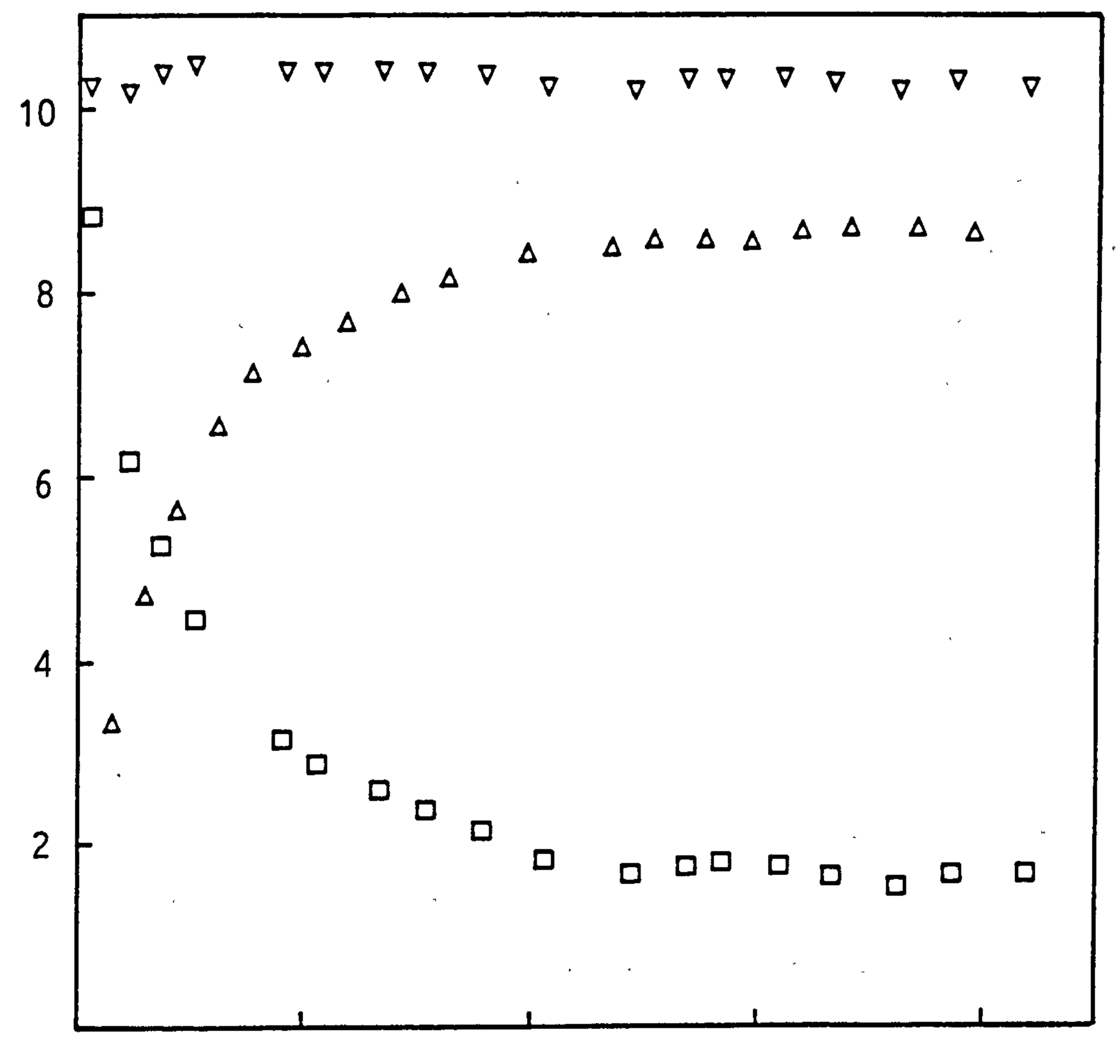

throughout the reaction, unlike the case for the similar study conducted using PNPA (Chapter 3) in which a temporary dip in concentration was observed, corresponding to a build up of the diacetyl peroxide. The maximum peracetic acid concentration (8.56 x 10^{-4} M) was attained after about 6500 seconds; the fall in hydrogen peroxide concentration mirrored the formation of peracetic acid, with 8.60 x 10^{-4} M being consumed in the reaction. The maximum yield of peracetic acid, 8.65 x 10^{-4}, compared to the theoretical maximum of 10 x 10^{-4} M, suggests that under these experimental conditions 13.5% of reactable acyl groups on the TAED underwent the hydrolysis reaction.

Although the results suggest that there is no build up of diacetyl peroxide during this reaction, this does not necessarily mean that peracetic acid is unreactive towards TAED; at pH 9.60, ignoring any buffer effects, and assuming normal pH dependence, the half-life for diacetyl peroxide hydrolysis is estimated as less than 10 seconds (based on the value for diacetyl peroxide hydrolysis reported in Table 3.11). Additionally, the pKa of peracetic acid is 8.2 and, consequently, at pH values above 8.2, the reaction of TAED with hydrogen peroxide will become proportionately larger than that with peracetic acid. This may explain the lack of any sigmoid nature in the curve describing peracetic formation which, even given the short half-life of diacetyl peroxide, might have been expected on the basis of the PNPA results, where reaction with peracetic acid was self-catalysing.

5.2 Determination of Rate Constants for the Reactions Occurring upon Mixing TAED and Hydrogen Peroxide Solutions

This section describes the measurement, where appropriate, of the rate constants corresponding to Equations 5.1 to 5.8 which, based on the results of a similar study using the 'model' activator, PNPA, are the reactions which might be expected to occur upon mixing TAED and hydro-

gen peroxide solutions. The experimental conditions used were identical to those used in the previous section, that is, pH 9.60 carbonate buffer, I = 0.1 M, 25°C.

Rate constants for the TAED and TriAED hydrolysis reactions (Equations 5.1 and 5.2) have already been determined (Chapter 4). Additionally, the results of preliminary experiments (not shown) indicated no detectable reaction between peracetic acid and TAED (Equations 5.5 and 5.6) under these experimental conditions; Figure 5.2 shows a second order plot of observed pseudo first order rate constants, k_{obs}, against peracetic acid concentration. These pseudo first order reactions, which were followed by measuring absorbance changes at 216 nm, corresponding to TAED, did, however, yield some interesting results. On plotting ln ($A - A_\infty$) against time, two phases to the reaction became apparent (see Figures 5.3 (a) - (d)). Examination of the data revealed that the two phases could not correspond to the differential rates expected for the reaction of TAED and TriAED with nucleophiles, as observed with hydrolysis; the percentage of the reaction that the initial 'fast' phase represented (up to 20%) was too small to correspond to the reaction of TAED with peracetic acid.

The initial fast phase of the reaction was found to be due to the reaction of TAED with hydrogen peroxide. Although hydrogen peroxide was removed from peracetic acid prior to the experiment (Section 3.2), under the alkaline conditions used in this study (pH 9.60), the peracetic acid can undergo alkaline hydrolysis to acetic acid and hydrogen peroxide.[112] Furthermore, the presence in the reaction solution of the very effective chelating agent, EDTMP, significantly reduces the extent of the trace metal ion catalysed reaction of hydrogen peroxide with peracetic acid, which would otherwise have occurred at pH 9.60.[111] This is demonstrated by Figure 5.4 which shows the effect of the pres-

Figure 5.2 Plot of pseudo first order rate constant (kobs) against nucleophile concentration for the reaction between peracetic acid and tetraacetylethylenediamine at 25°C in a pH 9.60 sodium carbonate -sodium hydrogen carbonate buffer (I = 0.1M): $[TAED]_o = 1x10^{-3}M$; $[EDTMP] = 1x10^{-5}M$.

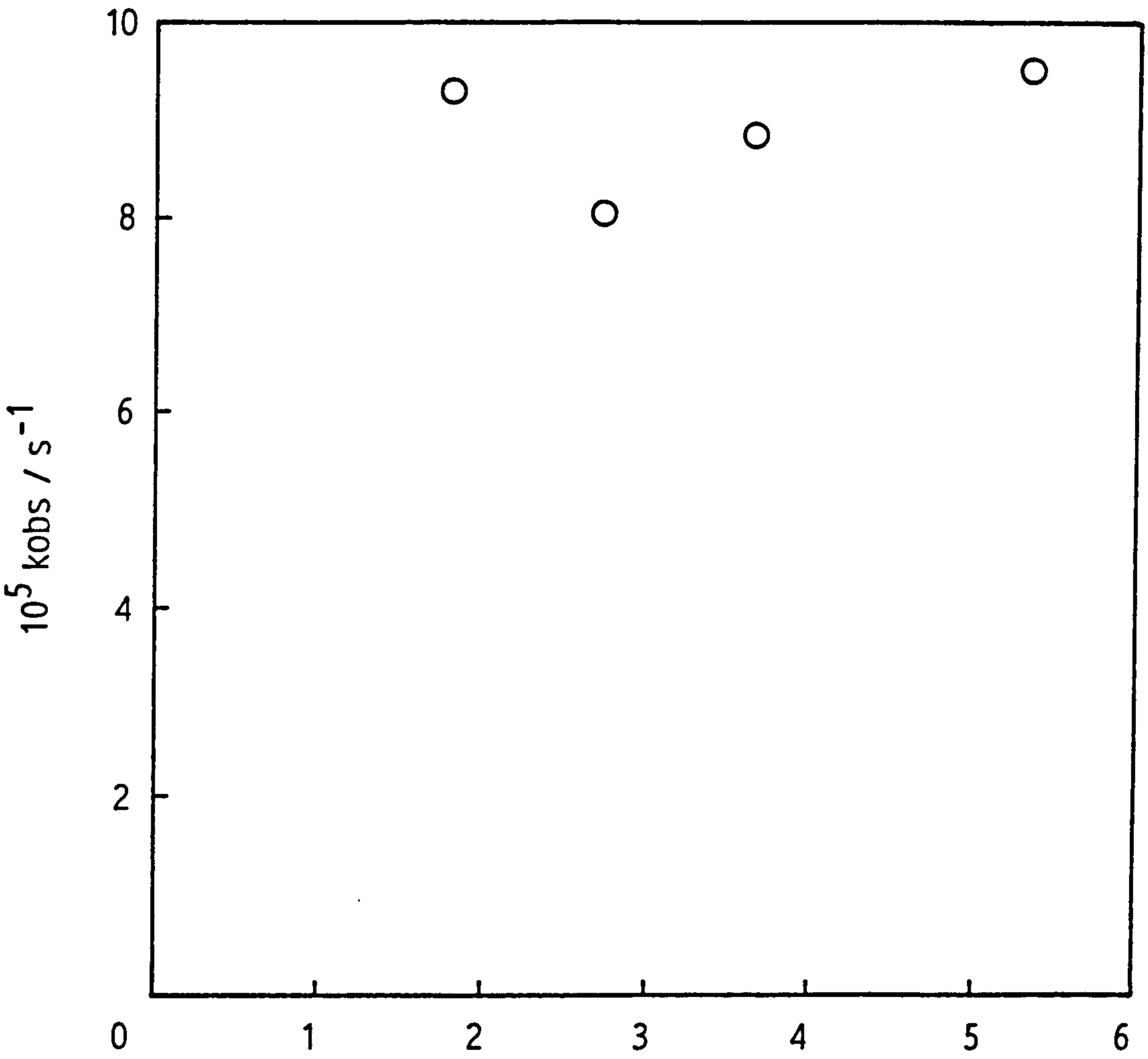

Figure 5.3 Pseudo first order plots for the reaction between tetraacetylethylenediamine and peracetic acid at 25°C in a pH 9.60 sodium carbonate - sodium hydrogen carbonate buffer (I = 0.1M): $[TAED]_o = 1x10^{-3}M$; $[EDTMP] = 1x10^{-5}M$. The lines represent the best fit using the linear least sqares method. Absorbance measurements were made at 216 nm.

(a) [Peracetic acid] = $1.800x10^{-3}M$

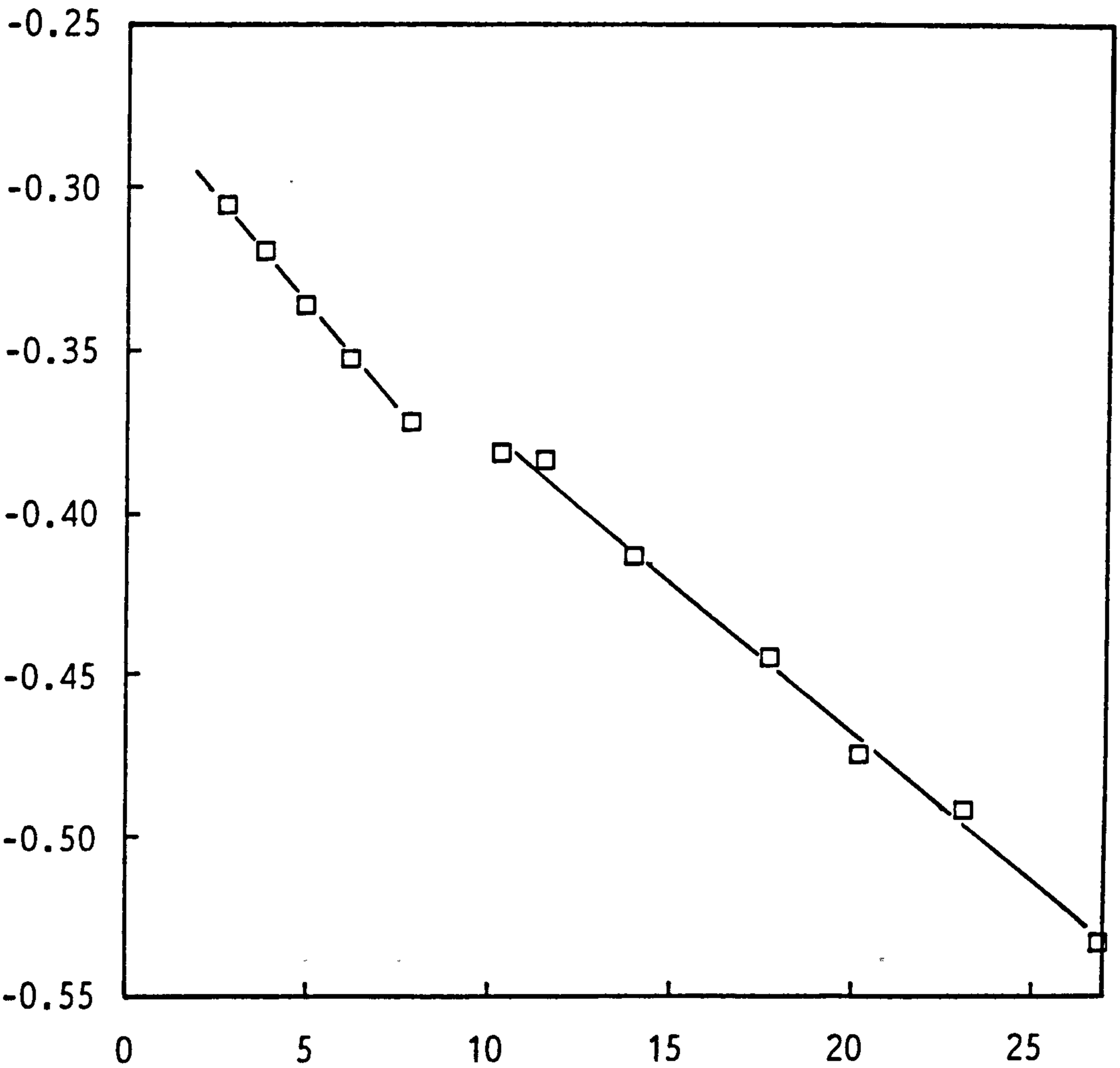

Figure 5.3(b) [Peracetic acid] = 2.716×10^{-3}M

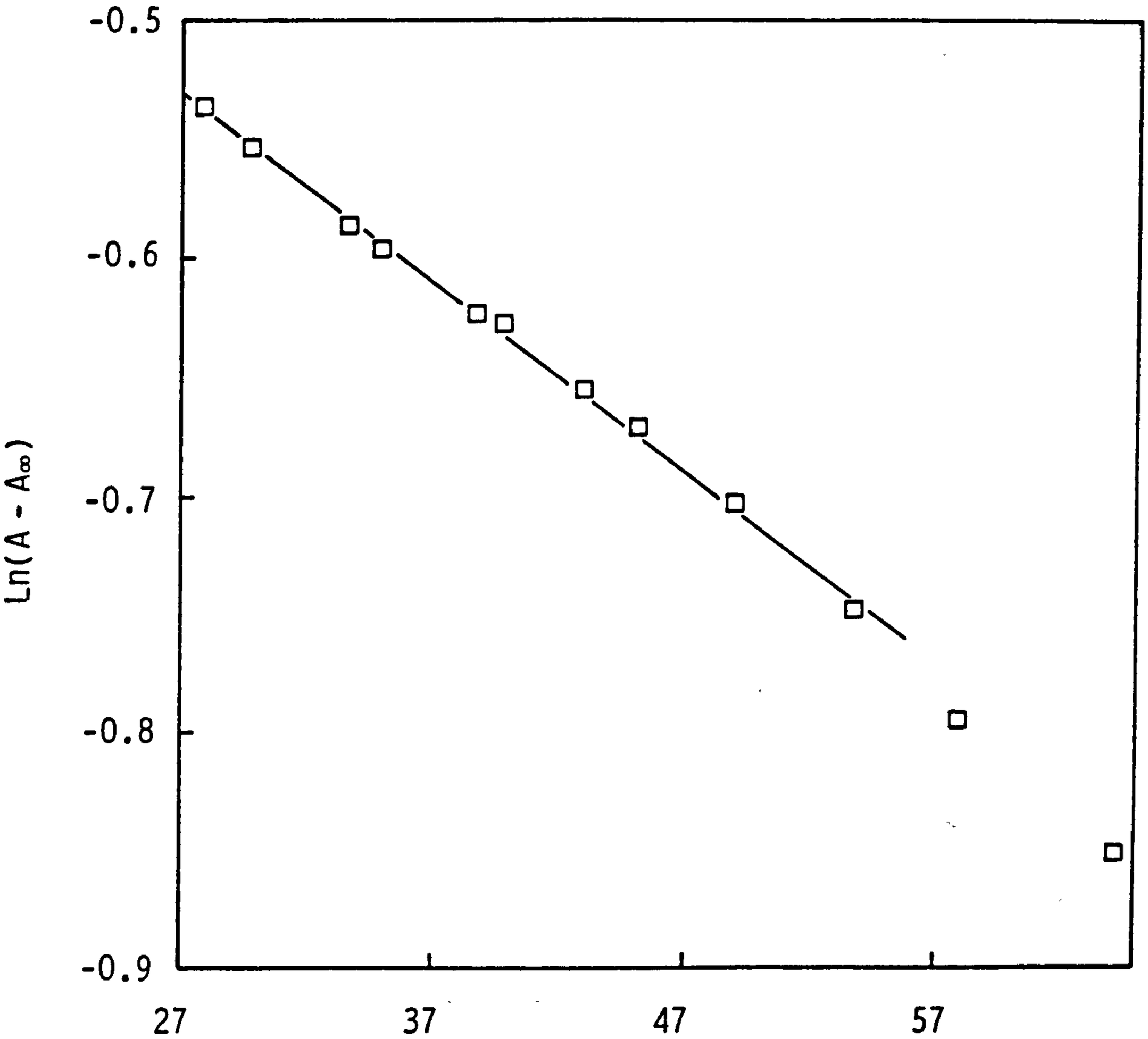

Figure 5.3(c) [Peracetic acid] = 3.636×10^{-3} M

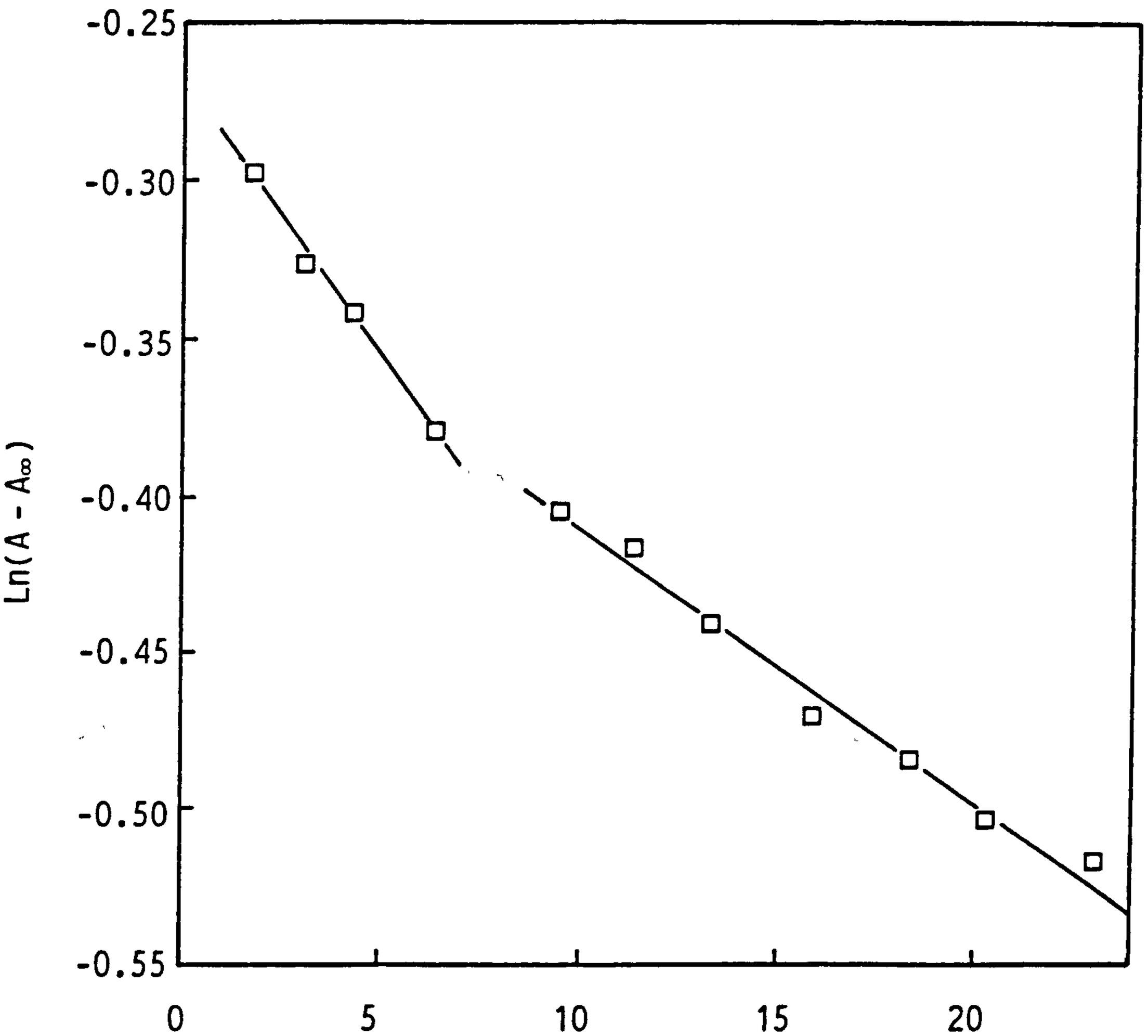

Figure 5.3(d) [Peracetic acid] = 5.328×10^{-3} M

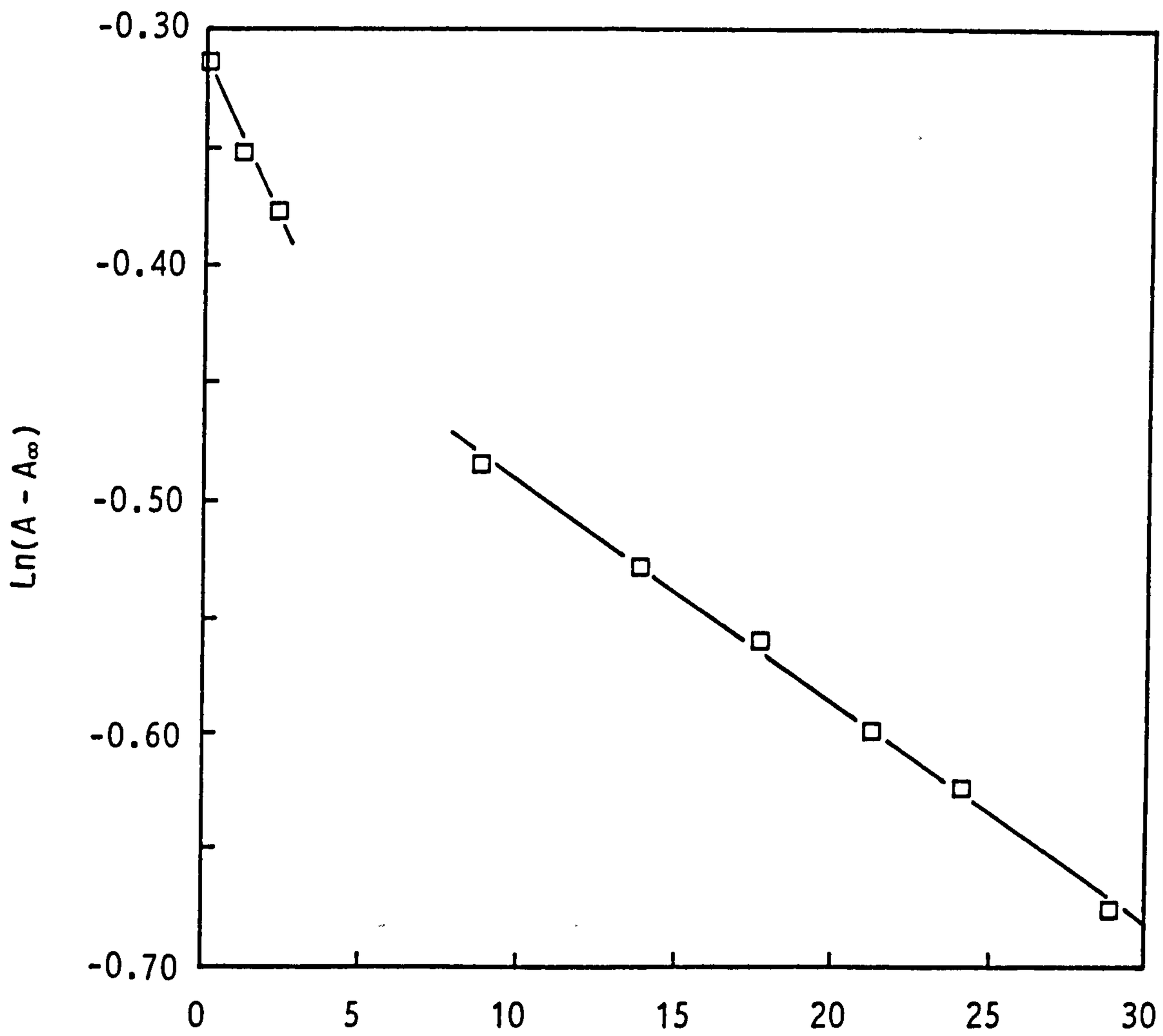

Figure 5.4 Time-course of hydrogen peroxide formation resulting from the hydrolysis of peracetic acid in a pH 9.60 carbonate buffer (I = 0.1M) at room temperature. The effect of the presence, □, and absence, Δ, of $1x10^{-5}$M EDTMP is shown. The initial concentration of peracetic acid was $5.54x10^{-3}$M.

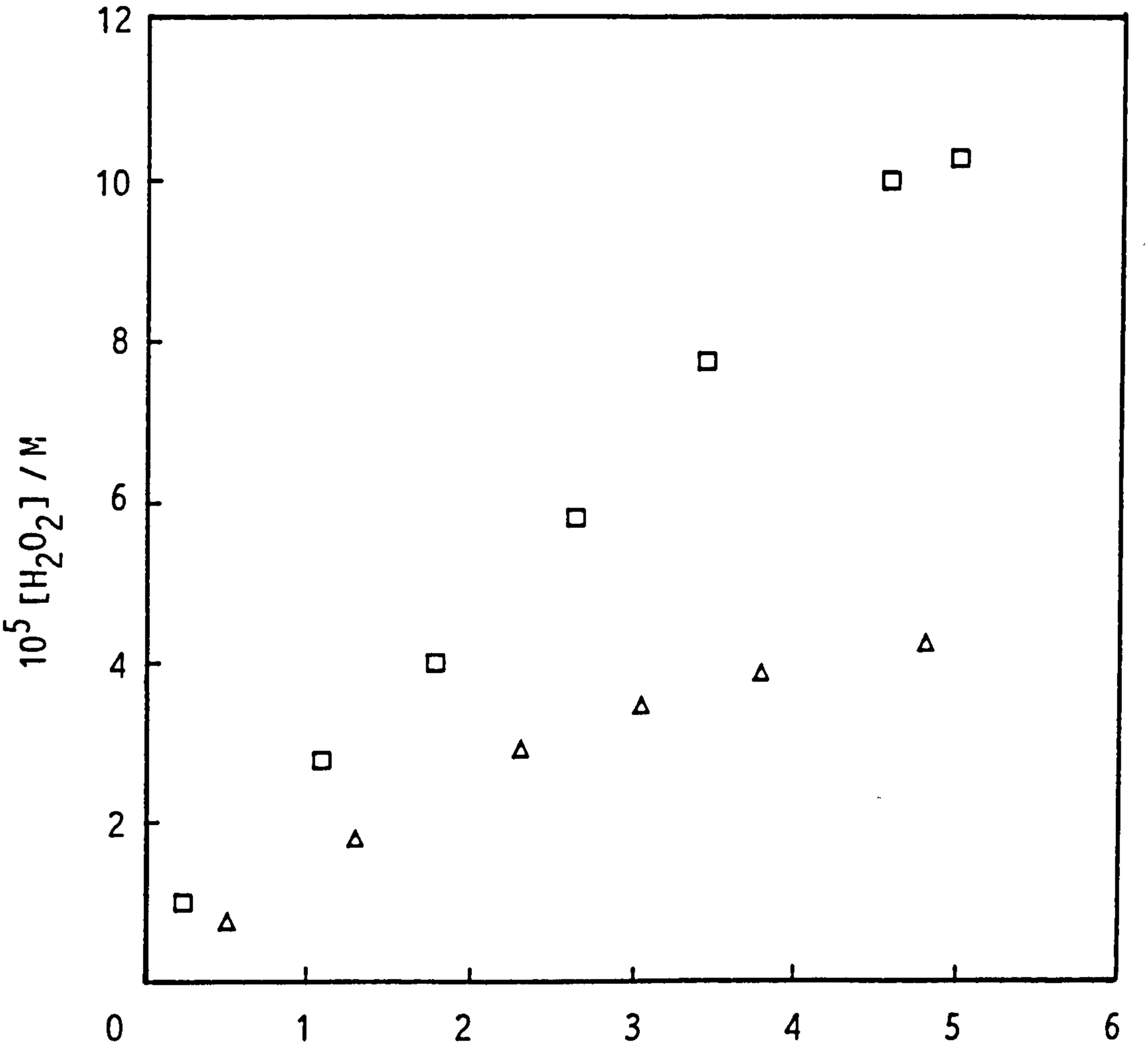

ence of EDTMP on the formation of hydrogen peroxide in a solution of peracetic acid (5.54×10^{-3} M in pH 9.60 carbonate buffer) from which hydrogen peroxide had initially been removed. Hydrogen peroxide was determined in the presence of excess peracetic acid using a H_2O_2 specific titanium sulphate assay.[97,98] Clearly, although hydrogen peroxide builds up in both solutions, in the presence of EDTMP the build up is greater; the reasons for this are discussed above. It was often the case that the peracetic acid/carbonate buffer solutions used in kinetic runs were prepared up to an hour before their use, thus giving time for the H_2O_2 build up.

In light of these results, the rate constants corresponding to Equations 5.5 to 5.8 are now not considered significant and were not determined. The rate constants corresponding to Equations 5.3 and 5.4, the reaction of TAED and TriAED with hydrogen peroxide, were determined as described in Sections 5.2.1 and 5.2.2, respectively.

5.2.1 Determination of the Observed Second Order Rate Constant for the Reaction of TAED with Hydrogen Peroxide

We have seen in the study of TAED hydrolysis (Chapter 4) that TAED hydrolyses 2.8 times faster than TriAED; the reasons for this have been discussed. It is expected, at least on statistical grounds, that TAED and TriAED will show differential rates of reaction with hydrogen peroxide.

The measurement of the reaction rates of TAED and TriAED with hydrogen peroxide presents practical problems, principally, in devising methods to separate the two rate constants. The method used to obtain two separate rate constants for TAED hydrolysis was found to be unsuitable in this case since, under pseudo first order conditions, the rate of reaction is likely to have been so rapid that only a few measurements

could be taken before the completion of the reaction.

The method used to obtain a rate constant for the reaction between TAED and hydrogen peroxide was to follow the liberation of peracetic acid in a solution containing TAED in excess over hydrogen peroxide under pseudo first order rate conditions. Under these conditions, with at least tenfold excess of TAED over hydrogen peroxide, then the contribution of TriAED perhydrolysis to the rate constant will be negligible.

Experimental

Materials

The preparation of TAED and carbonate buffer solutions has been described under Section 4.2. Solutions of hydrogen peroxide were standardized cerimetrically.[101] All solutions contained 1 x 10^{-5} M EDTMP.

Procedure

Under pseudo first order conditions, the release of peracetic acid was followed for solutions of hydrogen peroxide (4.3 x 10^{-5} M) in the presence of TAED (ranging from 0.5 x 10^{-3} to 0.9 x 10^{-3} M). The solution was maintained at pH 9.60 using a carbonate buffer (sodium salts). It should be noted that the range of TAED concentrations was restricted due to its low solubility.

Results

Figure 5.5 shows a typical plot of peracetic acid formation for the reaction of TAED with hydrogen peroxide. Pseudo first order rate constants were obtained from linear regression of ln ($[PA]_\infty$ - [PA]) against time. The plots, an example of which is shown in Figure 5.6, were linear up to at least 4 half-lives. The mean observed second order rate constant for reaction of TAED with hydrogen peroxide
(3.347 s^{-1} M^{-1}) was obtained by dividing the pseudo first order constants (listed in Table 5.1) by the nucleophile concentration. Figure

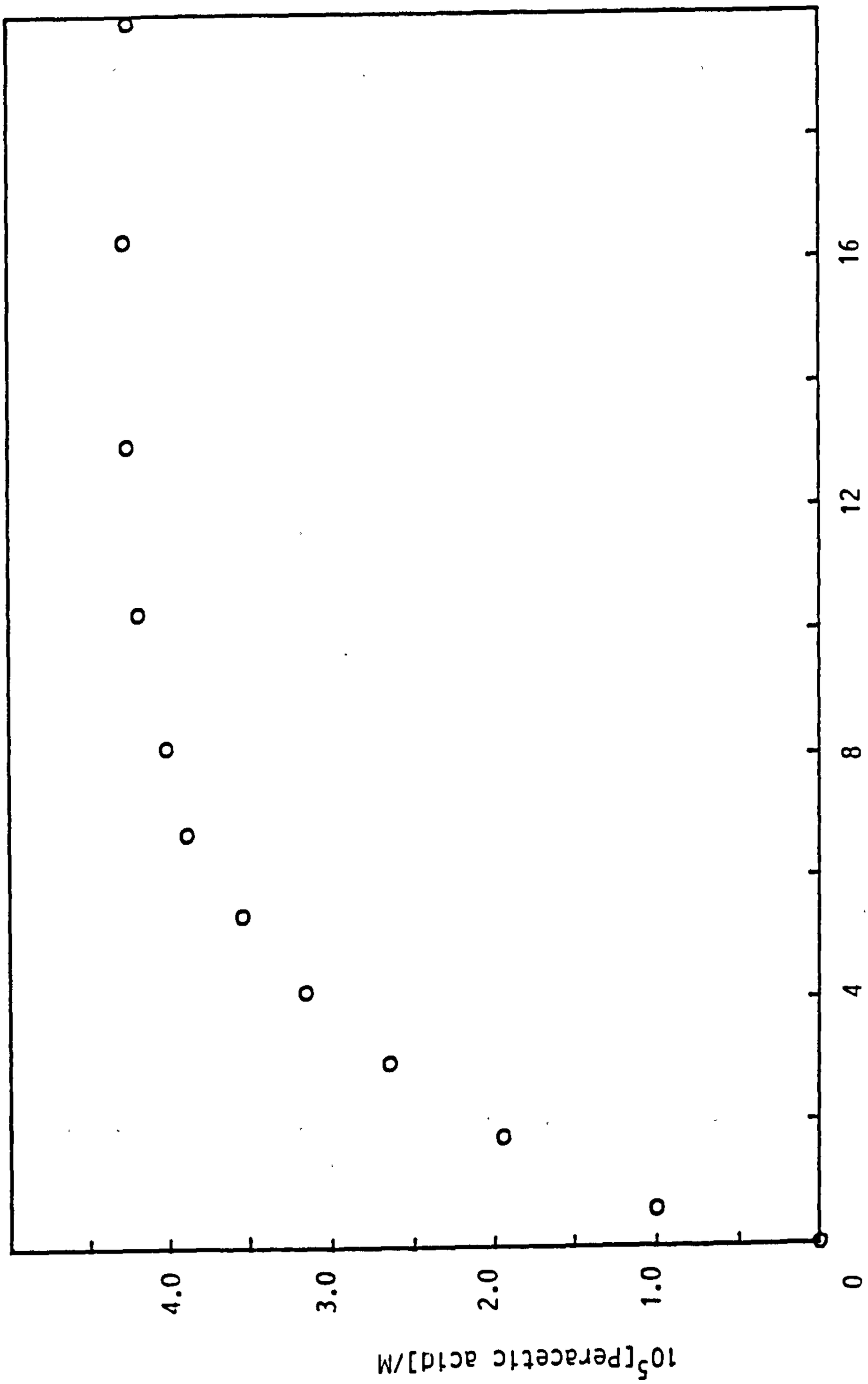

Figure 5.5 Plot showing the formation of peracetic acid during the reaction between hydrogen peroxide and excess tetraacetylethylenediamine at 25°C in pH 9.60 sodium carbonate - sodium hydrogen carbonate buffer (I = 0.1M): $[H_2O_2]_o = 4.3x10^{-5}$M; [TAED] = $0.9x10^{-3}$M; [EDTMP] = $1x10^{-5}$M.

Figure 5.6 Pseudo first order plot for the reaction between hydrogen peroxide and excess tetraacetylethylenediamine at 25°C in pH 9.60 sodium carbonate - sodium hydrogen carbonate buffer (I = 0.1M): $[H_2O_2]_o = 4.3x10^{-5}M$; $[TAED] = 0.9x10^{-3}M$; $[EDTMP] = 1x10^{-5}M$. The reaction was followed by measuring peracetic acid (PA) formation. The line represents the best fit using the linear least squares method for data over the initial linear region of the plot.

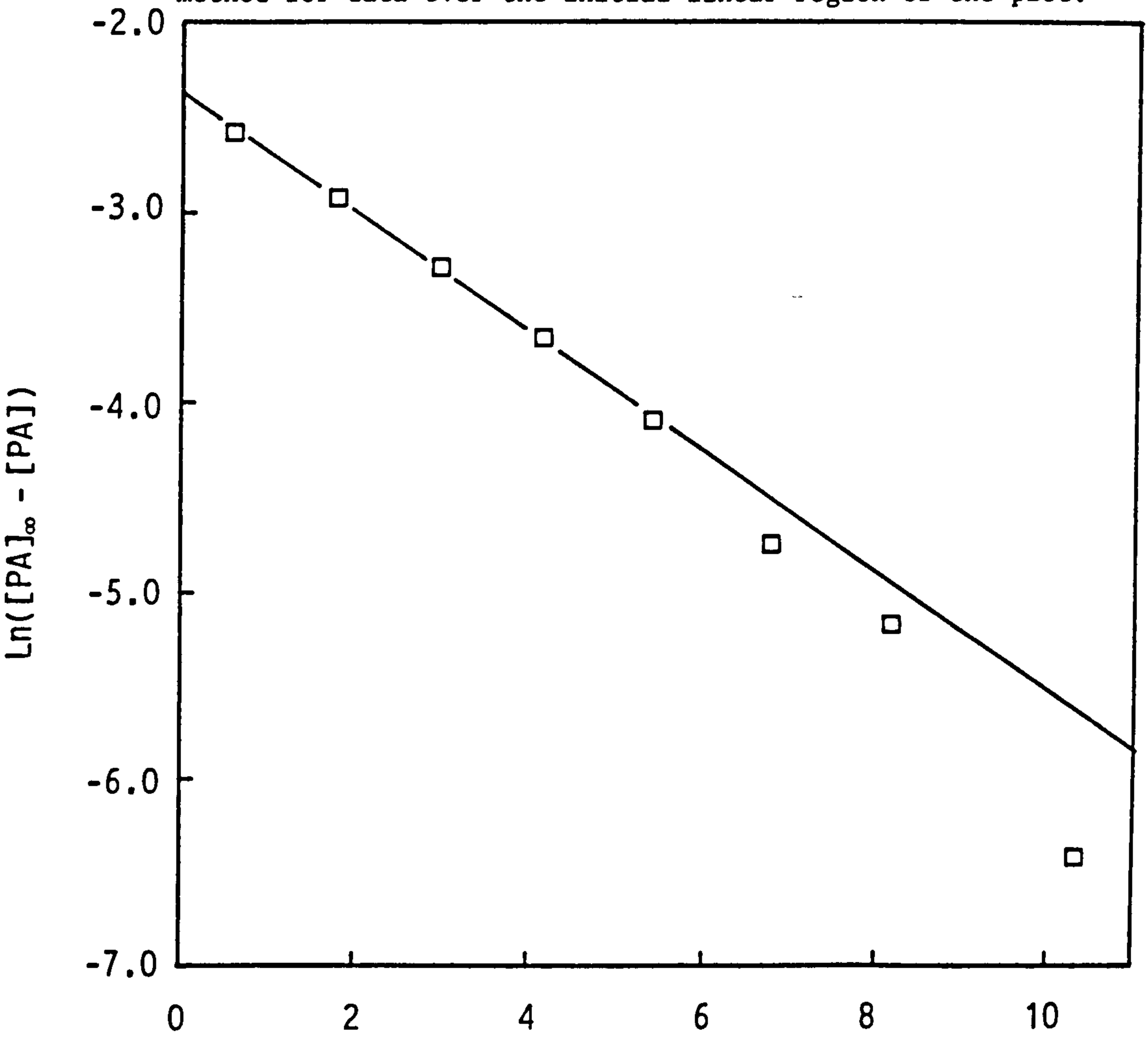

Table 5.1 Observed pseudo first order rate constants (kobs) for the reaction between tetraacetylethylenediamine (TAED) and hydrogen peroxide. Conditions were: pH 9.60 sodium carbonate - sodium hydrogen carbonate buffer (I = 0.1M); $[H_2O_2] = 4.3 \times 10^{-5}$M; [EDTMP] = 1×10^{-5}M; 25°C.

10^3[TAED]/M	10^3kobs/s^{-1}
0.5	1.610
0.6	2.073
0.7	2.294
0.8	2.636
0.9	3.141

5.7 shows the plot of pseudo first order rate constants against TAED concentration drawn with a slope defined by the mean observed second order rate constant.

5.2.2 Determination of the Observed Second Order Rate Constant for the Reaction of TriAED with Hydrogen Peroxide

Preliminary experiments were conducted (results not shown) in which peracetic acid liberation was followed in solutions containing TAED in the presence of excess hydrogen peroxide under pseudo first order conditions. In a biphasic reaction system, peracetic acid (PA) release is described by Equation 5.9:

$$[PA] = [PA]_\infty + [PA]_1 e^{-k1t} + [PA]_2 e^{-k2t} \qquad \text{Eqn 5.9}$$

where $[PA]_\infty$, $[PA]_1$, and $[PA]_2$ are constants and k_1 and k_2 are the pseudo first order rate constants corresponding to the reaction of H_2O_2 with TAED and TriAED, respectively. If $k_1 > k_2$ then, at some point in time, $[PA]_1 e^{-k1t}$ will approach zero and, after this point, a plot of $\ln ([PA]_\infty - [PA])$ against time will yield a slope corresponding to the rate of reaction of TriAED with hydrogen peroxide. It was found, however, that the peracetic acid liberation was too rapid and only a few measurements could be made during the course of the reaction. Consequently, a value for the rate of reaction of TriAED with hydrogen peroxide could not be accurately determined using this method.

A more reliable value was obtained by numerical solution to differential equations corresponding to Equations 5.1 to 5.4. Only these Equations are considered to be significant since it has been shown that peracetic acid reacts very slowly, if at all, with TAED.

Inputting the initial conditions of the TAED bleach activation study described in Section 5.1 (Figure 5.1) and the reliable values determined for the rate constants corresponding to Equations 5.1, 5.2, and 5.3,

Figure 5.7 Plot of pseudo first order rate constant (kobs) against substrate concentration for the reaction between hydrogen peroxide and tetraacetylethylenediamine at 25°C in pH 9.60 sodium carbonate - sodium hydrogen carbonate buffer (I = 0.1M): $[H_2O_2]_o = 4.3 \times 10^{-5}$M; [EDTMP] = 1×10^{-5}M. The line corresponds to the mean value of kobs / [TAED].

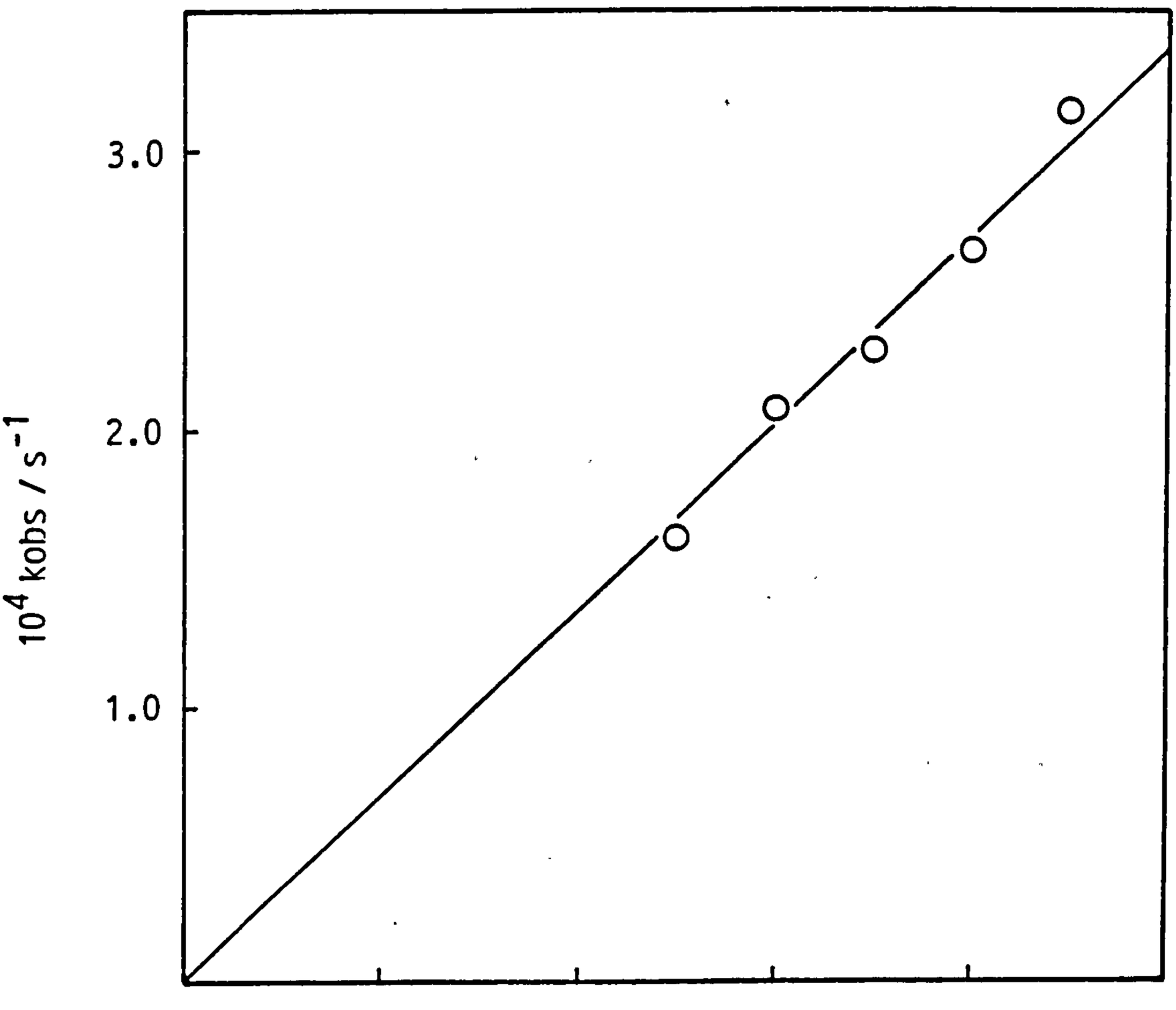

a computer program was used to calculate the numerical solution to the differential equations corresponding to these equations. A guessed value for the reaction corresponding to Equation 5.4 was used in the program, and this was modified until the best fit with the experimental data in Figure 5.1 was achieved (1.16 M^{-1} s^{-1}) (Figure 5.8). Figure 5.9 clearly demonstrates the high degree of sensitivity of the method in determining the rate of reaction of TriAED with hydrogen peroxide; the two sets of curves correspond to estimated values of 1.16 ± 0.16 M^{-1} s^{-1}. Table 5.2 contains a summary of the rate constants corresponding to Equations 5.1 to 5.4. The ratio of the rate constants for the reaction of TAED and TriAED with hydrogen peroxide, 2.88, is almost exactly the same as that observed for the respective hydrolysis reactions.

5.3 General Discussion

The reaction of TAED with hydrogen peroxide at pH 6.8 proceeded very slowly, and so it was necessary to conduct the study of TAED hydrolysis and perhydrolysis reactions at pH 9.6, where the rates of reaction could be practicably measured. From our discussion of the comparative reactivities of esters and amides, in Section 1.2, it should not be surprising that the activated ester PNPA is more reactive than TAED.

In Chapter 4, it was found that the ratio of rate constants for TAED and TriAED hydrolysis reactions was 2.8, and the reasons for this have been discussed. An almost identical ratio (2.88) was found for the respective reactions with hydrogen peroxide; this suggests that the same factors influencing the relative reactivity of TAED and TriAED towards the hydroxide ion are also influencing the reactivity towards hydrogen peroxide.

Figure 5.8 Change in the concentrations of: peracetic acid plus H_2O_2, Δ; peracetic acid, O; H_2O_2 calculated from the previous concentrations, □. Conditions were: pH 9.60 carbonate buffer (I = 0.1M); $[H_2O_2]_o = 1.015 \times 10^{-3}$; $[TAED]_o = 0.5 \times 10^{-3}$M; $[EDTMP] = 1 \times 10^{-5}$M; 25°C. The curves represent numerical solution to differential equations corresponding to Equations 5.1 to 5.4.

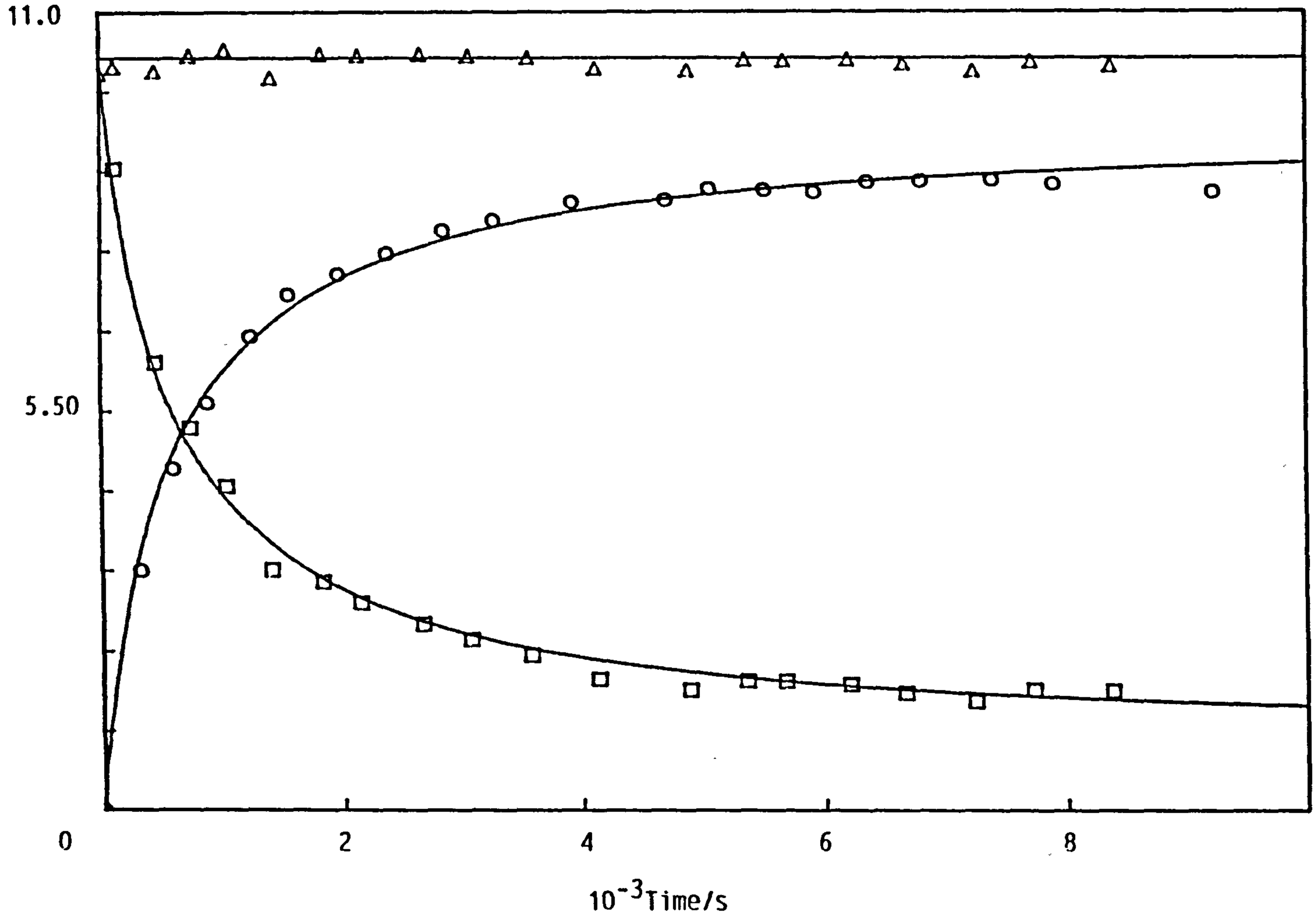

Figure 5.9 Change in the concentrations of: peracetic acid plus H_2O_2, Δ; peracetic acid, O; H_2O_2 calculated from the previous concentrations, □. The curves represent the numerical solution of differential equations corresponding to Equations 5.1 to 5.4. The two sets of curves correspond to values of $1.16 \pm 0.16\ M^{-1}s^{-1}$ for the rate constant corresponding to Equation 5.4.

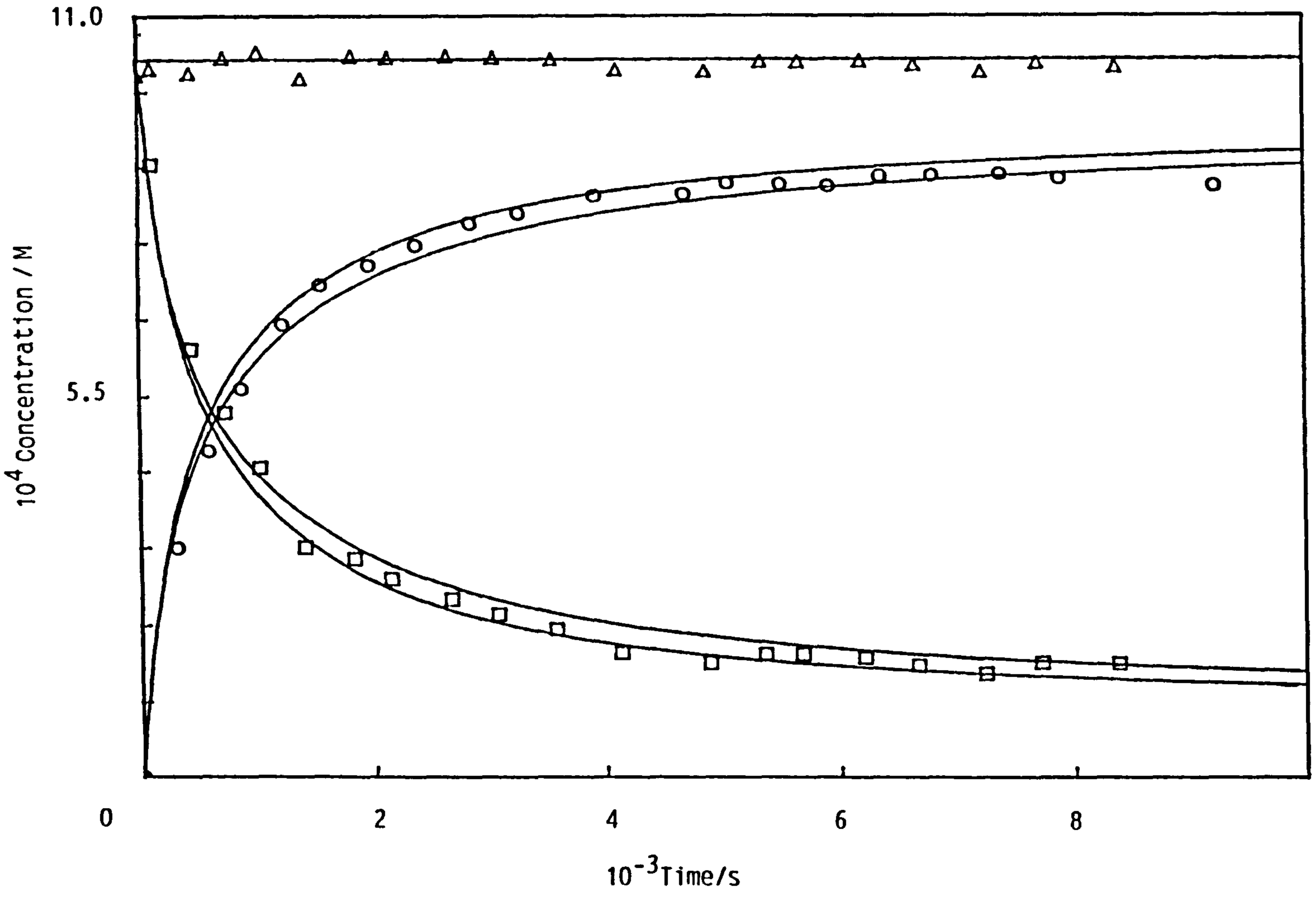

Table 5.2 Summary of rate constants for the main reactions which occur upon mixing hydrogen peroxide and TAED in a pH 9.60 carbonate buffer (I = 0.1M), 25°C.

Reaction		Rate constant
TAED + H_2O_2	(Eqn. 5.3)	$3.347 \pm 0.123\ M^{-1}s^{-1}$ *
TriAED + H_2O_2	(Eqn. 5.4)	$1.160 \pm 0.160\ M^{-1}s^{-1}$ **
TAED + H_2O	(Eqn. 5.1)	$1.400 \times 10^{-4}\ s^{-1}$
TriAED + H_2O	(Eqn. 5.2)	$0.499 \times 10^{-4}\ s^{-1}$

* 90% Confidence limits.

** Error obtained using numerical integtration method as described in the text.

Table 5.3 Predicted yields of peracetic acid for various initial H_2O_2 : TAED ratios.

Ratio of $[H_2O_2]_o$ to $[TAED]_o$	Predicted yield of peracetic acid (%)	
	$[TAED]_o = 5 \times 10^{-4}M$	$[TAED]_o = 1 \times 10^{-3}M$
2	91.0	94.0
3	95.8	97.7
4	97.2	98.6
5	97.9	98.9
10	99.0	99.5

Probably the most important result to emerge from this study is the unreactivity of peracetic acid towards TAED and TriAED, quite unlike the PNPA model study. Figure 5.2 shows a plot of pseudo first order rate constants against peracetic acid concentration for the reaction with TAED; clearly there is little correlation between the nucleophile concentration and rate. From linear regression of this data, an upper limit of (1.63 $\pm$ 8.19)* x 10^{-3} M^{-1} s^{-1} was obtained for the observed second order rate constant at pH 9.60. Given the low reactivity of peracetic acid with TAED (and TriAED), the reactions involving diacetyl peroxide, which were important for the PNPA system, are, consequently, insignificant for this system. It has been stated already that one reason for the relative unreactivity of peracetic acid towards TAED, compared to the reactivity of hydrogen peroxide, concerns the respective pKa values of the two peroxides (8.2 for peracetic acid and 11.6 for hydrogen peroxide). Assuming that it is the anionic forms of the peroxides which react, then at pH values above 8.2 the ratio of observed rate constants for the reactions of TAED with peracetic acid and hydrogen peroxide will be greater than at pH values below 8.2. It is doubtful, however, if this factor can solely account for the unreactivity of peracetic acid. Other explanations are therefore required.

It is possible that there is an unusually large dependence of nucleophilicity on basicity for these reactions. A study of the structure-reactivity relationships of the reactions of TAED and TriAED was, therefore, carried out, and this is described in the following two chapters. The theory behind the Brønsted-type relationships between nucleophilicity and basicity has been stated in Chapter 1. If such studies revealed a 'normal' relationship (β = 0.3 to 1.0) for series

---

* 90% confidence limits

of nucleophiles, including peroxides, then this would suggest that either hydrogen peroxide is reacting unusually fast, or that peracetic acid is sterically or, in some other way, hindered in its reaction with TAED and TriAED. A Brønsted-type plot with a slope substantially above 1.0 would, on the other hand, be consistent with the results.

Finally concerning the use of TAED as a commercial bleach activator, it is important to point out that the wasteful hydrolysis reaction is competing with the reaction of TAED and hydrogen peroxide. By varying the initial concentration of reactants, however, it is possible to decrease the comparative extent of the hydrolysis reaction. Using the computer simulation program of the TAED bleach activation system and the rate constants contained in Table 5.2, then it has been possible to calculate the percentage of the theoretical maximum yield of peracetic acid per mole of TAED for various hydrogen peroxide : TAED ratios (at pH 9.60) and these data are contained in Table 5.3; peracetic acid yields of 99%, or better, should be obtainable for a 10:1 mole ratio of hydrogen peroxide : TAED, under these controlled experimental conditions.

CHAPTER 6 REACTION OF TAED AND TriAED WITH A SERIES OF AMINES AND ALCOHOLS

The studies contained within this and the subsequent chapter have the aim of obtaining second order rate data for the reactions of a range of nucleophiles with TAED and TriAED; such data can then be used to construct Brønsted-type plots, from which it can be ascertained whether or not a 'normal' Brønsted-type relationship exists (ß = 0.3 to 1.0) for the reaction of nucleophiles with TriAED (and TAED); results obtained for studies described in the previous chapter, that is, the low reactivity towards TriAED of peracetic acid compared to hydrogen peroxide, suggested the possibility of an abnormally high dependence of nucleophilicity on basicity for reactions with TriAED (or TAED). This chapter examines the reaction of TAED and TriAED with primary amines and also with alcohols. These nucleophiles, particularly amines, have been widely used in the literature in determining the sensitivity of reactions to nucleophile basicity.

Section 6.1 describes the experimental protocol used in the studies described in this and the subsequent chapter. In Section 6.2, the study of the reaction of TriAED and TAED with glycine and n-butylamine is described, including details of a CO_2-free experimental protocol; this was necessary in order to alleviate problems encountered with CO_2 dissolution into buffer mixtures, causing a lowering of the pH. Section 6.3 gives an account of the study of the reaction of TriAED with methanol and with trifluroethanol. A general discussion of the aminolysis and alcoholysis studies is contained in Section 6.4.

All spectrophotometric measurements were made using the Hewlett Packard HP 8451 diode array spectrophotometer fitted with thermostatted cell holder.

6.1 Techniques for Conducting Experiments in CO_2-free Conditions

Preliminary experiments conducted on the reactions of n-butylamine (at pH 10.44) and glycine (at pH 9.83) with TriAED, in which the amine was used as both buffer and nucleophile, indicated that at amine concentrations below 0.1 M problems were encountered due to CO_2 dissolution into the solution. This has the effect of lowering the pH of the buffer solutions, with a consequent reduction in the fraction of free base. In addition, CO_2 is known to react with aqueous solutions of primary and secondary amines.[123] Figure 6.1 clearly demonstates the problems encountered during the reaction of TAED with n-butylamine under pseudo first order conditions in which CO_2-free conditions were *not* employed. There is deviation from linearity in the plot after less than one half-life.

In order to avoid such interference, CO_2-free conditions were employed; the experimental protocol for obtaining such conditions is described below. Unless otherwise stated, the experimental procedures detailed in this chapter employed CO_2-free conditions.

6.1.1 General Techniques

CO_2 was removed from distilled water by boiling for ten minutes; the water was stored in an aspirator which had previously been flushed with nitrogen for five minutes. The inlet of the aspirator was fitted with an absorption tube containing soda lime granules (BDH 'carbasorb' brand). All solutions were made up in CO_2-free distilled water. One M potassium hydroxide solution was prepared from a BDH 'Convol' solution and stored in an aspirator as with the distilled water. Buffers and nucleophile solutions were prepared in a sealed vessel under nitrogen.

6.1.2 Preparation of Buffer and Nucleophile Solutions

Buffer/nucleophile solutions were prepared under nitrogen at 25°C in a

Figure 6.1 Pseudo first order plot for the reaction between triacetylethylenediamine and n-butylamine at 25°C in a pH 10.44 sodium carbonate - sodium hydrogen carbonate buffer (I = 1.0M, with NaCl): $[TAED]_o = 1x10^{-3}M$; [n-butylamine] = $8.6x10^{-3}M$. The line represents the best fit using the linear least squares method for data in the initial linear region of the plot. Absorbance measurements were made at 230 nm.

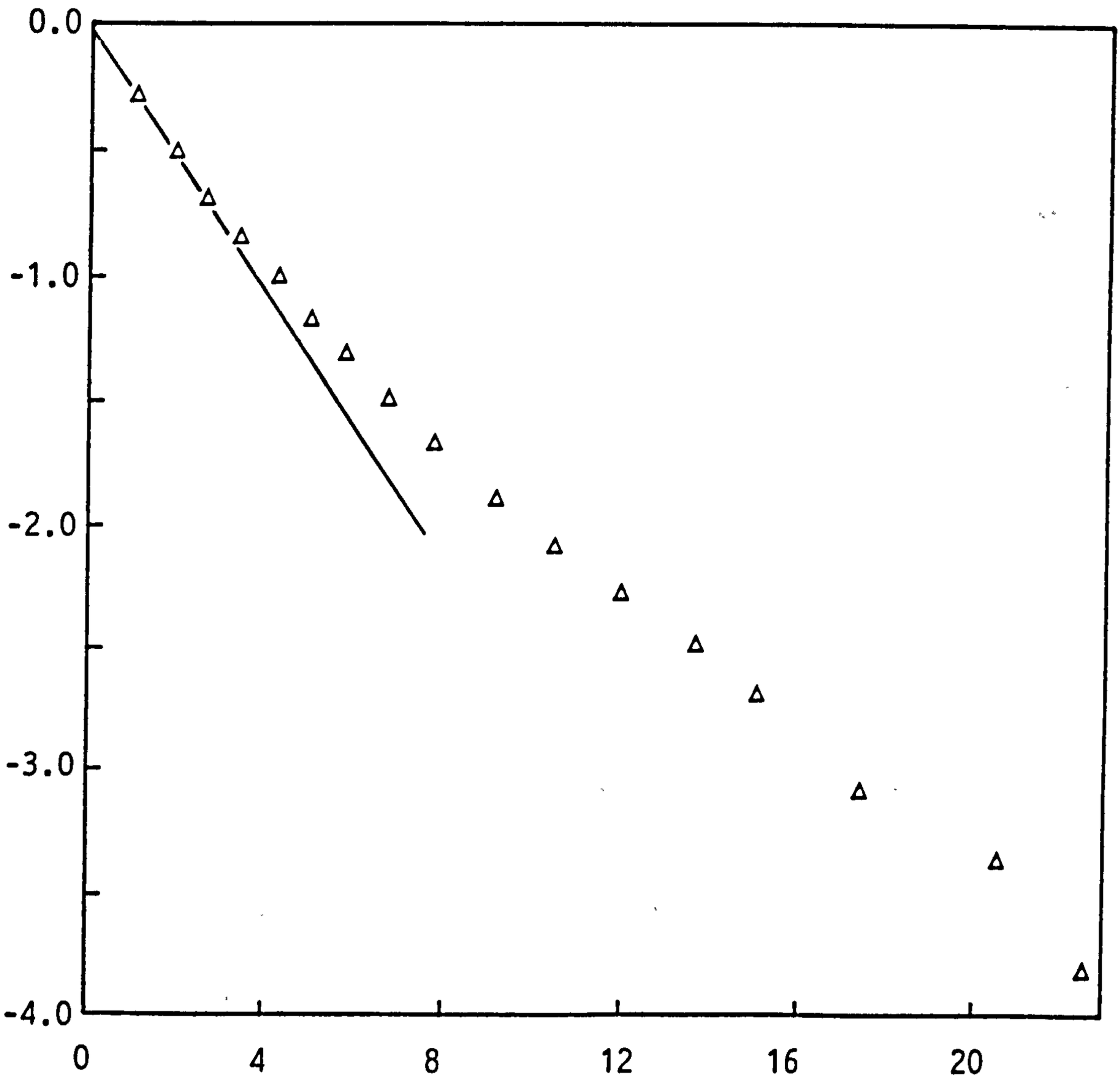

glass vessel fitted with pH meter and a self-sealing rubber cap, through which components of buffer solution (0.05 M $KHCO_3$, I = 1.0 M with KCl; 0.05 M K_2HCO_3, I = 1.0 with KCl) could be added using syringes. Buffer components were mixed in the vessel to obtain about 250 ml of buffer at the prescribed pH. One hundred ml of buffer was then transferred to a second, identical vessel containing a known quantity of nucleophile. It was usually necessary to adjust the pH of the nucleophile/buffer solution back to that of the original carbonate buffer, using a known volume of either HCl (1M) or KOH (1M) as required. From this stock nucleophile/buffer solution a range of dilutions could then be prepared by mixing appropriate quantities with the carbonate buffer solution in a mixing vessel flushed with nitrogen. It is advisable, when preparing these dilutions that, where practical, the concentration of the stock nucleophile/buffer solution is sufficiently high so that the dilutions can be made by mixing a small quantity of the stock solution with a much larger quantity of the carbonate buffer; this ensures that any slight difference between the pH of the carbonate buffer solution and that of the stock nucleophile/buffer solution will not produce any systematic pH difference during the dilutions. This is particularly important for the aminolysis and alcoholysis experiments (at low nucleophile concentrations) where the hydrolysis reaction is the major component of the observed pseudo first order rate constants. Where this is the case then, obviously, a systematic difference in pH would produce a systematic change in the rate of hydrolysis which would obviously affect any observed second order rate constant.

6.1.3 Kinetic Runs

Reactions were carried out as follows: two ml nucleophile/buffer solution was placed in a cuvette flushed with nitrogen. The cuvettes were firmly stoppered and equilibrated at 25°C in a thermostatted multiple

cell holder. The reaction was started by injecting 0.12 ml TAED or TriAED solution (2 x 10^{-3} M) into the nucleophile/buffer solution in the cuvette through which nitrogen was bubbled at the same time using glass capillary tube. Reactions were followed by measuring the absorbance decrease due to TAED or TriAED on the shoulder of the spectrum at 230 nm. Alternatively, some runs were carried out by following absorbance changes at 250 nm. In the later case, in order to obtain an adequate absorbance change, the reaction was started by mixing 1 ml each of TAED or TriAED solution with nucleophile buffer solution. This dilution of buffer does result in a slight increase in pH (~0.02 units) and this was routinely checked. The final ionic strength in all cases was 1.0 M. Where rates of reaction were rapid, then pseudo first order kinetic runs were conducted sequentially. However, where this was not the case then the runs were conducted in parallel.

6.1.4 pH Measurements

The kinetic studies conducted on TAED and TriAED were carried out in carbonate buffers over a pH range of 9.6 to 11.2. Consequently, in order to provide reliable calibration over the pH range of the experiments, the pH meter was standardized using reference solutions of pH 9.18 (at 25°C) and 12.45 (at 25°C). The pH 12.45 reference solution is a saturated solution of calcium hydroxide, which is listed as a secondary standard (Westcott[124]). Owing to the design of the pH meter used (PTI - 15), it was not possible, *electronically*, to calibrate the meter using these solutions, and, so, readings were made in millivolts, having obtained mV readings at each of the reference solutions and assuming a linear response of mV and pH between them.

6.1.5 Apparent pKa Determination for Glycine and n-Butylamine

Apparent pKa's for glycine and n-butylamine were determined under the same conditions under which the kinetic runs were carried out, that

is, I = 1M (at half neutralisation) and 25°C. The titrant was 1M KOH and the tabular method of pKa determination, described by Albert and Sergeant[125], was used. The titrations were carried out under nitrogen. The apparent pKa's of glycine and n-butylamine were determined as 9.803 and 11.098, respectively. The data for these calculations and the conditions used are contained in Tables 6.1 and 6.2 for glycine and n-butylamine, respectively. The literature values for the pka of glycine and n-butylamine are 9.78[126] and 10.59[126], respectively (25°C, I = 0 M)

6.2 Aminolysis Studies

6.2.1 Reaction of Glycine with TAED at High Amine Concentrations

This particular study was not conducted using CO_2-free conditions. The reaction of TAED with glycine was carried out using the amine as both nucleophile and buffer at the pKa of glycine. This was achieved by adding the appropriate amount of KOH.

Experimental

Reagents

A 2 x 10^{-3} M TAED solution was prepared as described in Chapter 4. The stock glycine buffer solution (pH 9.82, I = 2.0 M) contained 2M glycine, 1M NaOH and 1.5M NaCl. A range of glycine concentrations was prepared by diluting the stock solution with a 2M NaCl solution, thus maintaining the ionic strength. All solutions contained 1 x 10^{-5} M EDTMP. The contribution of the glycine zwitterion to the ionic strength was ignored since Jencks and Carriuolo[81] found that this introduced no serious errors at 1.0 M ionic strength for the glycinolysis of phenylacetate.

Procedure

Under pseudo first order conditions, the decrease in absorbance at 250 nm, corresponding to TAED and TriAED, was followed for solutions of

Table 6.1 Calculation of pKa for glycine. Conditions were: [glycine] = 7.168×10^{-2}M (100ml); I = 1.0M* at half neutralisation; 25°C; titrant was 1.0M KOH.

(1) Volume of KOH added	(2) pH	(3) 10^2 Co /M	(4) 10^2 (Co - (3)) /M	(5) 10^5 $\{OH^-\}$ /M	(6) $\frac{(3)+(5)}{(4)-(5)}$	(7) Log(6)	(8) pKa
0.000	-	7.168	0.000	-	-	-	-
1.005	9.016	6.163	1.005	1.040	6.140	0.788	9.804
1.995	9.383	5.173	1.995	2.420	2.597	0.414	9.797
3.005	9.654	4.163	3.005	4.510	1.389	0.143	9.797
3.585	9.807	3.583	3.585	6.410	1.003	0.001	9.808
4.000	9.908	3.168	4.000	8.090	0.796	-0.099	9.809
5.010	10.163	2.158	5.010	14.500	0.435	-0.361	9.801

*Ionic strength maintained at 1.0M using KCl.

Table 6.2 Calculation of pKa for n-butylamine. Conditions were: [n-butylamine hydrochloride] = 0.1945M (50ml); I = 1.0M* at half neutralisation; 25°C; the titrant was 1.0M KOH and the titration was carried out under nitrogen.

(1) Volume of KOH added/ml	(2) pH	(3) Co /M	(4) 10^2 (Co - (3)) /M	(5) 10^4 $\{OH^-\}$ /M	(6) $\frac{(3)+(5)}{(4)-(5)}$	(7) Log(6)	(8) pKa
0.000	-	0.1945	0.000	-	-	-	-
0.588	9.875	0.1833	1.120	0.7499	16.438	1.2158	11.091
0.786	10.044	0.1788	1.570	1.107	11.066	1.0598	11.104
1.053	10.180	0.1734	2.110	1.514	8.285	0.918	11.098
1.340	10.300	0.1677	2.680	1.995	6.312	0.800	11.100
1.626	10.400	0.1620	3.250	2.512	5.031	0.702	11.102
2.007	10.518	0.1544	4.010	3.290	3.891	0.590	11.108
2.541	10.637	0.1437	5.080	4.335	2.862	0.457	11.095
3.113	10.756	0.1322	6.230	5.702	2.151	0.333	11.089
3.891	10.908	0.1167	7.780	8.091	1.526	0.184	11.091
4.430	11.010	0.1059	8.860	10.230	1.221	0.087	11.097
5.150	11.145	0.0915	10.300	18.964	0.914	-0.039	11.100

*Ionic strength maintained at 1.0M using KCl.

TAED (1×10^{-3} M) in the presence of excess glycine (ranging from 0.2 to 1M). This procedure was repeated using potassium salts instead of sodium salts.

Results

Pseudo first order rate constants for the reaction of *TriAED* with glycine were obtained as follows. The absorbance change during the reaction is described by Equation 6.1.

$$A = A_\infty + A_1\, e^{-k_1 t} + A_2\, e^{-k_2 t} + A_B \qquad \text{Eqn 6.1}$$

where A_∞, A_B, A_1 and A_2 are constants and k_1 and k_2 are the pseudo first order rate constants for the reaction of TAED and TriAED, respectively. If $k_1 > k_2$, as is the case with the hydrolysis and perhydrolysis reactions, then, at some point in time, the absorbance will be described by $A = A_\infty + A_2\, e^{-k_2 t} + A_B$ and thus the pseudo first order rate constant can be obtained from linear regression of ln $(A - A_\infty)$ against time.

Typical pseudo first order plots of ln $(A - A_\infty)$ against time for TAED glycinolysis in the presence of sodium and potassium salts are shown in Figures 6.2 and 6.3, respectively. The initial curvature in the plots is due to the reaction of TAED with glycine, however, clearly, there is an obvious linear portion of the plot which will correspond to the region where $A = A_2\, e^{-k_2 t}$. Pseudo first order rate constants, k_{obs}, for the reactions are contained in Tables 6.3 and 6.4. Figure 6.4 shows a plot of k_{obs} against total amine concentration (the results for experiments conducted in sodium and potassium salts are shown). The plot indicates that the rate of aminolysis of TriAED by glycine increa-

Figure 6.2 Pseudo first order plot for the reaction between glycine and tetraacetylethylenediamine at25°C in a pH 9.82 glycine - sodium hydroxide buffer (I = 1.0M with NaCl); $[TAED]_o = 1x10^{-3}M$; [glycine] = 1.00M. Absorbance measurements were made at 250 nm. The line represents the best fit using the linear least squares method for data in the linear region of the plot.

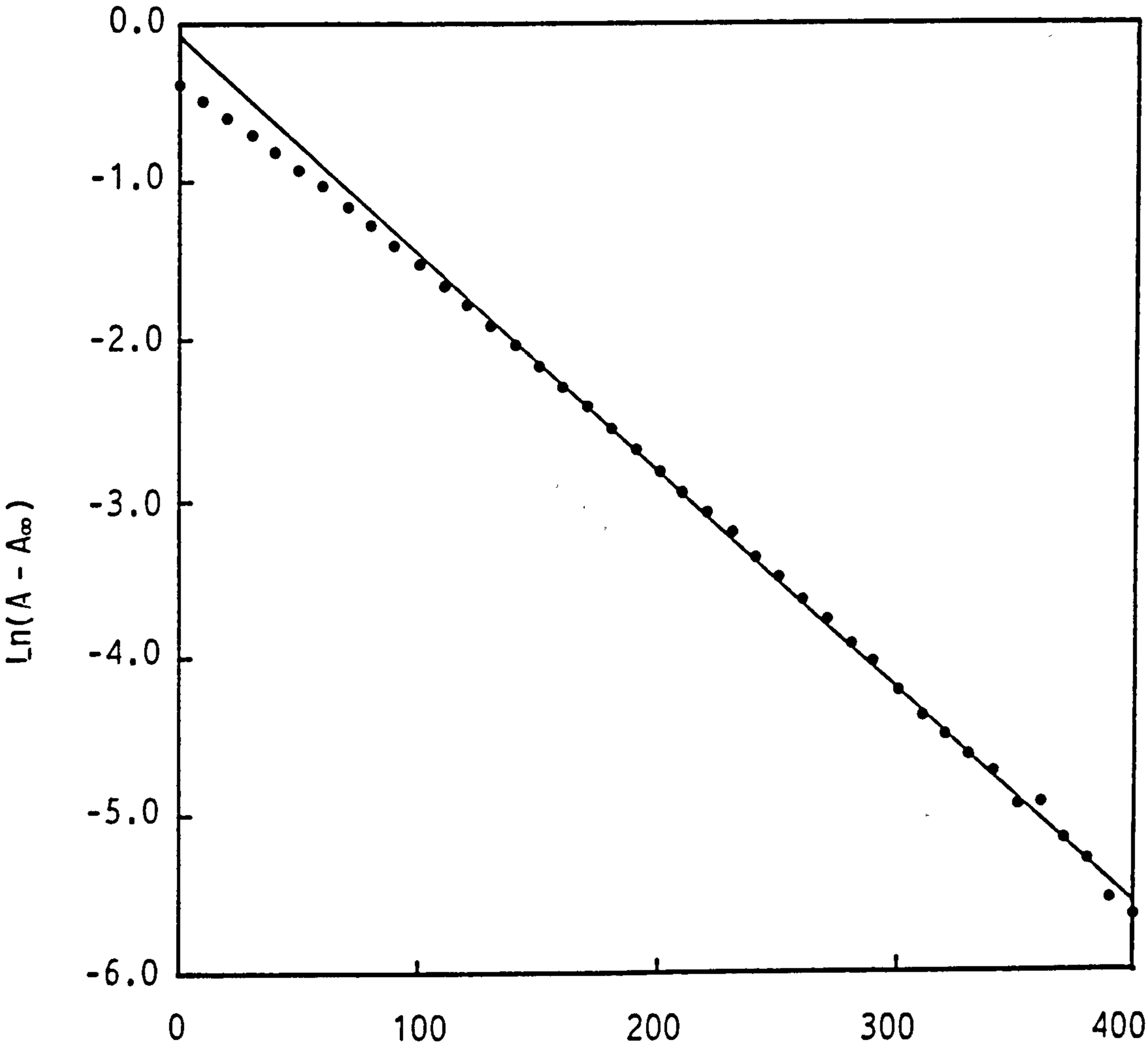

Figure 6.3 Pseudo first order plot for the reaction between glycine and tetraacetylethylenediamine at 25°C in a pH 9.82 glycine - potassium hydroxide buffer (I = 1.0M with KCl); $[TAED]_o = 1x10^{-3}M$; [glycine] = 0.951M. Absorbance measurements were made at 250 nm. The line represents the best fit using the linear least squares method for data in the linear region of the plot.

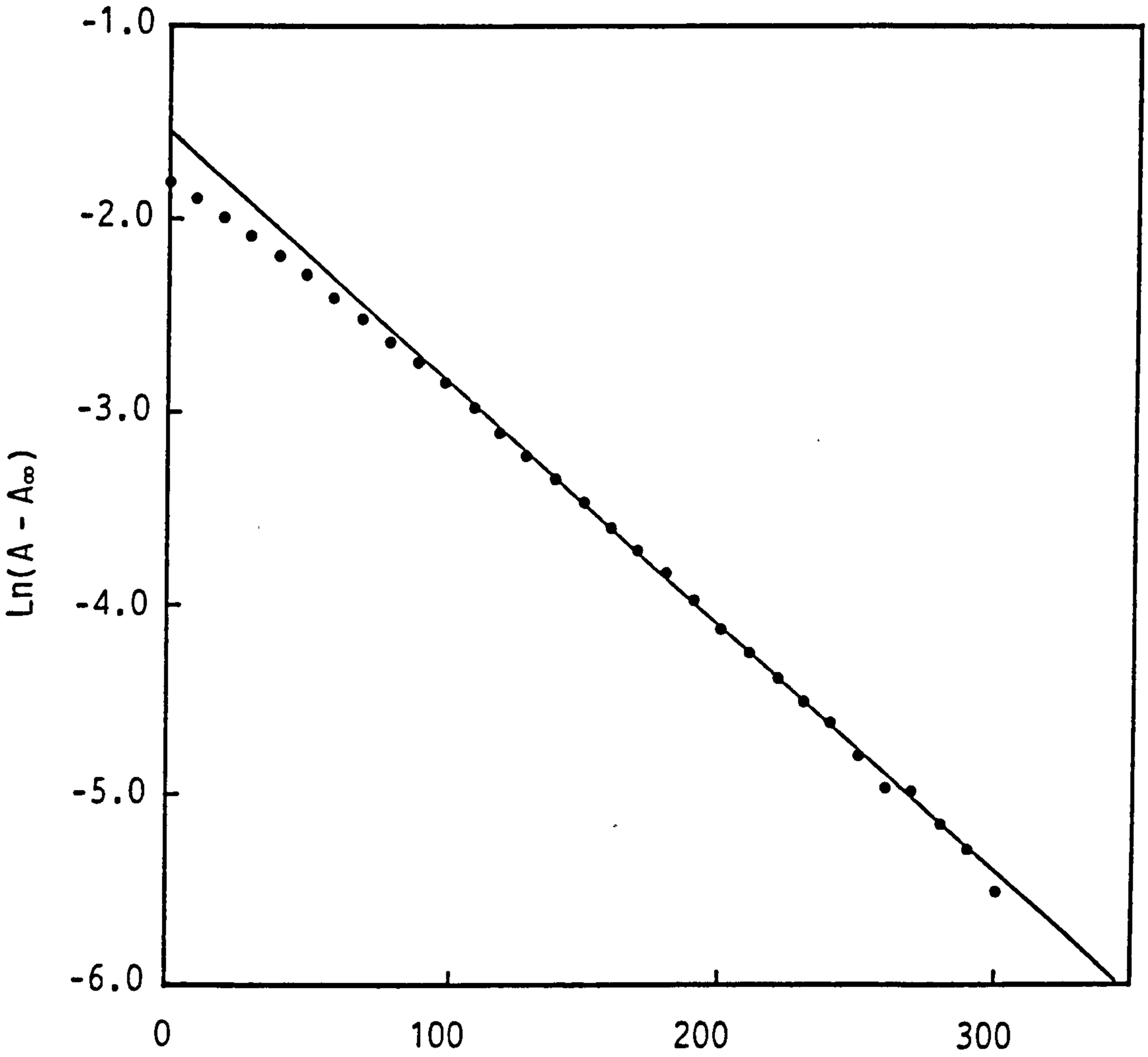

Table 6.3 Observed pseudo first order rate constants (kobs) for the reaction between triacetylethylenediamine (TriAED) and glycine. Conditions were: pH 9.82 glycine - KOH buffer (I = 1.0M with KCl); 25°C.

[glycine]/M	10^3kobs/s^{-1}	10^3(kobs/[glycine])/$M^{-1}s^{-1}$
0.476	3.063	6.434
0.571	4.346	7.611
0.666	5.882	8.832
0.761	8.167	10.732
0.856	10.451	12.209
0.951	13.242	13.924

Table 6.4 Observed pseudo first order rate constants (kobs) for the reaction between triacetylethylenediamine (TriAED) and glycine. Conditions were: pH 9.82 glycine - NaOH buffer (I = 1.0M with NaCl); 25°C.

[glycine]/M	10^3kobs/s^{-1}	10^3(kobs/[glycine])/$M^{-1}s^{-1}$
0.200	0.616	3.080
0.400	2.140	5.350
0.600	4.902	8.170
0.800	8.632	10.790
1.000	13.660	13.660

Figure 6.4 Plot of pseudo first order rate constant (kobs) against nucleophile concentration for the reaction between glycine and triacetylethylenediamine at 25°C and pH 9.82 in either a glycine-potassium hydroxide buffer (I = 1.0M, with KCl), □, or a glycine-sodium hydroxide buffer (I = 1.0M with NaCl), ■.

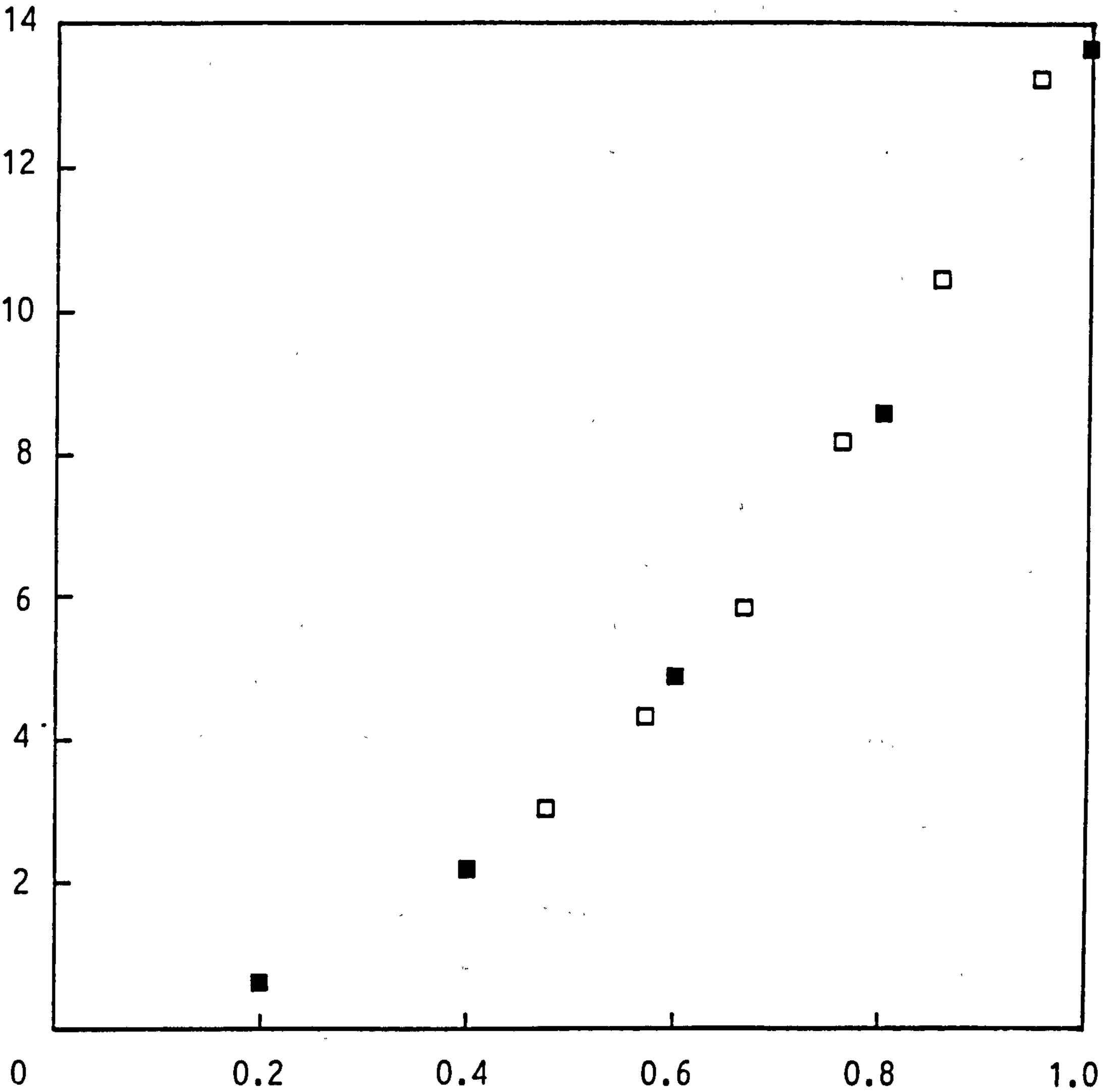

ses with more than the first power of [glycine]$_T$. This is well documented in the literature for esters[40,97] and amides[14,16] and is due to catalysis of the reaction by a second molecule of amine. From these literature studies it is generally accepted that the catalysis mechanism is general base catalysis by the free amine, RNH_2, although terms for general acid catalysis by RNH_3^+ have been detected.[16] General acid and base catalysis for this reaction will be discussed further in Section 6.4. For the moment, we will not presume which catalysis mechanism is operating.

Observed third order rate constants. Since the glycinolysis reaction of TriAED contains a significant third order component, then k_{obs}, the pseudo first order rate constant at any [Am]$_T$ is given by Equation 6.2.

$$k_{obs} = k_o + k_1 [Am]_T + k_2 [Am]_T^2 \qquad \text{Eqn 6.2}$$

Thus, a third order plot of $\frac{k_{obs} - k_o}{[Am]_T}$ against [Am]$_T$ yields k_2 as the slope and k_1 as the intercept. No value for k_o, the rate constant for TriAED hydrolysis was determined under these conditions, due to problems encountered with pH variations upon making glycine solutions from stock solutions; these problems are discussed later. However, at high glycine concentrations, $\frac{k_{obs} - k_o}{[Am]_T}$ approximates to $\frac{k_{obs}}{[Am]_T}$ and this function has been plotted against [Am]$_T$ in Figures 6.5 and 6.6, for k_{obs} data obtained from experiments using sodium and potassium salts, respectively. The observed third order rate constants were calculated from the mean of the $k_{obs}/[Am]_T$ values divided by [Am]$_T$. These values were $(1.385 \pm 0.046) \times 10^{-2}\ M^{-2}\ s^{-1}$ and $(1.390 \pm 0.080) \times 10^{-2}\ M^{-2}\ s^{-1}$ for the reactions carried out in the presence of potassium and sodium salts, respectively.

Figure 6.5 Plot of kobs/[nucleophile] against [nucleophile] for the reaction between triacetylethylenediamine and glycine at 25°C in a pH 9.82 glycine - potassium hydroxide buffer (I = 1.0M, with KCl). The line corresponds to the mean value of (kobs/[glycine] / [glycine]).

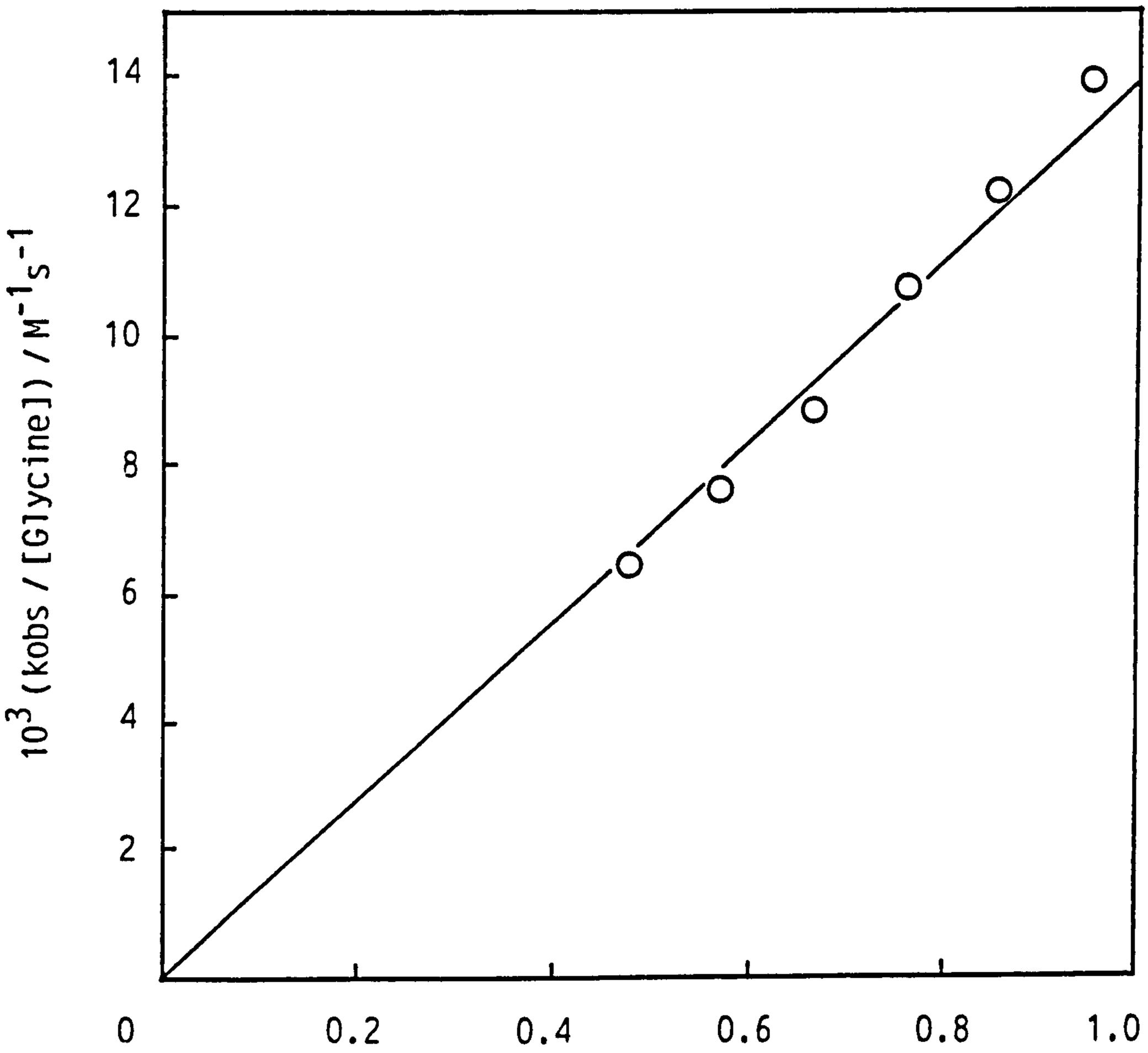

Figure 6.6 Plot of kobs / [nucleophile] against [nucleophile] for the reaction between triacetylethylenediamine and glycine at 25°C in a pH 9.82 glycine - sodium hydroxide buffer (I = 1.0M, with NaCl). The line corresponds to the mean value of (kobs / [glycine]) / [glycine].

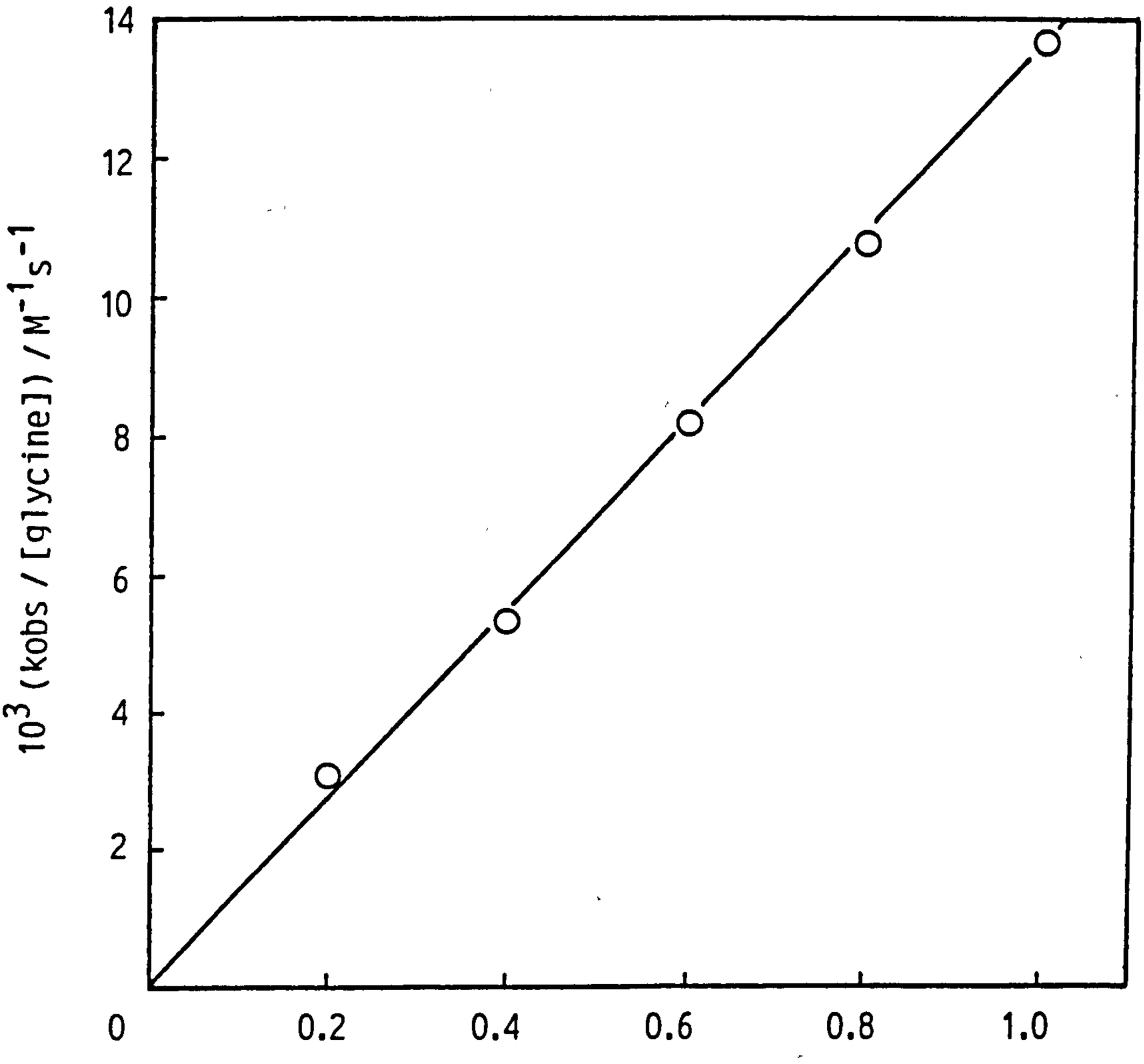

On Figure 6.4, the points for the reactions conducted in sodium and potassium salts appear to lie on the same curve at lower values of $[Am]_T$, however, at higher values there is a divergence.

pH Effects. The reason for using both sodium and potassium salts in the above studies was that erratic behaviour was observed when measuring the pH of the glycine buffer in the presence of sodium salts at the high ionic strengths used; this behaviour was not observed using potassium salts. In addition, sodium ions are believed to accelerate the rates of some reactions[8], as we have found with TriAED hydrolysis (Section 4.4). The other main problem encountered with pH was that on diluting the glycine stock solution with either KCl or NaCl to obtain a range of glycine concentrations, the pH was observed to change, even though the ionic strength was maintained constant. The pH difference between the highest and the lowest glycine concentrations was 0.18 units for the run using sodium salts, and a similar difference was obtained when using potassium ions. However, in both cases, it can be seen from Figures 6.5 and 6.6 plots of

$\frac{k_{obs}}{[Am]_T}$ against $[Am]_T$ yielded a linear relationship. Similar pH changes on dilution of amine buffer have been observed in the literature.[13]

6.2.2 Determination of Second Order Rate Constants for the Reaction of TriAED with Glycine and n-Butylamine

Because of the large third order component to the aminolysis reactions, kinetic runs were carried out at low glycine and n-butylamine concentrations in order to get a reliable value for the uncatalysed reactions of amines with TriAED. It was also found that by using low amine concentrations, yet still maintaining the ionic strength constant at 1M using KCl, then the pH variations observed in Section 6.2.1 - when diluting the stock solution with KCl - were alleviated. This method

for eliminating pH variations upon dilution of stock solutions has been used in the literature[87] and is more satisfactory than the alternative method of adjustment with KOH.

CO_2-free experimental techniques were used in all cases. Isolated TriAED (Obtained from Warwick International Ltd) was used for the experiments in the majority of cases. Observed second order rate constants were obtained at three different pH's for both glycinolysis and n-butylaminolysis reactions.

Experimental

Reagents

n-Butylamine was used in the form of n-butylamine hydrochloride which was prepared as follows. Fifty ml n-butylamine (BDH, GPR) was mixed to form a 50% solution with ethanol in a 250 ml round-bottomed flask. Whilst cooling the vessel under ice, approximately 50 ml 35% (w/v) hydrochloric acid was slowly added to the flask. The solvent was then evaporated off using a rotary condenser at 50°C. n-Butylamine was re-crystalized from ethanol, filtered, using a BÜchner funnel under vacuum and stored in a vacuum desicator for approximately one hour in order to remove traces of solvent. The yield was 15%. The n-butylamine crystalized in the form of leaflets as described in the literature.[127] A melting point determination gave a value of 211-213°C which is in agreement with the literature value (213-213.5°C)[82]. Purity was found to be 98% by titration of the butylamine hydrochloride with KOH. n-Butylamine stock solutions were made up with (a) the amine as both nucleophile and buffer (at the pKa of n-butylamine by adding the appropriate volume of KOH) and (b) the amine in a carbonate buffer. Dilutions from the stock solutions were made using either KCl, where the amine was used as buffer and nucleophile, or carbonate buffer where

carbonate buffer was used to maintain the buffering capacity. Glycine (BDH, biochemical) was used without further purification. All kinetic runs using glycine were conducted with carbonate buffer to maintain the buffering capacity. TAED and TriAED solution were prepared in distilled water as described in Section 4.2.

Procedure

Upon mixing TAED or TriAED with carbonate buffer/amine solution (or amine buffer solution alone), in a cuvette, the reaction was followed by measuring the decrease in absorbance on the shoulder of the TAED/-TriAED spectrum at either 230 or 250 nm as appropriate. In all cases, the final ionic strength of the reaction solution was 1 M (with KCl). The reaction of TriAED with n-butylamine was carried out at pH's 9.98, 10.03, and 10.39; the reaction of glycine with TriAED was carried out at pH's 9.80, 10.16, and 10.42. Full details of experimental conditions for each run are given in the results tables. At each pH, a rate constant for the hydrolysis of TriAED was obtained in carbonate buffer (I = 1 M, with KCl).

Absorbance measurements were followed until A_∞ had been reached and first and pseudo first order rate constants were obtained from linear regression of ln $(A - A_\infty)$ against time. In cases where TAED was used then the pseudo first order rate constant for the reaction of TriAED were obtained using the data treatment described in Section 6.2.1.

Results

Pseudo first order rate constants. It was noted from the first order plots of ln $(A - A_\infty)$ against time for n-butylaminolysis that where TAED was used, as opposed to isolated TriAED, there was some degree of positive curvature (Figure 6.7). The pH was found to be unchanged over the duration of the runs, and so the curvature is most likely to be attrib-

utable to the ratio of the rate constants for TAED and TriAED n-butylaminolysis being less than 2:1. If this was the case, then our previous assumption, when using TAED to obtain a k_{obs} value for TriAED, that in Equation 6.1 the term $A_1e^{-k_1t}$ approaches zero after a certain time may be incorrect. This would lead to an incorrect evaluation of the observed pseudo first order rate constant for TriAED aminolysis. We have estimated from glycinolysis experiments conducted at pH 9.80 that using TAED, as opposed to TriAED, may lead to an underestimation of the pseudo first order rate constant by up to 6%. Figure 6.7 demonstrates the slight curvature observed in a typical first order plot when using TAED as a substrate for n-butylaminolysis. The problem was alleviated upon using TriAED as the substrate, as is demonstrated by Figure 6.8 for n-butylaminolysis at pH 10.39. For the glycinolysis experiments, isolated TriAED was used at all pH's. Figure 6.9 shows a typical first order plot for TriAED glycinolysis at pH 9.80. Observed first order rate constants, k_{obs}, for the n-butylaminolysis and glycinolysis reactions are contained in Tables 6.5 and 6.6, respectively. Clearly, under these conditions, the rate of hydrolysis forms a significant proportion of the k_{obs} values.

Second order and observed second order rate constants. Figure 6.10 shows a plot of k_{obs} against total n-butylamine concentration at pH 10.03 and 10.39; Figure 6.11 shows the plot for the runs conducted at pH 9.98. For glycine, plots of k_{obs} against total amine concentration for runs conducted at pH 9.80, 10.16, and 10.42 are shown in Figure 6.12. The fact that for both n-butylamine and glycine the plots are linear indicates that at low amine concentrations, the contribution of the third order term $k[RNH_2]^2$ is negligible. It is interesting to note from Figure 6.11 that the k_{obs} values obtained for n-butylaminolysis in carbonate buffer appear to lie on the same line as those for n-butylam-

Figure 6.7 Pseudo first order plot for the reaction between n-butylamine and triacetylethylenediamine at 25°C in a pH 9.98 potassium carbonate - potassium hydrogen carbonate buffer (I = 1.0M, with KCl): $[TAED]_o = 1.2 \times 10^{-4}$M; [n-butylamine] = 49.3×10^{-3}M. Absorbance measurements were made at 230 nm. The line represents the best fit using the linear least squares method.

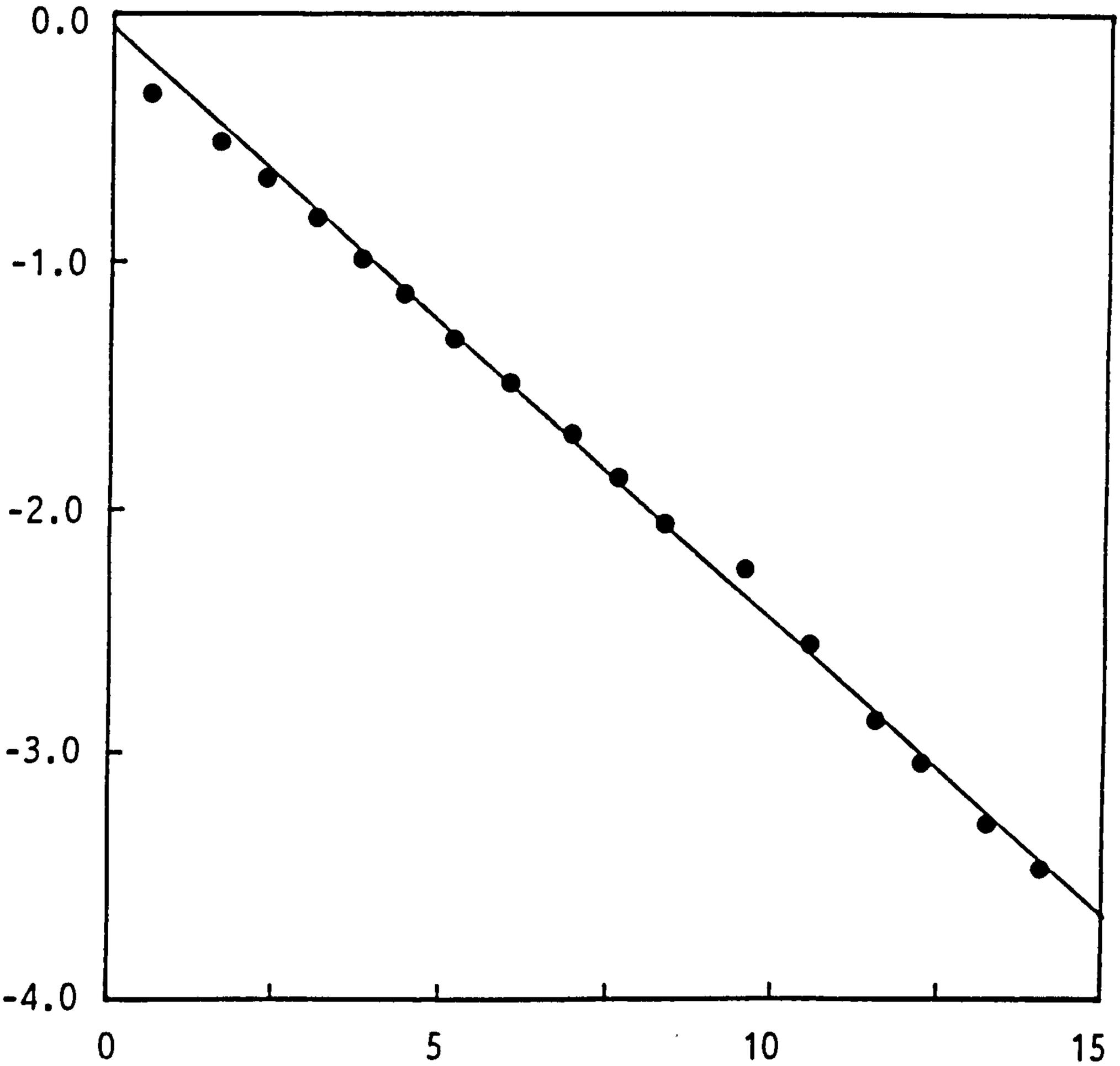

Figure 6.8 Pseudo first order plot for the reaction between n-butylamine and triacetylethylenediamine at 25°C in a pH 10.39 potassium carbonate - potassium hydrogen carbonate buffer (I = 1.0M, with KCl): $[TriAED]_o = 1x10^{-3}M$; [n-butylamine] = $19.572x10^{-3}M$. Absorbance measurements were made at 250 nm. The line represents the best fit using the linear least squares method.

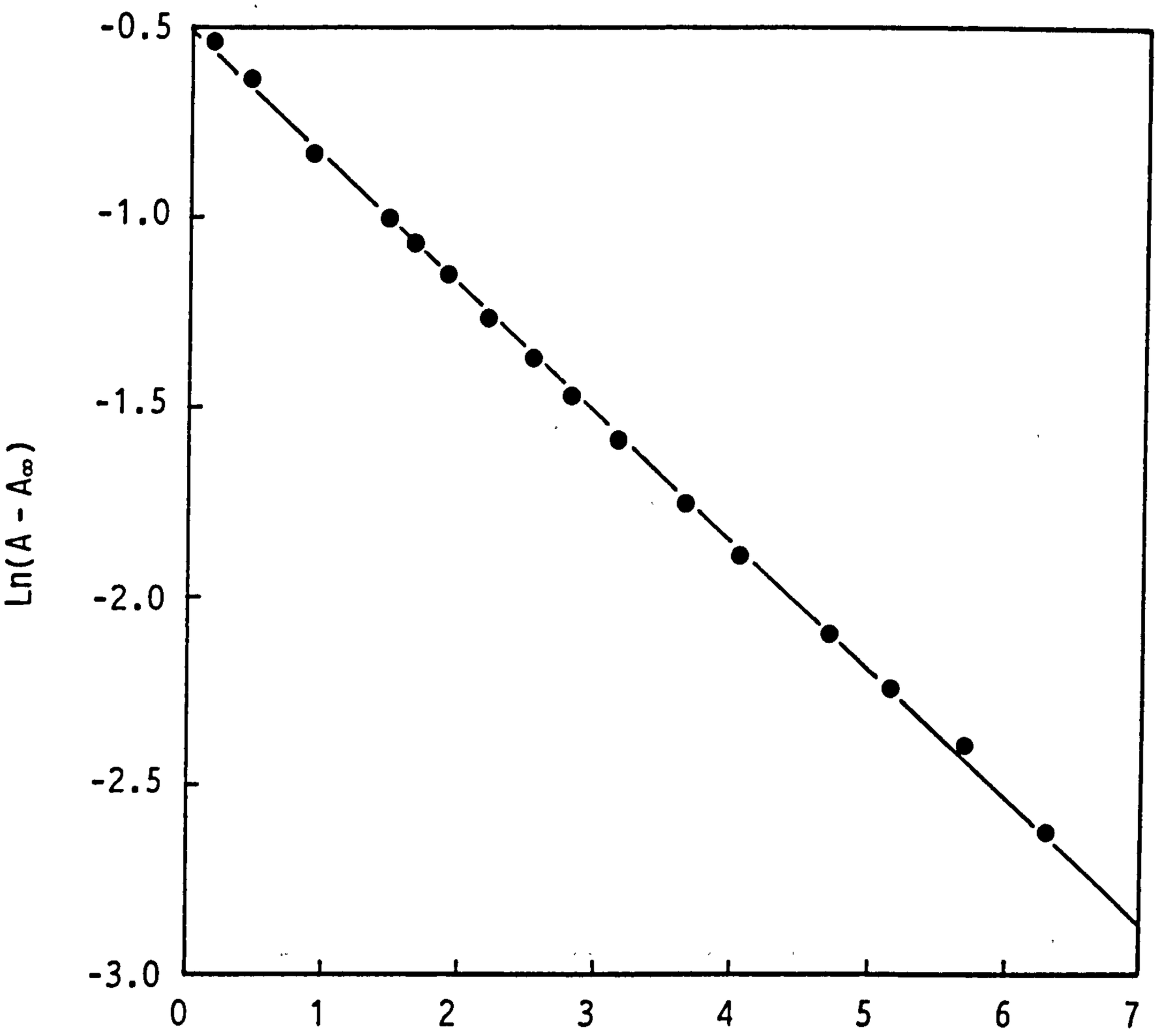

Figure 6.9 Pseudo first order plot for the reaction between gylcine and triacetylethylenediamine at 25°C in a pH 9.80 potassium carbonate - potassium hydrogen carbonate buffer (I = 1.0M, with KCl); $[TriAED]_o = 1.2x10^{-4}M$; $[glycine] = 64.23x10^{-3}M$. Absorbance measurements were made at 230 nm. The line represents the best fit using the linear least squares method.

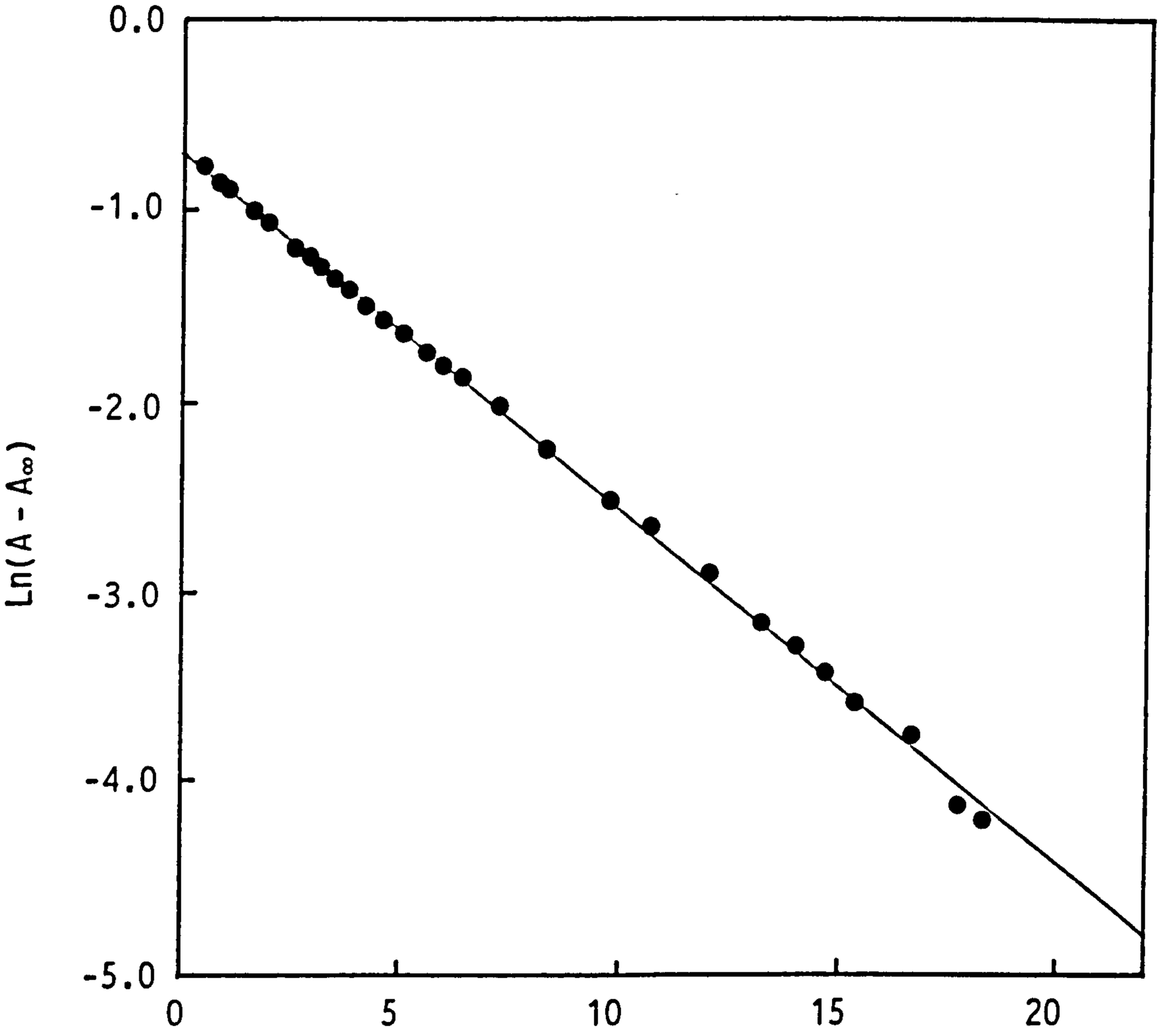

Figure 6.10 Plots of pseudo first order rate constabt (kobs) against nucleophile concentration for the reaction between n-butylamine and triacetylethylenediamine at 25°C in potassium carbonate - potassium hydrogen carbonate buffers of pH 10.028,O, and 10.39,□(I = 1.0M, with KCl): $[TriAED]_o = 1x10^{-3}M$. The lines correspond to the best fit using the linear least squares method.

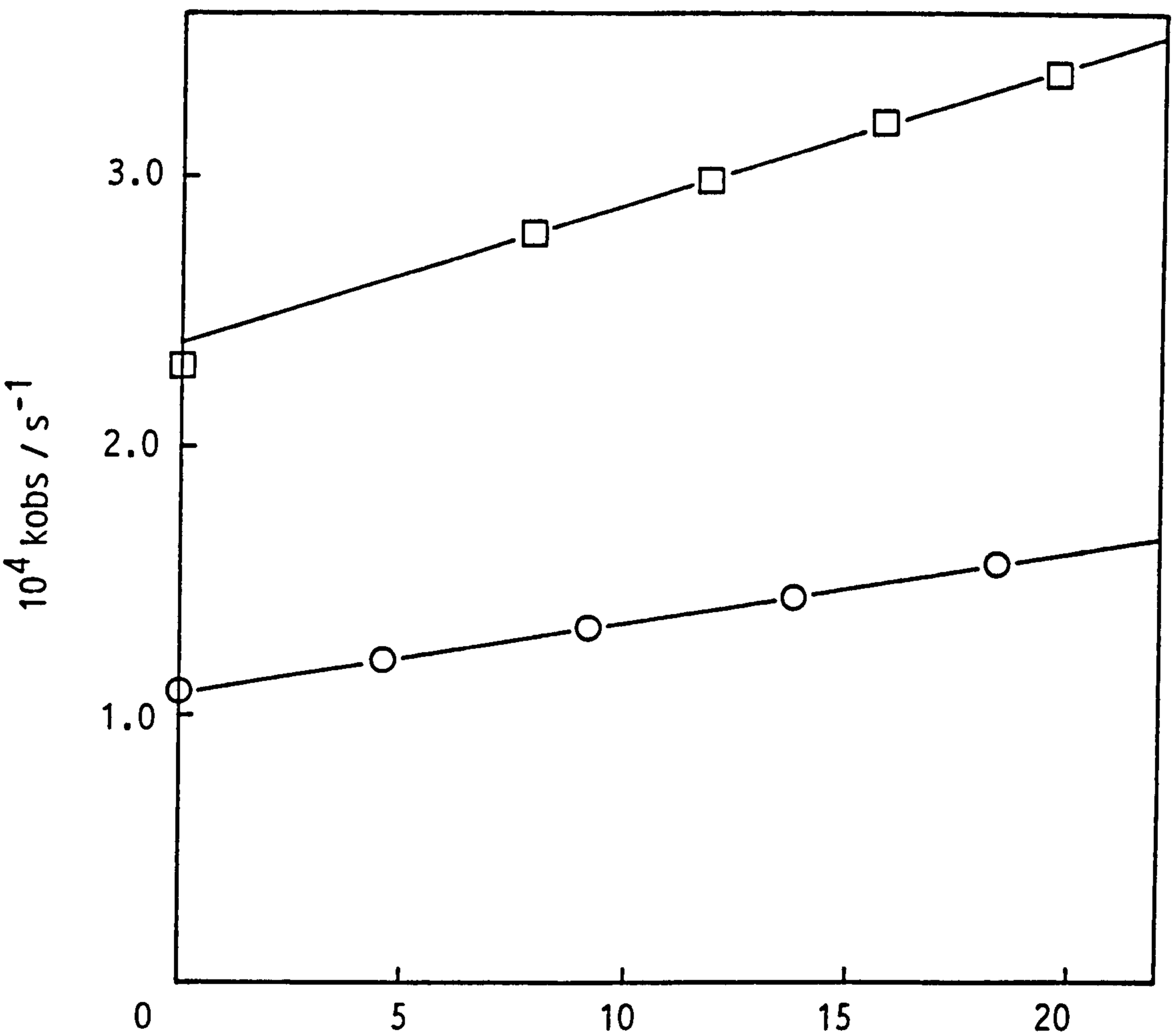

Figure 6.11 Plot of pseudo first order rate constant (kobs) against nucleophile concentration for the reaction between n-butylamine and triacetylethylenediamine at 25°C. The reaction was carried out at pH 9.98 in either potassium carbonate - potassium hydrogen carbonate buffer, O, or in a solution in which the amine was both buffer and nucleophile, ●, (I = 1.0 in both cases). The line represents the best fit using the linear least squares method.

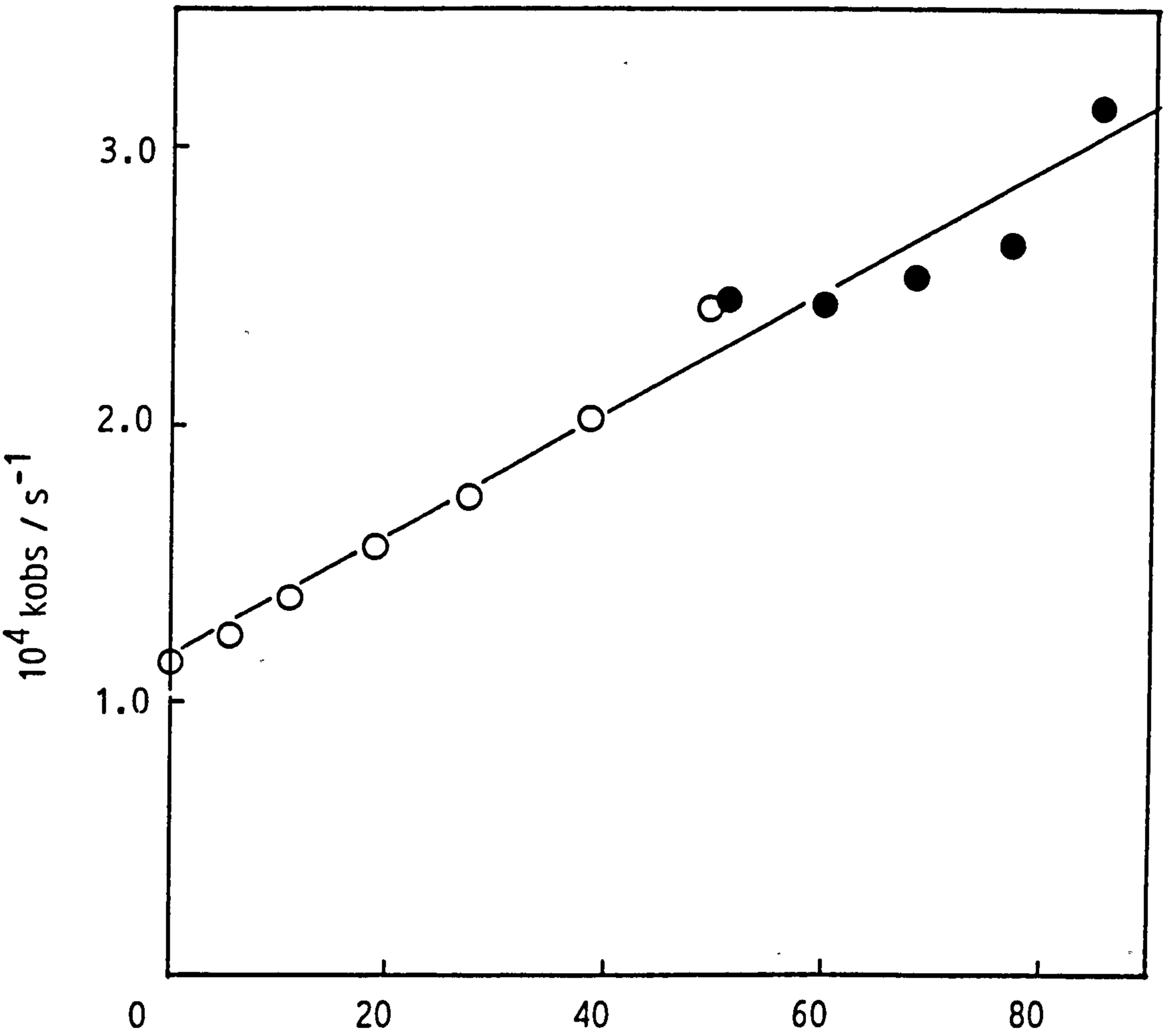

Figure 6.12 Plots of pseudo first order rate constant (kobs) against nucleophile concentration for the reaction between glycine and triacetylethylenediamine at 25°C in potassium carbonate - potassium hydrogen carbonate buffers of pH 9.80, □, 10.16, ○, and 10.42, △, (I = 1.0M with KCl). The lines correspond to the best fit using the linear least squares method.

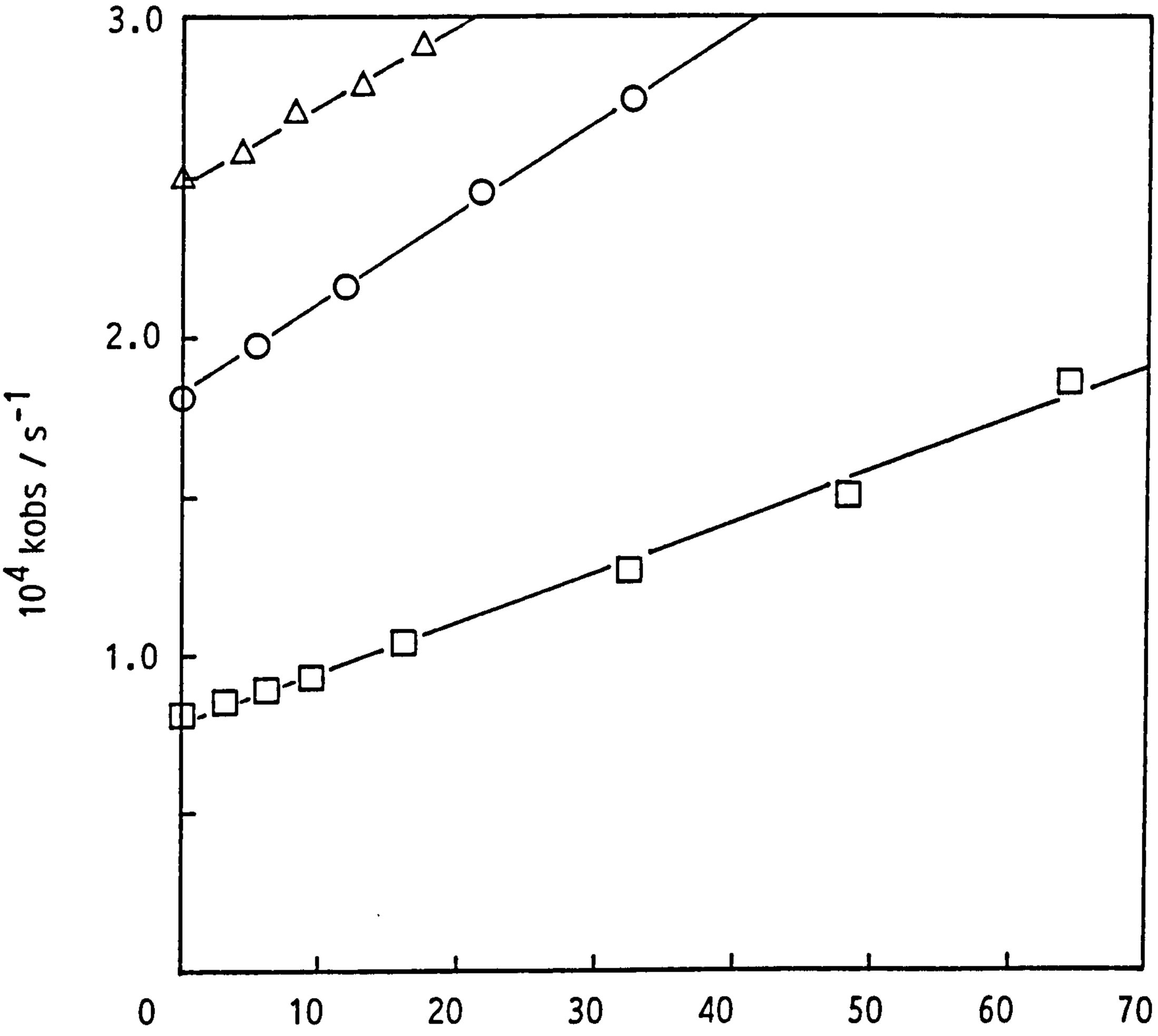

Table 6.5 Observed pseudo first order rate constants (kobs) for the reaction between triacetylethylenediamine (TriAED) and n-butylamine. Conditions were: pH, as indicated in table; 0.05M potassium carbonate - potassium hydrogen carbonate buffer (I = 1.0M with KCl); [TriAED] = $1x10^{-3}$M; 25°C. Absorbance measurements were made at 250nm.

pH	Fraction free base	10^3[n-butylamine]/M	10^4kobs/s^{-1}
9.98*	0.0708	0.000	1.140
		5.480	1.238
		10.940	1.377
		18.890	1.564
		27.390	1.743
		38.350	2.024
		49.300	2.416
		50.940**	2.449
		59.430**	2.433
		67.920**	2.529
		76.410**	2.648
		84.900**	3.145
10.028	0.0781	0.000	1.089
		4.585	1.203
		9.170	1.321
		13.755	1.437
		18.340	1.575
10.39	0.1718	0.000	2.302
		7.829	2.784
		11.743	2.984
		15.658	3.196
		19.572	3.375

*kobs values at this pH were obtained using tetraacetylethylenediamine as described in the text. [TAED] = $1.2x10^{-4}$M. Absorbance measurements were made at 230nm.

**The amine was used as both buffer and nucleophile, no carbonate buffer was present (I = 1.0M with KCl).

Table 6.6 Observed first order rate constants (kobs) for the reaction between triacetylethylenediamine (TriAED) and glycine. Conditions were: pH, as indicated on table; 0.05M potassium carbonate - potassium hydrogen carbonate buffer (I = 1.0M with KCl); [TriAED] = 1.2×10^{-4}M; 25°C. Absorbance measurements were made at 230nm.

pH	Fraction free base	10^3[glycine]/M	10^4kobs/s^{-1}
9.80	0.500	0.000	0.815
		3.134	0.854
		6.266	0.890
		9.400	0.930
		16.058	1.046
		32.116	1.275
		48.176	1.508
		64.234	1.856
10.16	0.696	0.000	1.809
		5.410	1.977
		11.719	2.158
		21.642	2.453
		32.446	2.740
10.42*	0.805	0.000	2.488
		4.313	2.576
		8.625	2.697
		12.938	2.781
		17.251	2.909

*[TriAED] = 1×10^{-3}. Absorbance measurements made at 250nm.

inolysis in amine buffer, suggesting that there is no observable catalysis of the n-butylaminolysis under these conditions. One should, however, bear in mind the points made previously about possible errors occurring in determining k_{obs} values for TriAED n-butylaminolysis when using TAED as the substrate. Observed second order rate constants, k_{2obs} for the reaction of TriAED with amines were obtained from linear regression of the first, and pseudo first order rate constants; these values are contained in Table 6.7. Equation 6.3 was used to estimate the second order rate constant, k_2, for the reaction assuming, according to precedent, that the free amine is the reactive species and using the apparent pka's of 11.10 and 9.803 determined by us for n-butylamine and glycine, respectively, under these conditions
(I = 1.0 with KCl). These values are also contained in Table 6.7.

$$k_2 = k_{2obs} \frac{K_a + [H^+]}{k_a} \qquad \text{Eqn 6.3}$$

It is clear from the k_2 values obtained at three different pH's, that the n-butylaminolysis of TriAED does not appear to show any general or specific catalysis under the conditions used in these runs; the observed second order rate constants simply show a dependence on free amine concentration. Note also, that the k_2 value for the run conducted using TAED as a substrate (at pH 9.98) is similar to those determined using isolated TriAED. This indicates that the errors introduced by curvature in the first order plots may not be very great. For glycine, the second order rate constants are not in good agreement. There is no clear trend, however, and it cannot definitely be stated that buffer effects exist. Nevertheless, on the basis of these results and those of the n-butylaminolysis results, one might be tempted to suppose that general acid-base and specific base catalysis mechanisms were negligible under these conditions. Finally, it should be noted from Table 6.5 for n-butylamine that, in the runs conducted at pH 10.03 and 10.39, the

Table 6.7 Second order (k_2) and observed second order (k_2obs) rate constants for the n-butylaminolysis and glycinolysis of TriAED at 25°C (I = 1.0M).

Amine	pH	$10^3 k_2obs / M^{-1}s^{-1}$ *	$10^3 k_2 / M^{-1}s^{-1}$
n-butylamine	9.98	2.210 ± 0.217 **	33.65
	10.03	2.628 ± 0.129	33.67
	10.39	5.495 ± 0.431	31.34
Glycine	9.80	1.581 ± 0.118	3.173
	10.16	2.873 ± 0.104	4.136
	10.42	2.425 ± 0.221	3.010

*90% Confidence Limits.

** Obtained using TAED, as described in the text.

lowest amine concentrations were not in tenfold excess over TriAED. Similarly, for glycine, in the run conducted at pH 10.42 (Table 6.6). This will not affect the K_{obs} values since the hydrolysis reaction is the major component of the observed first order rates at these low concentrations. The above results are discussed in Section 6.5.

6.3 Study of TriAED Alcoholysis

As well as determining the second order rate constants for the nucleophilic attack of glycine and n-butylamine on TriAED, it was also decided to study the reaction of TriAED with some alcohols. The study was prompted partially by the requirement to determine a rate constant for the reaction of methanol with TriAED; in Chapter 7, for the study of the reaction of methyl hydroperoxide with TriAED, methanol was present in the methyl hydroperoxide solution.

Precedent dictates that it is the anionic form of the alcohol which is the reactive species.[15,41,63,128] Consequently, alkyl alcohols are extremely unreactive due to their high pKa values. Nevertheless, there has been a number of studies conducted where rate constants for the alcoholysis of esters[41,63,128] and activated amides[15,16] have been determined. Rate constants are usually determined either by directly following the reaction using absorbance measurements or from product ratios. In the present study we have followed the reaction directly by observing the decrease in absorbance at 250 nm due to TriAED. Isolated TriAED was used in the studies. Two alcohols, methanol (pKa = 15.5[65]) and trifluoroethanol (pKa = 12.37[65]) were used in the study. Because of the unreactivity of these alcohols a large concentration of alcohol is required in the reaction solution in order to be able to detect a rate due to alcoholysis. There is the problem, however, that too large a concentration of alcohol will disrupt the structure of the water and lead to interfering solvent effects. In literature studies[41,63], where

the alcoholysis has been determined in aqueous solution, a maximum of about 8% v/v alcohol has been used. We have used a maximum of about 5% for the trifluoroethanol experiment and 2% for the methanol experiments.

Pseudo first order kinetic runs were conducted at pH 10.03, only, for both methanol and trifluoroethanol. The CO_2-free experimental protocol outlined in Section 6.1 was followed.

Experimental

Reagents

Methanol (GPR, 99% purity) and trifluoroethanol (Analar) were used without further purification. All kinetic runs were conducted using carbonate buffer to maintain the buffering capacity (I = 1.0 with KCl). It should be noted that in aqueous solution of alcohols, the alcohol, especially trifluoroethanol, is liable to decomposition.[63] Alcohol/buffer solutions were, therefore, prepared and used before appreciable decomposition could take place. TriAED and carbonate buffer solutions were prepared as described in Section 6.1.

Procedure

Upon mixing TriAED with carbonate buffer/alcohol solutions in a cuvette the reaction was followed by measuring the decrease in absorbance at 250 nm. Runs were conducted at pH 10.03 (I = 1.0) for both methanol and trifluoroethanol. The hydrolysis of TriAED at pH 10.03 was followed in carbonate buffer (I = 1.0 with KCl). Full details of concentrations and conditions used in the runs are given in the results tables. In all cases, A_∞ values were obtained. First and pseudo first order rate constants were calculated from linear regression of ln $(A - A_\infty)$ against time. Absorbance data were obtained over at least 3.5 half-

lives for the methanolysis reactions, and over at least 4 half-lives for the trifluoroethanolysis reactions.

Results

Pseudo first order rate constants. Typical plots of ln ($A - A_\infty$) against time are shown in Figure 6.13, for the methanolysis reactions, and in Figure 6.14, for trifluoroethanolysis reactions. For the methanolysis reaction the plots are linear for at least 2.7 half-lives after which, particularly for the lower concentrations, there was a positive deviation from linearity. For the trifluoroethanolysis plots there were also positive deviations from linearity in the pseudo first order plots. The plots were linear for at least 1.7 half-lives. These positive deviations are most likely attributable to decomposition of the alcohols since the pH of the solutions were found still to be 10.03 at A_∞. Pseudo first order rate constants, k_{obs}, were obtained from the initial linear regions of the plots and are contained in Table 6.8.

Second order rate constants. Plots of k_{obs} against total alcohol concentration are shown in Figures 6.15 and 6.16 for methanol and trifluoroethanol, respectively. There is slight negative curavture of the plots at the higher alcohol concentrations and this could be due to either an effect of the alcohol causing some degree of structure breaking in the aqueous solution, or alcohol decomposition in the aqueous solution. Observed second order rate constants, k_{2obs} for the reaction of TriAED with methanol and trifluoroethanol were calculated from linear regression of the first and pseudo first order rate constants listed in Table 6.8; the observed second order rate constants are listed in Table 6.9. Estimated second order rate constants, k_2, for the reaction of TriAED with the methoxide and trifluoroethoxide anions were calculated using Equation 6.3 and pKa values of 15.5[63] and 12.37[63] for methanol and trifluoroethanol, respectively.

Figure 6.13 Pseudo first order plot for the reaction between methanol and triacetylethylenediamine at 25°C in a pH 10.03 potassium carbonate - potassium hydrogen carbonate buffer (I = 1.0M with KCl): $[TriAED]_o = 1x10^{-3}M$; [methanol] = 0.583M. Absorbance measurements were made at 250 nm. The line represents the best fit using the linear least squares method over the initial linear region.

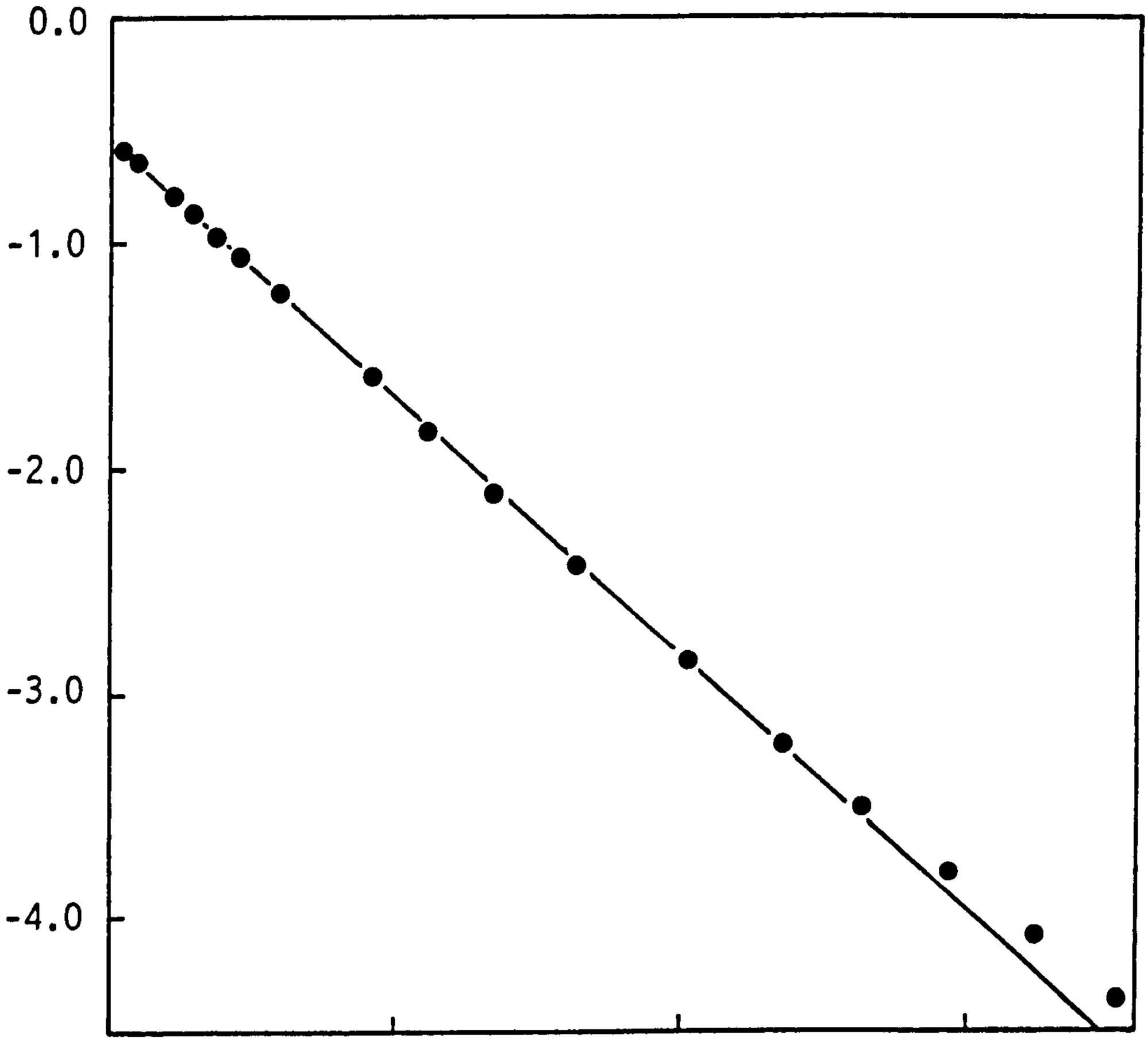

Figure 6.14 Pseudo first order plot for the reaction between trifluoroethanol and triacetylethylenediamine at 25°C in a pH 10.03 potassium carbonate - potassium hydrogen carbonate buffer (I = 1.0M with KCl): $[TriAED]_o = 1x10^{-3}M$; [trifluoroethanol] = 0.365M. Absorbance measurements were made at 250 nm. The line represents the best fit using the linear least squares method for data in the initial linear region of the plot.

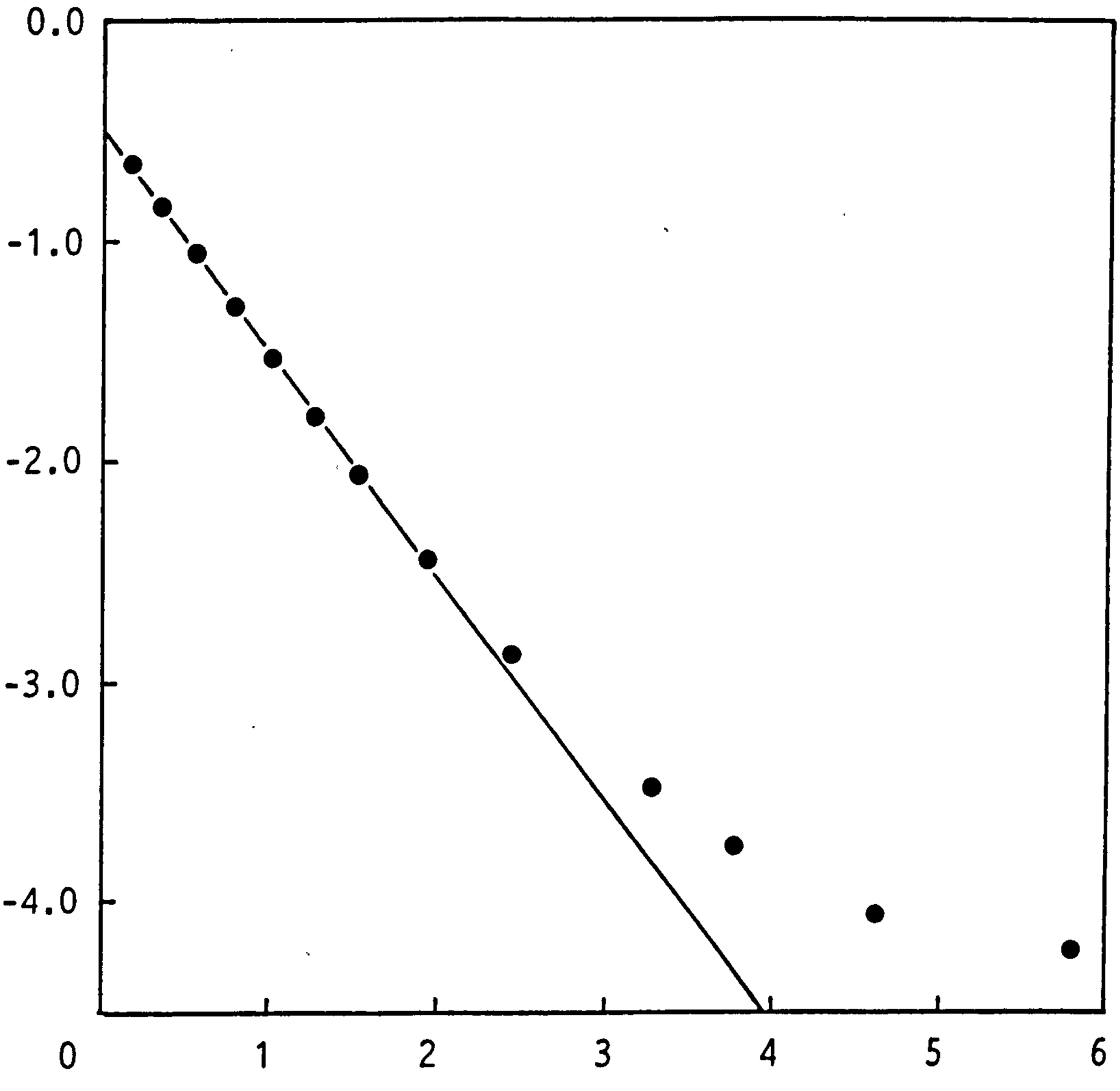

Figure 6.15 Plot of pseudo first order rate constant (kobs) against nucleophile concentration for the reaction between methanol and triacetylethylenediamine at 25°C in a pH 10.03 potassium carbonate - potassium hydrogen carbonate buffer (I = 1.0M with KCl): $[TriAED]_o = 1x10^{-3}M$. The line represents the best fit using the linear least squares method.

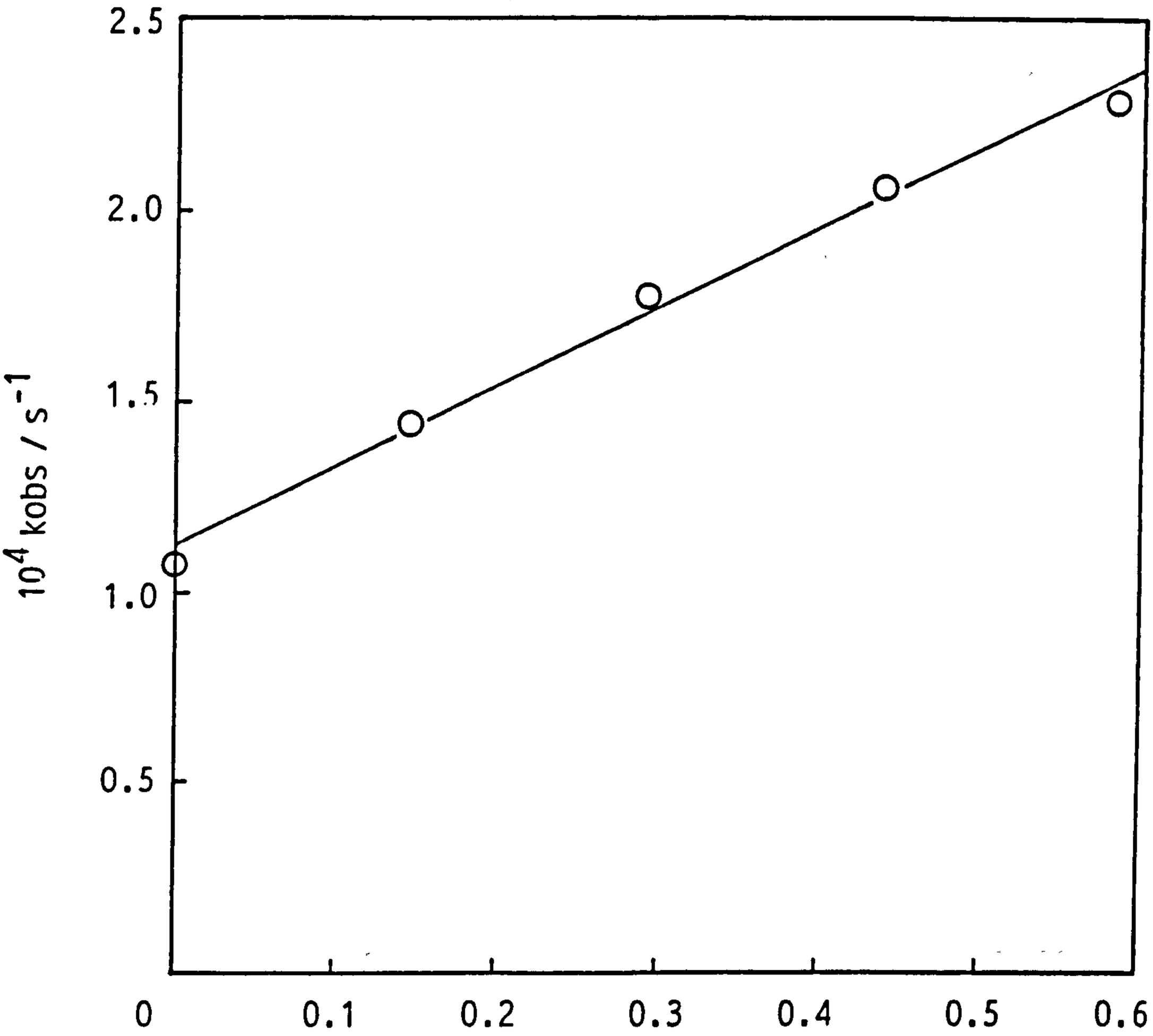

Figure 6.16 Plot of pseudo first order rate constant (kobs) against nucleophile concentration for the reaction between trifluoroethanol and triacetylethylenediamine at 25°C in a pH 10.03 potassium carbonate - potassium hydrogen carbonate buffer (I = 1.0M with KCl): $[TriAED]_o = 1x10^{-3}M$. The line represents the best fit using the linear least squares method.

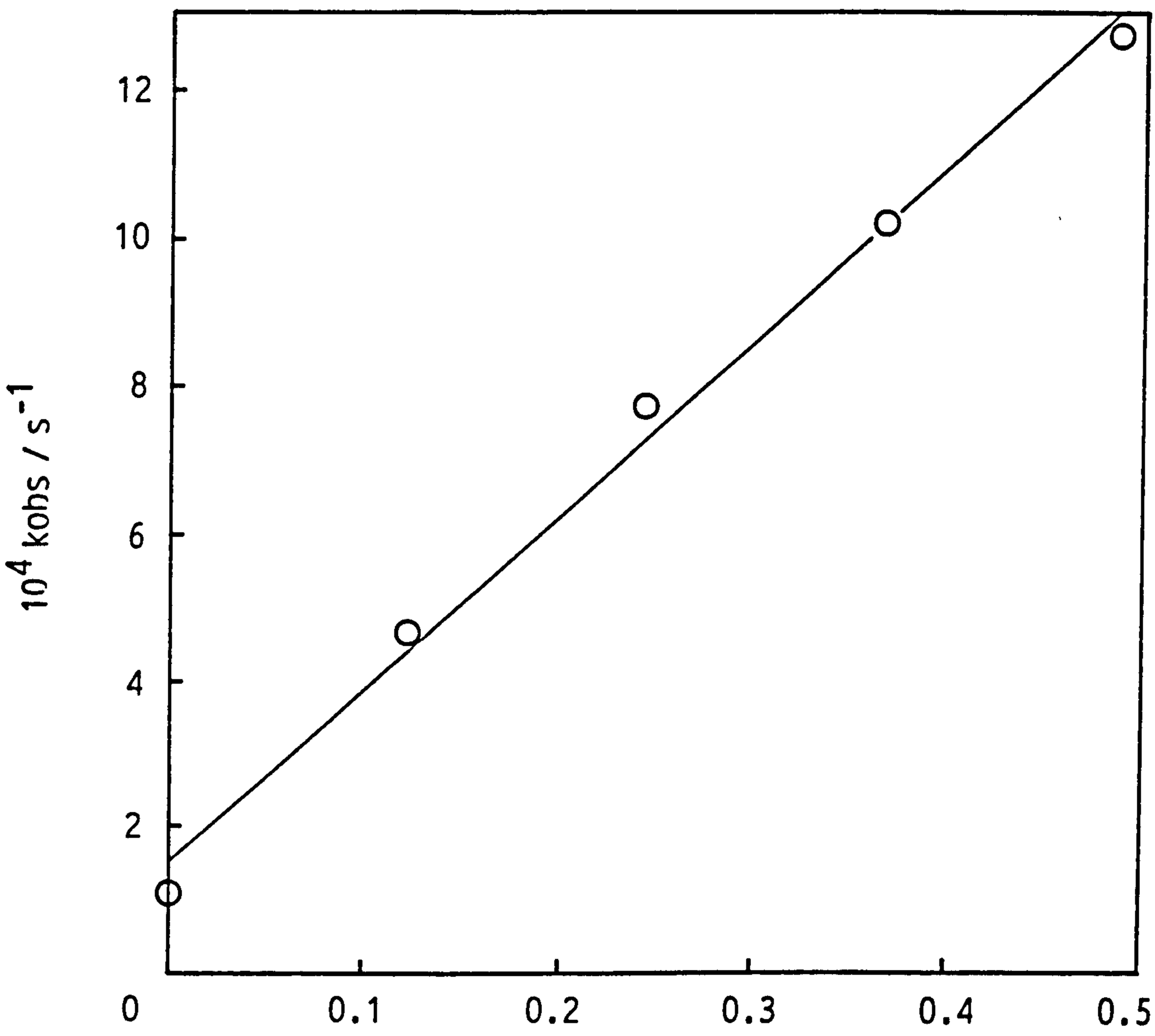

Table 6.8 Observed pseudo first order rate constants (kobs) for the reaction between triacetylethylenediamine (TriAED) and alcohols. Conditions were: pH 10.03; 0.05M potassium carbonate - potassium hydrogen carbonate buffer (I = 1.0M with KCl); [TriAED] = $1x10^{-3}$M; 25°C. Absorbance measurements were made at 250nm.

Alcohol	pKa	[alcohol]/M	10^4kobs/s^{-1}
Methanol	15.50	0.0000	1.079
		0.1458	1.444
		0.2916	1.776
		0.4374	2.056
		0.5832	2.285
Trifluoroethanol	12.37	0.0000	1.085
		0.1217	4.640
		0.2433	7.711
		0.3650	10.157
		0.4867	12.686

Table 6.9 Second order (k_2) and observed second order ($k_2$obs) rate constants for the reaction between alcohols and TriAED at 25°C (I = 1.0 M).

Alcohol	pKa	$10^4 k_2obs / M^{-1}s^{-1}$ *	$k_2 / M^{-1}s^{-1}$
Methanol	15.50	2.076 ± 0.256	61.220
Trifluoroethanol	12.37	23.604 ± 2.631	0.519

*90% Confidence Limits.

6.4 General Discussion

6.4.1 Aminolysis

The free amine, RNH_2, is likely to react with TAED or TriAED according to Scheme 6.1.

Scheme 6.1

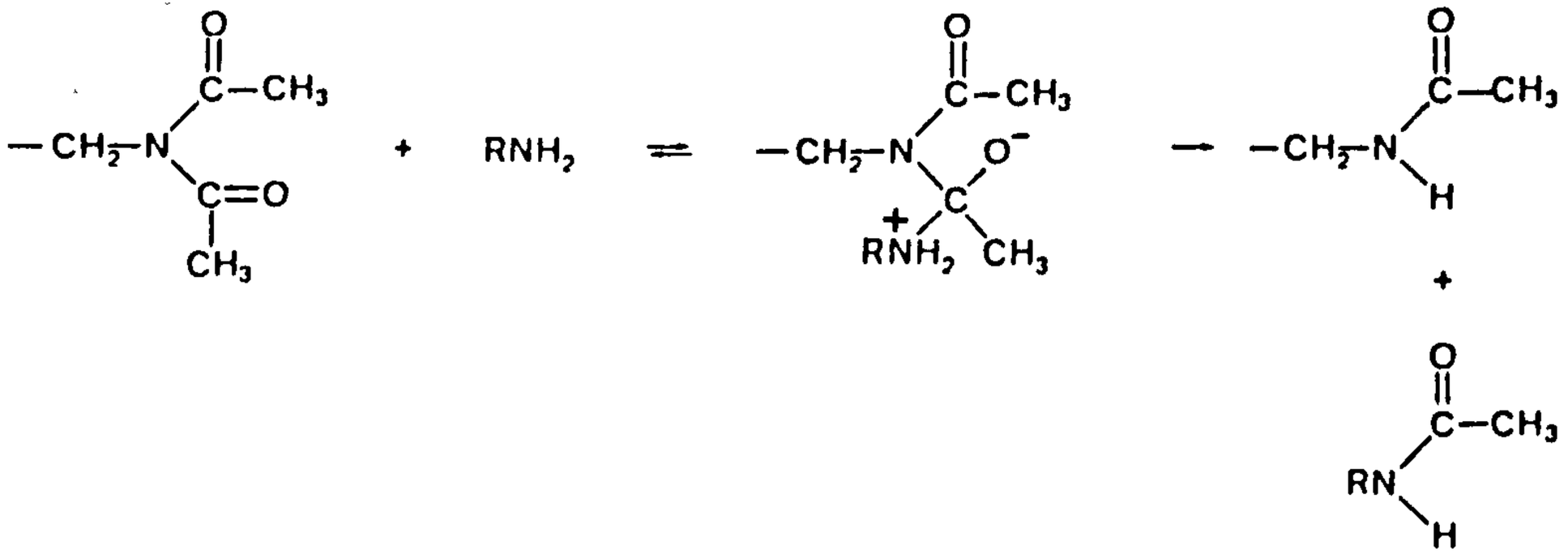

For the aminolysis experiments conducted at low amine concentrations using the CO_2-free experimental protocol, rate constants for the uncatalysed aminolysis reaction with TriAED were obtained at three pH values for both n-butylamine and glycine (Tables 6.4 and 6.5). For n-butylamine, the observed second order rate constant showed a simple dependence on free amine concentration, that is, the reaction was not subject to external catalysis under these conditions. For glycine, the pH dependence study was more variable although no clear trends were observed (Table 6.6); additional runs would have to be conducted, however, taken with the n-butylamine results, it appears likely that the second order rate constant for TriAED glycinolysis is also not subject to external catalysis under these conditions.

For the reactions conducted at high amine concentrations (glycine only) the rate was found to contain a term which is second order with respect to amine concentration, as is evidenced by the upward curvature in Figure 6.4. Aminolysis of esters and amides is, as we have discussed

in Chapter 1, subject to both general acid and general base catalysis. General acid catalysis is effectd by protonation of the carbonyl oxygen in esters[40] and, most likely, by protonation of the amide nitrogen in amides.[16,35] General base catalysis occurs by proton removal from the attacking amine[14,15,40,79] in the transition state. Kinetically, at a particular pH, both general acid and general base catalysis would result in a term in the observed rate which was second order with respect to the total amine concentration: $(k[Am]_T^2)$. Consider, for example, general base catalysis, in which the free amine is the nucleophile and the reaction is catalysed by a further molecule of free amine. The observed rate constant, ignoring hydrolysis (k_o), is defined by Equation 6.4.

$$K_{obs} = k_1 [RNH_2] + k_2 [RNH_2]^2 \qquad \text{Eqn 6.4}$$

For the case of general acid catalysis, where the free amine is the nucleophile and the reaction is catalysed by a molecule of RNH_3^+, then the observed rate constant is defined by Equation 6.5 since

$[RNH_3^+] = [RNH_2]\,[H^+]/K$

$$k_{obs} = k_1 [RNH_2] + k_2 [RNH_2]^2\,[H^+]\,1/K \qquad \text{Eqn 6.5}$$

Clearly, from Equations 6.4 and 6.5, a pH dependence study of the amine catalysed reaction would clarify the situation. Nevertheless, the literature suggests that, for both esters and amides, general base catalysis by a second molecule of free amine is the major catalytic component of observed rate constants. General acid catalysis by the RNH_3^+ species is either not kinetically observable or, at least, very small, compared to general base catalysis. For acetylimidazole[15], for example, the rate constant for general base catalysis by a second molecule of free glycine is 40 $M^{-2}\ s^{-1}$, whilst general acid catalysis by the RNH_3^+ species is an order of magnitude lower (3.33 $M^{-2}\ s^{-1}$). Our study has not included a pH dependence investigation of the *amine catalysed* aminolysis reaction and so it is not possible to definitely state

that general base catalysis is the major component in this case, although it seems likely from literature evidence.

6.4.2 Alcoholysis

The anionic form of the alcohol is likely to react with TAED or TriAED according to Scheme 6.2.

Scheme 6.2

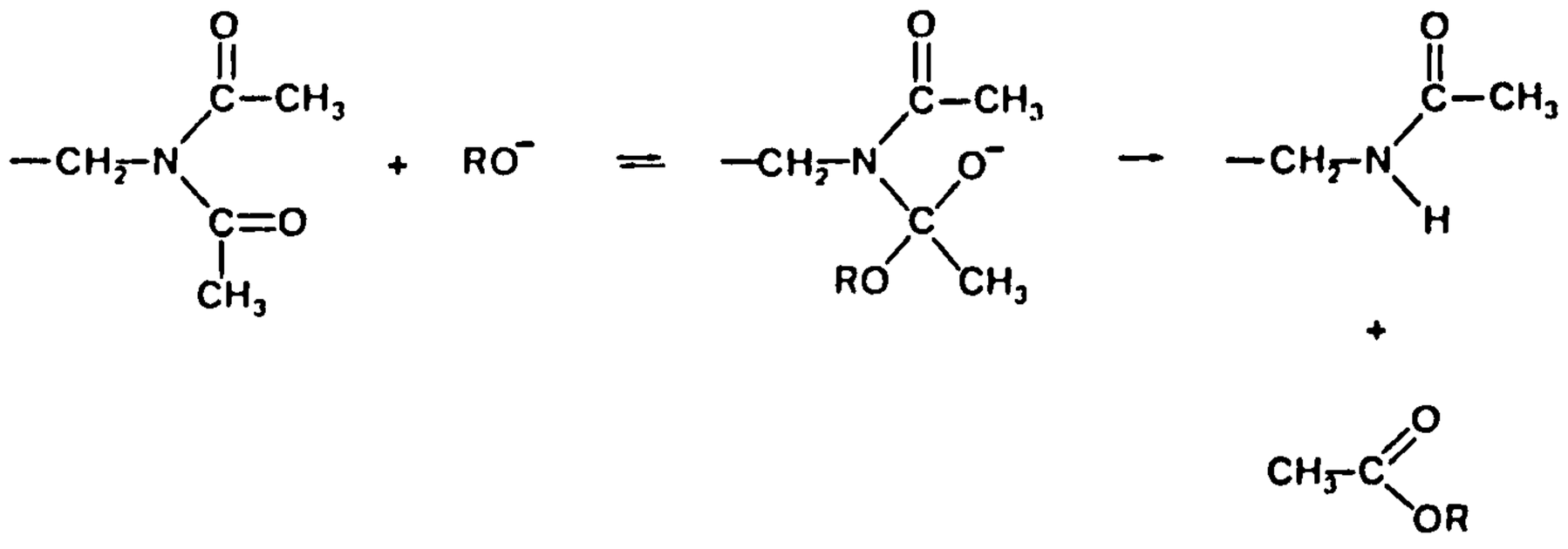

Subsequent hydrolysis of the product $CH_3C(O)OR$ will occur.[63]

The methanolysis and trifluoroethanolysis reactions were carried out at one pH value only and so it is not possible to comment on external catalysis reactions. Second order rate constants for the reactions were calculated from the observed second order rate constants at pH 10.03, as described in Section 6.2.2, assuming no buffer catalysis.

6.4.3 Linear Free Energy Studies

Having obtained second order rate constants for a series of alcohols and amines it is possible to present these data in the form of a Brønsted-type plot; this should give us information on whether a normal Brønsted-type relationship exists (β = 0.3 to 1.0) for the reaction of nucleophiles with TriAED and TAED. Brønsted-type relationships for the series of alcohols and amines examined in this chapter are discussed in Chapter 10, along with the results from a series of peroxides, which forms the subject of the next chapter.

CHAPTER 7 REACTION OF TAED AND TriAED WITH PEROXIDES

This chapter describes the study of the reaction of various peroxides with TriAED (and TAED). The second order rate constants obtained from such a study can be used to construct a Brønsted-type plot for the reaction of TriAED with a series of peroxides, and will complement similar studies conducted for a series of primary amines and a series of alcohols, as described in the previous chapter.

A detailed study of the reaction of hydrogen peroxide with TAED and TriAED, including both pH and temperature dependence studies is described in Section 7.1. From the temperature dependence studies, values for the activation enthalpy and entropy were obtained and these values are compared with literature values for similar reactions. The measurement of second order rate constants for the reaction of TriAED with Caro's acid and methyl hydroperoxide is described in Section 7.2 and 7.3, respectively. Section 7.4 describes the study of the reaction of hydrogen peroxide with the imidic bleach activator, triacetylethanolamine, which is structurally similar to TAED and TriAED. A general discussion of the above studies is contained in Section 7.5.

All spectrophotometric measurements were made using the Hewlett Packard HP 8451 diode array spectrophotometer fitted with thermostatted cell holder.

7.1 Study of the Reaction of TAED and TriAED with Hydrogen Peroxide

7.1.1 UV-Promoted Peroxide Decomposition

The kinetic runs in the pH dependence and temperature dependence studies described in this section were followed by the measurement of absorbance decrease of TAED or TriAED at 232 nm. Problems were, however, encountered due to UV interaction with the hydrogen peroxide and

buffer components of the reaction solution. Figure 7.1 shows absorbance decrease at 232 nm in a pH 9.99 carbonate buffer (I = 0.1); clearly, after the reaction appeared to be completed, there was still a steady decrease in absorbance. Hydrogen peroxide was found to be the component of the reaction mix responsible for this effect and this is clearly shown in Figure 7.2, where absorbance decrease at 232 nm was observed in a solution containing only hydrogen peroxide in distilled water. It is likely that this decrease in absorbance is caused by UV degradation of H_2O_2 since we have demonstrated (Figure 7.3) that, in a solution containing only H_2O_2 in pH 9.99 carbonate buffer, the frequency of illumination determines the rate of decrease in absorbance. It is known[129] that in the presence of UV radiation hydrogen peroxide dissociates into hydroxyl-free radicals (Scheme 7.1) and this may be the case here.

Scheme 7.1

$$H_2O_2 \xrightarrow{hv} HO. + HO.$$

In addition to interaction with the hydrogen peroxide, UV was also found to interact with some component of the carbonate buffer in combination with the hydrogen peroxide. Figure 7.4 shows that upon commencement of the illumination of a hydrogen peroxide/carbonate buffer solution there is an initial rapid increase in absorbance, followed by a subsequent decrease which is due to the H_2O_2, as described above. The initial increase is not observed for either hydrogen peroxide or carbonate buffers alone.

These problems encountered with UV interaction could not be alleviated by the use of a UV cut-off filter as they were with the UV photoxidative problems encountered with the iodimetric techniques described in Chapter 2; in this case measurements were to be made in the UV region of the spectrum. Instead, the number of measurements made during kine-

Figure 7.1 Absorbance decrease at 232 nm during the reaction between hydrogen peroxide and triacetylethylenediamine at 25°C in a pH 9.99 sodium carbonate - sodium hydrogen carbonate buffer (I = 0.1M): $[TAED]_o = 1x10^{-4}M$; $[H_2O_2] = 4.42x10^{-3}M$; $[EDTMP] = 1x10^{-5}M$.

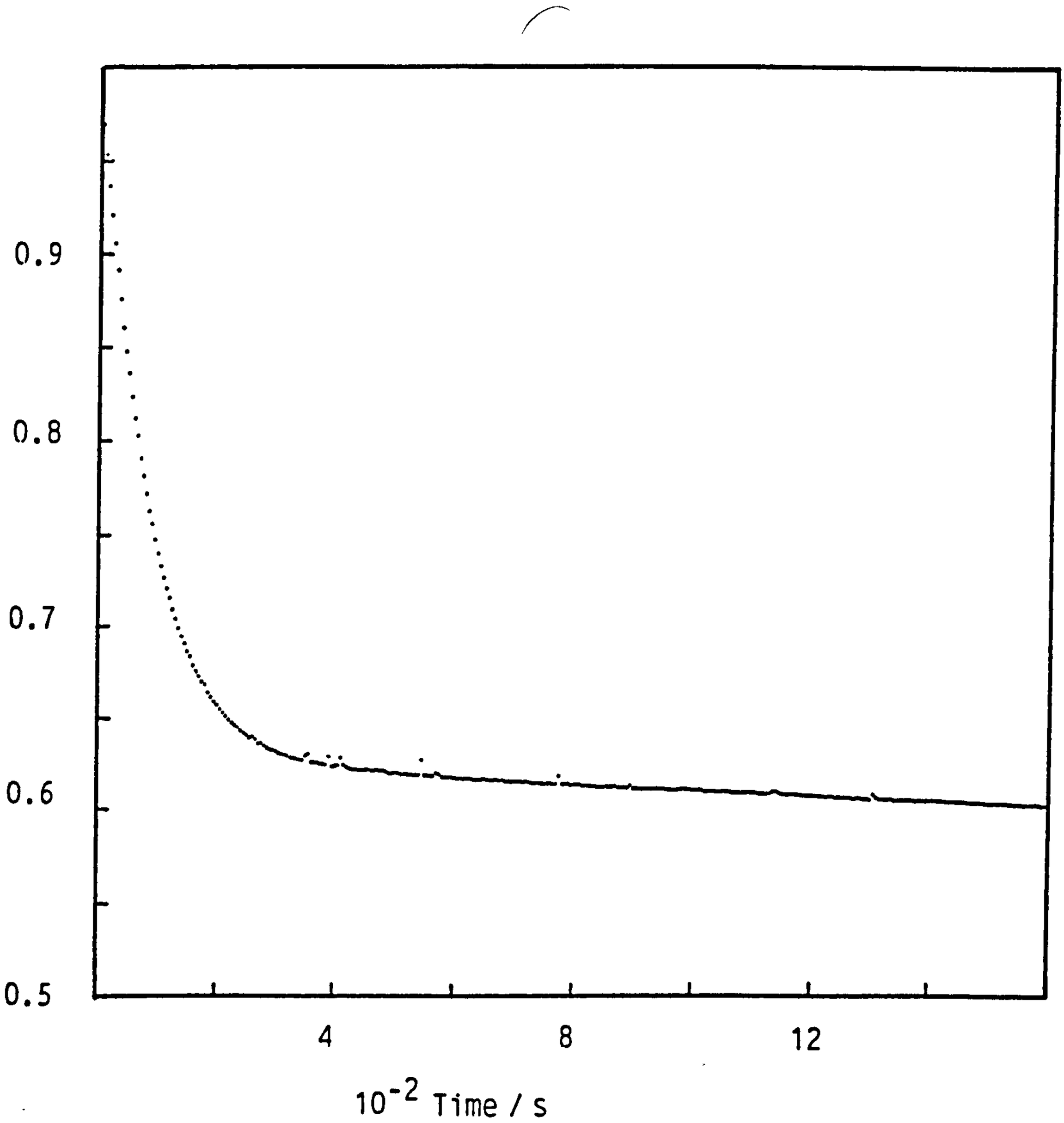

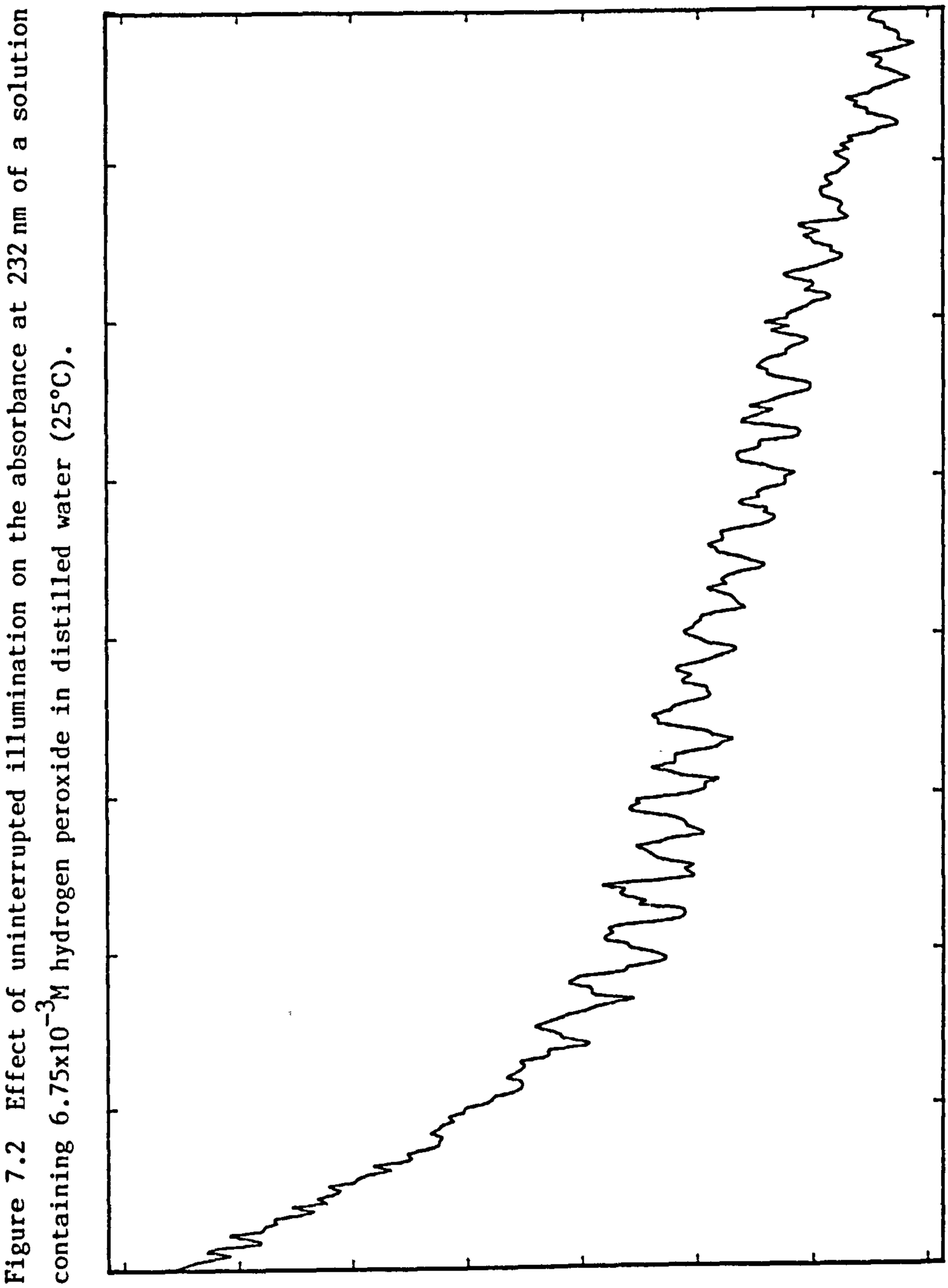

Figure 7.2 Effect of uninterrupted illumination on the absorbance at 232 nm of a solution containing 6.75×10^{-3} M hydrogen peroxide in distilled water (25°C).

Figure 7.3 Effect of the frequency of illumination on the rate of absorbance decrease at 232nm in a solution containing 6.75×10^{-3}M hydrogen peroxide in a pH 9.99 sodium carbonate - sodium hydrogen carbonate buffer (I = 0.1M, 25°C).

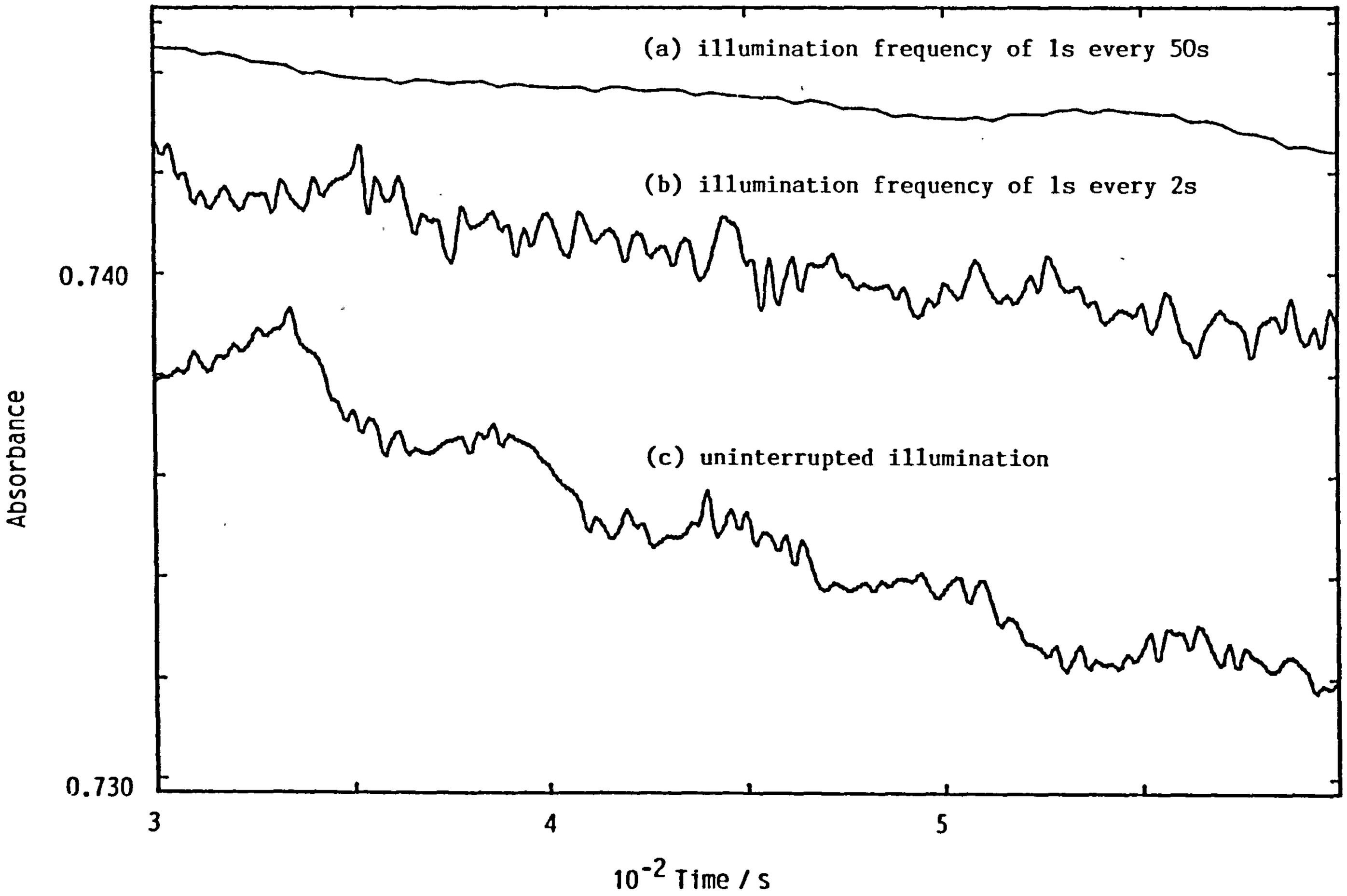

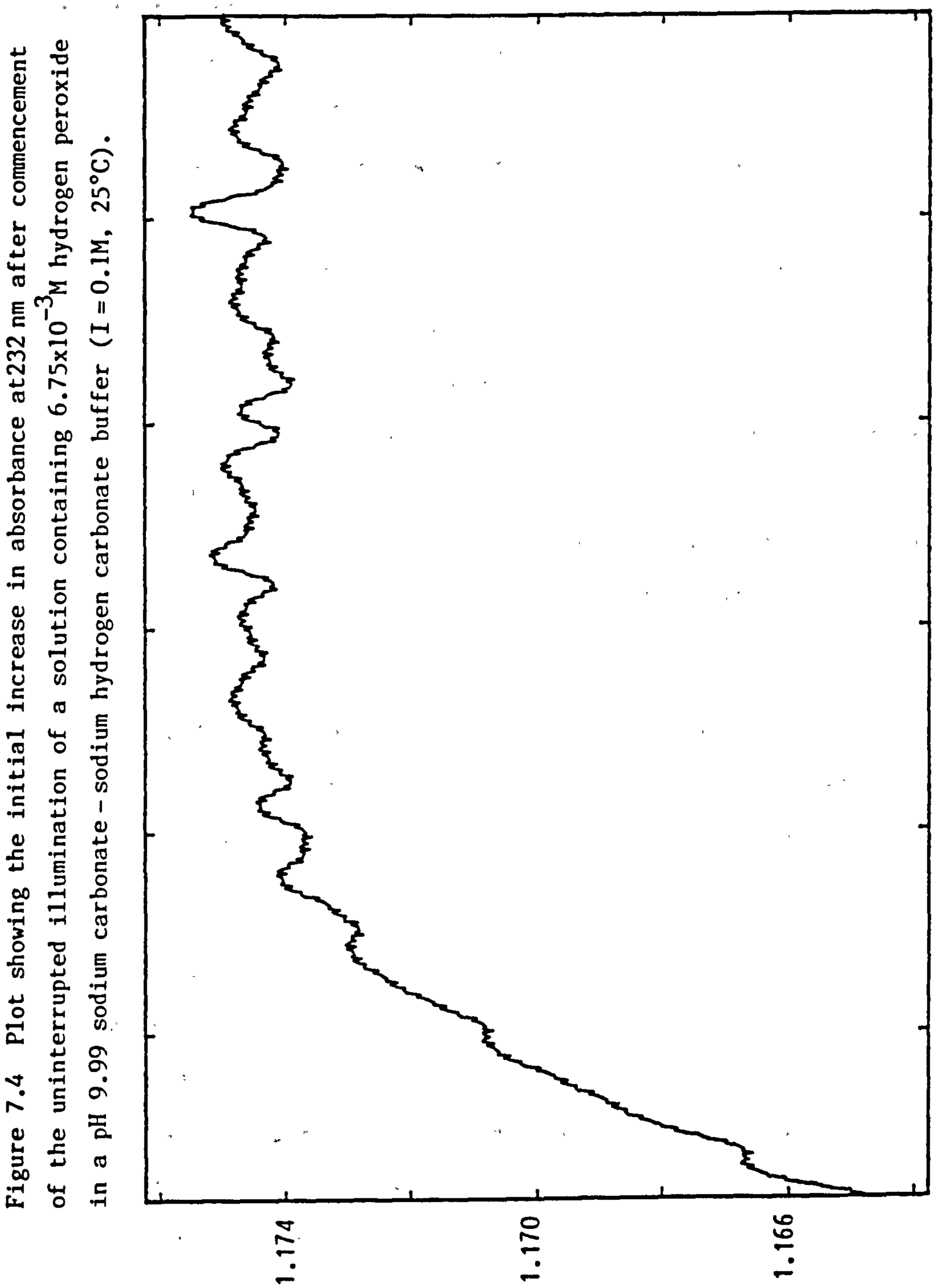

Figure 7.4 Plot showing the initial increase in absorbance at232 nm after commencement of the uninterrupted illumination of a solution containing $6.75x10^{-3}$M hydrogen peroxide in a pH 9.99 sodium carbonate - sodium hydrogen carbonate buffer (I = 0.1M, 25°C).

tic runs was kept to a minimum (20 to 30), thus reducing the level of UV radiation. In addition, because the UV interaction causes uncertainty in the value of A_∞, observed pseudo first order rate constants, k_{obs}, were calculated from non-linear regression using Equation 7.1

$$A = A_\infty + A_2\, e^{-k_2 t} + A_B \qquad \text{Eqn 7.1}$$

where k_2 is the observed pseudo first order rate constant for the reaction of H_2O_2 with TriAED; this equation adequately describes the absorbance changes when $A_1\, e^{-k_1 t}$ approaches zero (k_1 is the observed pseudo first order rate constant for the reaction of H_2O_2 with TAED). In practice, by the time the first absorbance measurements were taken in each run the absorbance data were already found to be described by Equation 7.2. Absorbance data for 4.5 lives were used although data over the initial 30-second period were eliminated because of the unexplained increase in absorbance observed, as discussed above.

7.1.2 pH Dependence Study

The objective of this study was to establish, according to precedent, that HOO^- is the reactive species; catalysis by buffer components might also manifest in such a study. The CO_2-free experimental protocol was *not* used during this study.

Experimental

Reagents

TAED solutions were prepared as described in Section 4.2. Carbonate buffers were prepared from sodium hydrogen carbonate and sodium carbonate. Hydrogen peroxide was standardized cerimetrically.[101] All solutions contained 1×10^{-5} M EDTMP.

Procedure

Under pseudo first order conditions, upon mixing TAED and carbonate buffer/hydrogen peroxide solutions in a cuvette, the reaction was fol-

lowed by measuring the decrease in absorbance on the shoulder of the TAED/TriAED spectrum at 232 nm. The reaction was conducted at pH 9.99 and 10.47 (I = 0.1). In addition, an observed second order rate constant has already been determined for this reaction at pH 9.60 (Chapter 5). At both pH's, a rate constant for the hydrolysis of TriAED was obtained in carbonate buffer (I = 0.1 M, sodium salts were used).

Results

Observed pseudo first order rate constants for TriAED perhydrolysis at pH 9.99 and 10.47 are contained in Table 7.1. Plots of pseudo first order rate constant against nucleophile concentration at pH 9.99 and 10.47 , which are linear, are shown in Figures 7.5 and 7.6, respectively. The observed second order rate constants at each pH were obtained from linear regression of the first, and pseudo first, order rate constants listed in Table 7.1 and, although the intercepts were negative, the 90% confidence limits included the value for TriAED hydrolysis in buffer alone. Table 7.2 contains the observed second order rate constants at pH 9.99 and 10.47, together with the value determined at pH 9.60 using the numerical integrative method described in Chapter 5.

On plotting the log of the observed second order rate constants against pH (Figure 7.7), a slope of 0.985 $\pm$ 0.084* is obtained; this is in fair agreement with the value of 1.00 expected for a reaction in which anionic form is the reactive species.

---

* 90% confidence limits

Table 7.1 Observed pseudo first order rate constants (kobs) for the reaction between triacetylethylenediamine* (TriAED) and hydrogen peroxide. Conditions were: pH, as indicated in table; sodium carbonate - sodium hydrogen carbonate buffer (I = 0.1M); $[TAED]_o$ = $1x10^{-4}$M; [EDTMP] = $1x10^{-5}$M; 25°C.

pH	$10^3[H_2O_2]$/M	10^2kobs/s^{-1}
9.99	0.000	0.0100
	2.292	0.5250
	4.419	1.1803
	7.817	2.1083
	9.664	2.8055
10.47	0.000	0.0257
	1.050	0.6670
	2.051	1.5255
	3.186	2.4698
	4.254	3.3780
	5.161	4.3295

*kobs values for the perhydrolysis of TriAED were obtained using TAED, as described in the text.

Table 7.2 pH dependence of observed second order rate constants for the reaction between TriAED and hydrogen peroxide (k_{TriAED}) and between TAED and hydrogen peroxide (k_{TAED}) at 25°C (I = 0.1 M).

pH	k_{TAED} / $M^{-1}s^{-1}$ *	k_{TriAED} / $M^{-1}s^{-1}$ *
9.60	3.347 ± 0.113	1.16 ± 0.16**
9.99	-	2.882 ± 0.272
10.47	-	8.364 ± 0.603

*90% Confidence Limits

**Error obtained using numerical integration method as described in the text.

Figure 7.5 Plot of pseudo first order rate constant (kobs) against nucleophile concentration for the reaction between hydrogen peroxide and triacetylethylenediamine at 25°C in a pH 9.99 sodium carbonate - sodium hydrogen carbonate buffer (I = 0.1M): $[TAED]_o = 1x10^{-4}M$; $[EDTMP] = 1x10^{-5}M$. The line represents the best fit using the linear least squares method.

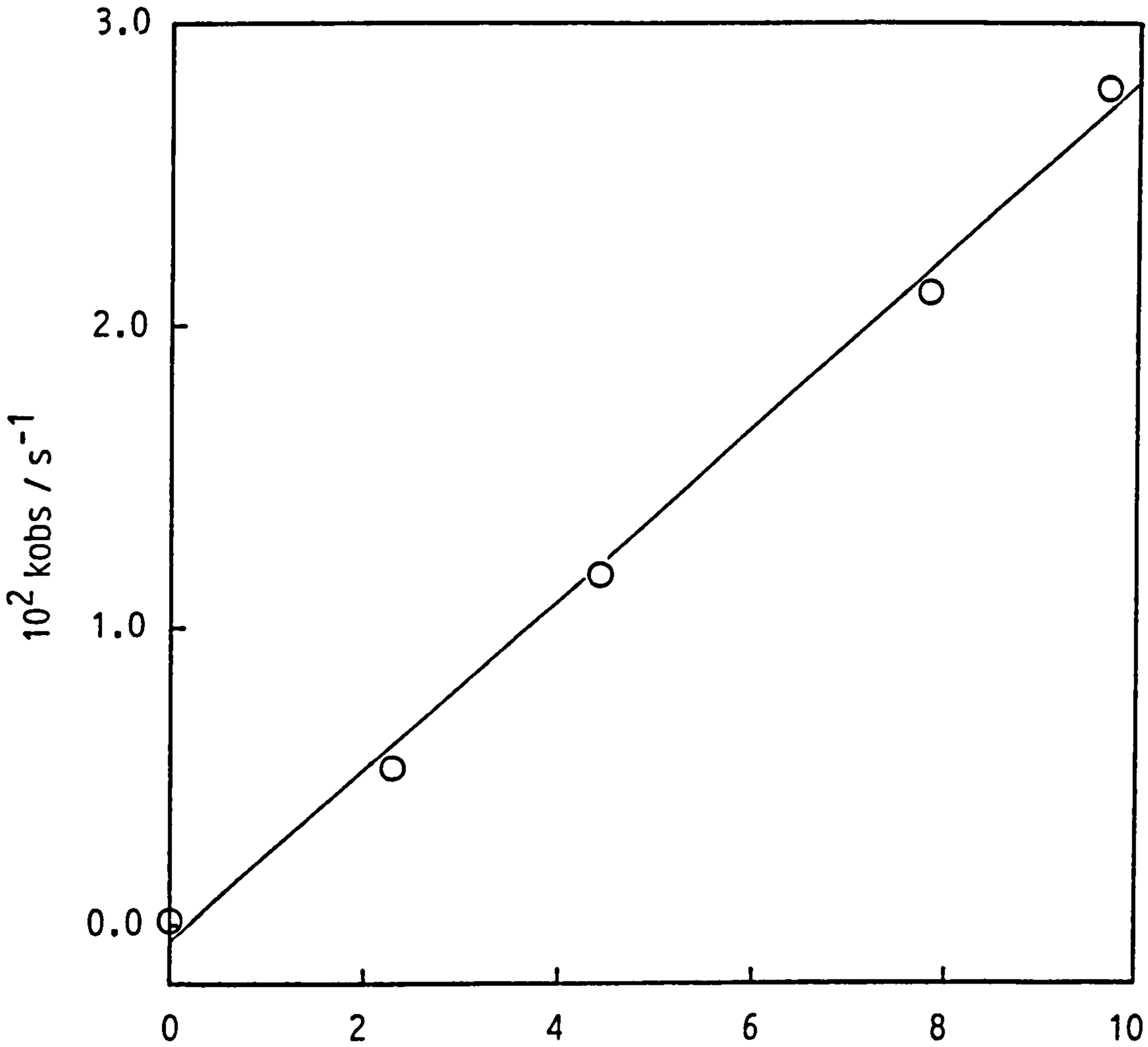

Figure 7.6 Plot of pseudo first order rate constant (kobs) against nucleophile concentration for the reaction between hydrogen peroxide and triacetylethylenediamine at 25°C in a pH 10.47 sodium carbonate - sodium hydrogen carbonate buffer (I = 0.1M): $[TAED]_o = 1x10^{-4}M$; $[EDTMP] = 1x10^{-5}M$. The line represents the best fit using the linear least squares method.

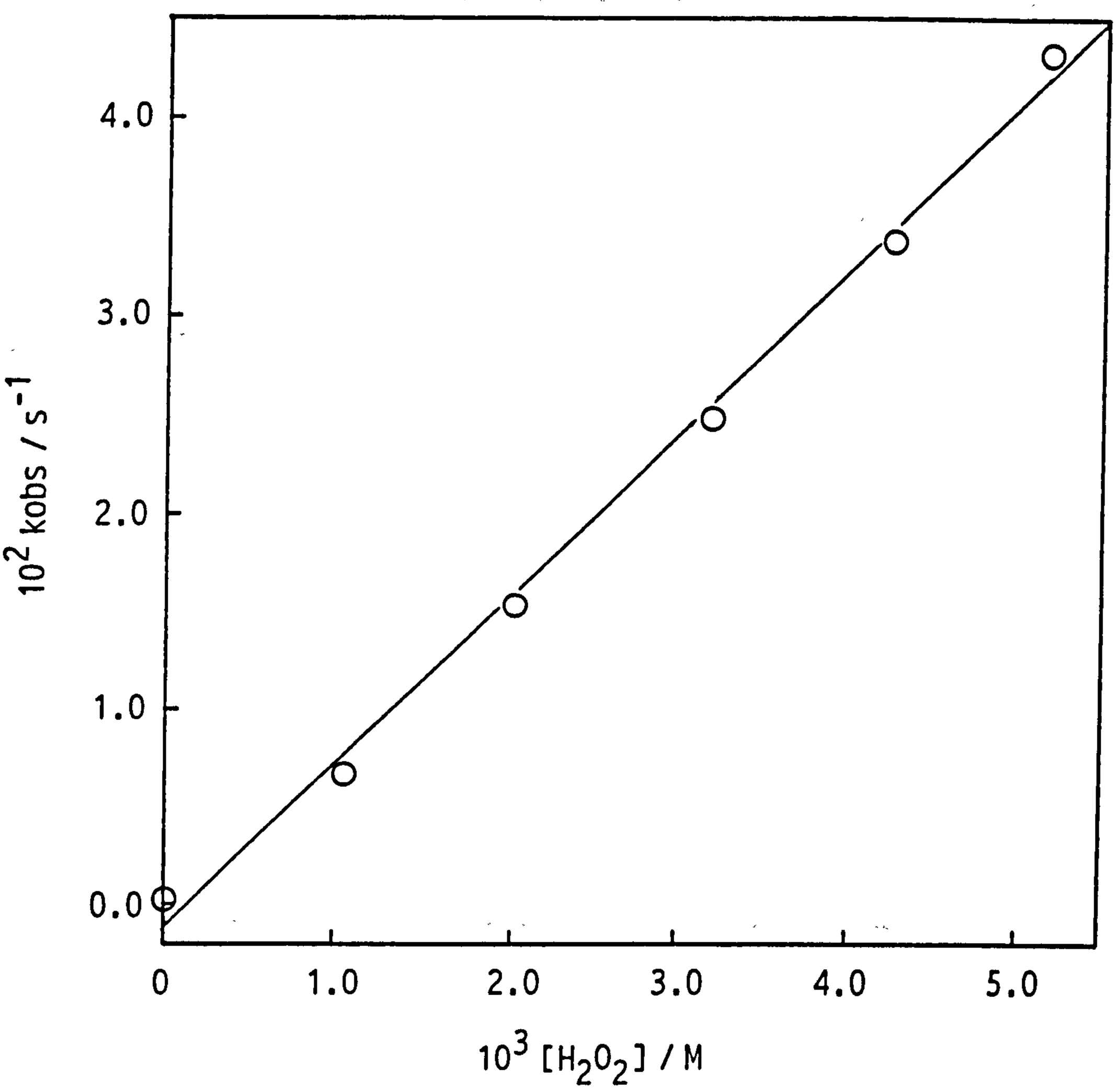

Figure 7.7 Plot showing the pH dependence of the reaction between hydrogen peroxide and triacetylethylenediamine ($k_2$obs) at 25°C. The reactions were carried out in sodium carbonate - sodium hydrogen carbonate buffers (I = 0.1M) which contained $1x10^{-5}$M EDTMP. The line represents the best fit using the linear least squares method.

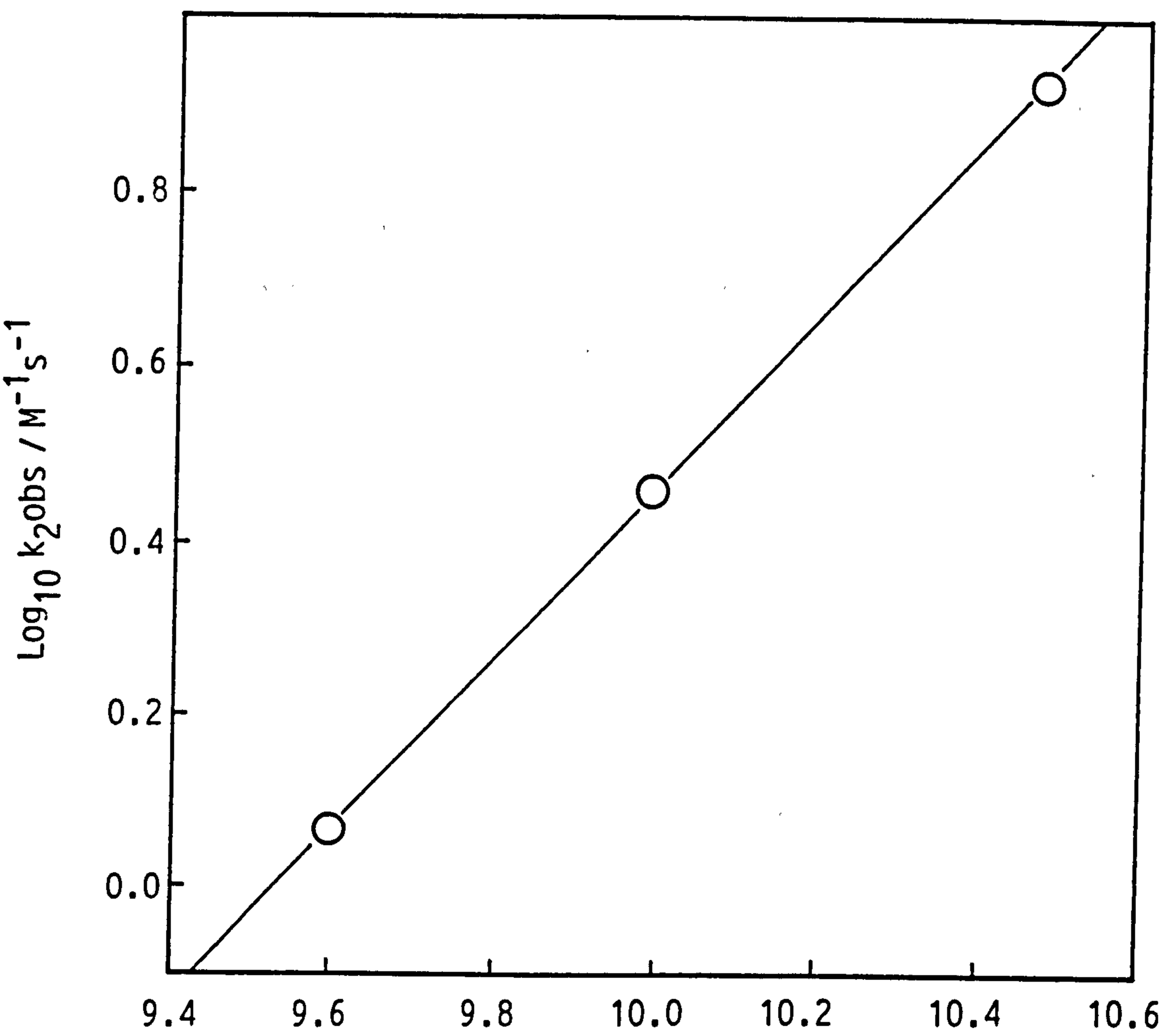

Finally, although the 90% confidence limits of the intercepts for the plots of k_{obs} against hydrogen peroxide concentration included the value for TriAED hydrolysis in buffer alone, the plots clearly indicate a systematic negative deviation in the determination of k_{obs} values. This is most probably an effect of the UV interaction with the H_2O_2/-buffer component which, although reduced by limiting the illumination of the cuvette, is not completely eliminated.

7.1.3 Temperature Dependence of TriAED Perhydrolysis

From a study of the relationship between temperature and second order rate constants for the reaction between TriAED and hydrogen peroxide, values for activation entropies and enthalpies can be obtained. The study of temperature dependence was carried out at pH 9.99 at five temperatures 15, 25, 35, 40, and 50°C (the experiment at 25°C had already been carried out as part of the pH dependence study). As with the pH dependence experimental, CO_2-free experimental techniques were not used.

A preliminary investigation was undertaken to assess the effect of temperature on pH of carbonate buffer solution. The pH of a carbonate buffer (I = 1.0 M, pH = 9.99 at 25°C) was determined at temperatures in the range 15 to 50°C. Measurements were made using a PT1-15 pH meter fitted with separate pH and reference electrodes. The meter was calibrated over two points using standard buffer solutions of 7.0 and 9.2 (at 25°C). The appropriate pH of the standard buffer solutions at each temperature, as listed in Table 7.3, was used in the calibrations. The pH variation of the carbonate buffer with temperature is plotted in Figure 7.8; clearly, there is a large dependence of pH on temperature for this particular buffer system.

Table 7.3 Variation with temperature of the pH of standard buffer solutions. (Information supplied by BDH technical services department, Poole, England)

	Standard buffer solution		
Temperature/°C	4.0*	7.0*	9.2*
10	-	-	9.34
15	-	7.015	-
20	4.00	6.96	9.205
25	4.005	6.95	9.18
30	4.011	6.86	9.08
35	4.020	6.82	9.00
40	4.031	6.78	8.94
45	-	-	-
50	-	6.70	8.82

*at 20°C

Figure 7.8 Effect of temperature on the pH of a sodium carbonate - sodium hydrogen carbonate buffer solution (I = 0.1M, pH = 10.025 at 25°C).

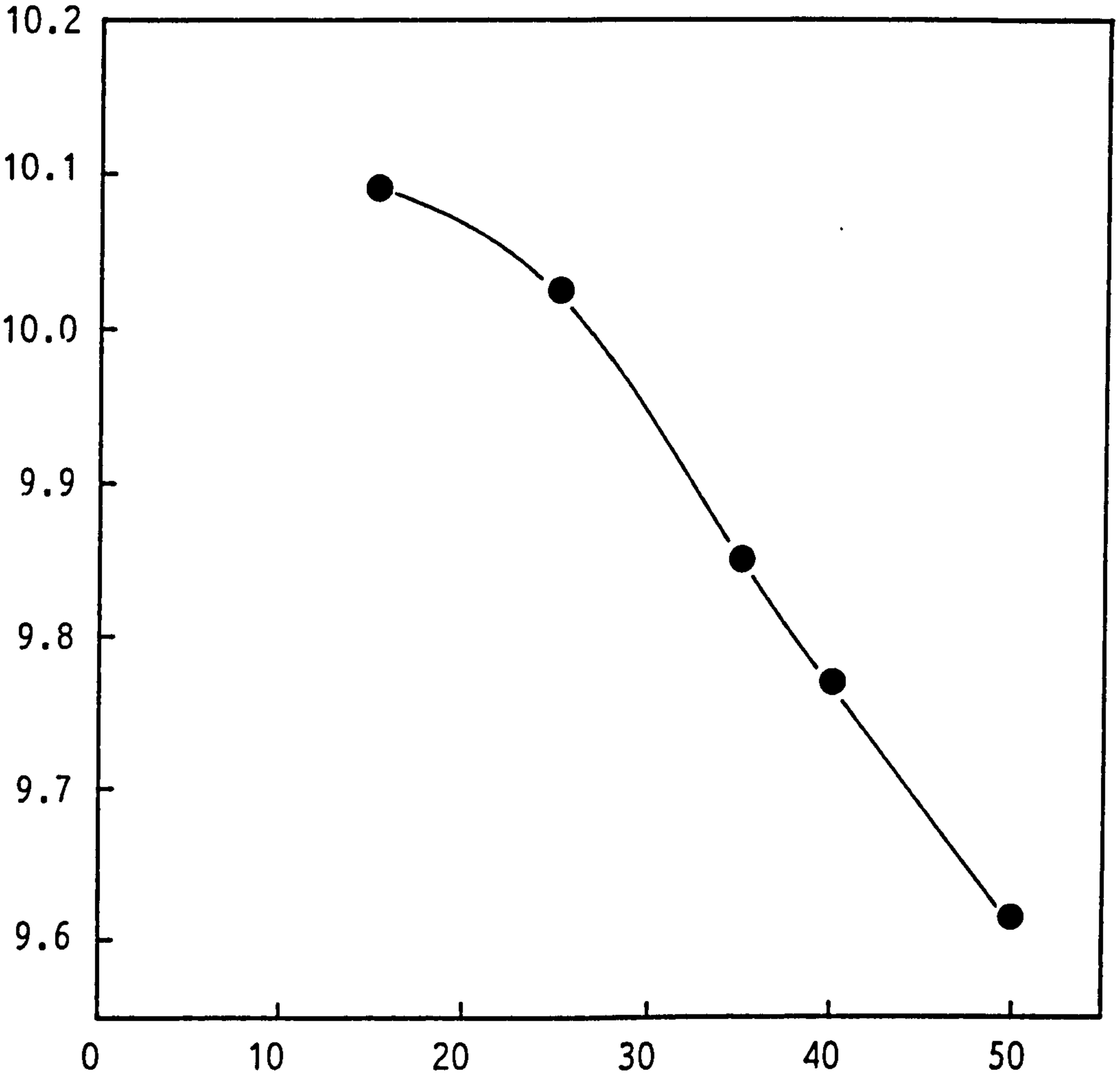

Experimental

Reagents

TAED solutions were prepared as detailed in Section 4.2. A pH 9.99 carbonate buffer was prepared from sodium hydrogen carbonate and sodium carbonate. Hydrogen peroxide was standardized cerimetrically.[101] All solutions contained 1 x 10^{-5} M EDTMP.

Procedure

Under pseudo first order conditions, with hydrogen peroxide in at least twentyfold excess over TAED, kinetic runs were followed by measuring the decrease in absorbance at 232 nm. The precautions against UV interference outlined in the previous section were followed and pseudo first order rate constants (for perhydrolysis of TriAED) were obtained from non-linear regresssion using Equation 7.1. Full details of concentrations and conditions in the runs are given in the results tables.

Results

Table 7.4 details the pseudo first order rate constants obtained at each temperature, for the perhydrolysis of TriAED. The observed second order rate constants at each temperature were obtained from linear regression of pseudo first order rate constants. These values are contained in Table 7.5. Plots of k_{obs} against hydrogen peroxide concentration are given in Figures 7.9 to 7.12 (that at 25°C was obtained as part of the pH dependence study in the previous section and is shown in Figure 7.5). Both negative and positive intercepts were obtained from these plots and although the hydrolysis rate constant was not determined at each temperature, it can be stated that the 90% confidence limits of the intercept include the origin for all but the run conducted at 15.15°C (-1.189 $\pm$ 0.969).

Table 7.4 Observed pseudo first order rate constants (kobs) for the reaction between triacetylethylenediamine* (TriAED) and hydrogen peroxide at several different temperatures. Conditions were: sodium carbonate - sodium hydrogen carbonate buffer (I = 0.1M); pH = 10.025 at 25°C**; $[TAED]_o = 1 \times 10^{-4}$M; [EDTPM] = 1×10^{-5}M.

Temperature/°C	$10^3[H_2O_2]$/M	10^2kobs/s^{-1}
15.15	2.307	0.304
	4.568	0.677
	8.956	1.431
	11.086	1.751
	15.224	2.573
25.0	0.000	0.010
	2.292	0.525
	4.419	1.180
	7.817	2.108
	9.664	2.806
35.0	2.294	1.305
	4.543	2.645
	6.747	4.270
	11.025	6.291
39.4	2.321	1.781
	4.595	3.495
	6.824	5.014
	9.009	7.140
	11.152	8.668
50.7	2.232	3.358
	3.330	5.850
	4.418	7.225
	5.495	9.307
	6.562	10.306

*kobs values were obtained using TAED as described in the text.

**see figure 7.8 for details of pH at other temperatures.

Table 7.5 Variation with temperature of observed second order rate constants ($k_2$obs) for the reaction between TriAED and hydrogen peroxide (I = 0.1 M).

Temperature / °C	$k_2$obs / $M^{-1}s^{-1}$ *	10^3 Intercept / s^{-1} *
15.15	1.740 ± 0.101	-1.189 ± 0.969
25.00	2.882 ± 0.272	-0.689 ± 1.629
35.00	5.749 ± 1.124	0.905 ± 7.817
39.40	7.888 ± 0.584	-1.288 ± 4.362
50.70	16.039 ± 2.864	1.402 ± 13.36

*90% Confidence Limits.

Figure 7.9 Temperature dependence study: Plot of pseudo first order rate constant (kobs) against nucleophile concentration for the reaction between hydrogen peroxide and triacetylethylenediamine at 15.5°C in a sodium carbonate - sodium hydrogen carbonate buffer ($I = 0.1M$, $pH = 10.09$) containing $1x10^{-5}M$ EDTMP: $[TAED]_o = 1x10^{-4}$. The line represents the best fit using the linear least squares method

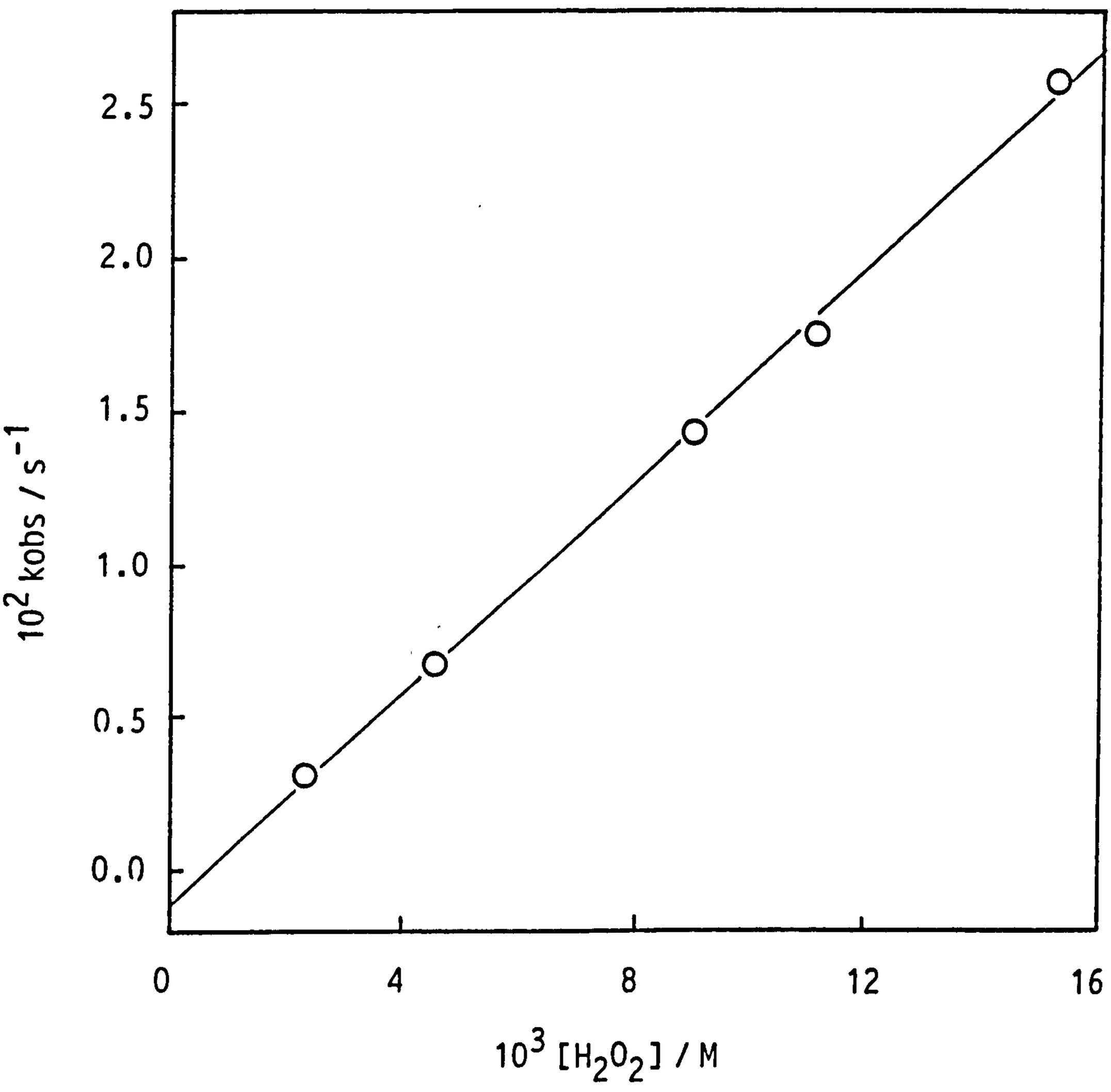

Figure 7.10 Temperature dependence study: Plot of pseudo first order rate constant (kobs) against nucleophile concentration for the reaction between hydrogen peroxide and triacetylethylenediamine at 35.0°C in a sodium carbonate - sodium hydrogen carbonate buffer (I = 0.1M, pH = 9.85) containing $1x10^{-5}$M EDTMP: $[TAED]_o = 1x10^{-4}$M. The line represents the best fit using the linear least squares method.

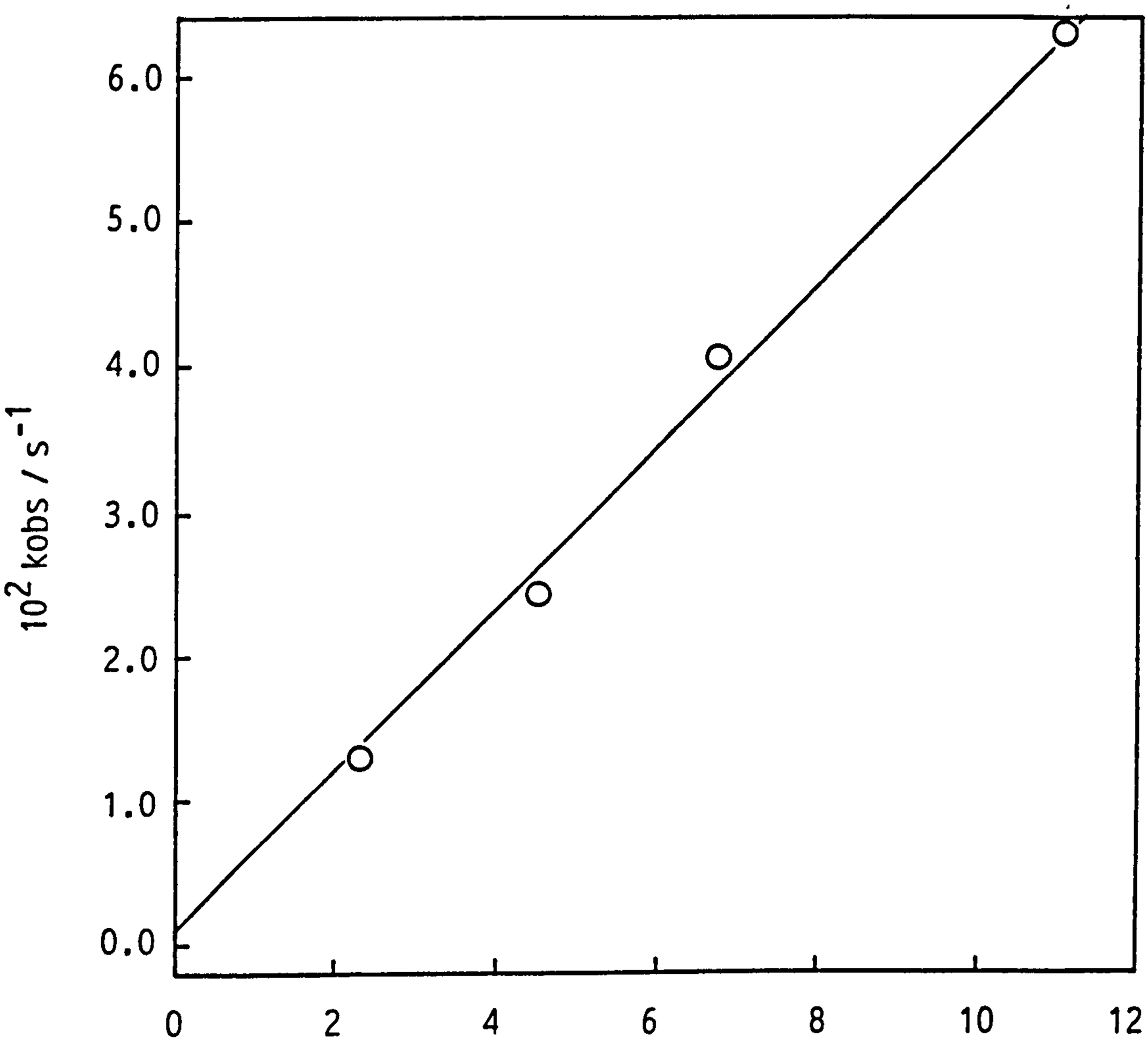

Figure 7.11 Temperature dependence study: Plot of pseudo first order rate constant (kobs) against nucleophile concentration for the reaction between hydrogen peroxide ans triacetylethylenediamine at 39.4°C in a sodium carbonate - sodium hydrogen carbonate buffer (I = 0.1M, pH = 9.77) containing $1x10^{-5}$M EDTMP; $[TAED]_o = 1x10^{-4}$M. The line represents the best fit using the linear least squares method.

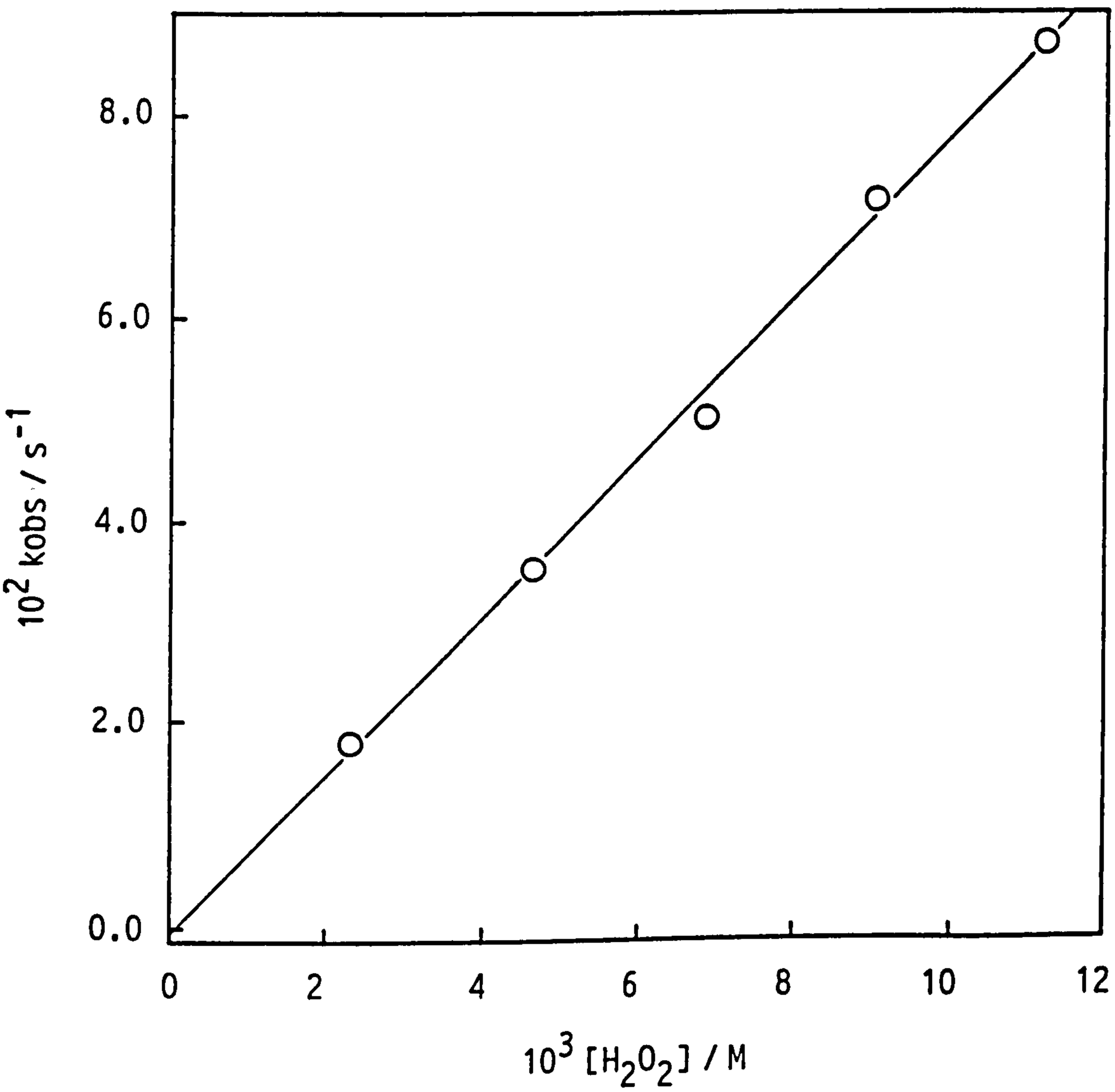

Figure 7.12 Temperature dependence study: Plot of pseudo first order rate constant (kobs) against nucleophile concentration for the reaction between hydrogen peroxide and triacetylethylenediamine at 50.7°C in a sodium carbonate - sodium hydrogen carbonate buffer (I = 0.1M, pH = 9.61) containing $1x10^{-5}$M EDTMP; $[TAED]_o = 1x10^{-4}$M. The line represents the best fit using the linear least squares method.

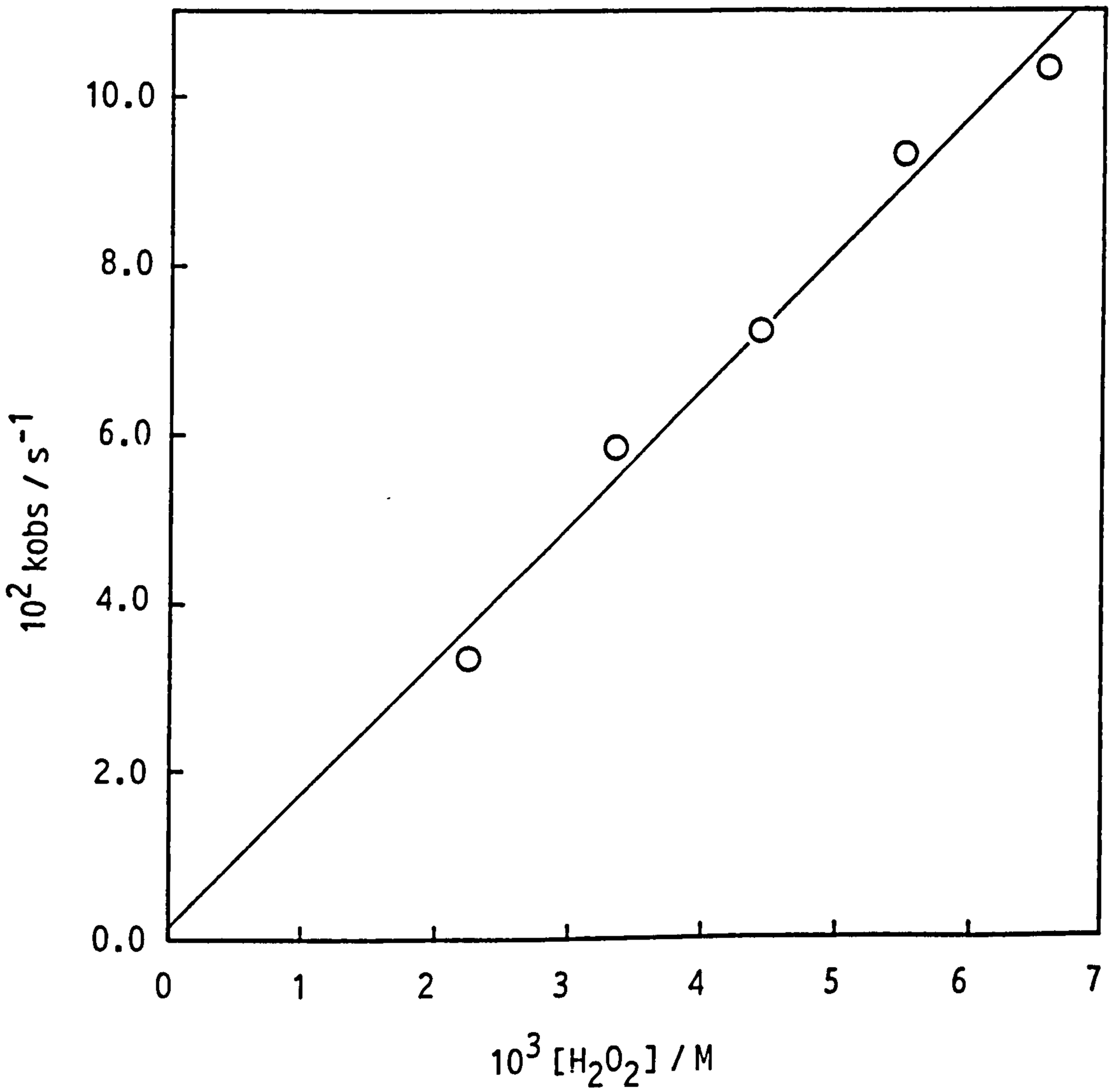

Calculation of $\Delta H^{\ddagger}$ and $\Delta S^{\ddagger}$ From a plot of ln (k_2/T) against 1/T, values of $\Delta H^{\ddagger}$ and $\Delta S^{\ddagger}$, the activation enthalpy and entropy, respectively, can be obtained using the relationship given in Equation 7.2

$$\ln \frac{k_2}{T} = \ln \left(\frac{k}{h} \right) + \frac{\Delta S^{\ddagger}}{R} - \frac{\Delta H^{\ddagger}}{R} \cdot \frac{1}{T} \qquad \text{Eqn 7.2}$$

where k and h are Boltzman's and Planck's constants, respectively, and R is the gas constant. k_2 is the second order rate constant and is related to the observed second order rate constant k_{2obs} by Equation 7.3

$$k_2 = k_{2obs} \frac{K + [H^+]}{K} \qquad \text{Eqn 7.3}$$

where K is the acid dissociation constant for HOOH which also shows a dependence on temperature as defined by Equation 7.4

$$\ln K = \frac{\Delta S^{\circ}}{R} - \frac{\Delta H^{\circ}}{R} \cdot \frac{1}{T} \qquad \text{Eqn 7.4}$$

where ΔS° and ΔH° are the standard entropy and enthalpy of dissociation, respectively. In 1948, Evans and Uri[130] measured the dissociation constant for hydrogen peroxide in aqueous solution over a temperature range of 15 to 35°C, and found that the plot of pKa against 1/T was linear. This indicates that ΔH° and ΔS° are independent of temperature over this range. From the data of Evans and Uri[130], ΔH° and ΔS° were calculated as 34.3 KJ mol^{-1} and -108.0 J mol^{-1} K^{-1}, respectively at zero ionic strength; we shall assume that the value for ΔH° is the same at I = 0.1 M. From these data it is possible to calculate the dissociation constant K at each temperature. Evans and Uri[130] obtained a pKa value of 11.65 for hydrogen peroxide, whereas throughout this thesis we have used a value at 11.60.[113] Table 7.6, therefore, contains two sets of values for pKa and k, calculated using the thermochemical data of Evans and Uri[130] and based on pKa values, at 25°C, of 11.6 and 11.65. From plots of ln (k/T) against 1/T (Figure 7.13, for the data based on pka = 11.6 only) $\Delta H^{\ddagger}$ and $\Delta S^{\ddagger}$ values were obtained and

Table 7.6 Thermochemical data for the reaction between triacetylethylenediamine and hydrogen peroxide.

pKa of HOOH at 25°C	Temperature/K	pH	pKa	*$k_2/M^{-1}s^{-1}$	$10^3(1/T)/K^{-1}$	$\ln(k_2/T)$
11.60	288.30	10.09	11.805	92.047	3.4686	-1.1417
	298.15	9.99	11.600	120.289	3.3540	-0.9078
	308.15	9.85	11.405	212.097	3.2452	-0.3735
	312.55	9.77	11.323	289.712	3.1994	-0.0759
	323.85	9.62	11.123	526.756	3.0878	0.4807
11.65	288.30	10.09	11.855	103.070	3.4686	-1.0286
	298.15	9.99	11.650	134.610	3.3540	-0.7952
	308.15	9.85	11.450	237.280	3.2452	-0.2613
	312.55	9.77	11.273	324.100	3.1994	-0.0363
	323.85	9.62	11.173	589.070	3.0878	0.5983

*calculated using Equation 7.3 and the observed second order rate constants contained in Table 7.5.

Table 7.7 Activation parameters for the reaction between TriAED and hydrogen peroxide.

pKa of HOOH	Slope of Figure 7.13	Intercept of Figure 7.13	$\Delta H^{\ddagger}$ / KJ mol^{-1}	$\Delta S^{\ddagger}$ / J mol^{-1} K^{-1}
11.60	−4384 ± 1038	13.938 ± 3.398	36.448 ± 8.630	−81.660 ± 28.250
11.65	−4333 ± 1071	13.867 ± 3.505	36.024 ± 8.904	−82.250 ± 29.140

Figure 7.13 Plot of $\ln(k_2/T)$ against $1/T$ for the reaction between hydrogen peroxide and triacetylethylenediamine, where k_2 is the second order rate constant for the reaction and T is the temperature (K). Reactions were carried out in carbonate buffer (I = 0.1M). The line represents the best fit using the linear least squares method.

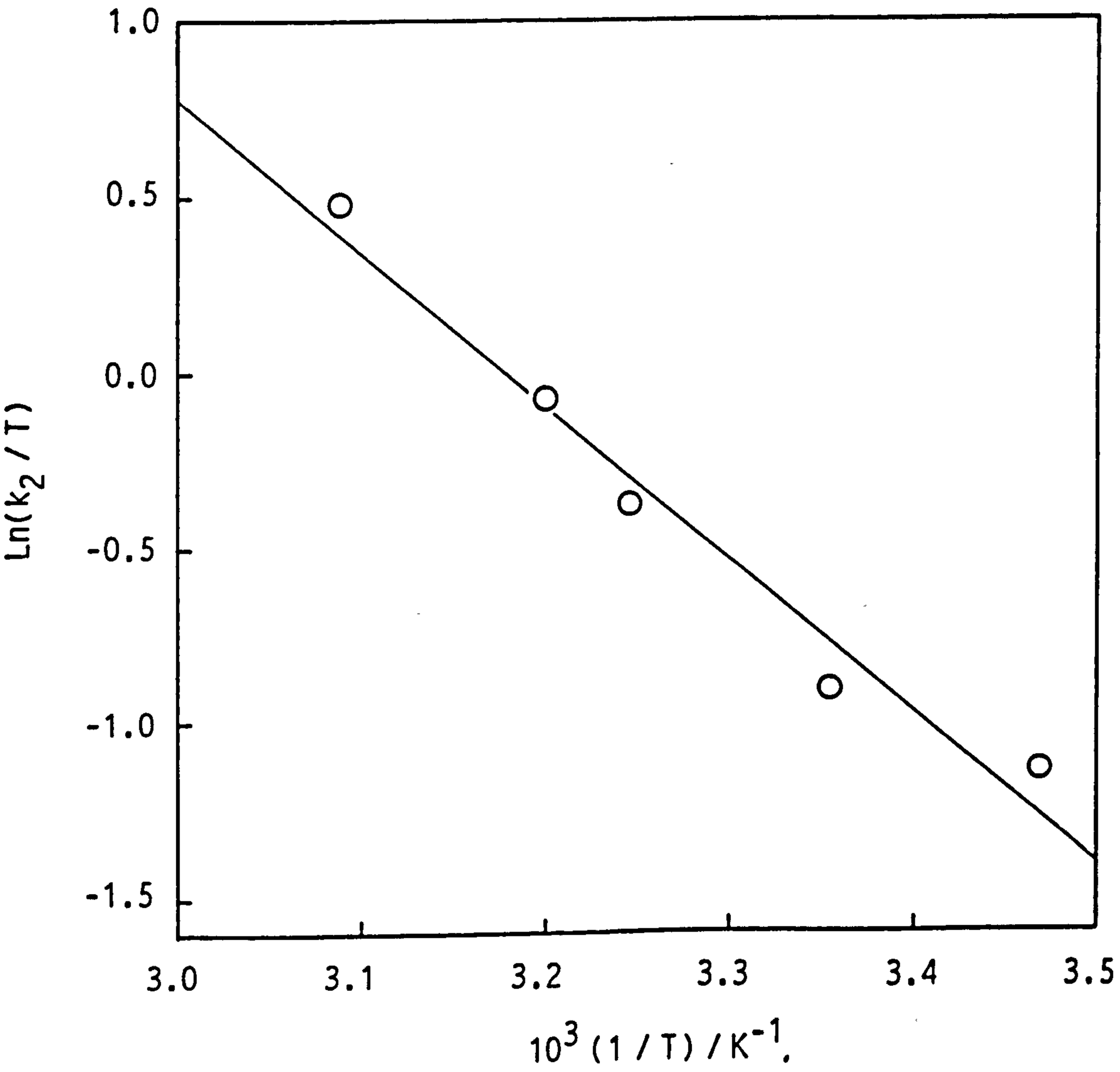

these are contained in Table 7.7. Clearly, the choice of pKa on which to base the calculation of k at each temperature, using the thermochemical data of Evans and Uri, does not significantly affect the evaluation of $\Delta H^{\ddagger}$ and $\Delta S^{\ddagger}$ for this reaction. The activation parameters are discussed in Section 7.4.

7.2 Study of the Reaction of a range of Peroxide Nucleophiles with TriAED

As part of the study to determine the reason for the low reactivity of peracetic acid towards TAED and TriAED, which includes the aminolysis and alcoholysis studies of the previous chapter, the reactivity towards TriAED of hydrogen peroxide, Caro's acid and methyl hydroperoxide was studied. From the results of these studies it should be possible to determine a Brønsted-type relationship for a series of peroxides, albeit a limited series.

Experimental

The techniques outlined in Section 6.1 for working in CO_2-free conditions were followed. Due to its availability isolated TriAED was used in these studies. All experimentals were conducted in carbonate buffer at an ionic strength of 1.0 (with KCl). Preliminary experiments on the reaction of TriAED with Caro's acid, of which the source is the potassium permonosulphate triple salt ($2\ KHSO_5.K_2SO_4.KHSO_4$), indicated that the kinetic runs should be conducted at pH 11.00; at this pH there was no detectable decomposition of Caro's acid over at least 15000 seconds, well beyond the length of time required for the kinetic runs (results not shown, EDTMP was present). Below this pH, however (~ pH 10.00) there was significant decomposition of Caro's acid. As a further protection against the effects of peroxide decomposition reactions, it should be noted that for all three peroxides, absorbance measurements

were made at 250 nm on the shoulder of the TriAED spectrum; at this wavelength the absorbance due to peroxides is minimal.

Reagents

TriAED and carbonate buffer solutions (potassium salts) were prepared under CO_2-free conditions, as detailed in Section 6.1. KCl was used to adjust the ionic strength of the buffer to the desired value. Hydrogen peroxide/buffer solutions were prepared as described in Section 6.1, and were standardized cerimetrically.[101] Solutions of Caro's acid in carbonate buffer were prepared using the procedure outlined in Section 6.1; the presence of sulphuric acid in the triple salt necessitated the readjustment of the pH back to 11.00 using a known volume of KOH. Caro-'s acid solutions were standardized iodimetrically, as described in Section 2.2. Methyl hydroperoxide was prepared by methylation of hydrogen peroxide using a modified version of the original preparation, described by Reiche and Hitz.[131] The procedure, which does not require a hazardous distillation, was carried out as follows: ensuring adequate cooling under ice and stirring using a magnetic stirrer, 37.5 g 30% H_2O_2 solution (BDH, Analar), 62.5 ml distilled water, and 25 g dimethyl sulphate (98%, BDH, GPR) were mixed in a resin pot fitted with condenser, dropping funnel and thermometer. Subsequently, 52.5 g 40% (w/w) potassium hydroxide solution was allowed to run into the reaction mix via a dropping funnel over about 40 minutes. Dimethyl peroxide, a byproduct of the reaction, escapes as a gas, and if the reaction mix is not adequately cooled, then much of the peroxides will be lost in this way. The reaction mix was not further treated.

Methods for monitoring peroxides in methyl hydroperoxide reaction mix. The peroxide content in the reaction mix was monitored as follows. The determination of the total peroxide content was based on the method of Behrman et al.[133]: samples were generally diluted tenfold and neutral-

ised with a few drops of 50% sulphuric acid. To a 5 ml sample was added 20 ml 4N sulphuric acid and 10 ml 100 g l^{-1} potassium iodide. A blank reaction was also carried out using distilled water. Immediately on adding the potassium iodide solution the assay mixtures were placed in the dark; this was found to slow down significantly the rate of colour development due to dissolved oxygen in the mixture. At regular intervals, 5 ml samples were withdrawn from the assay mixtures and titrated with 0.01 M sodium thiosulphate solution (BDH, CONVOL). The value was corrected for the blank reading corresponding to oxidation of iodide by dissolved oxygen. This process was continued until steady readings for the peroxide content were obtained indicating that all the peroxide had reacted to form iodine; usually, this was found to take about 90 minutes. The hydrogen peroxide content of the reaction mixture was determined spectrophotometrically using the specific titanium (IV) oxalate assay of Sellers[98]; this titanium assay gives a higher molar absorptivity (935 M^{-1} cm^{-1}) than the titanium (IV) sulphate assay[97] used in Section 5.2. Having obtained the total peroxide concentration and the hydrogen peroxide concentration, the methyl hydroperoxide concentration is then simply calculated from the difference between the two. All solutions contained 1 x 10^{-5} M EDTMP and were prepared immediately before use.

Variation in peroxide concentrations in the methyl hydroperoxide reaction mix. After several days, the hydrogen peroxide concentration was found to fall below detectable limits as can be seen from Table 7.8 which monitors the hydrogen peroxide and methyl hydroperoxide concentrations over 144 hours. After 144 hours, the methyl hydroperoxide concentration was in at least 2700-fold excess over hydrogen peroxide and could, therefore, be used in kinetic runs without significant interference by hydrogen peroxide. It is interesting to note from

Table 7.8 Variation with time of the concentrations of hydrogen peroxide and methyl hydroperoxide.

Hours after addition of KOH	$[H_2O_2]$/M	[MeOOH]/M
0	2.100	0.000
1	0.586	0.380
24	0.110	0.450
96	0.0027	0.396
144	1×10^{-4}	0.279

Table 7.8 that after 24 hours the methyl hydroperoxide concentration has increased, and this is likely to be attributable[132] to methylation of hydrogen peroxide by methanol under the alkaline conditions. Methanol is present in the reaction mix as a result of hydrolysis of the dimethyl sulphate. Dimethyl sulphate will itself have reacted with either H_2O or H_2O_2 very quickly and so the increase in [MeOOH] cannot be attributed to a lingering reaction with H_2O_2. After 144 hours the main components of the reaction mix will be methyl hydroperoxide, sulphate and methanol.

Procedure

Under pseudo first order conditions the decrease in absorbance at 230 nm corresponding to TriAED was followed for solutions of TriAED (1×10^{-4} M) in the presence of excess peroxide (ranging from 9.295×10^{-3} to 27.885×10^{-3} for MeOOH; 2.14×10^{-3} to 10.225×10^{-3} M for HOOH; and 3.458×10^{-3} to 10.375×10^{-3} M for Caro's acid). As with all the kinetic runs using peroxides, a minimum number of measurements was made during the course of the run in order to limit UV degradation of the peroxide. Pseudo first order rate constants were obtained from non-linear least squares using Equation 7.4. Absorbance data over 4.5 half-lives were used. In all cases, the pH was found to be unchanged over the duration of the runs. Rate constants for TriAED hydrolysis were obtained by following the absorbance decrease at 230 nm in carbonate buffer alone, at the same pH's as the kinetic runs using peroxides. Full details of experimental conditions and nucleophile concentrations are given in the results tables. In all cases, the runs were conducted at one pH only (10.03 for H_2O_2 and MeOOH and 11.04 for Caro's acid, I = 1.0).

Results

Figures 7.14, 7.15 and 7.16 show typical plots of absorbance decrease with time for reactions of TriAED with H_2O_2, MeOOH and Caro's acid, respectively. No significant problems were encounterd due to UV interaction with peroxide, although at higher concentrations of MeOOH, once A_∞ had apparently been reached a slight increase in absorbance with time was observed. Table 7.9 details the pseudo first order rate constants for each of the three peroxide nucleophiles. Observed second order rate constants for the reaction of TriAED with H_2O_2, 3.759 $\pm$ 0.211 M^{-1} s^{-1} ; MeOOH, 0.1937 $\pm$ 0.0160 M^{-1} s^{-1}, and Caro's acid (4.569 $\pm$ 0.358) x 10^{-2} M^{-1} s^{-1} were obtained from linear regression of the first, and pseudo first, order rate constants listed in Table 7.9. In all cases, the 90% confidence limit of the intercept included the rate of hydrolysis. Figures 7.17, 7.18, and 7.19 which are linear show plots of k_{obs} against nucleophile concentration. For the reaction of TriAED with Caro's acid it is clear that the hydrolysis reaction contributes a significant proportion to the observed pseudo first order rate constants. Another point concerning Caro's acid is the possibility that, as with the peracetic acid experimental (Section 5.2), hydrogen peroxide could be formed via a hydrolysis side reaction. We do not consider this reaction to have been significant in this case since, as well as the observed stability of Caro's acid at pH 11.00, no initial rapid absorbance decrease due to the reaction with H_2O_2 was observed on mixing TriAED with Caro's acid/buffer, unlike the peracetic acid runs.

90% confidence limits

Table 7.9 Observed pseudo first order rate constants (kobs) for the reaction between triacetylethylenediamine and various peroxide species. Conditions were: pH, as indicated in table; potassium carbonate - potassium hydrogen carbonate buffer (I = 1.0M with KCl); $[TriAED]_o = 1x10^{-4}M$; $[EDTMP] = 1x10^{-5}M$; 25°C.

Peroxide species	pH of runs	10^3[Peroxide]/M	10^3kobs/s^{-1}
H_2O_2	10.03	0.000	0.1084
		2.140	7.157
		4.130	15.009
		6.225	21.490
		8.260	30.650
		10.225	38.557
MeOOH	10.03	0.000	0.1084
		9.295	1.867
		13.943	2.958
		18.590	3.831
		23.237	4.514
Caros acid	11.04	0.000	1.120
		3.458	1.260
		6.916	1.430
		10.375	1.590

Figure 7.14 Plot of absorbance decrease at 230nm during the reaction between triacetylethylenediamine and hydrogen peroxide at 25°C in a pH 10.03 carbonate buffer (I = 1.0M with KCl). The curve represents the best fit to Equation 7.1. $[TriAED]_o = 1x10^{-4}M$; $[H_2O_2]_o = 4.13x10^{-3}M$; $[EDTMP] = 1x10^{-5}M$.

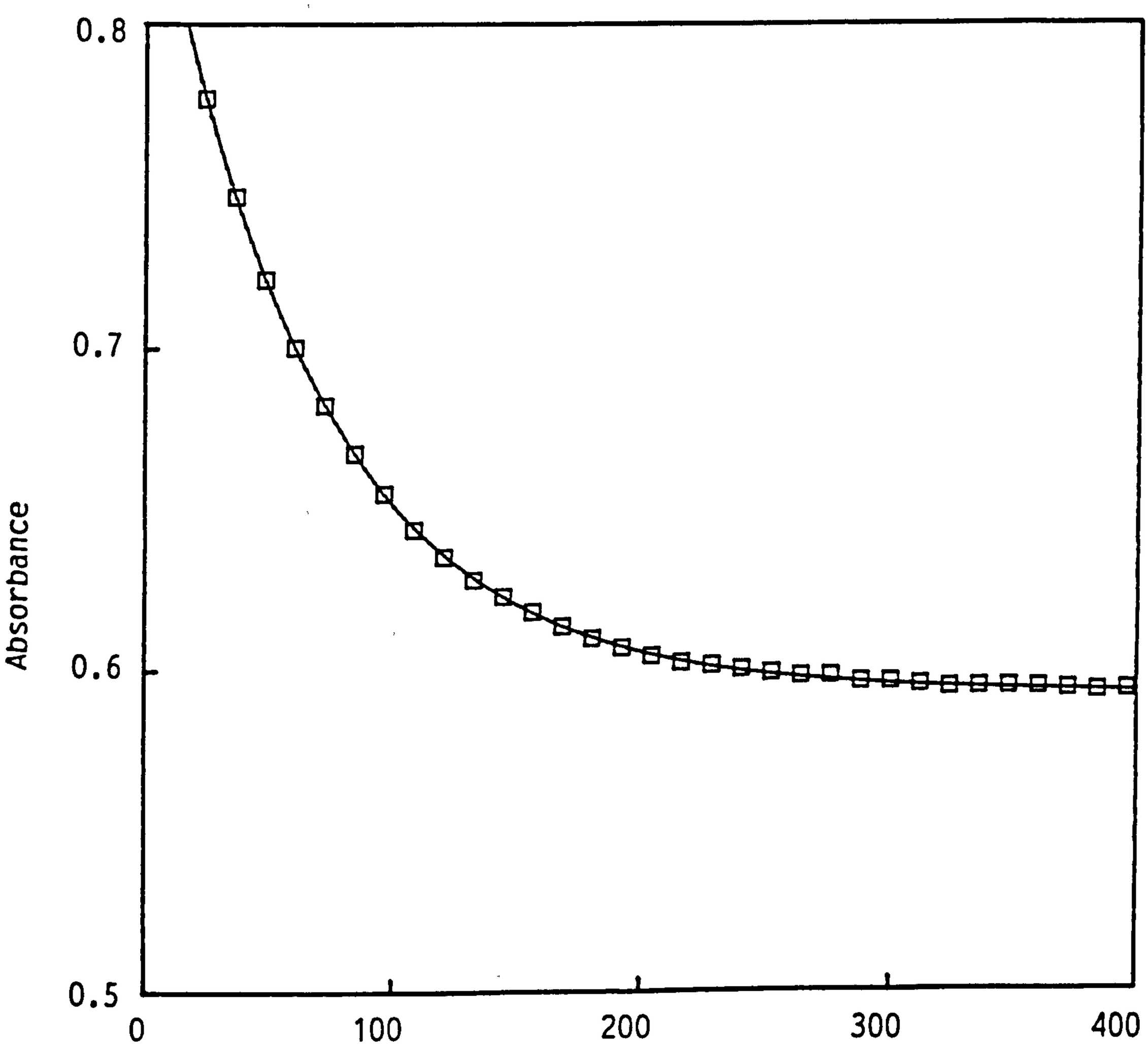

Figure 7.15 Plot of absorbance decrease at 230nm during the reaction between triacetylethylenediamine and methyl hydroperoxide at 25°C in a pH 10.03 carbonate buffer (I = 1.0M with KCl). The curve represents the best fit to Equation 7.1. $[TriAED]_o = 1x10^{-4}M$; $[MeOOH] = 18.59x10^{-3}M$; $[EDTMP] = 1x10^{-5}M$.

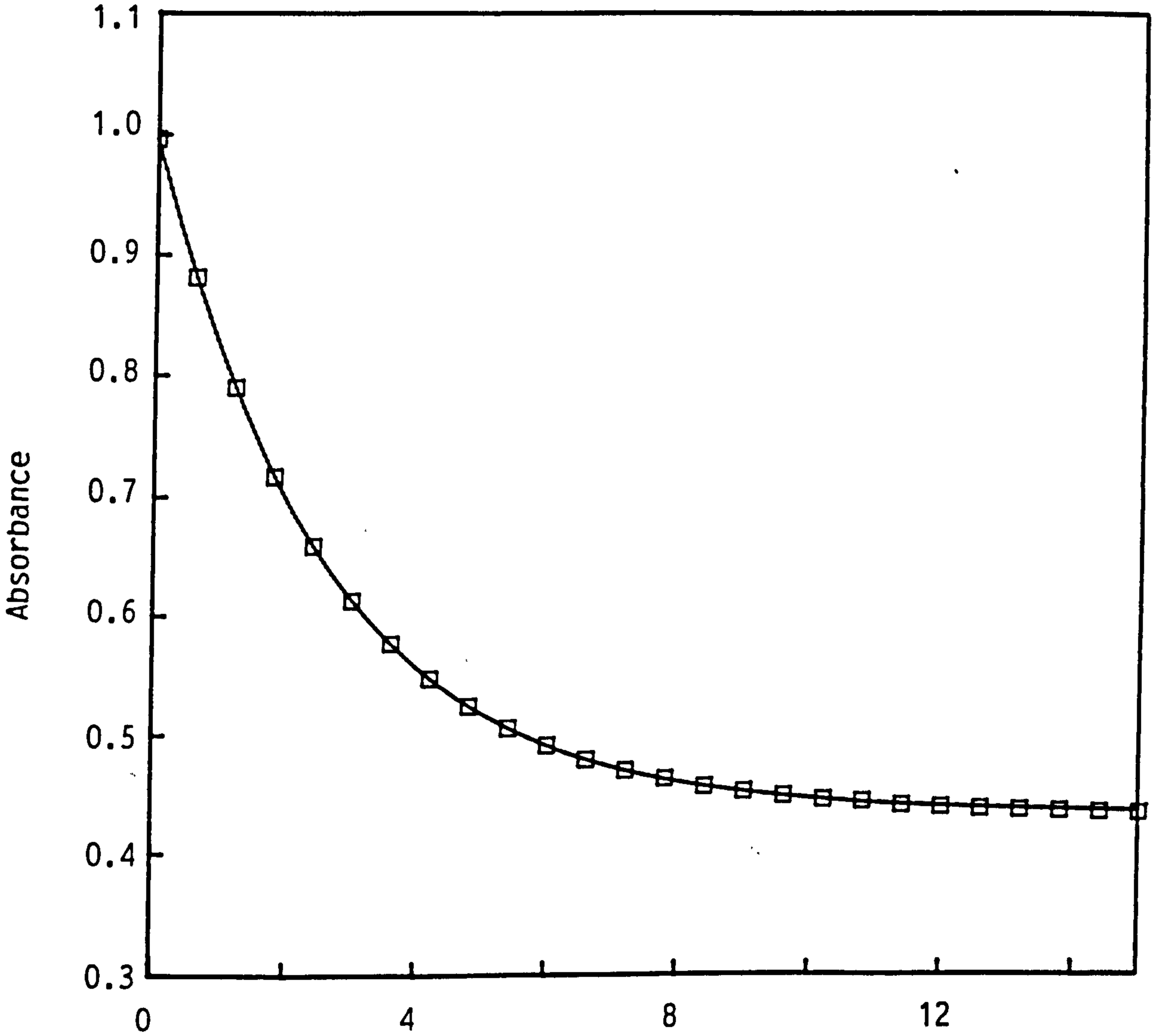

Figure 7.16 Plot of absorbance decrease at 230nm during the reaction between triacetylethylenediamine and Caro's acid at 25°C in a pH 11.04 carbonate buffer (I = 1.oM with KCl). The curve represents the best fit to Equation 7.1. $[TriAED]_o = 1x10^{-4}M$; $[Caro's\ acid]_o = 6.916x10^{-3}M$; $[EDTMP] = 1x10^{-5}M$.

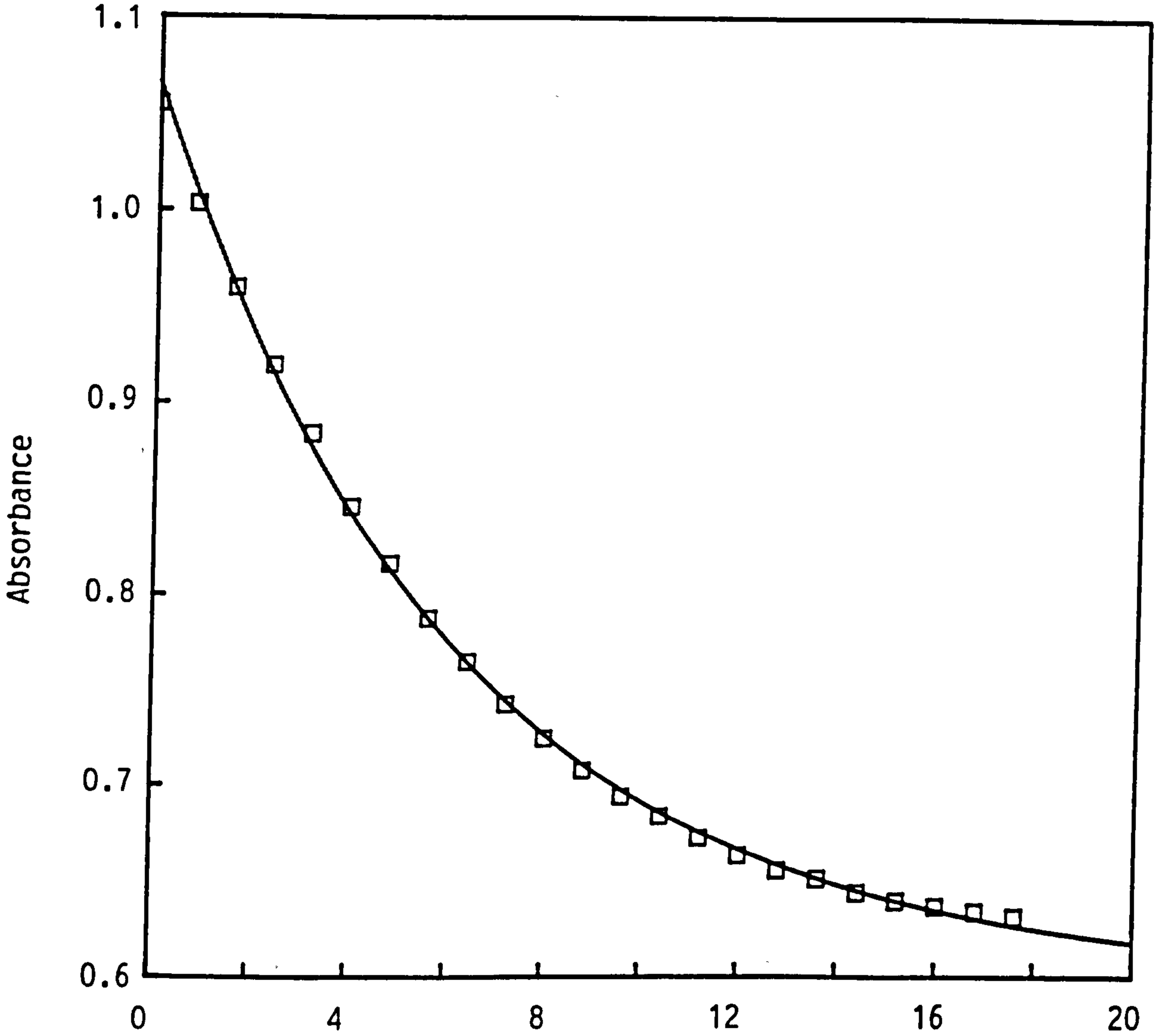

Figure 7.17 Plot of pseudo first order rate constant (kobs) against nucleophile concentration for the reaction between hydrogen peroxide and triacetylethylenediamine at 25°C in a pH 10.03 potassium carbonate - potassium hydrogen carbonate buffer (I = 1.0M with KCl) containing $1x10^{-5}$M EDTMP; $[TriAED]_o = 1x10^{-4}$M. The line represents the best fit using the linear least squares method.

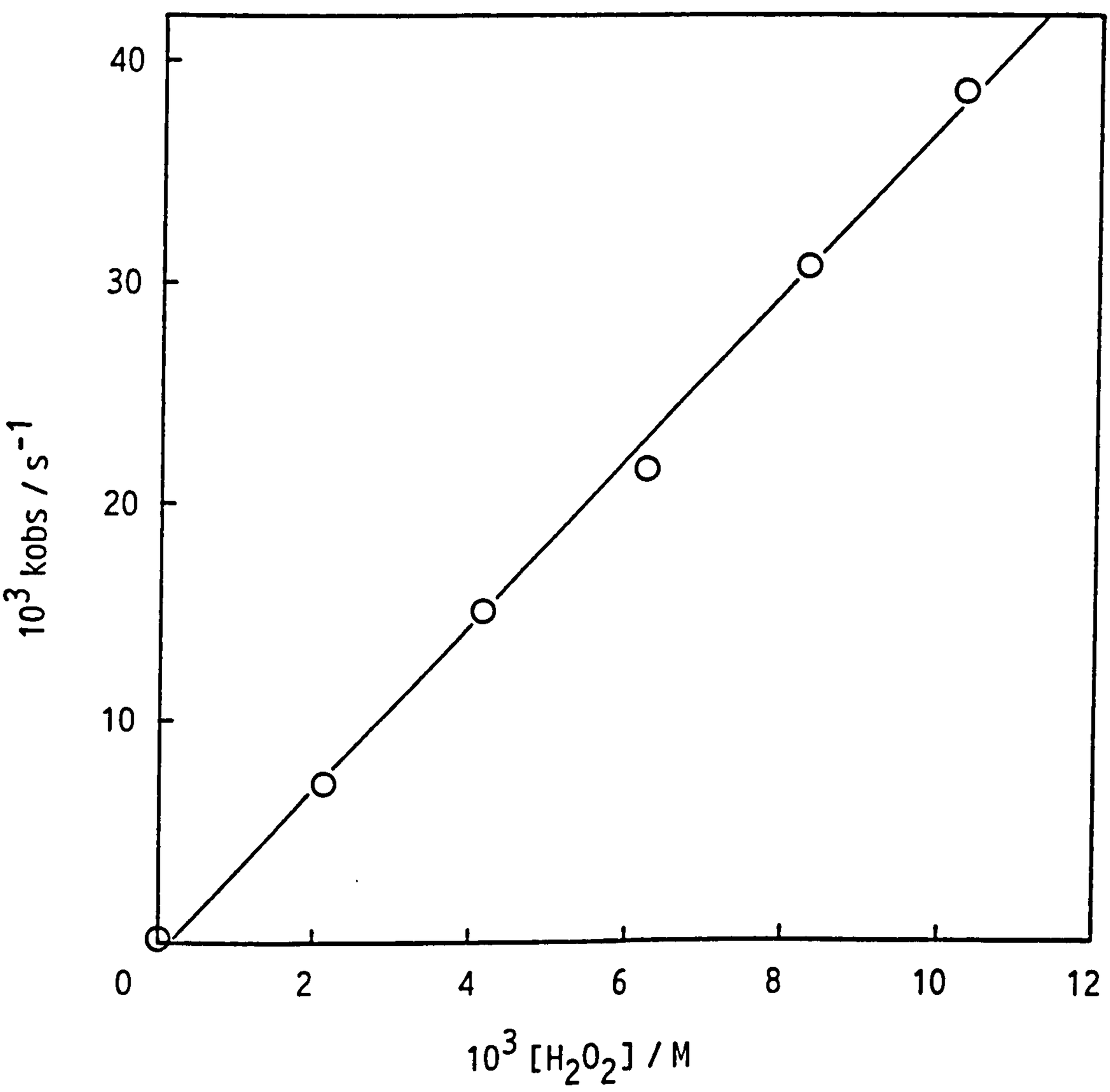

Figure 7.18 Plot of pseudo first order rate constant (kobs) against nucleophile concentration for the reaction between methyl hydroperoxide and triacetylethylenediamine at 25°C in a pH 10.03 potassium carbonate - potassium hydrogen carbonate buffer (I = 1.0M with KCl) containing $1x10^{-5}$M EDTMP; $[TriAED]_o = 1x10^{-4}$M. The line represents the best fit using the linear least squares method.

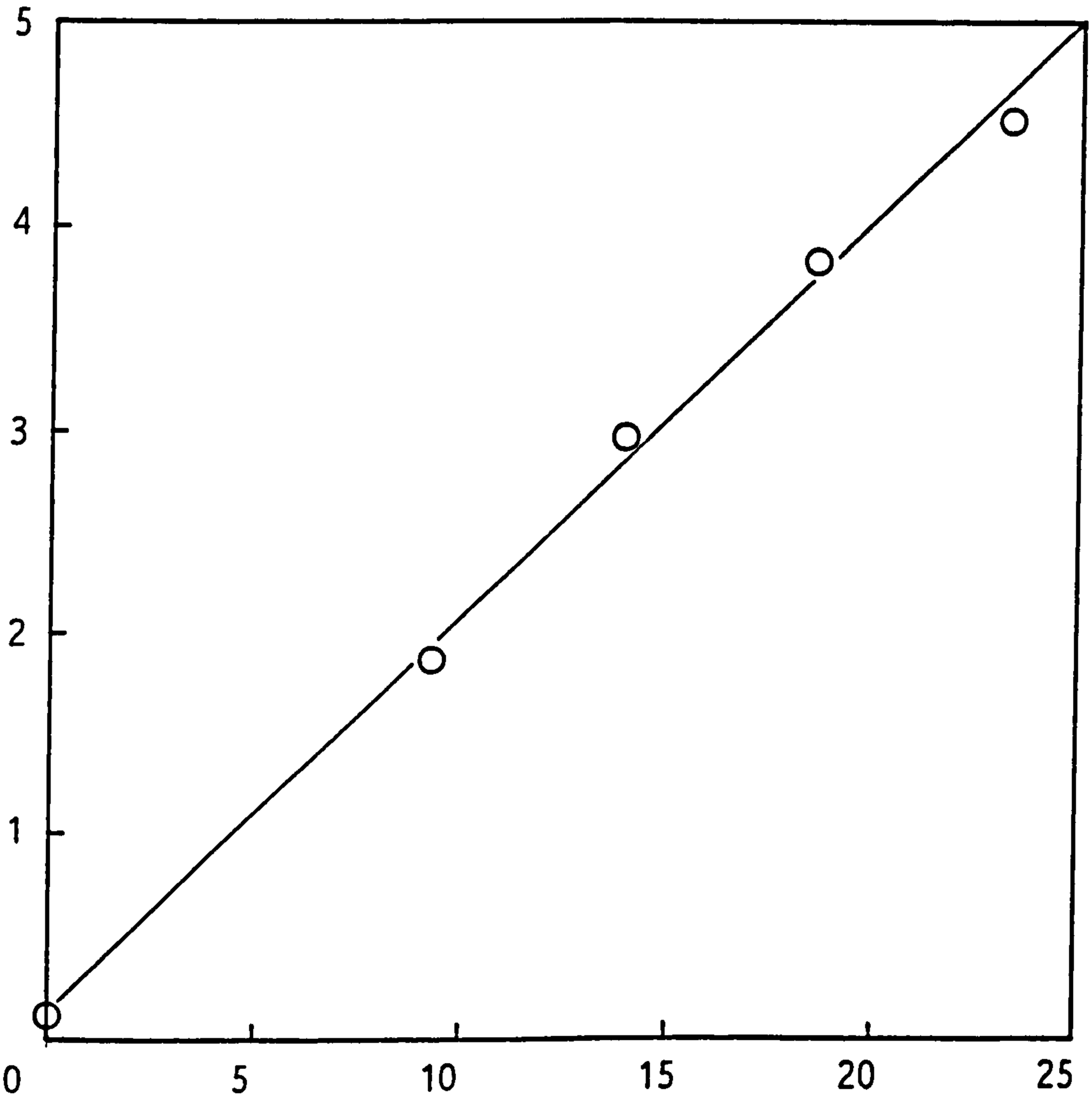

Figure 7.19 Plot of pseudo first order rate constant (kobs) against nucleophile concentration for the reaction between Caro's acid and triacetylethylenediamine at 25°C in a pH 11.04 potassium carbonate - potassium hydrogen carbonate buffer (I = 1.0M with KCl) containing $1x10^{-5}$M EDTMP; $[TriAED]_o = 1x10^{-4}$M. The line represents the best fit using the linear least squares method.

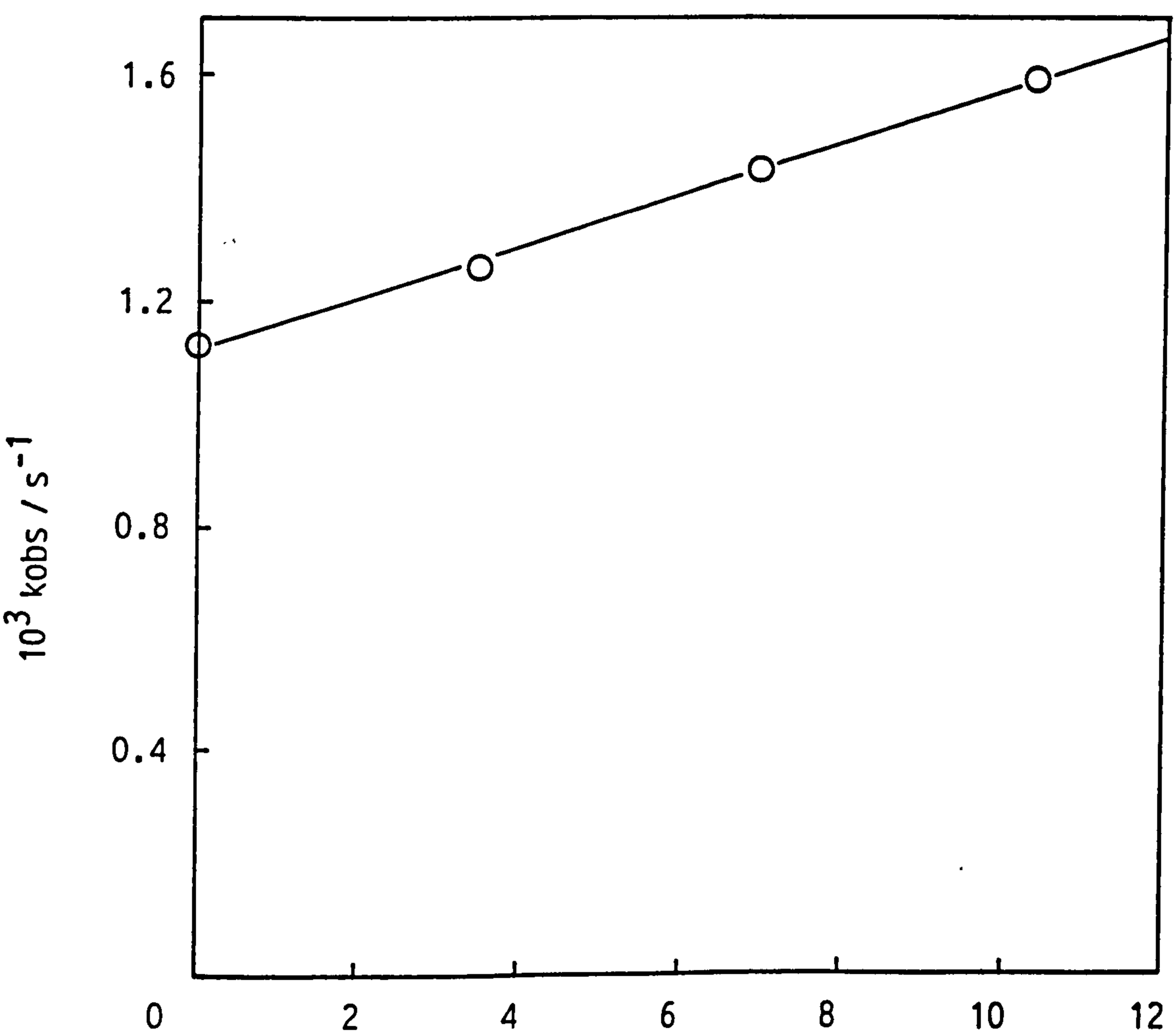

For the reaction of methyl hydroperoxide with TriAED we should address the contribution made to the pseudo first order rate constants from the methanol which is present in the methyl hydroperoxide solution. In the previous chapter, an observed second order rate constant for the reaction of methanol with TriAED was obtained under identical conditions to which these runs were conducted. The value obtained was 2.075×10^{-4} M^{-1} s^{-1} at pH 10.03 ($[Methanol]_o$ = 0.14 to 0.58 M). If we estimate that half the total dimethyl sulphate present in the methyl hydroperoxide preparation (~ 1.27 M) undergoes hydrolysis whilst the remainder is perhydrolysed to form methyl hydroperoxide and dimethyl peroxide, then this gives a potential concentration of 1.27 M methanol in the mixture. Consequently, at the highest methyl hydroperoxide concentration used in these runs, the concentration of methanol present would be 0.127 M. This would give a contribution of 2.645×10^{-5} s^{-1} towards the overall pseudo first order rate constant (5.465×10^{-3} s^{-1}), that is, 1/200 of the total. The exact concentration of methanol in the mixture is unknown, and so it is not possible to correct the pseudo first order rate constants obtained for methyl hydroperoxide, however, clearly, this will not create a significant error.

The results obtained for the reaction of peroxides with TriAED are discussed in Section 7.4.

7.3 Reaction of Hydrogen Peroxide with Triacetylethanolamine

7.3.1 Leaving Group Basicity

As well as studying the correlation between nucleophilicity and basicity as a means of gaining information about the nature of the transition state; a study of the effect of leaving group basicity on the rate of reaction will also give important information. The theory behind leaving group effects is discussed in the introductory chapter.

To study this effect it is necessary to look at the rate of reaction of nucleophiles, in this case hydrogen peroxide, with molecules possessing the imide function as in TAED and TriAED. Rate constants for the perhydrolysis of TAED and TriAED have already been determined. This section describes studies on triacetylethanolamine (TAE) [80] which resembles TAED, with the difference that one of the imide groups is replaced by an ester group.

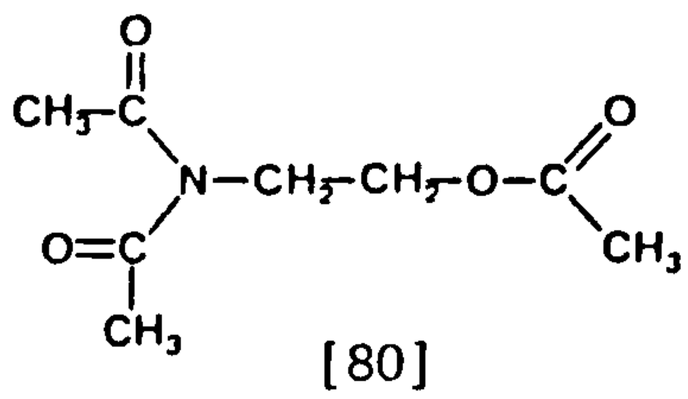

[80]

Figure 7.20 shows spectra of equimolar concentrations of DAED, TAED, and TAE in distilled water. TAE has a molar absorptivity at λmax of almost exactly half that of TAED, as expected, since there is only one imide group in TAE; the imide group is responsible for the absorption band at 218 nm. In addition, it should be noted that the maximum absorptivity of the group in TAE has shifted to 218 nm, compared to 216 nm in TAED. This is most likely due to the O-acetyl group in TAE being less electron withdrawing than the corresponding imide group in TAED. This has the effect of producing a bathochromic shift for the absorption due to the imide group in TAE, compared to that in TAED.

7.3.2 Stoichiometry of TAE Perhydrolysis

Before determining the rate constant for the reaction of hydrogen peroxide with TAE, it was necessary to determine the stoichiometry of the reaction by measuring peracetic acid release.

Figure 7.20 Spectra of equimolar (7.8×10^{-5}M) concentrations of tetraacetylethylenediamine (TAED), diacetylethylenediamine (DAED) and triacetylethanolamine (TAE) at 25°C in distilled water.

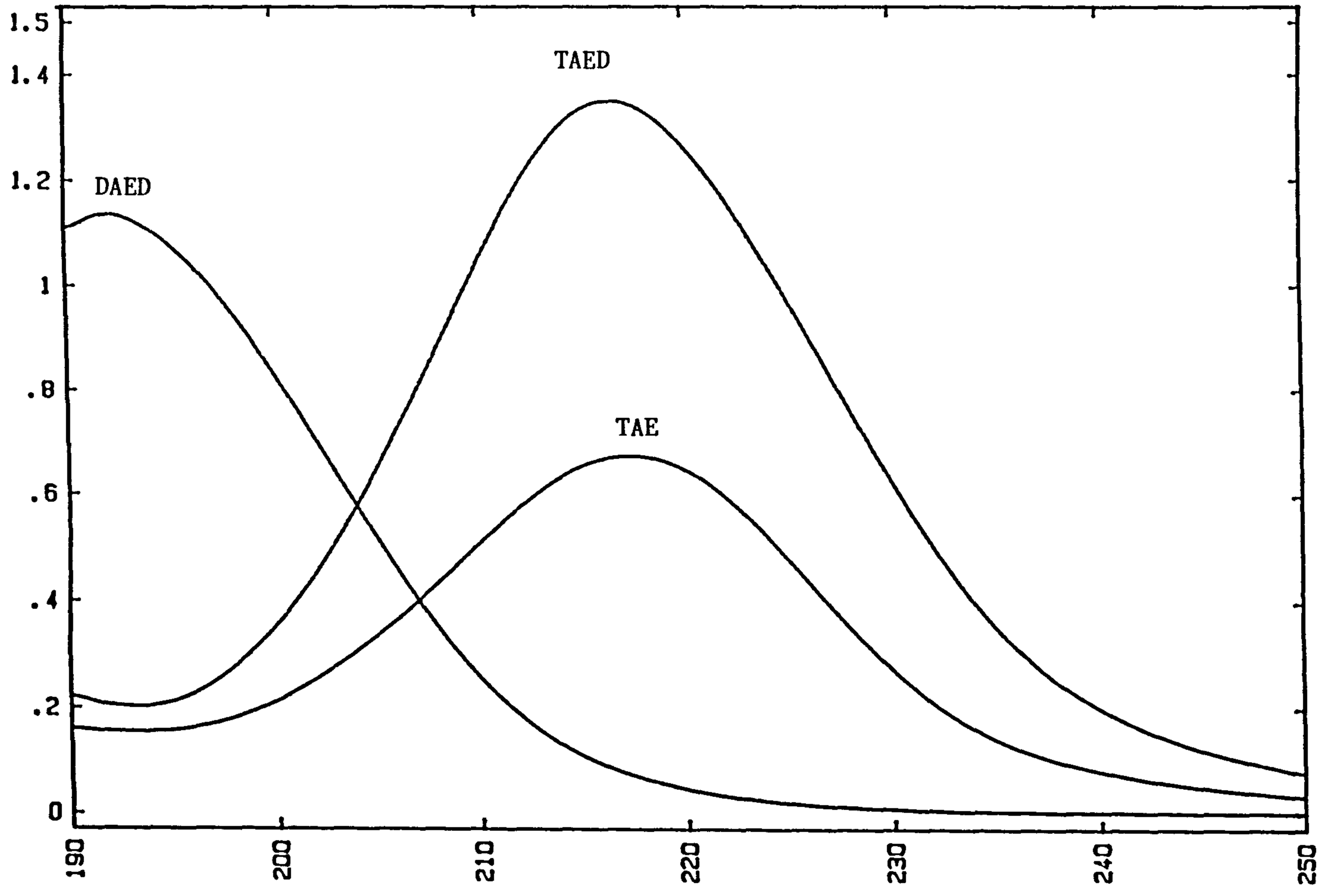

Reagents

TAE, which is a liquid, was obtained from Warwick Chemicals Ltd. and was found to be 95% purity by titration of residual HOAc with NaOH. Hydrogen peroxide was standardized cerimetrically.[101] Carbonate buffer (I = 0.2 M) was prepared from sodium carbonate (decahydrate) and sodium hydrogen carbonate. All solutions contained 1 x 10^{-5} M EDTMP. CO_2-free experimental techniques were not employed in this study.

Procedure

Upon mixing 50 ml each of the TAE and Hydrogen peroxide/buffer solutions, the peracetic acid and total iodide reactable peroxide concentrations were monitored until completion of the reaction after about 8000 seconds. Initial conditions were $[TAE]_o$, 0.95×10^{-3} M; $[H_2O_2]_o$, 2.14×10^{-3} M; pH 9.52 carbonate buffer (I = 1.0 M); $[EDTMP]_o$, 1×10^{-5} M.

Results and Discussion

The changes in peroxide concentration which occurred during the reaction are shown in Figure 7.21. The total iodide reactable peroxide concentration remained relatively constant throughout the course of the reaction, although there was a slight degree of peroxide loss. The maximum peracetic acid concentration attained was 0.85×10^{-3} M, suggesting that one molecule of percaetic acid is formed per moleçule of TAE; the shortfall on the theoretical maximum of 0.95×10^{-3} M being due to hydrolysis. This was confirmed by observing peracetic acid release at greater concentration ratios of hydrogen peroxide to TAE. With a tenfold excess of H_2O_2 over TAE, a maximum peracetic acid concentration of 0.942×10^{-3} M was obtained. It is one of the imide acetyl groups which reacts, as opposed to the ester group, since the peracetic acid liberation coincides with a decrease in the absorbance

Figure 7.21 Reaction of hydrogen peroxide with triacetylethanolamine. Plot showing the change in concentrations of: peracetic acid plus H_2O_2, Δ; peracetic acid, O; H_2O_2 calculated from the previous concentrations, ∇. Conditions were: pH 9.52 sodium carbonate - sodium hydrogen carbonate buffer (I = 0.1M) containing $1x10^{-5}$M EDTMP; $[H_2O_2]_o$ = $2.14x10^{-3}$M; $[TAE]_o = 0.95x10^{-3}$M; 25°C.

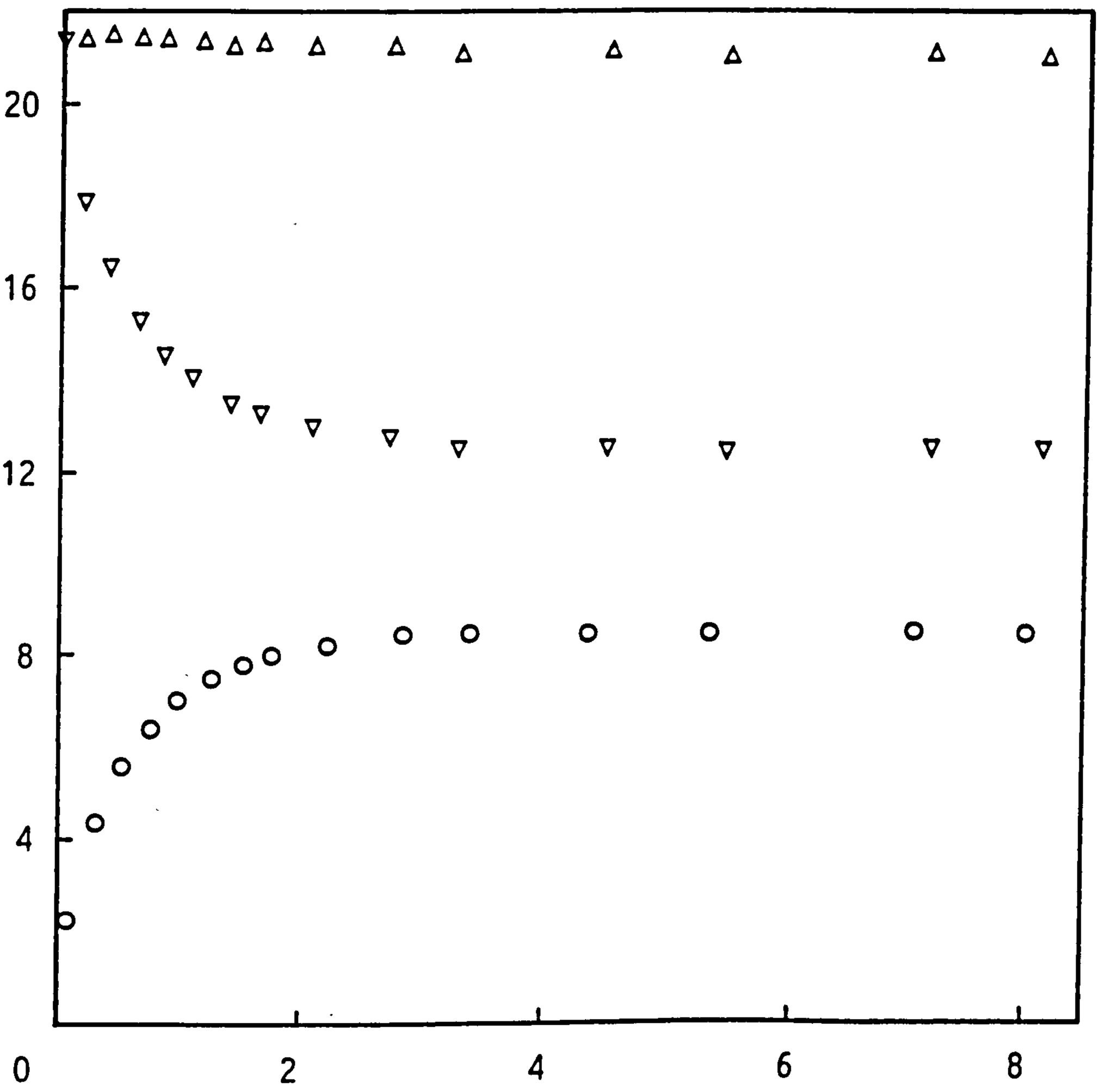

due to the imide group. This would be expected since the O-acetyl group is not activated (as, for example, it is in PNPA).

7.3.3 Determination of Second Order Rate Constants for the Reaction of TAE with Hydrogen Peroxide

The observed second order rate constant for the reaction of TAE with hydrogen peroxide was determined at pH 9.60 using an excess of the latter over the former under pseudo first order conditions and measuring the decrease in absorbance at 232 nm. Experimental procedures were the same as those detailed in Section 7.12 for TAED perhydrolysis. Initial conditions were $[TAE]_o$, 1×10^{-3} M; $[H_2O_2]$, ranging from 2.33×10^{-3} M to 10.30×10^{-3} M; pH 9.60 carbonate buffer (I = 0.1 M); $[EDTMP]_o$, 1×10^{-3} M; 25°C.

Pseudo first order rate constants were obtained from non-linear regression using Equation 7.5. This was used because of the problems of UV interaction with the H_2O_2/buffer components described previously. Absorbance data from 4.5 half-lives were used in the calculation.

$$A = A_\infty + A_1 e^{-k_1 t} \qquad \text{Eqn 7.5}$$

Results

Pseudo first order rate constants for TAE perhydrolysis are listed in Table 7.10, and a second order plot of k_{obs} against hydrogen peroxide concentration, which is linear, is shown in Figure 7.22. The observed second order rate constant for TAE hydrolysis (1.967 $\pm$ 0.0987) was obtained linear regression of the observed pseudo first order rate constants.

7.4 General Discussion

7.4.1 Reaction of Hydrogen Peroxide with TriAED and TAED

The pH dependence study (Section 7.1) has shown that it is, as expected from literature studies[41,62,133], the hydroperoxy anion which is the

Table 7.10 Observed pseudo first order rate constants (kobs) for the reaction between triacetylethanolamine and hydrogen peroxide. Conditions were: pH 9.60 sodium carbonate - sodium hydrogen carbonate buffer (I = 0.1M); $[triacetylethanolamine]_o$= $1x10^{-3}$M; [EDTMP] = $1x10^{-5}$M; 25°C.

$10^3[H_2O_2]$/M	10^3kobs/s^{-1}
2.233	4.338
4.488	8.452
6.628	13.270
8.786	16.998
10.300	20.160

Figure 7.22 Plot of pseudo first order rate constant (kobs) against nucleophile concentration for the reaction between hydrogen peroxide and triacetylethanolamine (TAE) at 25°C in a pH 9.52 sodium carbonate - sodium hydrogen carbonate buffer (I = 0.1M) containing $1x10^{-5}$M EDTMP; $[TAE]_o = 1x10^{-4}$M. The line represents the best fit using the linear least squares method.

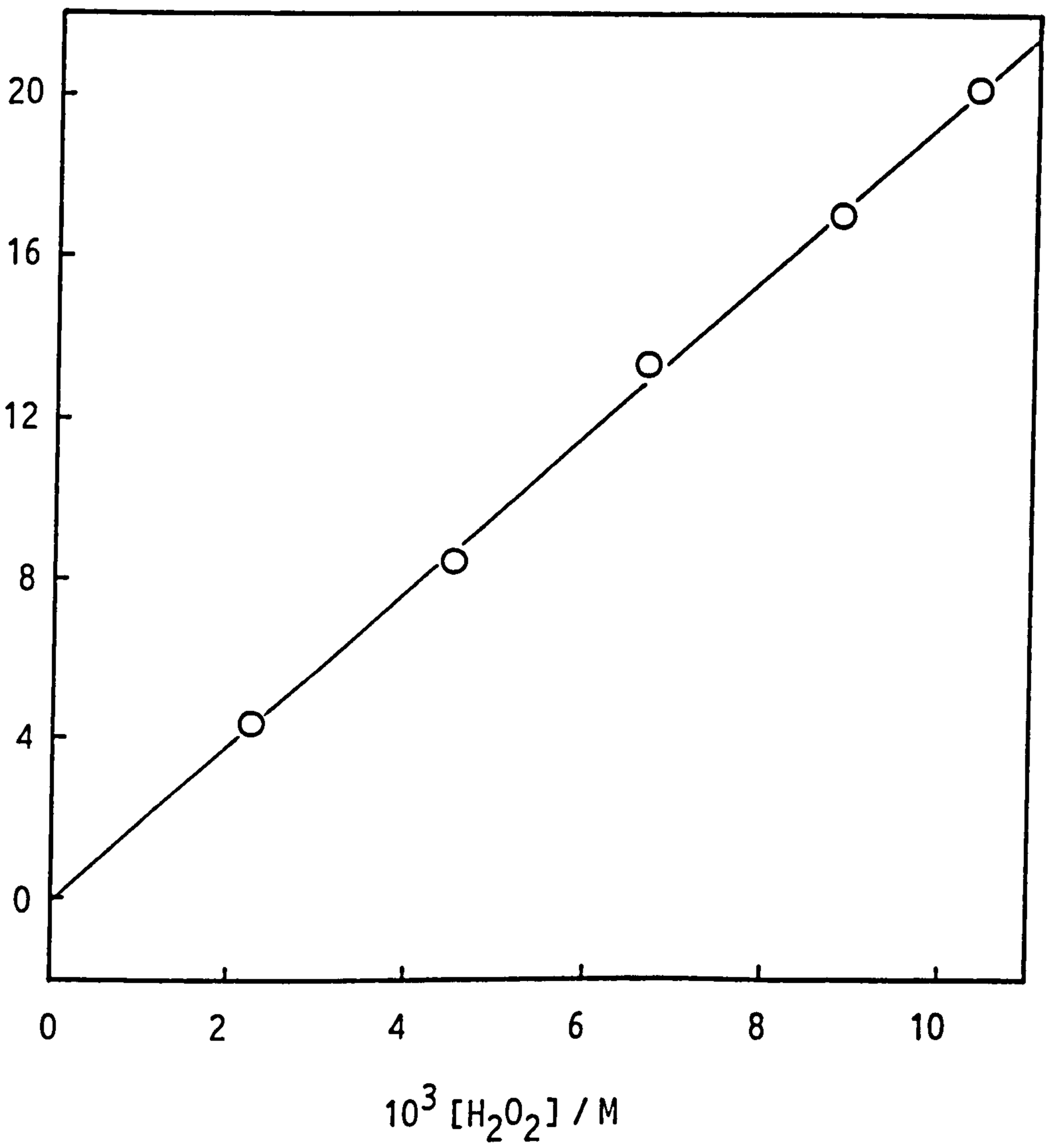

reactive form for the reaction with both TriAED and TAED; from a plot of k_{2obs} against pH a slope of 0.985 ± 0.084 was obtained indicating the likelihood of a simple dependence of the observed second order rate on [HOO^-]. The hydroperoxy anion most likely reacts with the imide group(s) of TAED and TriAED according to Scheme 7.2. Peracetic acid liberation and hydrogen peroxide consumption were measured for those reactions in Chapter 5 and are consistent with such a scheme.

Scheme 7.2

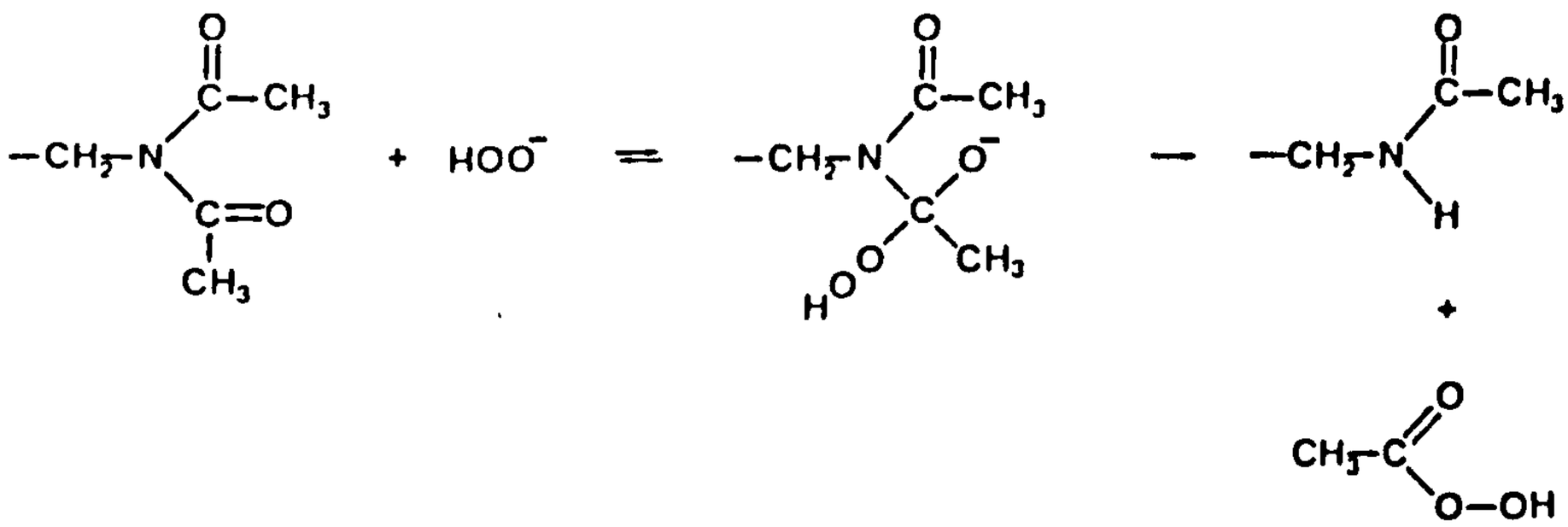

No external general acid and general base catalysis, by components of the carbonate buffer, was observed for this reaction. From studies conducted in Chapter 5 it was found that the ratio of second order rate constants for the reaction of HOO^- with TAED and TriAED was 2.88; almost identical to the ratio observed for the hydrolysis reaction (2.80). The reasons for these ratios, compared to the expected ratio of 2.0 on statistical grounds, has been discussed in Chapter 5, however, the implication is that the reaction mechanisms for the hydrolysis and perhydrolysis reactions are similar. On the other hand, the third order reaction of glycine and n-butylamine with TAED and TriAED gives a ratio of ~ 2.0 (results not shown), since it is the catalysis by a further molecule of free base which is the rate determining step, not nucleophilic attack of the amine. The observed ratio of 2.88 for hyd-

rogen peroxide has been shown to be unaffected by a change in pH, over the pH range used.

From the thermochemical data of Evans and Uri[130] the enthalpy and entropy of dissociation of hydrogen peroxide was calculated (Section 7.1). These values were ΔH^{o} = 34.3 k J mol^{-1} and ΔS^{o} = -108.0 J mol^{-1} K^{-1}. Using the data of Evans and Uri[130] and the results of a temperature dependence study for the reaction of HOO^{-} with TriAED (Section 7.1.3), it was possible to calculate the entropy and enthalpy of activation for the reaction. ($\Delta H^{\ddagger}$ = 36.448 $\pm$ 8.630 kJ mol^{-1}, $\Delta S^{\ddagger}$ = -81.660 $\pm$ 28.25 J mol^{-1} K^{-1}, with pKa = 11.6). In terms of free energy diagrams, the enthalpy of activation is a measure of the energy barrier which must be overcome by reacting molecules, whereas the entropy of activation is a measure of how many of these molecules that have this much energy can react.[8] The entropy of activation includes many factors which are often difficult to elucidate. Such factors include[8] steric orientation requirements (other reacting molecules must be in the correct orientation to react), the entropy of dilution, concentration effects and, very importantly, solvation effects. We have already seen the effects of solvation in the dissociation of hydrogen peroxide which resulted in a large negative entropy. Solvation effects have been discussed in Chapter 1 and should not be underestimated; they can manifest in (a) solvation of the reactant ions or molecules[58] and/or (b) solvation of the activated complex.[42] As we have discussed in Chapter 1, solvation effects are probably responsible for the downward curvature in Brønsted-type plots for the nucleophilicity of a series of oxygen nucleophiles with PNPA.[57] This is because the basic oxygen nucleophiles must become partially desolvated in the early stage of the reaction[57] and the desolvation requirements are reflected in the free energy changes in the formation of the transition state.

Consequently, for the above reasons, quantitative interpretation of $\Delta H^{\ddagger}$ and especially $\Delta S^{\ddagger}$ is unreliable. $\Delta S^{\ddagger}$ is, however, still a useful tool, such as in the distinction between monomolecular and bimolecular (or polymolecular) reactions when such distinctions cannot be directly made from kinetic studies. We have compiled a table of thermochemical data for the reaction of various nucleophiles with esters and amides (Table 7.11). Unfortunately, only a limited amount of thermochemical data for amides could be found, in addition to our own, however, there is a good range of data for esters. A survey of Table 7.11 will reveal that the values of $\Delta H^{\ddagger}$ and $\Delta S^{\ddagger}$ obtained for the reactions of HOO^- with TriAED are similar to those for the reactions of a series of peroxides with PNPA.[62] Indeed, for the general type of reaction involving nucleophilic attack by a neutral or anionic nucleophile at the carbonyl carbon of an amide or ester, our values of $\Delta H^{\ddagger}$ and $\Delta S^{\ddagger}$ are in the typical range observed. Beacause of the points raised in the above discussion, we will not attempt to interpret these data further.

Finally, concerning the temperature dependence study of the reaction of hydrogen peroxide with TriAED, it is useful from the commercial point of view of bleach activation to show the temperature dependence data uncorrected for the temperature dependence changes in buffer pH and hydrogen peroxide dissociation constant; this is shown in Figure 7.23. The plot is linear, indicating that the non-linear dependence on temperature of the carbonate buffer solution (Fig. 7.23) does not have a greatly significant effect on this relationship. Obviously, in terms of the bleaching of fabric stains at low temperatures, the temperature dependence of the bleach activation reaction is only one of the factors involved; the temperature dependence of the actual bleaching reactions must also be considered, as must the dissolution and local concentration effects of TAED and hydrogen peroxide in the wash liquor.

Table 7.11 Comparison of activation parameters for the reactions of various nucleophiles with esters and amides.

Substrate	Nucleophile	$\Delta H^{\ddagger}$ /KJ mol^{-1}	$\Delta S^{\ddagger}$ /J $mol^{-1}{}^{\circ}C^{-1}$	Ref
p-nitrophenylacetate	HOO^-	20.92	-117.2	62
	CH_3OO^-	35.56	-83.68	62
	$(CH_3)_3COO^-$	25.10	-129.70	62
	m-chloroperbenzoic acid	37.66	-71.13	62
	HO^-	33.47	-108.8	62
	$CH_3PO_3^{2-}$	78.24	-54.4	150
	CH_3CO^-	65.67	-119.2	150
	Imidazole	36.40	-125.5	150
	$N(CH_3)_3$	51.46	-88.28	150
	Ethylamine	34.3	-104.6	41
	Morpholine	44.8	-96.2	41
	Piperidine	31.0	-108.8	41
p-Nitrophenyl-3-bromopropionate	HO^-	46.86	-69.45	150
	$CH_3PO_3^{2-}$	78.66	-59.41	150
Phenylacetate	Ethylamine	36.0	-142.2	41
	Morpholine	59.8	-104.6	41
	Piperidine	38.1	-138.1	41
2,4-Dinitrophenylacetate	Ethylamine	31.8	-100.4	41
	Morpholine	38.1	-79.5	41
	Piperidine	29.7	-92.0	41
4-Nitrophenyl-cyanoacetate	H_2O	55.0	-130	134
Ethyl 4-nitrophenyl-malonate	H_2O	115.0	+79	134
Phenylthiolacetate	Piperidine	31.8	-111.7	136
	Piperazine	36.4	-113.0	136
	1-formyl-piperazine	38.5	-142	136
p-Nitrophenylthiol-acetate	Piperidine	41	-63.6	136
	1-formyl-piperazine	38.1	-111.3	136

Table 7.11 continued.

Substrate	Nucleophile	$\Delta H^{\ddagger}$ /KJ mol^{-1}	$\Delta S^{\ddagger}$ /J $mol^{-1}{}^{\circ}C^{-1}$	Ref
Bis(2,4-dinitrophenyl)-oxalate	H_2O	22.0	-242	135
Triacetylethylenediamine	HOO^-	36.0	-82.31	*
n-Methyldiacetamide	HO^-	46.37	-135.66	35**
Maleimide	HO^-	17.20	-151.0	37
N-Methylmaleimide	HO^-	21.02	-142.4	37
N-Ethylmaleimide	HO^-	24.85	-131.8	37
Hydroxymethylmaleimide	HO^-	13.37	-161.8	37

*This work

**Calculated from the data in reference 35.

Figure 7.23 Plot of $\ln(k_2obs/T)$ against 1/T for the reaction between hydrogen peroxide and triacetylethylenediamine, where k_2obs is the observed second order rate constant for the reaction, and T is the temperature (K). Reactions were carried out in carbonate buffer (I = 0.1M). The line represents the best fit using the linear least squares method.

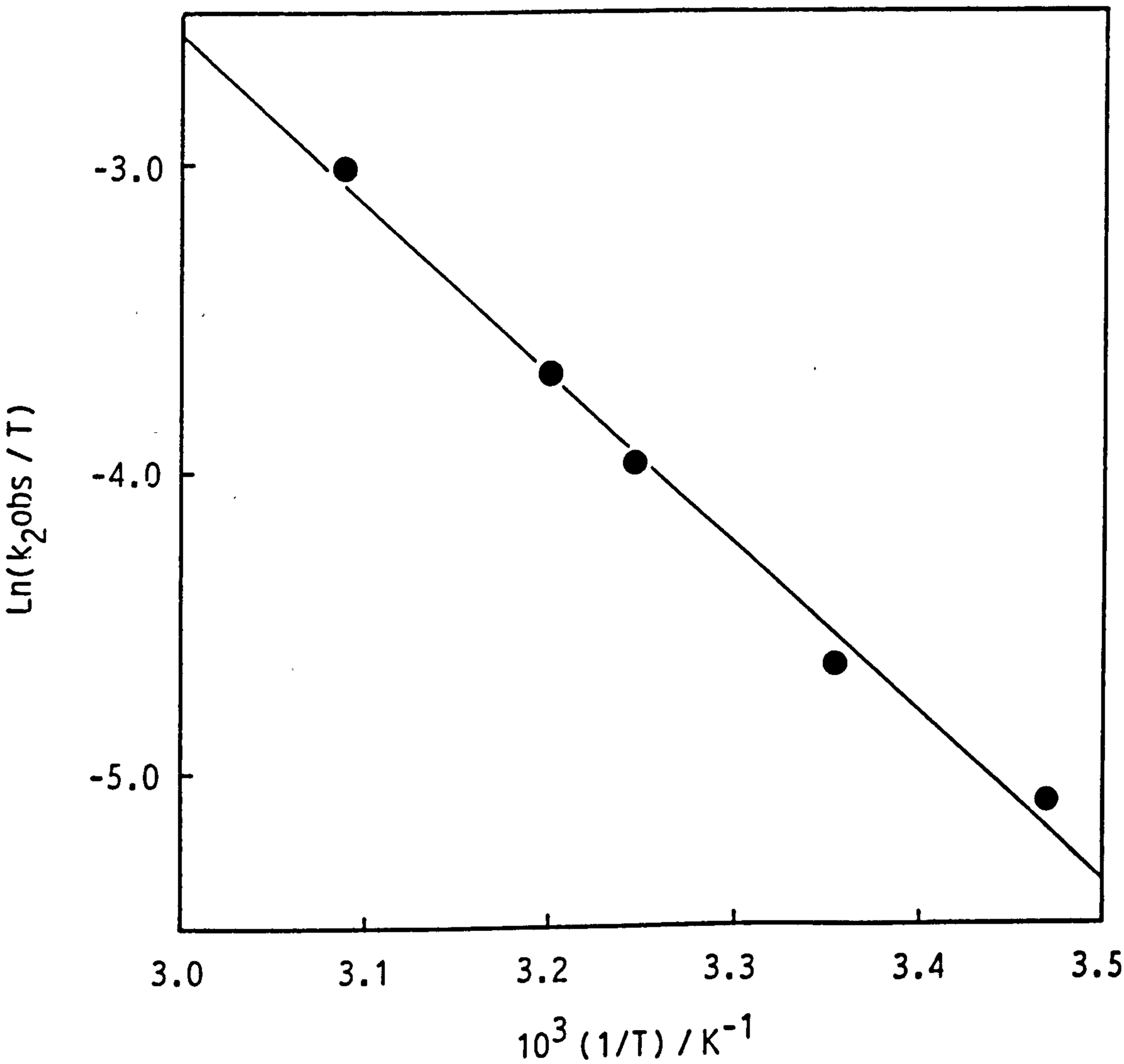

7.4.2 Reaction of Caro's Acid with TriAED

A rate constant was successfully determined for this reaction and, as far as we are aware, it is the first reported value for the reaction between a peroxyacid and an amide. The Caroate anion is likely to react with TAED and TriAED, according to Scheme 7.3.

Scheme 7.3

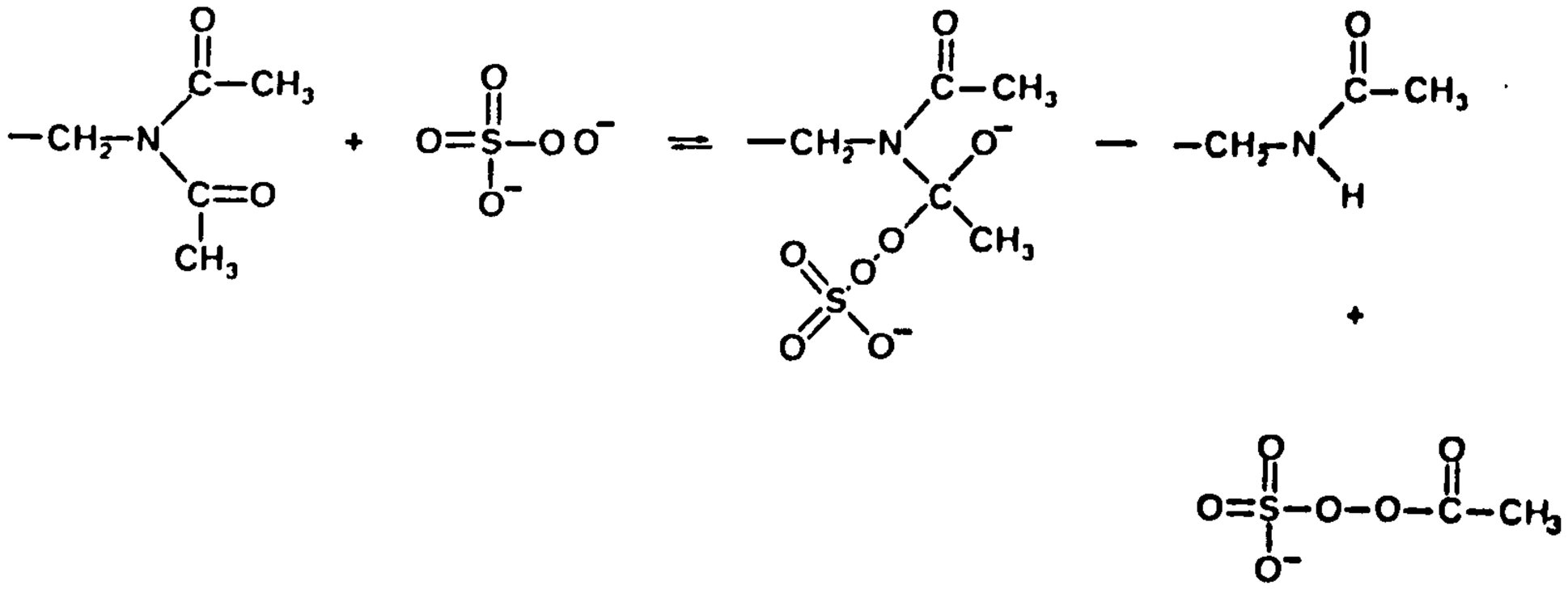

Subsequent hydrolysis of the anhydride of persulphate and acetic acid is likely. The fact that a rate constant for this reaction was obtained tends to indicate that other peroxyacids, such as peracetic acid, will also react with TAED and TriAED. We must assume, then, that, in the case of peracetic acid because of the problems encountered with hydrogen peroxide evolution during the reaction, due to peracetic acid hydrolysis, and the lower nucleophilicity of peracetic acid (pKa = 8.2), the reaction was masked. Even in the reaction with the caroate anion, TriAED hydrolysis contributed the major component of the pseudo first order rate constants.

7.4.3 Reaction of Methyl Hydroperoxide with TriAED

The standard method of Reiche and Hitz[131] for methyl hydroperoxide formation requires that, after addition of hydrogen peroxide, dimethyl sulphate and KOH, the reaction mixture is acidified and then distilled. This is followed by extraction into ether and, after drying, fractionation of the raw product to obtain the pure methyl hydroperoxide. Behr-

man et al.[133] modified this procedure by omitting the ether extraction and subsequent procedures, since the methyl hydroperoxide was to be used in aqueous solution. They obtained a small volume (20 ml) of 3.3 M methyl hydroperoxide. We have found that the potentially hazardous distillation of the acidified reaction mix is not necessary since if the reaction mix (*un*acidified) is left for several days, the hydrogen peroxide concentration falls to below detectable limits, whilst the methyl hydroperoxide concentration suffers only limited decomposition (Table 7.8). The only drawback to this modification of the original method is that it takes several days for the hydrogen peroxide to fall to below detectable limits. For the reactions of methyl hydroperoxide with TriAED, the methyl hydroperoxide was in at least 2700-fold excess over hydrogen peroxide. Quite a high concentration of methanol was also present during the kinetic runs, however, from a knowledge of the rate constants for the reaction of methanol with TriAED (Section 6.3), it was calculated that the contribution to the pseudo first order rate constants from methanolysis would be less than 0.5%. It is assumed, according to precedent[62,133] that it is the methyl hydroperoxy anion which is the reactive species. The reaction with TriAED most likely proceeds according to Scheme 7.4.

Scheme 7.4

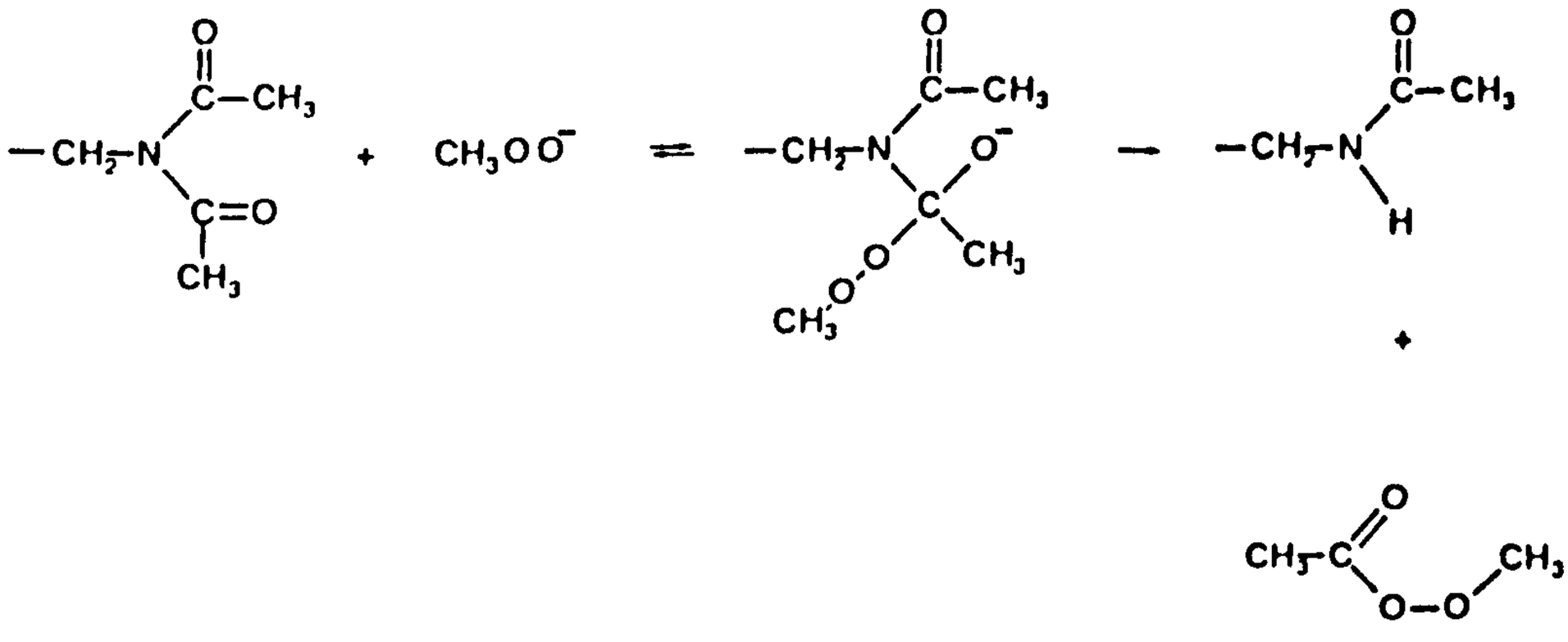

The perester will subsequently undergo hydrolysis. Our value for the rate constant for the reaction between methyl hydroperoxide and TriAED is, again, as far as we are aware, the first reported value for the reaction of methyl hydroperoxide with an amide.

7.4.4 Linear Free Energy Relationships

The Brønsted-type relationship shown for the reaction of the series of peroxides with TriAED is discussed in Chapter 10, together with the results from the study of reactions of a series of amines and alcohols with TriAED, as detailed in the previous chapter.

CHAPTER 8 DISCUSSION OF MECHANISMS FOR THE REACTION OF NUCLEOPHILES WITH TAED AND TriAED

The study of the reaction of nucleophiles with tetraacetylethylenediamine (TAED) has been detailed in Chapters 4 to 7. Based on the results of these studies, the discussion presented in this chapter attempts to examine the likely mechanisms occurring during the reactions, and draws upon literature evidence for additional support. Our principal proposal, and one for which we have very good evidence, is the idea of a cyclic intermediate structure for the reaction of hydrogen peroxide with TAED and TriAED. This cyclic structure involves the peroxide anion acting as both a nucleophile and a general acid catalyst for the reaction. Although similar speculative mechanisms for both esters[77,78] and amides[35] can be found in the literature, the results that we have obtained from our studies appear to be firm evidence for such a mechanism. Our proposed mechanism and its implications are also discussed with respect to the reaction of TAED and TriAED with the other nucleophiles that we have studied.

8.1 Concerted or Stepwise?

A review of current thinking on the timing of the bond formation and bond cleavage process during acyl transfer reaction is contained in Chapter 1. Briefly, it can be recalled that for the type of reactions that we have examined in these studies, the two relevant mechanisms are the concerted mechanism and the tetrahedral intermediate stepwise mechanism. For reaction types where the bond formation and bond cleavage processes occur simultaneously, then this is termed a concerted reaction; here, the lifetime of the tetrahedral intermediate is less than one molecular vibration and, consequently, can be said not to exist. The alternative reaction type is one in which bond formation between

nucleophile and carbonyl carbon is completed before the bond between the carbonyl carbon and leaving group begin to cleave; here, the lifetime of the tetrahedral intermediate is greater than one molecular vibration and, thus, it *can* be said to exist, although this existence is generally fleeting. Our studies have not enabled us to say which of these two reaction types apply to the reactions of the various nucleophiles with TAED and TriAED that we have examined, indeed, both reaction types may apply, depending on the nucleophile. Only for the reaction of TriAED with the hydroxide ion does any evidence exist, and this supports a stepwise process for this particular nucleophile; with increasing carbonate buffer concentration the rate increase for the hydrolysis reaction, due to buffer catalysis, was observed to level off. Such levelling off has also been observed[35] for the hydrolysis of the structurally-similar imide, N-methyl diacetamide. Khan[14] has interpreted such behaviour as a change in rate determining step, which in turn implies the formation of an intermediate along the reaction coordinate.

For the reaction of alcoholate anions, and peroxide anions with TAED and TriAED, literature evidence suggests that the reaction type is likely to be stepwise since concerted reaction types have only been proposed for circumstances where the nucleophile and substrate are structurally similar (phenolate ions with substituted phenyl esters[45,46] and amines with the imidazolium ion[15]). The reaction of amines with TAED and TriAED could conceivably occur via a concerted process.

8.2 Linear Free Energy Relationships

Table 8.1 summarises the second order rate constants obtained by us for the reaction of a range of nucleophiles with TriAED. Figure 8.1 shows these rate data expressed in the form of a Brønsted-type plot. The β_{nuc}

Table 8.1 A summary of second order rate constants (k_2) for the reaction of various nucleophiles with TriAED (I = 1.0 M, potassium salts used, 25°C)

Nucleophile	pKa	k_2 / $M^{-1}s^{-1}$	Log k_2 / $M^{-1}s^{-1}$
Glycine	9.803	3.439×10^{-3}	-2.464
n-Butylamine	11.098	3.289×10^{-2}	-1.483
Anion of			
Trifluoroethanol	12.37	0.5187	-0.285
Methanol	15.50	61.22	1.787
Hydrogen peroxide	11.60	143.41	2.157
Methyl hydroperoxide	11.50	5.910	0.772
Caros acid	9.3	4.652×10^{-2}	-1.332
Peracetic acid	8.2	1.8×10^{-2} [a,b]	-1.745
Water	15.75	1.017 [c]	0.0072

[a] Upper limit.

[b] I = 0.1 M, sodium salts used.

[c] From Chapter 4.

Figure 8.1 Bronsted-type plot for second order rate constants for the reaction of a range of nucleophiles with triacetylethylene-diamine in aqueous solution at 25°C. The points represent peroxides,■; primary amines,●; alcohols,▲; the hydroxide ion,▼. The abbreviations refer to glycine, Gly; n-butylamine, n-But; the Caroate anion, Car; peracetic acid, PA.

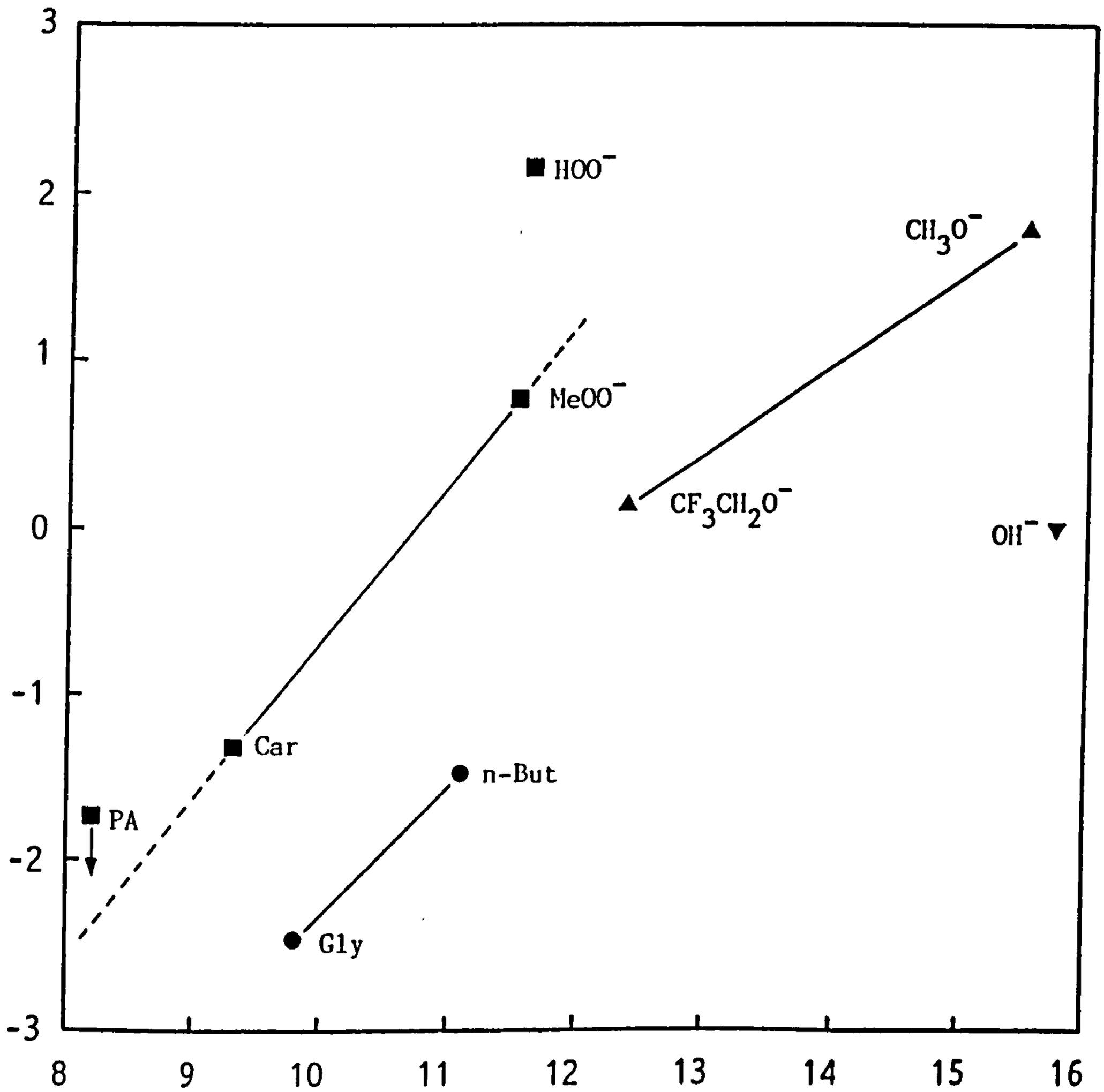

values obtained for the nucleophile series, each, unfortunately, based only on two points, are 0.66, 0.76, and 0.96 for the alcohols, amines, and peroxides (excluding hydrogen peroxide and peracetic acid), respectively. For the peroxides, a line with a slope of 0.96 is drawn connecting the points for Caro's acid and methyl hydroperoxide. We justify drawing the line between these two peroxides, rather than the other peroxides, for two reasons. Firstly, as is evident from Figure 8.2, in a study of the reaction of a series of peroxides (including peracetic acid[60,61]) with PNPA[41,62,64], the points for the peroxy acids showed a much better correlation with the point for methyl hydroperoxide[41], as compared to the correlation with the point for hydrogen peroxide[41]; there is quite a large positive deviation of the point for hydrogen peroxide from the Brønsted slope corresponding to the peroxy acids. The second reason is that, on the basis of the ßnuc values obtined for the alcoholysis and aminolysis experiments, a ßnuc value of 0.96 for a series of peroxides would not be unexpected. Obviously, in order to confirm this slope, it would be necessary to obtain further values for rates of reaction of peroxides with TriAED. The point for peracetic acid in Figure 8.1 is an upper limit value.

The ßnuc values obtained for the reaction of alcohols, amines, and peroxides with TriAED indicate the likelihood that the reactivity of TriAED towards nucleophiles is within the 'normal' range expected for these types of reactions (0.3 to 1.0). Thus, the enhanced reactivity of HOO^- towards TriAED compared to peracetic acid cannot be explained in terms of abnormal reactivity of TriAED. The Brønsted-type plot for the peroxide series clearly shows that when the pKa of hydrogen peroxide is statistically corrected (to 11.9), the point still clearly lies well above the extrapolated Brønsted slope. The subject of enhanced reactivity of HOO^- will be dealt with shortly. The second point

Figure 8.2 Bronsted-type plot for second order rate constants for the reaction of a range of substituted peroxybenzoic acids and other peroxides with p-nitrophenylacetate in aqueous solution at 25°C. The points represent p-NO_2-PBA,▽; m-NO_2-PBA,●; m-Cl-PBA,□; p-SO_3-PBA,▼; p-Cl-PBA,○; PBA,■; p-MeO-PBA,△; peracetic acid,▲; methyl hydroperoxide,◇; hydrogen peroxide,◆. The line represents the best fit using the linear least squares method for the peroxyacid points.

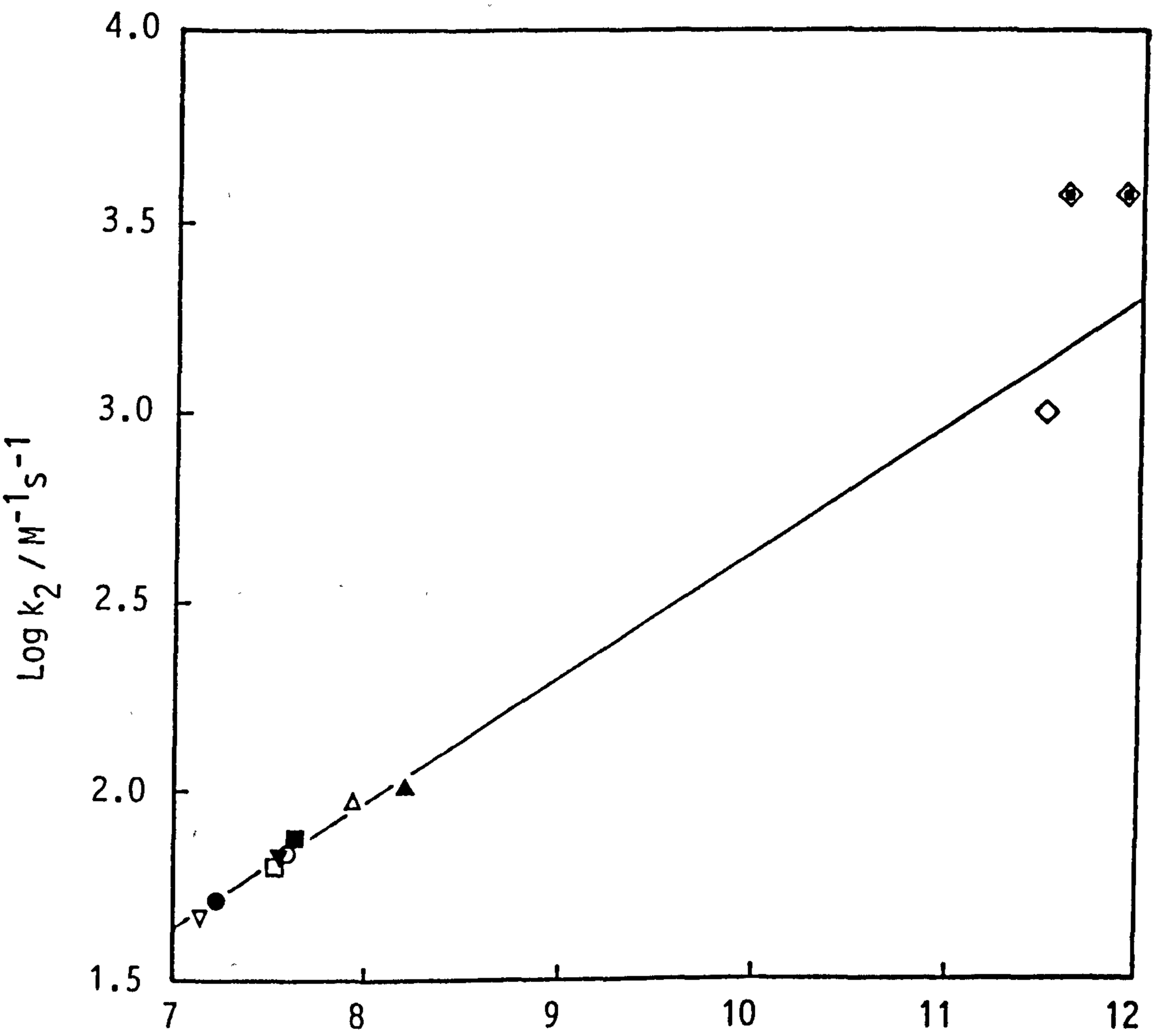

arising from the values obtained for ßnuc, for each of the nucleophile series, is that they are consistent with either a concerted mechanism, or a stepwise mechanism in which rate determining breakdown of the tetrahedral intermediate is the kinetically significant step. A leaving group pKa of 15.7 was calculated by us for TriAED (for details see Section 8.3), and so it is likely[9,10] that for nucleophiles with pKa's less than this, the breakdown of the tetrahedral intermediate is indeed rate determining. It is interesting to contrast this result with that obtained for a series of peroxy acids with PNPA[42] (Figure 8.2), where a ßnuc value of 0.3 was obtained. In this case, of course, the pKa of the PNPA leaving group (7.14 for PNP) is below the pKa of the peroxide nucleophile and a low ßnuc value is to be expected since formation of the tetrahedral intermediate is likely to be rate determining.

The relative position of the three series of nucleophiles on the Brønsted-type plot in Figure 8.1 is similar to that observed for the same series with PNPA (Figure 1.12); the peroxides as 'α nucleophiles' form the most reactive series; the value for HO^- (Chapter 4), as with PNPA, falls well below even the slope for the alcohols and must be considered as belonging to a separate series.

8.3 General Acid-base Catalysis: the Occurrence of Cyclic Intermediates

The conditions under which general acid-base catalysis should and should not be expected to occur has been discussed in Section 1.6 For the reaction of nucleophiles with esters, general acid catalysis is effected[9,10] by protonation of the carbonyl oxygen, thus 'trapping' the intermediate (if an intermediate exists) with respect to the back reaction to reactants (k_{-1}). Where an attacking nucleophile contains a proton which becomes acidic when the addition compound is formed, then

general base catalysis may occur via deprotonation of the nucleophile, again, 'trapping' the intermediate with respect to k-1. In the case of reactions involving carbonyl compounds in which the leaving ability of the leaving group is poor, as with TriAED, then there is a requirement for the leaving group to be protonated, making it a much better leaving group. Thus, in common with other amides[16], the reaction of TriAED with nucleophiles should be dominated by the requirement for protonation of the leaving group in order to avoid the unstable RN^- ion. General acid catalysis, in this case, therefore, unlike the esters, would be expected to be effected by protonation of the amide nitrogen rather than the protonation of the carbonyl oxygen.[16]

Where the conditions for the occurrence of general acid-base catalysis are met, as described in Section 1.6, then buffer components may act as general acids and general bases. (Some buffer components containing both acidic and basic groups act as both general acids and general bases in a concerted bifunctional mechanism.[85,87,120,121]) We propose, however, that for the reaction of hydrogen peroxide with TriAED, in which HOO^- displays greatly enhanced reactivity over other peroxides, that, as well as acting as a nucleophile, the peroxide ion also acts as a general acid catalyst, protonating the amide nitrogen [81]. Protonation of the amide nitrogen, as opposed to the carbonyl oxygen, is the most likely mechanism for general acid catalysis, in this case, for the reasons given previously.

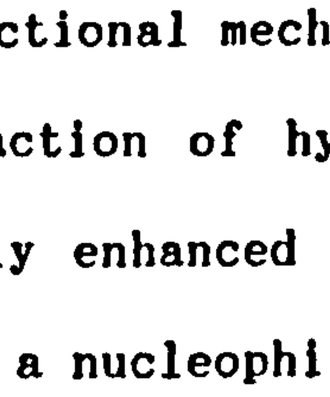

[81]

Such a mechanism applies whether the peroxide ion reacts via a concerted one-encounter process, or whether the protonation of the amide nitrogen occurs subsequent to the addition at the carbonyl carbon. Alternatively, the proton transfer could conceivably occur via solvent molecules in a proton switch mechanism.[10]

The above mechanism, [81], would explain the enhanced reactivity of HOO^- compared to the other peroxide anions studied since methyl hydroperoxide, peracetic acid, and the caroate ion do not contain a proton which becomes acidic during the addition reaction. The most significant evidence for this mechanism is the large rate enhancement observed for HOO^- compared to CH_3OO^- in which the relatively small methyl group has been substituted for a proton. HOO^- reacts 25 times faster than CH_3OO^-, yet the difference in pKa values is only 0.1 (0.4 if the pka of H_2O_2 is statistically corrected).

Table 8.2, compiled from the literature, contains a list of substrates for which the rate constants for the reaction with both HOO^- and CH_3OO^- have been determined. In all cases there is a rate enhancement for k_{HOO^-} compared to $k_{CH_3OO^-}$, however, the difference is clearly most significant for TriAED and also p-nitrophenylmethylphosphonicacid (PNPMP) [82].

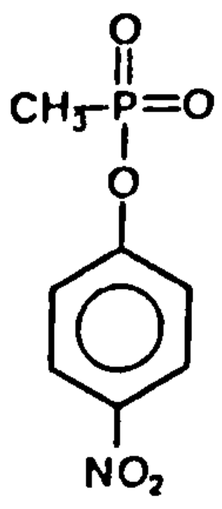

[82]

Jencks[41,137] has referred to rate difference of the reactions of HOO^- and CH_3OO^- with esters (PNPA, DNPA, AMPP, and PA) and has concluded

Table 8.2 Comparison of the reactivities of the anions of hydrogen peroxide and methyl hydroperoxide towards triacetyethylenediamine (TriAED), phenylacetate (PA), p-nitrophenylacetate (PNPA), 2,4-dinitrophenylacetate (DNPA), 1-acetoxy-4-methoxypyridinium perchlorate (AMPP) and the p-nitrophenylmethylphosphate anion (PNMP) at 25°C

Substrate	pKa lg	k_{HOO^-}	k_{MeOO^-}	$Log(k_{HOO^-} / k_{MeOO^-})$
TriAED	15.74	143.41 [a]	5.910 [a]	1.385
PA	10.00	533 [b]	105 [b]	0.705
PNPA	7.14	3540 [a]	1000 [b]	0.549
DNPA	4.3	16250 [b]	6000 [b]	0.4327
AMPP	2.2	2.333×10^{6} [b]	0.667×10^{6} [b]	0.544
PNMP	-	1.550×10^{-1} [c]	3.200×10^{-3} [c]	1.685

[a] This work.

[b] Reference 41

[c] Reference 133 (rate constants determined at 30°C)

that the hydrogen atom of the hydroperoxide anion does not cause a *large* rate enhancement by hydrogen bonding to the substrate. Suggestions of rate enhancement for HOO^- due to hydrogen bonding to substrates were originally proposed[77,78] to account for the large difference in reactivities of HOO^- and HO^-, bearing in mind the much greater basicity of the latter. Although a comparison of the reactivities of HOO^- and HO^- towards substrates is invalid since the nucleophiles belong to different Brønsted series, it is still useful for the purposes of this discussion to describe these original cyclic mechanisms. Epstein et al. in 1956[77], and Larson, in 1958[78], proposed similar mechanisms for the reaction of the hydroperoxide ion with phosphate esters. Stabilization of the transition state for the reactions (Scheme 8.1) was proposed to occur via a hydrogen bonding interaction between the hydroperoxide hydrogen and either the phosphoryl oxygen[77,78] [83] or the ester oxygen[77] [84].

Scheme 8.1

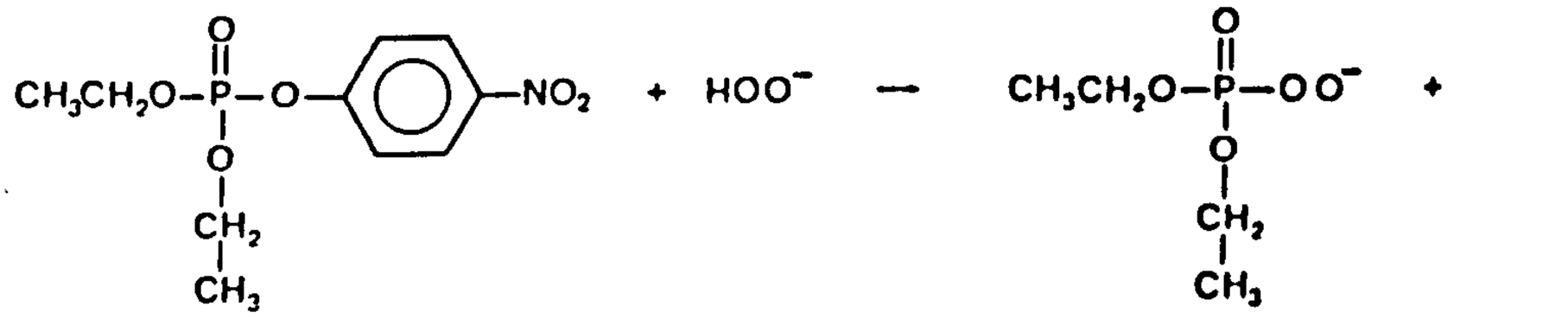

paraoxon
(0,0-diethyl-0-p-nitrophenyl phosphate)

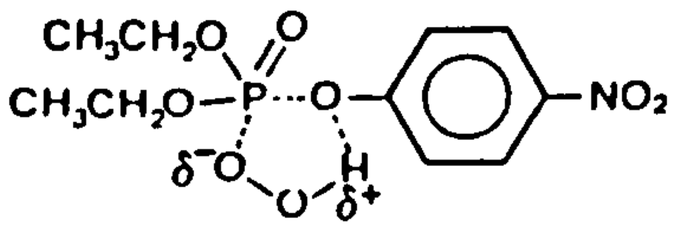

[83]

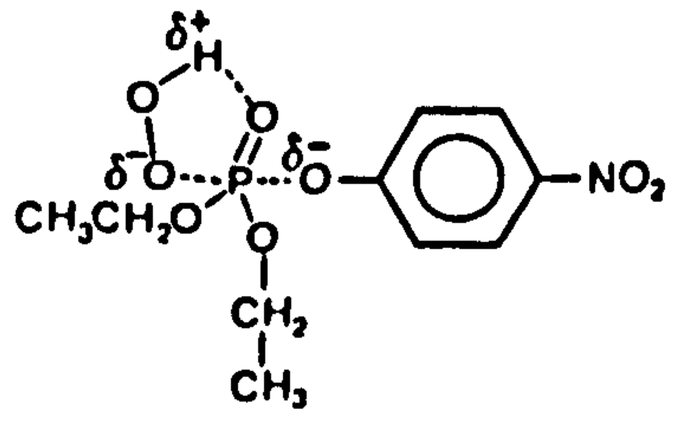

[84]

Epstein et al.[77] calculated that the interatomic distance involved would allow both the above mechanisms to be possible, however, no firm evidence for either is offered, other than the difference in reactivities of HOO^- and HO^- towards these substrates.

More recently, however, Behrman et al.[133] have investigated the reaction of a range of nucleophiles with the charged phosphate ester PNPMP [82]. Included in this study were the peroxides MCPBA, hydrogen peroxide, methyl hydroperoxide, and t-butyl hydroperoxide. It will be noted from Table 8.2 that the ratio log k_{HOO^-}/k_{MeOO^-} (1.685) is similar to the ratio that we obtained with TriAED (1.405). Behrman et al.[133] however, rather than invoking cyclic mechanisms for hydrogen bonding stabilization, ascribed this ratio to an increased dependence of reactivity on bulkiness of the nucleophile in displacements at the tetrahedral phosphorous, relative to the less crowded carbonyl carbon; the reactivities of HOO^-, CH_3COO^- and $(CH_3)COO^-$ towards PNPMP are in a ratio of 155:3:1, whereas for PNPA the ratio is 18:5:1. Nevertheless, the possibility remains of a hydrogen bonding interaction between the hydroperoxide hydrogen and either the phosphoryl oxygen, the ester oxygen or, in this case, also the anionic oxygen. It will be noted from the ratios quoted above that the ratio for the relative reactivities of CH_3OO^- and $(CH_3)_3COO^-$ is *higher* for PNPA (5:1) than it is for PNPMP (3:1). This is clearly inconsistent with the explanation of Behrman et al. which is based on increased steric effects for the reaction of nucleophiles at the tetrahedral phosphoryl phosphorous; if this were the case then one would have expected a much higher ratio for the relative reactivities of CH_3OO^- and $(CH_3)COO^-$ for the reaction with PNPMP compared to PNPA. Clearly, from these values, it is the increased reactivity of HOO^- towards the other peroxides which is the main factor, the difference between CH_3OO^- and $(CH_3)_3COO^-$ remaining relati-

vely unchanged. Finally, it must be stated, with regard to the study of Behrman et al.[133] that whilst correlations between nucleophilicity and basicity have been demonstrated for the reaction of structurally-similar nucleophile series with neutral phosphate esters (e.g. pyridines[138]), the rate constant for the reaction at MCPBA with PNPMP does not fit on a Brønsted-type plot with $MeOO^-$, unlike the case with PNPA.[64] Other factors regarding the reactivities of peroxides towards PNPMP are obviously involved.

For our own study with TriAED, we are fairly confident that the marginally increased steric effects for CH_3OO^- compared to HOO^- are not significant and do not account for the observed difference in reactivities of these compounds. This conclusion is based on the Brønsted-type relationship observed for the reaction of a series of peroxides with the ester PNPA[61,62,64] (Figure 8.2), where the steric demands of reactions at the carbonyl carbon should be similar to those for TriAED and TAED.

Further evidence supporting the proposal of the cyclic intermediate structure [81] for the reaction of hydrogen peroxide with TriAED (and also with TAED) comes from two sources, the first, from our own experimental results and, the second, from the literature.

(1) As described in Chapter 7, rate constants have been determined for the reaction of the hydroperoxide anion with TriAED, TAED, and triacetylethanolamine, which are structurally-similar imides. These data are summarised in Table 8.3. The pKa values for the imides have been calculated using Equation 8.1, and the data for σ^* presented by Perrin et al.:[139]

$$pKa = 22.0 - 3.1\ \Sigma\sigma^* \qquad \text{Eqn 8.1}$$

Equation 8.1 applies to any amide, R_1CONHR_2, for which σ^* constants of R_1CO and R_2 are known. Using the data in Table 8.3, a limited Brøns-

Table 8.3 Summary of second order rate constants (k_2) for the reaction between hydrogen peroxide and tetraacetylathylenediamine (TAED), triacetylethylenediamine (TriAED) and triacetylethanolamine (TAE) at 25°C (I = 0.1 M).

Substrate	pKa of leaving group	$k_2 / M^{-1}s^{-1}$	$\log k_2 / M^{-1}s^{-1}$
TAE	15.12	198.6	2.2980
TAED	15.24	170.0 [a]	2.2304
TriAED	15.68	117.2	2.0689

[a] this value was devided by two in order to correct for the statistical factor.

ted-type plot for leaving group basicity has been drawn for the reaction with HOO^- (Figure 8.3); this yields a value of $\beta lg = 0.398$. Whilst this value for βlg is not abnormally high or low it is inconsistent with the value of βnuc obtained (0.96) for the reactions of Caro's acid and methyl hydroperoxide with TriAED. We have already established in Chapter 1 that, on theoretical grounds, for a particular rate determining step of the reaction (where a tetrahedral intermediate mechanism exists), similar βnuc and βlg values are expected; this has been demonstrated in the literature.[17,40,53] Thus, for the reaction of peroxides with TriAED which gives a βnuc value of 0.96, then one would expect that the corresponding βlg value would correlate with this, which, clearly, the βlg value obtained for HOO^- (0.398) does not do. This supports the proposed cyclic intermediate mechanism [81] for the reaction of HOO^- with imides; the reason is that for a series of imides the same factors which affect the charge density at the carbonyl carbon, and thus the rate of reaction at the carbonyl carbon, also affect the charge density at the amide nitrogen and, thus, its requirement for protonation. If we take the example of methyl hydroperoxide, it is likely to react with TriAED, TAED, and TAE via a simple nucleophilic substitution reaction at the carbonyl carbon, in which there can be no hydrogen bonding interaction with the imide nitrogen. It is clear, therefore, that for $MeOO^-$ the only effect of electron withdrawing or donating groups (on the imide) that will influence the rate of reaction will be the charge density at the carbonyl carbon. For HOO^-, however, this is not the case, and, although electron withdrawing groups on the imide will tend to increase the rate of reaction by making the carbonyl carbon more electron deficient, this will be countered somewhat by the reduced electron density on the imide nitrogen which makes it less susceptible to protonation by the hydroperoxide hydrogen. This

Figure 8.3 Bronsted-type plot for second order rate constants for the reaction of hydrogen peroxide with a range of imides in aqueous solution at 25°C. The points represent triacetylethanolamine,O, tetraacetylethylenediamine,□, and triacetylethylenediamine,Δ. The line represents the best fit using the linear least squares method.

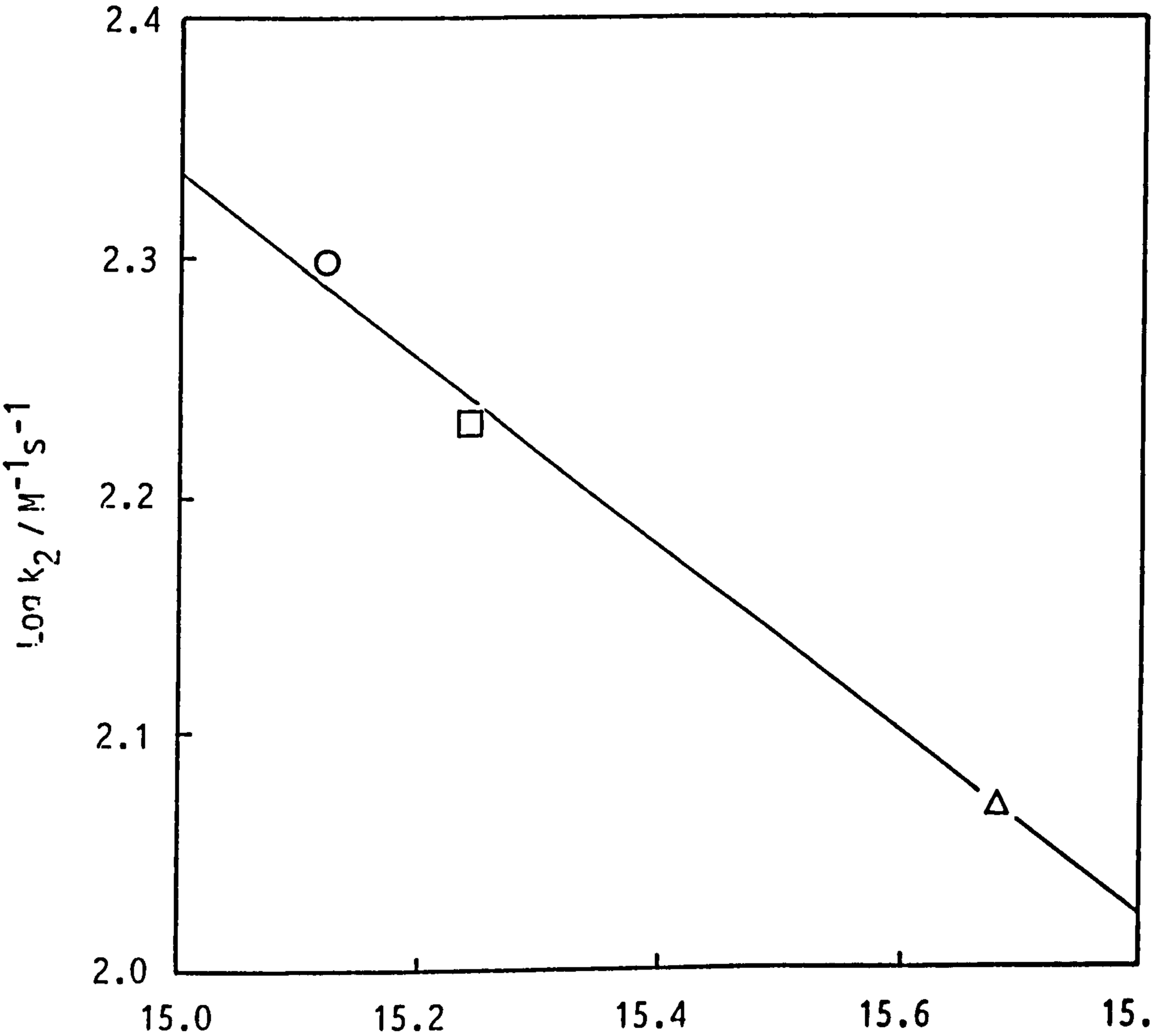

explains the low ßlg value obtained and supports the cyclic intermediate structure [81].

(2) Jencks[8,67], has suggested an analagous cyclic intermediate structure to explain the rapid o-acylation of hydroxylamine when reacting with activated acyl groups. Acylation of hydroxylamine on the oxygen rather than the generally much more reactive nitrogen atom was unexpected during the reaction with PNPA. The o-acylation reaction was much more rapid (~300-fold greater) than rates of reaction of PNPA with water, oxygen anions, and nitrogen nucleophiles of comparative basicity. The hydroxylamine, in the form of the dipole structure (Scheme 8.2).

Scheme 8.2

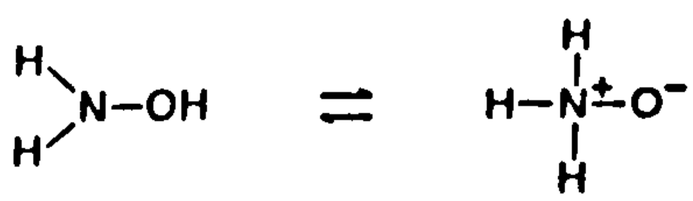

is proposed as the reactive form. This structure does not possess unusual polarisability[67], nor does it have a free electron pair adjacent to (α to) the nucleophilic oxygen. Consequently, the enhanced reactivity is ascribed to cyclic structures including hydrogen bonded interactions [85] and [86].

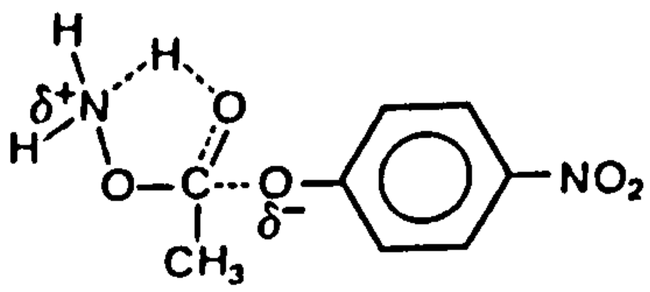

[85]

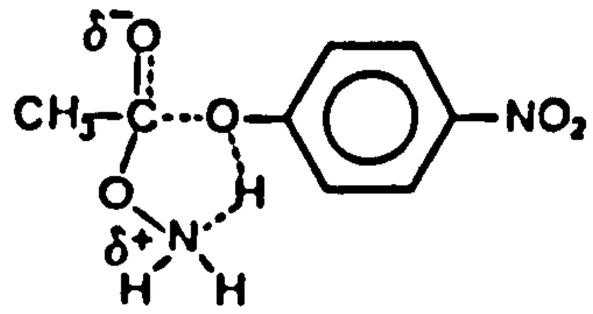

[86]

Obviously, mechanism [86] is very similar to the mechanism that we have proposed, since it involves a hydrogen bonded interaction with the leaving group. Jencks has called[8] these mechanisms internal (intramolecular) general acid-base catalysis since acylation of the oxygen is assisted by the neighbouring amine group. The subject of intramolecular general acid-base catalysis has been covered in Section 1.7.2 and has been shown to be responsible for large rate enhancements.[44] Our mechanism for the reaction of HOO^- with imides [81] should, like the mechanisms of Jencks[67], ([85] and [86]), also be regarded as an example of intramolecular general acid-base catalysis since the acyl transfer reaction is proposed to be catalysed by the hydrogen atom on the attacking nucleophile.

Finally, we can rule out the possibility that the enhanced reactivity of k_{HOO^-} over k_{MeOO^-} is due to concerted bifunctional mechanisms involving carbonate buffer components, rather than an intramolecular general acid-base catalysis mechanisms; this is because in the pH dependence study for the reaction of HOO^- with TriAED (Section 7.1) a slope of 0.985 ± 0.084 was obtained on plotting pH against log k_2 over a pH range of 9.60 to 10.47. This indicates an absence of buffer catalysis; if HCO_3^- was responsible for such large rate enhancements then changing the pH and, thus, $[HCO_3^-]$ should have resulted in a slope much less than 1.0.

8.4 Implications for Other Reactions

In this final section, the implications of our proposed mechanisms [81] for the reaction of HOO^- with TriAED are discussed regarding the reaction of other nucleophiles with TriAED. Also, some literature studies are re-examined regarding the possibility of the existence of hydrogen bonded cyclic intermediates for the reaction of hydrogen peroxide and amines with ester substrates.

8.4.1 Reaction of Amines with TriAED and Other Imides

Of the nucleophiles that we have studied, the group for which the proposed cyclic intermolecular mechanism [81] has greater relevance are the amines; in particular, the aminolysis reaction which is catalysed by a second molecule of amine. Although we have no evidence, it is possible that the amine catalysed reaction of glycine and n-butylamine with TriAED could proceed via a mechanism in which the second molecule of amine acts as a bifunctional catalyst, with catalysis effected in a concerted process.

Scheme 8.3

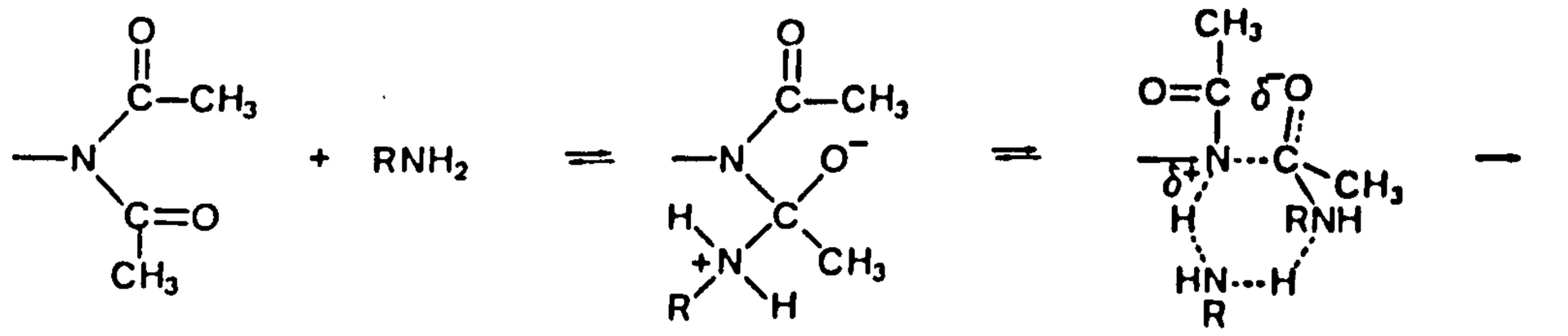

There is excellent evidence[87,120,121] for enhanced catalytic ability (over monofunctional catalysts) when catalysis is effected by a bifunctional catalyst acting via a fully concerted mechanism. (See Section 1.6.2.)

In the literature, similar cyclic structures have been proposed for ester aminolysis reactions[40,68,79,80,81,140], in which the leaving ester oxygen is protonated [87].

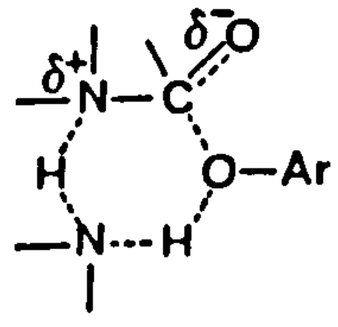

[87]

Satterthwait and Jenck[40] have, however, ruled out such structures on the grounds that tertiary amines (Quinuclidines) which have no transferable proton are more effective as general base catalysts than hydrazine, for the reaction of hydrazine with 2-chloroethylacetate and p-chlorophenylacetate.

8.4.2 Reaction of the Hydroxide Ion with TriAED

Nucleophilic attack of the hydroxide ion at the carbonyl carbon of TriAED, with intramolecular general acid-base catalysis occurring via protonation of the imide nitrogen by the hydroxide oxygen, in an analagous mechanism to the proposal for HOO^-, is possible, however, it would necessitate the formation of a four-membered ring. A more likely mechanism could involve a proton switch. A glance at the Brønsted-type plot in Figure 8.1, however, shows that the point for hydroxide ion, which is uncorrected for general acid-base catalysis by buffer components, shows no enhanced reactivity relative to the Brønsted-type slopes for amines and alcohols compared to the relationship for the ester PNPA (Figure 1.12). With a pKa of 15.75, of course, a significant proportion of the hydrolysis reaction could take place via uncatalysed nucleophilic displacement at the carbonyl carbon with rate determining formation of the tetrahedral intermediate being the kinetically significant step (if a tetrahedral intermediate exists); in such circumstances protonation of the amide leaving group to avoid the formation of the RN^- ion would not lead to any rate enhancement, since this step would occur after the kinetically significant transition state.

Nevertheless, we have demonstrated that general acid-base catalysis of alkaline hydrolysis of TriAED by buffer components does occur, and Laurent and Pellisier[35], working on the analagous N-methyldiacetamide, have also found such buffer catalysis. As discussed in Section 4.5, these authors found that in carbonate and phosphate buffers the hydrol-

ysis is likely to be catalysed only by the acid components of the buffers, HCO_3^- and $H_2PO_4^-$. It was proposed that the catalysis was effected via a concerted bifunctional mechanism with protonation of the imide nitrogen [88]. A proton switch mechanism is also suggested.

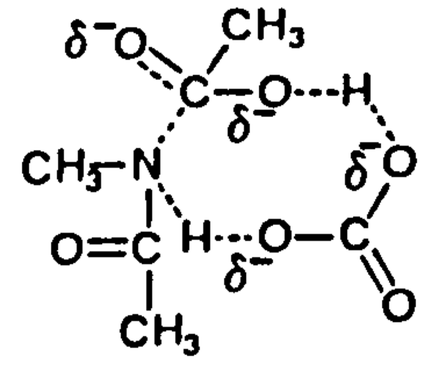

[88]

8.4.3 Reaction of HOO⁻ and MeOO⁻ with Esters

The possibility, in reactions with esters, that HOO^- may show some rate enhancement over $MeOO^-$, due to a hydrogen bonded interaction between the hydroperoxide hydrogen and either the leaving ester oxygen or the carbonyl oxygen, cannot be discounted from the literature data. Table 8.2 shows that for PA, PNPA, DNPA, and AMPP, in all cases, the value for k_{HOO^-} is significantly larger than k_{MeOO^-}, yet their basicities differ by only 0.1 of a unit (0.4 units if the pKa of H_2O_2 is statistically corrected). This is particularly noticeable for phenyl acetate which has a relatively poor leaving group. Also, note, that on Figure 8.2, a Brønsted-type plot for the reactions of a series of peroxides with PNPA, the value for HOO^- lies above the slope formed by the other peroxides (including $MeOO^-$), and this is true even if the pKa at H_2O_2 is statistically corrected. Although it has been stated[41] that the hydrogen atom of the hydroperoxide anion does not produce a *large* rate enhancement by hydrogen bonding to ester substrates, the results that we have obtained for the same reactions with amides, and the literature values for k_{HOO^-} and K_{MeOO^-} for esters, suggest that this effect may produce *some* rate enhancement.

CHAPTER 9 A STUDY OF THE BLEACH ACTIVATOR PENTAACETYL-D-GLUCOSE

Pentaacetyl-D-glucose (PAG) is a bleach activator which is used in some washing powder formulations (5.2% of 1986/87 market share[7]). The objective of the study contained in this chapter was to look at hydrolysis and perhydrolysis reactions of PAG and, in particular, to look at the mole ratio of peracetic acid release from PAG. Theoretically, there are five acetyl groups which could undergo a perhydrolysis reaction with hydrogen peroxide to yield peracetic acid, however, ratios of about 2.5 moles of peracetic acid per mole of PAG are usually obtained.[141] The methods and approach used in the study of the bleach activation reactions of PNPA and TAED were applied to this study.

PAG is an acetate derivative of D-glucose. Section 9.1 discusses the aspects of carbohydrate chemistry pertinent to this study, particularly structural considerations. The remaining sections describe the experimental study of PAG; Section 9.2 is an investigation of the time-course of peracetic acid release; and Sections 9.3 and 9.4 detail the procedure used to determine the number of acetyl groups which are available for hydrolysis and perhydrolysis reactions. Finally, Section 9.5 contains a discussion of the PAG results.

9.1 General Introduction and Structural Considerations

Penta-o-acetyl-D-glucose is an acetate derivative of D-glucose, with acetylation being effected[142] by acetic anhydride in the presence of a basic catalyst such as sodium acetate or pyridine. Acid catalysts such as zinc chloride may also be used.

Penta-o-acetyl-D-glucose (PAG) exists in the pyranose ring form but, unlike D-glucose, will not exhibit mutarotation in acid/base conditions

since it cannot form an acylated acetyldehydo-D-glucose intermediate. The two anomeric forms of PAG are shown below.

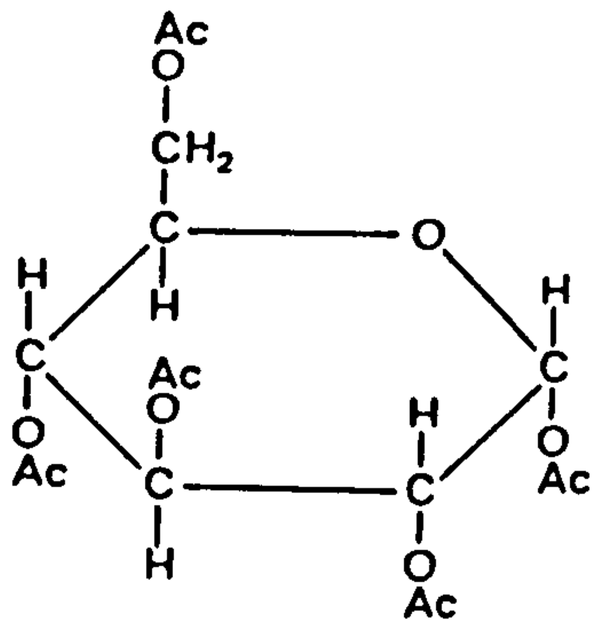

pentaacetyl-β-D-glucopyranose

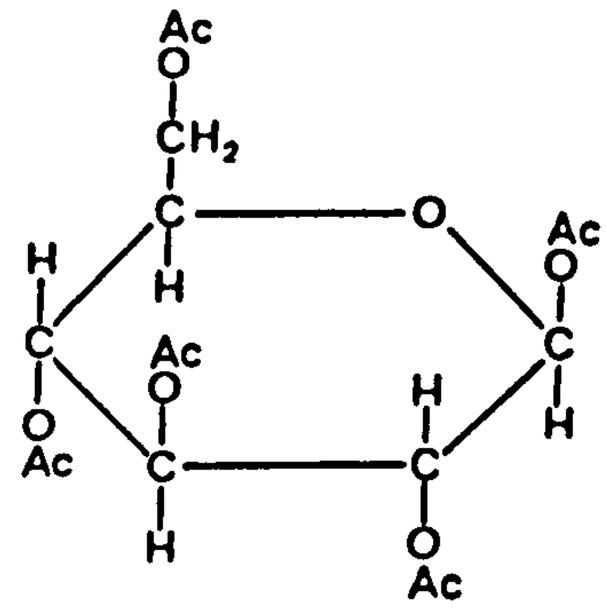

pentaacetyl-α-D-glucopyranose

Only if the acetyl group at the C_1 position is removed will the acid/-base catalysed mutarotation be possible.

If one examines the bond angle of a six-membered pyranose ring, as shown above, then it will be found that like cyclohexane derivatives it will only adopt structures which are free from angular strain if the ring is non-planar. There are three general ring structures which are free from angular strain, all of which have four of the ring atoms in one plane and the other two lying on opposite sides of the plane (chair and skew conformation) or on the same side (boat conformation).

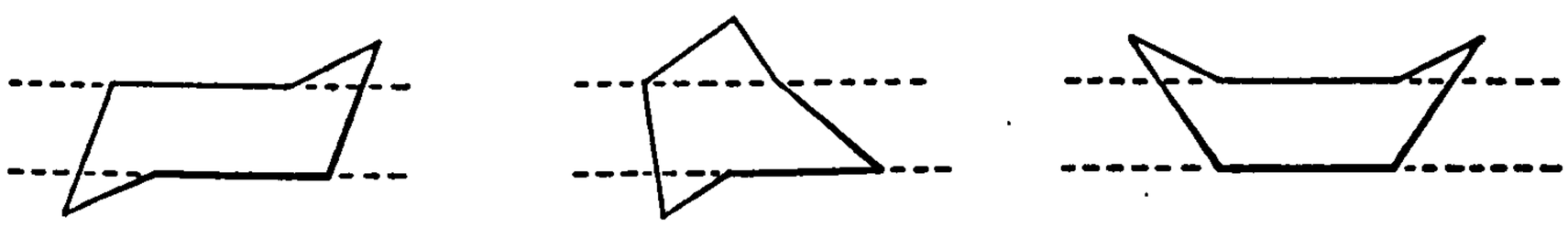

chair skew boat

Unlike the chair conformation, the boat and skew conformations are flexible and interchange freely, without introducing any angular strain (twisting and rotating conformation of bonds) in what is known as the flexible boat/skew cycle.[151] The basis of predicting the stability of various conformations comes from studies on cyclohexane derivatives.[142]

There are slight differences between cyclohexane and pyranoid geometries due to the carbon-to-oxygen bond (1.43 Å) being slightly less than the carbon-to-carbon bond (1.54 Å) and a slight difference in bond angles (~ 2°), however, for the most part, these can be ignored. It is stated in *Rodd's Chemistry of Carbon Compounds*[142], that the preferred or most populated conformation assigned to a molecule is that of lowest energy in which angular strain and non-bonded interactions between substituents are at a minimum.[142] The chair forms are the preferred conformation for D-glucose and its derivatives since the substituents attached to the ring are staggered. Boat conformations are only taken up under restraint since they represent the maximum energy state[142] due to strong repulsive interactions between substituent groups. The skew conformation has the minimum energy of the flexible form.[142] There are two possible chair conformations, as shown below.

Pentaacetyl-β-D-glucose

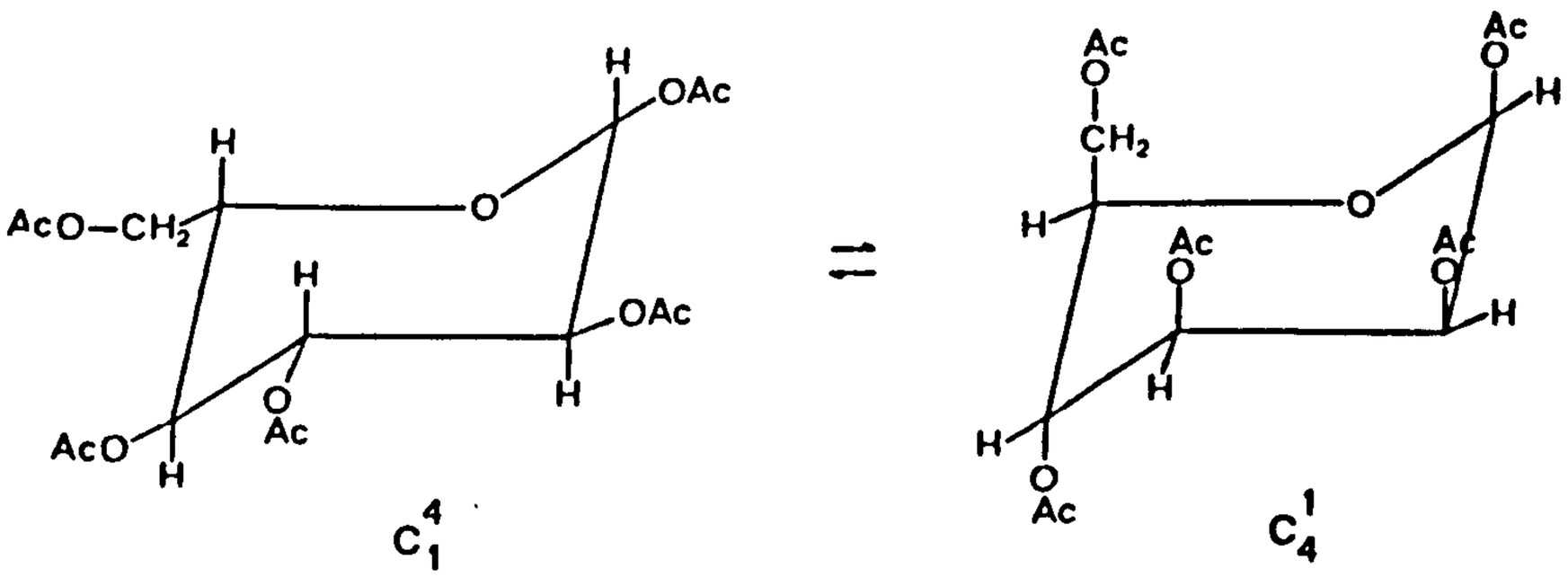

Pentaacetyl-α-D-glucose

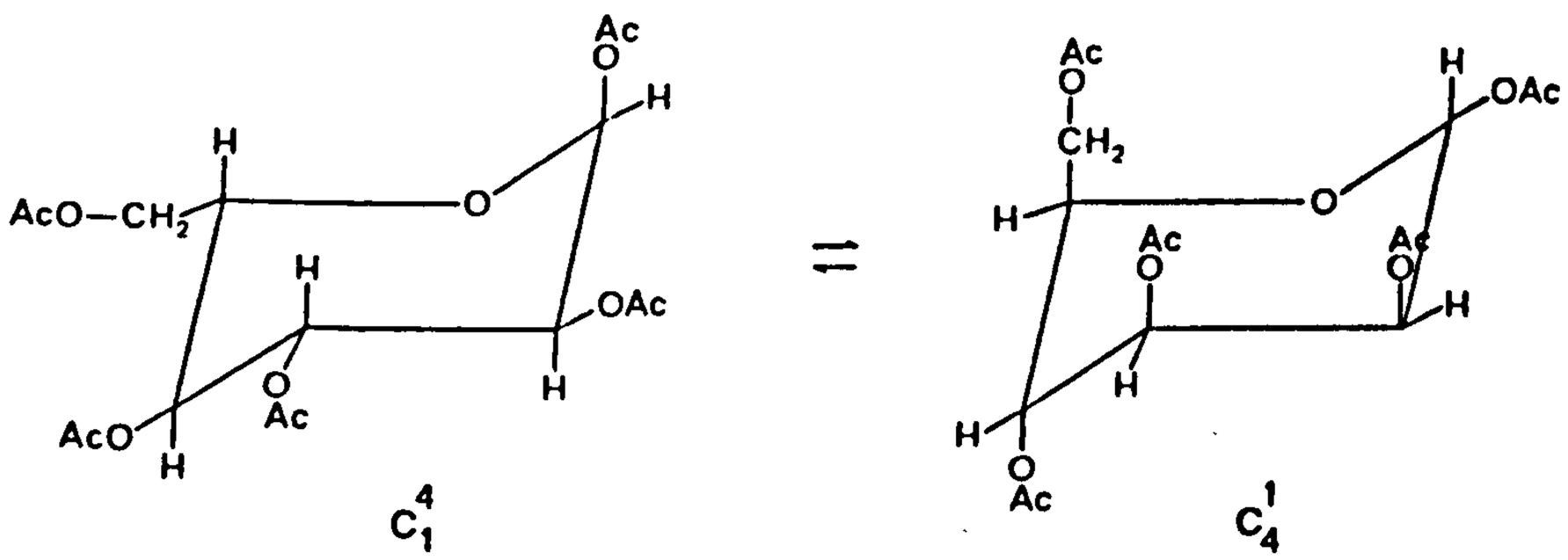

For the α and ß anomeric forms of PAG, the form where the acetyl groups are in the equitorial plane (C_1^4) is by far the most preferred since there are no 1-3 and 2-4 substituent interactions as there are with the substituents in the axial plane.[142]

9.2 Time-course of Peracetic Acid Release on Reaction of PAG with Hydrogen Peroxide

As with TAED and PNPA, the time-course of peracetic acid release was followed using the method described in Section 2.2. The procedure was conducted at two different hydrogen peroxide concentrations. CO_2-free experimental techniques were not used.

Reagents

Penta-o-acetyl-α-D-glucose, 6 x 10^{-4} M solution in distilled water. Prepared by stirring PAG (supplied by Aldrich Chemicals, 98%) in distilled water for about 3-4 hours. Sodium carbonate buffer, pH 9.45 (I = 0.2 M) containing 8.1753 gl^{-1} disodium carbonate (decahydrate) and 9.6012 gl^{-1} sodium hydrogen carbonate. The PAG and carbonate buffer solutions contained 1 x 10^{-5} M EDTMP.

Procedure

An appropriate amount of standardized hydrogen peroxide was added to the carbonate buffer to give either a 5.066 x 10^{-3} M or 8.614 x 10^{-4} M solution, 25 ml each of the hydrogen peroxide/buffer solution and the PAG solution were then mixed in a 50 ml conical flask. Initial conditions in the flask were: pH 9.45, I = 0.1 M, $[PAG]_o$ = 3 x 10^{-4} M, $[H_2O_2]_o$ = 2.533 x 10^{-3} M or 4.307 x 10^{-3} M. Peracetic acid formation and the total iodide reactable peroxide formation were followed until completion of the reaction.

Results

On plotting the time-courses of peracid release from PAG, at the two different hydrogen peroxide concentrations (Figure 9.1), the striking feature was the similarity in the pattern of peracid release for the two plots despite nearly a twofold difference in $[H_2O_2]_o$ The two runs were not conducted under pseudo first order conditions (i.e. a tenfold excess hydrogen peroxide over the concentration of the acetyl groups), since they were not initially intended to yield kinetic information. Using non-linear least squares, we have fitted tha data in Figure 9.1 to curves described by Equation 9.1 in which there are two exponential terms.

$$[PA] = [PA]_\infty + [PA]_1 e^{-k1t} + [PA]_2 e^{-k2t} \qquad \text{Eqn 9.1}$$

where

Figure 9.1 Plot showing the release of peracetic acid from the reaction of pentaacetyl-α-D-glucose with hydrogen peroxide: pH 9.45 sodium carbonate - sodium hydrogen carbonate buffer (I = 0.1M); $[H_2O_2]_o = 2.53 \times 10^{-3}$M, O, and 4.31×10^{-3}M, □; $[PAG]_o = 3 \times 10^{-4}$M; $[EDTMP] = 1 \times 10^{-5}$M; 25°C. The curves represent the best fit to Equation 9.1.

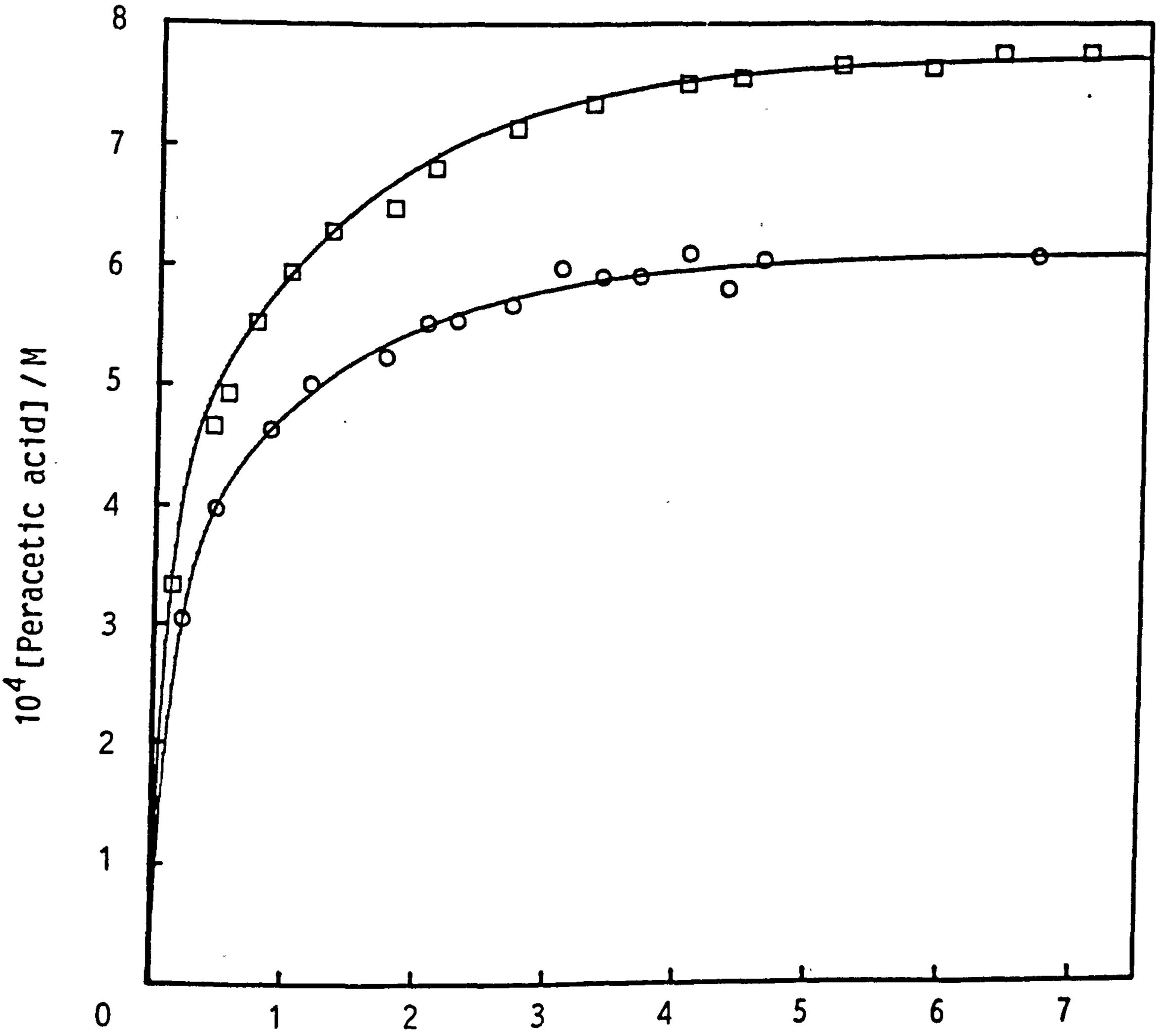

$[PA]_\infty$, $[PA]_1$ and $[PA]_2$ are constants and k_1 and k_2 are the observed first order constants. Table 9.1 lists the data for these plots. k_1, the observed first order rate constant for the initial fast phase of the reaction is clearly dependent on $[H_2O_2]_o$, however, k_2, the observed first order rate constant for the second phase appears to be independent of $[H_2O_2]_o$. Obviously, further work will have to be done to confirm this phenomenon, in particular, the runs should be repeated using a tenfold excess of hydrogen peroxide over the concentration of acetyl groups. We propose that a possible explanation for the apparent independence of the second phase on $[H_2O_2]_o$ is the presence of a rate limiting acetyl migration mechanism which occurs subsequent to the removal of the first acetyl group. This is discussed in Section 9.5

9.3 Determination of the Number of Acetyl Groups Available for Hydrolysis in PAG

Using paper chromatographic methods, Halonen et al.[143] have demonstrated that there is complete deacetylation of pentaacetyl-ß-D glucose in an acetone water (1:1) solution. Chromatograms (solvent of butyl alcohol - isopropyl alcohol - water) were prepared at various stages of deacetylation of PAG (as determined titrimetrically). Between the solvent front and glucose, a number of spots (7) were completely separated and all gave a positive reaction to the hydroxamate test of aldohexoses with diphenylamineaniline - phosphoric acid. The authors suggest that these spots corresponded to intermediate stages of deacetylation. The spots disappeared when deacetylation was carried out for a sufficient period of time.

We wished, independently, and directly, to verify the presence of D-glucose as an end product of acylated D-glucose hydrolysis, under the reaction conditions used in our experimental procedures. The simplest method by which this could be achieved appeared to be by using a gluc-

Table 9.1 Observed first order rate constants and linear constants calculated using the ELORMA program for data obtained during the reaction between hydrogen peroxide and penta-o-acetyl-α-D-glucose in a pH 9.45 sodium carbonate - sodium hydrogen carbonate buffer (I = 0.1M); $[PAG]_o = 3 \times 10^{-4}$M; $[EDTMP] = 1 \times 10^{-5}$M; 25°C.

$10^3[H_2O_2]_o$ / M	$10^4 k_1/s^{-1}$	$10^4 k_2/s^{-1}$	$10^4[PA]_1$ / M	$10^4[PA]_2$ / M	$10^4[PA]_\infty$ / M
2.538	72.38 ± 15.1	7.737 ± 1.563	-3.276	-2.806	6.082
4.310	104.30 ± 10.52	7.329 ± 0.473	-3.980	-3.741	7.723

Table 9.2 Results of glucose assays conducted after 4 and 22½ hours for various sample solutions.

Sample solution	Absorbance at 352 nm	
	4 hours	22½ hours
PAG / carbonate buffer	0.010	0.349
PAG / carbonate buffer	0.009	0.352
Carbonate buffer	0.010	0.011
PAG / distilled water	0.009	0.010

ose assay. Glucose oxidase (GOD) catalyses the oxidation of ß-D-glucose to D-gluconic acid in the following reaction

$$\text{ß-D-glucose} + O_2 + H_2O \xrightarrow{\text{GOD}} \text{D-Gluconic acid} + H_2O_2$$

The hydrogen peroxide can then be determined and thus gives a measure of the concentration of ß-D-glucose. The standard method (Sigma Chemicals) for hydrogen peroxide utilizes the following reaction

$$H_2O_2 + \underset{\text{colourless}}{\text{o-Dianisidine (reduced)}} \xrightarrow{\text{POD}} \underset{\text{red}}{\text{o-Dianisidine (oxidised)}} + O_2$$

where POD is the enzyme peroxidase. We have developed an alternative, iodimetric method, which has the advantage of increases sensitivity over the POD assay. Furthermore, the assay takes advantage of acid catalysed mutarotation of D-glucose and measures the total (α and ß) D-glucose concentrations rather then the ß - D glucose concentration alone.

9.3.1 Devlopment of an Iodimetric Method for Glucose Determination

Background to method

In the standard sigma method, the ideal assay mix for glucose determination contains both the glucose oxidase and reagents for hydrogen peroxide measurement. This is so that as soon as the hydrogen peroxide is formed it reacts with the peroxide assay, ensuring that decomposition by the small amount of catalase impurity present in the glucose oxidase is minimised. Recommended conditions for the glucose oxidase assay (Sigma Chemicals Ltd.) are pH 5.1 and 35°C, for which one unit of GOD will oxidise 1.0 mole of ß-D-glucose to D-gluconic acid per minute. We wished to determine the hydrogen peroxide iodimetrically, however, at the recommended pH of the GOD assay (5.1), the oxidation of iodide to iodine is extremely slow. We found that by using a more concentrated solution of glucose oxidase then reasonable enzyme activity can be

obtained under the conditions for iodimetric H_2O_2 determination that we have used throughout this thesis.

Materials and Methods

Reagents

0.05 M sodium acetate stock buffer solution, pH 5.1 at 35°C, prepared by adding 1.42 ml glacial acetic acid to 450 ml distilled water, adjusting to pH 5.1 at 35°C with 30% (w/v) NaOH and then diluting to 500 ml with distilled water.

0.005 M sodium acetate buffer, pH 5.1 at35°C, prepared from 0.05 M stock buffer.

Glucose oxidase solution, 0.05 g of Sigma glucose oxidase (ß-D-Glucose: oxygen 1-oxidoreductase; EC1.1.34; type II-S from *Aspergillus niger*; 25000 units g^{-1}) dissolved in 5 ml 0.005 M sodium acetate buffer solution.

Potassium hydrogen phthalate solution, 20 g l^{-1} in distilled water.

Potassium iodide solution, containing 66 g l^{-1} potassium iodide, 2 g l^{-} sodium hydroxide and 0.2 g l^{-1} ammonium heptamolybdate.

D-Glucose stock solution, 1 x 10^{-2} M in distilled water.

Assay

To a small test tube is added 1 ml hydrogen phthalate solution, 1 ml potassium iodide solution, 0.1 ml D-glucose solution (approximately 62% and 38% of the ß and α anomers, respectively, at equilibrium)[144] and 0.1 ml of the glucose oxidase solution. The tube is sealed using parafilm and incubated at 35°C in the dark for 2 hours, at which time it had been previously determined that the maximum colour development is attained. After cooling to 25°C the contents of the test tube are transferred by pasteur pipette to a silica UV optical cell and the absorbance due to triiodide formation measured at 352 nm.

Results

Using this assay, a 2-hour incubation period is required in order to reach A_∞ for triiodide. Figures 9.2 and 9.3 show the time-course of triiodide formation at 352 nm (35°C) for two different enzyme concentrations ($[glucose]_o = 8 \times 10^{-4}$ M). It becomes apparent at the highest enzyme concentration that the triiodide formation is biphasic, the second phase independent of the enzyme concentration. Also, the A_∞ value gives a hydrogen peroxide concentration exceeding the expected concentration of ß-D-glucose in the D-glucose solution, moreover, it corresponds to the total glucose concentration. This suggests that the initial phase is due to the rate limiting enzyme catalysed oxidation of ß-D-glucose to gluconic acid and hydrogen peroxide; from Figures 9.2 and 9.3, it is clear that this step is dependent on the enzyme concentration. Subsequently, the second phase, which is independent of enzyme concentration, is due to the acid-catalysed, rate-limiting mutarotation of the α to ß anomeric form to maintain the equilibrium as the ß form is oxidised. This interpretation is supported by the fact that in Figure 9.3 the end of the initial phase corresponds to about 63% of the total glucose concentration, in agreement with data for the percentage of the ß anomeric form in aqueous solution at equilibrium.[144]

9.3.2 Utilization of the Glucose Assay to Determine if Glucose is the End Product of Acetylated D-glucose Hydrolysis

Reagents

Penta-o-acetyl-α-D-glucose, 6×10^{-4} M in distilled water (supplied by Aldrich Chemicals, 99%).

Sodium carbonate buffer, pH 9.45, I = 0.2 M.

Assay reagents as described in previous section.

Procedure

The assay was calibrated by measuring the maximum absorbance values for

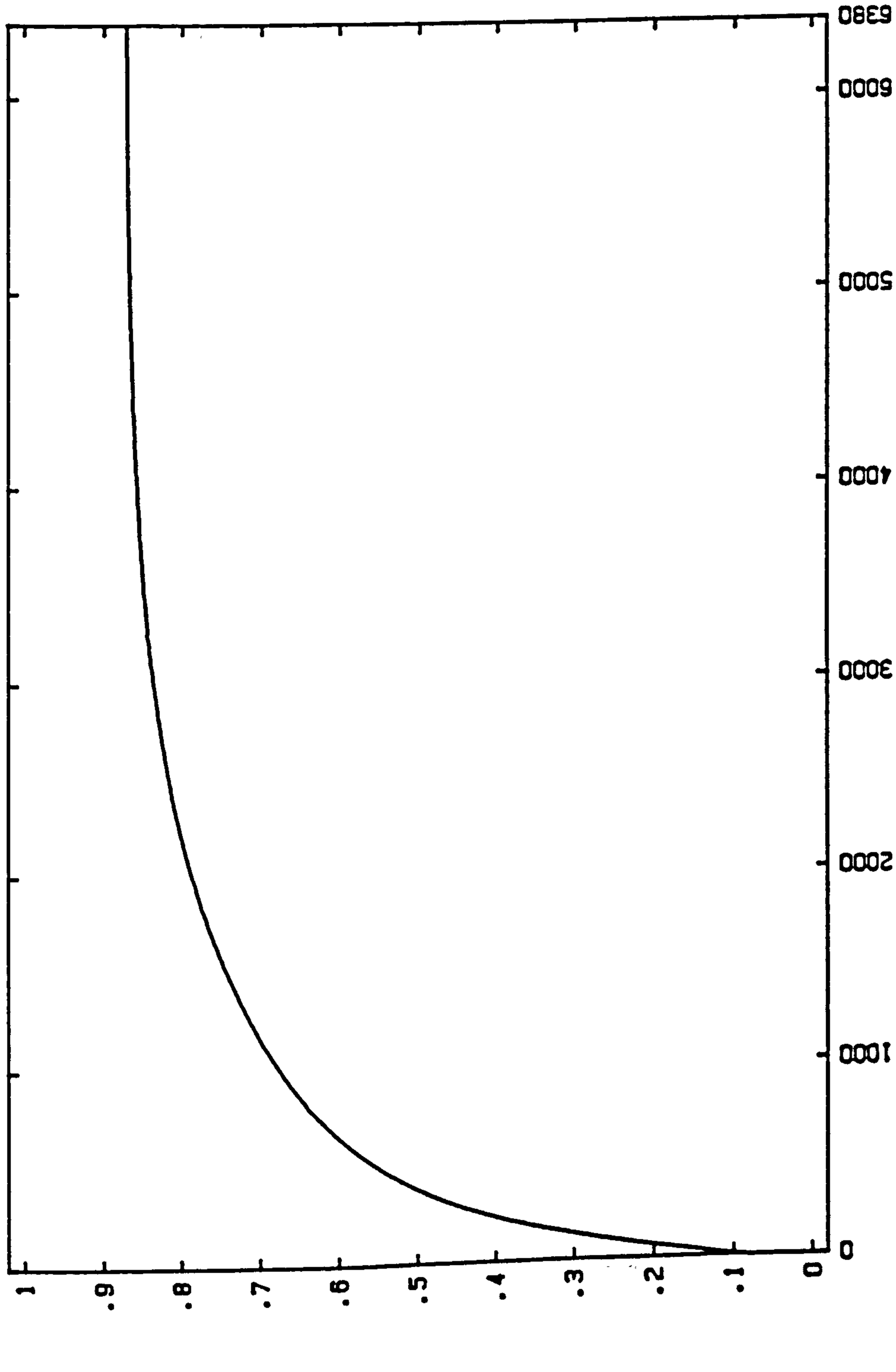

Figure 9.2 Absorbance increase at 352 nm due to triiodide formation resulting from the oxidation of iodide by hydrogen peroxide formed as a product of GOD catalysed glucose oxidation: phthalate buffer; $[D\text{-glucose}]_0 = 8 \times 10^{-4}$M; 0.05ml GOD; 25°C.

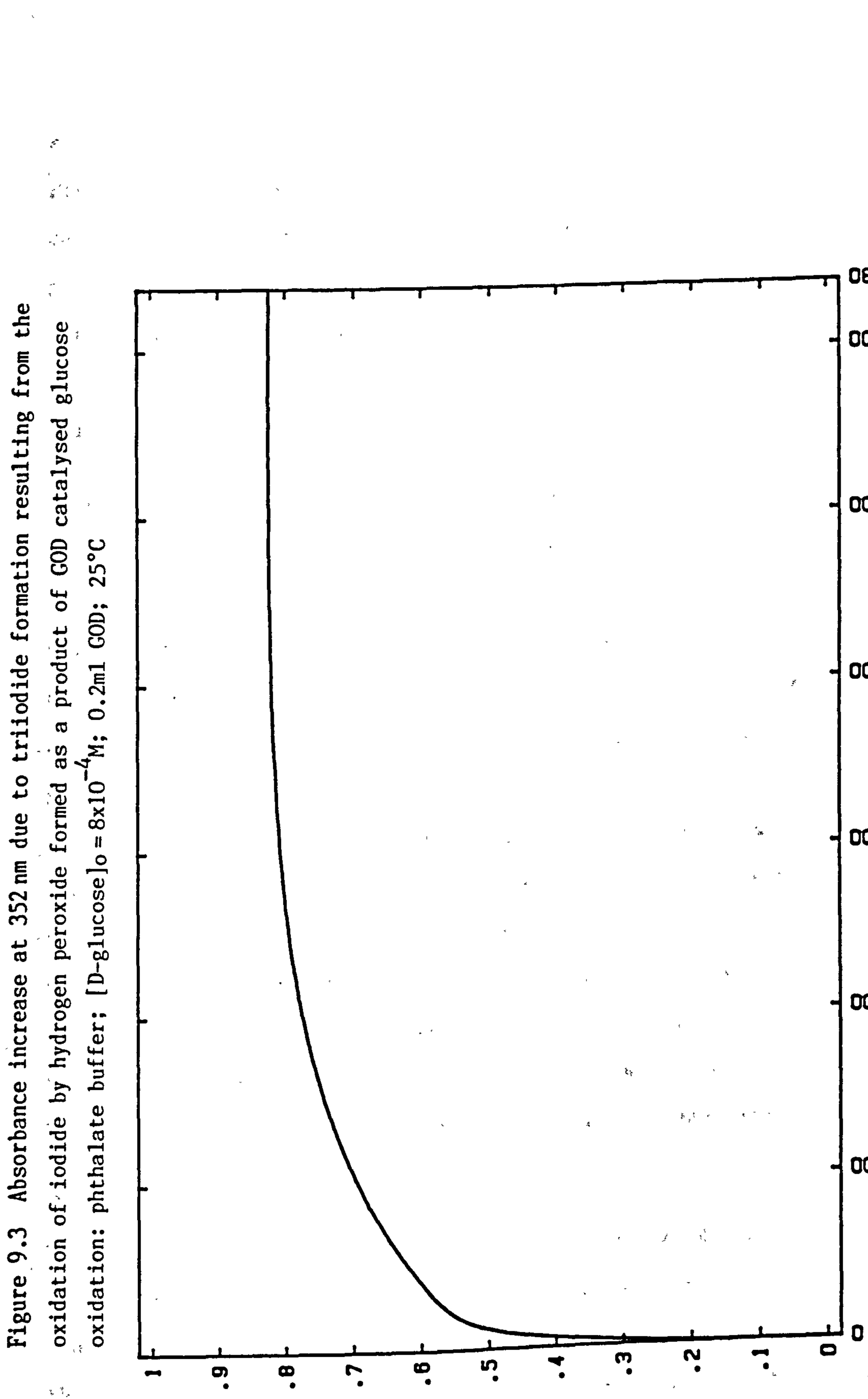

Figure 9.3 Absorbance increase at 352 nm due to triiodide formation resulting from the oxidation of iodide by hydrogen peroxide formed as a product of GOD catalysed glucose oxidation: phthalate buffer; $[D\text{-glucose}]_o = 8 \times 10^{-4}$M; 0.2ml GOD; 25°C

a range of D-glucose concentrations, the curve for which is shown in Figure 9.4. The values have not been corrected for the blank absorbance (enzyme + KI + phthalate) which was 0.013. The assay gave extremely good linearity over the concentration range used although there was a small negative intercept. This is most probably due to decomposition of hydrogen peroxide by the catalase impurity present in the glucose oxidase (~ 2.7 sigma units/mg solid).

25 ml of PAG and 25 ml of carbonate buffer were mixed in a 50 ml conical flask and maintained in a water bath at 25°C. Samples of the solution were analysed for glucose after 4 hours and 22.5 hours, using a slight modification of the previously described glucose assay: because of its low stability, the concentration of pentaacetyl-α-D-glucose in solution was only 3×10^{-4} M, which, if all converted to glucose, would give a maximum absorbance of approximately 0.3 units in the glucose assay. In order to increase the sensitivity of the assay, a 0.3 ml sample of the PAG/buffer solution was used. The KI concentration was corrected to give the same concentration of iodide in the assay mixture as the original procedure. In addition to the PAG/buffer mix, two additional samples were analysed for glucose using exactly the same procedure; (a) a solution of PAG in distilled water and (b) carbonate buffer, pH, I = 0.1 M. These samples will give a blank assay.

Results

Table 9.2 shows the results of the glucose assays at 4 and 22.5 hours for all solutions tested. Whilst at 4 hours we were unable to detect glucose in the hydrolysing PAG samples (absorbances were the same as in the blank solution), at 22.5 hours glucose was found to be present. The absorbance corresponded to a glucose concentration of about 1.13×10^{-4} M, or approximately 38% of the maximum glucose concentration expected for complete hydrolysis of PAG.

Figure 9.4 Calibration curve for the glucose assay. The line represents the best fit using the linear least squares method.

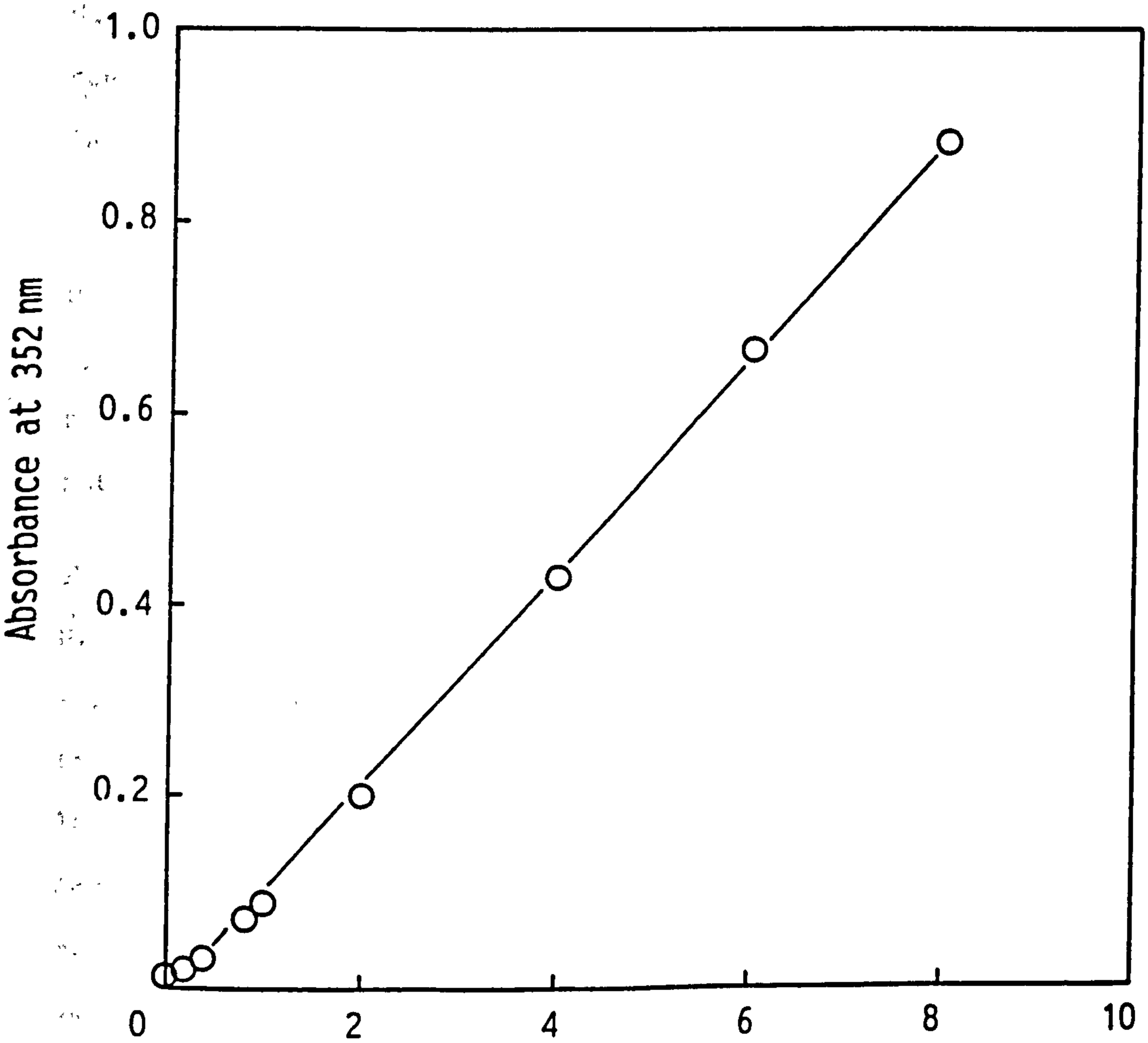

We have, therefore, confirmed that complete deacylation of PAG is possible during hydrolysis and this suggests that all the acetyl groups are also available for the perhydrolysis reactions. However, a considerable period of time is required for complete deacylation to occur (over 4 hours).

9.4 Effect of Hydrogen Peroxide concentration on Peracetic Acid Yield from Pentaacetyl-α-D-glucose

Having determined that PAG can be completely deacylated a study was conducted to see if the maximum yield of peracetic acid, on reacting PAG with hydrogen peroxide, was 5 moles per mole of PAG.

Reagents

Pentaacetyl-α-D-glucose, 6×10^{-4} M in aqueous solution.

Hydrogen peroxide solution, a range of concentrations in pH 9.45 carbonate buffer, I = 0.2 M.

Both solutions contained 1×10^{-5} M EDTMP.

Procedure

0.5 ml of PAG solution and 0.5 ml of hydrogen peroxide/carbonate buffer solution were mixed in a 1.5 ml plastic centrifuge tube. Concentrations of hydrogen peroxide in the tubes were (10^3/M): 5.32, 10.64, 15.96, 21.28, 26.6, 31.92, 37.24, 42.56, 47.88, and 53.2. Using 0.1 ml samples, the peracetic acid concentration was monitored until no further increase in concentration was observed (in most cases the maximum peracetic acid concentration $[PA]_\infty$, had been achieved by the time the first sample was taken.

Results

Figure 9.5 shows a plot of the five peracetic acid measurements made at several hydrogen peroxide concentrations. Clearly, there appears to be some peroxide decomposition after $[PA]_\infty$ has been reached. Figure 9.6

Figure 9.5 Plot showing the release of peracetic acid from the reaction of pentaacetyl-α-D-glucose with hydrogen peroxide at several hydrogen peroxide concentrations: pH 9.45 sodium carbonate - sodium hydrogen carbonate buffer (I = 0.1M); $[PAG]_o = 3x10^{-4}$M; 25°C; $[EDTMP]_o = 1x10^{-5}$M. The symbols refer to hydrogen peroxide concentrations of (10^3/M): 2.53,○, 4.31,■, 5.32,△, 10.64,●, 15.96,□, 21.28,▼, 26.6,▽, 53.2,◆.

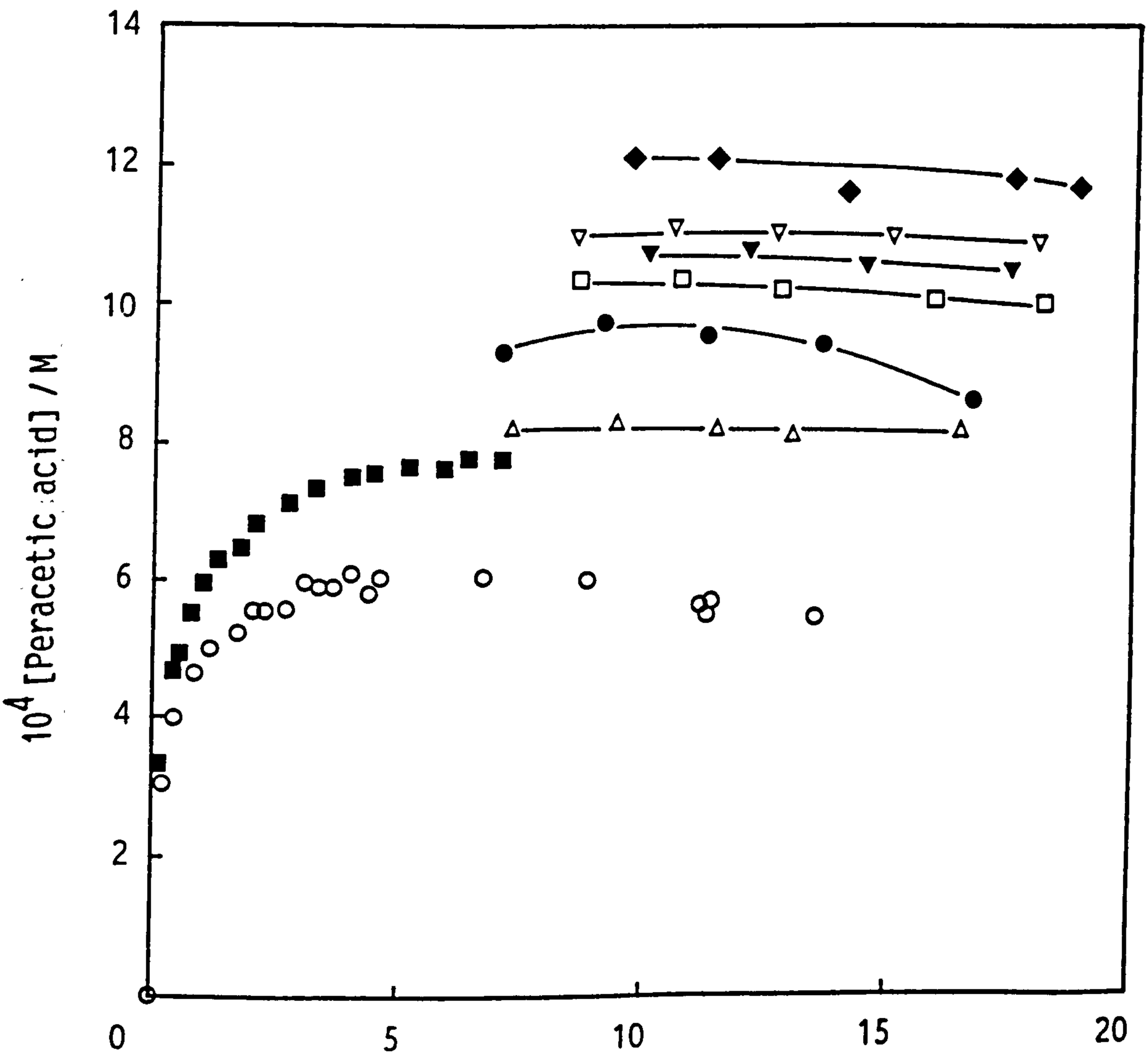

Figure 9.6 Plot showing the effect of hydrogen peroxide concentration on infinity concentrations of peracetic acid resulting from the reaction between pentaacetyl-α-D-glucose and hydrogen peroxide: pH 9.45 sodium carbonate - sodium hydrogen carbonate buffer (I = 0.1M); $[PAG]_o = 3 \times 10^{-4}$M; 25°C; $[EDTMP] = 1 \times 10^{-5}$M.

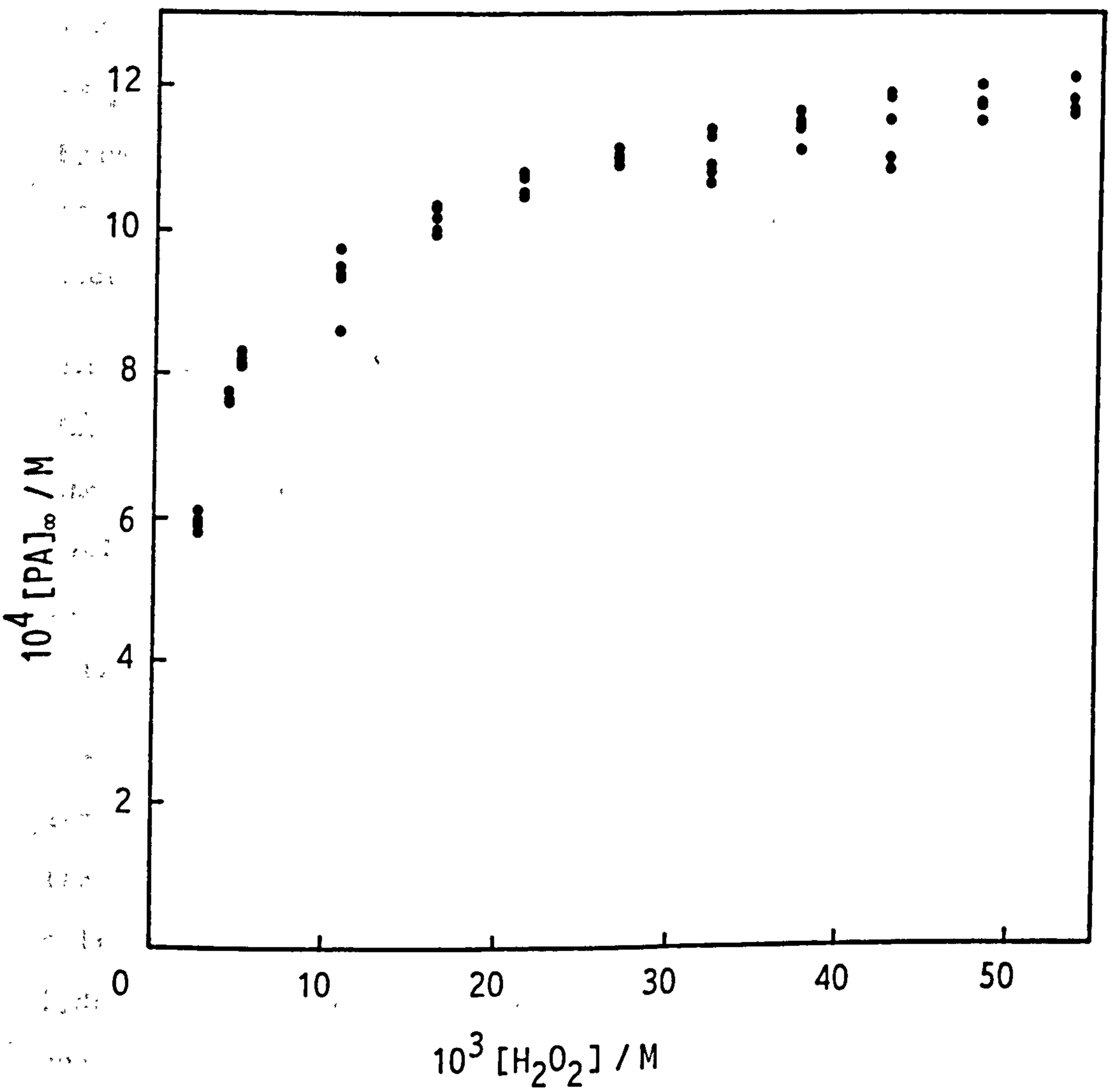

shows a plot of $[H_2O_2]_o$ against $[PA]_\infty$. All five peracetic acid measurements made at each $[H_2O_2]_o$ are displayed in the plot; clearly, as we increase $[H_2O_2]_o$, then $[PA]_\infty$ also increases.

From our own studies (Section 9.3) and also literature information[143], we know that all five acetyl groups are removed from PAG by hydrolysis to give glucose as a final product. It is, therefore, likely that all the acetyl groups are available for attack by the perhydroxyl anion, and a theoretical maximum of 5 moles of peracetic acid could be expected per mole of pentaacetylglucose, given a high enough concentration of hydrogen peroxide. From our data it seems that the maximum value for $[PA]_\infty$ has not been reached. These results are discussed further in Section 9.5.

9.5 Discussion of PAG Studies

The original aim of these studies was to determine whether all five of the o-acetyl groups of PAG were available to undergo hydrolysis to yield peracetic acid, bearing in mind the usually quoted ratio[141] of 2.5 moles of peracetic acid per mole of PAG when it is used as a bleach activator in detergent formulations.

Our initial studies of the time-course of percetic acid formation during reaction of PAG with hydrogen peroxide at pH 9.45 indicated that the peracetic acid formation is characterised by at least two kinetically-distinct phases, the second of which appears to be independent of hydrogen peroxide concentration. We propose that this phenomenon is due to rate limiting acetyl migration; acetyl migration is well documented in the literature.[141-8]

In all the various conformations of PAG there will be a large degree of congestion between the carbonyl carbons and methyl groups of neighbour-

ing acetyl groups. Consequently, attack of nucleophilic compounds at the carbonyl carbons will be hindered at the C_1 to C_4 positions. However, attack at the carbonyl carbon at the C_6 acetyl group will be less sterically hindered due to (a) the extra CH_2 group between the ring and the o-acetyl group compared to the acetyl groups at the C_1 to C_4 positions, and (b) the presence of only one neighbouring acetyl group. Consequently, attack at the C_6 acetyl group is most likely and the attack will probably be dependent on $[H_2O_2]_o$. Having removed one of the acetyl groups, acetyl migration to the C_6 position can subsequently occur. Doershuk, in 1952[145], has shown using C^{14} tracer experiments that the these rearrangements are intramolecular and not intermolecular. Acetyl migration is thought to proceed via cyclic ortho-acid intermediates and is catalysed by bases, and to a lesser extent by acids. For example, 1,2,3,4-tetra-o-acetyl-β-D-glucopyranose rearranges to the 1,2,3,6-tetra-acetate in a 1 x 10^{-3} N sodium hydroxide[142], as shown in Scheme 9.1

Scheme 9.1

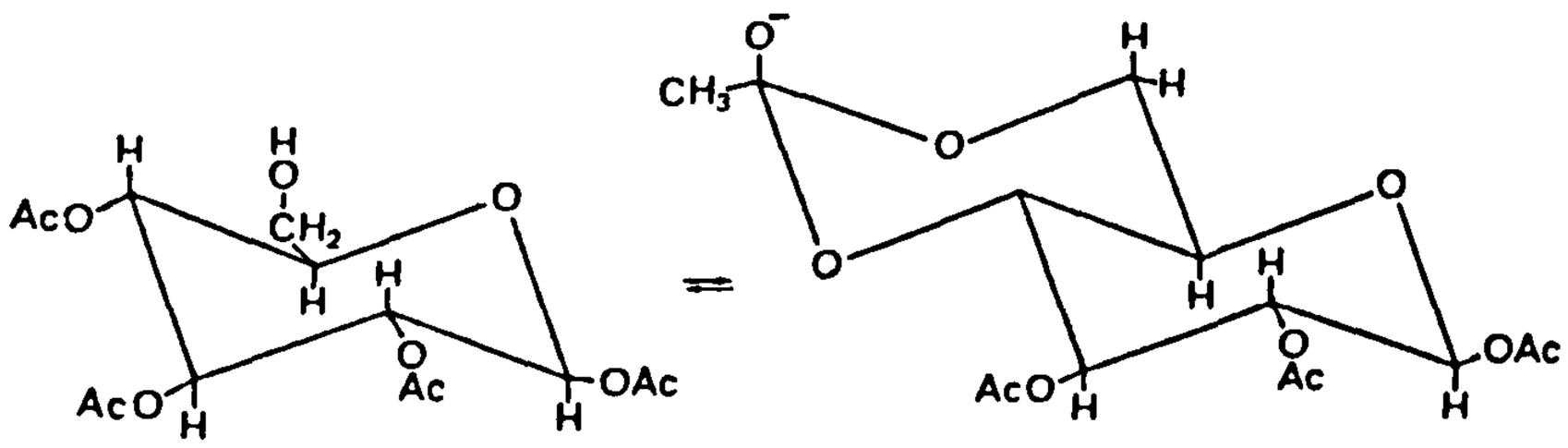

1,2,3,4-tetraacetyl-β-D-glucose ortho acid

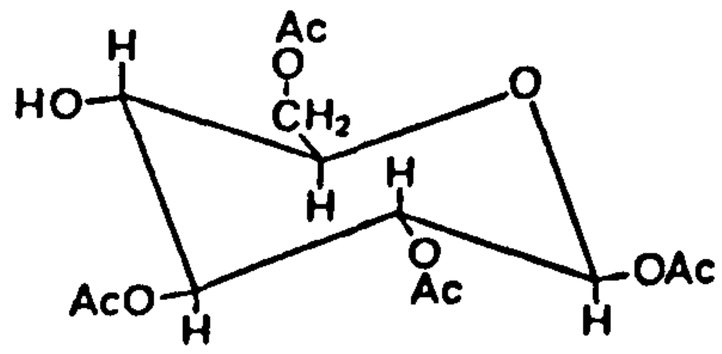

1,2,3,6-tetraacetyl-β-D-glucose

The ease with which ester migration occurs is dependent on the ease of formation of the cyclic intermediate. Once the acetyl group has migrated to the less sterically hindered C_6 position then it may undergo nucleophilic attack.

Although it is likely that nucleophilic attack of the HOO^- anion is possible at the carbonyl carbons of all the o-acetyl positions, we are suggesting that initially the main route to acetyl removal, subsequent to the removal of the first acetyl group, involves rate determining migration of the acetyl groups to the less sterically hindered C_6 position.

Using a Dreiding molecular model, Table 9.3 has been compiled for possible acetyl migrations involving strainless cyclic intermediates and the various conformations for which they apply. The number of ring atoms included in the cyclic ortho-acid intermediate is also given. It is known that there is a tendency for the acetyl group to migrate away from the anomeric centre (C_1). The following acetyl migrations have been observed in the literature for acylated D-glucose compounds or the corresponding migrations in similar compounds: 1 --> 2[146]; 4 --> 6[147]; 3 --> 6[147] (possibly) and 2 --> 4[142]. It is interesting that the 2 --> 4 transition has been observed (for 2,3,6 - triacetyl-ß-D-glucose[42]) since it is exclusively a migration belonging to the unfavourable $^1C_4$ conformation (for both anomers). The α anomer transitions may also apply to the ß-D-glucose pentaacetate since, as we have discussed, if the C_1 acetyl group is removed then the mutarotation can occur during the reaction which will eventually give an equilibrium of the anomers. It is clear from Table 9.3 that there is plenty of scope for acetyl migration to the less sterically hindered C_6 position where a nucleophilic displacement reaction may occur.

Table 9.3 Possible acetyl migrations for α and β anomers of acylated D-glucose compounds.

Anomer	Conformation		
	C_1^4 Chair	C_4^1 Chair	Skew / Boat
	4 → 6 (6)*	1 → 6 (7)	4 → 6 (6)
		3 → 6 (7)	3 → 6 (7)
		1 → 3 (6)	1 → 6 (7)
		2 → 4 (6)	
	4 → 6 (6)	3 → 6 (7)	4 → 6 (6)
	1 → 2 (5)	2 → 4 (6)	3 → 6 (6)

*Figures in parentheses donate the number of ring atoms involved in the cyclic orthoacid intermediate.

Rate constants for acetyl migration, quoted in the literature, are consistent with our proposal that such migrations are responsible for the rate independence of peracid formation on [H_2O_2] for the second phase. For example, Kamerling et al.[146] followed the acetyl migration from N-acetyl-7-o-acetyl neuraminic acid (Neu 5,7,Ac_2) to form N-acetyl-9-o-acetyl nuraminic acid (Neu 5,9,Ac_2). Using HPLC to measure conversion of Neu 5,7,Ac_2 to Neu 5,9,Ac_2, $t_{\frac{1}{2}}$ values were determined at pH values of 7.0, 7.5, 8.0, and 8.5 (Tris/HCl buffer at 37°C). On plotting log $t_{\frac{1}{2}}$ against pH, a slope of -1.37 was obtained, demonstrating the role of base catalysis in acetyl migration. At pH 8.5 the half-life for acetyl migration was 360 seconds (37°C).

From the studies conducted in Section 9.3, we have confirmed that complete deacylation of PAG is possible during hydrolysis and this suggests that all the acetyl groups are also available for the perhydrolysis reactions; the complete hydrolysis of PAG to glucose is, however, extremely slow, since after 4 hours at pH 9.45 no glucose could be detected, and after 22.5 hours only 38% of the acetyl groups had undergone hydrolysis. From the hydrolysis study, it should also be expected that all 5 o-acetyl groups of PAG are available to undergo reaction with HOO^-, suggesting that a maximum of 5 moles of peracetic acid per mole of PAG could be obtained. We have shown that by increasing the initial hydrogen peroxide concentration, the yield of peracetic acid ([PA]) also increases (Figure 9.6); this is because the extent of the competing hydrolysis reaction is decreased at higher hydrogen peroxide concentrations. From our experimental data, a maximum ratio of ~ 4 moles of peracetic acid per mole of PAG was achieved at the highest hydrogen peroxide concentration used (53.2×10^{-3} M). Figure 9.6 suggests that still higher peracetic acid yields could be obtained at higher hydrogen peroxide concentrations. It is possible from these data to predict a

value for $[PA]_\infty$ at $[H_2O_2]_\infty$. The theoretical considerations for this prediction are described below

From our previous discussions it is likely that the acetyl group at the C_6 position is the first to be removed.

$$PAG + H_2O \xrightarrow{k_o} 4AG + A$$

$$PAG + H_2O_2 \xrightarrow{k_1} 4AG + PA$$

where

A = acetic acid and PA = peracetic acid

Thus,

$$\frac{d[PA]}{dt} = k_1 [H_2O_2]_o [PAG]$$

$$\frac{d[A]}{dt} = k_o [PAG]$$

$$\frac{d[PA]}{d[A]} = k_1 \frac{[H_2O_2]_o}{k_o} \qquad \text{Eqn 9.2}$$

Integrating Eqn 9.2

$$[PA] = \frac{k_1 [H_2O_2]_o}{k_o} \cdot [A] + C$$

At boundary conditions t = 0, [PA] = 0, [A] = 0 and, therefore,

$$C = 0$$

Therefore,

$$\frac{[PA]}{[A]} = \frac{k_1 [H_2O_2]_o}{k_o} \qquad \text{Eqn 9.3}$$

After removal of the first acetyl group it is likely that in order for the next group to be removed rate determining acetyl migration to the C_6 position is required

$$4AG \xrightarrow{k} 4AG'$$

where k is the rate constant for acetyl migration. Hydrolysis and perhydrolysis can then occur at the C_6 acetyl group.

$$4AG' + H_2O \xrightarrow{k_o'} 3AG + A$$

$$4AG + H_2O_2 \xrightarrow{k_1'} 3AG + PA$$

making the steady-state approximation in [4AG]'

$$0 = \frac{d[4AG]'}{dt} = k[4AG] - k_o'\,[4AG]' - k_1'\,[4AG]'\,[H_2O_2]_o$$

$$k[4AG] = [4AG]'\,(k_o' + k_1'\,[H_2O_2]_o)$$

$$[4AG]' = \frac{k[4AG]}{k_o' + k_1'\,[H_2O_2]_o}$$

Thus,

$$\frac{d[A]}{dt} = \frac{k_o'\,k\,[4AG]}{k_o' + k_1\,[H_2O]_o}$$

and

$$\frac{d[PA]}{dt} = \frac{k_1'\,k\,[4AG]\,[H_2O_2]_o}{k_o' + k_1'\,[H_2O_2]_o}$$

$$\frac{d[PA]}{d[A]} = \frac{k_1'\,[H_2O_2]_o}{k_o'}$$

and . .

$$\frac{[PA]}{[A]} = \frac{k_1'\,[H_2O_2]_o}{k_o'} \qquad \text{Eqn 9.4}$$

Our results have suggested that there are at least two kinetically distinct phases to peracetic acid liberation, and it is possible that the removal of the third acetyl group from PAG also proceeds via rate limiting acetyl migration to the C_6 position and, therefore, we will get a similar relationship to Equations 9.3 and 9.4 for 3AG.

$$\frac{[PA]}{[A]} = \frac{k''\,[H_2O_2]}{k_o''} \qquad \text{Eqn 9.5}$$

It is unknown whether the removal of the fourth and fifth acetyl groups proceed mainly via this mechanism or via the non-acyl migration mechanism. However, it is likely that as more acetyl groups are removed from the molecule, then the steric hindrance at the carbonyl carbons of acetyl groups at the C_1 to C_4 positions will be reduced and, therefore, acetyl removal at these positions will become more favoured.

It would seem possible that

$$\frac{k_1}{k_o}[H_2O_2] = \frac{k_1'}{k_o'}[H_2O_2] = \frac{k_1''}{k_o''}[H_2O_2]$$

since the acetyl removal most likely occurs at the C_6 position after acetyl migration. We are going to make a further, and less certain assumption, that these ratios also hold for the removal of the fourth and fifth acetyl groups.

Thus,

$$\frac{[PA]_\infty}{[A]_\infty} = \frac{k_1^*\,[H_2O_2]}{k_o^*} \qquad \text{Eqn 9.6}$$

where k_1^* and k_o^* are composite rate constants for the removal of all five acetyl groups.

Now,

$$[A]_\infty = n[PAG]_o - [PA]_\infty$$

where n is the number of available acetyl groups.

Substituting into Equation 9.6.

$$\frac{[PA]_\infty}{n[PAG]_o - [PA]_\infty} = \frac{k_1^*\,[H_2O_2]_o}{k_o^*}$$

$$[PA]_\infty = \frac{n\,k_1^*\,[H_2O_2]_o\,[PAG]_o}{k_o^*} - \frac{k_1^*}{k_o^*}[H_2O_2]_o\,[PA]_\infty$$

$$[PA]_\infty \left(\frac{1 + k_1^*\,[H_2O_2]_o}{k_o^*}\right) = n\,\frac{k_1^*\,[H_2O_2]_o}{k_o^*}\,[PAG]_o$$

$$[PA]_\infty = \frac{k_o^*}{k_o^* + k_1^*\,[H_2O_2]_o}\; n\,\frac{k_1^*\,[H_2O_2]_o}{k_o^*}\,[PAG]_o$$

$$\frac{[PA]_\infty}{n[PAG]_o} = \frac{k_1^*\,[H_2O_2]_o}{k_o^* + k_1^*\,[H_2O_2]_o}$$

$$\frac{1}{[PA]_\infty} = \frac{1}{n[PAG]_o}\left(1 + \frac{k_o^*}{k_1^*} \cdot \frac{1}{[H_2O_2]_o}\right) \qquad \text{Eqn 9.7}$$

A plot of $1/[H_2O_2]_o$ against $1/[PA]_\infty$ gives an intercept of $1/n\,[PAG]_o$ and the slope divided by the intercept gives the ratio of the rate

constants k_1^*/k_o^*. This plot has been made for our data and is shown in Figure 9.7. Due to problems encountered with peroxide decomposition in this series of experiments, only the maximum values of [PA] for each $[H_2O_2]_o$ have been used in the plot. The data for the plot are contained in Table 9.4.

The plot is linear up to about 50 M^{-1}, however, at higher values of $1/[H_2O_2]_o$ the points show a negative deviation. From linear regression of the points up to $1/[H_2O_2] = 46.99\ M^{-1}$, the following parameters were obtained.

$$\frac{1}{n[PAG]_o} = 757.7 \pm 7.188^*$$

$$n[PAG]_o = (13.197 \pm 0.564) \times 10^{-4}*$$

$$n = 4.399 \pm 0.187^*$$

$$\text{slope} = 3.675 \pm 0.239^*$$

$$\underline{k_o^*} = 4.85 \times 10^{-3}$$
$$k_1^*$$

The main point arising from this is that although we have shown that all five acetyl groups in PAG can be removed by hydrolysis (and, therefore, most likely, also, by perhydrolysis), our data give a theoretical maximum (at $[H_2O_2]_o = \infty$) of only 4.4 acetyl groups. The most probable explanation for this value being less than five is that peroxide decomposition reactions masked the slow release of peracetic acid corresponding to the removal of the final acetyl group, giving a value of $[PA]_\infty$ lower than that expected. Alternatively, there could have been significant hydrolysis of the PAG solution while it was being prepared, since 3-4 hours are required to dissolve up a 6×10^{-4} M solution. We have found that peracetic acid does not react with glucose and, so, this can be ruled out as a reason for [PA] being less than 5 at $[H_2O_2]$.

---

* 90% confidence limits

Figure 9.7 Plot of $1/[PA]_\infty$ against $1/[H_2O_2]_o$ for the reaction between hydrogen peroxide and pentaacetyl-α-D-glucose: pH 9.45 sodium carbonate - sodium hydrogen carbonate buffer (I = 0.1M); $[PAG]_o = 3x10^{-4}M$; 25°C; $[EDTMP] = 1x10^{-5}M$: The line represents the best fit using the linear least squares method.

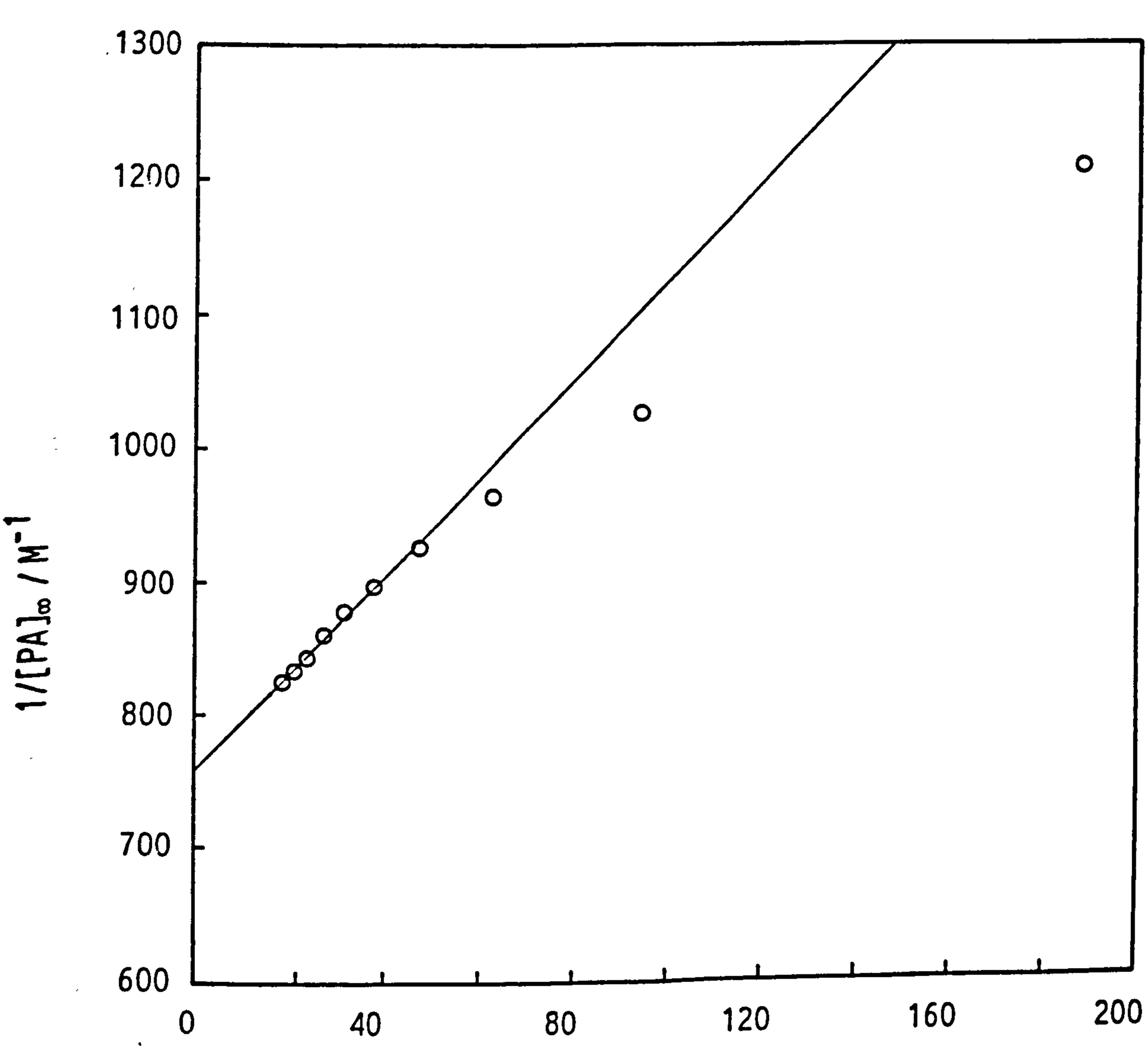

Table 9.4 Values of $1/[H_2O_2]_o$ and $1/[PA]_\infty$ for the reaction between hydrogen peroxide and pentaacetyl-α-D-glucose in pH 9.45 carbonate buffer (I = 0.1M).

$1/[H_2O_2]_o$ / M^{-1}	$1/[PA]_\infty$ / M^{-1}
18.80	825.0
20.89	833.4
23.50	842.6
26.85	859.6
31.33	877.0
37.59	898.0
46.99	926.8
62.66	964.4
93.98	1026.0
187.96	1207.0

CHAPTER 10 CONCLUSIONS AND RECOMMENDATIONS FOR FURTHER RESEARCH

10.1 General

This work has been concerned with kinetic and mechanistic studies of the process of peroxide bleach activation, that is, the *in situ* generation of peroxy acids (usually peracetic acid) from the reaction of hydrogen peroxide with a peroxyacid precursor (the bleach activator). Peroxyacids have a superior low temperature (below 60°C) bleaching performance to hydrogen peroxide, which was the traditional bleach used in European detergent formulations (in the form of sodium perborate).

Our approach to this study was, initially, to work on a bleach activator, paranitrophenylacetate (PNPA), for which the activation reaction scheme was relatively easy to elucidate; the methods and approach used in the study of this 'model' activator were then applied successfully to the study of two commercially-used bleach activators, tetraacetylethylenediamine (TAED) and pentaacetylglucose (PAG).

This chapter reviews the main conclusions of our research and offers some suggestions for the direction in which supplementary investigations might proceed. Generally, whilst there is always scope for additional work to be conducted on buffer effects, ionic strength effects, elucidation of thermodynamic parameters, etc. the emphasis of our recommendations lies in the further investigation of the reactivity, towards TAED, of hydrogen peroxide, compared to other peroxide nucleophiles. In particular, experiments are suggested which are designed to obtain further evidence in support of our proposed cyclic intermediate mechanism for the reaction of hydrogen peroxide with TAED. The other main area into which research should be concentrated is the role

that acetyl migration plays in the reaction of nucleophiles with o-acetylated pyranoses such as PAG.

10.2 Work on Paranitrophenylacetate (PNPA)

(1) The reaction of hydrogen peroxide with PNPA was followed by monitoring the levels of paranitrophenol, peracetic acid, and total iodide reactable peroxide. The maximum theoretical yield of peracetic acid was not observed during this reaction due to the competing PNPA hydrolysis reaction, which yields PNP and acetic acid as products. The ability to measure peracetic acid was made possible by an iodimetric spectrophotometric technique, developed during this work, which is capable of rapidly and accurately measuring peracetic acid concentrations as low as 1 x 10^{-5} M (in the cuvette) in the presence of up to a 1000-fold excess of hydrogen peroxide.

(2) In addition to the reaction of hydrogen peroxide with PNPA, we have shown that one of the products of this reaction, peracetic acid, reacts with a further molecule of PNPA to produce diacetyl peroxide. Diacetyl peroxide is unreactive towards iodide, even with the addition of the catalyst ammonium heptamolybdate, and its presence in the reaction solution was, therefore, indicated by a dip in the total iodide reactable peroxide concentration. Diacetyl peroxide can either undergo hydrolysis to yield peracetic acid and acetic acid, or can react with hydrogen peroxide to yield two molecules of peracetic acid.

(3) Using independently determined rate constants, computer-generated curves for the concentrations of PNP, H_2O_2, peracetic acid, and total iodide peroxide subsequent to mixing hydrogen peroxide and PNPA in a 2:1 mole ratio (pH 6.80, phosphate buffer) were in excellent agreement with the actual concentration changes observed in such a reaction; this indicates that the proposed scheme for this reaction (Scheme 3.2), and

the individually determined rate constants corresponding to it, adequately describe this system, under the conditions used.

(4) The observation of increased rates of reaction at higher phosphate buffer concentrations for all reactions corresponding to Scheme 3.2, apart from the reaction of peracetic acid with PNPA, is ascribed to general base catalysis by components of the phosphate buffer.

(5) Estimated second order rate constants for the reaction of HOO^- with PNPA in borate buffer are roughly four times lower than those observed in phosphate and carbonate buffers. This is attributed to the formation of a complex between hydrogen peroxide and borate.

$$B(OH)_3 + H_2O_2 \underset{}{\overset{K}{\rightleftharpoons}} (HO)_3BOOH^- + H^+$$

Our results are in agreement with the reported[115] equilibrium constant for the above equation.

10.3 Work on Tetraacetylethylenediamine (TAED) and Triacetylethylenediamine (TriAED)

10.3.1 General

(1) Crystalographic studies have shown that tetraacetylethylenediamine is a molecule consisting of two approximately planar imide groups in the E,Z configuration, separated by an ethylene group. One acetyl group of each imide group is capable of undergoing transfer to a suitable nucleophile; the successive deacylation stages yield, initially, triacetylethylenediamine (TriAED) and, finally, diacetylethylenediamine (DAED).

(2) TAED has a maximum absorptivity at 216 nm (molar absorptivity of 17240 M^{-1} cm^{-1}), whereas DAED has a maximum absorptivity below 192 nm; it is possible, therefore, to follow the reaction of TAED with nucleophiles by observing the decrease in absorbance at 216 nm, or on the shoulder of the TAED spectrum at higher wavelengths.

(3) Sequential spectra taken during the TAED hydrolysis reaction in a pH 9.6 carbonate buffer gave an isobestic point at 203.5 nm for TAED and DAED. Absorbance data obtained from the sequential spectra allowed the prediction of a spectrum for the intermediate, TriAED. The spectrum resembled that expected for a compound which half-resembled DAED and half-resembled TAED. Furthermore, the predicted spectrum resembled the actual spectrum of isolated TriAED very closely.

(4) The reaction of the nucleophiles hydrogen peroxide and water with TAED is biphasic; this is also likely to be true for other nucleophiles and is attributable to differential rates of reaction of TAED and TriAED with nucleophiles. On statistical grounds, a 2:1 ratio would be expected for the reactions of TAED and TriAED with nucleophile, however, for the reactions with hydrogen peroxide and water, the ratio is approximately 2.8:1; this higher-than-expected ratio is due to the electron withdrawing nature of the acetyl groups, and the effect of their removal on the electrophilicity of the carbonyl carbons of the remaining acetyl groups.

(5) A study of the pH dependence of TAED hydrolysis yielded a slope of 0.819 (I = 0.1 M, sodium salts used) on plotting log k_{obs} against pH. That the slope is less than the expected value of 1.0 for a simple first order dependence on hydroxide ion concentration suggests significant contributions to the rate from general acid - general base catalysis and/or a significant rate of reaction of the H_2O nucleophile. It is impossible at this stage to state which of these possibilities applies; extensive studies would have to be carried out in order to determine the contributions of k_{BH^+} $[OH^-]$, k_B- $[OH^-]$ and $k_{H2O}[H_2O]^n$ to the overall rate. We have, however, shown in another study that carbonate buffer does catalyse the hydrolysis of TriAED (isolated TriAED was

used). A more comprehensive pH dependence study of TriAED hydrolysis (I = 1.0 M, potassium salts) yielded a slope of 0.938 for which the above points also apply.

(6) We have found that the cation used in the buffer comnponents, and to maintain the ionic strength, influences the rate of hydrolysis of TriAED. Specifically, the use of sodium salts instead of potassium produced a 43% rate enhancement of TriAED hydrolysis (0.05 M carbonate buffer, pH 9.8, I = 1.0 M with KCl or NaCl). This is possibly due to either differential degrees of interaction of the hydrated cations with the transition state of the reaction (general acid catalysis), or the effect of the cation on the structure of water.

(7) In studies of the reaction of hydrogen peroxide with TAED and Tri-AED, problems were encountered with peroxide decomposition from two different sources. Transition metal ion-promoted decomposition reactions were alleviated by the use of ethylenediaminetetramethylene phosphonic acid hexasodium salt (EDTMP). UV-promoted decomposition reactions were reduced by decreasing the number of measurements taken during a particular kinetic run.

(8) A pH dependence study for the reaction of hydrogen peroxide with TAED yielded a slope of 0.985 $\pm$ 0.084 on plotting log k_{2obs} against pH; this suggests, as expected, that it is the hydroperoxy anion, HOO^-, which is the reactive form since the rate shows a simple dependence on $[HOO^-]$. Additionally, no external general acid - general base catalysis under these conditions is suggested by this result.

(9) The enthalpy and entropy of activation for the reaction of HOO^- with TriAED were determined as $\Delta H^{\ddagger} = 36.448 \pm 8.630$ KJ mol^{-1} and $\Delta S^{\ddagger} = -81.660 \pm 28.25$ J mol^{-1} K^{-1}, respectively; these values are in the typical range observed for the general type of reaction involving nuc-

leophilic attack by a neutral or anionic nucleophile at the carbonyl carbon of an amide or ester.

10.3.2 Linear Free Energy Studies

(1) Under CO_2-free experimental conditions, linear free energy studies were conducted for the reaction of three series of nucleophiles (peroxides, amines, and alcohols) with TriAED (isolated). ßnuc values were obtained for second order reactions (a third order reaction was also seen, as expected, for the reaction of amines with TriAED). For all three series of nucleophiles the ßnuc values were in the 'normal' range expected for reactions which proceed via a stepwise process; the values were 0.66, 0.76, and 0.96 for alcohols, amines, and peroxides (excluding hydrogen peroxide and peracetic acid), respectively, although only based on two points each. The fact that peroxides and other series of nucleophiles appear to show a 'normal' dependency of nucleophilicity on basicity rules out the possibility that the unexpectedly large difference in reactivity between hydrogen peroxide and peracetic acid is due to an abnormally large dependence of nucleophilicity on basicity for these reactions. Obviously, additional data are required in order to confirm the trends shown in the three Brønsted-type plots. This does, however, present practical problems from the point of view of the low reactivity of TriAED towards all but the most reactive nucleophiles. To expand the range of peroxides, for example, would necessitate the use of a range of peroxyacids which have pKa's mainly in the range 7.1 to 8.2. The peroxyacids will have a relatively low reactivity towards TriAED, and there is also the problem of equilibrium of peroxyacids with hydrogen peroxide, which was encountered during the reaction of peracetic acid with TAED. The formation of hydrogen peroxide in the reaction solution is due to alkaline hydrolysis of peroxyacids, and so it might be possible to work at a less alkaline pH, thus reducing the

extent of the hydrogen peroxide build up (and the rate of TriAED hydrolysis). Of course, if the pH was too near to the pKa of the peroxide then the additional problem of peroxyacid decomposition would be encountered. Another series of nucleophiles which would be interesting to look at is the thiols; for the reaction with esters such as PNPA, thiols show greater reactivity than amines. Figure 1.12, which shows Brønsted-type plots for the reaction of several series of nucleophiles with PNPA, should give a good idea of the additional range of nucleophiles which could be used to react with TriAED to expand our presently limited study.

(2) For a series of peroxides, the point for HOO^- lies significantly above the Brønsted slope drawn between the points for Caro's acid and methyl hydroperoxide, indicating enhanced reactivity of HOO^- compared to other peroxides. Furthermore, hydrogen peroxide is ~25 times more reactive than methyl hydroperoxide, yet the difference in pKa is only 0.1 (0.4 if the pKa of H_2O_2 is statistically corrected). The increased steric effects for methyl hydroperoxide, compared to hydrogen peroxide, are unlikely to account for this difference, although an idea of the extent of steric effects on the rate of reaction with TriAED could be obtained by comparing the reactivity of methyl hydroperoxide with other alkyl hydroperoxides, such as ethyl hydroperoxide and propyl hydroperoxide. The latter two hydroperoxides can be synthesized from n-alkyl methane sulphonates, according to the method of Williams and Mosher.[149]

(3) A cyclic intermediate mechanism [81] is proposed by us to explain the enhanced reactivity of HOO^- over other peroxides. The hydroperoxy anion, as well as acting as a nucleophile, also acts as a general acid catalyst, protonating the amide nitrogen. Such a mechanism is not possible for peroxides other than HOO^-.

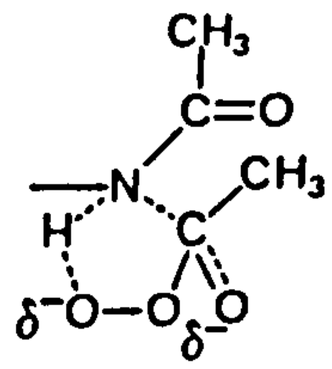

[81]

It might be possible to further test this proposal by looking at the reaction of a series of peroxides, including hydrogen peroxide, with an imidic activator in which the formation of a cyclic intermediate structure, such as [81], would be hindered due to congestion around the imide nitrogen. Such a situation would be provided in the case of N-t-butyldiacetamide [89]; if the cyclic intermediate proposal is correct, then for such a study the extent of the rate enhancement of hydrogen peroxide over other peroxides would be expected to be reduced.

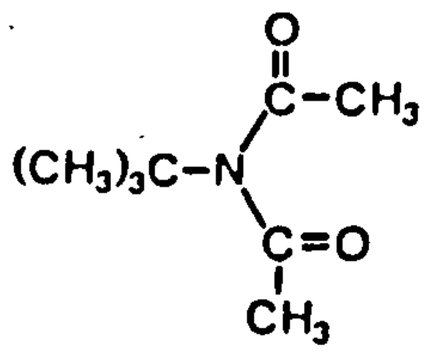

[89]

(4) A βnuc value of 0.398 was obtained for the reaction of hydrogen peroxide with a series of imidic activators with leaving group pKa's in the range 15.12 to 15.68. The value for βlg is inconsistent with the corresponding βnuc value for the reaction of peroxides with TAED (0.96); similar βnuc and βlg values are expected, for these types of reaction, as has been demonstrated in the literature.[17,40,53] This further supports the proposal of a cyclic intermediate mechanism since for a series of imides the same factors which decrease the charge density at the carbonyl carbon, thus making it more reactive, also decrease the charge density at the amide nitrogen and thus decrease its require-

ments for protonation. Whilst the latter effect will not have any bearing on the rate of reaction of peroxides, such as methyl hydroperoxide, it will affect the reactivity of hydrogen peroxide. This effect could be confirmed if similar ßlg and ßnuc values were obtained for the reaction of methyl hydroperoxide (or Caro's acid) with a range of imides with different leaving groups (preferably over a wider pKa range than that employed for the hydrogen peroxide study).

(5) Cyclic intermediate structures have also been proposed for the reaction of hydrogen peroxide with esters; in the case of PNPA, the point for HOO^- on a Brønsted-type plot lies above the slope formed by a series of other peroxides (including $MeOO^-$).

10.4 Work on Pentaacetylglucose (PAG)

(1) Despite the often-quoted ratio of 2.5 moles of peracetic acid liberated per mole of PAG, we have shown that all five acetyl groups are available for reaction by hydrolysis. Also, by increasing the mole ratio of H_2O_2:PAG, the yield of peracetic acid is found to increase. We have predicted a maximum yield of 4.5 moles of peracetic acid per mole of PAG; peroxide decomposition reactions during the runs probably account for the predicted maximum being less than five.

(2) Rate limiting acetyl migration has been suggested by our results to be an important factor in the reaction of nucleophiles with PAG; in a biphasic plot for the liberation of peracetic acid from PAG, the second phase was found to be independent of $[H_2O_2]$. It is likely that the initial attack of nucleophiles on PAG is at the least congested carbonyl carbon, that is, at the acetyl in the C_6 position; subsequent acetyl transfer reactions are limited, initially, by the rate of migration of acetyl groups to the C_6 position. It is, however, possible that the initial attck of nucleophiles is at the acetyl group in the C_1 posi-

tion. A possible method for determining whether the initial attack was at the C_6 or C_1 acetyl groups would be to measure the optical rotation of a solution of alkaline ß-D-penta-o-acetylglucose. It is impossible for the ß form to change into the α anomer whilst the C_1 position still has an acetyl group attached. Thus, depending on the results of the optical rotation measurements, one could predict whether acetyl removal occurred at the C_1 or C_6 position first. It is suggested that the role played by acetyl migration during the reaction of H_2O_2 with PAG can further be studied as follows: a value for the rate of reaction of H_2O_2 with the first acetyl group can be obtained under pseudo first order conditions by using a large excess of PAG over H_2O_2; under such conditions the main reaction will be that between H_2O_2 and the acetyl group in either the C_1 or C_6 positions. The rate constant for the rate of reaction of H_2O_2 with the second acetyl group can be obtained under pseudo first order conditions, with H_2O_2 in excess, by using a tetra-acetylglucose, preferably ß-1,2,3,4-o-acetylglucose; if acetyl migration is important then rate independence should be observed with increasing $[H_2O_2]$.

REFERENCES

1. Mecheels, J., Seifen-Oele-Fette-Wasche, 1982, 108, 31
2. Department of Energy, Digest of United Kingdom Energy Statistics, years 1969 - 1989, HMSO, London.
3. Parker, J. A., New Peroxygen Bleaching Systems, CSMA Detergent Seminar, Lake Harmony, 1985, June.
4. Hignett, G. J., Tenside Detergents, 1986, 23, 69.
5. Warwick International Ltd., Application Report 8602, 1986.
6. TAED Basic Patent: DAS 1 162 967.
7. Reinhardt, G., Shuler, W., and Quack, J. M., TAED - Manufacture, Effects and Environmental Properties, 20th Jornades del CED / AID, Barcelona, 1988, March.
8. Jencks, W. P., Catalysis in Chemistry and Enzymology, McGraw - Hill Book Company, New York, 1969.
9. Jencks, W. P., Accounts of Chemical Research, 1980, 13, 161.
10. Jencks, W. P., Accounts of Chemical Research, 1976, 9, 425.
11. Williams, A., and Douglas, K. T., Chemical Reviews, 1975, 75, 627.
12. Bender, M. L., Chemical Reviews, 1960, 60, 53.
13. Cline, G. W., and Hanna, S. B., Journal of Organic Chemistry, 1988, 53, 3583.
14. Khan, M. N., Journal of the Chemical Society, Perkin Transactions II, 1988, 1129.
15. Oakenfull, D. G., and Jencks, W. P., Journal of the American Chemical Society, 1971, 93, 178.
16. Oakenfull, D. G., Salvensen, K., and Jencks, W. P., Journal of the American Chemical Society, 1971, 93, 188.
17. Fersht, A. R., and Jencks, W. P., Journal of the American Chemical Society, 1970, 92, 5442.
18. Bender, M. L., and Thomas, R. J., Journal of the American Chemical Society, 1961, 83, 4183.
19. Tomilla, E., and Hinshelwood, C. N., Journal of the Chemical Society, 1953, 1801.

20. Eurento, E. K., Esterification and Ester Hydrolysis, in Patai, S., ed, The Chemistry of Carboxylic Acids and Esters, Interscience Publishers, London, 1969.

21. Bruice, T. C., Hegarty, A. F., Felton, S. M., Donzel, A., and Kundu, N. G., Journal of the American Chemical Society, 1970, 92, 1370.

22. Challis, B. C., and Challis, J. A., in Sutherland, I. O., ed., Comprehensive Organic Chemistry, Pergammon Press, Oxford, 1979.

23. Hine, J., King, R. S. M., Midden, W. R., and Sinha, A., Journal of Organic Chemistry, 1981, 46, 3186.

24. Edwards, J. T., and Terry, K. A., Journal of the Chemical Society, 1957, 3527.

25. Kirsch, J. F., and Jencks, W. P., Journal of the American Chemical Society, 1964, 86, 837.

26. Camilleri, P., Carey, J. V., Odell, B., and Williams, D. G., Journal of the Chemical Society, Perkin Transactions II, 1988, 591.

27. Hargreaves, M. K., Pritchard, J. G., and Dave, H. R., Chemical Reviews, 1970, 70, 439.

28. Feiser, L. F., and Feiser, M., Textbook of Organic Chemistry, D. C. Heath and Company, Boston, 1950.

29. Westheimer, F.H., and Metcalf, R. P., Journal of the American Chemical Society, 1941, 63, 1339.

30. Biecher, S. S., and Taft, R. W., Journal of the American Chemical Society, 1957, 79, 4927.

31. Jones, R. W. A., and Thomas, J. D. R., Journal of the Chemical Society (B), 1966, 661.

32. Huisgen, R., and Ott, H., Tetrahedron, 1959, 6, 253.

33. Packer, J., Thomson, A. L., and Vaughan, J., Journal of the Chemical Society, 1955, 2601.

34. Bender, M. L., Ginger, R. D. and Onik, J. P., Journal of the American Chemical Society, 1958, 80, 1044.

35. Laurent, E., and Pellissier, N., Bulletin de la Société Chemique de France, 1974, 9, 1904.

36. Hall, H. K., Brandt, M. K., and Mason, R. M., Journal of the American Chemical Society, 1958, 80, 6420.

37. Matsui, S., and Aida, H., Journal of the Chemical Society, Perkin II, 1978, 1277.

38. Khan, M. N., International Journal of Chemical Kinetics, 1987, 19, 143.

39. Hoagland, P. D., and Fox, S. W., Journal of the American Chemical Society, 1967, 89, 1389.

40. Satterthwait, A. C., and Jencks, W. P., Journal of the American Chemical Society, 1974, 96, 7018.

41. Jencks, W. P., and Gilchrist, M., Journal of the American Chemical Society, 1968, 90, 2623.

42. Pohl, E. R., Wu, D., and Hupe, D. J., Journal of the American Chemical Society, 1980, 102, 2759.

43. Hupe, D. J., Wu, D., and Sheppard, P., Journal of the American Chemical Society, 1977, 99, 7659.

44. Khan, M. N., Journal of the Chemical Society, Perkin Transactions II, 1989, 199.

45. Ba-Saif, S., Luthra, A. K., and Williams, A., Journal of the American Chemical Society, 1987, 109, 6362.

46. Ba-Saif, S., Luthra, A. K., and Williams, A., Journal of the American Chemical Society, 1989, 111, 2647.

47. Bender, M. L., Journal of the American Chemical Society, 1951, 73, 1626.

48. McClelland, R. A., and Santry, L. J., Accounts of Chemical Research, 1983, 16, 394.

49. Capon, B., Ghosh, A. K., and Grieve, D. McL. A., Accounts of Chemical Research, 1981, 14, 306.

50. Treffers, H. P., and Hammett, L. P., Journal of the American Chemical Society, 1937, 59, 1708.

51. Ladenheim, H., and Bender, M. L., Journal of the American Chemical Society, 1960, 82, 1895.

52. Olah, G. A., O'Brien, D. H., and White, A. M., Journal of the American Chemical Society, 1967, 89, 5694.

53. Hupe, D. J., and Jencks, W. P., Journal of the American Chemical Society, 1977, 99, 451.

54. Gresser, M. J., and Jencks, W. P., Journal of the American Chemical Society, 1977, 99, 6963.

55. Gresser, M. J., and Jencks, W. P., Journal of the American Chemical Society, 1977, 99, 6970.

56. Castro, E. A., and Santander, C. L., Journal of Organic Chemistry, 1985, 50, 3595.

57. Jencks, W. P., Brant, S. R., Gandler, J. R., Frendrich, G., and Nakamura, C., Journal of the American Chemical Society, 1982, 104, 7045.

58. Ritchie, C. D., Accounts of Chemical Research, 1972, 5, 348.

59. Edwards, J. O., and Pearson, R. G., Journal of the American Chemical Society, 1962, 84, 16.

60. Davies, D. M., and Deary, M. E., Journal of Chemical Research (M), 1988, 2720.

61. Davies, D. M., and Deary, M. E., Journal of Chemical Research (S), 1988, 354.

62. McIsaac, J. E., Subbaraman, L, R., Mulhausen, H. A., and Behrman, E. J., Journal of Organic Chemistry, 1972, 37, 1037.

63. Jencks, W. P., and Gilchrist, M., Journal of the American Chemical Society, 1962, 84, 2910.

64. Davies, D. M., and Jones, P., Journal of Organic Chemistry, 1978, 43, 769.

65. Ballinger, P., and Long, F. A., Journal of the American Chemical Society, 1960, 82, 795.

66. Edwards, J. O., Journal of the American Chemical Society, 1958, 80, 4585.

67. Jencks, W. P., Journal of the American Chemical Society, 1958, 80, 4585.

68. Bruice, T. C., Donzel, A., Huffman, R. W., and Butler, A. R., Journal of the American Chemical Society, 1967, 89, 2106.

69. Dixon, J. E., and Bruice, T. C., Journal of the American Chemical Society, 1972, 94, 2052.

70. DePuy, C. H., Della, E. W., Filley, J., Grabowski, J. J., and Bierbaum, W. M., Journal of the American Chemical Society, 1983, 105, 2481.

71. Buncel, E., and Um, I., Journal of the Chemical Society, Chemical Communications, 1986, 595.

72. Aubort, J. D., and Hudson, R. F., Journal of the Chemical Society, Chemical Communications, 1970, 937.

73. Aubort, J. D., and Hudson, R. F., Journal of the Chemical Society, Chemical Communications, 1970, 938.

74. Aubort, J. D., and Hudson, R. F., Journal of the Chemical Society, Chemical Communications, 1970, 1378.

75. Buncel, E., and Hoz, S., Tetrahedron Letters, 1983, 24, 4777.

76. Hoz, S., Journal of Organic Chemistry, 1982, 47, 3545.

77. Epstein, J., Demek, M. M., and Rosenblatt, D. H., Journal of Organic Chemistry, 1953, 21, 796.

78. Larsson, L., Acta Chemica Scandinavica, 1958, 12, 723.

79. Kirsch, J. F., and Kline, A., Journal of the American Chemical Society, 1969, 91, 1841.

80. Bruice, T. C., and Mayahi, M. F., Journal of the American Chemical Society, 1960, 82, 3067.

81. Jencks, W. P., and Carriulo, J., Journal of the American Chemical Society, 1960, 82, 675.

82. Bunnett, J. F., and Davis, G. T., Journal of the American Chemical Society, 1960, 82, 665.

83. Lowry, T. H., and Richardson, K. S., Mechanism and Theory in Organic Chemistry 3rd Ed, Harper and Row, 1987.

84. Jencks, W. P., Journal of the American Chemical Society, 1972, 94, 4731.

85. Barnett, R. E., and Jencks, W. P., Journal of the American Chemical Society, 1969, 91, 2358.

86. Drake, D., Schowen, R. L., and Jayaraman, H., Journal of the American Chemical Society, 1973, 95, 454.

87. Cox, M. M., and Jencks, W. P., Journal of the American Chemical Society, 1981, 103, 580.

88. Gold, V., Oakenfull, D. G., and Riley, T., Journal of the Chemical Society, 1968, 90, 5839.

89. Showen, R. L., and Behn, C. G., Journal of the American Chemical Society, 1968, 90, 5839.

90. Gopalakrishnan, G., and Hogg, J. L., Journal of Organic Chemistry, 1981, 46, 4959.

91. Khan, M. N., Journal of the Chemical Society, Perkin Transactions II, 1989, 233.

92. Blagoeva, I. B., Pojarlieff, I. G., Tashev, D. T., and Kirby, A. J., Journal of the Chemical Society, Perkin Transactions II, 1989, 347.

93. Hibbert, F., and Spiers, K. J., Journal of the Chemical Society, Perkin Transactions II, 1989, 377.

94. Briffett, N. E., and Hibbert, F., Journal of the Chemical Society, Perkin Transactions II, 1989, 765.

95. Aldersley, M. F., Kirby, A. J., Lancaster, P. W., McDonald, R. S., and Smith, C. R., Journal of the Chemical Society, Perkin Transactions II, 1974, 1487.

96. Frew, J. E., Jones, P., and Scholes, G., Anal Chim. Acta., 1983, 155 139.

97. Eisenberg, G. M., Industrial Engineering in Chemistry, Analytical Edition, 1943, 15, 327.

98. Sellers, R. M., Analyst, 1980, 105, 950.

99. Ogleby, J. W., and Williams, J., Analytical Proceedings, 1985, 22, 181.

100. Greenspan, F. P., and Mackellar, D. G., Analytical Chemistry, 1948, 20, 1061.

101. Hurdis, E. C., and Romeyn, H., Analytical Chemistry, 1954, 26, 320.

102. Sully, B. D., and Williams, P. L., Analyst, 1962, 87, 653.

103. DiFuria, F., Prato, M., Quintily, U., Salvagno, S., and Scorrano, G., Analyst, 1984, 109, 985.

104. Allen, A. O., Hochanadel, C. J., Gomathy, J. A., and Davis, T. W., Journal of Physical Chemistry, 1952, 56, 575.

105. Cohen, I. R., Purcell, T. C., and Altshuler, A. P., Environmental Science and Technology, 1967, 1, 247.

106. Saltzman, E., and Gilbert, N., Analytical Chemistry, 1959, 31, 1914.

107. Purcell, T. C., and Cohen, I. R., Environmental Science and Technology, 1967, 1, 431.

108. Vogel, A. I., Vogel's Macro and Semimicro Qualitative Inorganic Analysis 5th Ed., Longman Inc., New York, 1979.

109. Palmer, D. A., Ramette, R. W., and Mesmer, R. E., Journal of Solution Chemistry, 1984, 13, 673.

110. Brown, J. M., and Darwent, J. R., Journal of the Chemical Society, Chemical Communications, 1979, 171.

111. Evans, D. F., and Upton, M. W., Journal of the Chemical Society, Dalton Transactions, 1985, 1151.

112. Ogata, Y., and Sawaki, Y., Tetrahedron, 1967, 23, 3327.

113. Everett, A. J., and Minkoff, G. J., Transactions of the Faraday Society, 1953, 49, 410.

114. Potts, J. E., and Amis, E. S., Journal of the American Chemical Society, 1948, 71, 2112.

115. Pizer, R., and Tihal, C., Inorganic Chemistry, 1987, 26, 3639.

116. Lee, C. M., and Kumler, W. D., Journal of the American Chemical Society, 1961, 83, 4586.

117. Robin, M. B., Bovey, F. A., and Basch, H., in Zabicky, J., ed., The Chemistry of Amides Part One, Interscience Publishers, London, 1970.

118. Alcock, N. W., Benton, D. J., and Moore, P., Transactions of the Faraday Society, 1979, 66, 2210.

119. Scott, A. I., Interpretation of the UV Spectra of Natural Products, Pergammon Press Ltd., Oxford, 1964.

120. Fishbein, J. C., Baum, H., Cox, M. M., and Jencks, W. P., Journal of the American Chemical Society, 1987, 109, 5790.

121. Yang, C. C., and Jencks, W. P., Journal of the American Chemical Society, 1988, 110, 2972.

122. Pass, G., Ions in Solution 3: Inorganic Properties, Oxford University Press, Oxford, 1973.

123. Crooks, J. E., and Donnellan, J. P., Journal of the Chemical Society, Perkin Transactions II, 1989, 331.

124. Westcott, C. C., pH Measurements, Academic Press, New York, 1978.

125. Albert, A., and Serjeant, E. P., The Determination of Ionisation Constants, Chapman and Hall, London, 1984.

126. Evans, A. G., and Hamann, S. D., Transactions of the Faraday Society, 1951, 47, 34

127. Bunnett, J. F., and Davis, G. T., Journal of the American Chemical Society, 1960, 82, 665.

128. Bender, M. L., and Glasson, W. A., Journal of the American Chemical Society, 1959, 81, 1590.

129. Curci, R., and Edwards, J. O., in Swern, D., ed., Organic Peroxides Vol 1, Wiley Interscience, New York, 1969.

130. Evans, M. G., and Uri, N., Transactions of the Faraday Society, 1949, 45, 224.

131. Reiche, A., and Hitz, F., Berichte Deutschen Chemischen Gesellschaft, 1929, 62, 2458.

132. Rasburn, J., Personal Communication, 1989.

133. Behrman, E. J., Biallas, M. J., Brass, H. J., Edwards, J. O., and Isaks, M., Journal of Organic Chemistry, 1970, 35, 3069.

134. Isaacs, N. S., and Najem, T. S., Journal of the Chemical Society, Perkin Transactions II, 1988, 557.

135. Jennings, R. N., and Capomacchia, A. C., Anal. Chim. Acta, 1988, 207.

136. Castro, E. A., and Ureta, C., Journal of Organic Chemistry, 1989, 54, 2153.

137. Jencks, W. P., and Carriuolo, J., Journal of the American Chemical Society, 1960, 82, 1778.

138. Brass, H. J., Edwards, J. O., and Biallas, M. J., Journal of the American Chemical Society, 1970, 92, 4675.

139. Perrin, D. D., Dempsey, B., and Sejeant, E. P., pKa Prediction for Organic Acids and Bases, Chapman and Hall, London, 1981.

140. Bruice, T. C., and Willis, R. G., Journal of the American Chemical Society, 1965, 87, 531.

141. Warwick International Ltd., Personal communication, 1989.

142. Coffey, S., ed., Rodd's Chemistry of Carbon Compounds, Elsevier, London, 1967.

143. Halonen, A., Heinonen, K., and Visapaa, A., Pap. Puu, 1972, 54 (4A), 165.

144. Harman, R. E., ed., Asymmetry of Carbohydrates, Marcell Dekker Inc., New York, 1976.

145. Doerschuk, A. P., Journal of the American Chemical Society, 1952, 74, 4202.

146. Dick, W. E., Carbohydrate Research, 1972, 21, 255.

147. Rowell, R. M., Carbohydrate Research, 1972, 23, 417.

148. Kamerling, J. P., Shauer, R., Shukla, A. K., Stoll, S., Van Halbeek, H., and Vliegenthart, F. G., Journal of Biochemistry, 1987, 162, 601

149. Williams, H.R., and Mosher, H. S., Journal of the American Chemical Society, 1954, 76, 2984.

ACKNOWLEDGEMENTS

I wish to express my deepest appreciation to Dr Martin Davies for his support, guidance and friendship throughout this work. My sincere thanks are also due to Dr Tony Gradwell, Dr John Townend and Mr Darrel Crowther of Warwick International Ltd. for their stimulating contributions to this research. Finally, I wish to thank Warwick International Ltd. for funding this Research Assistantship.

Appendix 1 Table of data for Figure 1.12: Second order rate constants (k_2) for the reaction of a range of nucleophiles with p-nitrophenylacetate in aqueous solution at 25°C.

Nucleophile	pKa	k_2 / $M^{-1}s^{-1}$	Log k_2	Ref
Peroxybenzoates (PBA)	7.93	92.4	1.966	64
anion of:				
p-OMe-PBA	7.93	92.4	1.966	64
PBA	7.64	74.7	1.873	64
p-Cl-PBA	7.60	67.9	1.832	64
p-SO_3-PBA	7.56	67.1	1.827	64
m-Cl-PBA	7.53	62.6	1.797	64
m-Cl-PBA	7.40	69.7	1.843	62
m-NO_2-PBA	7.23	51.5	1.712	64
p-NO_2-PBA	7.14	47.1	1.673	64
Other peroxides				
anion of:				
HOOH	11.60	3666	3.564	41
MeOOH	11.50	1000	3.000	41
Peracetic acid	8.2	101	2.004	61
Thiols				
anion of:				
$CH_3CH_2CH_2SH$	10.53	29.7	1.473	53
CH_3CH_2SH	10.35	20.5	1.312	53
$HOCH_2CH_2SH$	9.61	12.08	1.082	53
$CH_3OC(O)CH_2CH_2SH$	9.33	11.25	1.051	53
$CH_3OC(O)CH_2SH$	7.91	8.8	0.944	53
CF_3CH_2SH	7.30	1.467	0.166	53
C_6H_5SH	6.43	0.357	-0.447	53
p-$AcNHC_6H_3SH$	6.08	0.138	-0.860	53
3,4-$Cl_2C_6H_3SH$	5.48	4.57×10^{-2}	-1.34	53
2,3,5,6F_4C_6HSH	2.75	1.983×10^{-4}	-3.70	53
F_5C_6SH	2.68	2×10^{-4}	-3.699	53

Appendix 1 continued.

Nucleophile	pKa	k_2 / $M^{-1}s^{-1}$	Log k_2	Ref
Alcohols				
anion of:				
Methanol	15.5	483	2.684	63
2-Chloroethanol	14.31	93.3	1.968	63
Ethanol	16.0	253	2.403	65
$HOCH_2CH_2OH$	15.1	172	2.236	65
$CH_3OCH_2CH_2OH$	14.8	60	1.778	65
$HC{\equiv}CCH_2OH$	13.55	122	2.086	65
F_3CCH_2OH	12.37	52.5	1.720	65
p-$CH_3C_6H_4OH$	10.07	1.883	0.275	41
2,2,3,3-$F_4CH_2CH_2CH_2OH$	12.74	61	1.785	63
$HSCH_2CH_2OH$	9.5	10.33	1.014	63
Phenolate ions				
substituents:				
4-Me	10.20	3.16	0.499	45
4-F	9.95	1.99	0.299	45
H	9.86	1.24	0.093	45
4-Cl	9.38	0.81	-0.092	45
3-Cl	9.02	0.32	-0.495	45
3,4-Cl_2	8.62	0.25	-0.602	45
2-Cl	8.48	0.063	-1.201	45
4-Ac	8.05	0.024	-1.620	45
4-CN	7.95	0.023	-1.638	45
2,3-Cl_2	7.71	0.019	-1.721	45
3,4,5-Cl_2	7.68	0.058	-1.237	45
4-CHO	7.66	0.014	-1.854	45
2,4,5-Cl_3	6.72	0.0084	-2.076	45
2,3,5-Cl_3	6.43	0.0038	-2.42	45
F_5	5.49	$6.4x10^{-4}$	-3.194	45
2,3,5,6-F_4	5.53	$9.2x10^{-4}$	-3.036	45
2,3,4,5-Cl_4	5.64	0.0012	-2.908	45

Appendix 1 continued.

Nucleophile	pKa	k_2 / $M^{-1}s^{-1}$	Log k_2	Ref
Other oxygen nucleophiles				
anion of:				
H_2O	15.75	9.5	0.978	41
$(CF_3)_2C(OH)_2$	6.45	$3.3x10^{-5}$	-4.48	57
$(CHF_2)_2C(OH)_2$	8.90	$1.3x10^{-3}$	-2.886	57
$(CF_3)_2CHOH$	9.22	2.1	0.322	57
$CH_3(CF_3)C(OH)_2$	10.45	$4.2x10^{-3}$	-2.377	57
Potassium carbonate	10.4	$1.76x10^{-2}$	-1.75	57
Primary amines				
Ethylamine	10.97	16	1.204	41
Propylamine	10.98	16	1.204	41
Ethylenediamine	10.18	8.93	0.951	41
Methoxyethylamine	9.72	2.667	0.426	41
Glycine	9.76	2.583	0.412	41
Glyglycine	8.25	0.172	-0.764	41
Glycine ethylester	7.90	0.067	-1.174	41
Ethylenediamine-H^+	7.42	0.0933	-1.030	41
Trifluoroethylamine	5.84	$7x10^{-4}$	-3.155	41
Aniline	4.85	$1.83x10^{-4}$	-3.74	41
Hydrazine	8.20	7.5	0.875	41
Semicarbazide	11.42	48.3	1.684	41
Secondary amines				
Piperidine	11.42	48.3	1.684	41
Piperazine	10.10	7.167	0.855	41
Morpholine	8.87	0.633	-0.198	41
Piperazine-H^+	6.01	$2.083x10^{-3}$	-2.68	41
Tertiary anines				
Imidazole	7.21	0.583	-0.234	41
Pyridine	5.52	$2.833x10^{-3}$	-2.55	41

Appendix 2 Program listing: Numerical solution of differential equations corresponding to Scheme 3.2, which pertains to the reactions occurring upon mixing solutions of hydrogen peroxide and p-nitrophenylacetate in a pH 6.80 phosphate buffer at 25°C.

```
10 CLEAR @ DISP "Large or Small
   Paper size? (L/S)"
11 INPUT S$
12 IF S$<>"S" AND S$<>"L" THEN
   GOTO 10
15 DISP "Value for dT?"
16 INPUT D2
20 DISP "Every Nth calculation
   will be   used. Value for N?
   "
21 INPUT N9
25 DISP "Output to printer ?(Y/
   N)"
26 INPUT P$
27 IF P$="Y" THEN PRINTER 2 @ G
   OTO 100
28 IF P$="N" THEN PRINTER 1 @ G
   OTO 100
29 GOTO 25
100 A8=0 ! PNP
200 B8=.0008698 ! PNPA
300 C8=0 ! H202
400 D8=.0018 ! PA
500 E8=0 ! DAP
600 K0=.000007323 ! PNPA+H20
700 K1=.05564 ! PNPA+H202=PA+PNP
800 K2=0 ! PNPA+H202=XX+PNP
900 K3=3.8716 ! PNPA+PA
910 K4=.4898 ! DAP+H202
920 K5=.0001584 ! DAP+H20
925 K6=0 ! PA+H202
1000 PLOTTER 705
1049 PRINT "K0  =";K0
1050 PRINT "K1  =";K1
1052 PRINT "K2  =";K2
1053 PRINT "K3  =";K3
1054 PRINT "K4  =";K4
1055 PRINT "K5  =";K5
1056 PRINT "DT  =";D2
1057 PRINT "PNPA=";B8
1058 PRINT
1200 N=0 @ T=0
1290 ON KEY# 1 GOTO 3000
1300 PRINT "T=";T
1301 PRINT "PNP=";A8
1302 PRINT "H202+PA=";C8+D8
1303 PRINT "H202=";C8
1304 PRINT "PA=";D8
1305 PRINT "DAP=";E8
1350 PRINT "▒▒▒▒▒▒▒▒Press k1  to
   stop▒▒▒▒▒▒▒▒"
1360 PRINT
1400 A9=(K0+(K1+K2)*C8+K3*D8)*B8
1401 A9=A8+A9*D2
1500 B9=(K0+(K1+K2)*C8+K3*D8)*B8
1501 B9=B8-B9*D2
1600 C9=C8-((K1+2*K2)*C8*B8+K4*E
   8*C8+K6*C8*D8)*D2
```

```
1700 D9=D8+(K1*B8*C8-K3*B8*D8+2*
     K4*E8*C8+K5*E8-K6*C8*D8)*D2
1800 E9=E8+(K3*B8*D8-K4*E8*C8-K5
     *E8)*D2
1900 T=T+D2
2000 A8=A9 @ B8=B9 @ C8=C9 @ D8=
     D9 @ E8=E9
2100 N=N+1 @ IF INT(N/N9)-N/N9=0
      THEN GOTO 1300
2200 GOTO 1400
3000 DISP @ DISP @ DISP
3010 DISP "Min, max values for x
      axis?"
3020 INPUT X1,X2
3030 DISP @ DISP "Min,max values
      for y axis?"
3040 INPUT Y1,Y2
3045 PLOTTER 705
3047 IF S$="S" THEN SCALE X1,3*X
     2/2,Y1,Y2 @ GOTO 3055
3050 SCALE X1,X2,Y1,Y2
3055 GOTO 4000
3060 XAXIS Y1,N9*D2,X1,X2
3070 YAXIS X1,(Y2-Y1)/10,Y1,Y2
3080 MOVE 0,0
3090 LABEL @ LABEL X1
3095 LABEL
3100 MOVE (X2-X1)/2-(X2-X1)*.025
      .0
3110 LABEL @ LABEL (X2-X1)/2
3120 MOVE X2-(X2-X1)*.07,0 @ LAB
     EL @ LABEL X2
3130 FOR Y=0 TO 10
3140 MOVE 0,Y*((Y2-Y1)/10)
3150 LDIR 3*PI/2
3160 LABEL @ LABEL @ LABEL @ LAB
     EL @ LDIR 0
3162 L=Y1+Y*((Y2-Y1)/10)
3163 IF LEN(VAL$(L))>8 THEN L=IN
     T(L*10^7+.5)/10^7
3164 LABEL L
3170 NEXT Y
3180 MOVE (X2-X1)/2-(X2-X1)/4*(S
     $="S"),0
3190 LABEL @ LABEL @ LABEL @ LAB
     EL "Time (seconds)"
3200 MOVE 0,(Y2-Y1)/2 @ LDIR 3*P
     I/2
3210 LABEL @ LABEL @ LABEL @ LAB
     EL @ LABEL @ LDIR PI/2 @ LA
     BEL "Concentration (M)"
3220 DISP "Title of graph?"
3230 INPUT T$
3240 IF T$="" THEN GOTO 4000
3250 MOVE (X2-X1)/3,Y2
3260 LDIR PI
3270 LABEL
3275 LDIR 0
3280 LABEL T$
3290 LDIR PI
```

```
3300 LABEL
3310 LDIR 0
3315 U$=""
3320 FOR I=1 TO LEN(T$)
3330 U$=U$&"_"
3340 NEXT I
3350 LABEL U$
4000 N=X2/(N9*D2)
4010 CHAIN "NEWDRAW"
9999 END
```

Program notes: The program initially asks for a time interval, dT, to be used in the calculations, and a value for N, whereby concentrations calculated for every Nth iteration are reported. Lines 100 to 925 set the initial conditions for the program, based on the experimental conditions used. Variables A8 to E8 are the initial concentrations of the principal species involved in the system, and variables K0 to K6 are the experimentally determined rate constants pertaining to reactions involving these species. K2 and K6 refer to rate constants for hypothesised reactions involving peroxide decomposition - peroxide decomposition was observed to occur during some of the experimentals (see Figures 3.21 to 3.23). The variables K2 and K6 were set at zero for the plots shown in Figures 3.19 to 3.23. Lines 1000 to 1058 output to printer the rate constants used during the program. Lines 1290 to 1360 outputs to printer the concentrations of the principal species at the end of every Nth iteration (key k1 is pressed to end the iterative process and output the data to plotter). Lines 1400 to 2000 calculate the concentration changes over the period dT for each of the principal species. Lines 3000 to 3290 set up the parameters for output of the data to the plotter so that the computer generated curves can be compared with actual data points as in Figures 3.19 to 3.23. Line 4000 chains the 'Newdraw' program which actually plots the curves.

Appendix 3 Copies of publications:

Davies, D. M., and Deary, M. E., Determination of Peracids in the Presence of a Large Excess of Hydrogen Peroxide Using a Rapid and Convenient Spectrophotometric Method, Analyst, 1988, 113, 1477.

Davies, D. M., and Deary, M. E., Kinetics of the Perhydrolysis of p-Nitrophenylacetate and the Formation, Hydrolysis, and Perhydrolysis of Diacetyl Peroxide, Journal of Chemical Research (S), 1988, 354.

Davies, D. M., and Deary, M. E., Iodimetric Method for Measuring Low Concentrations of Diacetyl Peroxide, Using Hydrogen Peroxide as a Catalyst, Analytical Proceedings, 1989, Nov., 367.

Determination of Peracids in the Presence of a Large Excess of Hydrogen Peroxide Using a Rapid and Convenient Spectrophotometric Method

D. Martin Davies* and Michael E. Deary
Department of Chemical and Life Sciences, Newcastle upon Tyne Polytechnic, Newcastle upon Tyne NE1 8ST, UK

Peracids can be determined in the presence of up to a 1000-fold excess of hydrogen peroxide by taking advantage of the much greater rate of reaction of the peracid with iodide. A fast, convenient and accurate spectrophotometric method is described that involves a simple linear extrapolation. The effects of a number of experimental variables on the accuracy, precision, sensitivity and selectivity of the method are described. The method has been applied to the determination of the peracetic acid formed during the perhydrolysis of *p*-nitrophenyl acetate.

Keywords: *Peracid determination; iodimetry; spectrophotometry; hydrogen peroxide*

Two methods are widely used to determine peracids in the presence of hydrogen peroxide. In the method of Greenspan and Mackellar[1] the hydrogen peroxide is first titrated with cerium(IV) sulphate and the residual peracid is then determined iodimetrically. The alternative method of Sully and Williams[2] utilises the much greater reactivity of iodide with peracid than with hydrogen peroxide. The liberated iodine is titrated with thiosulphate over a period of several minutes and the linear graph of titre *versus* time is extrapolated back to zero time to give a value, corrected for the slow reaction of hydrogen peroxide, which corresponds to the peracid. Recently, a gas - liquid chromatographic method,[3] based on the differential rate of oxidation of methyl *p*-tolyl sulphide by peracids and hydrogen peroxide, has been used to determine peracid concentrations in the presence of up to a 100-fold excess of hydrogen peroxide.

The spectrophotometric determination of I_3^- greatly enhances the sensitivity of the iodide-reduction methods used for peroxide determination.[4–7] Kinetic spectrophotometry has been used to determine mixtures of peroxides by following the release of I_3^- to completion and analysing the time course graphically.[7,8]

This paper describes a convenient and rapid spectrophotometric method for the determination of peracids in the presence of up to a 1000-fold excess of hydrogen peroxide. The method is analogous to the titrimetric method of Sully and Williams[2] and involves extrapolation of the absorbance change, due to the initial rate of the reaction between hydrogen peroxide and iodide, back to zero time to give a value that corresponds to the iodine formed from the reaction of the peracid with iodide.

The proposed method has been used to monitor the formation of peracetic acid during the perhydrolysis of *p*-nitrophenyl acetate.

Experimental

Apparatus

Absorbance measurements were made at 25 °C using a Hewlett Packard HP 8451A diode array spectrophotometer fitted with a 290-nm UV cut-off filter and thermostated cell holder.

Reagents

Analytical-reagent grade chemicals were used wherever possible. AnalaR (BDH) potassium iodide was recrystallised from distilled water. All solutions were prepared in distilled water. Solution A contained 6.6 g l^{-1} of potassium iodide and 2 g l^{-1} of sodium hydroxide. Solution B contained 20 g l^{-1} of potassium hydrogen phthalate.

m-Chloroperbenzoic acid (MCPBA) was dissolved in distilled water and filtered using a No. 4 sinter to give an approximately 5 mM stock solution. The peracid stock solution was assayed before use as follows. To a 5-ml aliquot of the MCPBA solution was added 10 ml of solution B and 5 ml of a 10 g l^{-1} potassium iodide solution and the liberated iodine was titrated with 0.0100 M sodium thiosulphate. Hydrogen peroxide, 30%, was determined cerimetrically.[9] Aliquots of hydrogen peroxide and of the peracid stock solution were mixed with water containing ethylenediaminetetramethylenephosphonic acid (EDTMP) in a calibrated flask and diluted to the mark to give sample solutions containing 0.1–1.4 mM peracid, up to 0.2 M hydrogen peroxide and 1 μM EDTMP.

Assay

A 0.1-ml aliquot of the sample solution is added to a 1-cm cuvette containing 1 ml of solution A and 1 ml of solution B and the timer on the spectrophotometer is started simultaneously. The cuvette is quickly stoppered and shaken and the liberated iodine is measured at $\lambda_{max.}$ = 352 nm for 0.1 s every 1.0 s for a total of 5 s. The absorbance at zero time is calculated by regression analysis, assuming a linear relationship between absorbance and time. The concentration of peracid is calculated from the absorbance at zero time using an apparent molar absorptivity of 24 100 l mol^{-1} cm^{-1}.

Results and Discussion

Experimental Procedure

The interval between starting the timer and taking the first absorbance reading is about 12 s. For peracid samples containing no hydrogen peroxide, the slope of a graph of absorbance *versus* time is zero. This shows that the reaction between the peracid and iodide is complete before the first absorbance measurement is made. It is essential to use the 290 nm cut-off filter with the diode array spectrophotometer otherwise UV radiation causes photo-oxidation of the iodide and a significant increase in absorbance with time.

An apparent molar absorptivity of 24 100 l mol^{-1} cm^{-1} at 352 nm is obtained for the iodine liberated by peracid samples of known concentration, and which contain no hydrogen peroxide.

Table 1 shows the linear response of the method. The presence of reducing impurities in the iodide, however, causes

* To whom correspondence should be addressed.

Table 1. Determination of *m*-chloroperbenzoic acid (MCPBA) in the presence of hydrogen peroxide; response of the assay. Concentrations in the cuvette: H_2O_2, 2.51 mM; KI, 3.1 g l^{-1}

10^5 [MCPBA]*/M†	98% Confidence limits‡ of 10^5 [MCPBA]/M
0.49	0.49 ± 0.01
0.98	0.97 ± 0.01
1.96	1.94 ± 0.01
2.83	2.96 ± 0.02
3.93	3.89 ± 0.04
4.92	4.89 ± 0.05
5.90	5.89 ± 0.07
6.88	6.83 ± 0.12

* Concentrations are those in the cuvette.
† Prepared by mixing known volumes of titrated solutions of MCPBA and H_2O_2.
‡ $n = 5$.

Table 2. Determination of MCPBA in the presence of hydrogen peroxide: effect of hydrogen peroxide concentration and amount of potassium iodide used

Ratio of $[H_2O_2]$ to [MCPBA]	10^5 [MCPBA]/M	98% Confidence limits of 10^5 [MCPBA]/M: Assay 3.1 g l^{-1} of KI	98% Confidence limits of 10^5 [MCPBA]/M: Alternative 31 g l^{-1} of KI
0	1.05	1.05 ± 0.01	1.06 ± 0.01
4.0	1.05	1.06 ± 0.01	1.08 ± 0.01
10.5	1.05	1.06 ± 0.01	1.10 ± 0.02
21.4	1.05	1.07 ± 0.01	1.14 ± 0.02
54	1.05	1.06 ± 0.02	1.17 ± 0.06
99	1.04	1.04 ± 0.05	1.23 ± 0.06
217	1.03	1.07 ± 0.05	—
530	1.03	1.12 ± 0.03	—
1050	1.03	1.06 ± 0.05	—

a fixed negative bias (results not shown). We found it necessary to recrystallise the AnalaR potassium iodide supplied by BDH, whereas a sample of the material supplied by Sigma was free of reducing impurities.

Table 2 shows that the assay is accurate, within experimental error, for ratios of hydrogen peroxide to peracid of up to 1000. The precision of the method is less at the higher ratios of hydrogen peroxide to peracid. The random error involved in starting the timer causes an error in the calculated absorbance at zero time; this error is larger at the higher hydrogen peroxide concentrations at which the change of absorbance with time is also larger.

If the time interval between starting the timer and taking the first absorbance reading is appreciably greater than about 12 s or if absorbance readings are taken for much longer than 5 s, then at high ratios of hydrogen peroxide to peracid a positive systematic error in the measured peracid concentration occurs (data not shown, but see below). This is because the measured absorbance change no longer represents adequately the initial rate of the reaction of hydrogen peroxide with iodide.

The proposed method is easily modified to allow the use of larger sample volumes of more dilute peracids. However, the concentration of iodide in the cuvette should always be 3.1 g l^{-1}.

Effect of Iodide Concentration and Catalyst

The apparent molar absorptivity of the liberated iodine depends on the concentration of iodide used in the assay (see Table 3); this effect has been observed previously.[7] The results obtained in this work are consistent with the reported[10] equilibrium constant for the formation of I_3^- from I_2 and I^-. Table 3 also gives the slightly different molar absorptivities obtained for MCPBA and hydrogen peroxide when assay solution A is replaced by solutions containing 2 g l^{-1} of sodium

Table 3. Apparent molar absorptivities (ε)

	ε*/l mol^{-1} cm^{-1}			
	MCPBA			
KI†/g l^{-1}	Uncatalysed	Catalysed	H_2O_2 Catalysed	Reference
3.1	24 100	24 400	23 700	This work
10‡	26 200	28 800	27 000	Reference 5
13	—	—	25 000	Reference 4
13	—	—	23 000	Reference 6
31	26 100	26 500	25 800	This work

* Determined in potassium hydrogen phthalate buffer unless stated otherwise.
† Concentrations are those in the cuvette.
‡ Potassium dihydrogen phosphate - disodium hydrogen phosphate buffer.

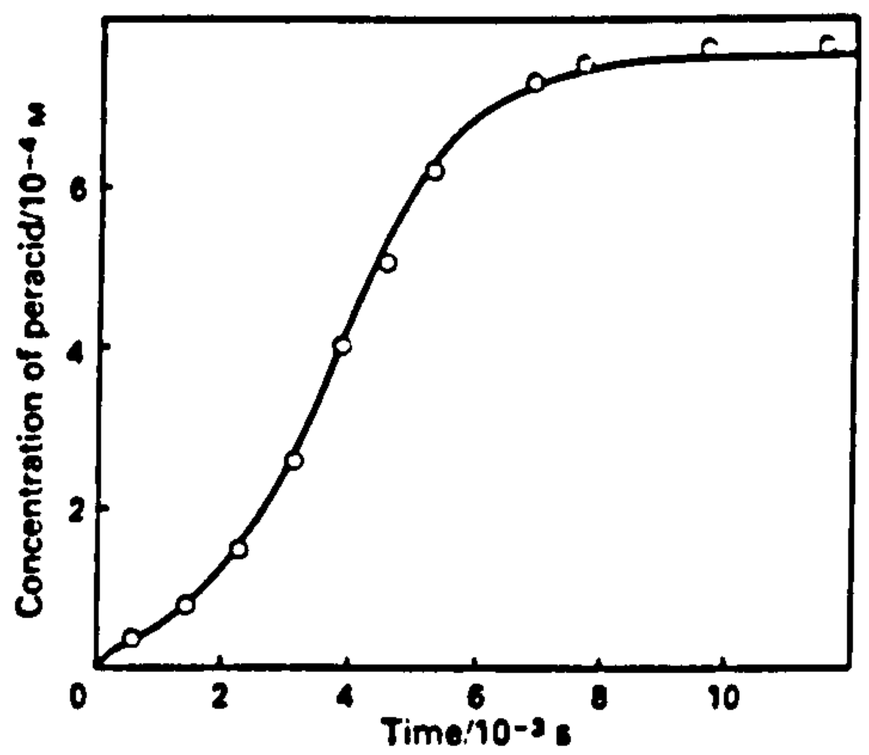

Fig. 1. Formation of peracetic acid during the perhydrolysis of *p*-nitrophenyl acetate. Concentrations are calculated from independently determined rate constants and data points are corrected for the assay dilution factor. Phosphate buffer, 0.1 M at 25 °C; pH = 6.8; $[H_2O_2]_0$ = 2.02 mM; and [PNPA]$_0$ = 0.91 mM

hydroxide, 0.2 g l^{-1} of ammonium heptamolybdate catalyst and either 6.6 or 66 g l^{-1} of potassium iodide. Similar effects have been observed previously.[5]

A set of results from an assay procedure in which solution A was replaced by an alternative solution containing ten times as much iodide is shown in Table 2. A positive systematic error occurs at the higher hydrogen peroxide to peracid ratios. This is because at the higher iodide concentration the time course of the reaction of hydrogen peroxide is faster and the initial rate phase of the reaction is complete before the first absorbance measurement has been made.

Application

The method was used to determine the concentration of the peracetic acid formed during the perhydrolysis of *p*-nitrophenyl acetate (PNPA). The absorbance readings were corrected for the background due to PNPA and *p*-nitrophenol, which was measured by adding the sample to a cuvette containing 1 ml of a 2 g l^{-1} sodium hydroxide solution and 1 ml of solution B. The sigmoidal-shaped curve shown in Fig. 1 is obtained. This is because[11] the peracetic acid formed initially reacts further with PNPA to form diacetyl peroxide, which ultimately reacts with hydrogen peroxide to yield two moles of peracetic acid. Hence, the perhydrolysis of PNPA is autocatalytic. A small amount of acetate is also formed owing to hydrolysis of PNPA and diacetyl peroxide. The agreement between the measured peracid concentration and that calculated using the rate constants for the individual reactions, determined independently,[11] confirms the validity of the proposed method and illustrates its utility.

We thank Warwick International Ltd. for funding a Graduate Research Assistantship (to M. E. D.).

References

1. Greenspan, F. P., and Mackellar, D. G., *Anal. Chem.*, 1948, 20, 1061.
2. Sully, B. D., and Williams, P. L., *Analyst*, 1962, 87, 653.
3. Di Furia, F., Prato, M., Quintily, U., Salvagno, S., and Scorrano, G., *Analyst*, 1984, 109, 985.
4. Allen, A. O., Hochanadel, C. J., Gomathy, J. A., and Davis, T. W., *J. Phys. Chem.*, 1952, 56, 575.
5. Cohen, I. R., Purcell, T. C., and Altshuller, A. P., *Environ. Sci. Technol.*, 1967, 1, 247.
6. Frew, J. E., Jones, P., and Scholes, G., *Anal. Chim. Acta*, 1983, 115, 139.
7. Saltzman, E., and Gilbert, N., *Anal. Chem.*, 1959, 31, 1914.
8. Purcell, T. C., and Cohen, I. R., *Environ. Sci. Technol.*, 1967, 1, 431.
9. Hurdis, E. C., and Romeyn, H., *Anal. Chem.*, 1954, 26, 320.
10. Palmer, D. A., Ramette, R. W., and Mesmer, R. E., *J. Solution Chem.*, 1984, 13, 673.
11. Davies, D. M., and Deary, M. E., *J. Chem. Res.*, submitted for publication.

Paper 8/00885J
Received March 7th, 1988
Accepted May 9th, 1988

Kinetics of the Perhydrolysis of *p*-Nitrophenyl Acetate and the Formation, Hydrolysis, and Perhydrolysis of Diacetyl Peroxide

J. Chem. Research (S), 1988, 354-355
J. Chem. Research (M), 1988, 2720-2736

D. Martin Davies* and Michael E. Deary

Department of Chemical and Life Sciences, Newcastle upon Tyne Polytechnic, Newcastle upon Tyne NE1 8ST, U.K.

Hydrogen peroxide bleach activators which contain an acyl functional group are of commercial interest. We have used *p*-nitrophenyl acetate (PNPA) as a model bleach activator because the *p*-nitrophenoxide leaving group is stable with respect to oxidation and, owing to its yellow colour, is easily measured spectrophotometrically without interference from peroxide species, which absorb only in the u.v. region.

Figure 1 shows the result of mixing H_2O_2 and PNPA in a

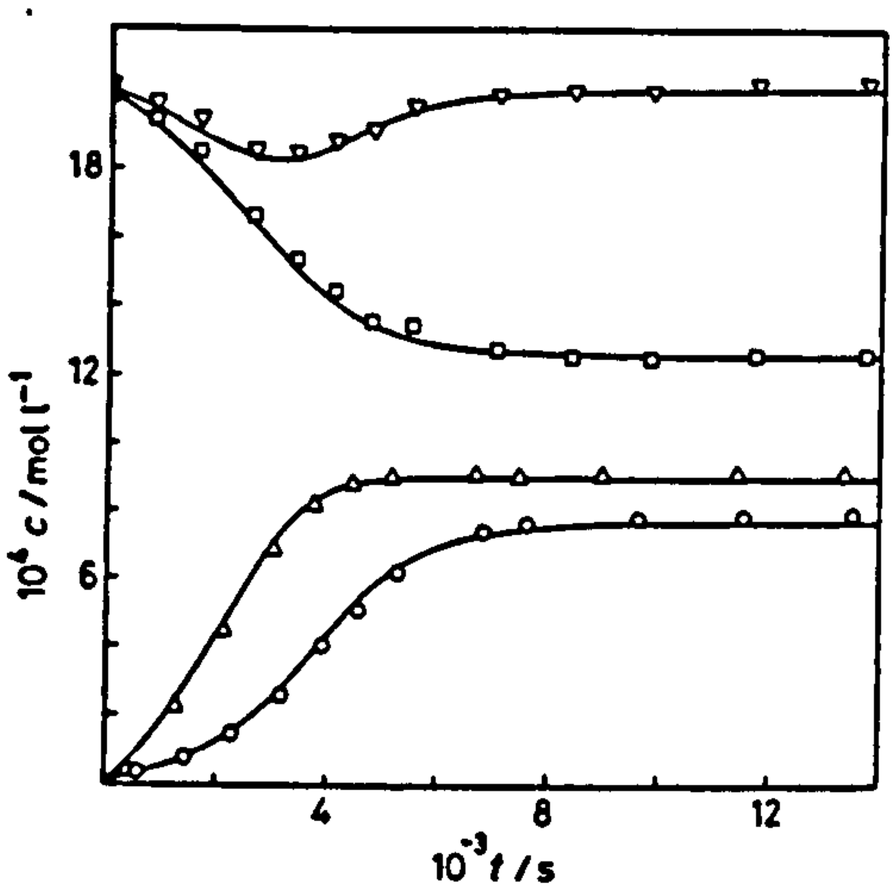

Figure 1 Change in the concentrations of: peracetic acid plus H_2O_2, ▽; peracetic acid, ○; H_2O_2 calculated from the previous concentrations, □; and *p*-nitrophenol, △: $[H_2O_2]_o$, 2.02×10^{-3} mol l^{-1}; $[PNPA]_o$, 9.10×10^{-4} mol l^{-1}; phosphate buffer pH 6.8, ionic strength 0.1 mol l^{-1} containing 1×10^{-5} mol l^{-1} EDTA; 25°C

2:1 mol ratio. Peroxide concentrations were measured iodometrically using a recently developed[7] spectrophotometric method. The lag in the formation of peracetic acid and the trough in the concentration of the iodide-reactable peroxide plot indicates that a less reactive peroxide is formed as an intermediate. Figure 2 shows that when peracetic acid and PNPA are mixed in a 2:1 mol ratio, a rapid loss of peracid and corresponding release of *p*-nitrophenol occurs, followed by a gradual regeneration of peracetic acid back to its original concentration. If H_2O_2 is added to the reaction solution after the peracid concentration has reached the minimum, then the rate of formation of peracetic acid is greater than the rate of its regeneration in the absence of H_2O_2 (Figure 3). Moreover, as shown in Figure 3, the peracetic acid concentration reaches an infinity value greater than the original peracid concentration, corresponding to the equation

$$[\text{peracid}]_\infty = [\text{peracid}]_o + 2([\text{peracid}]_{orig} - [\text{peracid}]_o)$$

in which the subscripts ∞, o, and orig indicate the final concentration, the concentration at any time after addition of hydrogen peroxide, and the original concentration (corrected for dilution by the addition of hydrogen peroxide) respectively.

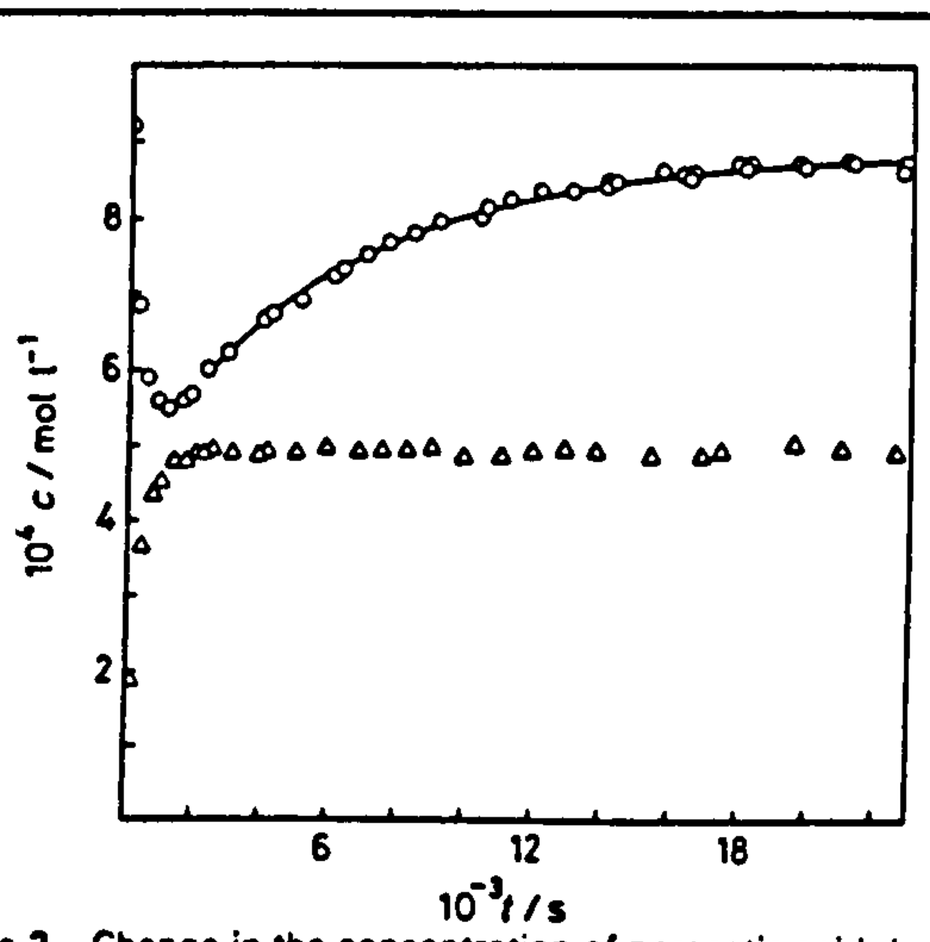

Figure 2 Change in the concentration of peracetic acid during and after its reaction with PNPA: peracetic acid, ○; *p*-nitrophenol, △: [peracetic acid]$_o$, 9.2×10^{-4} mol l^{-1}; [PNPA]$_o$, 4.9×10^{-4} mol l^{-1}; buffer as Figure 1. The curve represents the best fit to an exponential equation with [peracetic acid]$_\infty$, 8.81×10^{-4} mol l^{-1} and a pseudo-first-order rate constant, 1.72×10^{-4} s^{-1}

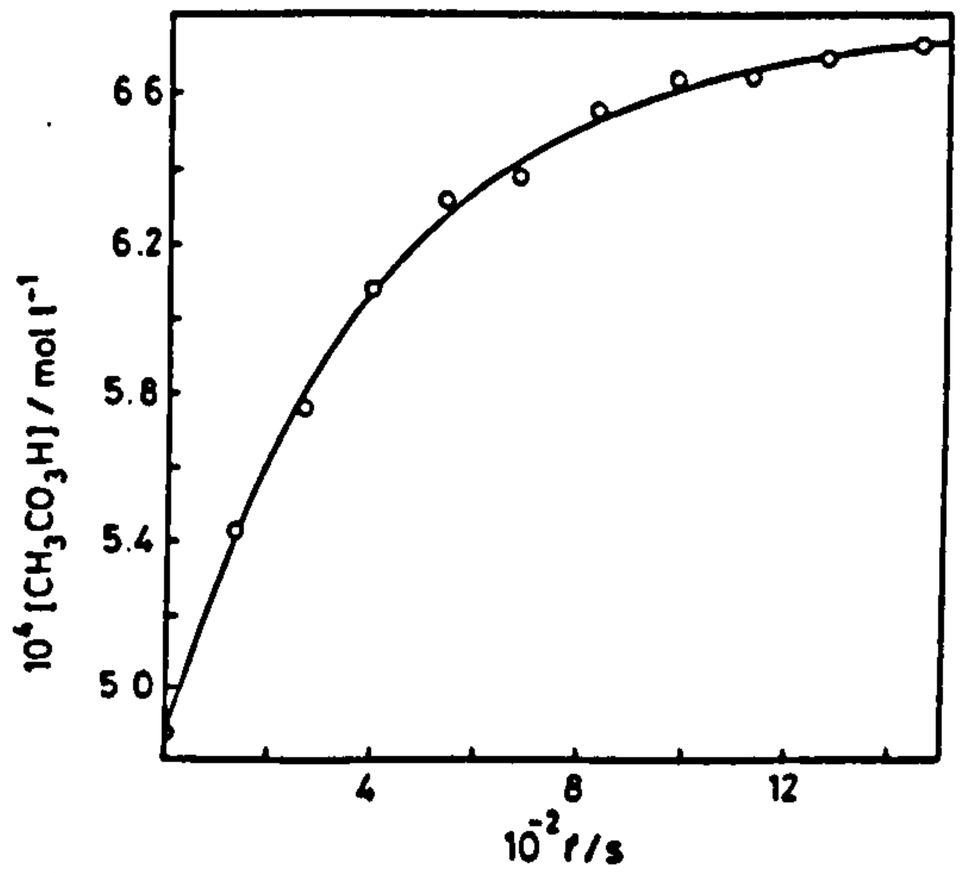

Figure 3 Increase in the concentration of peracetic acid after addition of excess H_2O_2, 5.06×10^{-3} mol l^{-1}, to diacetyl peroxide preformed from the reaction of PNPA and 5.58×10^{-4} mol l^{-1} peracetic acid; buffer as Figure 1. The curve represents the best fit to an exponential equation with [peracetic acid]$_\infty$, 6.77×10^{-3} mol l^{-1} and a pseudo-first-order rate constant, 2.49×10^{-3} s^{-1}

The above results are consistent with the reaction pathways shown in the Scheme, in which diacetyl peroxide is the intermediate. A similar reaction scheme has been suggested for the perhydrolysis of a surfactant *p*-nitrophenyl ester.[4]

The rate constants, shown in the Table, for the hydrolysis (k_o), perhydrolysis, and peracylation (k_{obs}: H_2O_2 and peracetic acid, respectively, in large excess) of PNPA were obtained by measuring spectrophotometrically the release of *p*-nitrophenol. The rate constants for the hydrolysis (k_o) and perhydrolysis (k_{obs}: H_2O_2 in large excess) of diacetyl peroxide were obtained by measuring the release of peracetic

*To receive any correspondence.

Table First-order rate constants (k_c) for the hydrolysis of PNPA and diacetyl peroxide and second-order rate constants (k_{obs}) for the reaction of PNPA with hydrogen peroxide and peroxyacetic acid and the reaction of diacetyl peroxide with hydrogen peroxide

Acyl species	Nucleophile	Buffer	pH	Ionic strength (mol l^{-1})	10^5[Acyl]$_o$ (mol l^{-1})	10^4[nucleophile] range (mol l^{-1})	k_c/s^{-1}	k_{obs}/l mol^{-1} s^{-1} [a]	k/l mol^{-1} s^{-1}
PNPA	Buffer	Phosphate	6.8	0.02	8.3	—	5.55×10^{-6}	—	—
PNPA	Buffer	Phosphate	6.8	0.10	10.9	—	7.32×10^{-6}	—	—
PNPA	HOO^-	Phosphate	6.8	0.02	8.3	360-1800	—	$(4.97 \pm 0.13) \times 10^{-2}$	3140
PNPA	HOO^-	Phosphate	6.8	0.10	10.9	170-960	—	$(5.61 \pm 0.14) \times 10^{-2}$	3540
PNPA	HOO^-	Borate	9.25	0.10	1.0	3.0-50	—	3.84 ± 0.26	862
PNPA	HOO^-	Carbonate	10.0	0.10	1.0	1.3-10	—	92.7 ± 5.36	3785
PNPA	$CH_3CO_3^-$	Phosphate	6.8	0.02	8.3	8-15	—	3.98 ± 0.16	104
PNPA	$CH_3CO_3^-$	Phosphate	6.8	0.10	9.1	14-37	—	3.94 ± 0.03	103
$(CH_3CO_2)_2$	Buffer	Phosphate	6.8	0.02	44	—	9.69×10^{-5}	—	—
$(CH_3CO_2)_2$	Buffer	Phosphate	6.8	0.10	20	—	16.5×10^{-5}	—	—
$(CH_3CO_2)_2$	HOO^-	Phosphate	6.8	0.02	44	44-120	—	0.358 ± 0.015	22600
$(CH_3CO_2)_2$	HOO^-	Phosphate	6.8	0.10	20	48-110	—	0.509 ± 0.028	32100

[a] 90% Confidence limit.

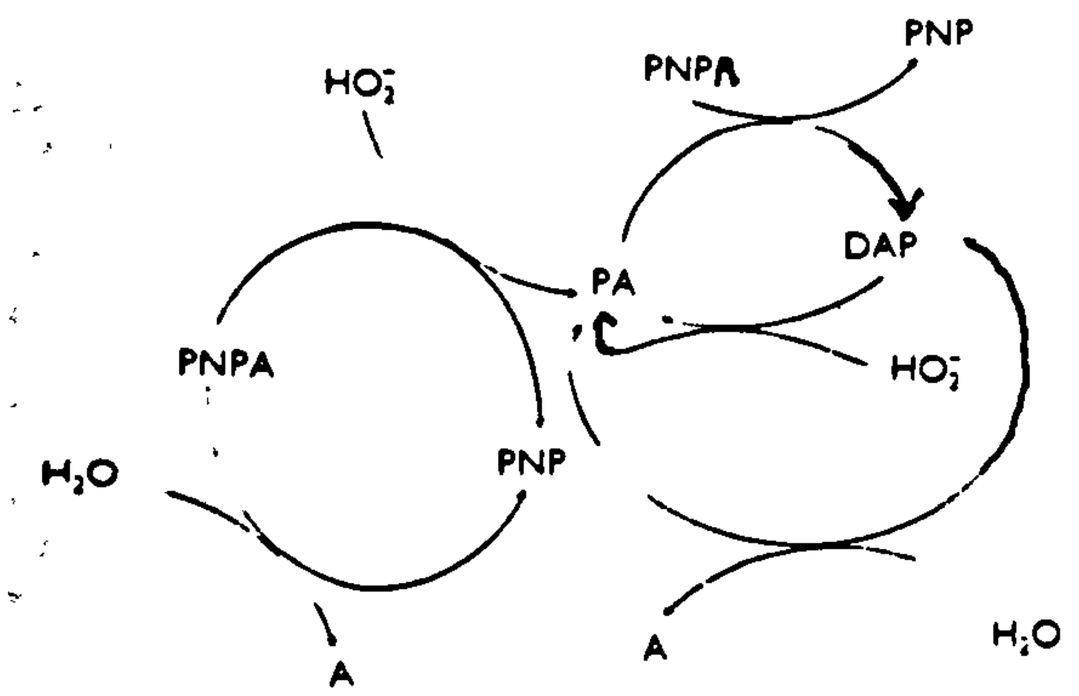

Scheme PNP = *p*-Nitrophenoxide; PA = peracetate; A = acetate; DAP = diacetyl peroxide

acid. The curves in Figure 1 represent the numerical solution of the differential rate equations corresponding to the Scheme. The agreement of the calculated concentrations with those observed indicates that the pathways shown in the Scheme completely describe the experimental system.

The rate constants k, shown in the Table, are calculated for the dependence on the concentration of the nucleophilic species, HO_2^-, and peracetate, using the pK_a values of H_2O_2 and peracetic acid. The findings in a variety of buffer systems are summarized as follows. The perhydrolysis of PNPA and diacetyl peroxide shows small but significant phosphate buffer effects whereas the peracylation of PNPA does not. It is likely that phosphate stabilizes the activated complex formed during hydrolysis by interacting with the hydrogen of HO_2^-. Rate constants for the perhydrolysis of PNPA in carbonate buffer are quite similar to those in phosphate but rate constants in borate buffer are about four times lower than those in phosphate. The low rate of perhydrolysis of PNPA in borate buffer can be explained by the formation of unreactive $(HO)_3BOOH^-$. Thus, using a recently determined[11] formation constant for $(HO)_3BOOH^-$ to calculate the concentration of HO_2^-, a rate constant of 3920 l mol^{-1} s^{-1}, which is quite similar to those found with the other buffers, is obtained.

The ratio of the rate constants in phosphate buffer, ionic strength 0.1 mol dm^{-3}, for the hydrolysis of diacetyl peroxide (after correction for the statistical factor) and PNPA is 11.2 and that for perhydrolysis of diacetyl peroxide (after correction, in addition, for the stoicheiometry) and PNPA is 2.2. Thus the hydrolysis and perhydrolysis reactions of diacetyl peroxide are faster than the corresponding reactions of PNPA, despite the fact that the pK_a of the parent acid of the peracetate leaving group is higher than that of *p*-nitrophenoxide. Acid anhydrides, however, are more reactive than the corresponding esters[14] and the rates of substitution on the carbonyl carbon of diacyl peroxides should parallel those for analogous anhydrides.

We thank Warwick International Limited for funding a Graduate Research Assistantship (to M. E. D.).

Techniques used: Spectrophotometry, iodometry

References: 14

Tables: 1

Figures: 3

Received, 7th March 1988; Paper E/8/03064B

References cited in this synopsis

4 J. M. Brown and J. R. Derwent, *J. Chem. Soc., Chem. Commun.*, 1979, 171.
7 D. M. Davies and M. E. Deary, *The Analyst*, 1988, 113, 1477.
11 R. Pizer and C. Tihal, *Inorg. Chem.*, 1987, 26, 3639.
14 J. F. Kirsch and W. P. Jencks, *J. Am. Chem. Soc.*, 1964, 86, 837.

the pH of the injected solution. The signals obtained when phosphate buffers with pH values above and below that of the carrier stream were injected are shown in Fig. 7. The effect of injecting 0.01 M potassium chloride solutions of various acidities into a neutral 0.01 M potassium chloride carrier stream is shown in Fig. 8. Injection of alkaline solutions dissolves the modifying surface.

Discussion

The studies so far indicate that 12-molybdophosphate is more readily reduced at a glassy carbon electrode having a film of reduced molybdophosphate than it is at a freshly polished electrode. To determine molybdate at this electrode, however, would require very close matching of the pH of the carrier stream and the injectate.

A further anomaly in this study is the fact that 12-molybdophosphate in the presence of excess of phosphate is not reduced to any great extent at +0.2 V as is the case when molybdate is in excess. This may mean that in the phosphate buffer solutions the major species present is not 12-molybdophosphate but another phosphate - molybdate species.

RZ thanks the Government of the People's Republic of China for financial support and leave of absence.

References

1 Fogg, A. G., and Bselsu, N. K., *Analyst*, 1982, 107, 560.
2 Fogg, A. G., and Alonso, R. M., *Analyst*, 1988, 113, 361.

Iodimetric Method for Measuring Low Concentrations of Diacetyl Peroxide, Using Hydrogen Peroxide as a Catalyst

D. Martin Davies and Michael Edward Deary
Department of Chemical & Life Sciences, Newcastle upon Tyne Polytechnic, Newcastle upon Tyne NE1 8ST

Peracids and, when ammonium heptamolybdate is present, hydrogen peroxide, react rapidly with iodide in acidic conditions to form iodine, which can be measured spectrophotometrically as I_3^- at 352 nm. Diacyl peroxides, however, react very slowly with iodide, even in the presence of the ammonium heptamolybdate catalyst.[1] Therefore, for iodimetric methods of measuring diacyl peroxide, interference from oxygen is a problem under the acidic assay conditions used, and the assay must be carried out under nitrogen.[2] When measuring very low concentrations of diacyl peroxides complete exclusion of oxygen is required, and this is very difficult.

We describe here a potential iodimetric spectrophotometric method for determining low concentrations of diacyl peroxides, which overcomes the problem of oxygen interference by using hydrogen peroxide as a catalyst. We have used the term "catalyst" to describe the role of hydrogen peroxide in this method, even though the hydrogen peroxide is itself consumed. However, as Moore and Pearson[3] state, "from a practical point of view, a catalyst is a substance that changes the rate of a desired reaction, regardless of the fate of the catalyst itself."

Experimental

Apparatus

Absorbance measurements were made at 25 °C using a Hewlett-Packard HP 8451 A diode array spectrophotometer, fitted with a 290 nm UV cut-off filter and thermostated cell holder.

Reagents

p-Nitrophenyl acetate (PNPA), 30% hydrogen peroxide (AnalaR) and buffer components of the best available grade were obtained from BDH. Peroxyacetic acid (Proxitane 4002) was kindly donated by Interox Ltd. Solutions were made up in distilled water and in general contained 1×10^{-4} M EDTA to inhibit metal-ion catalysed decomposition of the peroxides. The reaction of peracetic acid and hydrogen peroxide, which at high pH is catalysed by minute trace quantities of metal ions,[4] was utilised to remove hydrogen peroxide from the proxitane.[5] Diacetyl peroxide (DAP) was generated *in situ* by mixing, in equal volumes, solutions of PNPA (in distilled water) and peracetic acid (in pH 6.8 phosphate buffer, $I = 0.2$ M):

$$CH_3(CO)OC_6H_4NO_2 + CH_3(CO)OOH \rightarrow CH_3(CO)OO(CO)CH_3 + HOC_6H_4NO_2$$

Fig. 1 shows concentrations of peracetic acid and *p*-nitrophenol (PNP) during the course of the reaction. PNP was measured at 400 nm. Peracetic acid was determined by a spectrophotometric iodimetric method.[6] Since this required triiodide to be measured at 352 nm, it was essential that the absorbance was corrected for the interfering PNP absorbance at 352 nm. The formation of diacetyl peroxide in Fig. 1 is indicated by the initial rapid decrease in the concentration of peracetic acid.

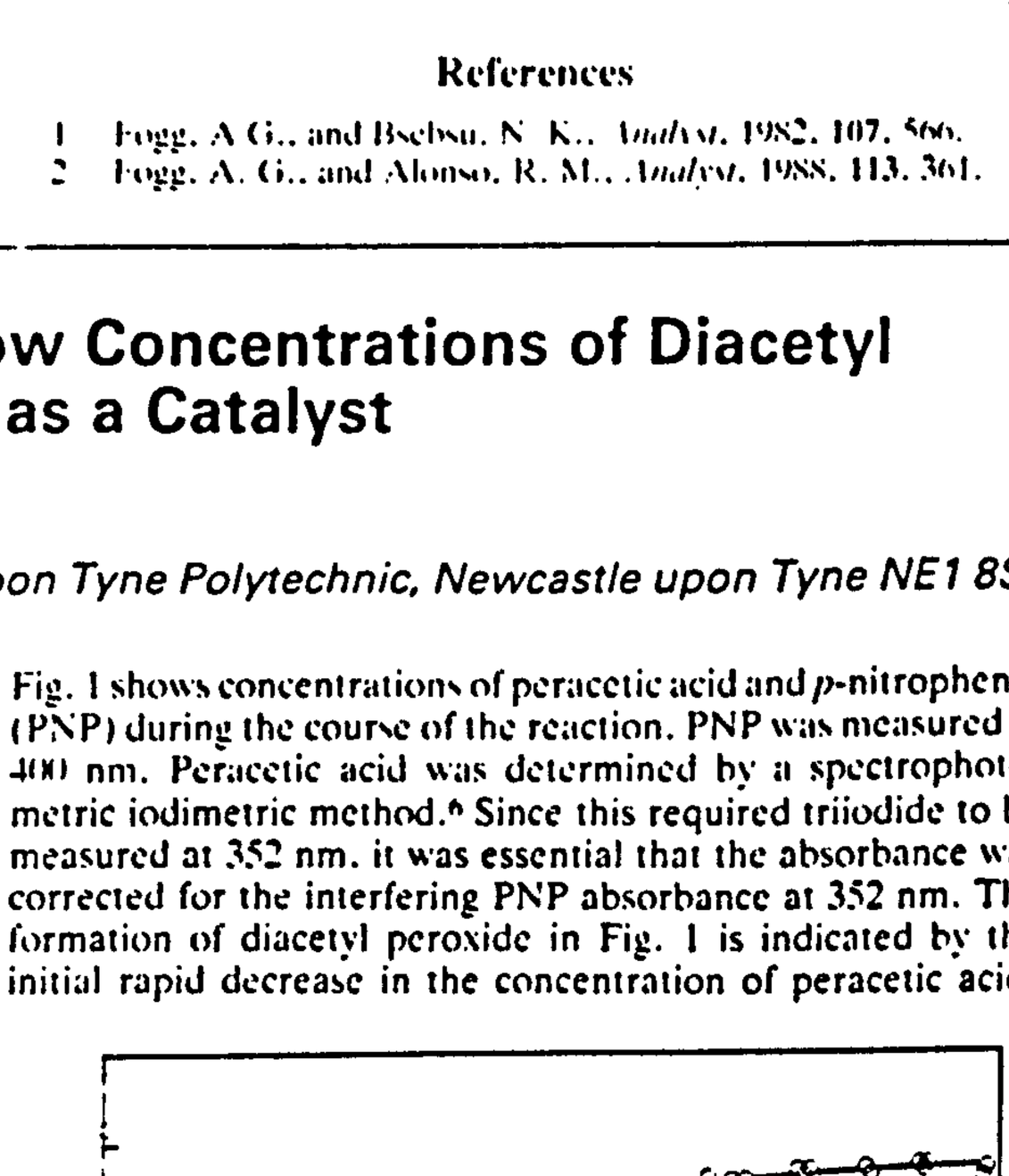

Fig. 1. Change in the concentration of peracetic acid during and after its reaction with PNPA: ○, peracetic acid concentration; △, *p*-nitrophenol concentration. $[PNPA]_0$ 4.9×10^{-4} mol l^{-1}, $[peracetic\ acid]_0$ 9.2×10^{-4} mol l^{-1}; phosphate buffer pH 6.8, $I = 0.1$ mol l^{-1} containing 1×10^{-4} mol l^{-1} EDTA. The curve represents the best fit obtained by using the non-linear least squares method

The concentration of peracetic acid subsequently rises due to regeneration *via* the hydrolysis reaction of diacetyl peroxide:

$$CH_3(CO)OO(CO)CH_3 + HO^- \rightarrow CH_3(CO)O^- + CH_3(CO)OOH + H^+$$

The concentration of peracetic acid eventually returns to the original level ($[PNPA]_0$).

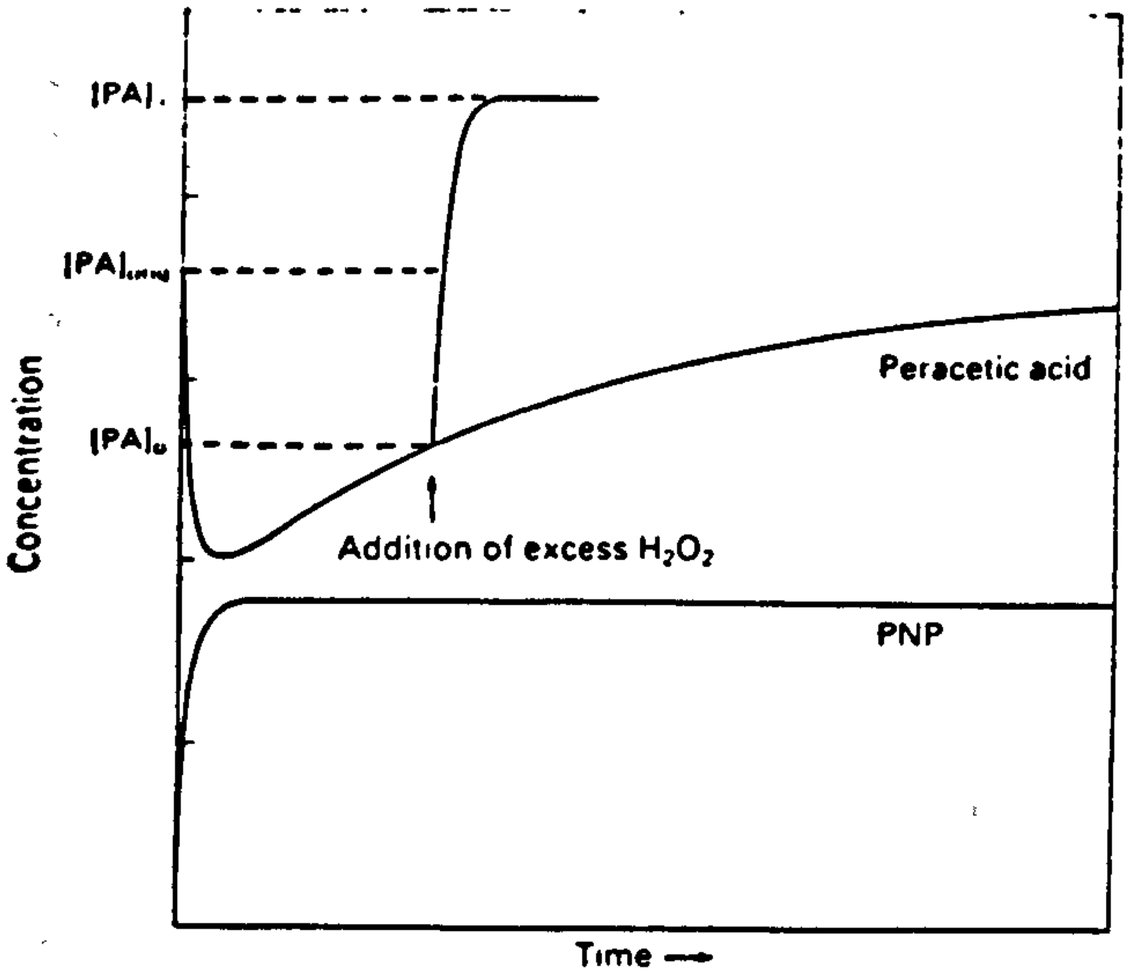

Fig. 2. Schematic representation of the release of peracetic acid from diacetyl peroxide upon addition of an excess of hydrogen peroxide. $[PA]_{add}$ is the concentration of peracetic acid used to react with the PNPA to form diacetyl peroxide. $[PA]_0$ is the peracetic acid concentration at the time of addition of hydrogen peroxide to the diacetyl peroxide, and $[PA]_\infty$ is the subsequent final concentration of peracetic acid attained

Assay Theory

Diacetyl peroxide is slowly hydrolysed at pH 6.8; however, it reacts much more rapidly with hydrogen peroxide to yield two molecules of peracetic acid:

$$CH_3(CO)OO(CO)CH_3 + HOO^- \rightarrow 2CH_3(CO)OO^- + H^+$$

If a small volume of hydrogen peroxide is added to a solution of diacetyl peroxide, as shown schematically in Fig. 2, and the subsequent increase in concentration of peracetic acid is measured by using a recently developed method for the determination of peracid in the presence of an excess of hydrogen peroxide,[6] then the diacetyl peroxide concentration can be calculated as follows:

$$[DAP] = \frac{\Delta[PA]}{2} \quad .. \quad .. \quad .. \quad (1)$$

where $\Delta[PA] = [PA]_\infty - [PA]_0$, $[PA]_0$ is the peracetic acid concentration at the time of addition of hydrogen peroxide to the assay mix and $[PA]_\infty$ is the final concentration of peracetic acid attained.

Equation (1) assumes negligible contribution to the peracetic acid increase from DAP hydrolysis reaction and negligible peroxide decomposition.

Assay

To a 10-ml aliquot of diacetyl peroxide solution, 0.05 ml of hydrogen peroxide of known concentration is added and the subsequent release of peracetic acid is followed until $[PA]_\infty$ is reached. This is shown in Fig. 3 for a hydrogen peroxide concentration of 2.54×10^{-4} M (concentration in cuvette). $[PA]_0$ is obtained immediately before addition of the hydrogen peroxide.

Results and Discussion

The assay was carried out for a range of diacetyl peroxide concentrations. Also, a range of hydrogen peroxide concentrations was used to react with DAP in order to obtain a second-order rate constant for the reaction.[5,7]

Fig. 4 shows a plot of observed against expected diacetyl peroxide concentrations. The expected DAP concentration was obtained from $[PA]_\infty - [PA]_0$. The slope was 1.2 ± 0.08* although a negative y intercept was observed [$(0.40 \pm 0.29^*) \times 10^{-6}$ mol l^{-1}], most probably due to the contribution of DAP hydrolysis to peracetic acid regeneration, assumed by equation (1) to be negligible.

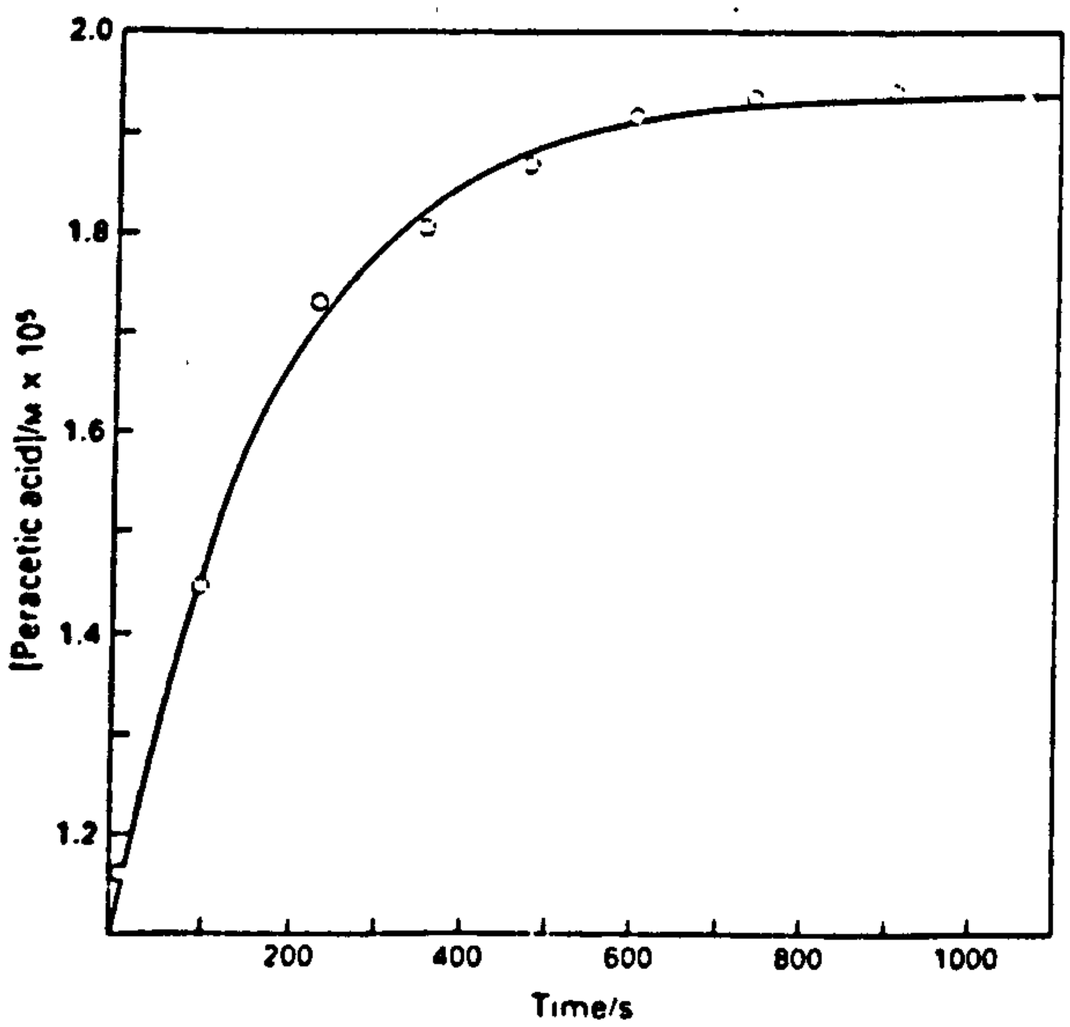

Fig. 3. Increase in the concentration of peracetic acid after the addition of an excess of hydrogen peroxide to diacetyl peroxide [H_2O_2]. 2.542×10^{-4} mol l^{-1} phosphate buffer pH 6.8, $I = 0.1$ mol l^{-1} containing 1×10^{-5} mol l^{-1} EDTA. The curve represents the best fit obtained by using the non-linear least squares method. Peroxide concentrations are those in cuvette

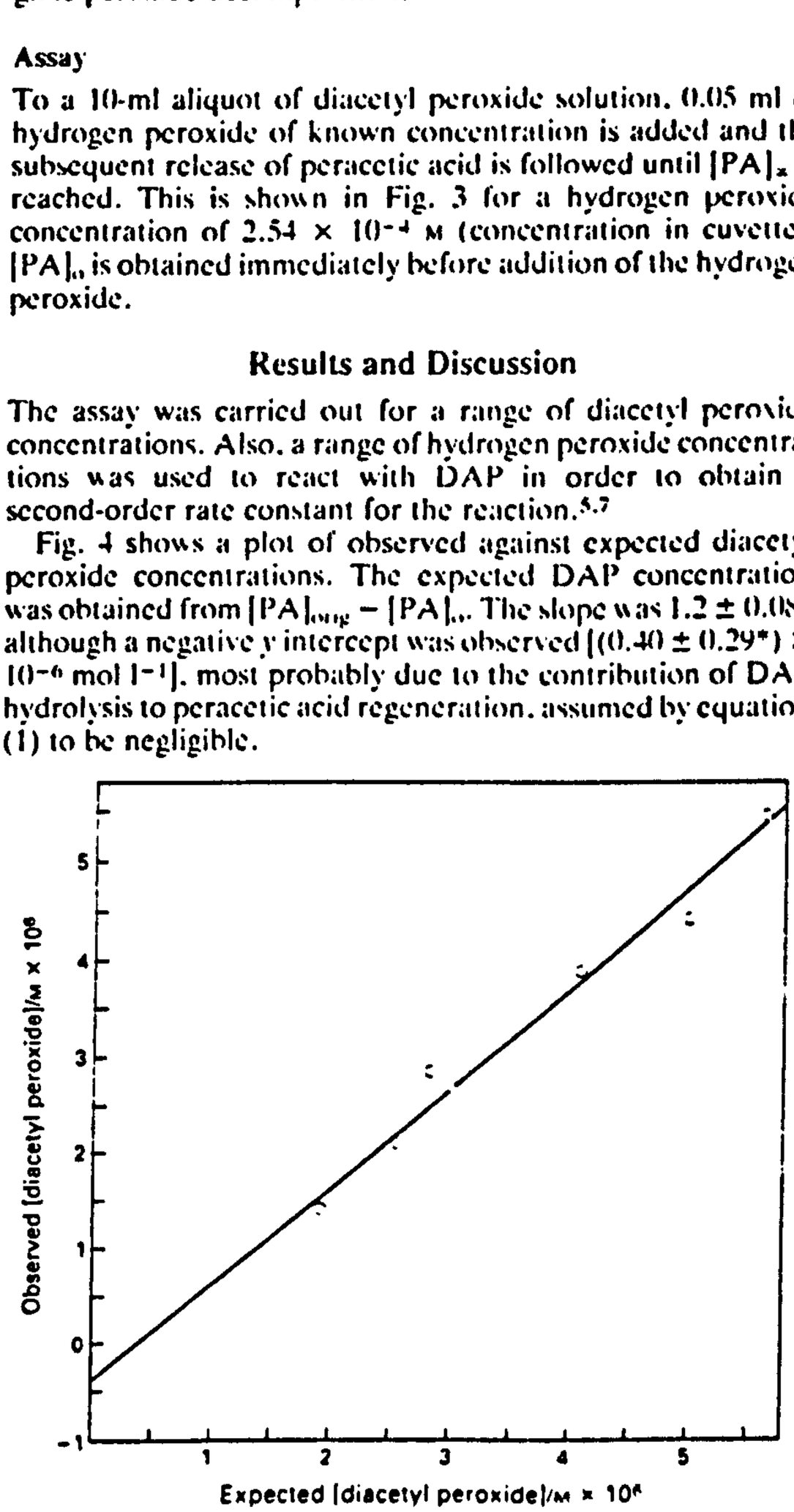

Fig. 4. Observed *versus* expected diacetyl peroxide concentrations. The line represents the best fit obtained by using the linear least squares method

In Fig. 3 an assay time of approximately 1000 s was required to reach $[PA]_\infty$. It would be possible by using a recently published method[6] to determine peracetic acid accurately in the presence of at least 10 times the concentration of hydrogen peroxide shown in Fig. 3. This would achieve a rapid assay time (~ 100 s) and eliminate the slight negative bias caused by DAP hydrolysis during the assay.

We plan to carry out further development and characterisa-

* Best fit ± σ.

tion of this assay using diacetyl peroxide, or analogous compounds such as benzoyl peroxide, standardised by an established method.[2]

We thank Warwick International Limited for funding a Graduate Research Assistantship (to MED).

References

1. Purcell, T. C., and Cohen, I. R., *Environ. Sci. Technol.*, 1967, **1**, 431.
2. Welcher, F. J., *Editor*, "Standard Methods of Chemical Analysis," Sixth Edition, Volume 2, Part A, D. Van Nostrand Company Inc, New York, 1962, p. 411.
3. Moore, J. W., and Pearson, R. G., "Kinetics and Mechanism," Third Edition, Wiley, New York, 1981.
4. Evans, D. F., and Upton, M. W., *J. Chem. Soc., Dalton Trans.*, 1985, 1151.
5. Davies, D. M., and Deary, M. E., *J. Chem. Res. (M)*, 1988, 2720.
6. Davies, D. M., and Deary, M. E., *Analyst*, 1988, **113**, 1477.
7. Davies, D. M., and Deary, M. E., *J. Chem. Res. (S)*, 1988, 354.

Chemiluminescence Detection of a Benzodiazepine

Anthony R. J. Andrews and Alan Townshend
School of Chemistry, University of Hull, HU6 7RX

Chemiluminescence is the term for light emitted during chemical reactions. These reactions are nearly always oxidation reactions. Light is emitted if a reaction product or intermediate is formed in an electronically excited state, which then relaxes to the ground state by emission of a photon:

$$A + B \rightarrow P^* \rightarrow P + \text{Photon}$$

The efficiency of this process can often be increased by using a suitable fluorescent molecule (S) which has an excitation spectrum overlapping the emission spectrum of the donor molecule. This energy exchange, called sensitisation, is shown below.

$$P^* + S \rightarrow P + S^*$$
$$S^* \rightarrow S + \text{Photon}$$

The advantages of chemiluminescence detection are its high sensitivity, selectivity and low cost, particularly when using flow injection methods in conjunction with chemiluminescence detection.

Flow injection is frequently used for chemiluminescence studies.[1-17] It has been found greatly to facilitate chemiluminescence monitoring because it permits the rapid and reproducible mixing of the sample and reagents in a light-tight cell with minimal sample-handling problems. Very rapid emissions, which commonly occur in chemiluminescence systems, are easily accommodated by construction of an appropriate detector assembly. Such a set-up is also readily applicable to HPLC detection.

Chemiluminescence is being investigated for the detection of various drugs. Examples of drugs that can presently be detected in this way are morphine,[1,18] tetracycline[2] and *N,N*-dimethyltryptamine.[19] In an attempt to extend this range, another class of drugs, the benzodiazepines, was investigated.

The benzodiazepines are now the most frequently prescribed psychotropic drugs in the world.[20] Their widespread use has led to problems of both dependence and abuse. All benzodiazepines marketed around the world are analogues of the basic structure shown in Fig. 1. It is this similarity between the available benzodiazepines, and the need for a universal detection technique, that led to chemiluminescence being investigated for their possible detection.

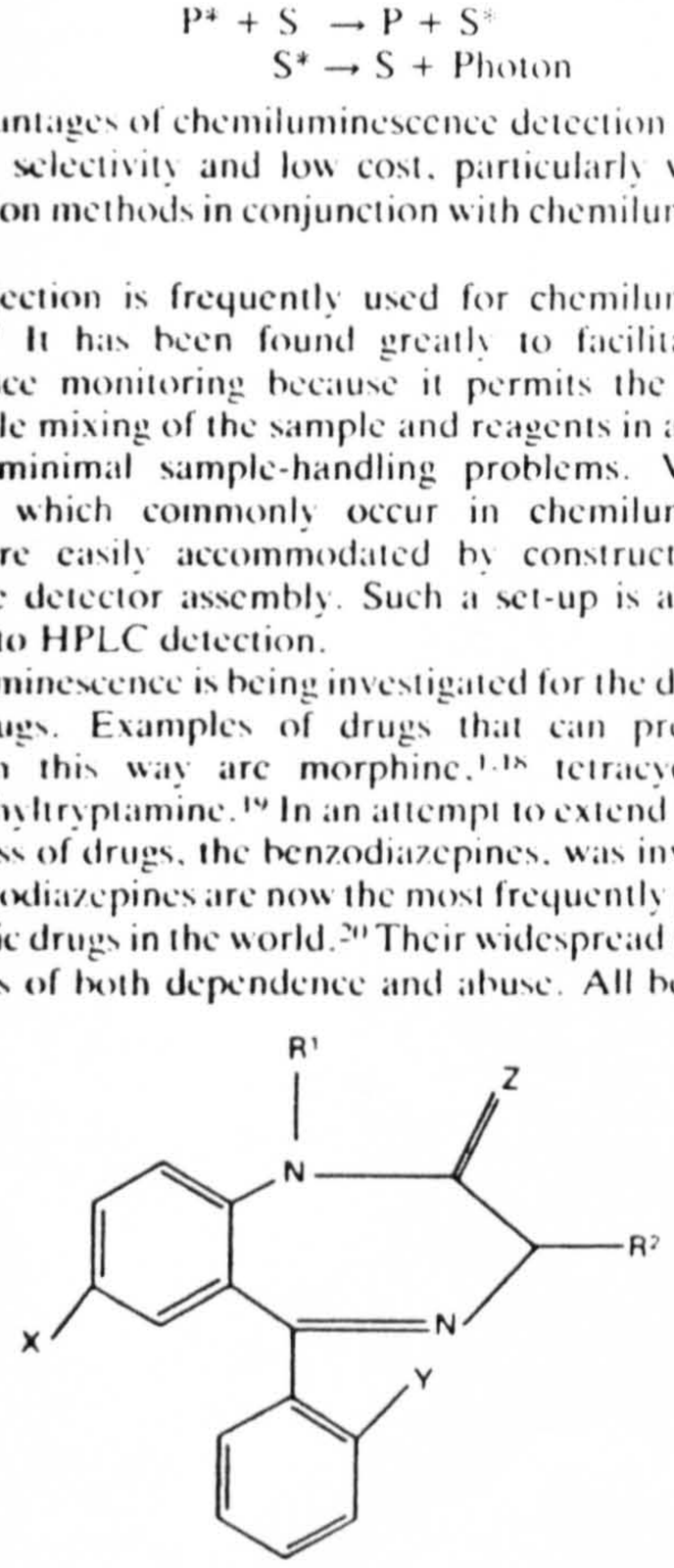

X and Y can be halogen, nitro or amine groups
Z is usually oxygen
R¹ and R² are alkyl groups

Fig. 1. General benzodiazepine structure

Experimental

The benzodiazepines were screened for chemiluminescence by using the flow injection manifold and detector assembly shown in Fig. 2. The flow cell and detector were as described previously.[1,11]

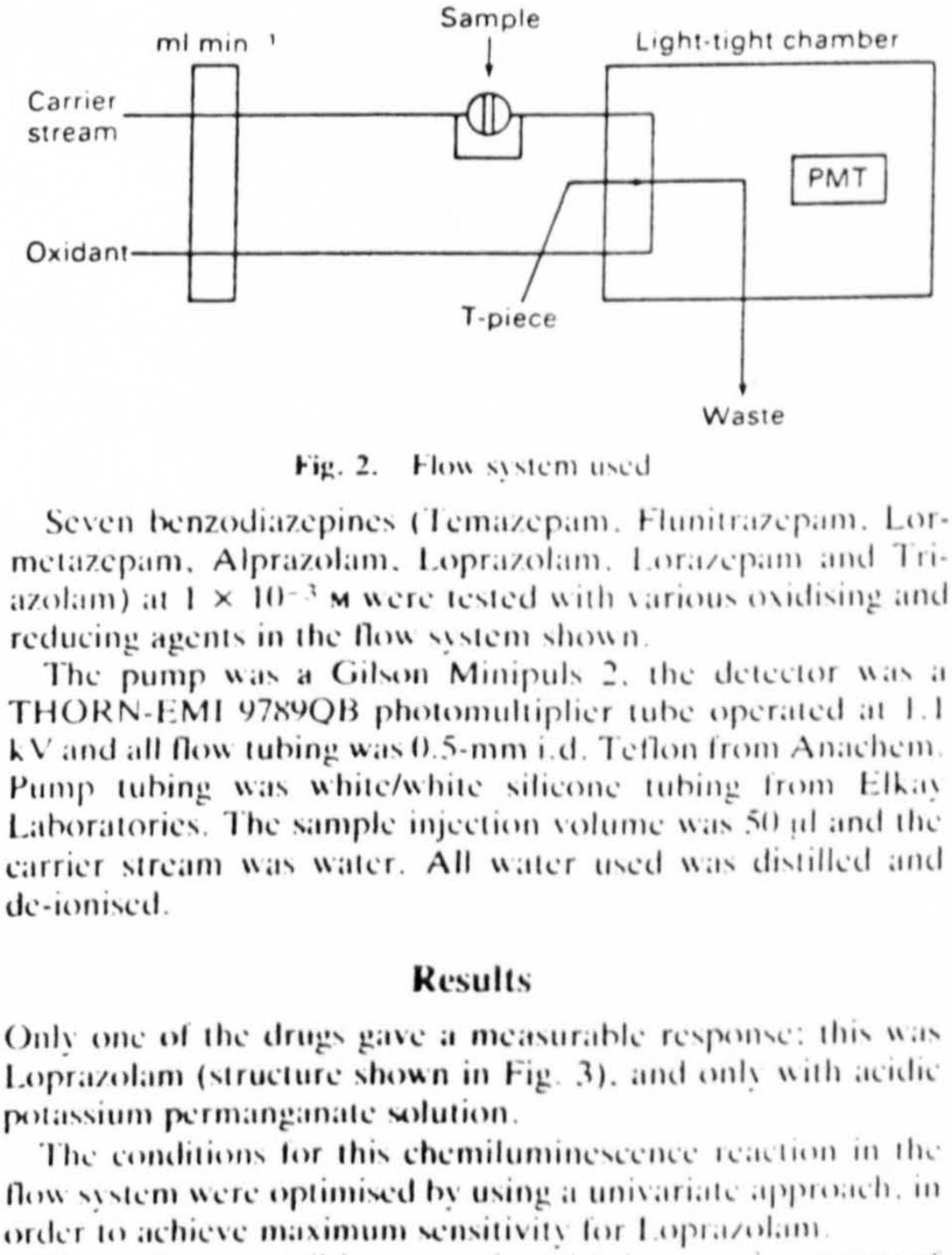

Fig. 2. Flow system used

Seven benzodiazepines (Temazepam, Flunitrazepam, Lormetazepam, Alprazolam, Loprazolam, Lorazepam and Triazolam) at 1×10^{-3} M were tested with various oxidising and reducing agents in the flow system shown.

The pump was a Gilson Minipuls 2, the detector was a THORN-EMI 9789QB photomultiplier tube operated at 1.1 kV and all flow tubing was 0.5-mm i.d. Teflon from Anachem. Pump tubing was white/white silicone tubing from Elkay Laboratories. The sample injection volume was 50 µl and the carrier stream was water. All water used was distilled and de-ionised.

Results

Only one of the drugs gave a measurable response; this was Loprazolam (structure shown in Fig. 3), and only with acidic potassium permanganate solution.

The conditions for this chemiluminescence reaction in the flow system were optimised by using a univariate approach, in order to achieve maximum sensitivity for Loprazolam.

The optimum conditions were found to be a carrier stream of 0.94 M formic acid at pH 0.9 (adjusted with hydrochloric acid), 2×10^{-4} M potassium permanganate, and a pump speed of 600, which avoids excessive reagent consumption, as it corresponds to a flow-rate of 1.3 ml min^{-1} in each line.

Water was used as the solvent for Loprazolam. Although ethanol gave rise to more intense emissions (relative CL, 2.9:1, ethanol:water), problems arose with the use of ethanol